ANL-83-4
NEANDC(US)-214/L

ANL-83-4
NEANDC(US)-214/L

Proceedings of the NEANDC/NEACRP Specialist's Meeting on Fast-Neutron Capture Cross Sections

April 20-23, 1982, at Argonne National Laboratory

Edited by
A. B. Smith and W. P. Poenitz
Argonne National Laboratory

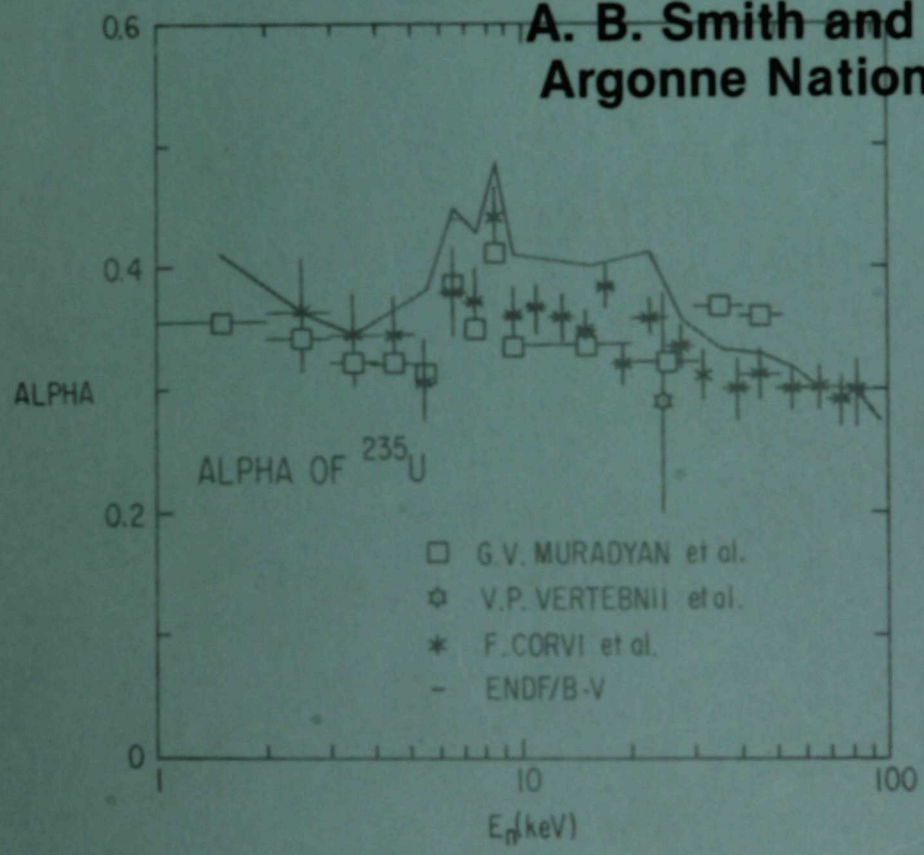

BASE TECHNOLOGY

ARGONNE NATIONAL LABORATORY, ARGONNE, ILLINOIS

Operated for the U. S. DEPARTMENT OF ENERGY
under Contract W-31-109-Eng-38

DISCLAIMER

This report was prepared as an account of work sponsored by an agency of the United States Government. Neither the United States Government nor any agency thereof, nor any of their employees, makes any warranty, express or implied, or assumes any legal liability or responsibility for the accuracy, completeness, or usefulness of any information, apparatus, product, or process disclosed, or represents that its use would not infringe privately owned rights. Reference herein to any specific commercial product, process, or service by trade name, trademark, manufacturer, or otherwise, does not necessarily constitute or imply its endorsement, recommendation, or favoring by the United States Government or any agency thereof. The views and opinions of authors expressed herein do not necessarily state or reflect those of the United States Government or any agency thereof.

Printed in the United States of America
Available from
National Technical Information Service
U. S. Department of Commerce
5285 Port Royal Road
Springfield, VA 22161

NTIS price codes
Printed copy: A99
Microfiche copy: A01

Distribution Category:
LMFBR Physics: Base
Technology (UC-79d)

ANL-83-4
NEANDC(US)-214/L

ARGONNE NATIONAL LABORATORY
9700 South Cass Avenue
Argonne, Illinois 60439

Proceedings of the NEANDC/NEACRP Specialist's Meeting on FAST-NEUTRON CAPTURE CROSS SECTIONS

April 20-23, 1982
at Argonne National Laboratory

Cosponsored by

Argonne National Laboratory
and the
Organization for Economic Cooperation and Development

Edited by

A. B. Smith and W. P. Poenitz
Argonne National Laboratory

NOTICE

The Organization for Economic Co-operation and Development (OECD) was set up under a Convention signed in Paris on 14th December, 1980, which provides that the OECD shall promote policies designed:

- to achieve the highest sustainable economic growth and employment and a rising standard of living in Member countries, while maintaining financial stability, and thus to contribute to the development of the world economy:
- to contribute to sound economic expansion in Member as well as non-member countries in the process of economic development.
- to contribute to the expansion of world trade on a multilateral, non-discriminatory basis in accordance with international obligations.

The Members of OECD are Australia, Austria, Belgium, Canada, Denmark, Finland, France, the Federal Republic of Germany, Greece, Iceland, Ireland, Italy, Japan, Luxembourg, the Netherlands, New Zealand, Norway, Portugal, Spain, Sweden, Switzerland, Turkey, the United Kingdom and the United States.

The OECD Nuclear Energy Agency (NEA) was established on 20th April 1972, replacing OECD'S European Nuclear Energy Agency (ENEA) on the adhesion of Japan as a full Member.

NEA now groups all the European Member countries of OECD and Australia, Canada, Japan, and the United States. The Commission of the European Communities takes part in the work of the Agency.

The primary objectives of NEA are to promote co-operation between its Member governments on the safety and regulatory aspects on nuclear development, and on assessing the future role of nuclear energy as a contributor to economic progress.

This is achieved by:

- encouraging harmonization of governments' regulatory policies and practices in the nuclear field, with particular reference to the safety of nuclear installations, protection of man against ionizing radiation and preservation of the environment, radioactive waste management, and nuclear third party liability and insurance;
- keeping under review the technical and economic characteristics of nuclear power growth and of the nuclear fuel cycle, and assessing demand and supply for the different phases of the nuclear fuel cycle and the potential future contribution of nuclear power to overall energy demand;
- developing exchanges of scientific and technical information on nuclear energy, particularly through participation in common services;
- setting up international research and development programs and undertakings jointly organized and operated by OECD countries.

In these and related tasks, NEA works in close collaboration with the International Atomic Energy Agency in Vienna, with which it has concluded a Co-operation Agreement, as well as with other international organizations in the nuclear field.

LEGAL NOTICE

The Organization for Economic Co-operation and Development assumes no liability concerning information published in this Bulletin.

Organizing Committee

D. Gayther, Atomic Energy Research Establishment (UK)
G. Grenier, Centre d'Etudes de Nucleaires, Bruyéres-le-Châtel (France)
F. Froehner, Kernforschungszentrum Karlsruhe (FRG)
R. Peelle, Oak Ridge National Laboratory (US)
W. Poenitz, Argonne National Laboratory (US)
A. Smith, Argonne National Laboratory (US)
S. Tanaka, Japan Atomic Energy Research Institute (Japan)
N. Tubbs/C. Nordborg, Organization for Economic Cooperation and Development

Meeting Chairman

A. Smith, Argonne National Laboratory

Scientific Secretary

W. Poenitz, Argonne National Laboratory

Working Group Chairmen

Group 1, Fertile and Fissile Nuclei; R. Peelle, Oak Ridge National Laboratory

Group 2, Structural Materials; F. Froehner, Kernforschungszentrum Karlsruhe

Group 3, Fission-Product Nuclei; H. Gruppelaar, Netherlands Energy Research Foundation

Arrangements

M. Holden, Argonne National Laboratory

PROGRAM AND TABLE OF CONTENTS

INTRODUCTION

Welcoming Remarks-- C. Till, Associate Laboratory Director, Argonne National Laboratory

Administrative Comments-- A. Smith

TECHNICAL SESSIONS

Page

I. APPLICATION AND BASIC OVERVIEWS--

A. Smith, Chairman

A. APPLICATIONS

A-1. Neutron Capture Data and FBR Performance Predictions--P. Collins, Argonne National Laboratory 1

B. BASIC CONCEPTS

B-1. A Review of the Fundamentals of the Neutron-Capture Reaction--R. Chrien, Brookhaven National Laboratory. 18

B-2. Fast-Neutron Capture Mechanisms for Neutron-Energies Between 0.5 and 6.0 MeV--S. Joly, G. Grenier and J. Voignier, Centre d'Etudes de Nucleaires, Bruyères-le-Châtel. 57

B-3. E1-Gamma Strength from (γ,n) Measurement in ^{95}Mo--C. Coceva and M. Magnani and M. Stefanon, ENEA, Bologna. 63

C. CALCULATIONAL MODELS AND METHODS

C-1. Current Status of Fast-Neutron Capture Calculations--D. Gardner, Lawrence Livermore National Laboratory. 67

C-2. Calculation of Average Capture Cross Sections for Actinides: Level-Statistical vs. Global Approach--F. Froehner, B. Goel and U. Fischer, Kernforschungszentrum Karlsruhe 116

C-3. The use of ABAREX for Neutron Capture Calculations--P. Moldauer, Argonne National Laboratory 125

C-4. Total Gamma-ray Spectra and Isomeric-Ratio Calculations in Fast-Neutron Radiative Capture--G. Reffo, ENEA, Bologna. 133

II. REFERENCE-STANDARD CAPTURE CROSS SECTIONS--

A. Smith, Chairman

The Gold Standard Capture Cross Section from 100 keV to 15 MeV--T. Ryves, National Physical Laboratory. 144

III. EXPERIMENTAL TECHNIQUES AND MEASUREMENTS--

C. Nordborg, Chairman

A. ABSORPTION AND ACTIVATION TECHNIQUES

A-1. On Absorption and Activation Techniques in Measurements of Fast-Neutron Capture Cross Sections--I. Bergqvist, University of Lund . . 162

A-2. Absolute Measurements of the Fast Neutron Capture Cross Section of ^{115}In--D. Grady, G. Knoll and J. Robertson, University of Michigan 179

A-3. Measurements and Model Calculations of the ^{110}Cd(n;γ)^{111m}Cd Cross Section--D. Smith, J. Meadows, P. Moldauer and W. Poenitz, Argonne National Laboratory. 186

A-4. Neutron-Capture-Activation Cross Sections of ^{94,96}Zr and ^{98,100}Mo at Thermal and 30 keV Energies--J. Wyrick and W. Poenitz, Argonne National Laboratory. . . . 196

B. PROMPT-DETECTION TECHNIQUES

B-1. Prompt Gamma-ray Detectors for the Measurement of Neutron Capture Cross Sections--D. Gayther and R. Thom, Atomic Energy Research Establishment 205

B-2. Fast-Neutron Capture-Cross-Section Measurements with the ANL Large-Liquid-Scintillator Tank--W. Poenitz, Argonne National Laboratory. 239

B-3. Fast-Neutron Capture-Cross-Section Measurements Using a NaI Detector--S. Joly, G. Grenier and J. Voignier, Centre d'Etudes de Nucleaires, Bruyères-le-Châtel 248

Page

B-4. Fast-Neutron Capture-Cross-Section Measurement with the Pulse-Height-Weighting Technique--N. Yamamuro, M. Igashira and M. Shimizu, Tokyo Institute of Technology 255

B-5. Gamma-rays from Radiative-Capture Reactions in ^{133}Cs, ^{181}Ta and ^{197}Au--N. Yamamuro, M. Igashira, H. Shirayanagi, Y. Fujita and K. Kobayashi, Tokyo Institute of Technology and Kyoto University. 262

C. EXPERIMENTAL CORRECTIONS AND ASSESSMENTS

C-1. Averaging $\sigma(n,\gamma)$ in the Transition Region E_n= 1-150 keV— R. Macklin, Oak Ridge National Laboratory 275

C-2. Correction Techniques for Cross Section and Angular-Distribution Measurements in Fast-Neutron Capture--S. Joly, G. Grenier, and J. Voignier, Centre d'Etudes de Nucleaires, Bruyères-le-Châtel. 281

IV. FISSILE AND FERTILE CAPTURE--

S. Whetstone, Chairman

A. FERTILE CAPTURE

A-1. Fast-Neutron Capture in ^{238}U and ^{232}Th--W. Poenitz, Argonne National Laboratory 288

A-2. Absolute Measurement of the Cross Section for 23-keV Neutron Activation of Thorium--G. Baldwin and G. Knoll, University of Michigan. 302

B. FISSILE CAPTURE

B-1. Status of Neutron Capture Data of ^{233}U, ^{235}U and ^{239}Pu in the Unresolved-Resonance Region--F. Corvi, Bureau Central de Measures Nucleaires 314

B-2. Fast-Neutron Capture in Actinide Isotopes; Recent Results from Karlsruhe--K. Wisshak, F. Käppeler, G. Reffo and F. Fabbri, Kernforschungszentrum Karlsruhe 336

Page

B-3. Measurement of Neutron-Capture Cross Section and Alpha of ^{235}U from 2-85 keV--F. Corvi, L. Calabretta, M. Merla, T. van der Veen and M. Moore, Bureau Central de Measures Nucleaires. 347

C. CAPTURE IN OTHER IMPORTANT ACTINIDES

C-1. Review of Fast-Neutron Capture Cross Sections of the Higher-Plutonium Isotopes and ^{241}Am--L. Weston, Oak Ridge National Laboratory 355

C-2. Actinide Integral Measurements in the CFRMF and Integral Tests for ENDF/B-V--R. Anderl, Y. Harker and J. Rodgers, Idaho National Engineering Laboratory. 369

C-3. Some Aspects of the Evaluation of ^{237}Np, ^{238}Pu and ^{241}Am Capture-Cross-Sections in the Unresolved Region--H. Derrien, Centre d'Etudes Nucleaires, Cadarache 379

V. STRUCTURAL-MATERIAL CAPTURE--

D. Gayther, Chairman

1. Status of Structural Data in the Resolved Resonance Region--G. Rohr, Bureau Central de Measures Nucleaires 394

2. Neutron Capture Widths of S-Wave Resonances in ^{56}Fe, $^{58,60}Ni$ and ^{27}Al--K. Wisshak, F. Käppeler, G. Reffo and F. Fabbri, Kernforschungszentrum Karlsruhe 417

3. Evaluation of the Radiation Width of the 27.7 keV Resonance in ^{56}Fe--B. Allen, Lucas Heights (AAEC). 431

VI. FISSION-PRODUCT CAPTURE--

R. Schenter, Chairman

A. DIFFERENTIAL MEASUREMENTS

A-1. Differential Fission-Product-Capture Measurements Since Bologna--R. Block, Rensselaer Polytechnic Institute 437

A-2. Average Capture Cross Sections of the Fission-Product Nuclei ^{105}Pd and ^{108}Pd--G. Rohr, C. Bastian, F. Cornelis, R. Shelley, T. van der Veen and G. Vanpraet, Central Bureau de Measures Nucleaires 464

Page

A-3. Status of Recent Fast-Capture-Cross-Section Evaluations for Important Fission-Product Nuclides--H. Gruppelaar, Netherlands Energy Research Foundation 473

B. INTEGRAL MEASUREMENTS AND TESTS

B-1. Integral Measurements and Tests of Fission-Product Neutron Capture Cross Sections--R. Anderl, Idaho National Engineering Laboratory. 518

VII. SUMMARY PLENARY SESSION

A. REPORTS OF THE WORKING GROUPS

A-1. Fast-Neutron Capture in Fissile and Fertile Nuclides--Chairman R. Peelle, Oak Ridge National Laboratory 557

A-2. Fast-Neutron Capture in Structural Materials--Chairman F. Froehner, Kernforschungszentrum Karlsruhe 564

A-3. Fast-Neutron Capture Cross Sections for the Most Important Fission-Product Nuclei--Chairman H. Gruppelaar, Netherlands Energy Research Foundation 570

B. SOME SUMMARY REFLECTIONS

A. B. Smith, Argonne National Laboratory 586

List of Participants 590

NEUTRON CAPTURE DATA AND FBR PERFORMANCE PREDICTIONS

by

Peter J. Collins
Argonne National Laboratory
Idaho Falls, Idaho, USA

Abstract

The accuracy requirements for Physics parameters in fast breeder reactors and the extent to which they are achieved through tests with integral experiments are reviewed. Sensitivities to capture cross sections are discussed for calculations of fuel enrichment, breeding ratio, reactivity, safety parameters, power distributions, and control rod worths.

I. Introduction

Uncertainties in the prediction of physics parameters result in increased design margins to cover operational and safety requirements which lead to economic penalties. There is general agreement on what target accuracies are achievable. Table 1 shows the requirements for commercial plants from reviews in the U.S.[1], France[2], and the U.K.[3]. In addition to uncertainties due to basic nuclear data and bias factors applied, account must be taken of approximations in calculation methods and engineering limitations. To ensure that requirements are met with about 95% confidence, it is common to design for two standard deviation variations about the nominal values.

The target accuracies have been approached or achieved for many basic parameters in fresh cores through the extensive use of critical experiments. The integral data are used either to provide bias factors or alternatively in the production of adjusted data libraries which adequately fit the experimental results. Data adjustment had its origins in fitting measurements in relatively simple benchmark cores. Subsequent testing in more realistic mock-up experiments or with data from operating power reactors may require a re-adjustment or the additional use of bias factors. Sensitivity analyses, in varying degrees of detail, are used to obtain uncertainty estimates for the predicted parameters. These analyses use nuclear data uncertainties to treat the mismatch between experimental data and the design reactor.

Not all requirements can be met by integral data. Significant limitations arise from material inventories and in the reproduction of temperature effects. These are covered to some extent by zone experiments and studies of samples of materials in small amounts. Further improvements in nuclear data will have important impact in several areas; optimization of designs for commercial size reactors, operation and fuel-cycle related parameters, design for new concepts which may step significantly out of the range of cores for which data is now available.

Recent reviews of nuclear data needs for LMFBRs have been given by Hammer[2] and Rowlands[3]. In this paper, the present accuracies obtained for basic fast reactor parameters are reviewed in relation to the target accuracies and the influence of uncertainties in capture cross sections is discussed.

II. Critical Mass and Breeding Ratio

The calculated eigenvalue and breeding ratio in a plutonium uranium fueled fast reactor are strongly correlated because of the common reaction rates which occur in their formulation. Predictions of the critical mass at room temperatures can be made to better than one percent through the use of integral assemblies. The extension to operating temperatures introduces additional uncertainties due to expansion and Doppler effects. Further uncertainties arise in calculating the reactivity change over a burnup cycle. These are discussed in the next section. Uncertainties in the critical mass require increased fuel enrichments to guarantee operation over the designed fuel cycle. Uncertainties in the breeding ratio have an impact on design studies and economic planning.

Sensitivities (fractional change in a parameter divided by the fractional change in a cross section) are generated in detail by generalized perturbation methods. The energy integrated sensitivities for k_{eff} and breeding ratio (with no k-reset) for the initial loading of the Clinch River Breeder Reactor (CRBR) and for a U.S. conceptual design for a 1200 MWe heterogeneous core, taken from Kallfelz[4], are shown in Table 2. The CRBR initial core contains plutonium feed enrichment of 11% and the CDS design is for mid-equilibrium cycle. Similar sensitivities for a 1200 MWe conventional LMFBR design at equilibrium cycle are given by Marable[5]. The sensitivities are quite similar, apart from those for the higher plutonium isotopes, which reflect the higher content of ^{240}Pu and ^{241}Pu in the fuel for the commercial designs.

The integrated sensitivities can be used to give an estimate of the relative importance of the capture cross section integrated over the LMFBR spectra. Table 3 shows the percent change in cross sections which would lead to a 0.25% change in k_{eff} and 1% in breeding ratio. These variations result from similar cross section changes in the principal plutonium isotopes and in ^{238}U. The internal and external breeding ratios are sensitive to different energy ranges for ^{238}U capture because of the softer spectra in blanket zones. In making full use of sensitivity information it is necessary to consider correlations between the cross sections. Correlations between ^{238}U capture and ^{239}Pu fission are especially important because of their high sensitivities.

A study of the k_{eff} and breeding ratio biases and uncertainties for a large conventional LMFBR is described in detail by Marable et al. in Ref. 5. This work included covariance information for the fission, capture and ν data of ^{239}Pu, and ^{238}U, and ^{235}U. A data adjustment procedure was used, with benchmark integral data for k_{eff} and reaction rate ratios, to predict k_{eff} and breeding ratio biases and their uncertainties. Their results are shown in Table 4. The estimated standard deviations due to evaluated nuclear data were 3% for k_{eff} and 7% for breeding ratio. The standard

deviations making use of integral experiments reduced to 0.5% and 2% and approach the design goals. These results are similar to those obtained in other studies, for example Rowlands[6].

III. Fuel Cycle Reactivity

Changes in reactivity over a burnup cycle result from changes in heavy metal concentrations in the core, production of plutonium in blanket regions and capture in fission products. Integral data related to burnup effects are limited or indirect. However results are becoming available from the operating reactors themselves. The CARNAVAL adjusted data set utilizes integral measurements in zones with high ^{240}Pu content, irradiations of samples in PHENIX and RAPSODIE and integral data for fission product samples[7]. The ENDF/B-V fission product data for fast reactors included adjustment from integral measurements[8].

The method of determining the enrichments for the first loading of Superphenix is described by Giacometti[9]. Table 5, taken from the results in this reference, shows the reactivity changes and uncertainty components over the first cycle. The uncertainty in fission product reactivity results from an 8% uncertainty (1σ) in the CARNAVAL pseudo-FP data. The uncertainty due to heavy atom evolution in the core results from an uncertainty of 0.003 in the internal breeding gain of -0.013. These uncertainties are taken into account by an increase in enrichment of 3.9% (increase of 220 kg plutonium) and result in a 25% increase in the reactivity loss per cycle and a 17% decrease in breeding gain.

The fuel enrichment specification for CRBR (heterogeneous core) is described by Lake[10]. After the first cycle of 128 efpd for the initial core, three blanket assemblies are replaced by fresh fuel and the second cycle occupies 200 efpd. The calculated burnup reactivity swings for the two cycles are shown in Table 6. The total excess reactivities and uncertainties including fuel fabrication and calculation uncertainties etc., are (1.335 ± 0.407) and (1.885 ± 0.727)% Δk at the end of each cycle. No bias is taken for the core conversion ratio and a conservative estimate of 5% uncertainty is assumed. A conservative estimate of 25% (1σ) is also assumed for the lumped fission product data for ENDF/B-III used in the calculations.

Recent analysis for CRBR using the ENDF/B-V fission product data and covariance matrices[11] shows a negligibly different reactivity bias (0.02% Δk the end-of-cycle-four) compared with the Version III fission product data. However the uncertainty is reduced by a factor of four to 6.4% (1σ).

Codes are becoming available to calculate sensitivities by time-dependent generalized perturbation theory[12,13]. These will provide economic means to study the fuel cycle problems in detail.

Recent reviews of nuclear data needs for actinides and fission products have been given by Kusters[14], Rowlands[15], and Hammer[16].

IV. Sodium Void Reactivity

Sodium void coefficients for input to fast reactor safety codes are usually calculated with fairly simple methods such as first order diffusion-perturbation theory with few energy groups. Such techniques introduce errors of the order of 10% but are sufficient in relation to the complication of the accident analysis. A target accuracy of 20% on the maximum positive sodium void reactivity is commonly regarded as acceptable. The target accuracies have been achieved through the large number of measurements made in mock-up experiments over the past decade. The uncertainties in extrapolation to the power reactors are taken into account. However, comparisons with experiment show consistent overpredictions of 10% to 15% with ENDF/B-IV data[17] and calculations with Version V data are only a few percent different. The source of this discrepancy is presumed to lie in the nuclear data.

Calculations with adjusted data sets show better agreement with experiment than for ENDF/B data. However bias factors significantly different from unity are obtained. Table 7 compares the non-leakage and leakage bias factors for FGL5[18], CARNAVAL-IV[19] and ENDF/B-IV. Note that the bias factors are also dependent upon the calculation methods employed.

In the operating reactor, control rods are withdrawn as fission products build up. A number of experiments have been made to study sodium voiding around boron control rods. The predictions are similar to those for cores with the rods withdrawn, provided transport corrections of the order of 10% are made.

Energy-integrated senstivities for voiding the inner core zone of a 1200 MWe conventional core are shown in Table 8. These were generated taking into account the spectrum change on complete voiding of the zone in an rz model. Relatively high sensitivities are found for capture cross sections, including those of structural materials and fission products. Figure 1 shows the energy variation of the sensitivities for capture in lumped fission products, ^{238}U, iron and molybdenum. The sensitivities are particularly large in the vicinity of the 2.8 KeV sodium resonance. The profiles for lumped fission products and uranium are similar because of the group-averaged data employed. Capture resonances in this energy range may have significant effects on sodium void reactivity. In the case of iron, the sensitivity around the 1.2 KeV resonance is an order of magnitude greater than elsewhere.

The spectrum changes upon sodium voiding must be taken into account when assessing the uncertainty due to fission products. Integral measurements of fission product worths and capture cross sections are required in both normal and voided spectra to high accuracy to provide these data. Experiments on sodium voiding in the presence of a fission product mixture have been made in the FCA assembly[20]. While the fission product worth was well predicted, the change in sodium void worth in the presence of this material was predicted badly compared with in zones containing Mo and Nb. It was concluded that more precise data for the capture cross section of fission product material was required in the 100 eV to 10 KeV range.

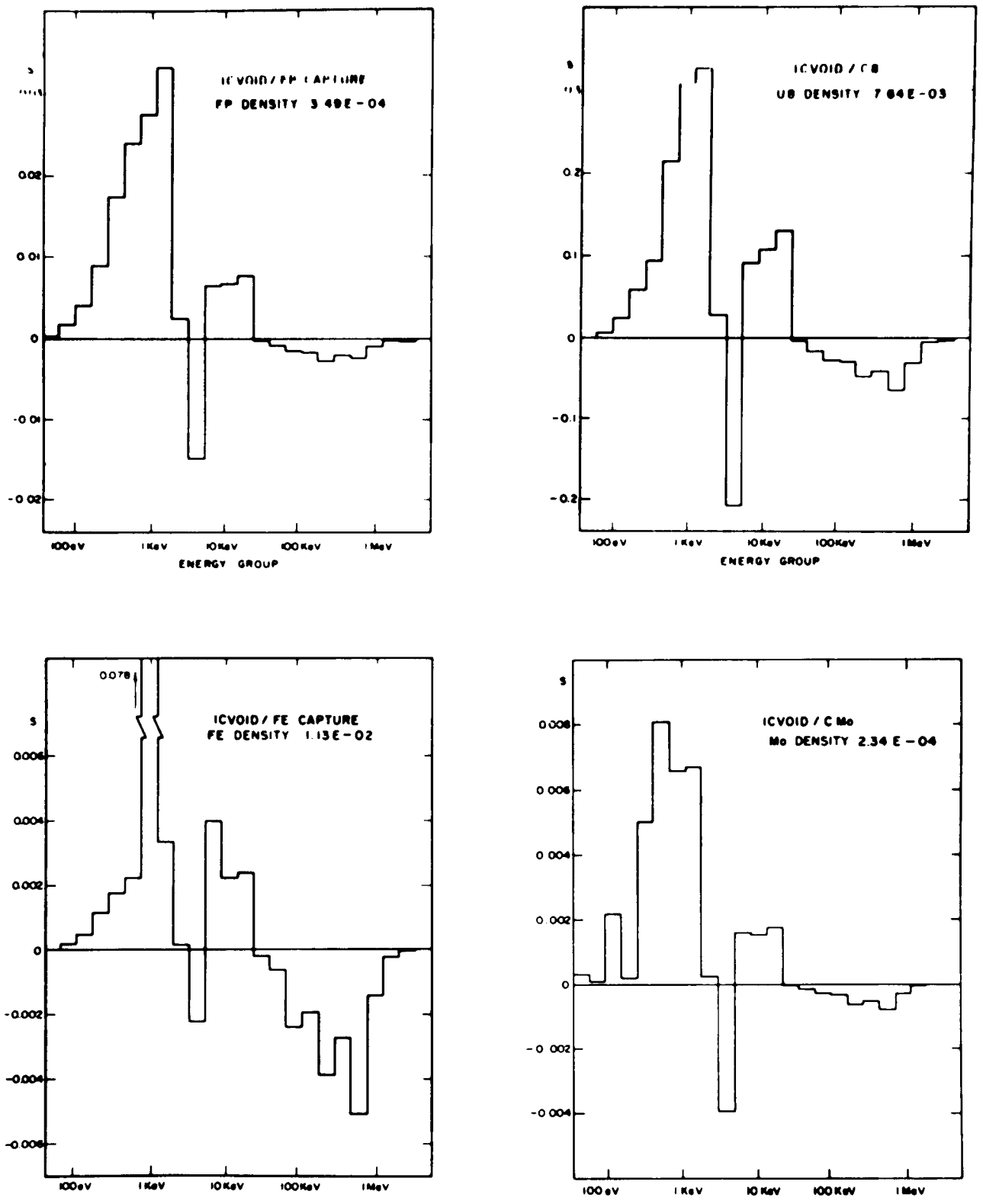

Fig. 1. Sensitivities of inner core sodium void to capture in lumped fission product, ^{238}U, iron, and molybdenum.

V. Doppler Effect

The Doppler coefficient of reactivity in fast reactors is due principally to resonances in ^{238}U. The energy range from 200 eV to 10 KeV accounts for 80-90% of the total Doppler effect. Uncertainties in the Doppler coefficient, apart from those due to the ^{238}U resonance parameters, arise from calculation of the fraction of neutrons in this energy range. For other materials an increase in capture cross sections decreases the Doppler effect.

Tests of calculated Doppler coefficients rely on the SEFOR experiments[22] supplemented by small sample Doppler measurements in critical experiments. Uncertainties of 12% to 15% result from these analyses when extrapolated to power reactors. Butland[21] has given estimates of additional uncertainties for extrapolation to the equilibrium fuel cycle. Fission products decrease the Doppler coefficient by 10%. An uncertainty in fission product capture of 10% results in uncertainties of 0.5% to 1.5% through the cycle for a two batch refuelling scheme. Uncertainties in the higher plutonium isotope data, 20% to 30% for capture, give uncertainties in the Doppler effect of 1% in the fresh core to 3% at full burnup.

The Doppler effect in steel may contribute as much as 10% to 15% of the isothermal Doppler coefficient in an LMFBR and its uncertainty must be considered. The Doppler effect in the converter region of the proposed U.S. safety test facility was due almost entirely to steel isotopes. Recent work has lead to improved algorithms for calculation of structural Doppler effects[23].

VI. Power Distributions

In the 300 MWe size conventional cores, little discrepancy in fission rate distributions in core regions has generally been found and target accuracies of about ±2% on the form factors have been satisfied with no bias factor requirements. Reaction rates deep into the blanket regions are often mispredicted, by as much as 5% to 10%.

The heterogeneous core designs and larger conventional cores show higher sensitivities. This is evident for the NEACRP sponsored intercomparison calculations[24], where marked differences were found among the contributors solutions. Table 9 shows a comparison of integrated sensitivities for a 300 MWe core and the 1200 MWe benchmark. Sensitivities for the larger core are much higher, sometimes by a factor of four. The ^{238}U capture sensitivity is dominant among the absorption reactions. However effects due to capture components of steel are not negligible in view of variations of up to 60% among processed multigroup libraries.

Sensitivities for the heterogeneous core designs at initial loading may be larger than for the conventional cores. However, the sensitivities decrease with burnup due to production of plutonium in the internal blankets leading to increased coupling between the fuel rings[25].

VII. Control Rod Worths

Target accuracies of 5% are achievable after bias factors are employed. However the rod worths are sensitive to approximations in the calculation methods. These must be carefully taken into account in the application of bias factors. Uncertainties of about 5% in the reactivity scale must be taken into account if a sufficiently faithful mock-up is not available. The most refined calculations tend to show a bias in comparison with experiment with some data sets[26]. The NEACRP comparison showed discrepancies in the central control rod worths of as much 30% between calculations using precisely specified methods. As in the case of power distributions, the ^{238}U capture sensitivity predominates among the absorption reactions but non-negligible components are found for capture in the diluent materials.

As might be expected from power shape misprediction, different biases are sometimes found, in the more sensitive cores, for control worths as a function of radius. C/E values for outer ring rod banks may be 5 to 10% higher than for inner rod positions. These discrepancies diminish after considerable refinements in calculation but discrepancies remain with the ENDF/B data[27]. Table 10 shows the energy-dependent sensitivities for a central rod and for the outer control rod bank in a conventional core of intermediate size. Because of the different signs in sensitivities between the two positions, a change in capture cross sections of 5% can change the relative predictions of the rod worths by 2%.

VII. Conclusion

At the present stage the data from integral experiments are essential in meeting target accuracies either in deriving bias factors or in the production of adjusted data sets. However, this information is limited in many areas and does not generally produce significant improvements in knowledge of differential data over the energy ranges corresponding to the group widths used in fast reactor analysis.

Reductions in the accuracies presently obtained are required in design parameters for the optimization of future commercial plants and in calculating burnup effects. Improved differential data is essential in achieving these objectives and in resolving discrepancies that still exist between calculation and integral experiments.

The target accuracies (1σ) for principal capture cross sections averaged over the LMFBR spectra are summarized as follows[2,3]:

^{238}U, ^{240}Pu	3%
^{235}U, ^{239}Pu	4%
^{241}Pu, ^{241}Am	5%
Fe, Cr, Ni	5% to 10%
Primary fission products	5% to 10%

Requirements for secondary transactinides are determined by calculation of the activity of irradiated fuel rather than by core performance. Target accuracies for priority 1 materials are typically 10%.

The correlations between the data are also important. The high accuracy requirements for k_{eff} and breeding ratio require the spectrum averaged value of ^{238}U capture relative to ^{239}Pu fission to an accuracy of about 1.5%. Further reduction in uncertainties of Doppler and sodium void reactivities can be achieved through improved knowledge of resonance parameters and of capture data in specific energy ranges.

REFERENCES

1. P. Greebler and B.A. Hutchins, "Significance of Integral Parameters in the Design and Performance of Fast Breeder Reactors," New Developments in Reactor Physics and Shielding, CONF-720901, 1972, p. 928.

2. Ph. Hammer, "Nuclear Data Needs for Plutonium Breeders," Proc. Nuclear Cross Sections for Technology, Tennessee, NBS Special Publication 594 1979 p. 6.

3. J.L. Rowlands, "Nuclear Data for Reactor Design, Operation and Safety," International Conference on Neutron Physics and Nuclear Data, Harwell 1978, p. 7.

4. J.M. Kallfelz et al., "Design and Sensitivity Analysis of a CDS-Type Heterogeneous Core," Proc. 1980 Advances in Reactor Physics and Shielding, Sun Valley, Idaho (1980) p. 467.

5. J.M. Marable et al., "Uncertainty in the Breeding Ratio of a Large Liquid Metal Fast Breeder Reactor: Theory and Results," Nucl. Sci. Eng. 75, 1980, p. 30.

6. J.L. Rowlands et al., The Production and Performance of the Adjusted Cross-Section Set FGL5," Proc. Int. Symp. on Physics of Fast Reactors, Tokyo, 1973, p. 1133.

7. J.P. Chandat et al., "Data Adjustments for Fast Reactor Design" Trans. Am. Nucl. Soc. 27, 1977, p. 877.

8. P.F. Rose, "ENDF/B Fission Product Data," Trans. Am. Nucl. Soc. 38, 1981, p. 655.

9. C. Giacometti et al., "Characteristiques Neutroniques du Reactor Super-Phenix 1 de Creys-Malville," Symp. Fast Reactor Physics Aix-en-Provence, IAEA-SM-244/24, 1979, Vol. I, p. 3.

10. J.A. Lake, "Fuel Enrichment Requirements for the Clinch River Breeder Reactor," Proc. 1980 Advances in Reactor Physics and Shielding, Sun Valley, Idaho, 1980, p. 480.

11. J.R. White and R.E. Schenter, "Analysis of the Lumped Fission Product Uncertainty in CRBR," Trans. Am. Nucl. Soc. 39, 1981, p. 931.

12. J.R. White et al., "On the Implementation, Verification, and Application of Multicycle Depletion Perturbation Theory," Proc. 1980 Advances in Reactor Physics and Shielding, Sun Valley, Idaho, 1980, p. 769.

13. J.C. Estiot et al., "Application of Sensitivities to Actinide Build-up Problems," Paper to NEACRP Annual Meeting 1980.

14. H. Kusters, "Nuclear Data Needs for the Analysis of Generation and Burn-up of Actinide Isotopes in Nuclear Reactors," Proc. Nuclear Cross Sections for Technology, Tennessee, NBS Special Publication 594, 1980, p. 18.

15. J.L. Rowlands, "Needs and Accuracy Requirements for Fission Product Nuclear Data in the Physics Design of Power Reactor Cores," Proc. Fission Product Nuclear Data-1977 IAEA-213, p. 41.

16. Ph. Hammer, "Besoins en donnees nucleaires des products de fission et actinides pour les calculs des reacteurs de puissance a neutrons rapides, "International Conference on Neutron Physics and Nuclear Data, Harwell, 1978, p. 551.

17. C.L. Beck et al., "Sodium Void Reactivity in LMFBRs: A Physics Assessment", Trans. Am. Nucl. Soc. 39, 1981, p. 924.

18. A.T.D. Butland et al., "An Assessment of Methods of Calculating Sodium-Voiding Reactivity in Plutonium-Fuelled Fast Reactors," Symp. Fast Reactor Physics Aix-en-Provence, IAEA-SM-244/24, 1979, Vol. I, p. 281.

19. F. Lyon et al., "Sodium Void Reactivity Effect in Fast Neutron Critical Facilities: Uncertainties due to the Transposition to Power Reactors," Specialists Meeting on Design Features Affecting Dynamic Behavior of Fast Reactor Core, Rome, 1981.

20. K. Koyama et al., "Effect of Fission-Product Accumulation on Sodium-Void Worth," Symp. Fast Reactor Physics Aix-en-Provence, IAEA-SM-244/24, 1979, Vol. I, p. 583.

21. A.T.D. Butland et al., "An Assessment of Methods of Calculating Doppler Effects in Plutonium-Fuelled Sodium-Cooled Fast Reactors," Symp. Fast Reactor Physics Aix-en-Provence, IAEA-SM-244/24, 1979, Vol., p. 257.

22. L. Caldarola et al., "SEFOR Experimental Result and Applications to LMFBRs," Proc. Conf. on Engineering of Fast Reactors for Safe and Reliable Operation, Karlsruhe 1972, p. 1312.

23. R.N. Hwang et al., "Improved Algorithms for the Calculation of Resolved Resonance Cross Sections with the Applications to the Structural Doppler Effect in Fast Reactors," ANL-80-104, 1980.

24. L.G. LeSage et al., "Proc. NEACRP/IAEA Specialists Meeting on the International Comparison Calculation of a Large Sodium-Cooled Fast Breeder Reactor," ANL-80-78, 1979.

25. M.J. Lineberry et al., "Physics Studies of a Heterogeneous Liquid-Metal Fast Breeder Reactor," Nucl. Technology 44, 1979, p. 21.

26. H.F. McFarlane et al., "ZPPR Studies of Control Rod Worths in Large Heterogeneous LMFBRs," Proc. 1980 Advances in Reactor Physics and Shielding, Sun Valley, Idaho, 1980, p. 546.

27. P.J. Collins et al., "Experimental Studies of 350 MW(e) Heterogeneous Cores at ZPPR," Symp. Fast Reactor Physics, Aix-en-Provence, IAEA-SM-244/24, 1979, Vol. II, p. 57.

TABLE 1. Accuracy Requirements for Design Parameters (1σ)

Parameter	Greebler[1]	Hammer[2]	Rowlands[3]
Critical Mass	1% (Pu Enr.)	0.5% Δk	0.5-1.0% Δk
Peak/Average Power Density	2%	1.5%	1%
Control Rod Worth	2%	5%	5%
Doppler Coefficient	7%	7.5%	10-15%
Sodium Void Reactivity	0.3$	10%	10-15%
Reactivity Loss per Cycle	- -	0.25% Δk	5% of reactivity
Total Breeding Gain	- -	0.015	0.03

TABLE 2. Sensitivities for k_{eff} and Breeding Ratio in Two Heterogenoues Cores

Data		k_{eff}		Breeding Ratio	
		CRBR[a]	CDS[b]	CRBR[a]	CDS[b]
^{239}Pu	ν	0.840	0.691	-0.033	-0.013
	σ_f	0.598	0.501	-0.760	-0.668
	σ_c	-0.0563	-0.049	-0.174	-0.174
^{240}Pu	ν	0.0295	0.051	-0.0020	-0.003
	σ_f	0.0204	0.035	-0.0012	-0.002
	σ_c	-0.0081	-0.015	0.0244	0.047
^{241}Pu	ν	0.0265	0.120	-0.0008	-0.006
	σ_f	0.0191	0.088	-0.0233	-0.112
	σ_c	-0.0013	-0.006	-0.0040	-0.019
^{242}Pu	ν	0.00041	0.005	-0.00003	<0.001
	σ_f	0.00028	0.003	-0.00002	<0.001
	σ_c	-0.00009	-0.002	0.00003	<0.001
^{235}U	ν	0.0099	0.009	0.0073	0.004
	σ_f	0.0072	0.007	-0.013	-0.013
	σ_c	-0.0008	<0.001	-0.0069	-0.006
^{238}U	ν	0.116	0.124	0.0281	0.018
	σ_f	0.071	0.077	0.0180	0.011
	σ_c	-0.191	-0.219	0.677	0.756
Na	σ_c	-0.0016	-0.002	-0.0014	<0.001
Fe	σ_c	-0.0109	-0.012	-0.0090	-0.005
Cr	σ_c	-0.0081	-0.005	-0.0060	-0.003
Ni	σ_c	-0.0037	-0.005	-0.0031	-0.003
Mn	σ_c	-0.0017		-0.0041	
Mo	σ_c	-0.0036		-0.0026	

[a]CRBR at beginning of Cycle 1.

[b]CDS at mid-equilibrium cycle from Ref. 4.

TABLE 3. Changes in Capture Cross Sections Producing Variations of Approximately 0.25% in k_{eff} and 1% in Breeding Ratio

Capture Cross Section	k	BR
^{239}Pu	5	6
^{240}Pu	15	20
^{241}Pu	40	50
^{242}Pu	125	1000
^{235}U	250	150
^{238}U	1.1	1.3
Na	125	700
Fe	20	100
Cr	30	150
Ni	50	300
Mn	125	250
Mo	60	400

TABLE 4. k_{eff} and Breeding Ratio Prediction for a 1200 MWe Conventional LMFBR[a]

	k_{eff}	Breeding Ratio
Calculated value with ENDF/B-IV	1.000	1.15
Standard deviation based on evaluated data and methods biases	3.1	7.3
Change in calculated value due to data adjustment, %	+1.4	-5.5
Standard deviation of adjusted value, %	0.5	2.0

[a]From Marable, Ref. 4.

TABLE 5. Uncertainty Components for Superphenix k_{eff}[a]

	k_{eff}	Δk	Uncertainty (2σ)
Fresh core calculation corrected	1.03497		0.00350
Fuel fabrication uncertainty			0.00650
Fission product buildup		-0.02183	0.00350
Burnup in core		-0.01186	0.00500
Buildup in blankets		+0.00729	0.00100
Control reserve		-0.00300	- -
Final k	1.00557		

[a]First cycle 480 efpd (JEPP), Ref. 9.

TABLE 6. Burnup Reactivity Swing for Cycles 1 and 2 of CRBR

	Cycle 1		Cycle 2	
	Δk	1σ	Δk	1σ
Calculation with corrections[a]	0.01358	0.00019	0.02180	0.00035
Fission product worth		0.0011		0.0018
Release of gaseous FPs	-0.00023		-0.00036	
Core conversion ratio		0.00185		0.00331
Total	0.01335	0.00216	0.02144	0.00378

[a]Includes fission product worths of 1.4$ and 3.4$ at the end of each cycle. See Ref. 10 for details.

TABLE 7. Sodium Void Coefficient Bias Factors

Component	FGL5[a]	CARNAVAL-IV[b]	ENDF/B-IV[c]
Non-Leakage	1.04 ± 0.05	0.92 ± 0.03	0.89 ± 0.01
Axial Leakage	0.89 ± 0.08	1.02 ± 0.03	0.90 ± 0.01
Radial Leakage	1.00 ± 0.20	1.00 ± 0.06	0.90 ± 0.01

[a]Ref. 18, for conventional power reactor at operating conditions, U.K. calculation methods with diffusion theory.

[b]Ref. 19, for Super-Phenix corrected for transport and anistotropy effects.

[c]Fitting 48 results in integral experiments with a single leakage component.

TABLE 8. Energy Integrated Sensitivities for Inner Core Void Reactivity in a 1200 MW Conventional Core

Material	Capture Sensitivities	Fission Sensitivities
^{239}Pu	0.426	-0.701
^{240}Pu	0.112	0.036
^{241}Pu	0.042	-0.267
^{242}Pu	0.0092	0.0041
^{235}U	0.0061	-0.016
^{238}U	0.924	0.128
F.P.[a]	0.112	
Fe	0.076	
Cr	0.026	
Ni	0.009	
Mn	0.035	
Mo	0.028	
Na	0.067	

[a]Lumped fission products after a burnup 360 days.

TABLE 9. Sensitivity Coefficients for the Maximum/Minimum Fission Distribution in the Inner Core of Conventional LMFBRs[a]

Data		350 MWe Core	1200 MWe Core
^{239}Pu	σ_f	+0.0005	+0.020
	σ_c	-0.015	-0.022
^{240}Pu	σ_f	-0.0033	-0.024
	σ_c	-0.0016	0.004
^{241}Pu	σ_f	+0.0010	+0.026
	σ_c	N/A	-0.001
^{242}Pu	σ_f	N/A	-0.0027
	σ_c	N/A	-0.0005
^{238}U	σ_f	+0.010	0.036
	σ_c	-0.084	-0.365
Fe	σ_c	-0.0063	-0.020
Cr	σ_c	-0.0032	-0.010
Ni	σ_c	-0.0011	-0.007

[a]350 MWe reactor with 11% ^{240}Pu fuel, 1200 MWe reactor with 20% ^{240}Pu fuel.

TABLE 10. Control Rod Worth Sensitivities to ^{238}U Capture[a]

Lower Energy	Central Rod	Outer Ring Rod Bank
1.4 MeV	0.003	0.005
500 KeV	0.002	0.011
180 KeV	-0.008	0.009
67 KeV	-0.029	0.007
25 KeV	-0.051	0.009
1.2 KeV	-0.178	0.003
Thermal	-0.097	0.005
Total	-0.358	0.049

[a]70 MWe conventional core. Central rod worth 2.6$, rod bank worth 10$.

Discussion

QUESTION: R. Schenter
Why aren't the control rod worths sensitive to ^{10}B cross sections?
ANSWER: P. Collins
The boron is in large lumps and is very strongly shielded so the rod worths show a lower sensitivity.

QUESTION: R. Macklin
Are the target accuracies in the final summary viewgraph 1 sigma, 2 sigma or something else?
ANSWER: P. Collins
One sigma.

QUESTION: R. Peelle
For a commercial-size breeder (~ 1 GWe), what neutron-energy ranges are important for capture in structure materials and fissile and fertile materials? For example, what are median energies of sensitivity for the most important responses?
ANSWER: P. Collins
It will depend on the parameter of interest. For the heavy isotope captures important for k_{eff} and breeding ratio the range would be 10 to 100 keV. For the safety coefficients the range of higher sensitivity is 500 eV to 10 keV. The structural-material capture occurs mainly in resonances at particular energies.

QUESTION: A. B. Smith
What do you attribute to integral-calculation uncertainty for, say, k_{eff}?
ANSWER: P. Collins
It is important that these be carefully evaluated both for data adjustment and in deriving bias factors. Uncertainties in k_{eff} range from 0.2% for simple benchmarks to about 0.5% in complex power reactor geometries.

QUESTION: W. Poenitz
Didn't you indicate that if you adjust the cross sections to obtain agreement with some type of integral measurement, that you then observe discrepancies with others?
ANSWER: P. Collins
Yes, that is true. Basically, the adjustments are made with very simple parameters, e.g. k_{eff}, reaction rate ratios, etc. We adjust to fit the integrated values over the whole energy range. If we then come to other specific experiments which have sensitivities in other energy ranges adjustments still have to be made.

QUESTION: A. B. Smith
I would like to ask a question which probably should be directed to Leo LeSage. One figure referred to the NEACRP benchmark comparison. What do these differences reflect? Differences in calculation techniques and methods or data?

ANSWER: L. LeSage
Probably P. Collins can answer this.

P. Collins:
The differences came not only from the data, much came probably from processing.

L. LeSage:
Yes, as you probably recall, several calculations used ENDF/B and came up with quite different answers. As far as the large differences in the power distributions are concerned, you can trace this to differences in k.

QUESTION: A. B. Smith
What enrichment (^{240}Pu) are you assuming for your CRBR comparisons?
ANSWER: P. Collins
The sensitivity data were for the initial core loading of CRBR where the plutonium will contain 11% ^{240}Pu. The other data for commercial cores was for plutonium with 20% ^{240}Pu.

A REVIEW OF THE FUNDAMENTALS OF THE NEUTRON CAPTURE REACTION

by

R. E. Chrien
Brookhaven National Laboratory
Upton, New York, 11973, USA

Abstract

Fifty years of research into the nature of the radiative capture reaction mechanisms is briefly summarized. A variety of such mechanisms is exploited to explain neutron capture over nine decades of neutron energy.

I. Introduction

The topic of neutron capture is as old as the discovery of the neutron. This year marks the 50th anniversary of that discovery, which as we all know has profoundly influenced the course of human history. The purpose of this review is to offer a brief introduction to the understanding of the reaction mechanisms for neutron capture, which plays an important and central role in the variety of applications which this meeting will address. We note that historically the neutron capture has enriched our understanding of the nuclear many-body probes, and continues to add to that understanding even at this late stage in the development of nuclear physics. Equally important is its role in applications and it is worthwhile remarking on the fact that in few other areas of nuclear physics is the link between fundamental research and applications so close.

Radiative neutron capture reactions have been observed in almost every known stable target nuclide and are often the dominant reaction in the energy region just above particle threshold.

Neutron capture γ-ray measurements extend over nine decades of energy, from cold and thermal neutron fluxes to the d(t,n) reaction near 15 MeV. In these nine decades of energy (Fig. 1), the capture cross section varies from well separated resonances with complex configurations, to the unresolved resonance regions, where giant resonance structures may be found.

Based on the incorporation of photons into basic dispersion theory, Lane and Lynn [LL 60] recognized three components of the resonance capture cross section: the compound nucleus (or resonance internal), channel (or resonance

external), and direct capture (hard sphere potential and distant resonances). The last two components preferentially feed single particle final states.

Resonant processes can be divided into valence, doorway, and statistical mechanisms (Fig. 2). In the entrance channel configuration, the valence neutron can undergo a radiative transition without perturbing the core. Radiative decay can also occur from the doorway configurations of a resonance, either by a particle-hole annihilation or by particle transition in the presence of an excited core. All other decay modes are grouped together under the heading of statistical interactions.

Average capture cross sections can be calculated from the average resonance parameters or measured directly in low resolution measurements at keV neutron energies. These quantities play an important role in fast reactor design and stellar nucleosynthesis, and exhibit systematic mass dependences which are markedly affected by odd-even mass numbers and the magic neutron numbers.

II. Photon Channels

Early reaction theories deal only with particle channels. Lane and Thomas [LT 58] showed that photons were not identical to particle channels, and employed perturbation theory, using the weak coupling of nucleons to the electromagnetic field.

The radiative transition probability T between a resonance λ in state ψ and final state Φ is given by the perturbation theory expression [Hei 54]:

$$T = \frac{2\pi d\rho}{\hbar} \left|\langle\psi|H'(A)|\Phi\rangle\right|^2$$

where H'(A) is the electromagnetic perturbation operator written in terms of the vector potential A, and $d\rho$ is the density of photon states within the solid angle $d\Omega$.

The photon width amplitude is related to the electromagnetic perturbation operator

$$e^{i\phi_\gamma}\Gamma_{\lambda\gamma}^{1/2} = \left(\frac{2\pi d\rho}{\hbar}\right)^{1/2} \hbar^{1/2} \int d\tau X_\lambda^* H'(A)\Phi$$

In R-matrix theory the states X_λ are defined only for the internal region of configuration space (bounded by the channel radii a_c) so that the eigenstates X_λ can have a one-to-one correspondence with resonances; nevertheless there is a contribution to the photon width amplitudes from the external region, $r > a_c$.

The contribution of the external region to the transition probability must be included in evaluating the width in the equation above. The complete expression for the collision matrix element includes a sum of resonant and non-resonant components,

$$U_{c\gamma} = U_R + U_{HS},$$

where $$U_R = ie^{-i(\phi_c+\phi_\gamma)} \sum_{\gamma\mu} A_{\lambda\mu}\Gamma_\mu^{1/2}\Gamma_{\lambda\gamma}^{1/2},$$

and $$U_{HS} = \frac{2\pi d\rho}{\hbar}^{1/2} \int_{r_c=a_c}^{\infty} (I_c - e^{-2i\phi_c} O_c) H'\Phi d\tau_c.$$

The product of the photon width amplitude and phase factor is expressed as the sum of internal, open-external and closed-external amplitudes respectively, i.e.,

$$e^{-i\phi_\gamma}\Gamma_{\lambda\gamma}^{1/2} = -(2\pi d\rho)^{1/2}\{ \int d\tau X_\lambda^* H'\Phi$$

$$+ h^{-1/2}\sum_{c^+} e^{-i\phi c^+}\Gamma_{c^+}^{1/2}\int_{r_{c^+}=a_{c^+}}^{\infty} d\tau_{c^+} O_{c^+}'^* H'\Phi$$

$$+ \sum_{c^-} \frac{2M_{c^-}a_{c^-}}{\hbar^2}^{1/2} \gamma_{\lambda c^-}\int_{r_{c^-}=a_{c^-}}^{\infty} d\tau_{c^-} \frac{O_{c^-}'(r_{c^-})}{O_{c^-}'(a_{c^-})} \phi_{c^-} H'\Phi\}$$

These expressions show not only that the radiation width includes contributions from both open and closed channels in the external region (i.e., channel capture), but also that the capture amplitude includes a non-resonance part U_{HS} analogous to the potential scattering contribution to the elastic scattering amplitude.

In the semi-classical theory of radiation, the perturbation Hamiltonian can be written in terms of the canonical momenta, $\bar{p} - e\bar{A}/c$, of the interacting particles. The complete expression for a system of A nucleons, written in a way so as to suppress the translational mode of the center of mass of the system, is as follows:

$$H'(\underline{A}) = (4AM_c)^{-1} \sum_{j,k} \{\underline{P}_j - \underline{P}_k - \frac{e_j}{c} \underline{A}(r_j) + \frac{e_k}{c} \underline{A}(r_k)\}^2$$

$$+ V' - \left(\frac{e\hbar}{2M_c} \right) \sum_j \mu_j (\underline{\sigma}_j \cdot \mathrm{curl}\ \underline{A}_j)$$

This operator is linearized by dropping terms of the order of A^2, which is equivalent to consider the interaction in terms of a single photon; the last term above describes the interaction of the intrinsic magnetic moments of the nucleus. The electromagnetic field is expanded into its various multipoles and the multipoles can be divided into two groups.

(a) parity $(-)^L$; these are electric multipole operators (because they arise mainly from the charge terms);

(b) parity $(-)^{L+1}$; magnetic multipole operators (because of the contribution from the magnetic moments).

The components of the electromagnetic perturbation operator are proportional to irreducible tensor operators denoted by H_{TM} where T denotes the parity.

Thus the partial radiation amplitude for a photon channel with multipolarity LM (in which the photon carries L units of angular momentum and M units of angular momentum projection on the z axis) is

$$\Gamma^{1/2}_{\lambda(\gamma LM)} = \frac{(8\pi)^{1/2} k_\gamma^{L+1/2} (L+1)^{1/2}}{L^{1/2}(2L+1)!!} \langle X^{\ell}_{\lambda Jm} | H^L_{TM} | \phi_{\mu j' m'} \rangle$$

for the transition from a state λ with angular momentum J and Z-projection m to a final state μ with angular momentum J' and projection m'.

In M^{th} component $H_{TM'}$ the general subscript T has to be specialized to either electric or magnetic radiation according to the parity difference $(-1)^L$ or $(-1)^{L+1}$ respectively, of the initial or final state.

In the long wave length approximation ($k_\gamma a \ll 1$), forms of the operator H^L_{TM} for E1 and M1 transitions (for $E_\gamma < 10$ MeV) are

$$H'_{E-1} = \sum_k r_k Y^1_\mu(\theta_k, \phi_k)$$

$$H'_{M-1} = \frac{e\hbar}{2M_c} \left(\frac{3}{4\pi} \right)^{1/2} \sum_k (L_{kM} + \mu_k \sigma_{kM})$$

Practical experience has shown that for neutron capture only E1 and M1 multipoles are of any importance; only a few E2 transitions have been observed, and no M2 or other multipole orders have ever been detected.

To carry this discussion further we must provide some prescription to evaluate the photon widths. The electromagnetic operator is well known; the nuclear wave functions are not known, particularly at the excitation energy required. Nevertheless there are certain simplifying assumptions that can be made to arrive at width distributions and systematics. Some of these are discussed below.

III. THE STATISTICAL THEORY

The foundation of the statistical model is expressed in the Bohr condition [Boh 36] that the lifetime of an excited state is much longer than the time required for a nucleon to orbit the nucleus. The probability of forming the excited state E_λ in channel c is therefore independent of the probability of decay in channel c'.

The reaction cross section is expressed in terms of the collision matrix $U_{cc'}$ which contains the R-matrix expression,

$$R_{cc'} = \frac{\gamma_{\lambda c}\gamma_{\lambda c'}}{E_\lambda - E}$$

The resonance wave functions $|\lambda\rangle$ are considered to be complicated, with only a small overlap with the channel wave functions, i.e. $\langle\lambda/c\rangle^2 \approx 10^{-4}$ to 10^{-7}. In the approximation the $\gamma_{\lambda c}$ can be considered as random variable.

The fundamental assumptions of the statistical model are:

(a) $\gamma_{\lambda c}$ and $\gamma_{\lambda c'}$ have random signs such that $\sum_\lambda \gamma_{\lambda c}\gamma_{\lambda c'} = 0$.

(b) $\gamma_{\lambda c}$ and $\gamma_{\lambda c'}$ are independent and uncorrelated such that the linear correlation coefficient is zero, i.e., $p(\gamma_{\lambda c}, \gamma_{\lambda c'}) = 0$.

(c) The strength function for channel c is independent of energy over the range ΔE, i.e., $1/\Delta E \sum_\lambda \gamma^2_{\lambda c}$ = constant.

Because $\gamma_{\lambda c}$ is the coupling amplitude of entrance channel c with the resonance state at energy E_λ, the above assumptions imply that the statistical properties of the exit channel c' contain no 'memory' of the entrance channel amplitude.

To evaluate the partial radiative width, under these assumptions, one can adopt the "black" nucleus picture of Blatt & Weisskopf [BW 52]; for a spinless particle in a bound S-state, the E1 transition width to a low-lying P state is

$$\Gamma_{s\gamma p} = \frac{16\pi k_\gamma^3}{9} \left|\langle J=0 \| Y^1 \| J=1\rangle \left\{\langle e\rangle \int_0^\infty dr\ r\ u_0\ (r) u_1(r)\right\}\right|^2$$

where $\langle e\rangle$ is the effective charge of a particle in a system of particles (for a neutron $\langle e\rangle = -Z/A\ e$; proton $\langle e\rangle = N/A\ e$). The photon wave number is $k_\gamma = E_\gamma/\hbar c$.

In the statistical model the initial single particle state is dissolved among the compound nucleus states over an energy interval corresponding to the spacing of the single particle states, D_s.

If the radial wave functions are assumed uniform within the nuclear radius (a) and zero outside, an estimate of the integral above is

$$\int_0^\infty dr\ r\ u_0(r) u_1(r) = 3a/4 \ ;\ \text{hence}$$

$$\Gamma_{\lambda\gamma p} = 3/4\ \langle e^2\rangle\ (E_\gamma/\hbar c)^3\ a^2 \langle D_o\rangle / D_s$$

for an electric dipole transition of energy E_γ to a p-wave single particle state. This width is further reduced if the p-wave single particle state is diluted over many low-lying states μ. The estimate for $\Gamma_{\lambda\gamma p}$ above is to be understood as an average value; the actual $\Gamma_{\lambda\gamma p}$ exhibited by fine structure resonances will fluctuate about the average. Abundant experimental evidence confirms the expectations of the statistical model that this fluctuations is adequately described by the Porter-Thomas distribution; i.e., a chi-square distribution with one degree of freedom.

The intensity of primary E1 radiation from thermal neutron capture, $f_1(E_\gamma)dE_\gamma$, in the γ-ray energy interval E_γ to $E_\gamma + dE_\gamma$, is obtained by multiplying I.70 by the level density of p-wave states, i.e.,

$$f_1(E\ )dE\ = \frac{3}{4}\ \langle e^2\rangle\ (E_\gamma/\hbar c)^3\ a^2 \cdot \frac{1}{D_s}\ \frac{\rho(E_{th}-E_\gamma)}{\rho(E_{th})}\ dE_\gamma,$$

where $D_o = 1/\rho(E_{th})$ and E_{th} is the total energy of the thermal capture reaction (i.e., binding energy), and $\rho(E_{th}-E_\gamma)$ is the level density of states at the intermediate energy.

The shape of the primary spectrum is dependent on the opposing $E^3{}_\gamma$ and $\rho(E_{th}-E_\gamma)$ factors. For heavy nuclides a bell-shaped curve is observed, peaking about 2 to 3 MeV and decreasing rapidly at higher and lower γ-ray energies. These spectra cannot be compared directly with experimental results because of the presence of secondary and higher order cascade γ rays, as shown in Fig. 3.

The average total radiation width $\langle\Gamma_\gamma\rangle$ of resonances λ with spin J is just the sum of the average partial radiation widths $\langle\Gamma_{\gamma\mu}\rangle$ to final states μ with spin I,

$$\langle\Gamma_\gamma\rangle(J) = \sum_\mu \langle\Gamma_{\gamma\mu}\rangle$$

$$\approx \sum_{I=|J-1|}^{J+1} \int_0^{E_c} dE_\gamma \cdot \rho\{(E_c-E_\gamma),I\}\Gamma_{\lambda\gamma\mu}(E_\gamma,J)$$

Cameron [Cam 59] has estimated average radiation widths as a function of mass number using a shell model form for the final state level density. These calculations predict the observed peaks in $\langle\Gamma_\gamma\rangle$ in the mass regions just below magic neutron numbers. Cameron's estimate of mean partial radiation width as a function of energy, mass number and level density is

$$\langle\Gamma_{\gamma\mu}\rangle = C\ 10^{-9}\ E_\gamma^3\ (\mathrm{MeV})\ A^{2/3}\ D\ (\mathrm{eV})$$

where C = 0.33.

Average radiation widths compiled by Bird et al. [Bir + 76] for resonances for nuclides from A = 19 to 243 are shown in Fig. 4.

Some broad features of the data are immediately evident. s-wave radiation widths reach maximum values in the $40 \leq A \leq 70$ region (i.e., N = 20, 28), $A \approx 140$ (N = 82) and $A \approx 200$ (N = 126). These regions correspond to peaks of the s-wave neutron strength function and occur when the 3s and 4s single particle states become unbound. A similar effect occurs for p-wave radiation widths, in the 2p and 3p mass regions (N = 14, 50).

Clearly nuclear structure effects play an important role in determining average radiation widths. Level density effects are also important, because average radiation widths for odd-A target nuclides are substantially less than those for neighboring odd-N nuclides. However, the odd-A targets have radiation strength functions $\langle\Gamma\rangle/D$ which are much larger than the even-A targets. Odd-Z, even-N targets have larger γ-ray strength functions and odd-odd targets have the largest values of all. This is because the radiation widths vary slowly with mass number, while resonance spacings depend markedly on the position of the closed neutron shells. Consequently, radiative strength functions exhibit deep minima at the magic neutron numbers as well as odd-even effects.

There are large differences between s- and p-wave radiation widths in the 3s and 3p regions. In the 3s region s-wave widths are on average three times those observed for p-wave resonances. In the 3p region the situation is reversed. While large s- and p-wave radiation widths are associated with

peaks in the 3s and 3p neutron strength functions, s-wave widths in the 4s region are not enhanced. The presence of low-lying single-particle states to which E1 transitions can proceed appears to be an important requirement. These occur just above the magic neutron numbers at N = 20, 28, 50 and 82, and have negative parity in the 3s and 4s regions and positive parity in the 3p region. In the 3s and 4s regions, high energy E1 transitions from s-wave resonances will be much stronger than M1 transitions to the same final states from p-wave resonances. The statistical model will therefore predict in those cases a significant enhancement of s-wave radiation widths over p-wave radiation widths [AM 79]. Johnson has shown that the opposite occurs in the 3p region [Joh 79].

IV. Departures from Statistical Capture

As previously noted, the photon collision matrix elements can be separated into internal and external parts (with respect to the nuclear radius), and the latter into resonant and non-resonant components, i.e.,

$$U = U(\text{internal}) + U(\text{external})$$

$$U(\text{external}) = U(\text{resonant}) + U(\text{non-resonant})$$

These last terms are respectively called channel (or valence) capture and direct or potential capture, and represent the non-statistical part of the capture process in that they are dependent on the single particle strengths

$$\Gamma_{\lambda\mu}(\text{Ch}) = \frac{16\pi}{9} k_\gamma^3 (2/a)^2 \; \theta_\mu^2 \theta_\lambda^2 (\langle e\rangle a/k_\mu)^2 \; \frac{\langle J_\lambda || Y^{(1)} || J_\mu \rangle^2}{2J_\lambda+1}$$

In resonant channel capture, the partial radiation width is jointly proportional to the single particle strengths of the resonance and final states, and a manifestation of this effect is the observation of correlations between the reduced neutron widths ($\Gamma^\ell_{\lambda n}$) and partial radiative widths $\rho(\Gamma^\ell_{\lambda n}, \Gamma_{\lambda\mu})$, and between the reduced partial radiative widths and the final state spectroscopic factors $\rho(2J+1)\theta^2_\mu, \Gamma_{\lambda\mu}/E_\gamma^3)$.

Non-Resonant Capture

In the strong coupling model, there is no free motion of the neutron in the target nucleus. The neutron and radiation amplitudes have random signs, and the contribution of distant resonances is zero. Background capture results from hard sphere scattering alone in which the incident neutron is scattered by the nuclear potential into a bound, single particle final state. The potential capture cross section $\sigma_{\gamma\mu}(\text{HS})$ barn for an E1 transition to final state μ is given by [LL 60]:

$$\sigma_{\gamma\mu}(HS) = \frac{0.062}{a\sqrt{E_n}} \cdot \left(\frac{Z}{A}\right)^2 \cdot \theta_\mu^2 y^2 \left(\frac{y+3}{y+1}\right)^2,$$

where E_n is the neutron energy in eV, a is the nuclear radius in fm; $y = k_\mu a$ and k_μ is the neutron wave number for the single particle state bound by energy E_γ, defined above.

The hard sphere cross section is proportional to y^2 or E_γ. Since this cross section is proportional to

$$k_\gamma^3 [\langle\theta_\lambda || D || \theta_\mu\rangle]^2 ,$$

the dipole matrix element must be proportional to E^{-1}.

Kopecky et al. [SK 74, SK 76] have shown that direct capture occurs in the 3s region at thermal energies. The final state correlations between the (n,γ) and (d,p) cross sections are greatly improved by the use of an E_γ energy dependence for the radiative strength, rather than the usual E^3_γ factor, when nearby resonances have no influence on the cross section.

In the intermediate coupling model, single particle motion of the incident neutron is assumed to persist in the nucleus, the single particle effect is observed in the size resonances of the s- and p-wave neutron strength functions which occur close to the zero binding of single particle neutron levels.

In the intermediate coupling model, a contribution to the potential or non-resonant collision matrix element arises from the tails of distant resonances, i.e.,

$$U(P) = U(HS) + U(DR).$$

The distant resonance component U(DR) is normally zero owing to the random nature of the sign and magnitude of the partial radiation width amplitudes, as predicted by the statistical model. But when channel capture is dominant, the amplitudes can add coherently.

The mass dependence of the non-resonant capture cross section in the 3s and 4s regions has been obtained from calculations using R-matrix theory with intermediate coupling [LL 60] and, more recently, using optical and shell model formulations of the valence model [CM 75, Cug 76]. In the 3s region at thermal energy, σ^P peaks at 0.9 barn for A ≈ 52, dropping sharply to zero at A ≈ 58 and recovering to a second maximum of 0.3 barn at A ≈ 67 (Fig. 6). A similar pattern is found in the 4s region with peaks at A ≈ 150 and 195, and a minimum at A ≈ 170. These results were obtained with an imaginary potential W_0 = 3.30 MeV and are sensitive to variations in this quantity.

Examples of nuclides showing potential capture are ^{130}Te and ^{136}Xe, as shown in Fig. 5 [MC 79].

Valence Capture

First formulated by Lane and Lynn [LL 60], and demonstrated experimentally by Mughabghab et al. [Mug + 71], the valence model describes the change of state of the incident neutron in the entrance channel by the emission of dipole radiation in the field of a spectator target.

The partial radiative width for an E1 transition from resonance λ to final state μ is given by [Lyn 68]

$$\Gamma_{\lambda\mu} = \frac{16\pi k_\gamma^3}{9} \frac{\left|X_\lambda(J_\lambda)\right|\left|H_E^{\,1}\right|\left|X_\mu(J_\mu)\rangle\right|^2}{(2J_\lambda+1)} ,$$

where k_γ is the photon wave number, and $H_E^{\,1}$ is the electric dipole operator D.

The basis functions χ can be expanded in terms of radial wave functions for a set of single particle states defined in the spin-orbit coupling scheme. Neglecting core transitions [Lan 59], the partial valence radiative width becomes

$$\Gamma^V_{\lambda\mu} = \frac{16\pi k_\gamma^3}{9} \theta^2_\lambda \theta^2_\mu \left|\langle e\rangle \int dr\, u_\lambda\, r u_\mu\right|^2 \cdot \frac{\left|\langle j' I_\alpha J_\lambda\right|\left|Y^{(1)}\right|\left|j'' I_\alpha I_\mu\rangle\right|^2}{2J_\lambda+1}$$

where $\theta^2_\lambda, \theta^2_\mu$ are the dimensions reduced widths of the resonance and final state, $\theta_\lambda = \Gamma_{\lambda n}\ [2kRP_\ell\Gamma_W]^{-1}$, where Γ_W is the Wigner single particle limit, R the nuclear radius and P_ℓ the penetrability; θ^2_μ is the (d,p) spectroscopic factor; u_λ, u_μ are the resonance and final state single particle radial wave functions, and ⟨e⟩ is an effective charge equal to Z/A times the electron charge.

For a zero spin target ($I_\alpha = 0$), the angular part of the matrix element for a transition from the initial state $(J_\lambda, j'\ell')$ to the final state (J_μ, j'', ℓ'') becomes

$$\frac{3}{4\pi}(2J_\mu+1)\begin{pmatrix} j' & j'' & 1 \\ -1/2 & 1/2 & 0 \end{pmatrix}\frac{1}{2}\left[1+(-1)^{\ell'+\ell''+1}\right] .$$

The valence model can be formulated in terms of optical model parameters as first pointed out by Lane and Mughabghab [LM 74]. Done in this way, the valence model avoids the problem of wave function normalization which occurs for an unbound state.

$$\Gamma^V_{\lambda\mu} = \left[\frac{\mathrm{Im}\langle u_\mu | D | U_E(\mathrm{opt})\rangle}{\mathrm{Im}\ \tan\delta(\mathrm{opt})} \right]^2 \cdot \Gamma_\lambda ,$$

where u_μ is the final state wave function and $U_E(\mathrm{opt})$ is the optical model initial state wave function at neutron energy E. The dipole operator is denoted by D and $\delta(\mathrm{opt})$ is the optical model phase shift. Removing the energy dependence from $\Gamma_{\lambda n}$ and explicitly showing the $E^3{}_\gamma$ dependence, we obtain

$$\Gamma^V_{\lambda\mu} = q_{\lambda\mu}(E_n) \cdot E^3_{\lambda\mu} \cdot \theta^2_\mu \cdot Z^2/A^2 \cdot \Gamma^\ell_{\lambda n} ,$$

where $\Gamma^\ell{}_{\lambda n} = \Gamma_n(P_\ell\sqrt{E})^{-1}$ eV and the reduced partial valence width $q_{\lambda n}(E_n)(\mathrm{MeV})^{-3}$ is an energy dependent parameter calculated from the optical model and contains the radial integration and geometrical factors. In this formulation the energy dependence of the valence capture width is explicitly introduced with the $q_{\lambda\mu}$ factor above.

The valence process is expected to be important when the resonances (or initial states) have large reduced widths, corresponding to even-even target nuclides with large level spacings in the regions of the neutron strength function maxima; and when E1 transitions can excite final states with large spectroscopic factors which occur near closed neutron shells.

The reduced partial valence widths (q) and E1 transitions from resonances with the appropriate (ℓ,J) are calculated at thermal energies for s-, p- and d-wave capture assuming zero spin targets. These data are given in graphical form in Fig. 7 as a function of mass number. For non-zero spin targets, the reduced valence width is given by

$$q(I_\alpha) = (2J_\lambda+1)(2J_\mu+1) \begin{pmatrix} j' & J_\lambda & I_\alpha \\ J_\mu & j'' & 1 \end{pmatrix}^2 \cdot q(I_\alpha=0).$$

Since the valence process predominantly arises outside the nuclear radius, the reduced valence widths are dependent on the variation with energy of the external part of the initial and final state wave functions. As the final state becomes more tightly bound, the external part decreases which results in a decrease in the dipole overlap integral.

The dependence on the final state single particle binding energy has been investigated by observing the variation of the reduced valence width with changes in the central potential. A γ-ray dependence of $E^{-1}{}_\gamma$ is observed, resulting in an overall $E^2{}_\gamma$ dependence for valence transitions, in agreement with the prediction for channel capture.

The experimental confirmation of the marked energy dependence of q predicted in the 3s and 4s regions is extremely difficult to achieve. A large energy range is required for nuclides which also exhibit a dominant valence effect. To date, an adequate check of the theory has been possible in ^{54}Fe [All + 77a] where the capture data have been analyzed to 500 keV.

Width Correlations and Doorway States

Several authors have studied the underlying basis of width correlations in resonance neutron capture. Beer [Bee 69] used a two group expansion of the resonance wave function to account for the Porter-Thomas distribution of the reduced neutron widths, the narrow distributions of partial radiative widths and the correlations between reduced neutron and partial radiative widths, and between pairs of partial radiative widths. In the case of ^{169}Tm, one group of orthogonal basis functions contained the single particle component of the neutron resonances, while the other contained a small number of doorway or collective states.

Beer went on to apply the projection operator formalism [Bee 71], using the doorway state assumption. The transition matrix is divided up into direct, semi-direct and compound nucleus terms, and the same doorways contributing to the semi-direct term are also involved in the resonance term. The partial radiative amplitude is expanded into single particle, doorway and statistical components and expressions are obtained for the correlation coefficients $\rho_I(\Gamma^o{}_{\lambda n},\Gamma_{\lambda\mu})$, $\rho(\Gamma_{\lambda\mu},\Gamma_{\lambda\mu'})$ and $\rho_F(\theta^2{}_\mu,\Gamma_{\lambda\mu}/E_\gamma{}^3)$; ($\rho_I$ and ρ_F are the initial and final state width correlations). The first two correlations are predicted to be unity if the resonance reaction proceeds through an isolated radiative doorway state.

Soloviev [Sol 74] expands the wave function into few quasi-particle components and notes that if these were considered as doorways, then a correlation between channels occurs for common doorways. In strongly deformed nuclides, large correlations should be expected between K-allowed transitions to the ground and low-lying quasi-particle rotational levels.

A detailed treatment of doorway states and correlations has been developed by Lane [Lan 71]. Because of space limitations, we will not discuss that treatment here. Suffice it to say that large and symmetric initial and final state correlations are expected in the case of a single doorway with two-quasiparticle character. If the doorway has a particle-vibration character, the final state correlations will be reduced. When several overlapping doorways are present, ρ_I is reduced by 1/n, where n is the number of doorways, but in the case of twoquasiparticle doorways, the final state correlations will remain large.

V. AVERAGED CAPTURE CROSS SECTIONS AND WIDTHS

Many capture cross section measurements do not have sufficient resolution to resolve individual resonances, and instead provide data on the capture cross section averaged over a finite energy range. It is of interest to observe the energy and mass dependence of average capture cross sections to obtain further information on the neutron capture mechanism, and to provide

data needed for reactor and astrophysical calculations. The average cross section can be fitted by a formalism using average parameters for s-, p- and d-wave resonances, obtained from high resolution measurements, and by taking into account competition with inelastic neutron scattering when this is energetically possible. Consequently, high resolution and average capture measurements provide complementary data.

The role of fission products in the burnup of reactors is of great interest and, particularly for fast reactors, it is important to have systematic capture cross section data available. Where no such measurements exist, theoretical or semi-empirical estimates can be made; these must be extrapolated from existing data.

Summing over J and ℓ, the average capture cross section can be written in the form:

$$\sigma(E) = \frac{\pi^2 \lambda\!\!\!^{-2}}{(2I+1)} \cdot \sum_{j=|I-1/2|}^{j=|I+1/2|} \sum_J (2J+1) \frac{\langle \Gamma_{\lambda J(\gamma)} \rangle}{\langle D_{\lambda J} \rangle} \cdot$$

$$\sum_{\ell=|J-j|}^{\ell=|J+j|} \frac{\langle \Gamma_{\lambda J(n\ell j)} \rangle / \langle D_{\lambda J} \rangle}{\langle \Gamma_{\lambda J} \rangle / \langle D_{\lambda J} \rangle} \cdot S,$$

when $\Gamma_n \gg \Gamma_{\lambda\gamma}$, $\Gamma_n \approx \Gamma_\lambda$,

$$\sigma(E) \propto \sum_J (2J+1)\, S_{J\gamma}(E)$$

where $S_{J\gamma}(E) = \langle \Gamma_{\lambda J(\gamma)} \rangle / \langle D_{\lambda J} \rangle$ is the radiative strength function for spin state J.

Where the symbols have their usual meanings and S is the fluctuation factor which is introduced to account for the correlation between partial and total widths when averaging the single-level Breit Wigner formula [LL 57].

The partial and total capture cross sections expected for an even target are shown in Fig. 8. The s-wave cross section varies as λ^2, (i.e., 1/E) and the $\ell > 0$ cross sections increase with increasing penetrability at higher energies. Competition with higher order ℓ waves and the decrease in λ^2 lead to a decrease in the cross sections.

The observation of s- and p-wave size resonances reveals that single particle motion continues in the compound nucleus resonances. The definition of a γ-ray or photon strength function is most useful in investigating the role of single particle and giant dipole resonance models and other reaction mechanisms. Unlike the neutron case, there are a number of photon strength

functions defined in the literature. Bartholomew and co-workers [Bar + 73] defined the γ-ray strength function, in analogy to the neutron strength function, to be

$$f_{X\ell}(E_\gamma) = \frac{\langle \Gamma^{XL}_{\lambda\gamma\mu} \rangle}{D_\lambda(\mathrm{eV}) E_\gamma^{2\ell+1}(\mathrm{MeV})}$$

This function is directly related [Lon 79] to the reduced transition probability defined by Bohr and Mottelson [BM 69]

$$B(E1) = \sum_{\Delta=1\ \mathrm{MeV}} B(E1)^{\downarrow} = 0.956 \times 10^6\ f_{E1}(E_\gamma)\ [e^2 fm^2 MeV^{-1}]$$

$$B(M1) = \sum_{\Delta=1\ \mathrm{MeV}} B(M1)^{\downarrow} = 8.63 \times 10^7\ f_{ML}(E_\gamma)\ [e\hbar/2Mc)^2\ MeV^{-1}]$$

$$B(E2) = \sum_{\Delta=1\ \mathrm{MeV}} B(E2)^{\downarrow} = 1.25 \times 10^{12}\ f_{E2}(E_\gamma)\ [e^2 fm^4 MeV^{-2}]$$

Blatt and Weisskopf [BW 52] assume a uniform distribution of single particle configurations to obtain these estimates.

$$\Gamma_{\lambda\gamma\mu(E1)} = 6.8 \times 10^{-8}\ E_\gamma^3\ A^{2/3}\ D_\lambda D^{-1}$$

$$\Gamma_{\lambda\gamma\mu(M1)} = 2.1 \times 10^{-8}\ E_\gamma^3\ D_\lambda D^{-1}$$

$$\Gamma_{\lambda\gamma\mu(E2)} = 5.9 \times 10^{-14}\ E_\gamma^5\ A^{4/3}\ D_\lambda D^{-1} \quad ,$$

where Γ_γ, D_λ are in eV, E_γ, D are in MeV. It is assumed that the single particle strength is fragmented such that $\Gamma_i/D_i = \Gamma_{sp}/D_{sp}$. The single particle level spacing D was estimated at ≈0.5 MeV by Blatt and Weisskopf, but observations require this to be much larger, ≈20 MeV. Bartholomew [Bar 61] used these estimates to define the dipole reduced widths and the following expression for photon strengths have been in common use since then:

$$k(E1) = \Gamma_{\lambda\gamma\mu} \; [D_\lambda E_\gamma^3 A^{2/3}]^{-1}$$

$$k(M1) = \Gamma_{\lambda\gamma\mu} \; [D_\lambda E_\gamma^3]^{-1}$$

It was recognized by Axel [Axe 62] that the E1 giant resonance results in a redistribution of radiative strength in nuclei, and that a proper formulation of reduced widths should reflect that redistribution. An expression for the radiative strength function is readily developed from the Lorentzian expression for the photoabsorption cross section:

$$\frac{\Gamma_{\gamma\mu}(E_\gamma, J_\mu)}{\langle D\rangle(J_\mu)} = \frac{4}{3\pi} \frac{NZ}{A} \frac{e^2}{\hbar c} \frac{1+0.8x}{M\,c^2} \frac{(\Gamma_G E_\gamma)^2}{(E_\gamma^2 - E_G^2)^2 + \Gamma_G E^2)^2}$$

and the much quoted Axel approximation, evaluated at $E_\gamma \approx 7$ MeV, is

$$\frac{\Gamma_{\gamma\mu}}{D}(\approx 7\ \text{MeV}, J_\mu) = 2.2 \times 10^{-5} \left(\frac{E}{7\ \text{MeV}}\right)^5 \left(\frac{A}{100}\right)^{8/3} \left(\frac{\Gamma_G}{5\ \text{MeV}}\right).$$

The commonly stated Brink hypothesis [Bri 55] is that the γ-ray strength function for excited states is similar to that for the ground state. Thus the expression for the radiative strength valid only for ground state transitions is presumed by the hypothesis to be applicable also to transitions to excited states of the nucleus. The Axel expression is correspondingly used to produce the following form for the E1 photon strength function,

$$S(E1) = \langle\Gamma_{\lambda\gamma\mu}\rangle \; [D_\lambda E_\gamma^5 A^{8/3}]^{-1}$$

$$\langle S(E1)\rangle \approx 6.1 \times 10^{-15}\ \text{MeV}^{-5}\ .$$

The Weisskopf single particle model (SPM) predicts an $A^{2/3}$ dependence and the Axel GDR parameterization an $A^{8/3}$ dependence of the E1 strength function. A compilation of the dependence of E1 strengths has been presented by McCullagh, Stelts and Chrien [MSC 79]. Results from (n,γ), (γ,n) and (γ,γ') measurements on discrete resonances were examined for about 50 data sets, with renormalization of some results to more recent values of absolute partial widths. The E1 A-dependence is compared to the predictions of the SPM and GDR. Results for the latter are shown in Fig. 10 where the solid and dashed lines indicate the unweighted average value and the Axel GDR prediction. (Note (γ,γ') data are not included in the average because of their poor statistical accuracy.) Errors reflect the number of transitions contributing to each datum point.

The average ratio of observed and GDR strength functions is 0.69 ± 0.06, indicating that the GDR calculation overestimates the experimental data by about 30%.

Measurements of the energy dependence of the E1 strength function in the threshold region indicate that intermediate structure is superimposed on the tail of the giant electric dipole resonance (GDR). Data from (n,γ), (γ,n) and (γ,γ) reactions are shown in Fig. 11 for the compound nuclides ^{Nat}Tl, ^{204,205,206}Tl [Ear + 76] and ^{198}Au [Lon 79]. With respect to the GDR extrapolation (dashed curve) a surplus of E1 strength is observed in ^{205}Tl at 5 to 6 MeV. A maximum occurs in ^{206}Tl at the same energy, but with a marked deficit at lower energies. For ^{198}Au, the strength function also peaks at 5 to 6 MeV, but in general the E1 strength function is well below the GDR extrapolation.

The structure at 5 to 6 MeV has been studied extensively and there is widespread support for its existence [Bar + 73]. It appears in (d,pγ) and (n,γ) experiments in the 180 < A < 205 mass region (Fig. 12, for N = 82 nuclides (^{139}La, ^{141}Pr) [AM 79], and in the 120 < A < 134 mass region [Sta 64], at thermal, keV and MeV neutron energies. Its primary nature has been confirmed in many instances by observation of the shift in γ-ray energy with incident neutron energy in the keV region. In spite of this, the gross structure remains independent of energy over several MeV. The fine structure comprising the anomalous bump has also been observed with high resolution Ge(Li) detectors [Ear + 72] in ^{205}Tl. The interpretation of this effect has been related to p-h components which have escaped elevation into the GDR. The structure is not, however, observed in inelastic neutron scattering experiments [Ber + 66] when the γ-ray spectrum is basically statistical in character.

The situation for M1 giant resonance influences on the observed M1 strengths in nuclei is far from clear, both experimentally and theoretically.

For nuclides in the 100 < A < 180 region, the averaged resonance γ-ray data [Bol 73] exhibit an energy dependence for M1 transitions which is similar to the E^5_γ observed in the same mass range for E1 transitions. The ratio of average E1 and M1 radiation widths is found to be independent of mass number with an average value $\langle\Gamma_{E1}\rangle/\langle\Gamma_{M1}\rangle = 7 \pm 1$ for 110 < A < 240. There is no theoretical explanation for this observation.

Kopecky [Kop 79] has extended the ratio data down to A = 20, using thermal data where non-statistical capture mechanisms may occur. These data are shown in Fig. 13 with errors derived from the Porter-Thomas statistics. The three dashed curves indicate the expected A dependences for the Weisskopf or single particle model (SPM); the SPM but using the empirical constants k(E1) = 3 x 10^{-9}, k(M1) = 20 x 10^{-9}; and the E1 Axel prediction divided by the single particle value for M1 (GDR).

IV. Fast Neutron Capture

For capture in the energy region above 1 MeV, the cross sections extrapolated from lower energies or the basis of the compound-nucleus statistical

model are inadequate to explain the experimental data. The importance of direct excitations relative to compound nucleus formation becomes more and more important with increasing neutron energy. The best example is direct capture of a neutron into a single-particle orbit. We describe it as a one-step reaction leaving the other nucleons unperturbed. Another example is the direct excitation of the giant dipole state caused by the incident neutron, which at the same time is inelastically scattered into a bound single-particle orbit. In the next step, the giant dipole state may deexcite by the emission of γ-rays. This reaction is called "semidirect". It turns out that direct and semidirect reactions play a dominating role at neutron energies higher than about 5 MeV.

The direct-semidirect and the compound nucleus models represent the extremes on the reaction-time scale. Nevertheless, with proper choice of parameters the models provide a reasonable description of the experimental data. We shall first discuss the direct-semidirect model in some detail.

The driving force for polarizing the nucleus into a collective dipole vibration is provided by the symmetry potential, which expresses the fact that the force between neutron protons is, on the average, somewhat stronger than that between neutron and neutrons. Lane [Lan 62] has written the nuclear potential as,

$$V = V_o + \frac{V_1}{A} \vec{t} \cdot \vec{T}_{A-1}$$

where $\vec{t}$ is the nucleon isospin and $\vec{T}_{A-1}$ the isospin of the rest of the nucleus. The first term is the usual central potential and the second is referred to as the symmetry or isospin term. V_o and V_1 are the depths of the potentials which often are assumed to have the same radial dependence (Woods-Saxon form).

In the case where the nucleus is in the ground state, $\vec{t} \cdot \vec{T}_{A-1}$ can be replaced by $1/2\ t_z\ (N-Z)$ and one gets

$$V = V_o + \frac{1}{2} t_z \frac{N-Z}{A} V_1$$

The size of V_1 can be inferred from the symmetry energy term in the semi-empirical mass formula, and it is approximately 100 MeV. For a heavy nucleus like Pb, the size of the polarizing term in the potential is about $1/11(44)100 \approx 5$ MeV.

To see the effect of the symmetry potential, let us consider nucleon capture. The nucleon, in addition to the (isoscalar) potential V_o, is subject to a potential $NV_1/4A$ from the N target neutrons and $ZV_1/4A$ from the Z protons and these potentials have opposite signs. An incident neutron, for example, will by the action of the symmetry potential repel the N neutrons

and attract the Z protons. Hence, there will be a polarizing force between the neutrons and the protons of the target nucleus as the incident nucleon approaches the nucleus. The force is parallel to the force on the incident nucleon.

In nucleon capture, the symmetry potential is responsible for exciting simple, collective modes of motion in which the neutrons and protons move in opposite phases. The most important of these isovector (T=1) motions is the giant dipole resonance.

The Direct-Semidirect Cross Section

The symmetric force, in terms of the hydrodynamical model considered here, causes the neutron and proton spheres to separate, with a restoring force governed by the symmetry potential (Fig. 14).

The cross section is proportional due to square of the radiative amplitude,

$$\Gamma = \frac{ex_n}{2}\,(1 - Z\,\ddot{\xi}/\ddot{x}_n)$$

where the term in parenthesis represents the enhancement of the radiative amplitude due to target polarization.

The magnitude of $\ddot{\xi}/\ddot{x}_n$ can be estimated using the classical equations for a forced harmonic oscillator driven by the force between the incident neutron and the nucleus, and the restoring force due to the symmetry force. One must include a damping term which describes the function between the oscillating spheres. The result is

$$T = -\frac{ex_n}{2}\,\left(1 - \frac{2k\hbar^2/m}{E_D^2 - E_\gamma^2 - iE_\gamma\Gamma}\right)$$

where E_D is the giant dipole resonance energy, Γ the dipole width, and k a coupling constant. The constant can be evaluated from considering the spacing between single particle levels, E_o, and the neutron-proton residual interaction. The results are

$$T = T_d\,\left(1 - \frac{E_D - E_o}{E_D - E_\gamma - i\Gamma/2}\right)$$

and finally, since the cross section is proportional to the square of the amplitude,

$$\sigma^{dsd} = \sigma^{d}\left|1- \frac{\Delta E}{E_D-E_\gamma-i\Gamma/2}\right|^2$$

where $\Delta E = E_D - E_o$.

To illustrate the results let us consider the reaction $^{208}Pb(n,\gamma)^{209}Pb$, i.e. with the $2g_{9/2}$ ground state as the final state. The parameters of the giant dipole resonance, E_D = 13.42 MeV, Γ = 4.05 MeV, are taken from experimental data. The neutron binding energy is 3.94 MeV. The results in Fig. 15 show not only the direct-semidirect cross section, σ^{dsd}, but also the part which is due to the polarization charge. The latter is referred to as the semidirect cross section, σ^{sd}. We notice that σ^{sd} exhibits a symmetric resonance shape. On the other hand σ^{dsd} is asymmetric around the resonance energy, E_n = 9.5 MeV. The asymmetry arises because the direct and semidirect amplitudes, rather than cross sections, are added. The absolute square of the amplitudes contains a cross term which subtracts (destructive interference) from the quantity $\sigma^{sd} + \sigma^{dsd}$ below the giant dipole resonance. Above the peak of the resonance the interference is constructive.

The derivation outlined above is carried out using a classical approach, but also may be derived quantum-mechanically, as shown by Brown [Bro 64]. The results may be modified to include the isospin splitting of the giant resonance [AF 71, FG 70], and may be extended to deformed nuclei [BJ 72].

More discussion is appropriate to the role of the coupling constant which multiplies the semi-direct component of the DSD cross section.
In the classical derivation of the semidirect cross section we found that the incident neutron, by the action of the symmetry potential, forces a separation of the target neutrons from the protons. Moreover, we adopted the Goldhaber-Teller model to picture the giant dipole resonance as an oscillation of neutron and proton spheres against each other. If we let $U_1(r)$ denote the symmetry potential, then this model leads to a coupling which is proportional to $dU_1(r)/dr$ [CLR 65, Sat 72]. Alternatively, if one adopts the Jensen-Steinwedel model to describe the dipole resonance, one obtains a coupling function proportional to $rU_1(r)$ [Sat 72, LS 72, Pot 73]. A microscopic derivation of the semidirect cross section [Zim 70] results in a coupling in which the dominating term also is of volume form, $rU_1(r)$.

The symmetry potential, $U_1(r)$, must in the general case be assumed to be complex [Sat 71] even though the understanding of the imaginary term is not as obvious as for the central (spin and isospin independent) optical potential, U_o. The radial dependence of $U_1(r)$ is uncertain. Usually it is assumed that the real part has the same form as the central real potential but it has been suggested [TS 63, Sat 72] that the potential may be peaked at the nuclear surface.

In the model employed by Potokar [Pot 73], the symmetry potential is assumed to be

$$U_1(r) = V_1 f(r) - i\, W_1\, 4a\, df(r)/dr$$

where V_1 and W_1 are the depths of the real and imaginary parts of the potential. The Woods-Saxon form

$$f(r) = (1 - \exp \frac{r-R}{a})^{-1}$$

is usually taken to be the same for the real and imaginary terms, for simplicity. In the general case one should assume a different form for the imaginary term.

Giant resonances are highly collective modes of excitation which can be described in simple models like the hydrodynamical model. The giant dipole mode is only one form of oscillation that can occur in a nucleus. Another form which is well established is the quadrupole oscillation where the shape of the nucleus oscillates from prolate to oblate. Still higher order forms of nuclear shape oscillations are octupole and hexadecapole. The lowest form, which is of particular interest with regard to the nuclear compressibility, is the monopole oscillation described as a "breathing" mode.

The direct-semidirect model has been extended to include the excitation of other giant multipole resonances by applying the same formalism as for E1 transitions. The results of calculations for various multipoles [Pot 76, SLG 78, SG 78, SFG 79] indicate that the effect of the quadrupole resonance would be appreciable in the angular distribution of the γ rays. The interference between radiation of opposite parity, in this case E1-E2, causes a fore-aft asymmetry which is expected to be very large near the isovector E2 resonance predicted at $E_Q \approx 120\ A^{-1/3}$ MeV. (The isovector mode is characterized by an oscillation of neutrons and protons in opposite phases.) The asymmetry should also be observable near the isoscalar (when neutrons and protons move in phase) E2 resonance at $E_Q \approx 63\ A^{-1/3}$ MeV.

The experimental studies to search for the giant multipole resonances and to explore their properties involve many different kinds of reactions. Neutron capture reactions may also be used in these studies, particularly when polarized neutron sources are available, and the spin-depend effects may be investigated.

Experimental Results

Experiments on fast neutron capture include measurements of γ-ray spectra, partial cross sections for γ rays to individual states, angular distributions of γ rays and total capture cross sections by the activation method.

The measurements cover a neutron energy range up to about 15 MeV. Extension to still higher energies is in progress.

The measurements of γ-ray spectra offer an attractive possibility to gain insight into capture reaction processes. For example, one of the characteristics of a direct-semidirect reaction is that γ-ray transitions take place to single-particle states; e.g. the intensity of the γ ray is proportional to the spectroscopic factor. Compound-nucleus processes, at the other extreme, are non-selective. The resulting γ-ray spectra rather reflect the energy dependence of the total density of levels.

Three of the partial cross sections for neutron capture in ^{208}Pb are shown in fig. 16, namely for the $g_{9/2}$ ground state, the $i_{11/2}$ first excited state and the $g_{7/2}$ + $d_{5/2}$ states at 2.49 and 2.54 MeV, respectively [Ber 72]. All of them exhibit the resonance structure predicted by the directsemidirect model. It was noted in the preceding section that the cross section for ground state γ rays in ^{209}Pb would be expected to have its maximum at E_n = 9.5 MeV. The cross section for capture into each of the other single-particle states should peak at a neutron energy shifted upwards by the excitation energy of the state. Thus, we would expect the maximum cross-section for the $i_{11/2}$ state to occur at E_n = 10.3 MeV and for the $g_{7/2}$ + $d_{3/2}$ states at E_n = 12.0 MeV. The results are compatible with the Brink hypothesis [Bri 55] which prescribes that a giant dipole resonance is built on each excited state and that it has the same shape and magnitude as the one built on the ground state. The present results show that this is valid for the neutron single-particle states in ^{209}Pb.

Comparison with theoretical predictions for neutron capture by ^{208}Pb was first made with a surface-peaked coupling function [CLR 65]. We show in fig. 16 the direct-semidirect cross section obtained with this coupling function and a strength V_1 = 160 MeV of the symmetry potential (solid curves). Despite the rather high strength value, the calculated cross sections are too low and, furthermore, there is a disturbing discrepancy in the neutron energy dependences. A much better description of the data is obtained with a complex coupling function. The results (dashed curves) are taken from a calculation [Pot 73] with V_1 = 70 MeV and W_1 = 140 MeV.

The importance of direct and semidirect reactions in other nuclei can be estimated from fig. 17, which displays the partial cross sections for ground state γ rays in several nuclei (in the cases of ^{32}S and ^{89}Y also the first excited states are included in the cross sections). The results show that semidirect reactions are prominent in nuclei down to calcium. However, the contribution of direct-semidirect reactions in silicon is expected to be low in comparison with other reactions. It is obvious from the figure that compound nucleus reactions may play a significant role in sulfur and silicon. In these nuclei one should also expect structure due to reactions through single-particle doorway states [MC 78].

The success of the complex coupling model in describing the energy variation of the partial cross section is clear from the above figures, but the large imaginary potential, from 100 to 150 MeV required to fit the data is worthy of special mention.

The real coupling results in an interference between the direct and semidirect amplitudes which is destructive on the low-energy side of the giant resonance and constructive on the high-energy side. The effect of the imaginary term of the complex coupling is to restore the more symmetric resonance shape of the cross section. The problem is that the theoretical cross section, obtained with the large W_1-values, is dominated by the imaginary part of the coupling [Ber + 78].

The physical interpretation of the imaginary part of the coupling is that it describes the indirect excitation of the giant dipole resonance through more complicated reaction sequences than the polarization effect accounted for by the real term. These reaction sequences are probably typical only for capture reactions and, hence, the W_1-values applicable to these reactions may be quite different from those derived from other reactions. It is surprising that indirect excitations seem to dominate the scene for heavy nuclei. At present, it is an open question whether the large W_1-values reflect deficiencies in the direct-semidirect model or contributions from other reaction modes for the excitation of the giant dipole resonance.

Acknowledgements

The author has prepared this review based on material provided for a monograph on neutron capture sponsored by the NEANDC and to be published by Pergamon Press. Most important were the contributions of Barry Allen and Ingvar Bergqvist, but the advice and encouragement of Don Gardner and Wolfgang Poenitz are also acknowledged.

Research has been performed under contract DE-AC02-76CH00016 with the U.S. Department of Energy.

References

[AF 71] R. O. Akyuz and S. Fallieros, Phys. Rev. Lett. 27, 1016 (1971).

[All + 76b] B. J. Allen and A. R. deL. Musgrove, Nucl. Phys. A283, 37 (1977); J. W. Boldeman and R. L. Macklin, Nucl. Phys. A269, 408 (1976).

[AM 79] B. J. Allen and A. R. deL. Musgrove in "Neutron Capture Gamma-ray Spectroscopy", eds. R. E. Chrien and W. R. Kane, Plenum Press, New York, 1979, p. 538.

[Axe 62] P. Axel, Phys. Rev. 126, 671 (1962).

[Bar + 73] G. A. Bartholomew, E. D. Earle, A. J. Ferguson, J. W. Knowles and M. A. Lone, Advances in Nuclear Physics, Vol. 7 (Plenum Press, New York, 1973) p. 229.

[BDM 72] I. Bergqvist, D. M. Drake and D. K. McDaniels, Nucl. Phys. A191, 64 (1972).

[Bee 69] M. Beer, Phys. Rev. 181, 1422 (1969).

[Ber + 66] I. Bergqvist, B. Landborg, L. Nilsson and N. Starfelt, Nucl. Phys. 80, 198 (1966).

[Bir + 76] J. R. Bird, B. J. Allen, J. W. Boldeman, M. J. Kenny, A. R. de L. Musgrove, Proc. Int. Conf. Neutrons with Nuclei, Lowell (1976) Ed. E. Sheldon, CONF-760715 P1, 76.

[BJ 72] J. P. Boisson and S. Jang, Nucl. Phys. A189, 334 (1972).

[BM 69] A. G. Bohr and B. R. Mottelson in "Nuclear Structure", Vol. 1, W. A. Benjamin, New York and Amsterdam (1969) p. 382.

[Boh 36] N. Bohr, Nature 137, 344 (1936).

[Bol 73] L. M. Bollinger, Int. Conf. Photonuclear Reactions, Asilomar, CONF-730301, 783 (1973).

[Bri 55] D. M. Brink, Doctoral Thesis, Oxford University, 1955.

[Bro 64] G. E. Brown, Nucl. Phys. 57, 339 (1964).

[BW 52] J. M. Blatt and V. F. Weisskopf, "Theoretical Nuclear Physics", John Wiley and Sons, New York, 1952.

[Cam 59] A. G. W. Cameron, Can. J. Phys. 37, 322 (1959).

[CLR 65] C. F. Clement, A. M. Lane and J. R. Rook, Nucl. Phys. 66, 273 (1956).

[CM 75] J. Cugnon and C. Mahaux, Ann. Phys. 94, 128 (1975).

References - Page 2

[Cug 76] J. Cugnon, Nucl. Phys. A263, 61 (1976).

[FG 70] S. Fallieros and B. Goulard, Nucl. Phys. A147, 593 (1970).

[FKL 67] H. Feshbach, A. K. Kerman, R. H. Lemmer, Ann. Phys. 41, 239 (1967).

[Hei 54] W. Heitler, Quantum Theory of Radiation, Oxford University Press (1954).

[Joh 77] C. H. Johnson, Phys. Rev. C16, 2238 (1977).

[Kop 79] J. Kopecky, "Neutron Capture Gamma-ray Spectroscopy", R. E. Chrien and W. R. Kane, eds., Plenum Press, New York, 1979, p. 665.

[KSL 74] J. Kopecky, A. M. J. Spits and A. M. Lone, Phys. Lett. 49B, 323 (1974).

[Lan 59] A. M. Lane, Nucl. Phys. 11, 625 (1959).

[Lan 62] A. M. Lane, Nucl. Phys. 35, 676 (1962).

[Lan 71] A. M. Lane, Ann. Phys. 63, 171 (1971).

[LL 57] A. M. Lane and J. E. Lynn, Prog. Phys. Soc. (London), 70A, 557 (1957).

[LL 60] A. M. Lane and J. E. Lynn, Nucl. Phys. 17, 553, 586 (1960).

[LL 60a] A. M. Lane and J. E. Lynn, Nucl. Phys. 17, 553, 586 (1960).

[LM 74] A. M. Lane and S. F. Mughabghab, Phys. Rev. C10, 412 (1974).

[Lon 79] M. A. Lone in "Neutron Capture Gamma-ray Spectroscopy", R. E. Chrien and W. R. Kane, eds., Plenum Press, New York, 1979, p. 161.

[LS 68a] G. Longo and F. Saporetti, Nuovo Cimento 56B, 264 (1968).

[LS 72] G. Longo and F. Saporetti, Phys. Lett. 42B, 17 (1972).

[LT 58] A. M. Lane and R. G. Thomas, Rev. Mod. Phys. 30, 257 (1958).

[Lyn 68] J. E. Lynn, Theory of Neutron Resonance Reactions, Clarendon Press, Oxford (1968) 225.

[MC 79] S. F. Mughabghab and R. E. Chrien in "Neutron Capture γ-ray Spectroscopy", eds. R. E. Chrien and W. R. Kane, Plenum Press, New York, 1979.

References - Page 3

[Mug + 71] S. F. Mughabghab, R. E. Chrien, O. A. Wasson, G. W. Cole and M. R. Bhat, Phys. Rev. Lett. 26, 1118 (1971).

[Pot 73] M. Potokar, Phys. Lett. 46B, 346 (1973).

[Pot 76a,b] M. Potokar, Proc. Intern. Conf. on the Interactions of Neutrons with Nuclei (ERDA CONF, 760715, P2) Lowell 1976, p. 1436; M. Potokar, Phys. Lett. 46B, 346 (1976).

[Sat 71] G. R. Satchler, Phys. Lett. 35B, 279 (1971).

[Sat 72] G. R. Satchler, Nucl. Phys. A195, 1 (1972).

[SFG 79] F. Saporetti, F. Fabbri and R. Guidotti, Nucl. Phys. A321, 354 (1979).

[SG 78b] F. Saporetti and R. Guidotti, Nucl. Phys. Lett. A311, 284 (1978).

[SK 76] A. M. J. Spits and J. Kopecky, Nucl. Phys. A264, 63 (1976).

[SLG 78] F. Saporetti, G. Longo and R. Guidotti, Phys. Lett. 76B, 15 (1978).

[Sol 74] V. G. Soloviev in "Neutron Capture Gamma-ray Spectroscopy", Reactor Centrum Nederland, Petten, Netherlands (1974).

[Sta 64] N. Starfelt, Nucl. Phys. 53, 397 (1964).

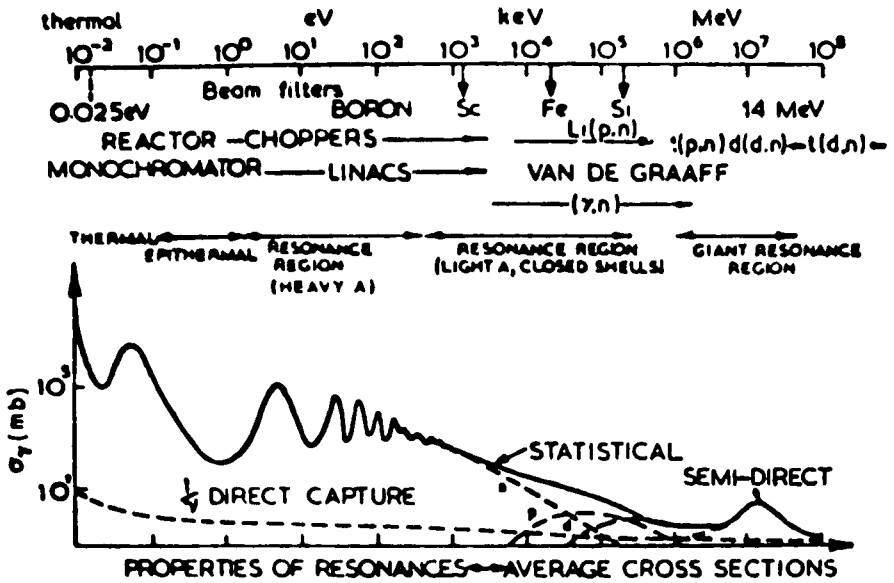

Fig. 1 Neutron capture research over nine orders of magnitude. Thermal, chopped and filtered beams from reactors are complemented by linear accelerator and Van de Graaff measurements in the keV and MeV ranges.

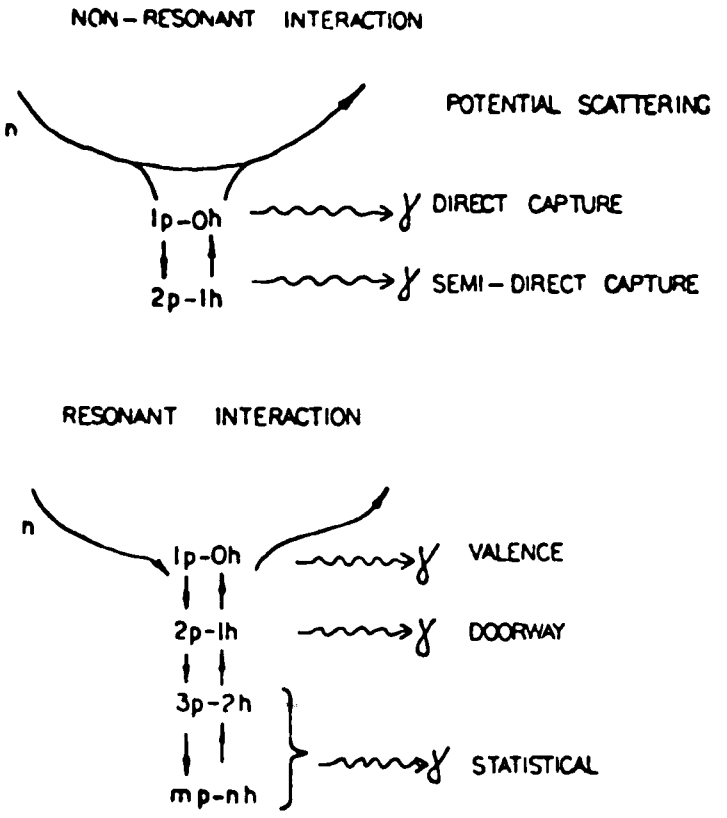

Fig. 2 Schematic representation of non-resonant and resonant neutron capture. Two-body interactions excite valence doorway and higher order particle-hole configurations. Radiative decay can occur from all components of the long-lived resonance state.

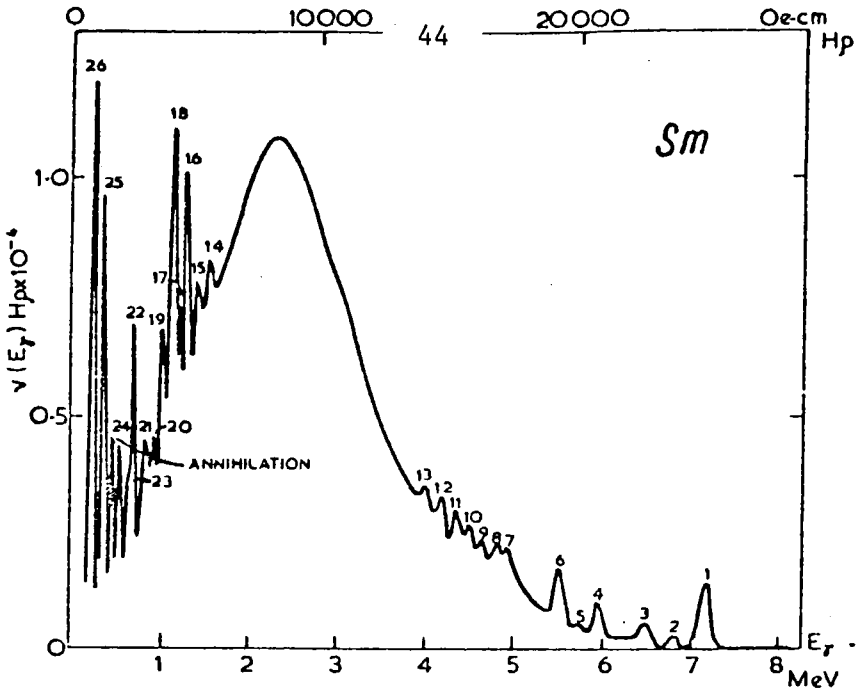

Fig. 3 Thermal capture γ-ray spectrum in Sm. The magnetic spectrometer can resolve only the high energy primary transitions and low energy cascade transitions. Note the ordinate is the energy weighted intensity $\nu(E_\gamma)\cdot E_\gamma$ [Gro + 59].

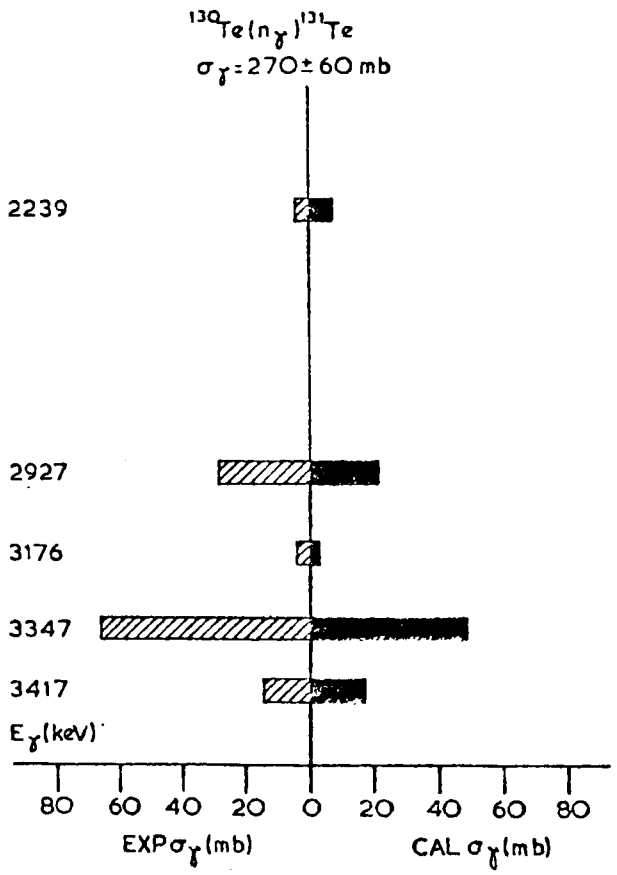

Fig. 5 Comparison of hard sphere and experimental partial capture cross sections at thermal energy for ^{130}Te. Only p-wave final states are shown [MC 79].

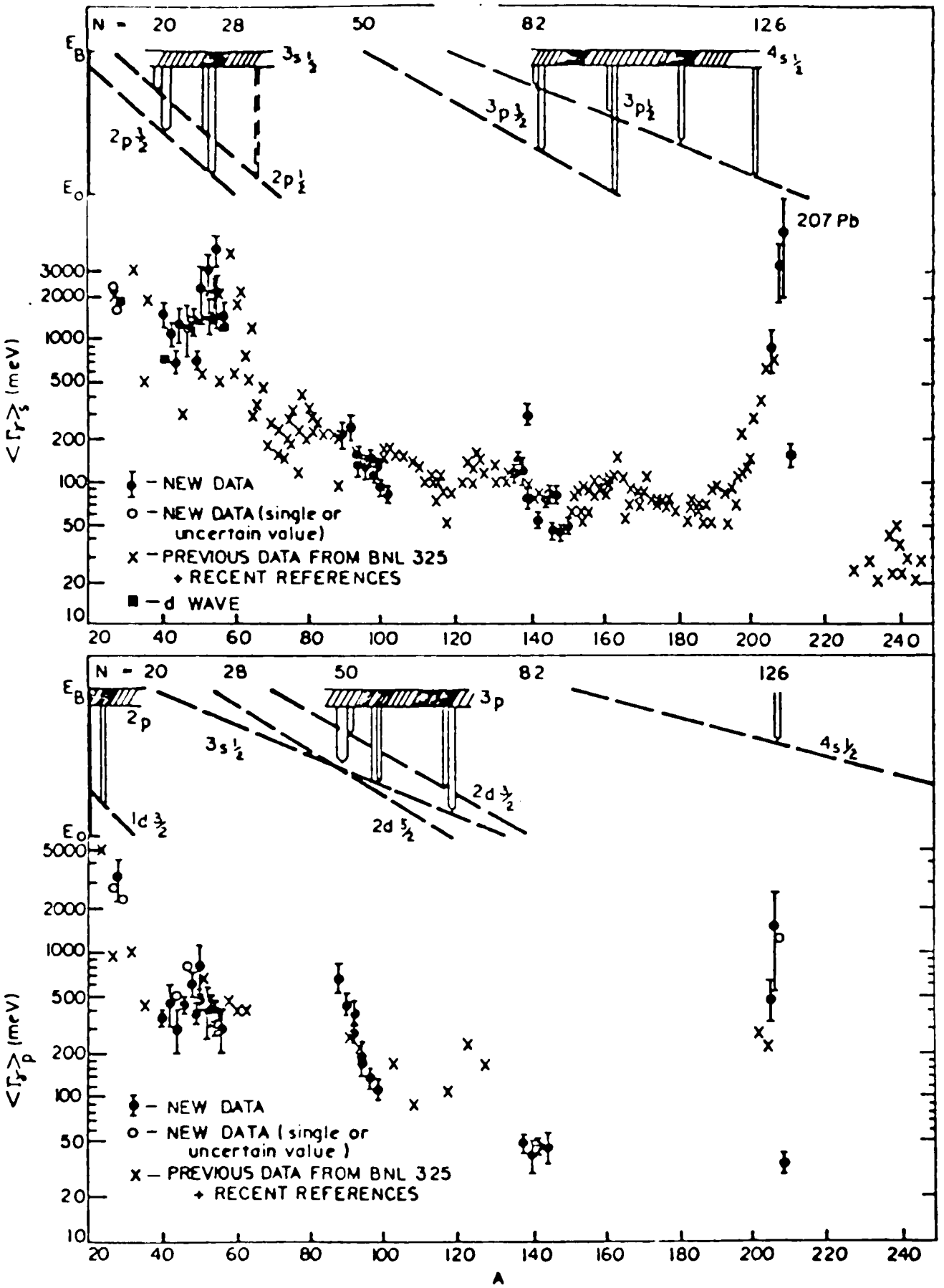

Fig. 4 Dependence of average radiation widths for s-wave (upper) and p-wave (lower) resonances. Schematic representations of the relevant E1 transitions between single particle shells are shown in each case, together with the A-dependence of the neutron strength function (hatched band) [Bir + 76].

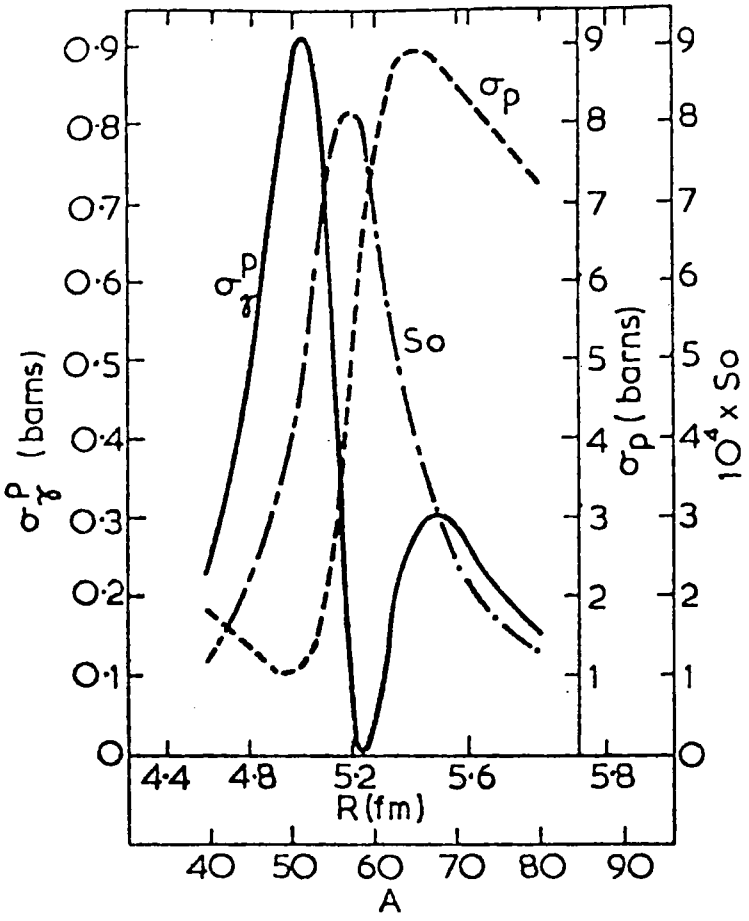

Fig. 6 Radial or mass dependence of the potential capture cross section ($\sigma^P{}_\gamma$), s-wave strength function (S_o) and potential scattering cross section (σ_p) for the 3s and 2p neutron orbitals. Imaginary potential W_o = 3.36 MeV [LL 60].

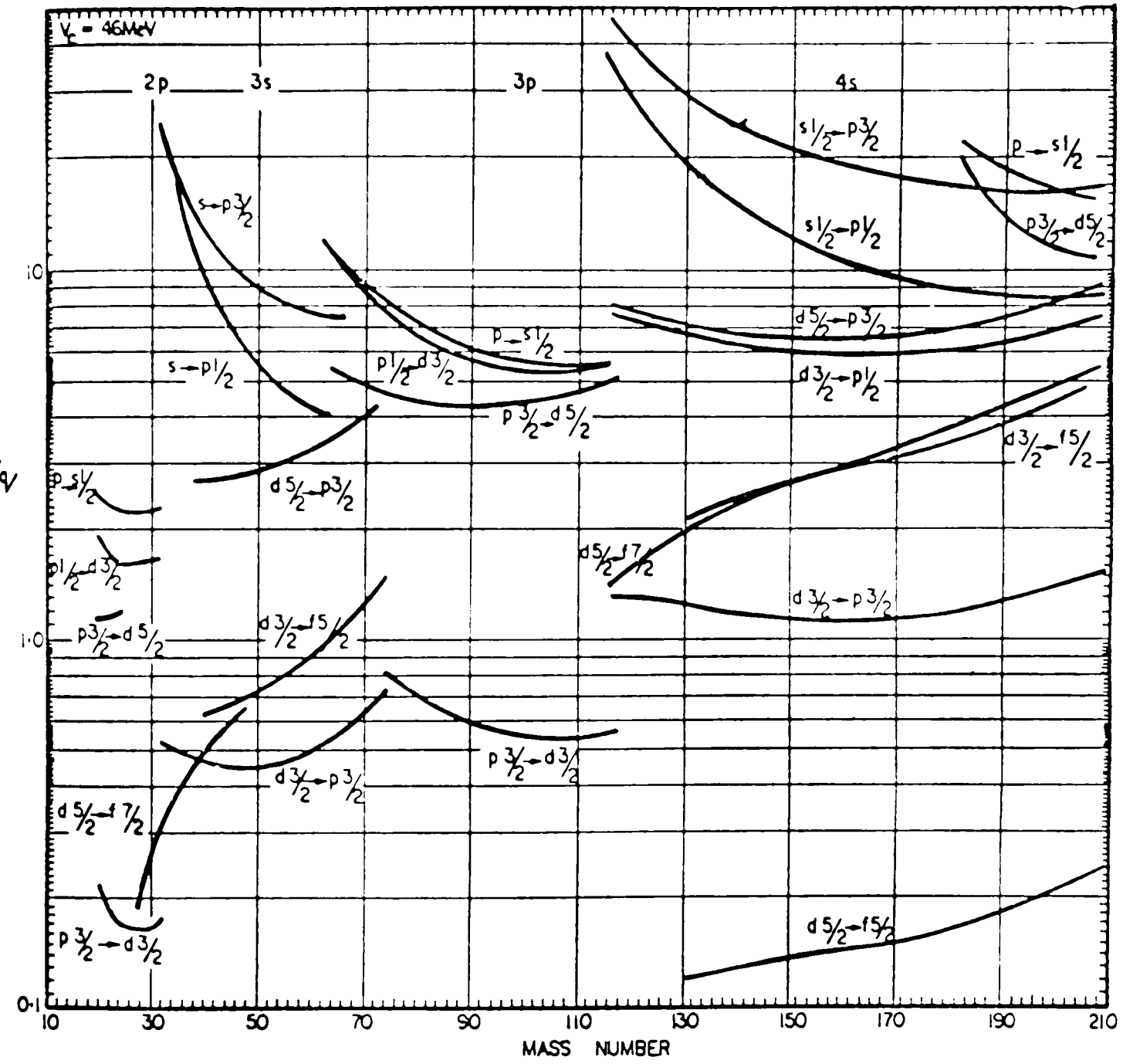

Fig. 7 Reduced valence widths (10^4q) for E1 transitions between s, p, d and f-wave single particle states. The largest values occur for s → p3/2 and p → s1/2 transitions [AM 78].

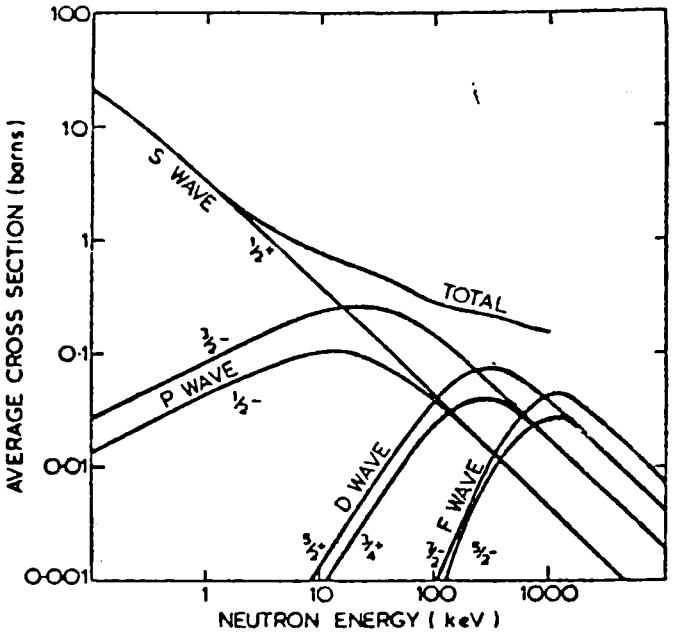

Fig. 8 Synthetic neutron capture cross section for A≈100. Partial capture cross sections for s, p, d and f-waves to the compound states are shown [CLS 63].

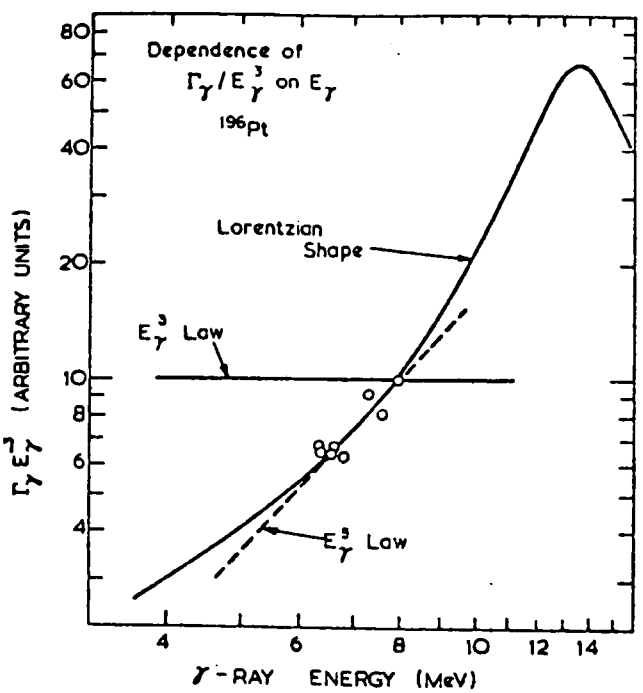

Fig. 9 Schematic representation of the energy dependence of reduced partial radiation widths. The E^5_γ rule, applicable only in the threshold region, is observed for resonance averaged γ-ray transitions in ^{196}Pt [BT 67].

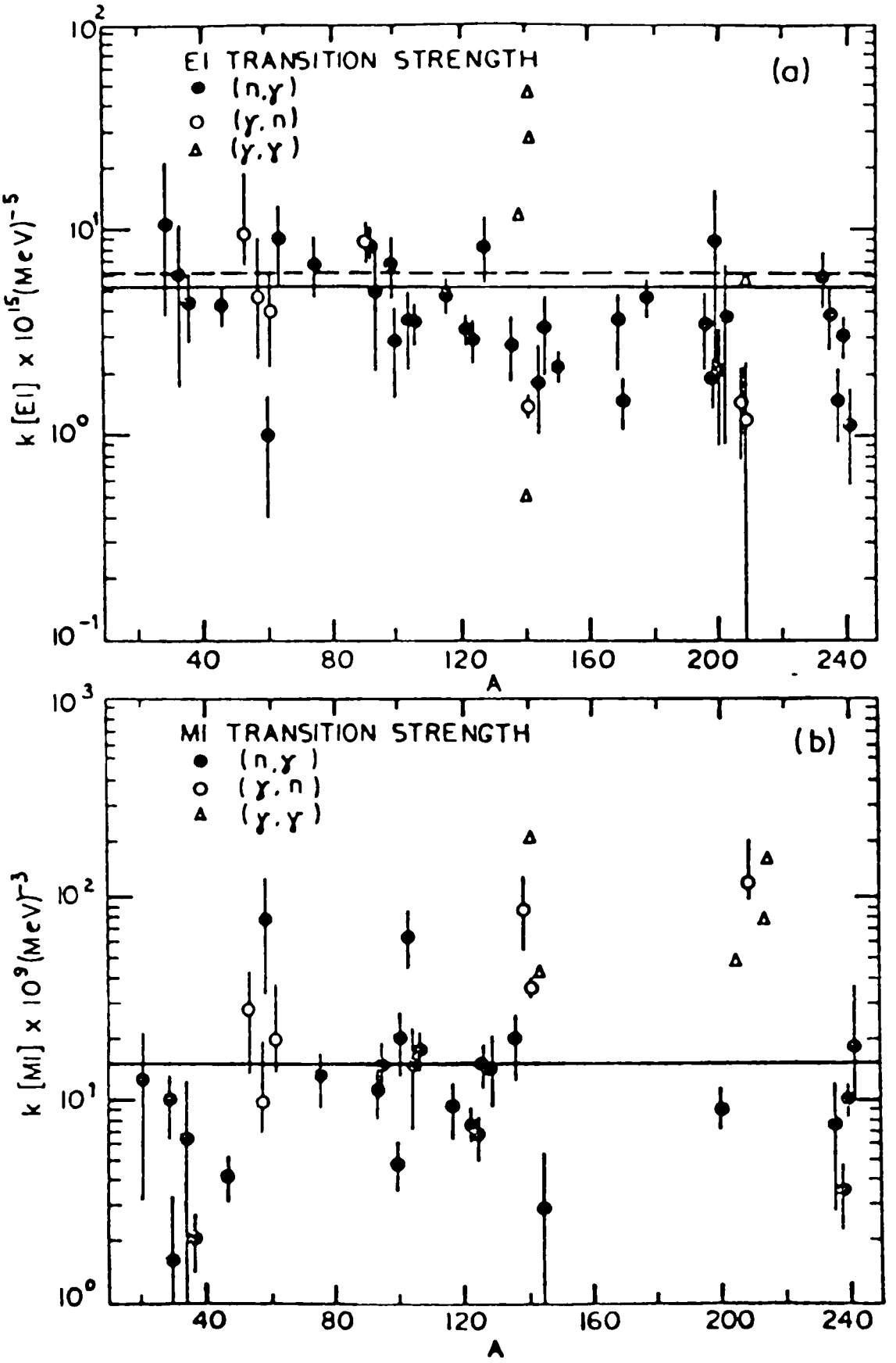

Fig. 10 Mass dependence of (a) E1 and (b) M1 transitions averaged over discrete resonances in (n,γ), (γ,n) and (γ,γ') reactions. Predictions of the giant dipole resonance model for E1 transitions (dashed line) are compared with the unweighted average (solid line) [MSC 79].

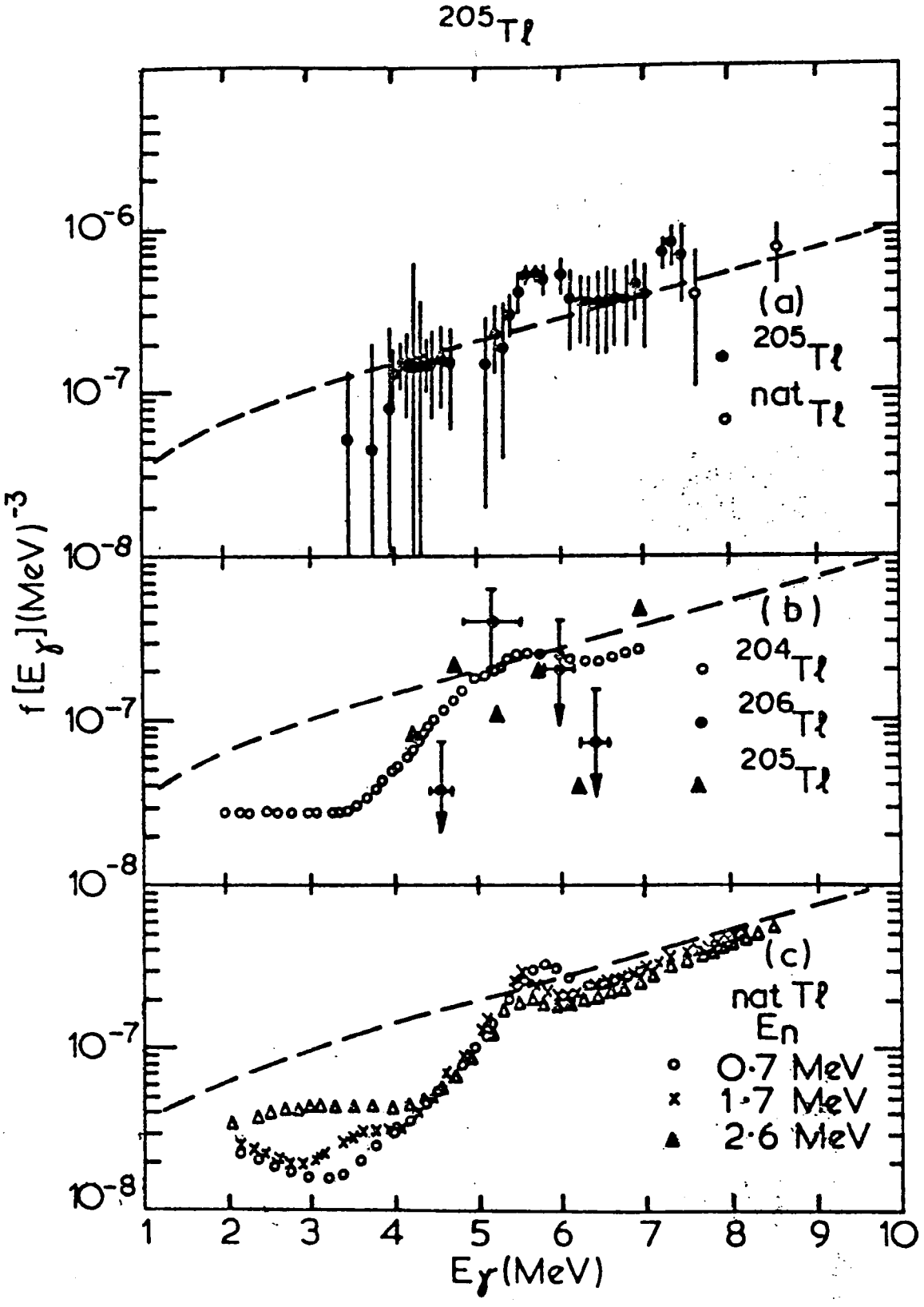

Fig. 11 Photon strength functions in Tl determined from photo excitation, (d,pγ), thermal, resonance and fast neutron capture are compared with that calculated from the Lorentzian tail of the giant dipole resonance [Ear + 76, Lon 78].

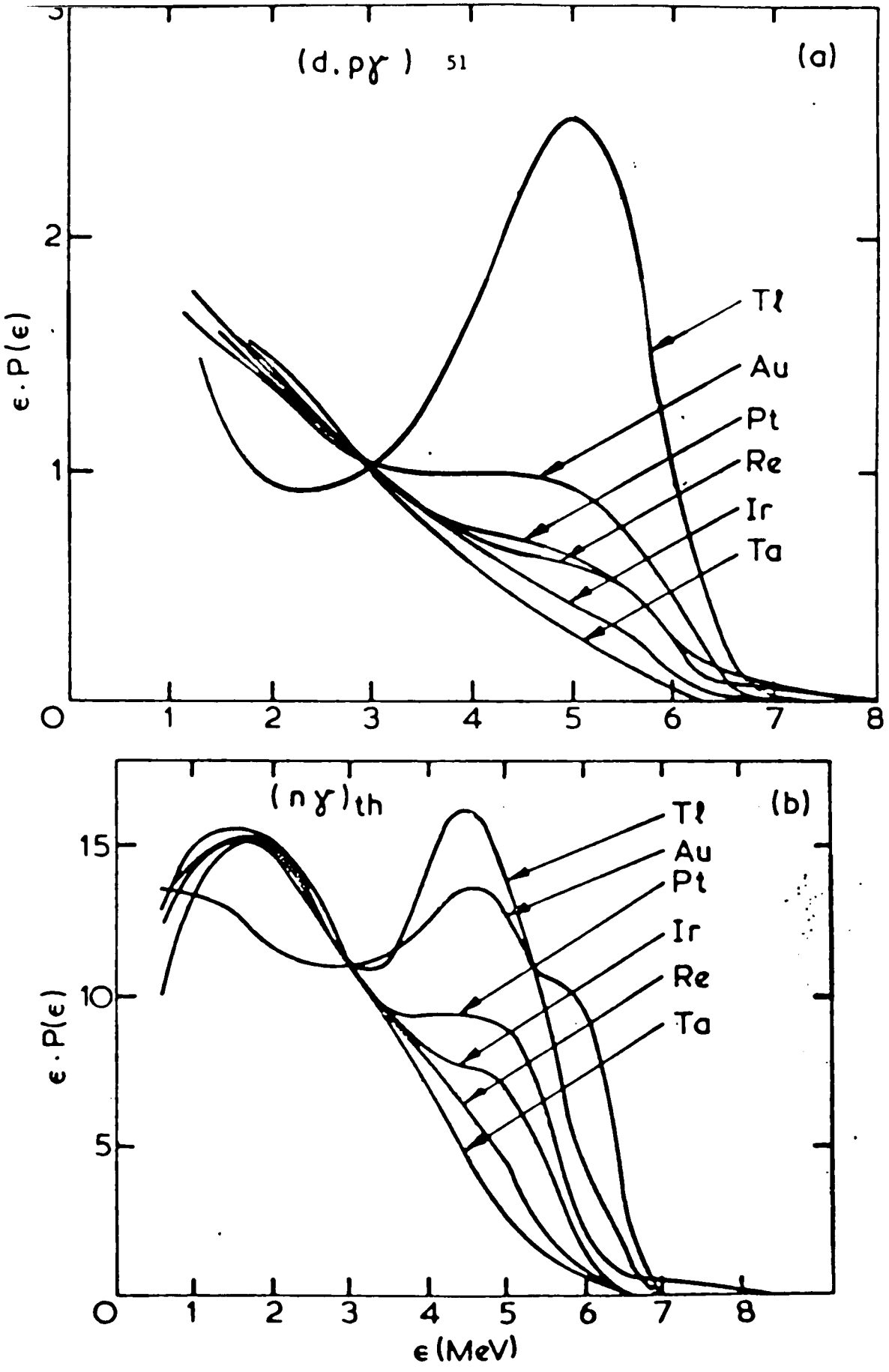

Fig. 12 Energy weighted NaI γ-ray spectra in the 181 < A < 205 mass region for (d,pγ) and thermal neutron capture reactions. All spectra are normalized to equal intensity at 3 MeV and smoothed to remove statistical effects [Bar + 73].

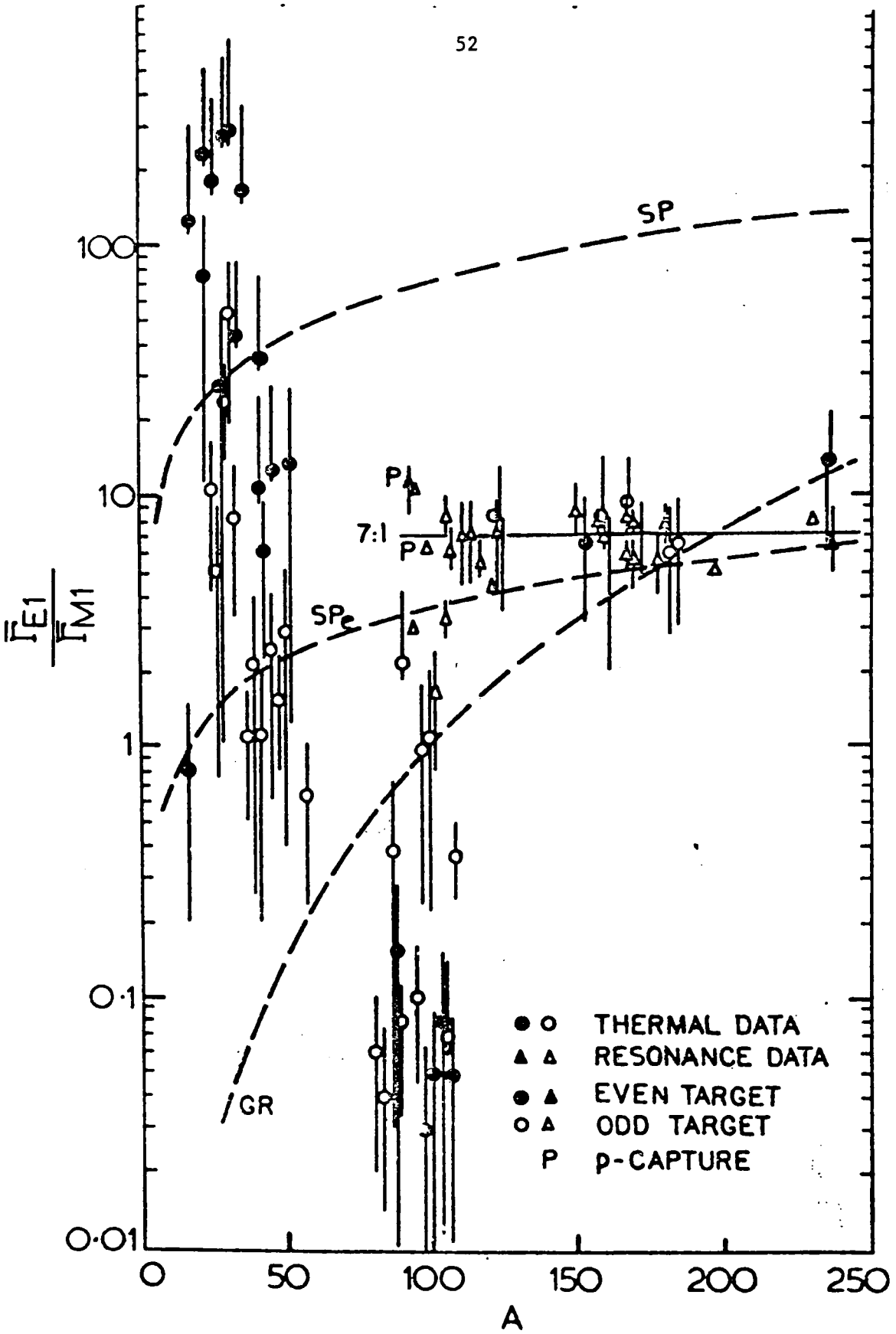

Fig. 13 A-dependence of the ratio of average E1 and M1 partial radiation widths. The expected dependences are shown for the single particle model (SP), the single particle model with empirical constants (SPe) and the giant dipole resonance model for E1 transition divided by the single particle value for M1 transitions (GR)

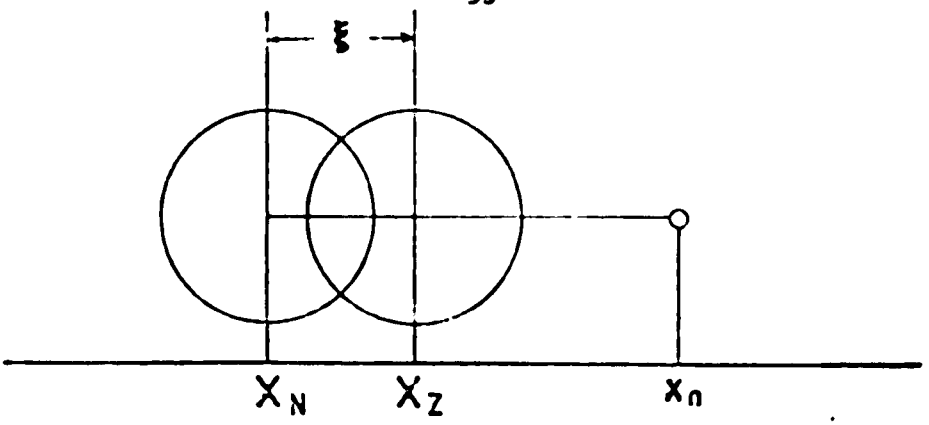

Fig. 14 Schematic representation of the target polarization due to an incident neutron.

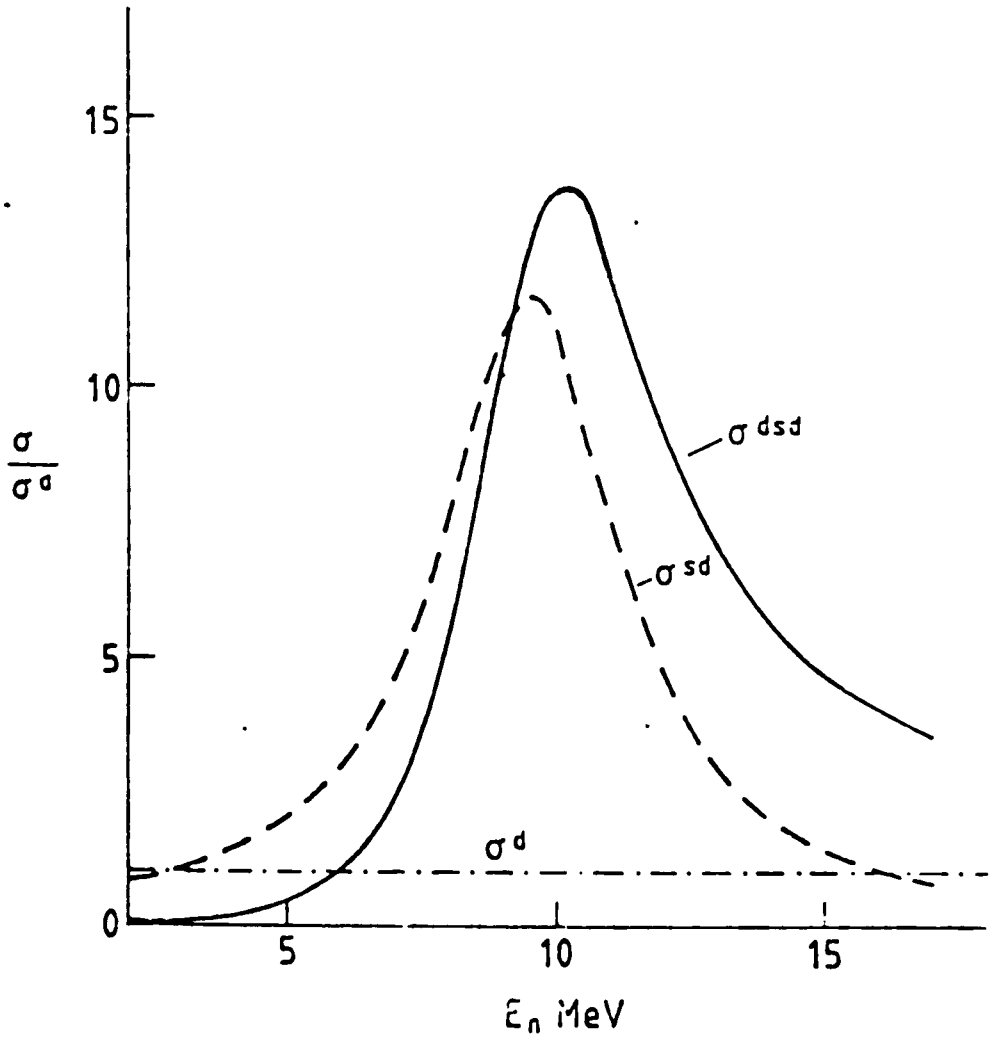

Fig. 15 Predicted shapes for the semidirect, σ^{sd}, and direct-semidirect, σ^{dsd}, cross sections of $^{208}Pb(n,\gamma)^{209}Pb$.

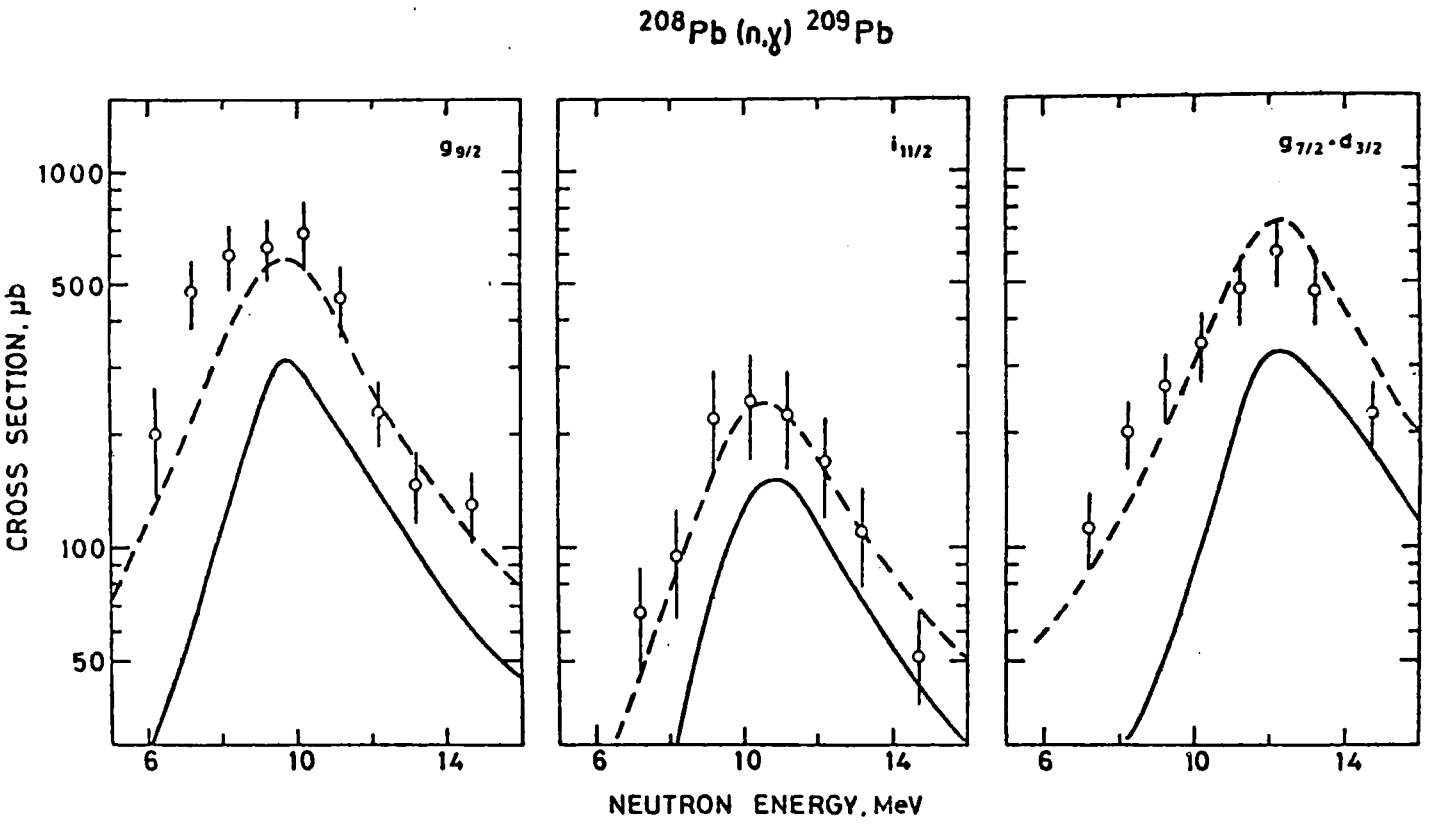

Fig. 16 Cross sections for γ-ray transitions to single-particle states of ^{209}Pb. The curves are direct-semidirect cross sections calculated with a surface-peaked (solid lines) and with a complex coupling function (dashed lines) [Pot 73].

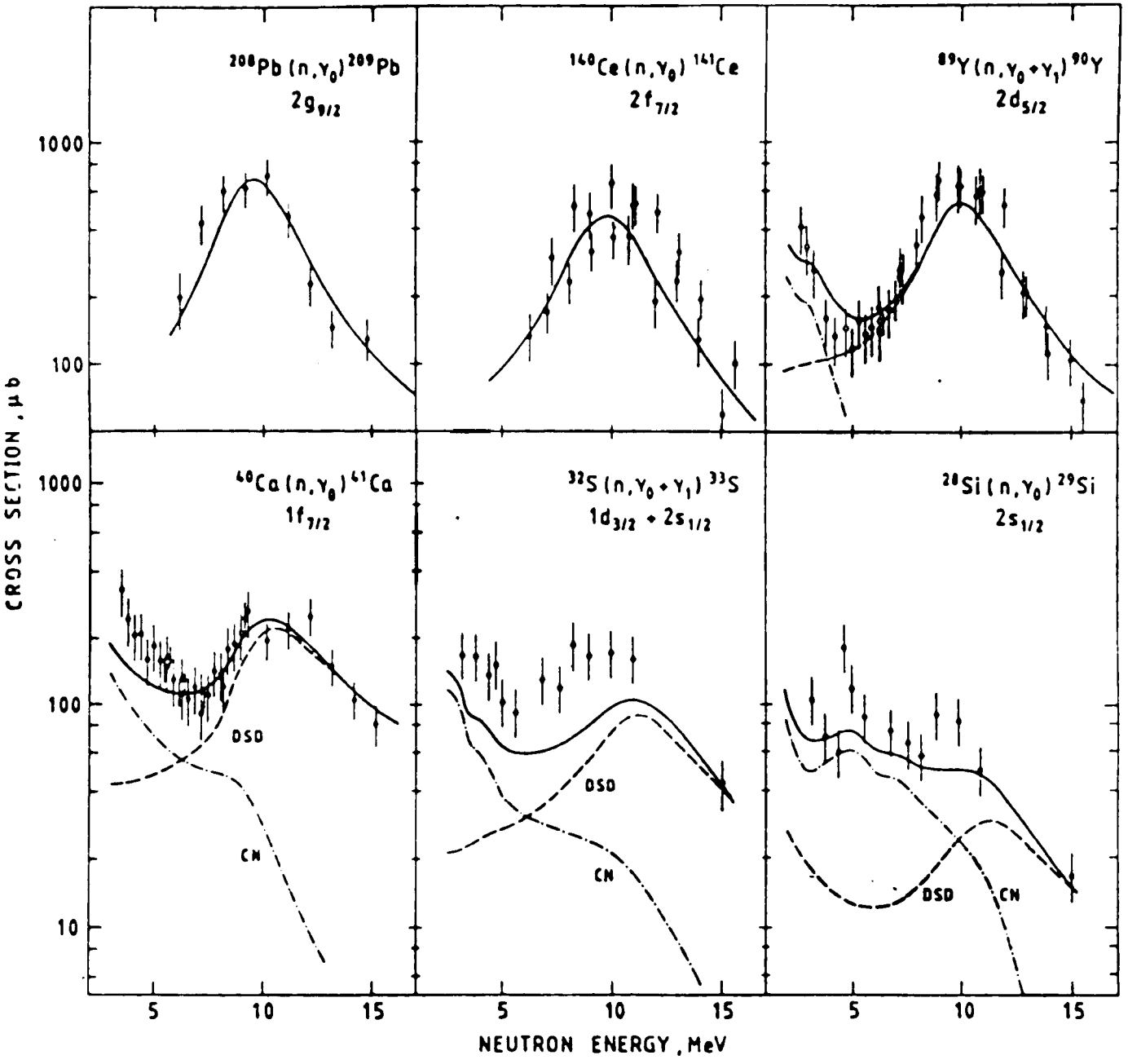

Fig. 17 Experimental and theoretical (n,γ_0) cross sections—or $(n,\gamma_0+\gamma_1)$, cross sections for ^{32}S and ^{89}Y—in the giant resonance region. The filled and open circles represent experimental results obtained at Los Alamos and Uppsala, respectively. The curves show the results of theoretical calculations with the direct-semidirect (DSD) and the compound nucleus (CN) models.

Discussion

COMMENT: S. Mughabghab
I would like to stress that the hard sphere term is only a part of the direct capture term. The full direct capture term includes a contribution from the tail of distant resonances. The full simplified expression is given, for example, in our paper presented at the Third (n,γ) Conference held at Brookhaven.

QUESTION: R. Block
A very mundane question - how accurately can one now calculate fast capture cross sections, for example, fission products?
ANSWER: R. Chrien
This type of calculation always involves extrapolation from a known base of experimental data. In this case the known data lie in the valley of stability; the unknown cross sections refer to nuclides off the valley. It is disturbing to note that extrapolations of binding energies or nuclear mass formulas, do not work particularly well far from stability.

QUESTION: R. Schenter
In calculating wave functions in the nuclear interior did you use the usual phenomenological local optical model potentials? It has been shown from microscopic models that the wave function is "damped" in the nuclear interior from that given by an equivalent local potential. Also phenomenological nonlocal optical-model potentials show this feature ("Perey Effect").
ANSWER: R. Chrien
As far as I know only local phenomenological potentials have been used. I am not sure how important nonlocal effects would be.

QUESTION: G. Rohr
What is the experimental evidence for valence nuclear transitions in the 3s-region?
ANSWER: R. Chrien
Perhaps the most evidence comes from the Australian group of Allen and his collaborators, for example in ^{54}Fe.

S. Mughabghab:
There are some nice cases in the 3s region, not so much looking for correlations but particular resonances (for example ^{50}Cr, ^{54}Fe) and calculating the magnitude. The agreement with calculations is very good.

R. Chrien:
You have cases where it seems to be valance and some where its not, so it is difficult to judge.

FAST NEUTRON CAPTURE MECHANISMS FOR NEUTRON ENERGIES BETWEEN 0.5 AND 6.0 MeV

by

S. Joly, G. Grenier and J. Voignier
Service de Physique Neutronique et Nucléaire
Centre d'Etudes de Bruyères-le-Châtel
B.P. N° 561
92542 MONTROUGE CEDEX, France

Abstract

Capture cross sections below 3 MeV are known to be mainly due to the compound-nucleus (CN) process. On the other hand, the direct and semi-direct (DSD) mechanisms were introduced to account for the excitation functions observed at higher energies, in the region of the giant dipole resonance (GDR). However, there are very few measurements in the region between 0.5 and 6.0 MeV. Data in this range are important as they help in deducing the strength of the complex particle-vibration coupling in the DSD model as well as restricting parameter variations involved in the CN calculations.
We present results obtained for the $^{89}Y(n,\gamma_o+\gamma_1)$ and $^{208}Pb(n,\gamma_o)$ reactions.

I. Introduction

The DSD model has been found to be fairly successful in describing the observed cross sections in the region of the GDR [1]. However, the strength W_1 of the imaginary coupling necessary to have a good fit with the data is larger than that found in typical optical potentials. The Pure Resonance (PR) model introduced later [2] is much less sensitive to the coupling form factor. A large contribution from compound-nucleus processes in the low-energy part of the GDR would result in a reduction of the strength W_1. It is thus of importance to measure cross sections in the region between 0.5 and 6.0 MeV. The CN process is predominant in the low-energy part of this region whereas CN and DSD processes are contributing by about the same amount around 6.0 MeV. A better estimate of the CN contribution should be possible in the region around 6.0 MeV and, consequently, the W_1-strength could be deduced with a better confidence.

Another interesting question concerns the excitation of giant resonances apart from the well known GDR ; for the region of interest these are the giant magnetic dipole (GMR) and the isoscalar component of the giant quadrupole (GQR). However, the excitation of the GDR is so large that a possible excitation of these resonances could be observed only through the interference with the E1 radiation causing forward-backward asymmetries.

Cross section and angular distribution measurements in the 0.5 to 6.0 MeV range are very difficult for several reasons : i) the capture cross section decreases to a minimum around 5.0 MeV, ii) because of the low D(d,n) reaction cross section the neutron flux is fairly small and, iii) finally, the 6.8 MeV γ-ray from thermal and slow neutron capture in the NaI crystal disturbs the high-energy part of the measured pulse-height distribution.

We report here on the results obtained for the $^{89}Y(n,\gamma_0+\gamma_1)$ and $^{208}Pb(n,\gamma_0)$ reaction cross section measurements as well as asymmetry factor measurements in the $^{208}Pb(n,\gamma_0)$ reaction at 3.8 and 5.9 MeV. These experiments have been made in collaboration with Leif Nilsson and coworkers from Uppsala.

II. Experiments

The experimental conditions are described in another contribution to this Meeting. Measurements of the $^{89}Y(n,\gamma_0+\gamma_1)$ cross section have been performed at Bruyères-le-Châtel for neutron energies between 0.5 and 3.0 MeV. The sample was a cylinder 4.8 cm in diameter and 1.6 cm in thickness made of elemental yttrium. Because of the 202 keV difference between the γ_0 and γ_1 transitions, they cannot be separated using a NaI γ-ray detector and are considered together in the theoretical calculations as well [3]. The cross sections obtained for the capture to the 2 $d_{5/2}$ ground-state doublet in ^{90}Y are presented in fig.1 along with previous data [4].

The $^{208}Pb(n,\gamma_0)$ cross section was measured from 0.8 to 5.9 MeV. The lead sample, enriched at 98.7% in ^{208}Pb, was a cylinder 3.9 cm in height and 3.5 cm in diameter with its vertical axis at 8.3 cm from the target. The angle-integrated capture cross sections for the γ-ray transition to the $g_{9/2}$ ground-state level of ^{209}Pb are presented in fig. 2 and compared with previous data in the GDR region [5]. Around 6.0 MeV the agreement between the two sets of data is quite good.

III. Compound-nucleus calculations

According to the compound-nucleus model, the neutron radiative capture cross section $\sigma(n,\gamma_f)$ for transitions to a final state f can be expressed by :

$$\sigma(n,\gamma_f) = \sum_\lambda \sigma_\lambda T_{\gamma\lambda f} \Big/ \sum_i T_i$$

where σ_λ is the cross section for the formation of the compound state λ, $T_{\gamma\lambda f}$ is the transmission coefficient for the γ-transition from the compound state λ to the final state f and T_i represents the transmission coefficient associated to each open channel. At the considered neutron energies, only neutron, proton and α-particle channels are open. These transmission coefficients are calculated by means of an optical model code using optical model parameters found in the literature. The γ-ray transmission coefficient is obtained using the γ-ray strength function deduced from photo-absorption cross section data. The γ-ray strength function deduced from the capture energy distribution by means of the spectrum fitting method [6] can also be used when possible. Generally, excited states in the residual nuclei, and their characteristics, are not known except for the low excitation energy region and we have to rely on level density estimates thus introducing uncertainties in compound-nucleus calculations. Moreover, different expressions are possible for the calculation of the elastic enhancement factor [7] which is difficult to estimate for the $^{208}Pb(n,\gamma_0)$ reaction at low neutron energies where few channels are open.

The results of these calculations are presented in figs. 1-2, for the $^{89}Y(n,\gamma_0+\gamma_1)$ and $^{208}Pb(n,\gamma_0)$ reactions, respectively. The agreement between calculated and observed cross sections is not that bad with regards to the uncertainties quoted previously.

IV. DSD calculations

In the DSD model the reaction amplitude is given by the sum of the direct and semi-direct (or collective) processes. The transition amplitude for capture of the incident neutron from the continuum optical-model state $|\chi_E^+\rangle$ to the single-particle state $|\varphi_{n\ell j}\rangle$ can be written in the form :

$$T = \langle\varphi_{n\ell j}|M|\chi_E^+\rangle + \langle\varphi_{n\ell j}\,|\,\frac{V_M}{E_\gamma - E_R + \frac{i}{2}\Gamma_R}\,|\chi_E^+\rangle$$

where M represents the single-particle multipole operator and V_M the form factor for the excitation of the giant resonance with excitation energy E_R and width Γ_R. The introduction of an imaginary term in the form factor gives the symmetry of the calculated excitation functions [1]. In figs. 1 and 2 are presented the results of the DSD calculations for the $^{89}Y(n,\gamma_0+\gamma_1)$ and $^{208}Pb(n,\gamma_0)$ reactions ; the solid line represents the sum of the CN and DSD calculations. For the $^{89}Y(n,\gamma_0+\gamma_1)$ reaction, a good agreement with the data is obtained with a real strength V_1 = 75 MeV and an imaginary strength W_1 = 110 MeV. The same real strength was kept for the $^{208}Pb(n,\gamma_0)$ reaction but a larger value W_1 = 140 MeV of the imaginary coupling term was necessary to reproduce the shape and the magnitude of the data. Unfortunately, the DSD calculated cross sections are also strongly dependent on the optical-model parameters used to generate the continuum wave functions. This, in turn, affects the strength of the deduced imaginary coupling term.

The possible excitation of the M1 and IVGQR resonances was investigated

in the $^{208}Pb(n,\gamma_0)$ reaction by means of the DSD calculations. The asymmetry factor, defined as the ratio between the difference and the sum of the forward and backward yields, was measured at 3.8 and 5.9 MeV energies where strong effects, if any, should show up according to DSD predictions [8]. Non zero values have been obtained [9] but several objections can be made to the DSD calculations. As can be seen from fig. 2, the DSD contribution in the region below 6.0 MeV is small compared to the CN contribution which should be subtracted first before comparison. On the other hand, interference between direct and statistical mechanisms may modify the predictions. As far as the M1 resonance is concerned, only fragments have been observed in heavy nuclei and it is not easy to define its characteristics (strength, energy and width).

V. Conclusion

Fast neutron capture cross section measurements in the neutron energy range from 0.5 to 6.0 MeV, combined with previous data in the GDR region, have shown the relative contribution of the compound-nucleus and direct semi-direct mechanisms. These are very difficult experiments and an accuracy better than 20% would not be easy to get.

Several problems remain to be worked out in the different models. We have seen that statistical calculations were very sensitive to level-density estimates, transmission coefficients (particles and γ-rays as well) and to the level width correction factor. The PR model was introduced to cover up some of the main objections to the DSD model (sensitivity to the optical-model parameters and to the imaginary coupling W_1). The good results obtained with this model suggest its preferential use for cross section estimates in the GDR region. Finally, further work is necessary to study the interference between direct and compound-nucleus contributions.

References

[1] - M. Potokar, Phys. Lett. 46B (1973) 346.

[2] - F.S. Dietrich and A.K. Kerman, Phys. Rev. Lett. 43 (1979) 114.

[3] - A. Lindholm et al., Nucl. Phys. A339 (1980) 205.

[4] - I. Bergqvist et al., Nucl. Phys. A295 (1978) 256.

[5] - I. Bergqvist, D.M. Drake and D.K. McDaniels, Nucl. Phys. A291 (1972) 641.

[6] - S. Joly, D.M. Drake and L. Nilsson, Phys. Rev. C20 (1979) 2072.

[7] - H.M. Hofmann et al., Z. Phys. A297 (1980) 153.

[8] - F. Saporetti and R. Guidotti, Nucl. Phys. A311 (1978) 284.

[9] - S. Joly et al., to be published in Nucl. Phys.

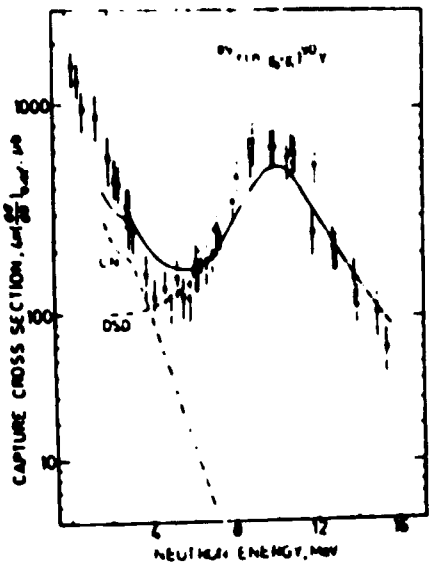

FIG. 1 - Comparison between compound-nucleus (CN) and direct-semi-direct (DSD) calculations with observed cross sections for the $^{89}Y(n,\gamma_0+\gamma_1)$ reaction.

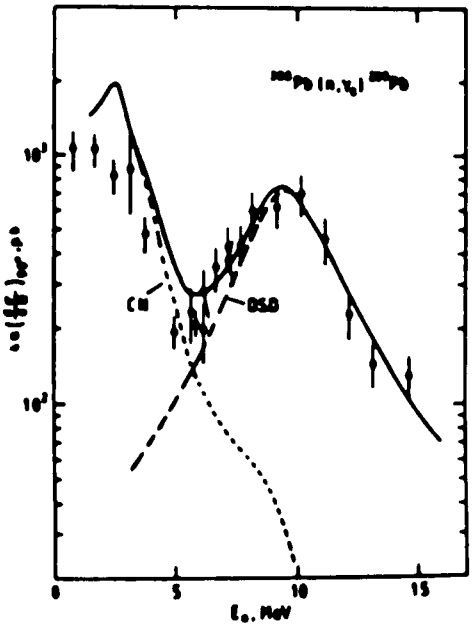

FIG. 2 - Comparison between CN and DSD calculations with observed cross sections for the $^{208}Pb(n,\gamma_0)$ reaction.

Discussion

QUESTION: R. Chrien
Has the use of bismuth germanated detectors (BGO) for high-energy capture γ-ray measurements been contemplated?
ANSWER: S. Joly
Yes, people in Los Alamos and in Oak Ridge are starting to use BGO for fast-neutron capture experiments as these detectors offer advantages over NaI crystals.

QUESTION: A. B. Smith
Do you have any evidence as to the energy-dependence of the iso-vector potential?
ANSWER: S. Joly
In the calculations we used an energy independent potential. However, in order to get good agreement with experiment, one has to assume the imaginary part of the potential to be relatively large so that it dominates which is puzzling. Even if one had allowed the potential to vary substantially with energy, it's likely that a large value of the imaginary part of the potential would have been necessary as well.

QUESTION: H. Gruppelaar
Your calculation only gives the partial capture cross section. How difficult it it to calculate total capture cross sections with the direct - semi-direct theory?
ANSWER: S. Joly
These calculations are possible for total capture cross sections as well as for spectroscopic factors when all bound states are known which is normally not the case except for nuclei near closed shells.

E1 GAMMA STRENGTH FROM (γ,n) MEASUREMENT IN ^{95}Mo*

by

C. Coceva, M. Magnani and M. Stefanon
ENEA, Bologna, Italy

Abstract

Threshold photoneutron measurements of the reaction $^{95}Mo(\gamma,n_o)$ were carried out in the neutron-energy interval 50-300 keV. Gamma-rays were obtained by bremsstrahlung of electrons accelerated by a low-energy linac; neutron energy was measured by time-of-flight. The cross-section is obtained by calibration with known $^{208}Pb(\gamma,n)$ resonances. An estimate of the electric dipole average gamma strength is deduced.

The threshold photoneutron technique was applied for a determination of the electric dipole gamma strength at about 7.5 MeV in the nucleus ^{95}Mo, for which no previous measurement was available in the literature.

The measured quantity is the cross-section for the (γ,n_o) process, in which a gamma-ray with energy above the neutron threshold is absorbed by the target nucleus, and a neutron is emitted, leaving the residual nucleus in its ground state. Such a cross-section is related to the gamma strength $\langle\Gamma_{\gamma o}/D\rangle$ through the equation

$$\bar{\sigma}_{\gamma,n}(E_\gamma) = 2\pi^2 \lambda\!\!\!^{-}{}_\gamma^2 \left(g \frac{\Gamma_n}{\Gamma} \frac{\Gamma_{\gamma o}}{D}\right) \qquad (1)$$

where $\Gamma_{\gamma o}$ is the width of the gamma transition between the ground state and the level at excitation E_γ of the target, and the other symbols have the usual meaning.

In the measurement, $\sigma_{\gamma n}(E_\gamma)$ is determined by time-of-flight spectrometry of the emitted neutrons. Gamma-rays incident on the target were obtained by bremsstrahlung of 7.8 MeV electrons issued by a low-energy linear accelerator. Electron pulses had a peak current of 3 A, a width of 6 ns and a repetition frequency of 650 Hz. The target consisted of metallic ^{95}Mo powder, with a 96.5% enrichment.

Two neutron detectors were placed at the end of two flight-paths, 10.3 m long, placed at 90° and 135° with respect to the incident gamma-rays. Each

detector consisted of seven ^{6}Li loaded glass scintillators having a diameter of 110 mm and a thickness of 12 mm.

The cross-section is deduced from the t.o.f. spectra using calibration measurements of ^{208}Pb(γ,n) resonances whose values of $\Gamma_{\gamma o}$ are taken as known standards from ref. [1].

The smoothed plot of fig. 1 shows the cross-section integrated over 4π, deduced from the two measurements at 90° and 135°.

The ground state of the target nucleus ^{95}Mo has $J^{\pi} = 5/2^+$. The most probable process leading to the emission of a low-energy neutron consists in the excitation of a $3/2^-$ resonance by absorption of E1 radiation, followed by p-wave neutron emission, leaving the residual ^{94}Mo in its 0^+ ground state. In the measured neutron energy range from 50 to 300 keV, emission of p-wave neutrons is much more probable than γ-decay. For this reason, in eq. (1) $\Gamma_n/\Gamma = 1$ as far as E1 radiation is concerned. Next in importance is the excitation of $3/2^+$ and $5/2^+$ levels by M1 radiation, followed by the emission of d-wave neutrons. This contribution increases with neutron energy; however in our range it is weaker than the E1 part for two reasons:

1) The M1 strength is smaller than the E1 one.

2) The factor Γ_n/Γ in eq. (1) is substantially smaller than unity because of the low penetrability factor for d-wave neutrons.

The whole energy range of the experiment was divided into three parts. The average measured cross-section and the expected M1 contribution in each interval are given in table 1. The M1 contribution and its uncertainty were calculated assuming that the gamma and neutron strength are

$10^8\ k(M1) = 1.2\ ^{+1.3}_{-0.7}\ MeV^{-3}$ and $10^4\ S_2 = 0.3 \pm 0.2$, respectively.

These values were estimated from the systematic behaviour of k(M1) and S_2 in the mass region around A = 95 (refs. [2] and [3] for k(M1) and [4] for S_2).

In the last column of tab. 1, the cross-section is given for E1 absorption in $3/2^-$ resonances; the indicated errors take into account the uncertainties of k(M1) and S_2 only, not including calibration errors mainly due to uncertainties of the assumed standard values.

The consistency of the σ_{E1} values in the three energy intervals indicates that the assumed k(M1) and S_2 are basically correct. Anyway, in order to deduce the E1 strength, we have used the σ_{E1} value obtained in the first energy interval, which has the lowest correction. The result is

$$k(E1) = \frac{\langle \Gamma_{\gamma o} \rangle}{D\ E_{\gamma}^3\ A^{2/3}} = 2.6\ ^{+0.2}_{-0.5}\ 10^{-9}\ MeV^{-3}$$

in good agreement with the systematics.

The experimental method here presented shows that values of the gamma strength can be simply deduced from the measurement. However, the attainable precision is at present limited by the large uncertainties in the $\Gamma_{\gamma o}$ values assumed as reference.

References

[1] R.J. Holt et al., Phys. Rev. C20 (1979) 93.
[2] O.A. Wasson and G.G. Slaughter, Phys. Rev. C8 (1973) 297.
[3] C.M. McCullagh, M. Stelts and R. Chrien, Phys. Rev. C23 (1981) 1394.
[4] A.R. de L. Musgrove, AAEC/E198 (1969).

* This contributed paper was not orally presented.

Table 1

E (keV)	$\bar{\sigma}_{exp}$ (γ,n_o) (mb)	$\bar{\sigma}_{calc}$ (M1) (mb)	$\bar{\sigma}$ (E1) (mb)
50 - 100	1.16	$0.11^{+0.21}_{-0.09}$	$1.05^{+0.09}_{-0.21}$
100 - 200	1.22	$0.28^{+0.42}_{-0.21}$	$0.94^{+0.21}_{-0.42}$
200 - 300	1.46	$0.39^{+0.49}_{-0.27}$	$1.07^{+0.27}_{-0.49}$

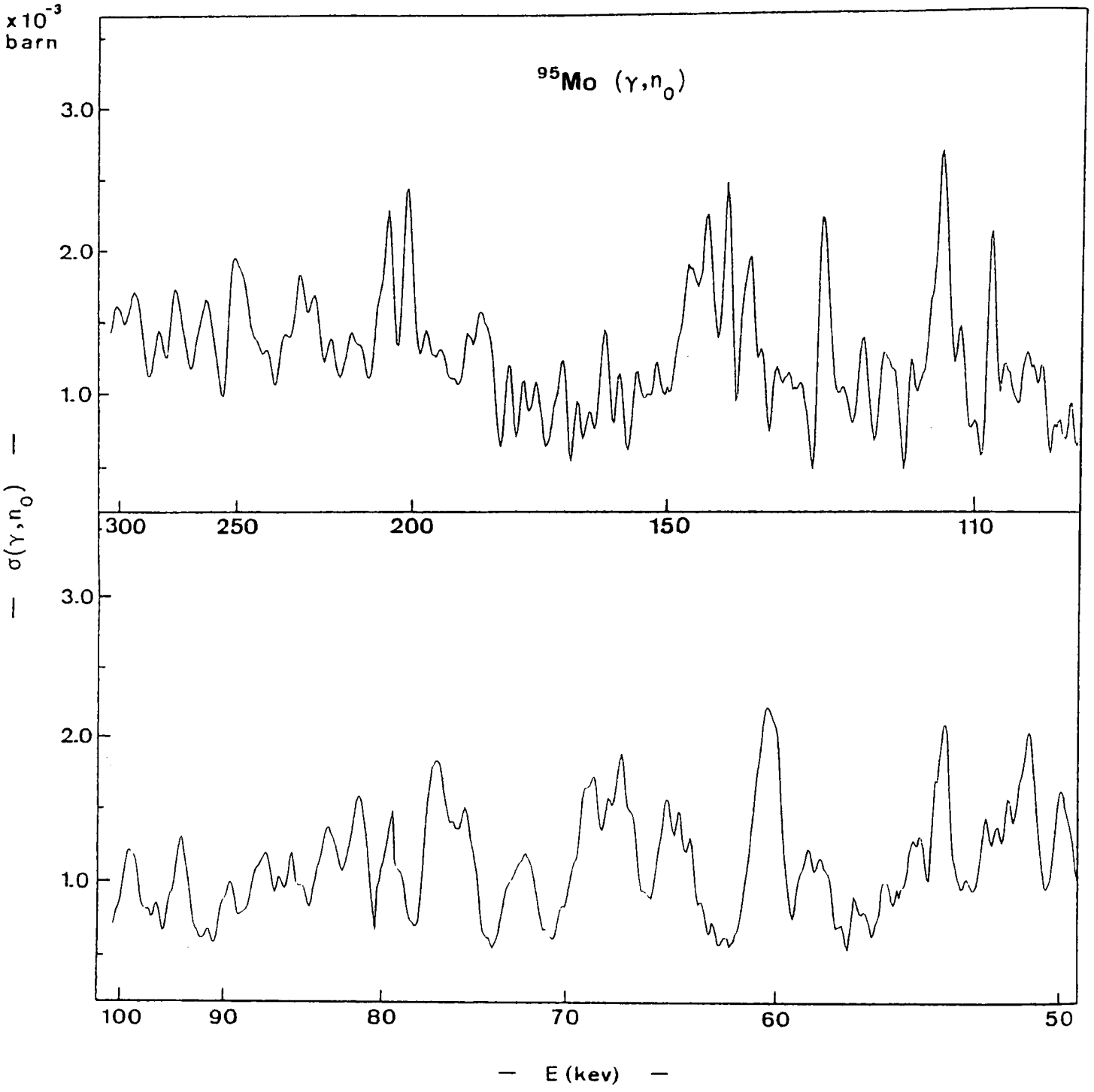

Fig. 1 - Cross-section of $^{95}Mo(\gamma,n_0)$ reaction.

CURRENT STATUS OF FAST NEUTRON CAPTURE CALCULATIONS*

by

Donald G. Gardner
Lawrence Livermore National Laboratory
Livermore, CA 94550, USA

Abstract

This work is primarily concerned with the calculation of neutron capture cross sections and capture gamma-ray spectra, in the framework of the Hauser-Feshbach statistical model and for neutrons from the resonance region up to several MeV. An argument is made that, for applied purposes such as constructing evaluated cross-section libraries, nonstatistical capture mechanisms may be completely neglected at low energies and adequately approximated at high energies in a simple way. The use of gamma-ray strength functions to obtain radiation widths is emphasized. Using the reaction $^{89}Y + n$ as an example, the problems encountered in trying to construct a case that could be run equivalently on two different nuclear reaction codes are illustrated, and the effects produced by certain parameter variations are discussed.

I. Introduction

A great deal of progress has occurred in recent years in the development of computer codes for calculating neutron capture cross sections and gamma-ray energy spectra over a wide range of incident neutron energies. Both statistical and nonstatistical capture mechanisms may be treated in varying degrees of detail. For medium-weight and heavy (but not fissile) nuclei, and for neutron energies up to several MeV, it is fair to say that the accuracy of neutron capture calculations is not limited by the available computer codes and the physics models which they contain, but by the input data. Modern codes properly conserve angular momentum and parity, and calculate all competing reactions concurrently. However, without accurate and complete input information such codes may produce substantially inferior results than often are available from greatly simplified calculations or even clever systematics. Although our modern codes demand a corresponding excellence in the nuclear physics information upon which their calculations are based, under favorable conditions they can produce remarkable results. More importantly, perhaps, they can provide insight into the reaction processes that could never come from simpler treatments.

*Work performed under the auspices of the U. S. Department of Energy by the Lawrence Livermore National Laboratory under contract number W-7405-ENG-48.

The orientation of this report is towards applications and not toward theory. We will be concerned mainly with statistical model calculations of the Hauser-Feshbach type, for incident neutron energies in the region from overlapping resonances up to several MeV. Nonstatistical capture mechanisms will be mentioned, but for many applications they may either be omitted from cross-section evaluations or treated rather simply. Much of the information summarized here was treated in more detail and given historical perspective in an unpublished report [Gar 81a], which will appear as a chapter in the monograph Radiative Neutron Capture (R. E. Chrien, editor), Pergamon Press, to be published this year. For other general descriptions of capture cross-section calculations, see Refs. [Dov+65, BR 69, SS 73, Rib+75, GJD 76, Iij+77, Ref 78]. For neutrons in the 5-20 MeV range, capture cross-section calculations based on the direct-semidirect model are discussed by Longo and Saporetti [LS 75]. Two major subjects will not be treated here at all. The first of these, capture calculations involving fissile nuclei, has already been covered in depth by Lynn [Lyn 74, Lyn 76, Lyn 81]. The second concerns error estimation and the construction of covariance matrices derived from sensitivity studies of the calculations. Some reports are available, for example, [Gru 75, Dra+77, Sch 78], but a comprehensive review appears to be lacking.

There exists a number of statistical model, nuclear reaction codes which can accurately calculate radiative neutron capture cross sections, gamma-ray spectra, and isomer populations. Two representative codes, COMNUC [Dun 70] and STAPRE [Uhl 70, US 76], were used in this work. Information on other codes may be obtained from the Nuclear Energy Agency Computer Program Library [SG 76]. When a properly designed test problem was formulated, the COMNUC and STAPRE codes reproduced each other's results to within a few percent. The problems encountered in constructing a test case which could be treated equitably by each code will be described; such problems seem to militate against the possibility of one test case being used to evaluate several different codes, except at a superficial level. Using the reaction $^{89}Y + n$ as an example, we will illustrate the sensitivity of results to certain model and parameter variations.

The most important input quantity for a capture calculation is the ratio of the radiation width to the level spacing, $\langle\Gamma_\gamma\rangle/D$, and its dependence on the excitation energy and the spin and parity of the radiating compound nuclear state. In the absence of experimental data, we believe this quantity may best be estimated from systematics involving the gamma-ray strength function rather than from systematics of the radiation width itself. Our current understanding of E1 strength function systematics will be reviewed in the final section of this report, and simple expressions will be given to estimate this quantity, as a function of energy, over a very wide mass range.

II. Nonstatistical Capture Mechanisms

For many years after Bohr proposed his compound nucleus picture of nuclear reactions [Boh 36], it was generally assumed that neutron capture reactions proceeded in a statistical way via this mechanism. Beginning in the late 1950's, and particularly in the last decade, a large body of theoretical and experimental evidence has been accumulated that shows conclusively that alternate mechanisms can contribute to the capture process. The point of concern here is -- how important are these mechanisms relative to the compound nucleus

capture process? From an evaluator's point of view, to what extent must they be considered when constructing an evaluated excitation function? In answering this question it is convenient to divide the energy range of the incident neutron into three parts: the low-energy resonance region, the region from the overlapping resonances up to, say, 5 MeV, and the high-energy region above 5 MeV, although the direct capture mechanisms functions in all energy regions.

II.A. Direct and Valence Neutron Capture

In 1959, Lane [Lan 59] published an extension of his work with Lynn [LL 57] on the derivation of both direct and compound nucleus capture mechanisms from dispersion theory. This work was followed immediately by two publications, [LL 60a, LL 60b] which formed the basis of much of the subsequent development of the theory of direct and valence capture. Four review papers in this area have appeared recently [Bir+76, Mug 78, MC 78, AM 79]. Subsequent to these reviews, a paper by Halderson and Castel was published [HC 79]. This was of particular interest because they compared three of the alternate theoretical approaches to the valence model treatment of Lane and Lynn. They investigated the case of $^{28}Si(n,\gamma)$, and concluded the most useful formulation was the optical model approach of Lane and Mughabghab [LM 74].

In simple terms, both direct capture and valence (or channel) capture arise from the overlap of initial and final state wave functions in the entrance channel region, primarily external to the surface of the target nucleus. The emission of dipole radiation occurs in the field of a spectator nucleus. Figure 1 illustrates the difference between direct and valence capture. When the incident neutron energy is on resonance, the capture probability is, in general, greatly enhanced over that for off-resonance (direct) capture.

The partial width for valence capture of an incident ℓ-wave neutron of energy E_n from an initial resonance, λ, to a final state, μ, may be expressed as

$$\Gamma^V_{\gamma\lambda\mu} = q_{\lambda\mu}(E_n)\ E_\gamma{}^3\theta_\mu{}^2 \left(\frac{Z}{A}\right)^2 \Gamma^\ell_{n\lambda}\ . \tag{1}$$

Here $q_{\lambda\mu}(E_n)$ corresponds to a reduced partial <u>valence</u> width, $\Gamma^\ell_{n\lambda}$ is the reduced neutron width for that partial wave, θ_μ is the reduced width of the final single-particle state, and E_γ is essentially the binding energy of the neutron in that final state. Summing over the final states, μ, the total valence width from resonance λ is

$$\Gamma^V_{\gamma\lambda} = \sum_\mu \Gamma^V_{\gamma\lambda\mu} \equiv Q_\lambda\ \Gamma^\ell_{n\lambda}\ . \tag{2}$$

Written in terms of ℓ-wave neutron strength functions, S_ℓ,

$$\langle\Gamma_\gamma\rangle^V_{\ell J} = Q_\ell\ S_\ell\ \langle D\rangle_{\ell J}\ . \tag{3}$$

The average spacing of resonances with the same $J\pi$ is $\langle D\rangle_{\ell J}$. The usual assumption is made that the total radiation width, $\langle\Gamma_\gamma\rangle$, is composed of a statistical part, $\langle\Gamma_\gamma\rangle^S$, and a nonstatistical part, $\langle\Gamma_\gamma\rangle^R$,

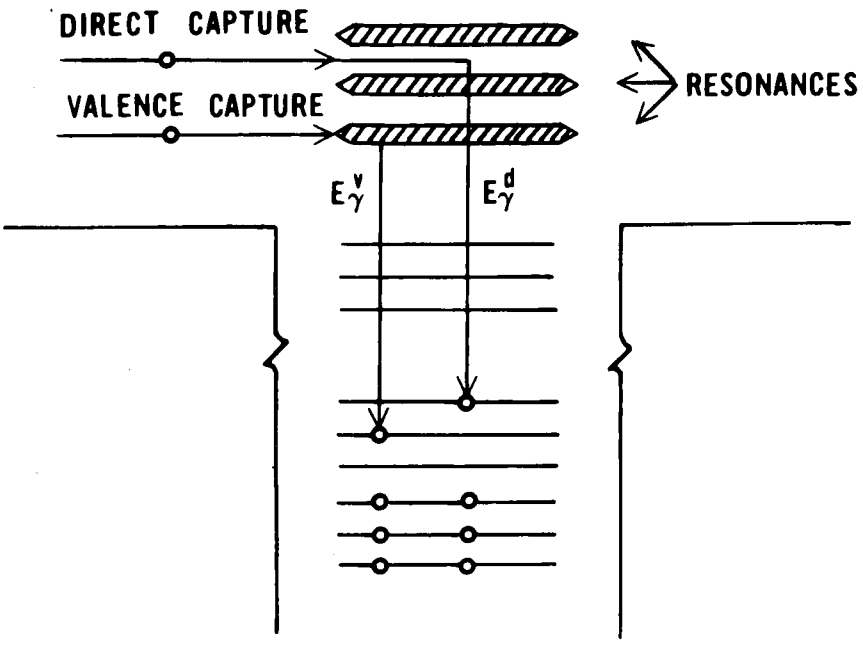

Fig. 1. Incident neutron undergoing direct or valence capture to a single-particle final state.

$$\langle\Gamma_\gamma\rangle = \langle\Gamma_\gamma\rangle^S + \langle\Gamma_\gamma\rangle^R , \tag{4}$$

and

$$\langle\Gamma_\gamma\rangle^R = \langle\Gamma_\gamma\rangle^V + \text{other nonstatistical terms.} \tag{5}$$

One would thus expect that partial valence widths would show correlations with the reduced widths of the initial and/or final states, and that the total valence capture width will be particularly enhanced for targets with large level spacings around maxima in the neutron strength functions.

Another assumption that is frequently made [AM 79] is that the difference between s-wave and p-wave radiation widths is attributable to nonstatistical capture mechanisms. In the mass region around A = 100, the 3-p neutron strength function reaches a maximum, and the nonstatistical contribution to the p-wave radiation width might thus be 50% or more. If this were true, it could severely limit our ability to calculate capture cross sections for nuclei where experimental data are lacking. However, the difference between s-wave and p-wave radiation widths cannot be due entirely to nonstatistical effects. Large differences can arise merely because of the spin and parity distributions of the discrete levels in the capture daughter nucleus. Also, the uncertainty in the average value of a partial-wave radiation width depends on the number, N, of the resonances that are averaged. In order to tell if s-wave and p-wave radiation widths really differ significantly a large number of resonances must be averaged, and there is no experimental evidence to suggest that valence

effects persist over a great many resonances. In fact, we have shown that, for the case of ^{98}Mo + n, which is the classic example [Chr+76] of undisputed correlations between transition strengths and reduced widths, all valence effects disappear completely when even a small number of resonances are averaged [Gar 81b].

We have made the most complete Hauser-Feshbach calculations that we can for the reaction ^{98}Mo + n, for neutrons in the 1 keV to 3 MeV energy range, using our latest versions of the statistical model codes STAPRE and COMNUC. The important aspects of our calculations include the use of absolute gamma-ray strength functions and detailed nuclear level information. In addition, we have modified the STAPRE code to print out partial wave results.

The spherical optical model potential used to produce the neutron transmission coefficients was that of Lagrange [Lag 77]. The level density parameters for ^{98,99}Mo were of the Gilbert-Cameron type [GC 65], as given by Cook et al. [CFM 67]. These were modified to reproduce the discrete levels in each nucleus: 26 levels up to 2.68 MeV in ^{98}Mo and 29 levels up to 1.25 MeV in ^{99}Mo. This structure information [Hen 79] represents evaluations in which experimental data were supplemented with theoretical calculations. The structure information for ^{99}Mo is shown in Table I, where the energies have been rounded to 50 keV.

The absolute gamma-ray strength functions were generated as follows: The E1 transitions utilized the energy-dependent Breit-Wigner line shape and the double-peak giant dipole resonance by Gardner et al. [GGD 80], which will be discussed further at the end of this report. The M1 transitions were taken to be single-particle in nature, and to represent about 15% of the total s-wave radiation width.

In the incident neutron energy range of 1-100 keV, our calculated capture cross sections agree well with those of Lagrange [Lag 77] which, in turn, fit the experimental measurements of Musgrove et al. [Mus+76]. Our calculations are still at a preliminary stage, but some of our tentative results are shown in Tables II and III, and compared with experiment where possible. The quantity S_ℓ in Table II is the neutron strength function for the ℓth partial wave. The gamma-ray strength functions are given in Table III. Because the calculated E1 strength function is energy dependent, the indicated range in values corresponds to the range of gamma-ray energies of 3.6-5.9 MeV.

In Fig. 2 we show the partial wave contributions to the total capture cross section for ^{98}Mo. In our current version of the STAPRE code these partial wave calculations are made without the width fluctuation correction and are thus somewhat larger than the correct values; however, the relative contribution of each partial wave is not greatly distorted. Figure 3 shows the high-energy end of the calculated gamma-ray spectra following the capture of 25-keV s-wave and p-wave neutrons. The experimental results of Chrien et al. [Chr+76] for the primary transitions to the first 8 levels in ^{99}Mo were averaged, and these are also plotted in Fig. 3. The s-wave data came from only 2 or 3 resonances, while the p-wave data included up to 15 resonances. The agreement between calculation and experiment is excellent in the p-wave case, and while the relative intensities are predicted well in the s-wave case the absolute intensities we calculate are low by a factor of 2 or 3. Our calculated s-wave radiation width is also low, compared with experiment,

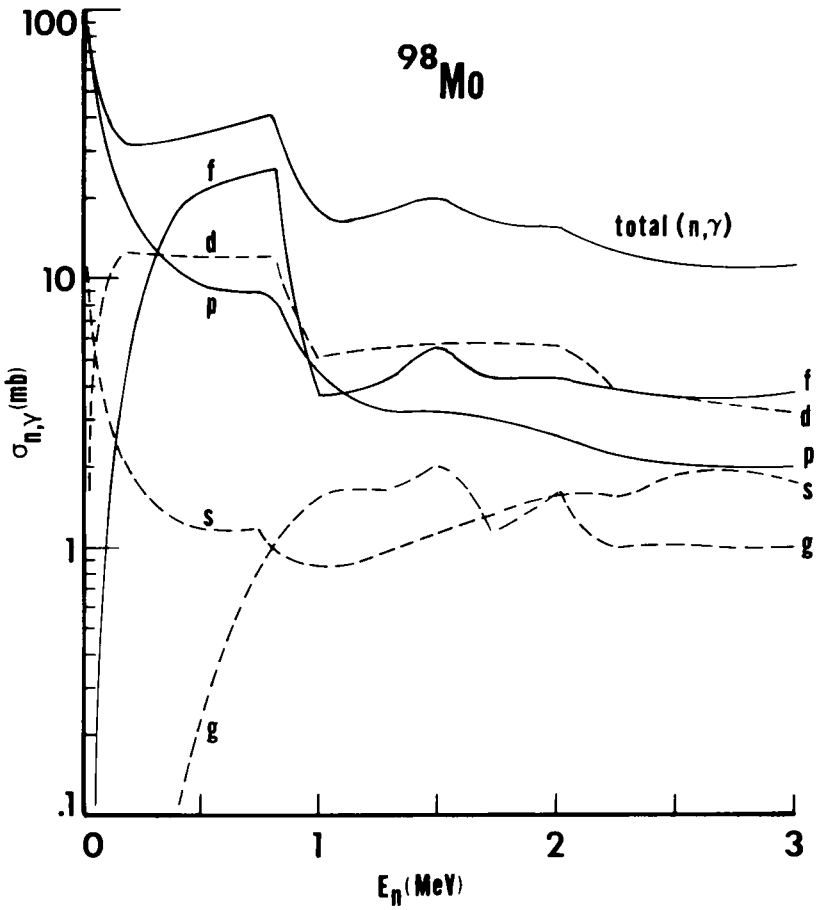

Fig. 2. Partial wave contributions to the total neutron capture cross section of ^{98}Mo. No width fluctuation correction was applied.

while the p-wave width is well calculated. The ^{99}Mo levels in Table I cannot be reached by primary E1 transitions following s-wave capture; including a possible $3/2^-$ level near 1.30 MeV might improve the calculated s-wave radiation width, but would not help the calculated gamma-ray spectra. One possibility would be to greatly increase the M1 gamma-ray strength function, which now is assumed to contribute 15% of the total s-wave radiation width. However, Fig. 2 shows that the s-wave contribution to the capture cross section is almost a decade less than that for p-waves, and so it is also possible some s-wave resonances with small radiation widths were not included in the experimental averages.

We conclude that we can calculate, on a purely statistical basis, the capture cross section and the average radiation width for s-wave and p-wave neutrons, in good agreement with experiment. Furthermore, the calculated intensities of primary gamma-rays to the first eight levels in ^{99}Mo agree well with recent averaged p-wave resonance measurements, even though the individual resonances may show large nonstatistical effects. It would appear that such nonstatistical effects disappear when even a small number of resonances are averaged, and so for evaluation purposes they may safely be ignored.

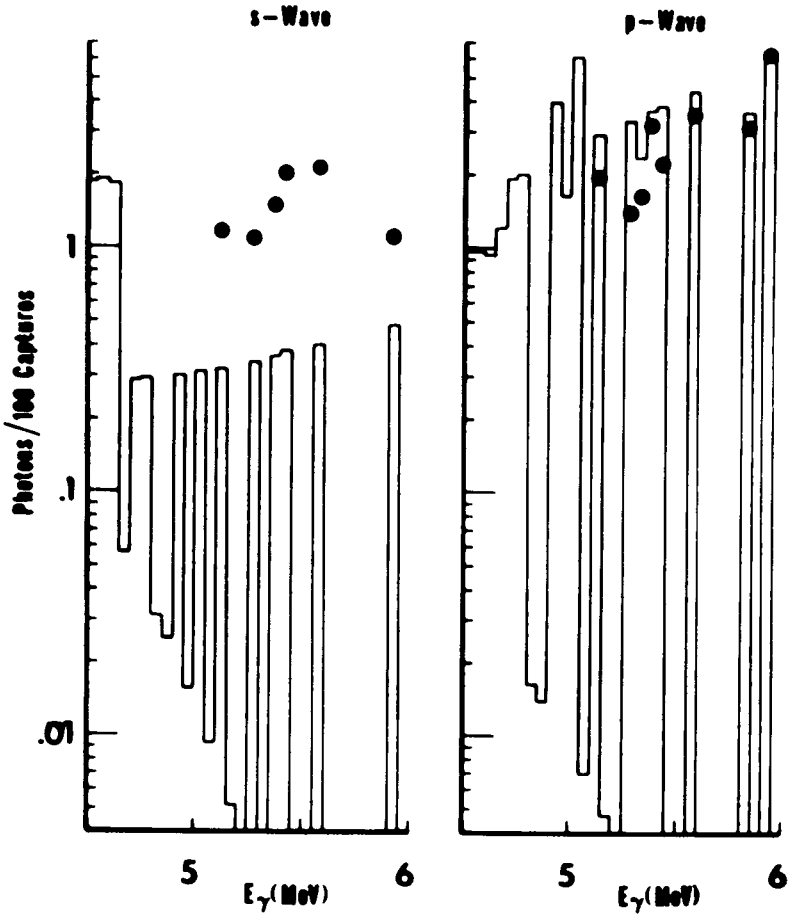

Fig. 3. High-energy portions of ^{98}Mo + n capture gamma-ray spectra for 25-keV s-wave and p-wave neutrons. Circles are experimental data [Chr+67].

II.B. Fast Neutron Capture

By fast neutron capture we generally mean capture of neutrons with energies above an arbitrary value of 5 MeV. The cross sections for capture are usually quite small, a few millibarns or less. The general situation for a medium-weight nucleus is illustrated in Fig. 4. Here we try to convey a feeling of the magnitude of the relative contributions to the capture cross section by the different capture mechanisms. The position of the peak arising from the semidirect mechanism depends on the energy of the giant dipole resonance, but it is in the neighborhood of 14 MeV, where the capture cross section is typically one millibarn.

While the capture cross sections are small for fast neutrons, the emitted gamma rays can clearly have energies in the 10-20 MeV region, or greater. In fusion reactors, neutrons with energies around 14 MeV are produced by the (d,t) reaction, and the shielding of the resulting high-energy gamma rays is important, not only to protect fusion reactor components but to satisfy biological safety requirements as well. Furthermore, as Bowman points out [BEG

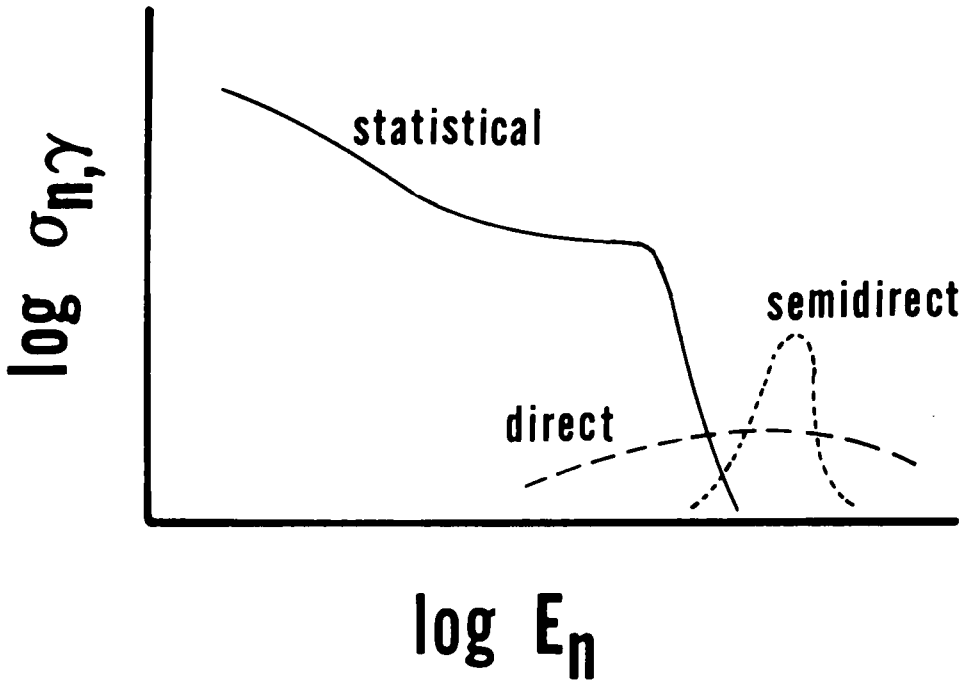

Fig. 4. Hypothetical example of neutron capture by a medium-weight nucleus, where the approximate contributions from the different capture mechanisms are indicated.

78], photofission of isotopes of U and Th present in various fission reactor systems can produce serious backgrounds that can interfere with threshold fission foil measurements.

The initial work by Lane and Lynn [Lan 59, LL 59] showed that the compound nucleus contribution to the capture of 14-MeV neutrons by heavy elements was much too small to account for the observed results. The direct contribution improved the agreement, but the calculations were still low by an order of magnitude. The breakthrough came in 1964 when Brown [Bro 64] pointed out that semidirect capture through the dipole states of nuclei can be even more important than direct capture when the energies were in the region of the giant dipole resonance (GDR). The reaction can be pictured as a high-energy neutron dropping into a low-lying final state, with the concurrent collective excitation of the GDR. A more detailed development of the semidirect capture model was published by Clement, Lane, and Rook [CLR 65].

An interesting feature of Brown's work is that he showed that the semidirect capture component could be expressed, approximately, as a term, F_{SD}, by which the direct capture was enhanced. Thus

$$\sigma_{n\gamma}^{DSD} \approx F_{SD} \cdot \sigma_{n\gamma}^{D} , \qquad (6)$$

where $\sigma_{n\gamma}^{DSD}$ is the direct + semidirect capture cross section, and $\sigma_{n\gamma}^{D}$ is the direct part alone. Actually, F_{SD} is the square of an amplitude, of the form

$$F_{SD} = |1 + \Delta E/(\varepsilon_\ell + E_\gamma - E_R + i\,\Gamma_R/2)|^2, \tag{7}$$

where ΔE is an energy shift associated with the dipole state. Implicit in Eq. 7 is an interference between the direct and semidirect capture mechanisms. This was neglected in the early theoretical treatments, but was later investigated by Longo and Saporetti [LS 68]. Review papers [Ber 74, LS 75, LS 76] summarize the recent advances in the DSD theory. Beyond these we might mention the recasting of the DSD model into an equivalent form, termed the "pure resonance model" by Dietrich and Kerman [DK 78].

Except where the details of the high-energy capture gamma-ray spectrum is important, we feel that for applied purposes the DSD component of the capture cross section can be adequately modeled using the approach of Benzi and Reffo [BR 69]. They recommend an expression that incorporates the factorization of $\sigma_{n\gamma}^{DSD}$ into two parts, along the lines of Eq. 6. They give, for incident neutron energy, E_n,

$$\sigma_{n\gamma}^{DSD}(E_n) = K\left[6\,(Z/A)^2\,\frac{(E_n^{1/2}\,R^4\,E_\gamma^3 \cdot 10^{-10})}{(2 + E_n/2 + 16.8\,E_n^{1/2}/R)}\right] \cdot \left[1 + \frac{0.75\,E_R\,E_\gamma - 0.61\,E_R^2}{(E_\gamma - E_R)^2 + (\Gamma_R/2)^2}\right]. \tag{8}$$

Here R is the nuclear radius, E_R and Γ_R refer to the energy and width of the GDR, and K is a normalizing constant that depends on the single-particle level spacing at the Fermi energy in the capture daughter nucleus. This can be estimated in different ways, or obtained by fitting Eq. 8 to 14-MeV cross-section data. For the parameter E_γ, Benzi and Reffo use

$$E_\gamma = E_n + S_n/2, \tag{9}$$

where S_n is the neutron separation energy in the daughter nucleus. Sometimes this shifts the position of the DSD peak up too far in energy, and using $E_\gamma = E_n + S_n$ may produce better results.

III. Statistical Model Calculations

For the purpose of constructing an evaluated excitation function for an (n,γ) reaction, it is acceptable to ignore nonstatistical capture mechanisms entirely in the overlapping resonance region, and to model them in a simple way above about 5 MeV incident neutron energy. In the energy region where the compound nucleus, statistical model pertains, the situation is quite different. In general, Hauser-Feshbach calculations must be done carefully, in which angular momentum and parity are conserved and all competing reactions are calculated concurrently. If we are only interested in the neutron capture reaction, then certain conditions are relaxed somewhat. For example, we do

not have to be concerned with precompound particle or gamma-ray emission, because they both become evident only at high energies, above 5 MeV, where the statistical capture process has nearly vanished anyway. Neither do we have to treat direct inelastic scattering with deformed nuclei in great detail, as long as we are confident that the neutron optical potential used to generate the transmission coefficients yields acceptable s-wave and p-wave neutron strength functions and a good compound nucleus formation cross section.

We will now set down the familiar Hauser-Feshbach and statistical model equations, and comment on some of the quantities and models that enter into such calculations. The reaction $^{89}Y + n$ will be used as an example. We have recently completed a careful comparison of the two statistical model codes, COMNUC and STAPRE, using this reaction as the test case. The main features of these two codes are summarized in Table IV. Some of the difficulties encountered in constructing a test case that can be run equitably on two or more different codes will become apparent as we discuss the sensitivity of the calculations to different parameters and nuclear models.

III.A. The Hauser-Feshbach Equations

The cross section for a compound-nucleus-type reaction with entrance and exit channels, c and c', respectively, may be expressed as

$$\sigma_{cc'}(E_c) = \frac{\pi \lambda\!\!\!^{-2}}{(2s+1)(2I+1)} \sum_{J\pi} (2J+1)\, \sigma^{J\pi}_{cc'}(E_c) \ , \tag{10}$$

where

$$\sigma^{J\pi}_{cc'}(E_c) = \left\langle \frac{\theta_c \theta_{c'}}{\theta} \right\rangle^{J\pi} \ , \tag{11}$$

$$= \frac{\langle\theta_c\rangle^{J\pi} \langle\theta_{c'}\rangle^{J\pi}}{\langle\theta\rangle^{J\pi}} S^{J\pi}_{cc'} \ , \tag{12}$$

and $\langle\theta\rangle^{J\pi} = \sum_{c'} \langle\theta_{c'}\rangle^{J\pi}$. All sums are taken to insure conservation of angular momentum and parity, and the symbols have their usual meaning. The collision matrix parameters, θ_c, are averaged over the resonances in the compound nucleus, $\langle\theta_c\rangle$, and approach the limiting value

$$\langle\theta_c\rangle^{J\pi} \rightarrow 2\pi \ \langle\Gamma_c\rangle^{J\pi}/D^{J\pi} \ . \tag{13}$$

The width fluctuation factor, $S^{J\pi}_{cc'}$, converts the average of a quotient of values, in Eq. 11, to a quotient of averaged values, in Eq. 12, which, in turn, may be related to optical model transmission coefficients, $T_c \approx \langle\theta_c\rangle$.

The averages over the partial widths are made under the assumption that they are distributed according to a χ^2-distribution, with ν_c degrees of freedom, except for the radiation width which is assumed to be nonfluctuating. We will consider different assumptions concerning the magnitude and behavior of ν_c later.

For a single particle channel we have identified $\langle\theta_c\rangle$ with the transmission coefficient, T_c. When the particle is emitted to a continuum of final states,

$$\langle\theta_x(E)\rangle_{c'}^{J\pi} = \sum_{c'} \langle\theta_{xc'}(E)\rangle^{J\pi} , \tag{14}$$

or in terms of transmission coefficients, and using a level density expression, $\rho(E)$, to represent the continuum, we replace the sum in Eq. 14 by an integral

$$\langle\theta_x(E)\rangle^{J\pi} = \sum_{c'} \int_0^{E_{max}} T_{c'}(E')\rho(J', \pi', (E_{max}-E'))dE'. \tag{15}$$

For the specific case of neutron capture,

$$\sigma_{n\gamma}(E_n) = \frac{\pi\lambda\!\!\!^{-2}}{2(2I+1)} \sum_{J\pi}(2J+1)\ \sigma^{J\pi}_{n\gamma}(E_n) , \tag{16}$$

and

$$\sigma^{J\pi}_{n\gamma}\ (E_n) = \frac{\langle\theta_{no}\rangle^{J\pi}\langle\theta_{cap}\rangle^{J\pi}}{\langle\theta\rangle^{J\pi}}\ S^{J\pi} . \tag{17}$$

By $\langle\theta_{no}\rangle$ we mean neutron emission to the target state, and $\langle\theta_{cap}\rangle$ is used to indicate the gamma-ray emission probability that leads to the daughter nucleus. Thus, we distinguish $\langle\theta_{cap}\rangle$ from $\langle\theta_\gamma\rangle$, to account for the possibility that the gamma-ray cascade in the compound nucleus is terminated by particle emission or fission before the ground state of the target nucleus is reached

$$\langle\theta_{cap}\rangle^{J\pi} = \langle\theta_\gamma\rangle^{J\pi} - \langle\theta_{\gamma n}\rangle^{J\pi} - \langle\theta_{\gamma p}\rangle^{J\pi} - \ldots \tag{18}$$

At sufficiently low incident neutron energies, the average capture width is due entirely to s-wave interaction, and it is $\langle\Gamma_\gamma\rangle$ at the neutron separation energy, S_n, that is often used to normalize gamma-ray transmission coefficients. Suppressing spin and parity notation and considering only dipole transitions,

$$\theta_\gamma(S_n) = \frac{2\pi\Gamma_\gamma}{D} = \int_0^{S_n} (T_\gamma^{E1} + T_\gamma^{M1})\rho(S_n-E_\gamma)dE_\gamma . \tag{19}$$

The normalization is accomplished by performing the appropriate integration for each compound spin state produced by s-wave neutron capture, and equating the results to the quotient of the experimental quantities, $\langle\Gamma_\gamma\rangle$ and D_{ob}.

$$\frac{\langle\Gamma_\gamma\rangle}{D_{ob}} = \frac{1}{2\pi} \sum_J \theta_\gamma^J . \tag{20}$$

More often we have knowledge of the gamma-ray strength function, $f_{x\ell}$, for multipole type $x\ell$, rather than the transmission coefficient, T_γ, and then we can rewrite Eq. 19 as

$$\theta_\gamma(E) = \int_0^E [f_{E1}(E_\gamma) + f_{M1}(E_\gamma)]\ E_\gamma^3\ \rho(E-E_\gamma)dE_\gamma. \tag{21}$$

III.B. Sensitivity of Capture Calculations to Model Parameter Variations

We have chosen the reaction $^{89}Y + n$ to illustrate some aspects of statistical model calculations. There are isomers in both ^{89}Y and ^{90}Y. This will test the ability of the STAPRE code to calculate isomer populations, and will also provide a reason for making calculations in which the isomeric state in ^{89}Y is the target state. However, the problem was not specified to yield the most accurate physical results, nor does it necessarily contain our preferred models or parameters; it was designed merely to compare two codes, and was simplified accordingly.

The neutron spherical optical model potential was that of Lagrange [Lag 79]. As with the ^{98}Mo case mentioned above, the level density expression was of the Gilbert-Cameron form [GC 65], with the parameters of Cook et al. [CFM 67] adjusted to agree with discrete level information, some of which appears in Tables V and VI. The Yrast limit, J_{max}, was defined approximately as

$$\hbar^2\ J_{max}^2 \approx 2\ I\ (E-\delta) \geqslant \hbar^2\ J_{min}^2. \tag{22}$$

The moment of inertia, I, is derived from the energy-dependent spin cut-off parameter, $\sigma^2(E)$. Just as $\sigma^2(E)$ is not allowed to decrease below a minimum value, $\sigma^2(E) \geqslant (6/\pi^2)\langle m^2\rangle$, so too we impose a minimum Yrast spin value, J_{min}. Lacking additional information, we usually assume J_{min} is independent of parity and we set it to either 3 or 7/2.

The gamma-ray strength function for ^{90}Y was assumed to have the Lorentz energy dependence of a single-peak GDR, with E_R = 16.69 MeV and Γ_R = 3.31 MeV. The strength was normalized to yield $\langle\Gamma_\gamma\rangle/D_{ob} = 3.659 \times 10^{-5}$ for s-wave neutrons by adjusting the capture calculation to agree with experimental measurements, as shown in Fig. 5. For comparison, an absolute calculation using the energy-dependent Breit-Wigner for the GDR [GGD 80, GG 81] yields a value of $\langle\Gamma_\gamma\rangle/D_{ob} = 4.25 \times 10^{-5}$, which is 16% greater than the value actually used.

The level density parameters give a value for D_{ob} of 5.01 keV at the assumed neutron separation energy of 6.85 MeV. This value depends on the choice made for $\langle m^2\rangle$, the mean spin projection used in the expression for the spin cut-off parameter. The test case used $\langle m^2\rangle = 0.24\ A^{2/3}$, a value favored by Reffo [Ref 78]. The more commonly used value of $\langle m^2\rangle = 0.146\ A^{2/3}$, yields D_{ob} = 2.97 keV, which is closer to the experimental values [MG 73, GP 72]. Since the ratio $\langle\Gamma_\gamma\rangle/D_{ob}$ was normalized to a given value, the actual magnitude of D_{ob} is not critical to the code comparison. However, the choice of $\langle m^2\rangle$ determines the spin cut-off parameter, which, in turn, can affect the calculated results regardless of the normalization. Also, if we wish to compare the partial radiation widths from the calculation with experimental values, then the numerical value of D_{ob} becomes important.

Before proceeding with the parameter sensitivity studies, we show next some calculations made with the COMNUC code, with the target nucleus ^{89}Y in its $1/2^-$ ground state and in its $9/2^+$ isomeric state. In Fig. 6, three kinds

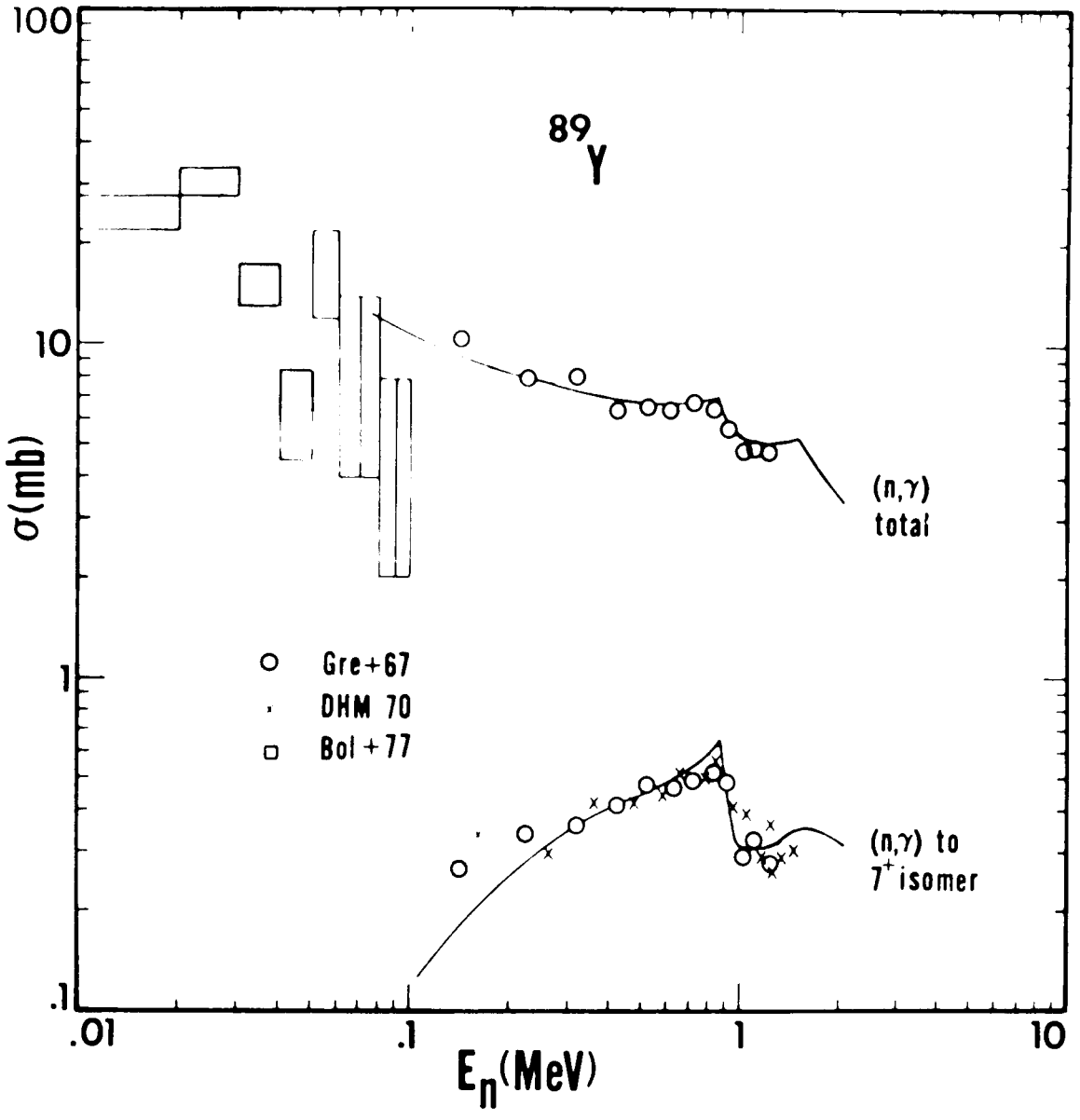

Fig. 5. Comparison of the STAPRE code calculation for the capture reaction $^{89g}Y(n,\gamma)^{m,g90}Y$ with experimental data.

of cross sections, the reaction, the inelastic scattering, and the total capture cross section are compared. The major difference occurs for the inelastic scattering cross section. With the isomeric state as target, scattering to the ground state can always occur with d-wave or higher ℓ-wave neutrons, resulting in a very low-energy effective threshold. The reason that both the capture and the inelastic scattering cross sections from the isomer can be larger than from the ground state is that the compound elastic scattering cross section from the isomer is less.

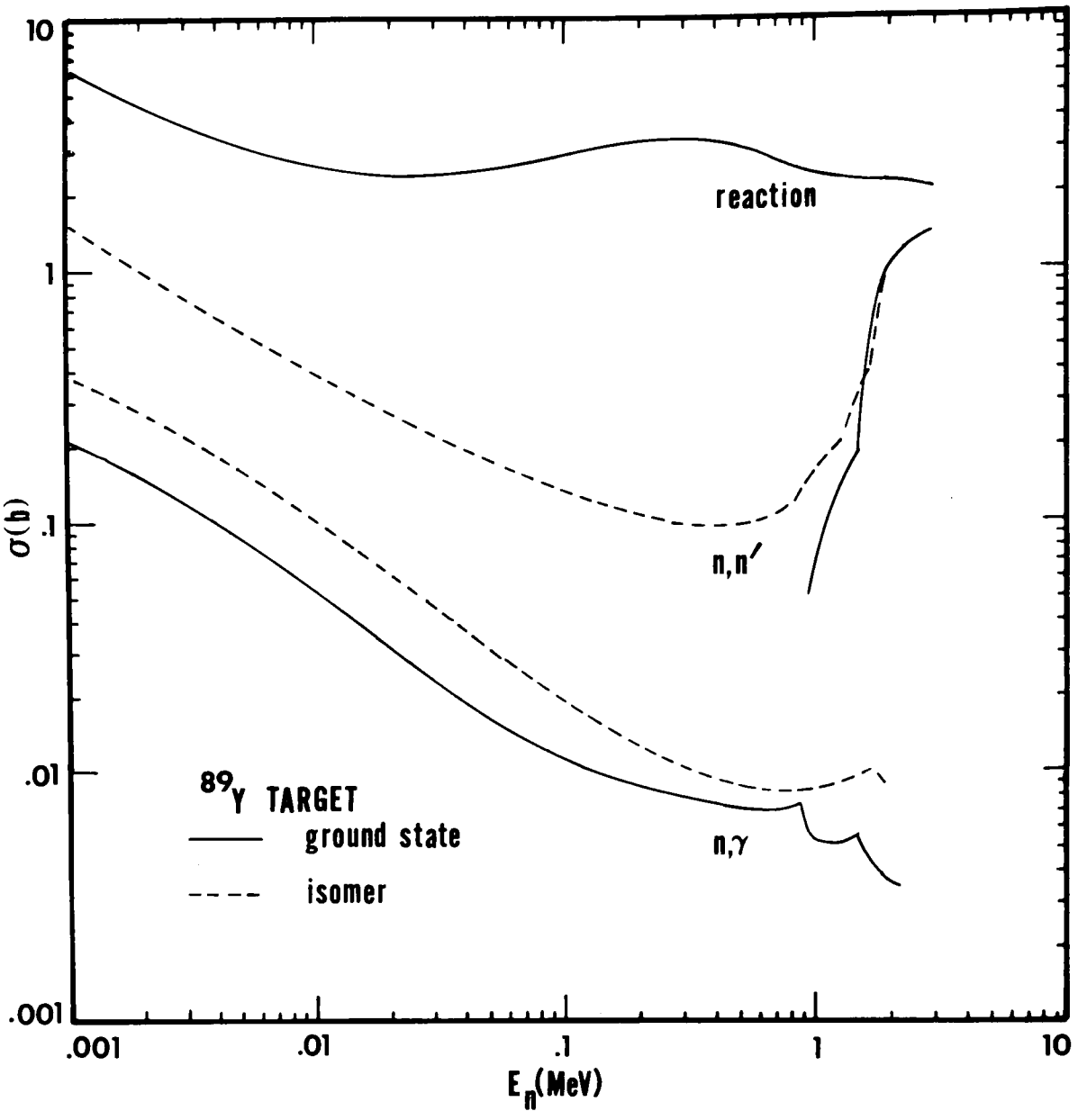

Fig. 6. Some reactions with ^{89}Y target nucleus in its ground state and in its isomeric state.

III.B.1. Width Fluctuation Correction

The correction factor, $S^{J\pi}_{cc'}$, which appears in Eqs. 12 and 17, has been calculated in a number of ways [Mol 61, THW 74, GR 77, Mol 78, Mol 80]. Both of our codes calculate the correction for a single channel by integrating an expression of the form

$$S^{J\pi}_{cc'} = \int_0^\infty dt \left(1 + 2\,\frac{\delta_{cc'}}{\nu_c}\right) \left[f^{J\pi}_c f^{J\pi}_{c'} \prod_{c''} (f^{J\pi}_{c''})^{\nu_{c''}/2}\right]^{-1}, \tag{23}$$

with

$$f_c^{J\pi} = 1 + 2t \langle\theta_c\rangle^{J\pi}/(\nu_c\langle\theta\rangle^{J\pi}) \ . \tag{24}$$

There are two questions here concerned with the number of degrees of freedom, ν_c, which describes the distribution of the partial widths. For a single channel in the weak absorption limit [Mol 64], ν_c should be about unity, while in the strong absorption limit [KKM 73], $\nu_c \approx 2$. The first question is, what is the behavior of ν_c between these limits? Tepel and coworkers [THW 74] suggest

$$\nu_c = 1 + \sqrt{\theta_c} \ ,$$

or in terms of transmission coefficients

$$\nu_c = 1 + \sqrt{T_c} \ . \tag{25}$$

Recently, Moldauer [Mol 80] suggested a form for ν_c which is a function of both T_c and the sum $\Sigma T_{c'}$ for all competing channels

$$\nu_c \ (T_c, \ \Sigma T_{c'}) = 1.78 + (T_c^{1.212} - 0.78)\exp(-0.228 \ \Sigma T_{c'}) \ . \tag{26}$$

In the strong absorption limit this also predicts $\nu_c \approx 2$. For most situations of interest here, where inelastic scattering competes effectively with neutron capture, the functional form for ν_c affects mainly the competition between compound elastic and inelastic scattering. The effect on the capture cross section is very small indeed, and so the expression given by Eq. 25 is quite adequate.

The second question is -- to what extent may individual channels be summed to form a "group", with a corresponding "group" degree of freedom? This concept is discussed by Gruppelaar and Reffo [GR 77], and was incorporated over a decade ago by Dunford, for example, in his COMNUC code. Dunford takes the extreme position of considering only compound elastic and inelastic neutron scattering to the discrete target levels as individual channels. All particle emission to a continuum of levels, such as expressed in Eq. 15, are considered one single group. For proton or alpha-particle emission, even the discrete level transitions are lumped together with the transitions to the continuum, and not considered separately. The same is true with discrete fission channels and continuum fission. For such groups, the group degree of freedom is given by

$$\nu_{group} = 2 \sum_c \langle\theta_c\rangle^{J\pi} > 1 \ . \tag{27}$$

The COMNUC code uses a Gaussian quadrature integration technique, which has been shown [Bee 73] to be accurate and efficient for the type of integral given in Eq. 23. As you well may imagine, the width fluctuation correction calculation requires very little computation time in COMNUC.

The STAPRE code, on the other hand, divides the energy range of the problem into equal size energy bins, and uses the trapezoidal integration method. Each $J\pi$ state in each continuum energy bin is treated separately, along with the discrete levels reached by particle emission from the first

compound nucleus. For the continuum bins, the single channel ν_c values are multiplied by the number of levels in the bin at energy E

$$\nu_{group} = \nu_c \rho(E,J,\pi)\Delta E. \tag{28}$$

The integral in Eq. 23 is evaluated at least twice, the second time by doubling the number of mesh points. This doubling is repeated until the answer remains constant to within a prescribed accuracy (such as 1%) or until the number of grid points reaches a set limit. If convergence was not obtained, an error message is printed.

In both codes, the width fluctuation correction is calculated separately for each $J\pi$ state in the compound nucleus. When the number of open channels available to each $J\pi$ compound state exceeds some limit, all of the correction factors for that state can be set to unity. In our experience, that limit should be in the range 100-200 before the correction becomes negligible.

In general, we have found that the width fluctuation correction calculation in STAPRE requires a great deal more computer time than it does in COMNUC, perhaps by as much as an order of magnitude. When there are no convergence problems in STAPRE, the cross sections calculated by the two codes agree to within a few percent. No convergence problems were encountered with the test problem as defined above, but we will show later that such problems appeared when the number of discrete levels were reduced to just the ground state in the nuclei $^{89,90}Y$.

The effect of the width fluctuation correction is shown in Fig. 7 for the compound elastic and inelastic scattering cross sections for ^{89}Y, and in Fig. 8 for the capture cross section. In the latter case there is virtually no difference in the results when $\nu_c = 1 + \sqrt{T_c}$ or just $\nu_c = 1$. Because the correction is different for each compound $J\pi$ state, it can affect isomer ratio calculations. In our test case, omitting the correction entirely had a 10% maximum effect on the calculated m/g ratio in ^{90}Y; at most energies the effect was much less than 10%.

III.B.2. Neutron Transmission Coefficients

Current statistical model codes use transmission coefficients which are specified either as functions of orbital angular momentum, T_ℓ, as does STAPRE, or of channel spin, T_j, as does COMNUC. The use of T_j values is correct, while the use of T_ℓ values is an approximation which can affect the calculated capture cross sections in the energy range of interest here. The source of the error is mainly the different spin distributions that the two types of transmission coefficients produce in the first compound nucleus.

There are two ways by which T_ℓ values may be obtained from an optical model program. The poorer of the two methods is merely to set the spin-orbit term in the potential to zero. The compound nucleus formation cross section produced by such T_ℓ values may differ from the correct value by an amount that varies with energy. In our case, the difference may be 4% or more, as is shown in Fig. 9.

The better way to average the T_j values is given in Eq. 29 for spin 1/2 particles

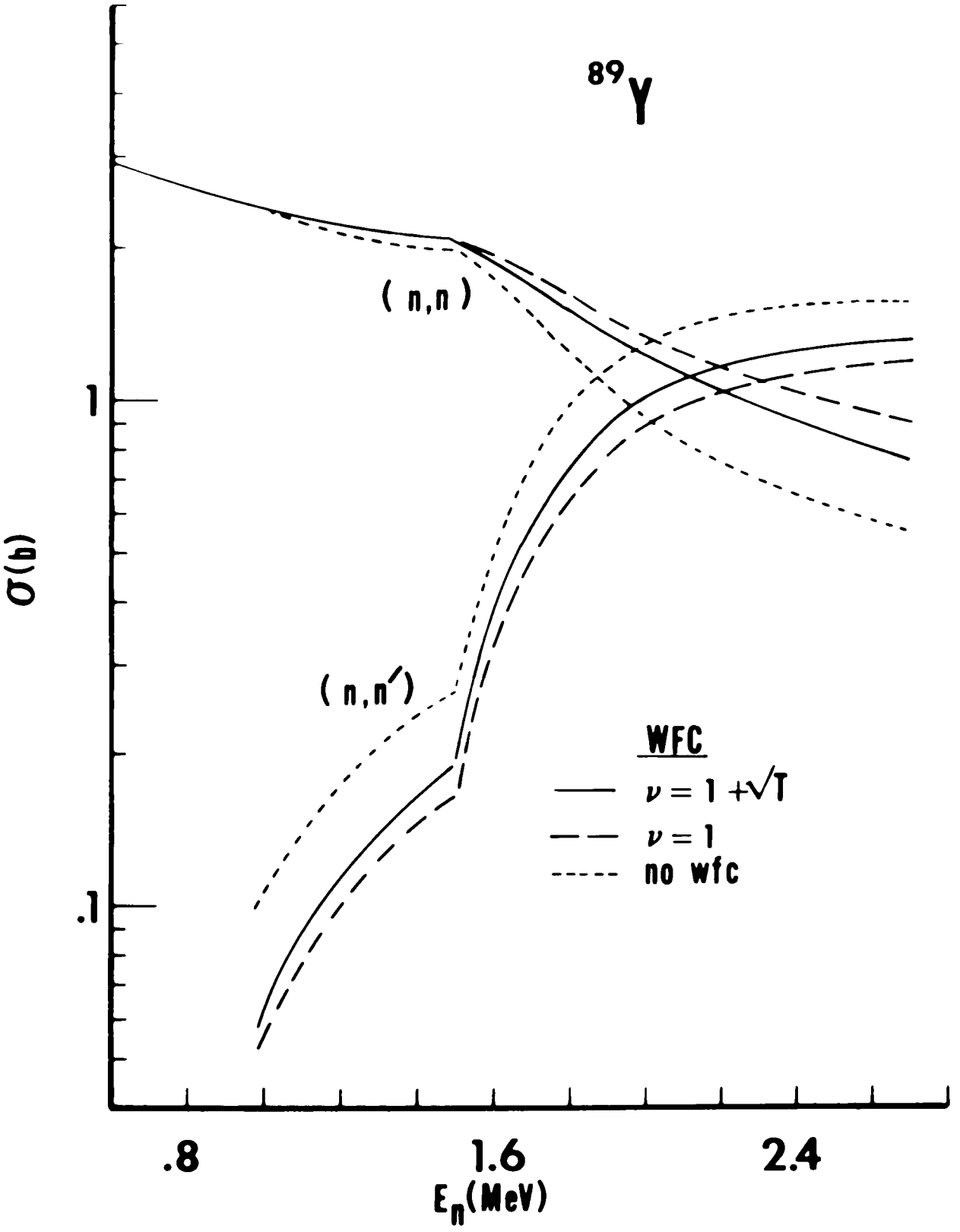

Fig. 7. Effect of the width fluctuation correction on the compound elastic and inelastic scattering cross sections for $^{89}Y + n$.

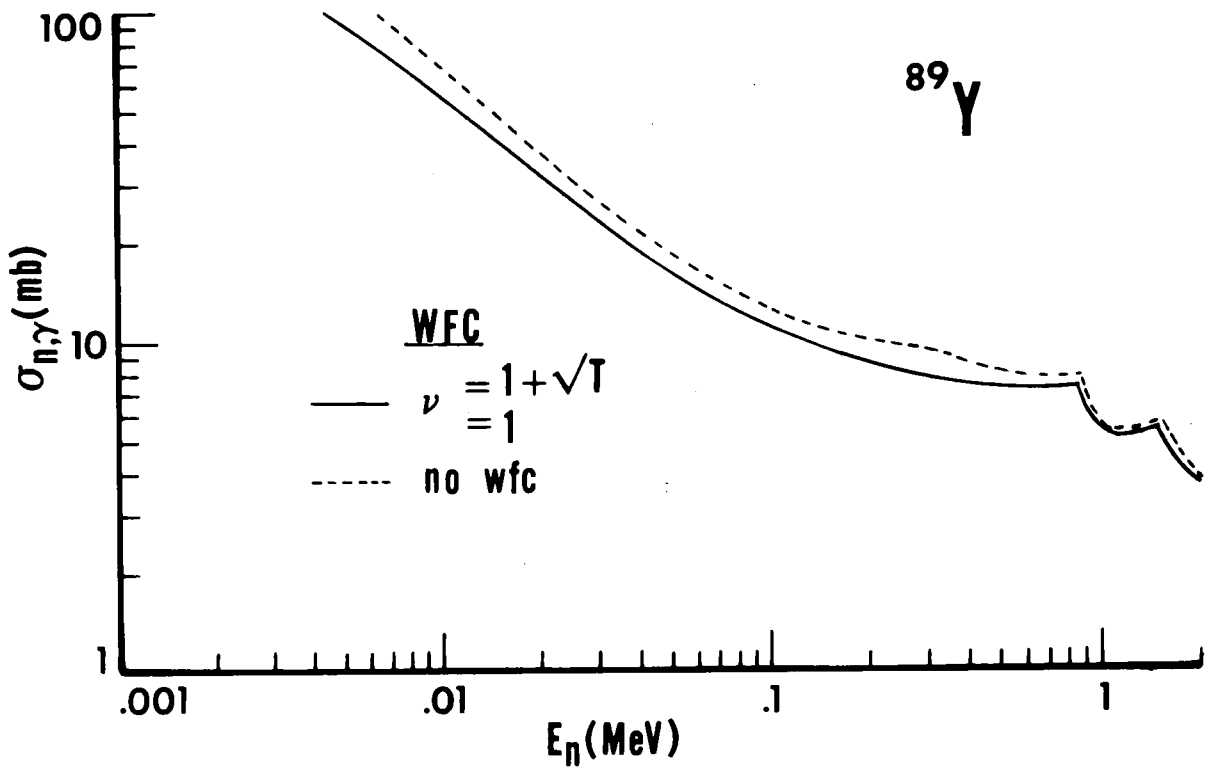

Fig. 8. Effect of the width fluctuation correction on the $^{89g}Y(n,\gamma)$ reaction.

$$T_\ell = [(\ell+1)T_{j=\ell+1/2} + (\ell)T_{j=\ell-1/2}]/(2\ell+1). \tag{29}$$

However, the spin distribution produced by even these T_ℓ values will not be the same as that produced by the original T_j values. An example is given in Fig. 10, for a 1-MeV neutron incident on ^{89}Y. Two curves are plotted, one for each parity state. Each is the ratio of the population of a given compound spin state calculated from T_j values divided by the population from T_ℓ values. For spin state 4^+ in ^{90}Y, the ratio exceeds 1.45. This sort of effect becomes even more pronounced at lower energies, and diminishes at higher energies. With 2.1 MeV neutrons, the ratio for the 4^+ state is still 1.25, and a considerably higher incident energy is required before the effect disappears.

There are two principal ways in which these spin distribution differences can affect the calculated capture cross sections (although second-order effects can enter in other ways, such as through the width fluctuation correction). First, the inelastic scattering competition back to the discrete target levels is quite sensitive to the spin distribution as well as to the spins and parities of the discrete levels. Changes in the inelastic scattering can affect, in turn, the capture cross section. Second, in the case where neutron capture leads to the population of isomers, the calculated isomer ratio will depend directly on the compound nucleus spin distribution. For the ^{89}Y test case, as specified above, the spin distribution effect

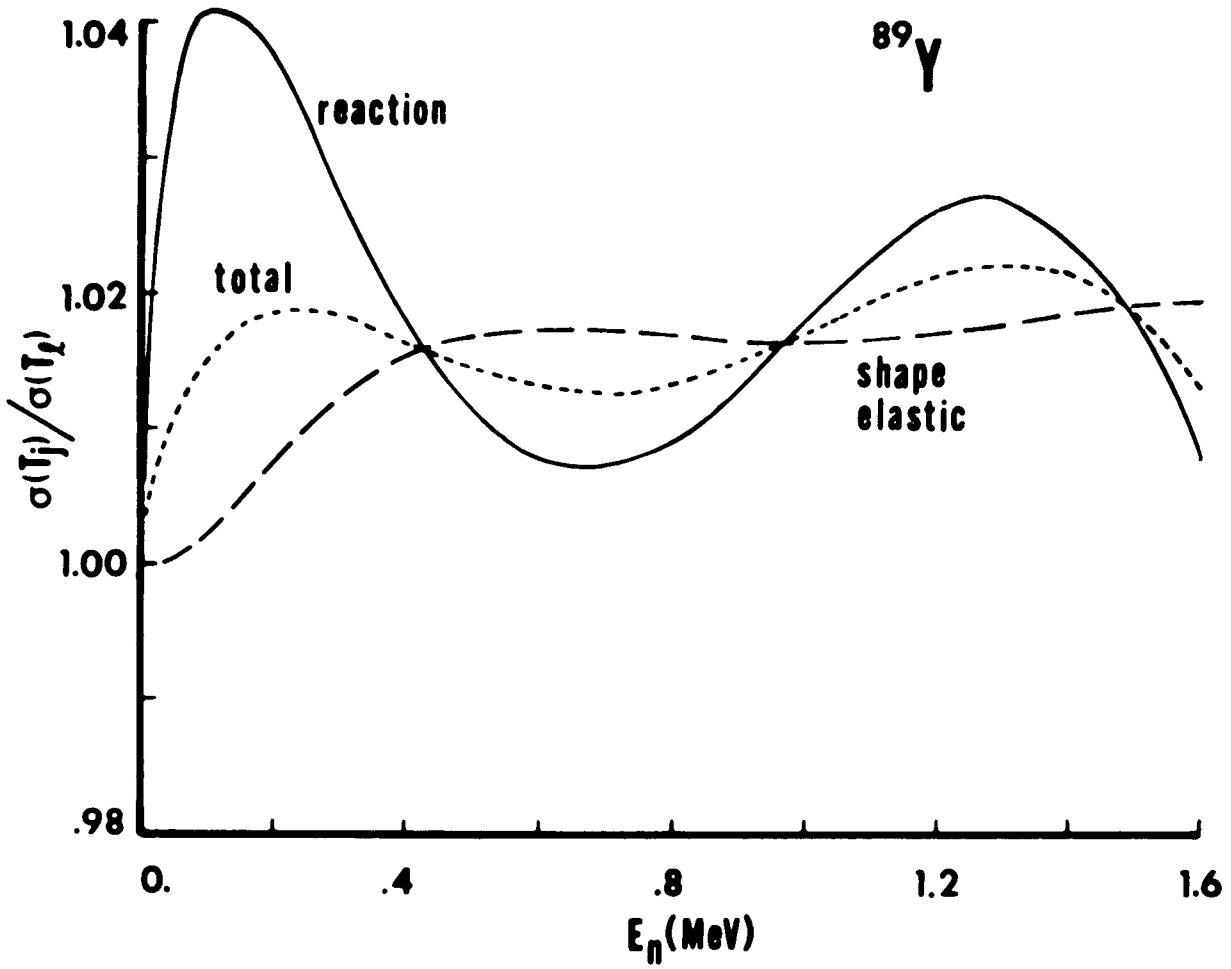

Fig. 9. The effect on the total, shape elastic, and reaction cross sections produced by setting the spin-orbit term to zero in the Lagrange neutron optical potential.

modified the total capture cross section by no more than 5%, but the isomer ratio in ^{90}Y changed by as much as 20%. The inelastic cross section was modified by 11% near threshold, but this dropped to 6% at 0.5 MeV above threshold and disappeared altogether after about 1 MeV above threshold.

One final comment concerning the accuracy of the neutron transmission coefficients is that the required accuracy is less at lower energies, below the inelastic scattering threshold, than at higher energies. From Eq. 17 it may be seen that when the compound elastic width is large compared with the radiation width, the capture cross section is determined essentially by $2\pi\langle\Gamma_\gamma\rangle/D$. As long as the width fluctuation correction is important, the capture cross section does not scale linearly with the compound nucleus formation cross section. Different sets of neutron transmission coefficients that produce compound nucleus formation cross sections that differ by factors of 2 or 3 for neutrons in the keV region may well produce capture cross sections that differ by only 10 or 20%. At higher energies accurate transmission coefficients are needed not only to compute the proper total reaction cross section, but also to obtain the correct inelastic scattering competition.

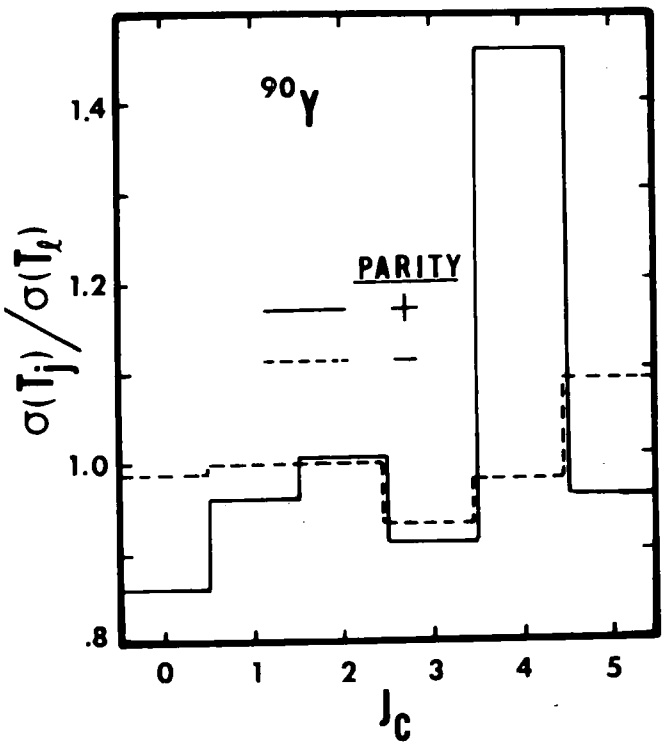

Fig. 10. Ratio of the populations of compound spin states produced by T_j and T_ℓ neutron transmission coefficients, for incident neutron energy of 1 MeV.

III.B.3. Nuclear Level Densities

This field is too vast to be summarized in a short report, and so we will limit our comments to the effects produced by only two features of level density formulations -- the spin cut-off parameter and the Yrast limit.

In our calculations we generally use the Gilbert-Cameron level density formulation, in which a constant temperature expression at low energies is smoothly joined to a Fermi gas expression at higher energies. The spin cut-off parameter appears in the spin distribution function

$$\rho(J,E) = \frac{(2J+1)}{\sigma^3\sqrt{8\pi}} \exp[-(J+1/2)^2/2\sigma^2] \ , \tag{30}$$

where $\sigma \equiv \sigma(E)$, and

$$\sigma^2(E) = \frac{6}{\pi^2} \langle m^2 \rangle \ [a(E-\delta)]^{1/2} \ . \tag{31}$$

We have already mentioned that we do not let $\sigma^2(E)$ fall below the value $(6/\pi^2)\langle m^2\rangle$, and have given two common estimates for the mean square spin projection, $\langle m^2\rangle$. One may also estimate σ^2 from the low-lying discrete levels, if there are enough of them

$$\sigma^2 = (1/2N) \sum_{i=1}^{N} (J_i+1/2)^2 \quad . \tag{32}$$

In the case of ^{89}Y and ^{90}Y, there are too many low-lying, high-spin levels to make this approach useful, and so the arbitrary choice was made that $\langle m^2 \rangle = 0.24\ A^{2/3}$. Calculations with our test case spanned the incident neutron energy range of 1 keV-3 MeV, and so continuum level densities appeared only in ^{90}Y. Since we have normalized the calculations with a value for $\langle \Gamma_\gamma \rangle / D_{ob}$, the capture calculations for the ground state of ^{89}Y are insensitive to the choice of $\langle m^2 \rangle$. When the high-spin isomer of ^{89}Y is the target state, the effect of different choices for $\langle m^2 \rangle$ can produce variations of up to 50% in the capture cross section, as is shown in Fig. 11. The same size effects are also observed in the isomer ratios calculated for ^{90}Y, which are displayed in Fig. 12.

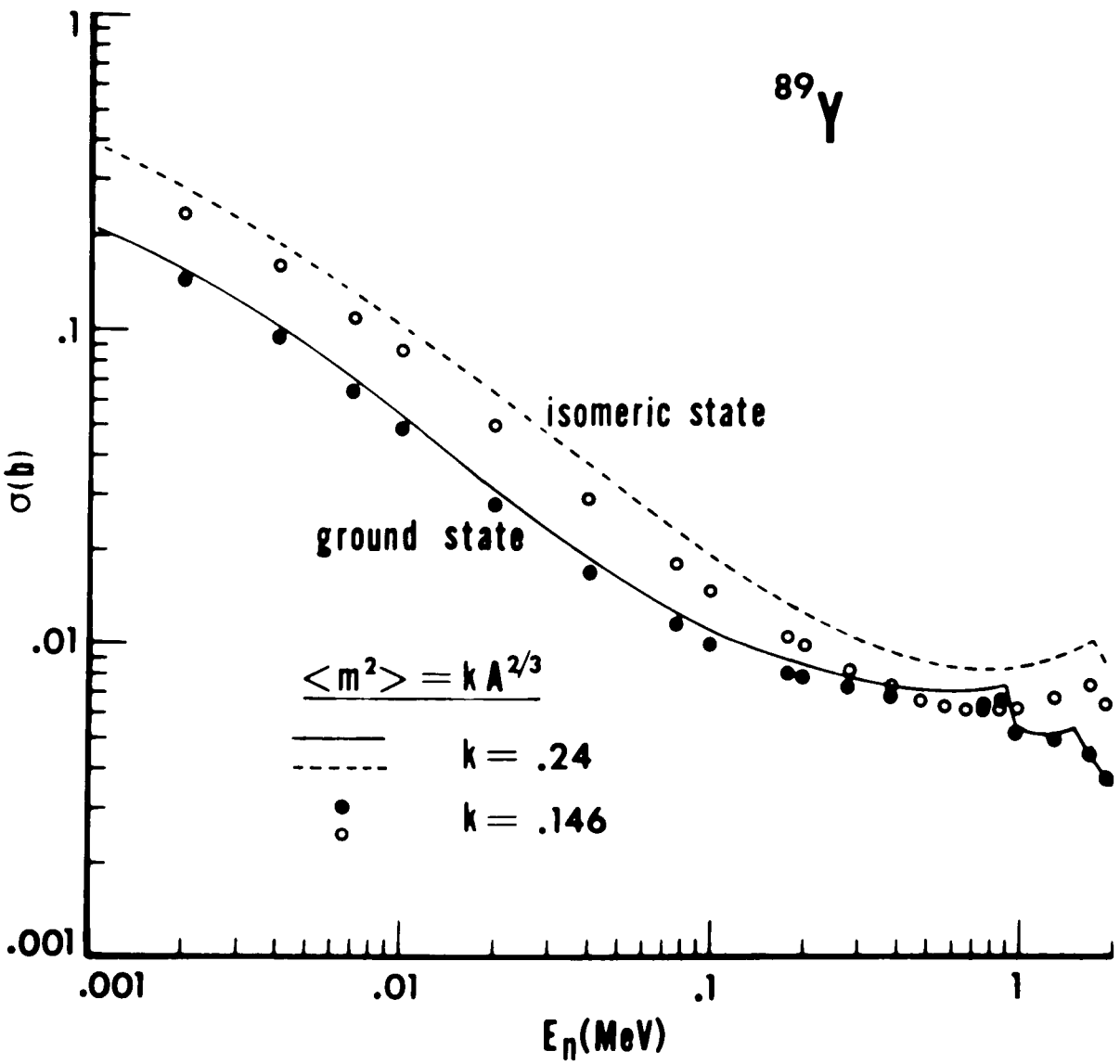

Fig. 11. Effect produced by different spin cut-off parameter values on total capture cross sections.

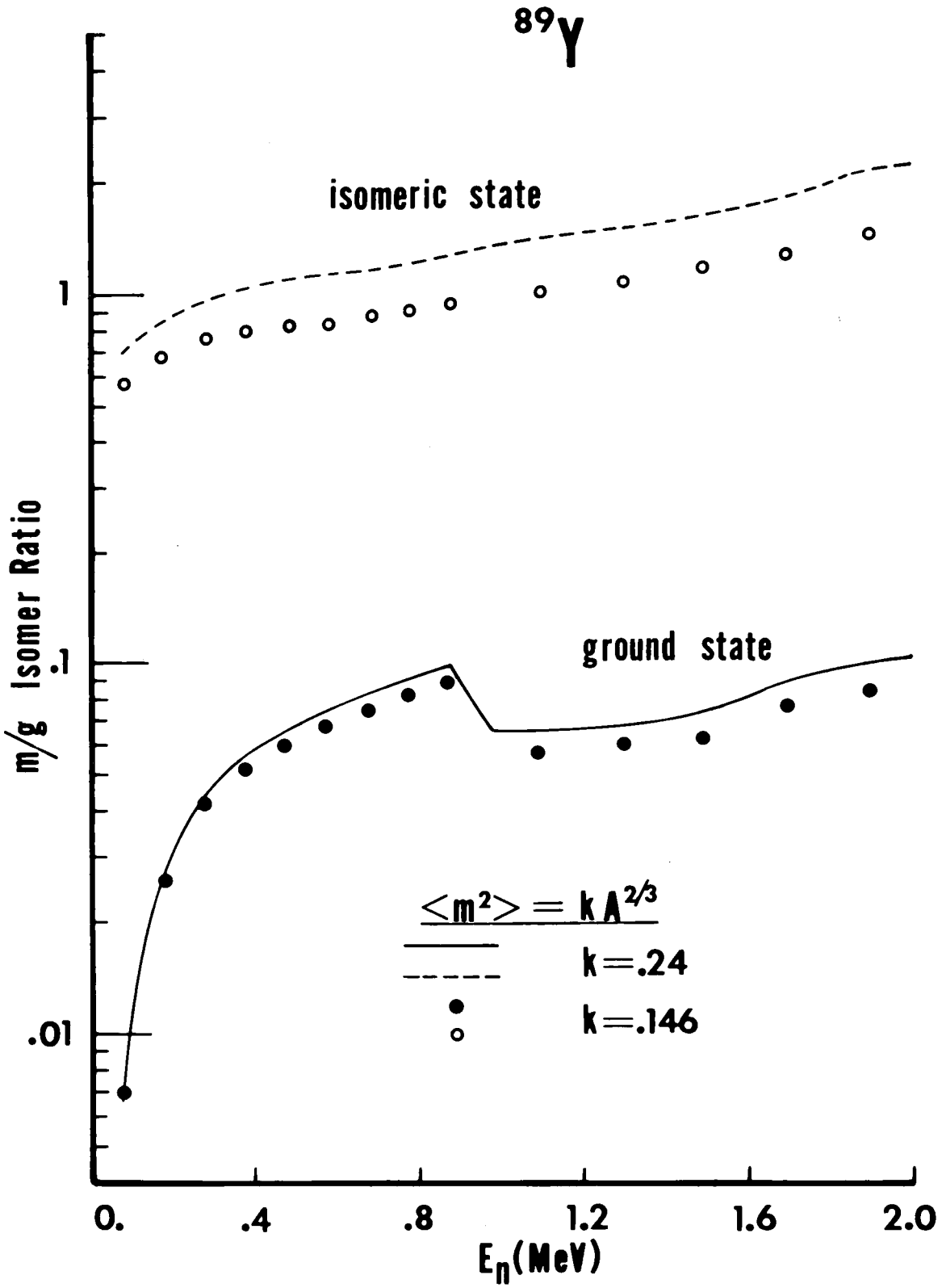

Fig. 12. Effect produced by different spin cut-off parameter values on the m/g ratio in ^{90}Y.

It might appear surprising that the Yrast limit would be of concern in low-energy neutron capture calculations. It can be when the pairing gap in the target nucleus is large and the discrete level information is scant. The usual Yrast models are statistial descriptions that lose their meaning at lower energies, particularly in the neighborhood of the pairing gap. If a continuum is used to represent the levels below the pairing energy, δ, some minimum number of levels must be allowed to exist, as we have indicated in Eq. 22. If not, the inelastic scattering competition to the capture process will be underestimated. The ^{89}Y test case does not show this effect because the maximum incident neutron energy used here, 3 MeV, still lies among the discrete target levels. Therefore, to illustrate the Yrast effect we have modified the test case so that only the ground states in $^{89,90}Y$ are specified, with the continuum beginning immediately above. Two calculations were made -- one in which $J_{min} = 1/2$ and the other in which $J_{min} = 7/2$ in the target nucleus. The apparent enhancement in the capture cross section for ^{89}Y in its ground state is shown in Fig. 13, and amounts to a 100% effect in the MeV region. Increasing J_{min} beyond 7/2 did not change the results appreciably. Tables such as the one by Gough [Gou 72] are useful for guidance in choosing J_{min}, or one might wish to be internally consistent and estimate J_{min} from the minimum spin cut-off value. In our case, this would be

$$J^2_{min} = \frac{18}{\pi^2} \sigma^2_{min} \quad . \tag{33}$$

III.B.4. Discrete Nuclear Levels

We believe that there is no adequate way to represent the first 10 or 20 levels in a typical nucleus with any level density expression. They are vital in providing the correct inelastic competition to the neutron capture process. Figure 14 shows the effect produced by representing all of the levels in $^{89,90}Y$ above the ground states by level density expressions. Two effects should be noted. First, even for incident neutron energies in the keV region, the capture cross section without the discrete excited states is less than that calculated with 25 levels in ^{90}Y. This is not due to inelastic scattering competition, but to the calculated partial radiation widths being all about the same in magnitude. In Table VII we see that with 25 levels in ^{90}Y, the p-wave width (and the f-wave width) is about twice as large as the s-wave width, thus producing a large capture cross section. The partial wave contributions to the total capture cross section of ^{89}Y, and to the production of the 7^+ isomer of ^{90}Y, are displayed in Fig. 15.

The second effect appears around 30-40 keV incident energy, when the inelastic scattering to the continuum representing the target levels begins to be important. Actually, the first inelastic level occurs around 0.9 MeV, and no (n,n') reaction can occur until then. However, with the continuum extending down to the ground state, the (n,n') cross section is calculated to be almost 400 mb at 0.9 MeV. As the figure shows, this has a profound effect on the capture cross section.

One additional comment should be made concerning discrete nuclear levels, even though it does not pertain to the ^{89}Y test case. In the deformed mass regions, where rotational bands are built on low-lying single-particle levels such as the ground state and any isomeric states, it is important that all

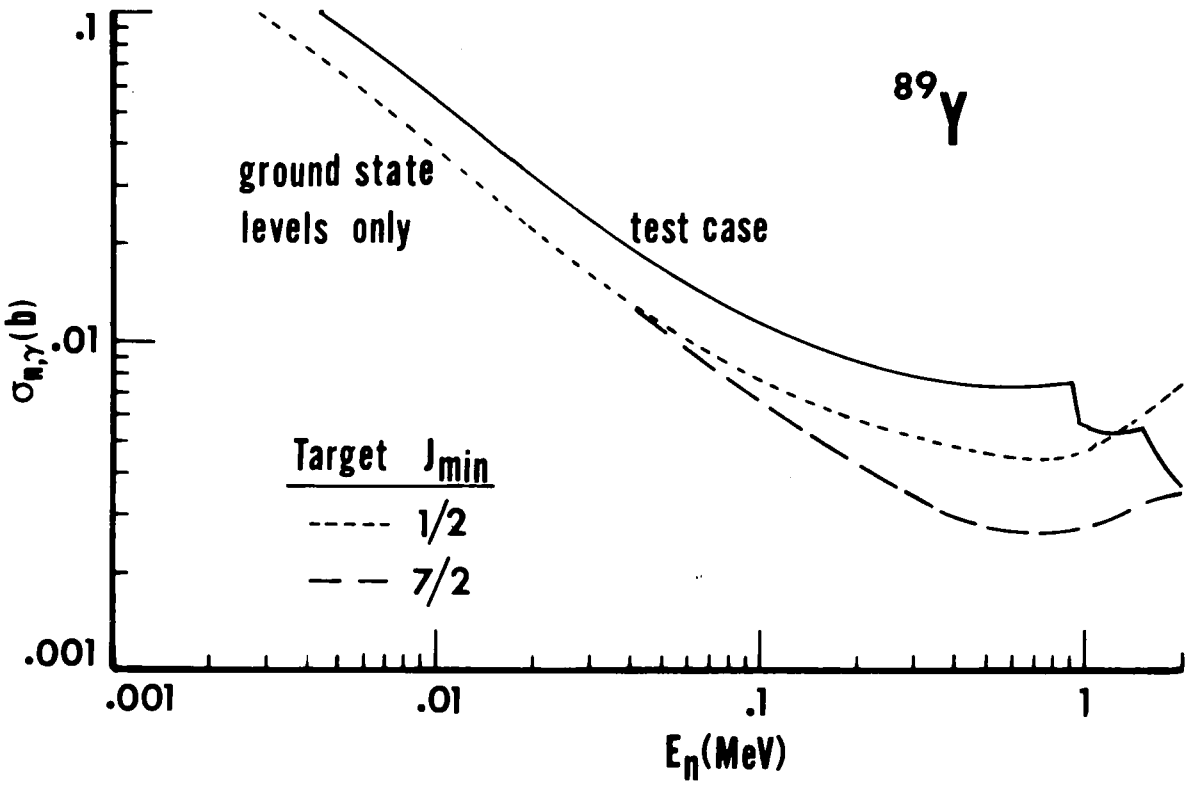

Fig. 13. Effect produced on the $^{89}Y(n,\gamma)$ reaction by reducing J_{min} in the target nucleus from 7/2 to 1/2. Only ground states were specified.

bands are extended up to a high enough spin so that each band fairly samples the spin distribution in the compound nucleus. Among these discrete levels the gamma-ray cascades proceed down each band, with interband crossings occurring mainly near the band heads. Therefore, if one wishes to calculate isomer populations accurately, care must be taken to insure that some particular band that happens to begin with a high-spin member does not receive an unfairly large portion of the capture cross section merely because the high-spin continuum states could not decay to the other bands [Gar 80].

But there is a dilemma here. While it may be possible to locate and characterize the first 5 or even 10 or more bands, and to estimate the position of their high-spin members, rather quickly one will overlook and omit other single-particle levels and their band members. As the lower bands are extended up in energy, the missing levels will begin to constitute the major fraction of the total number of true levels. The extension of the lower bands is required if the isomer ratios are to be calculated correctly, but the missing levels will distort the absolute magnitudes of the isomer populations. If the missing levels are in the daughter nucleus produced by neutron capture, the distortion may not be too large because of the size of the neutron separation energy and the very large number of levels in the continuum above the discrete levels. However, if the missing levels are in the target nucleus, and it is desired to calculate an isomer population following inelastic scattering, then the distortion may be very serious indeed. The missing target

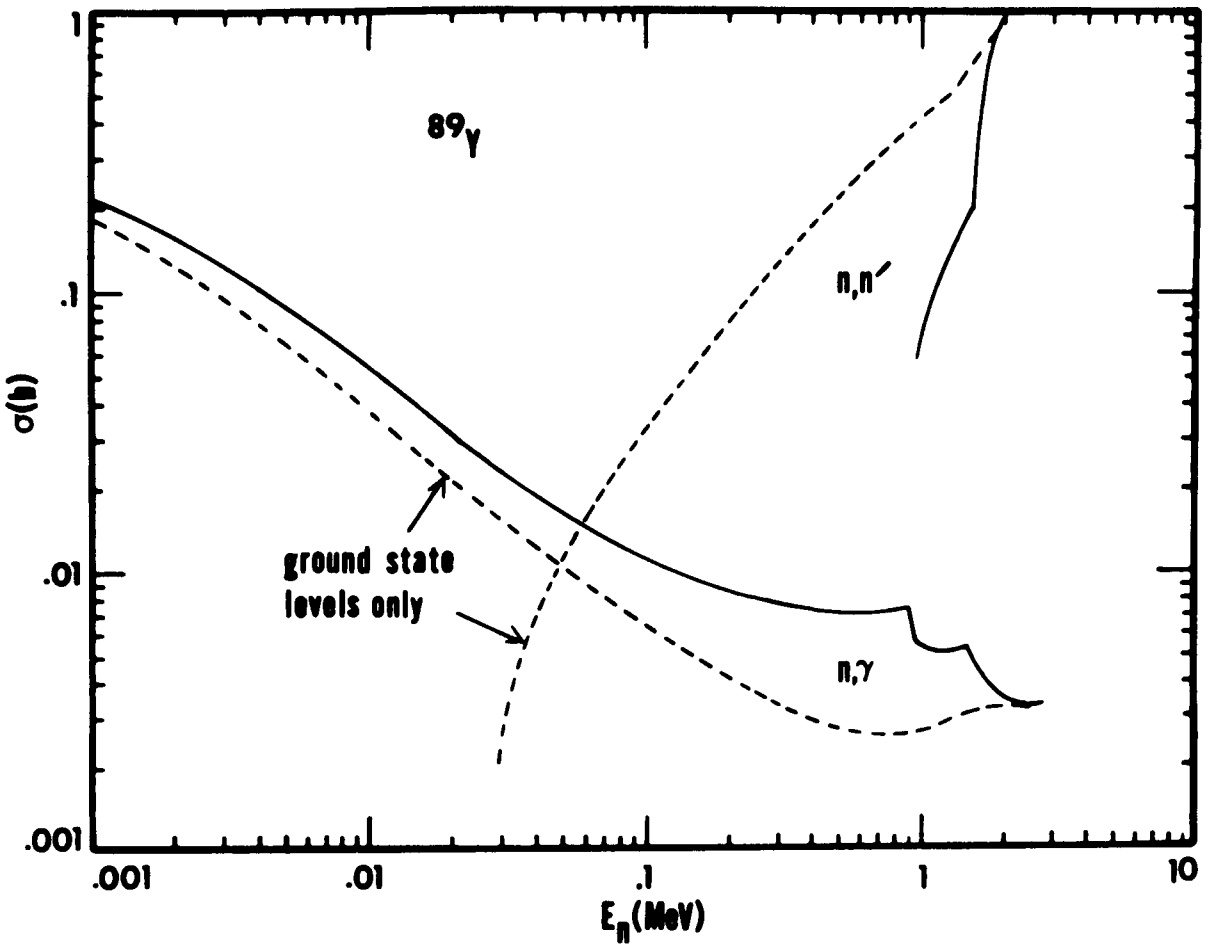

Fig. 14. The effect on the capture and inelastic scattering cross sections of ^{89}Y when only the ground states are specified in $^{89,90}Y$.

levels could cause a serious underestimation of the inelastic scattering cross section. We have found no universal solution to this problem, and we usually have to make a number of calculations with ad hoc modifications of the discrete levels in the hope of finding a compromise.

III.C. Some COMNUC-STAPRE Code Comparison Results

There are various ways in which a comparison between two computer codes may be made. We have chosen to try to construct a test case that could be run equivalently on the two codes, and then to compare as many intermediate and final results as possible to see how well the codes reproduced each other at the percent level. Another approach is to admit that there are model differences between the two codes, and to run similar (if not equivalent) problems to see by just how much the results differ. The problem, then, is to try to interpret the differences that are certain to occur, particularly if they arise from multiple (and perhaps unknown) sources. Other than determining if one or the other code contains some large error, it is difficult to see value of the latter approach.

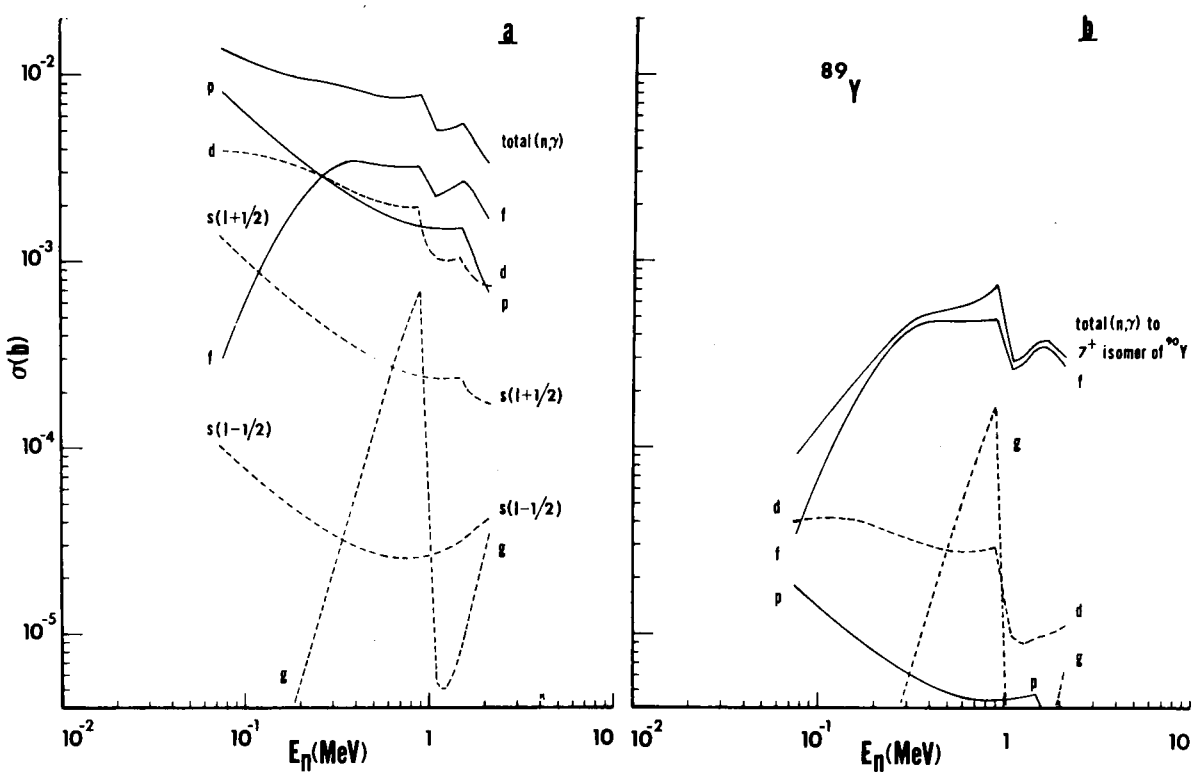

Fig. 15. Partial wave contributions to a) the total capture cross section of ^{89}Y, and to b) the production of the 7^+ isomer of ^{90}Y.

The ^{89}Y + n test case used here was formulated to compare two specific codes -- COMNUC and STAPRE. The level energies and the neutron separation energies were rounded to 50 keV because STAPRE bins all energies and 50 keV was the bin size used in our calculations. Only E1 gamma-ray transitions were allowed, because of a variety of problems in the gamma-ray subroutine in COMNUC. It turned out that we couldn't even use equal strengths for E1 and M1 transitions because of these problems. The test case was normalized to a given value for $\langle\Gamma_\gamma\rangle/D_{ob}$, again because of the inflexibility of the COMNUC code.

We have shown the sensitivity of some of the calculations to variations in the width fluctuation model, and to changes in the specifications of the spin cut-off parameter and Yrast limit. If one code used the Gilbert-Cameron level density formulation while the other used, say, the back-shifted Fermi gas model, one would undoubtedly observe differences in the magnitude and energy dependence of the results. If one code used the Brink-Axel energy dependence for E1 gamma-ray transitions while the other code used the Weisskopf single-particle energy dependence, there again would be differences in the results, particularly for the capture cross section in the MeV region.

We have attempted to use the same physics models where possible, but certain features will remain different. The use of T_j vs T_ℓ neutron transmission coefficients is an example. Once the spin distributions produced by each were examined, it was possible to explain the observed difference in the

calculated inelastic scattering cross sections. If the COMNUC and STAPRE codes used transmission coefficients obtained from different optical model programs, different results might be observed. We have observed differences due to various choices of integration step size and matching radius, and at least one optical model code in use has unity for the mass of the neutron. Our two codes use different methods for correcting the (n,γ) cross sections for reactions such as (n,γn') which do not lead to capture. In order to do this properly, the COMNUC code requires input from a separate code called CASCADE. With this input, however, the COMNUC results match those from STAPRE, as we can see from Fig. 16.

A more exact comparison of the two codes appears in the next two tables. In Table VIII, we list the ratio of the results from COMNUC to that from STAPRE for the following cross sections on the ground state of ^{89}Y: reaction (or compound nucleus formation), compound elastic, inelastic and total capture. Recalling that the STAPRE calculation used a bin size of 50 keV, it is impressive how well the two codes agree at low energies. We have also compared the values calculated by the two codes for the quantity $2\pi\langle\Gamma_\gamma\rangle/D$ in the compound nucleus ^{90}Y. Results for two incident neutron energies are given in Table IX; again the agreement is excellent. We have previously reported a COMNUC-STAPRE code comparison for the reaction ^{90}Zr + n, with neutrons up to 20 MeV in energy [Gar 80]. In that work no precompound particle emission was allowed, but a wide variety of reactions were compared: total, reaction, compound elastic, inelastic, capture, (n,2n), (n,3n), (n,p), (n,np), (n,pn), (n,α), (n,nα), (n,αn). In all cases the results agreed to better than 5-10%. By such comparisons we are convinced that the LLNL versions of the COMNUC and STAPRE codes are operating as their authors had planned.

An interesting situation occurred during the code comparison when only the ground states in ^{89,90}Y were specified, and all excited states were represented by a continuum level density expression. Very large differences were observed in both the capture and the inelastic scattering cross sections. Without the width fluctuation correction, the (n,n') reaction at 0.076 MeV produced cross sections that differed by a factor of 6, while with the WF correction the same cross sections differed by a factor of 12! The STAPRE code always experienced convergence problems calculating the WF correction when only the ground state was specified in each nucleus. This accounts for some of the discrepancy, but not for all of it. Eventually, the problem was traced to the fact that the STAPRE code begins the continuum one bin above the last specified discrete level. When the continuum was set in COMNUC at 50 keV above the ground state, the calculations without the WF correction again agreed to a few percent. However, with the WF correction, the capture cross sections differed by up to 25%, and the (n,n') cross sections varied by up to a factor of 2.

A limited study was carried out with the STAPRE code on the effect produced by changing the energy bin size. With a larger bin size, the computer storage size and run times are reduced. Limitations arise with large bin sizes, because reaction thresholds and discrete level energies are affected. We have tried the test problem with bins up to 250 keV in size, and the effect on the capture cross sections was generally less than 10%. When the test problem was run with only ground states, the apparent threshold for the (n,n') reaction seemed to depend on the bin size. For energy bins of 50 and 150 keV, one result was obtained, while bins of 200 and 350 keV produced a different

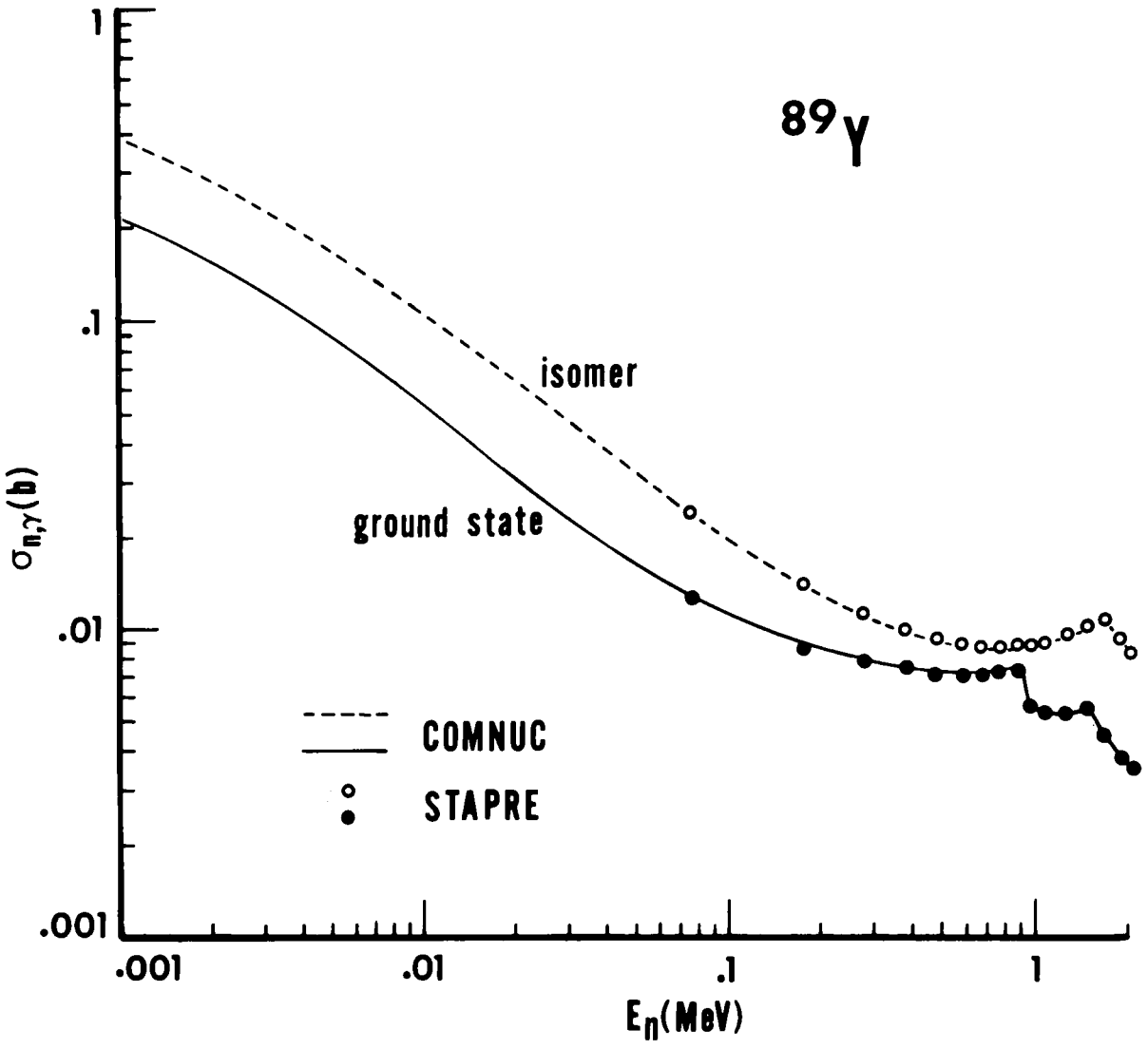

Fig. 16. Comparison of the neutron capture cross sections for the ground and isomeric states of ^{89}Y, as calculated by the COMNUC and STAPRE codes.

result. This is shown in Fig. 17. The corresponding capture cross sections also fell on two curves which joined together fairly well around E_n = 1 MeV. Further work will have to be done to understand this behavior.

IV. Gamma-Ray Strength Functions

As we have mentioned above, the most important quantity required for a low-energy neutron capture calculation is the ratio Γ_γ/D and its energy dependence. Usually $\langle\Gamma_\gamma\rangle/D_{ob}$ is evaluated at the neutron separation energy for s-wave neutrons, and is then used to normalize the gamma-ray transmission coefficients, as indicated in Eq. 19.

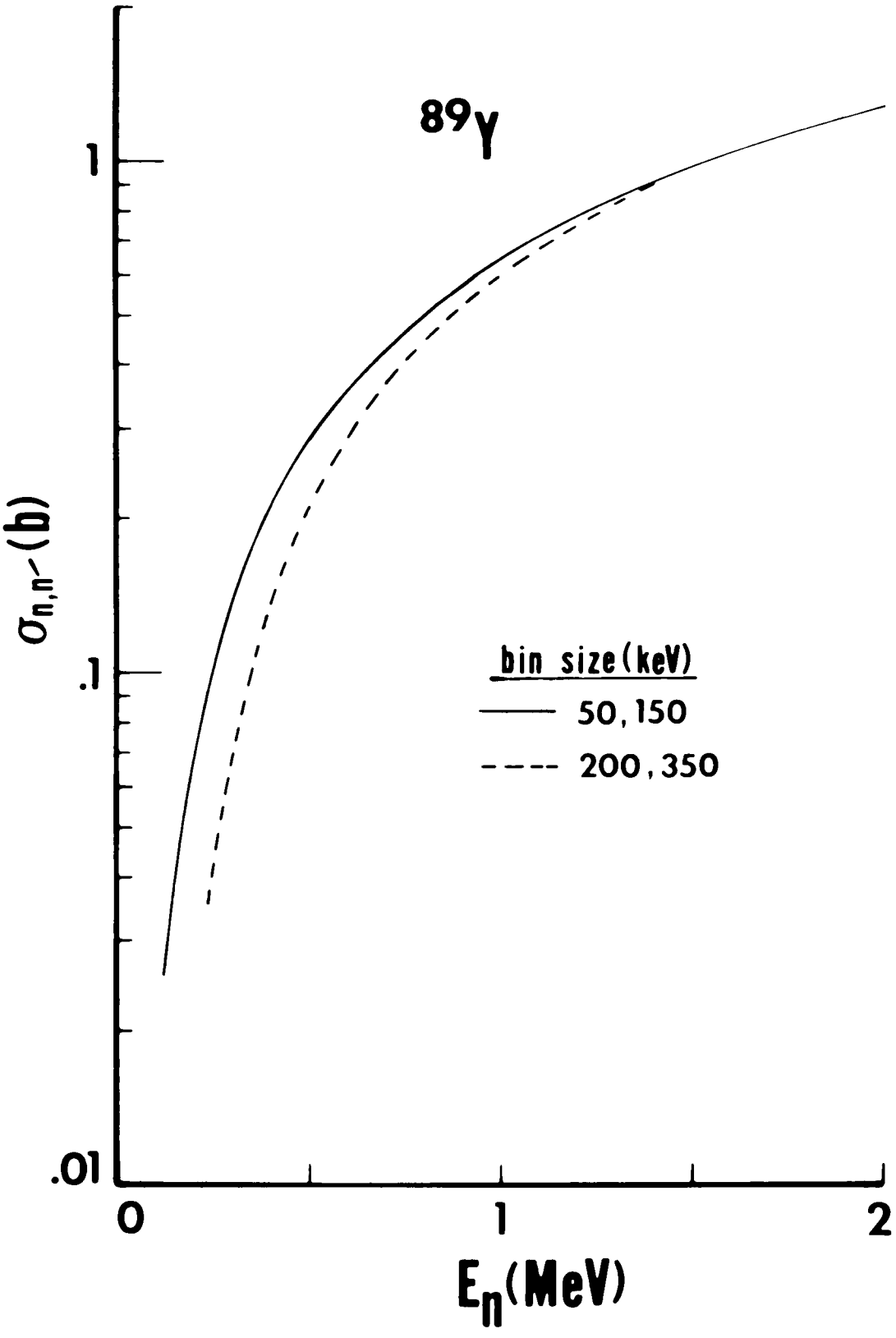

Fig. 17. The effect of bin size in the STAPRE code on the calculated (n,n') cross section.

Over the years, there have been many attempts to develop systematics for $\langle\Gamma_\gamma\rangle$. In 1951, Heidmann and Bethe [HB 51] suggested the form

$$\langle\Gamma_\gamma\rangle = C_1 \; A^{-C_2} \; (\mathrm{eV}), \tag{34}$$

with estimates for the constants of $C_1 = 5 \times 10^3$ and $C_2 = 2.3$. Almost 30 years later, comparison with recent compilations shows that Eq. 34 is not a bad estimate, except for light nuclei and nuclei near doubly closed shells. Until a few years ago, we used a recipe by Stolovy and Harvey [SH 57]

$$\langle\Gamma_\gamma\rangle = K \; A^{2/3} \; (S_n-\delta)^\alpha \; [D(S_n-\delta)]^\beta \; . \tag{35}$$

Here K, α, and β are constants, $S_n-\delta$ is the neutron separation energy corrected for the pairing energy, and D(U) is the level spacing per spin state at $U = S_n-\delta$. We have determined values for the constants in different mass ranges [Gar 75], and all of this was built into our COMNUC and STAPRE codes. Other recent evaluations include [BRV 74, Joh 77, Ref 78, Ben 78, Moo 78, ZS 78, Mug 79].

Due to the rapid variation of the neutron separation energy and the level density with proton and neutron number, and to the great importance of the discrete levels below the continuum (as we have seen in Table VII), one cannot expect to find any smooth behavior of the radiative width over any large mass range. The effective energy dependence of the radiative width depends not only on the intrinsic energy dependence of the partial radiative width, but also on the spin distribution in the radiating nucleus and also on its discrete levels and continuum level density. For these and other reasons, it appears more fruitful to us to try to develop systematics for the gamma-ray strength function, which underlies the radiative width, than to parameterize the radiative width itself. In fact, one of the examples that we have used in the past [GGD 80] concerns the neutron capture cross sections for ^{85,87}Rb. The capture cross sections for the two isotopes differ by a factor of 10, and the $\langle\Gamma_\gamma\rangle/D_{ob}$ values differ by a factor of 27, and yet they both have the same E1 strength function.

For neutron capture calculations, dipole transitions are the only ones of major importance among continuum states and for transitions from the continuum to the low-lying discrete levels. Of the dipole transitions, the E1 transitions far outweigh M1 transitions. Studies of capture gamma-ray spectra have shown that, for medium-weight and heavy nuclei, an E1 strength function with an energy dependence related to the shape of the GDR is more realistic than the constant strength function derived from the Weisskopf single-particle treatment. The situation for M1 strength functions is less clear; some investigators believe there is evidence for an M1 resonance shape. Recent reviews that bear on this question include [Lon 79, Kop 79, MSC 81].

In our treatments we have used the following expression for the E1 gamma-ray strength function, together with the Brink hypothesis,

$$f_{E1}(E_\gamma) = 3.32 \times 10^{-6} \; \frac{NZ}{A} \; \frac{F_{SR}}{E_\gamma} \; \frac{G_R(E_\gamma,E_R,\Gamma_R)}{\Gamma_R} \; . \tag{36}$$

Here $G_R(E_\gamma,E_R,\Gamma_R)$ is the GDR line shape function with a peak value of unity, and E_R and Γ_R are the energy and width of the GDR. We combine the contributions to the dipole sum rule of exchange terms, and of the extent to which the sum rule is exhausted, into the parameter, F_{SR}. If a double-peaked GDR with equal peak heights is assumed, then the term $G_R(E_\gamma,E_R,\Gamma_R)$ may be replaced by $\Sigma_i\, G_{Ri}(E_\gamma,E_{Ri},\Gamma_{Ri})/\Sigma_i\, \Gamma_{Ri}$. For M1 transitions, we generally assume f_{M1} = constant, and that the M1 radiation width is about 15% of the total s-wave radiations width at the neutron separation energy.

The Lorentz line shape is a commonly-used functional form for G_R. Another form that we have investigated recently [GGD 80, GG 81] might be called the energy-dependent Breit-Wigner (EDBW) shape.

<u>Lorentz</u>

$$G_R(E_\gamma,E_R,\Gamma_R) = [1 + (E_\gamma^2-E_R^2)^2/(E_\gamma\Gamma_R)^2]^{-1} \ . \tag{37}$$

<u>Energy-Dependent Breit-Wigner</u>

$$G_R(E_\gamma,E_R,\Gamma_R,E_x) = [1 + 4(E_\gamma-E_R)^2/(\Gamma(E_\gamma\Gamma_R)]^{-1} \ , \tag{38}$$

with

$$\Gamma(E_\gamma) = \Gamma_R\ [2E_\gamma/(E_x+E_R)]^2 \ ;\ E_\gamma < (E_x+E_R)/2,$$

$$= \Gamma_R \qquad\qquad ;\ E_\gamma > (E_x+E_R)/2,$$

and with $E_x \approx 5$ MeV. We will compare these two shapes after we have further discussed the EDBW form.

Our development of the systematics for the EDBW treatment of E1 gamma-ray strength functions is based on a number of assumptions:

1. All nuclei with A > 40 behave like prolate spheroids, and their GDR shapes may be approximated as the sum of two peaks of equal height, σ_{01} and σ_{02}, even when the peaks are not resolved.

2. $\Gamma_{R1}\,\sigma_{01} = 0.5\,\Gamma_{R2}\,\sigma_{02}$, and hence $\Gamma_{R1} = 0.5\,\Gamma_{R2}$.

3. The average energy of the two peaks is $E_R = (E_{R1} + 2\,E_{R2})/3$, and according to ref. [BF 75], $E_R = 31.2\,A^{-1/3} + 20.6\,A^{-1/6}$ MeV. Also, the separation of the two peaks may be related to the deformation parameter, β_2,

$$E_{R2}/E_{R1} = 0.95\left[\frac{2.126 + 0.822\,\beta_2}{2.126 - \beta_2}\right] .$$

4. The widths, Γ_{R1} and Γ_{R2}, are not functions of β_2, but are mass dependent. For masses up to about 160, we use $\Gamma_{R2} = 29.7\,A^{-1/3}$, and for higher mass we use $\Gamma_{R2} = 66.1\,A^{-1/2}$. The mass 160 separation point is arbitrary and rather uncertain.

5. The parameter, F_{SR}, we now take as unity, if both isospin states are available. For neutron capture, only $T^<$ states can be reached, and so we use [FG 70]

$$F_{SR} = \frac{T_o}{T_o+1} (1 + 1.5\ A^{-2/3}) \quad ,$$

where

$$T_o = (N-Z)/2.$$

Our latest finding is that, for β_2 values in the range 0.1-0.3 and for gamma-ray transitions up to at least 7 MeV in energy, the calculated E1 strength function is quite insensitive to nuclear deformation. Therefore, it should be possible to go back to Eq. 36 and develop a useful single-peak approximation to our double-peak systematics. We have made the following approximations:

1. $NZ/A \approx A/4$.

2. The mass range was arbitrarily divided at A = 160, and

   <u>A < 160</u>

   $$\sum \Gamma_{Ri} = 1.5\ (29.7\ A^{-1/3}) = 44.6\ A^{-1/3}\ .$$

   $$F_{SR} = 1.5 - 2.8\ A^{-1/3}\ .$$

   <u>A ⩾ 160</u>

   $$\sum \Gamma_{Ri} = 1.5\ (66.1\ A^{-1/2}) = 99.1\ A^{-1/2}\ .$$

   $$F_{SR} = 0.99\ .$$

3. $\sum G_{Ri}\ (E_\gamma, E_{Ri}, \Gamma_{Ri}) = 2\ G_R^*(E, E_R, \Gamma_R^*)$.

4. $E_R = 31.2\ A^{-1/3} + 20.6\ A^{-1/6}$.

The functional forms for G_R^* were to be as before, the EDBR form up to the energy $(E_R+5)/2$, and the normal Breit-Wigner form from $(E_R+5)/2$ up to the peak energy, E_R. It turned out that it was necessary to introduce a slight energy dependence in Γ_R^* to better represent the sum of two Breit-Wigner expressions at the higher energies. Our final results are as follows:

Energy Range	Functional Form
$E_\gamma < (E_R+5)/2$	$G_R^*(E_\gamma) = \left[1 + \frac{(5+E_R)^2\ (E_\gamma-E_R)^2}{(E_\gamma\ \Gamma_R^*)^2}\right]^{-1}.$
$E_R > E_\gamma > (E_R+5)/2$	$G_R^*(E_\gamma) = \left[1 + \frac{2}{\Gamma_R^*}^{\ 2}\ (E_\gamma-E_R)^2\right]^{-1}.$

Mass Range	Functional Form
$40 < A < 160$	$f_{E1}(E_\gamma) = 3.72 \times 10^{-8}\ A^{4/3}\ \frac{(1.5-2.8A^{-1/3})}{E_\gamma}\ G_R(E_\gamma).$
	$\Gamma_R^* = 22.3\ A^{-1/3} \left(1.052 - 6.0 \times 10^{-5}\ \frac{E_\gamma{}^4}{E_R}\right)$.
$A > 160$	$f_{E1}(E_\gamma) = 1.66 \times 10^{-8}\ \frac{A^{3/2}}{E_\gamma}\ G_R^*(E_\gamma)$.
	$\Gamma_R^* = 49.6\ A^{-1/2} \left(1.052 - 6.0 \times 10^{-5}\ \frac{E_\gamma{}^4}{E_R}\right)$.

The above expressions represent the average behavior of $f_{E1}(E_\gamma)$, including the isospin correction, near the line of stability, in both spherical and deformed mass regions. Figure 18 shows $f_{E1}(E_\gamma)$, as a function of mass, for gamma-ray energies of 3, 5, and 7 MeV. It is not obvious from this figure, but the energy dependence of $f_{E1}(E_\gamma)$, for gamma-ray energies in the range 3-7 MeV, is about E_γ^2. There are two common ways to plot f_{E1} values, to attempt to remove the energy and/or mass dependencies:

$$k_{E1} = f_{E1}(E_\gamma)\ A^{-2/3}\ , \tag{39}$$

and

$$S_{E1} = f_{E1}(E_\gamma)\ A^{-8/3}\ E_\gamma^{-2}\ . \tag{40}$$

In Fig. 19, we show the average behavior of $f_{E1}(E_\gamma)$, again for $E_\gamma = 3$, 5, and 7 MeV, but now plotted as k_{E1} and S_{E1}. The calculations are compared with resonance neutron capture data from the compilation of McCullagh et al. [MSC 81]. Figure 19 shows our calculated $f_{E1}(E_\gamma)$ values to be in generally good agreement with the measurements in both spherical and deformed mass regions, and that plots of S_{E1} from Eq. 40 should be useful in correlating data because the energy dependence of the E1 strength function is effectively removed, at least for the most commonly encountered range of gamma-ray energies.

In our last graph, Fig. 20, we compare the E1 strength function for ^{90}Y in the Lorentz form as specified in the ^{89}Y + n test case, with $f_{E1}(E_\gamma)$ for ^{90}Y from the calculation using the average EDBW expressions and with some measurements by Szeflinska et al. [SSW 79]. While the average trend with energy of the data points tends to follow the EDBW curve better than the Lorentz curve, the points lie below both curves in the range from 0 to 6.8 MeV over which the radiation width was normalized. It would seem from these data that the EDBW expressions given above yield $f_{E1}(E_\gamma)$ values that are too large by perhaps 30%. An examination of Fig. 19, leads one to conclude that a 30% decrease in S_{E1} might fit those data better as well. A further study is underway to try to reach some definite conclusion in this matter.

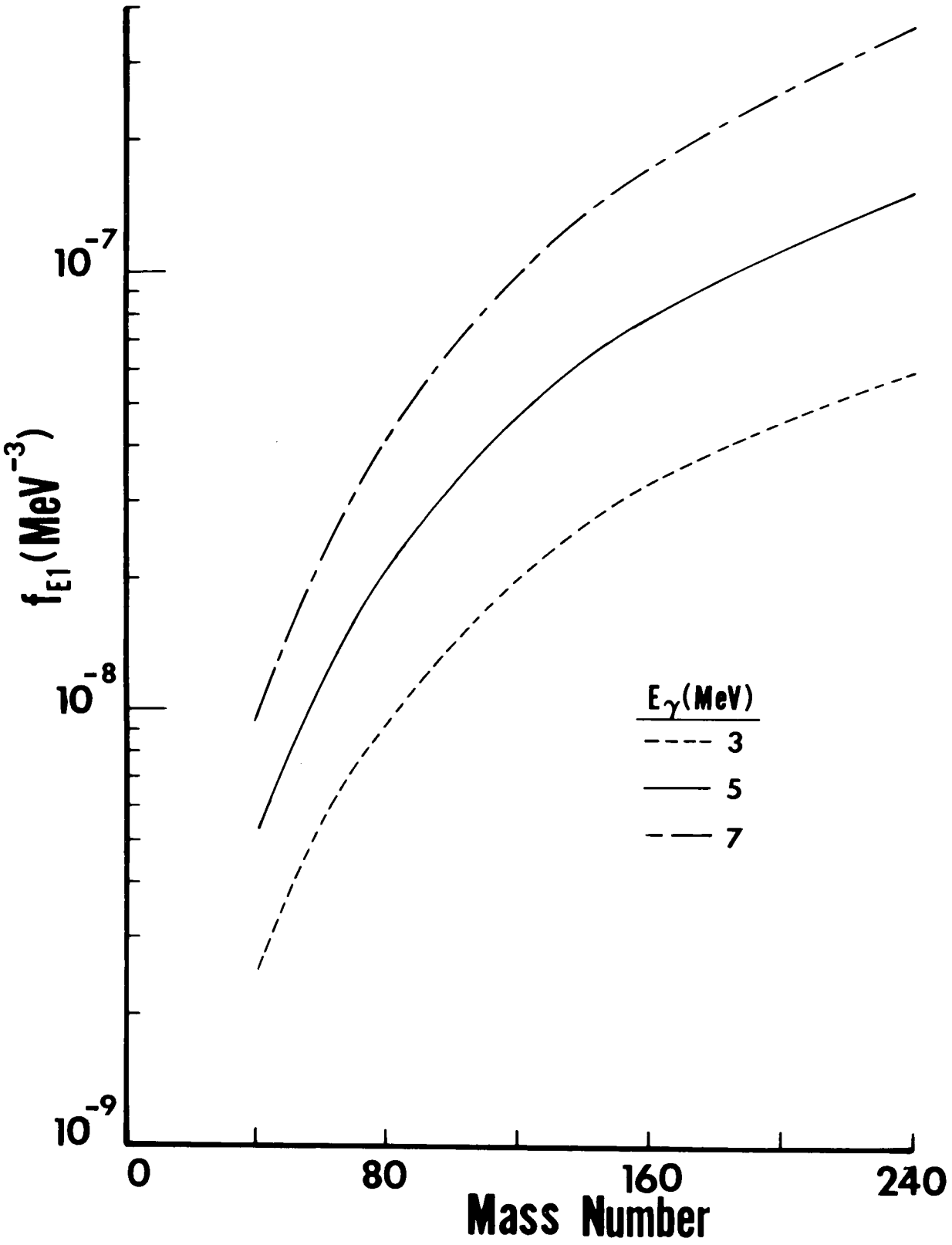

Fig. 18. Average behavior of $f_{E1}(E_\gamma)$ as a function of mass for E_γ = 3, 5, and 7 MeV.

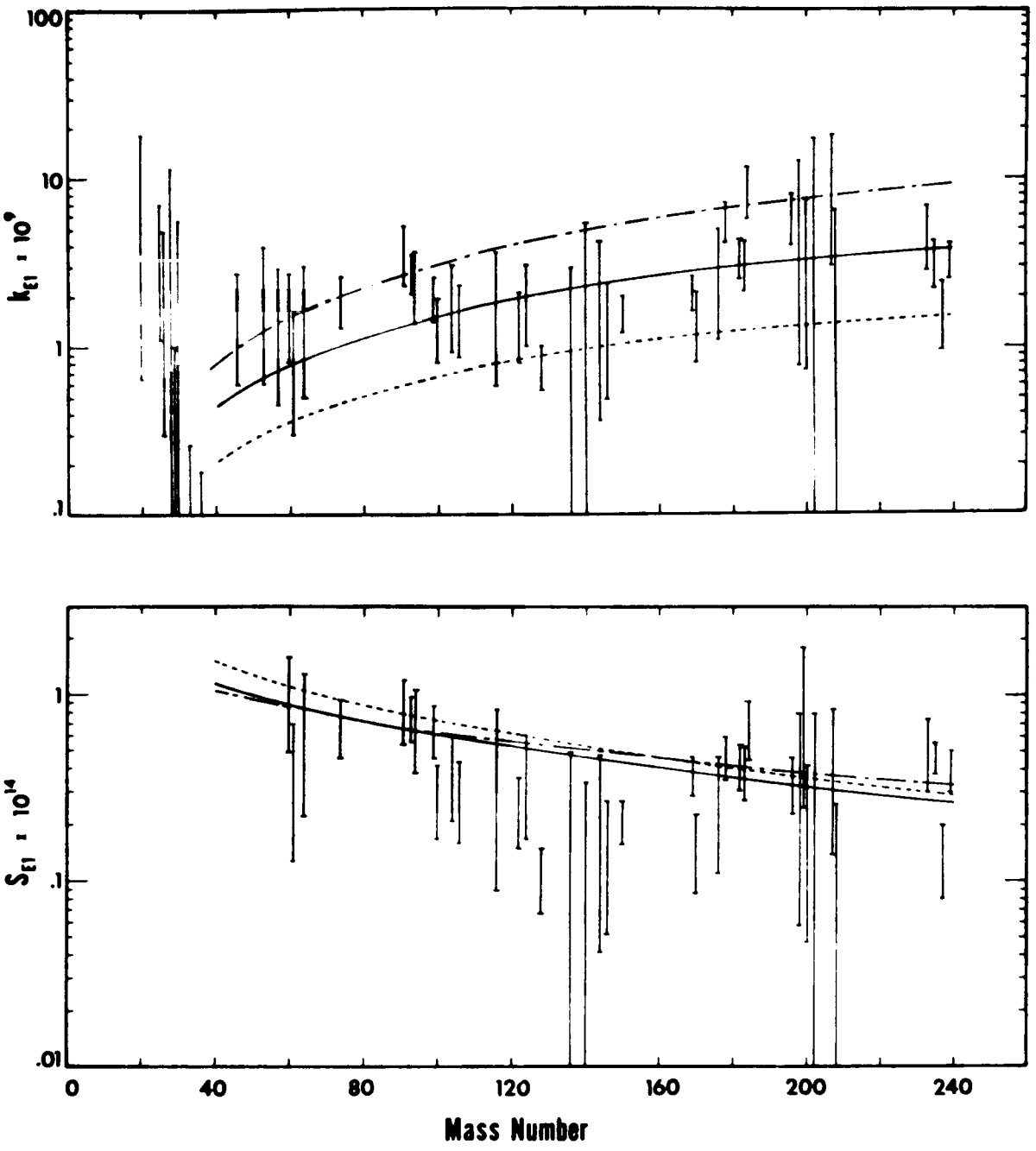

Fig. 19. Comparison of average $f_{E1}(E_\gamma)$, expressed as $k_{E1} = f_{E1}(E_\gamma)\ A^{-2/3}$ and $S_{E1} = f_{E1}(E_\gamma)\ A^{-8/3}\ E_\gamma^{-2}$, with average resonance neutron capture data from the compilation of McCullagh et al. [MSC 81]. Calculated $f_{E1}(E_\gamma)$ values are for E_γ = 3 MeV (short dash line), 5 MeV (solid line), and 7 MeV (short and long dash line).

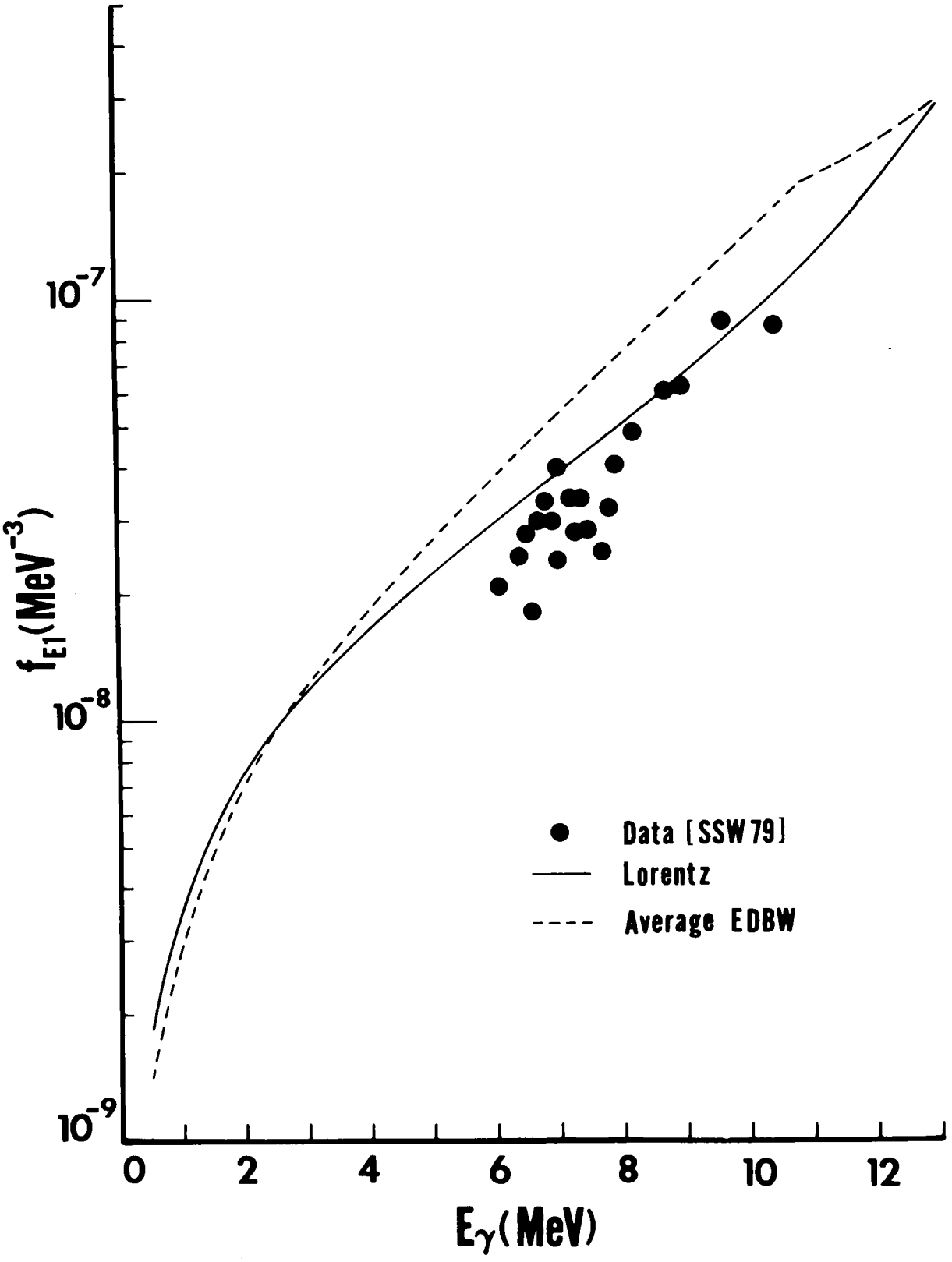

Fig. 20. Comparison of $f_{E1}(E_\gamma)$ for ^{90}Y in the Lorentz form specified by the ^{89}Y + n test case (solid line), with $f_{E1}(E_\gamma)$ for ^{89}Y from the average calculation (dash line), and with experimental measurements [SSW 79] (circles).

REFERENCES

[AM 79] B. J. Allen and A. R. Musgrove, Advances in Nuclear Physics, Vol. 10 (M. Baranger and E. Vogt, editors), Plenum Press, New York, 1979.

[Bee 73] M. Beer, Nucl. Sci. Eng. 50, 171 (1973).

[BEG 78] C. D. Bowman, C. M. Eisenhauer, and D. M. Gilliam, Proc. 2nd ASTM-EURATOM Symposium on Reactor Dosimetry, Palo Alto, CA, 1977, NUREG/CP-0004, Vol. 2., 1978, p. 575.

[Ben 78] V. Benzi, Neutron Physics and Nuclear Data, OECD Nuclear Energy Agency, 1978, p. 288.

[Ber 74] I. Bergqvist, Proc. Int. Symp. on Neutron Capture Gamma-Ray Spectroscopy and Related Topics, Petten, Sept. 1974, p. 199.

[Bir+76] J. R. Bird, et al., Proc. Int. Conf. on Interactions of Neutrons with Nuclei, Lowell, July 1976, CONF-760715-PL (E. Sheldon, editor), p. 76.

[Boh 36] N. Bohr, Nature 137, 344 (1936).

[Bol+77] J. W. Boldeman, et al., Nucl. Sci. Eng. 64, 744 (1977).

[BR 69] V. Benzi and G. Reffo, "Fast Neutron Radiative Capture Cross Sections of Stable Nuclei with $32 < Z < 66$," CCDN-NW/10, Dec. 1969.

[Bro 64] G. E. Brown, Nucl. Phys. 57, 339 (1964).

[BRV 74] V. Benzi, G. Reffo, and M. Vaccari, "On the Calculation of Total Radiative Widths of Neutron Resonances," Fission Product Nuclear Data, IAEA-169, Vol. III, 1974, p. 123.

[Chr+76] R. E. Chrien, et al., Phys. Rev. C13, 578 (1976).

[CLR 65] C. F. Clement, A. M. Lane, and J. R. Rook, Nucl. Phys. 66, 273 (1965); and 66, 293 (1965).

[CFM 67] J. L. Cook, H. Ferguson and A. R. Musgrove, "Nuclear Level Densities in Intermediate and Heavy Nuclei," AAEC/TM392, June 1967.

[DHM 70] N. D. Dudey, R. R. Heinrich, and A. A. Madson, J. Nucl. Energy 24, 181 (1970).

[DK 78] F. S. Dietrich and A. K. Kerman, "Direct-Semidirect and Pure Resonance Model Calculations of Fast Neutron Capture on ^{208}Pb," UCRL-81498, Aug. 1978; "A Pure-Resonance Model for Radiative Capture of Fast Nucleons," UCRL-82362, Jan. 1979.

[Dov+65] A. G. Dovbenko, et al., At. Energ. (USSR) 18, 114 (1965).

[Dra+77] J. B. Dragt, et al., Nuc. Sci. Eng. 62, 117 (1977).

[Dun 70] C. L. Dunford, "A Unified Model for Analysis of Compound Nucleus Reactions," AI-AEC-12931, July 1970.

[Gar 75] D. G. Gardner, Nuclear Cross Sections and Technology, NBS Special Publication 425, Vol. II, 1975, p. 651.

[Gar 80] D. G. Gardner, "Recent Developments in Nuclear Reaction Theories and Calculations," UCRL-84369, 1980, p. 25.

[Gar 81a] D. G. Gardner, "Methods for Calculating Capture Cross Sections and Gamma-Ray Spectra," UCRL-86982, Feb. 1981.

[Gar 81b] D. G. Gardner, "Statistical vs Valence Neutron Capture in ^{98}Mo," UCRL-86267, June 1981.

[GC 65] A. Gilbert and A. G. Cameron, Can. J. Phys. 43, 1446 (1965).

[GG 81] M. A. Gardner and D. G. Gardner, "Continued Study of the Parameterization of the E1 Gamma-Ray Strength Function," UCRL-86265, June 1981.

[GGD 80] D. G. Gardner, M. A. Gardner, and F. S. Dietrich, "A Study of Gamma-Ray Strength Functions," UCID-18759, Aug. 1980.

[GJD 76] H. Gruppelaar, A. J. Janssen, and J. W. Dekkor, "Intercomparison of Recent Evaluations for the Capture Cross Sections of Some Fission-Product Nuclides," ECN-112, Nov. 1976.

[Gou 72] R. A. Gough, "Yrast Tables," LBL-624, Feb. 1972.

[GP 72] M. Gyulassy and S. T. Perkins, "An Atlas of Unresolved Neutron Resonance Parameters," UCRL-50400, Vol. 13, Sept. 1972.

[GR 77] H. Gruppelaar and G. Reffo, Nuc. Sci. Eng. 62, 756 (1977).

[Gre+67] H. A. Grench, et al., Nucl. Phys. A94, 157 (1967).

[Gru 75] H. Gruppelaar, Nuclear Theory in Neutron Nuclear Data Evaluation, Trieste, IAEA-190, Vol. II, 1976, p. 61.

[HB 51] J. Heidmann and H. A. Bethe, Phys. Rev. 84, 274 (1951).

[HC 79] D. Halderson and B. Castel, Phys. Rev. C18, 1542 (1979).

[Hen 79] E. Henry, LLNL, private communication, 1979.

[Iij+77] S. Iijima, et al., J. Nucl. Sci. Techn. (Japan) 14, 161 (1977).

[Joh 77] C. H. Johnson, Phys. Rev. C16, 2238 (1977).

[KKM 73] M. Kawai, A. K. Kerman, and K. W. McVoy, Ann. Phys. 75, 156 (1973).

[Kop 79] J. Kopecky, Neutron Capture Gamma-Ray Spectroscopy (R. E. Chrien and W. R. Kane, editors), Plenum Press, New York, 1979, p. 665.

[Lag 77] C. Lagrange, CEA-N-1984, 1977.

[Lag 79] C. Lagrange, "On Optical Model Calculations in the Mass Region A = 80 to A = 170," Specialists' Meeting on Neutron Cross Sections on Fission Product Nuclei, Bologna, Dec. 1979, p. 233.

[Lan 59] A. M. Lane, Nuc. Phys. 11, 625 (1959).

[LL 57] A. M. Lane and J. E. Lynn, Prog. Phys. Soc. (London) 70A, 557 (1957).

[LL 59] A. M. Lane and J. E. Lynn, Nucl. Phys. 11, 646 (1959).

[LL 60a] A. M. Lane and J. E. Lynn, Nucl. Phys. 17, 563 (1960).

[LL 60b] A. M. Lane and J. E. Lynn, Nucl. Phys. 17, 586 (1960).

[LM 74] A. M. Lane and S. F. Mughabghab, Phys. Rev. C10, 412 (1974).

[Lon 79] M. A. Lone, Neutron Capture Gamma-Ray Spectroscopy, (R. E. Chrien and W. R. Kane, editors), Plenum Press, New York, 1979, p. 161.

[LS 68] G. Longo and F. Saporetti, Nuovo Cimento 56B, 264 (1968).

[LS 75] G. Longo and F. Saporetti, Nuclear Theory in Neutron Nuclear Data Evaluation, Trieste, IAEA-190, Vol. I, 1976, p. 191.

[LS 76] G. Longo and F. Saporetti, Nucl. Sci. Eng. 61, 40 (1976).

[Lyn 74] J. E. Lynn, "Systematics for Neutron Reactions of the Actinide Nuclei," AERE-R-7468, Nov. 1974.

[Lyn 76] J. E. Lynn, "Theoretical Calculation of Transactinium Isotope Nuclear Data for Evaluation Purposes," IAEA-186, Vol. 3, 1976, p. 201.

[Lyn 81] J. E. Lynn, Nuclear Fission and Neutron-Induced Fission Cross Sections, (A. Michaudon, editor), Pergamon Press, Oxford, 1981, Chapter V.

[MC 78] S. F. Mughabghab and R. E. Chrien, "Nonstatistical Effects in Neutron Capture, A Review of Recent Experiments," BNL-NCS-25448, Sept. 1978.

[MG 73] S. F. Mughabghab and D. I. Garber, "Resonance Parameters," BNL-325, Vol. 1, 1973.

[Mol 61] P. A. Moldauer, Phys. Rev. 123, 968 (1961).

[Mol 64] P. A. Moldauer, Phys. Rev. 135, 642 (1964).

[Mol 78] P. A. Moldauer, "Statistical Theory of Neutron Nuclear Reactions," ANL/NDM-40, Feb. 1978.

[Mol 80] P. A. Moldauer, Nucl. Phys. A344, 186 (1980).

[Moo 78] M. S. Moore, Neutron Physics and Nuclear Data, OECD Nuclear Energy Agency, 1978, p. 313.

[MSC 81] C. M. McCullagh, M. L. Stelts, and R. E. Chrien, Phys. Rev. C23, 1394 (1981).

[Mug 78] S. F. Mughabghab, "Non-Statistical Effects in Neutron Capture," BNL-NCS-24249-R, April 1978.

[Mug 79] S. F. Mughabghab, "Status of Radiative Widths, Neutron Strength Functions and Improved Evaluation Using the Lane-Lynn Theory," BNL-NCS-27050, 1979.

[Mus+76] A. R. Musgrove, et al., Nucl. Phys. A270, 108 (1976).

[Ref 78] G. Reffo, "Parameter Systematics for Statistical Calculations of Neutron Reaction Cross Sections," ICTP Trieste Winter Course on Nuclear Physics and Reactors, 17 Jan. to 10 March, 1978.

[Rib+75] P. Ribon, et al., "Evaluation des Sections Efficaces de Capture et de Diffusion Inelastique de 26 Produits de Fission," CEA-N-1832, Dec. 1975.

[Sch 78] F. Schmittroth, Theory and Application of Sensitivity and Uncertainty Analysis, ORNL/RSIC-42, 1978, p. 145.

[SG 76] E. Sartori and L. Garcia De Viedma, Nuclear Theory in Neutron Nuclear Data Evaluation, IAEA-190, Vol. II, 1976, p. 253.

[SH 57] A. Stolovy and J. A. Harvey, Phys. Rev. 108, 353 (1957).

[SS 73] F. Schmittroth and R. E. Schenter, "Fast Neutron Capture Cross Sections for Fission Product Isotopes," HEDL-TME-73-63, Aug. 1973; F. Schmittroth, "Neutron Capture Calculations for E_n = 100 keV to 4 MeV," HEDL-TME-73-79, Nov. 1973.

[SSW 79] G. Szeflinska, Z. Szeflinska, and Z. Wilhelmi, Nucl. Phys. A323, 253 (1979).

[Str+79] G. Struble, et al., LLNL, private communication, 1979.

[THW 74] J. W. Tepel, H. M. Hofman, and H. W. Weidenmuller, Phys. Lett. 49B, 1 (1974).

[Uhl 70] M. Uhl, Acta Phys. Austriaca 31, 245 (1970).

[US 76] M. Uhl and B. Strohmaier, "STAPRE, A Computer Code for Particle Induced Activation Cross Sections and Related Quantities," IRK 76/01, 1976.

[ZS 78] D. F. Zaretskii and V. K. Sirothkin, Sov. J. Nucl. Phys. 27, 808 (1978).

Table I. Discrete level information for ^{99}Mo.

Energy (MeV)	Jπ	$T_{1/2}$	Gamma-Ray Branching: Final level energy (MeV) (branching fraction)
0.00	$1/2^+$	66 h	--
0.10	$5/2^+$	16 μs	0.00 (1.00)
0.25	$7/2^+$		0.10 (1.00)
0.35	$3/2^+$		0.00 (0.42), 0.10 (0.58)
0.50	$1/2^+$		0.00 (0.53), 0.10 (0.24), 0.35 (0.23)
0.55	$3/2^+$		0.00 (0.29), 0.10 (0.61), 0.35 (0.10)
0.60	$5/2^+$		0.25 (0.24), 0.35 (0.76)
0.65	$3/2^+$		0.00 (0.72), 0.10 (0.22), 0.35 (0.06)
0.70	$11/2^-$	0.8 μs	0.25 (1.00)
0.70	$7/2^+$		0.10 (0.81), 0.25 (0.19)
0.75	$9/2^+$		0.10 (0.74), 0.25 (0.26)
0.80	$3/2^+$		0.00 (0.29), 0.10 (0.39), 0.35 (0.32)
0.90	$5/2^+$		0.00 (0.38), 0.10 (0.50), 0.35 (0.12)
0.90	$7/2^+$		0.10 (0.50), 0.25 (0.50)
0.90	$1/2^+$		0.00 (0.21), 0.10 (0.50), 0.35 (0.29)
0.90	$11/2^+$		0.25 (1.00)
0.90	$9/2^+$		0.10 (0.50), 0.25 (0.50)
0.90	$5/2^+$		0.00 (0.50), 0.10 (0.50)
0.95	$7/2^+$		0.10 (0.20), 0.25 (0.80)
0.95	$5/2^+$		0.00 (0.15), 0.10 (0.37), 0.35 (0.17), 0.55 (0.31)
0.95	$7/2^-$		0.10 (0.80), 0.25 (0.05), 0.70 (0.15)[a]
1.00	$1/2^+$		0.00 (0.15), 0.10 (0.38), 0.35 (0.30), 0.50 (0.08), 0.60 (0.09)
1.05	$5/2^+$		0.65 (1.00)
1.15	$15/2^-$		0.70 (1.00)[a]
1.15	$3/2^+$		0.00 (0.50), 0.65 (0.50)
1.20	$3/2^+$		0.10 (0.50), 0.50 (0.50)
1.20	$7/2^+$		0.10 (0.30), 0.35 (0.12), 0.60 (0.58)
1.20	$9/2^+$		0.70 (0.92)[a], 0.95 (0.08)[b]
1.25	$5/2^+$		0.35 (1.00)

(a) 0.70 MeV level with Jπ = $11/2^-$.
(b) 0.95 MeV level with Jπ = $7/2^-$.

Table II. Comparison of some calculated quantities with experiment for the reaction $^{98}Mo + n$.

Quantity	Partial wave	Calculation	Experiment: Chrien et al. [Chr+76]	Experiment: Musgrove et al. [Mus+76]	Evaluation: Gruppelaar [Gru 75]
$\overline{\Gamma}_\gamma$ (mV)	s	64	85.6	93 ± 11	86
	p	128	121	117 ± 15	120
$\overline{D}$ (eV)	s	820	900	950 ± 150	800
	p	290			
$S_\ell \times 10^4$	s	0.48	0.7 ± 0.2	0.44 ± 0.12	0.35
	p	6.24	7 ± 1	3.3 to 6.7	7

Table III. Gamma-ray strength functions.

E_γ = 3.6 - 5.9 MeV	Calculation	Chrien et al. [Chr+76]
$k_{E1} = \Gamma_{\gamma E1}\ D^{-1}\ E_\gamma^{-3}\ A^{-2/3}$	$(1\text{-}3) \times 10^{-9}$	1.8×10^{-9}
$k_{M1} = \Gamma_{\gamma M1}\ D^{-1}\ E_\gamma^{-3}$	1.8×10^{-9}	4.9×10^{-9}

Table IV. Comparison of current LLNL versions of two statistical model codes.

	Comments	COMNUC [DUN 70]	STAPRE [Uhl 70, US 76]
1.	Hauser-Feshbach with width fluctuation correction	Yes	Yes
2.	Built-in spherical optical model program	Yes	No
3.	Transmission coefficients	T_j	T_ℓ
4.	Computes shape elastic and total cross sections	Yes	No
5.	All possible cross sections always calculated	Yes	No
6.	Entrance channel always neutrons	Yes	No
7.	Integration method	Gaussian quadrature	Trapezoidal rule

Table IV. (Continued)

	Comments	COMNUC [DUN 70]	STAPRE [Uhl 70, US 76]
8.	Gilbert-Cameron level density formulation	Yes	Yes, or back-shifted Fermi gas
9.	Simple Yrast model	Yes	Yes
10.	Computes elastic and discrete inelastic angular distributions	Yes	No
11.	Precompound evaporation allowed	No	Yes
12.	Calculates energy spectra of emitted particles	No	Yes
13.	Gamma-ray competition at each compound nucleus	Yes	Yes
14.	Maximum number of compound nuclei in evaporation sequence	3	6
15.	Calculates gamma-ray spectra and production cross sections	No	Yes
16.	Weisskopf and/or Brink-Axel energy dependence of radiation width	Yes	Yes
17.	Absolute gamma-ray strength functions allowed	No	Yes
18.	Estimates direct-semidirect neutron capture	Yes	No
19.	Discrete levels allowed in all nuclei considered	Yes	Yes
20.	Computes isomer populations	No	Yes
21.	Permits isomers as target states	Yes	Yes
22.	Fission competition allowed	Yes	No
23.	Accepts input from coupled-channel codes	Yes	No

Table V. Level density parameters and discrete level information for ^{89}Y.

Level density parameters for Gilbert-Cameron expression

$$a = 9.36532 \text{ MeV}^{-1}$$
$$\delta = 1.89899 \text{ MeV}$$
$$E_X = 6.08438 \text{ MeV}$$
$$T = 0.87914 \text{ MeV}$$
$$E_o = 1.01917 \text{ MeV}$$
$$\sigma^2(E) = 5.81692\ [a(E-\delta)]^{1/2} \geqslant 5.81692$$
$$S_n = 11.450 \text{ MeV}$$

Discrete level information[a]

Energy (MeV)	J^π	$T_{1/2}$	Gamma-ray branching Final level energy (branching fraction)
0.00	$1/2^-$	Stable	--
0.90	$9/2^+$	16 s	0.00 (1.00)
1.50	$3/2^-$		0.00 (1.00)
1.75	$5/2^-$		0.00 (1.00)
2.20	$5/2^+$		0.90 (0.70), 1.50 (0.30)
2.55	$7/2^+$		0.90 (1.00)
2.55	$11/2^+$		0.90 (1.00)
2.60	$9/2^+$		0.90 (1.00)
2.85	$7/2^+$		0.90 (1.00)
2.90	$3/2^-$		0.00 (0.00)
2.90	$13/2^+$		0.90 (1.00)
3.05	$3/2^-$		0.00 (1.00)

(a) Ref. [Str+79].

Table VI. Level density parameters and discrete level information for ^{90}Y.

Level density parameters for Gilbert-Cameron expression

$$a = 9.75940 \text{ MeV}^{-1}$$
$$\delta = 0.51461 \text{ MeV}$$
$$E_X = 4.68128 \text{ MeV}$$
$$T = 0.85438 \text{ MeV}$$
$$E_o = -0.40013 \text{ MeV}$$
$$\sigma^2(E) = 5.86041\ [a(E-\delta)]^{1/2} > 5.86041$$
$$S_n = 6.850 \text{ MeV}$$

Discrete level information[a]

Energy (MeV)	J^π	$T_{1/2}$	Gamma-ray branching: Final level energy (branching fraction)
0.00	2^-	64.1 hr	--
0.20	3^-		0.00 (1.00)
0.70	7^+	3.2 hr	0.00 (0.004), 0.20 (0.996)
0.80	2^+		0.00 (0.78), 0.20 (0.22)
0.95	3^+		0.00 (0.42), 0.80 (0.58)
1.05	5^+		0.70 (1.00)
1.20	4^+		0.95 (0.89), 1.05 (0.11)
1.20	0^+		0.00 (1.00)
1.30	6^+		0.70 (0.95), 1.05 (0.05)
1.35	1^-		0.00 (1.00)
1.40	0^-		0.00 (1.00)
1.55	3^-		0.00 (1.00)
1.65	1^-		0.00 (1.00)
1.70	4^-		0.00 (1.00)
1.75	2^-		0.00 (1.00)
1.80	3^-		0.00 (1.00)
1.85	5^-		0.20 (1.00)
1.95	5^+		0.70 (1.00)
2.05	2^-		0.00 (1.00)

Discrete level information[a] (Continued)

Energy (MeV)	J^{π}	$T_{1/2}$	Gamma-ray branching Final level energy (branching fraction)
2.10	4^+		0.80 (1.00)
2.10	4^-		0.00 (1.00)
2.20	1^-		0.00 (1.00)
2.25	6^+		0.70 (1.00)
2.30	1^-		0.00 (1.00)
2.35	1^-		0.00 (1.00)

(a) Ref. [Str+79].

Table VII. Partial radiation widths for ^{90}Y.

Neutron partial wave	Calculated (mV) 25 levels in ^{90}Y	Calculated (mV) 1 level in ^{90}Y	Measured (mV) [Bol+77]
s	183	183	115
p	342	170	307
d	186	152	
f	251	132	
g	179	113	

Table VIII. Comparison of some cross sections calculated by COMNUC and STAPRE for the ^{89}Y + n test case.

E_n^{lab} (MeV)	Ratio of cross-section values, COMNUC/STAPRE			
	Reaction	Compound elastic	Inelastic	Total capture
0.076	0.95	0.95		1.01
0.177	0.99	0.99		1.03
0.278	0.99	0.99		1.03
0.379	0.99	0.99		1.02
0.480	0.99	0.99		1.03
0.581	0.99	0.99		1.03
0.683	0.99	0.99		1.03
0.784	0.99	0.99		1.03
0.885	0.99	0.99		1.03
0.986	0.99	0.99	1.11	1.04
1.087	0.99	0.99	1.11	1.04
1.289	0.99	0.98	1.08	1.04
1.492	0.99	0.98	1.06	1.04
1.694	0.99	0.99	0.99	1.04
1.896	0.99	1.00	0.98	1.04
2.098	0.99	1.00	0.98	1.05

Table IX. Comparison of values of $(2\pi\Gamma_\gamma/D) \times 10^4$ for some $J\pi$ compound nucleus states in ^{90}Y as calculated by COMNUC and STAPRE.

E_n^{lab} = 1.087 MeV

Spin	COMNUC/STAPRE ratio + parity	COMNUC/STAPRE ratio - parity
0	1.04	1.02
1	1.04	1.03
2	1.04	1.03
3	1.04	1.03
4	1.03	1.03
5	1.03	1.03
6	1.03	1.03

E_n^{lab} = 0.076 MeV

Spin	COMNUC/STAPRE ratio + parity	COMNUC/STAPRE ratio - parity
0	1.04	1.02
1	1.04	1.03
2	1.04	1.03
3	1.04	1.03
4	1.04	1.03
5	1.03	1.03
6	1.03	1.03

Discussion

QUESTION: W. Poenitz
Yttrium might not have been a good test case for comparison of different formulations of the width-fluctuation correction because the correction itself seemed to be small in this case. There are others where it is much larger and maybe they would have shown a difference.
ANSWER: D. Gardner
Possibly, but the difference between choices (for example, P. Moldauer's expression for the degrees of freedom, or others) is so small, you can't see a difference.

QUESTION: S. Mughabghab
You carried out the calculations for ^{98}Mo, and did not obtain agreement with experimental values for the total radiation width for S-wave resonances. The p-wave resonances agreement you obtained is not important. I would draw a different conclusion and that is that the calculations are uncertain. Did you make an evaluation of the uncertainties of the calculations; I mean, did you check what kind of changes you get if you vary the parameters?
ANSWER: D. Gardner
I did some of this for Yttrium, not for ^{98}Mo.

QUESTION: R. Chrien
When you calculate your spectrum you are averaging over a number of final states, is that correct?
ANSWER: D. Gardner
We calculate the entire cascade. For the final state these are direct transitions which form the high energy part of the spectrum.
COMMENT: H. Gruppelaar
I only want to comment. In the case of ^{98}Mo the p-wave component of the total-average-capture width is only a small part (15 meV compared with 120 or so). I agree, you cannot expect to see it.

CALCULATION OF AVERAGE CAPTURE CROSS SECTIONS FOR ACTINIDES - LEVEL-STATISTICAL VS. GLOBAL APPROACH

F.H. Fröhner, B. Goel and U. Fischer

Kernforschungszentrum Karlsruhe
Institut für Neutronenphysik und Reaktortechnik
P.O.Box 3640, D-7500 Karlsruhe
West Germany

Abstract

Average neutron capture cross cross sections have been calculated in the unresolved resonance region for many actinides, with two different methods: (1) with energy-dependent neutron strength functions obtained from a spherical optical potential adjusted to ^{238}U data, radiation strengths from the giant dipole resonance model with global parameters, and width fluctuation corrections according to Tepel et al., (2) with constant neutron strength functions and energy-dependent radiation strengths, both from resolved resonances, and width fluctuation corrections according to Moldauer (1980). Results from the two methods are compared with each other and with experimental data.

1. Introduction

Evaluation of neutron capture cross sections in the unresolved resonance region must rely heavily on theoretical calculations where measured data are scarce, inaccurate or completely lacking. Two main avenues are open, (i) extrapolation from the resolved resonance region towards higher energies with the level-statistical model based on average parameters extracted from resolved resonances, (ii) utilisation of more global information embodied in an optical model for the neutron channels and in a giant dipole resonance model for the radiation channels. If fission competes significantly one also needs information on fission barrier parameters. Both avenues merge where average resonance parameters or transmission coefficients are inserted in a capture cross section formula of the Hauser-Feshbach type. We report here on our experiences in the actinide region with both avenues and on a convenient way to utilise both in a consistent manner.

2. Prediction with Global Systematics

An evaluation of neutron capture cross section data cannot be performed in splendid isolation. Consistency demands that all cross section types are evaluated in parallel. This is quite obvious in the resolved resonance region where the same resonance parameters appear in the reso-

nance formulae for all open channels connected by the same compound state. For essentially the same reason it is true also in the unresolved resonance region. The total cross section plays a key role in each case because (a) it constrains all partial cross sections, (b) it can be measured absolutely and (c) it can be calculated from the entrance-channel parameters alone. In the unresolved region these are the effective radius for potential scattering and the strength function, or, equivalently, the complex optical-model collision function. Moreover, the total cross section is the only observable data type that can be directly calculated from an optical model. In contrast the shape-elastic and the compound nucleus formation cross section are related to observable cross sections only via branching ratios and width fluctuation factors which require additional information.

In spite of this usefulness for consistent data evaluation the total cross sections of many actinides are quite badly known in the keV region. When we started evaluating Am and Cm data in 1977 there were no measured total cross sections at all for these nuclides, and the data for neighbor nuclei like ^{242}Pu, ^{240}Pu and ^{238}U differed widely below 100 keV although one expects, in the spirit of the optical model, that they are almost equal for nuclei so similar in nucleon numbers and other properties. We therefore looked for guidance from optical model calculations. Since the quality of the data did not warrant more sophistication a spherical potential was chosen. The global potential established by Wilmore and Hodgson [1], with energy-dependent real and imaginary potential depths V and W, Woods-Saxon form for V and derivative Woods-Saxon form for W was taken as a first guess. This was refined by adjustment to ^{238}U total cross section data below 15 MeV and checked against elastic and inelastic cross sections and angular distributions for ^{238}U, with the code ABACUS [2] and a modified form of HAUSER-4 [3], as described in [4]. The adjusted potential has the parameters

$$V = 47.01 \text{ MeV} - 0.267 \text{ E} - 0.00118 \text{ MeV}^{-1} \text{ E}^2 ,$$

$$W = 9.0 \text{ MeV} - 0.53 \text{ E} ,$$

$$R_r = 1.21 \text{ fm } A^{1/3} , \qquad R_i = 1.298 \text{ fm } A^{1/3} ,$$

$$a_r = 0.66 \text{ fm} , \qquad a_i = 0.48 \text{ fm} .$$

Figs. 1 and 2 show total and differential elastic cross sections calculated with this potential together with measured data. It should be noted that the experimental data by Phillips and Howe [5] in Fig. 1 became available only after the potential had been finalised.

Fission transmission coefficients for single-hump fission barriers were calculated as sums over Hill-Wheeler barrier penetrabilities [6]. For double-hump barriers the usual strong-coupling approximation [7] was employed, viz. addition of inverse penetrabilities for the two barriers to get the inverse total penetrability. The barrier heights and curvatures were obtained by fitting fission cross section data which, in contrast to total cross sections, existed in all cases of interest. The transition state densities needed for the summations were described

by a Fermi-gas formula with energy-dependent a-parameter, following Ignatyuk et al. /8/. This permitted a simpler description than the composite transition state densities recommended by Lynn /9/.

The capture transmission coefficients were calculated with Brink-Axel giant dipole resonance profiles according to the global prescription of Holmes and Woosley /10/ and width fluctuation corrections for all partial cross sections according to Tepel et al. /11/. An example of a capture cross section curve calculated along these lines with HAUSER-4 (KfK version) is shown in Fig. 3 together with results based on information from resolved resonances.

The first comparisons with experimental data and also evaluations seemed to indicate that these global calculations were not too reliable below 50-80 keV. As better data became available, e. g. the total cross sections of Phillips and Howe /5/ and especially those of Poenitz et al. /12/, confidence in the results grew. Furthermore, the level-statistical approach described in the next section gave very similar cross sections, showing that our global approach is reasonably consistent with information extracted from resolved resonances also below 50 keV.

3. Extrapolation with Level Statistics

Averaging R-matrix formulae over many resonances one finds the level-statistical equivalent to the optical-model collision function for a particle channel $c \equiv \{Jls\}$ as

$$\langle U_{cc}\rangle = e^{-2i\phi_c}\,\frac{1-\bar{R}_{cc}L_c^{o*}}{1-\bar{R}_{cc}L_c^{o}}\,, \qquad (1)$$

with

$$\bar{R}_{cc} = R_c^{\infty} + i\pi s_c \qquad (2)$$

where ϕ_c is the hard-sphere scattering phase, R_c the distant-level parameter (related to the effective radius), s_c the pole strength (proportional to the strength function) and otherwise conventional notation is used (cf. /13/). The corresponding transmission coefficient is

$$T_c \equiv 1 - |\langle U_{cc}\rangle|^2 = \frac{4\pi s_c P_c}{|1-\bar{R}_{cc}L_c^{o}|^2}\,, \qquad (3)$$

These equations are valid if direct reactions are negligible as is the case in the keV range. The transmission coefficients for photon and fission channels are essentially the ratios of the correponding average partial widths to the mean level spacing,

$$T_\gamma = 2\pi\frac{\langle\Gamma_\gamma\rangle}{D_c}\,, \qquad T_f = 2\pi\,\frac{\langle\Gamma_f\rangle}{D_c}\,. \qquad (4)\ (5)$$

Thus the transmission coefficients for Hauser-Feshbach calculations involve average resonance parameters which, at least for s-wave reactions, can be determined in the resolved-resonance region. For extrapolation into the unresolved region the strong energy dependence of the level

spacing must be taken into account, e. g. with the Gilbert-Cameron formula [14], whereas strength functions and the distant-level parameters can be taken as constant over energy intervals of 2-300 keV.

Such calculations, based on level statistics for specific nuclei, should be capable of reproducing individual cross sections better than global prescriptions. The results, however, cannot be better than the input. For instance the level spacings must be carefully corrected for missing levels (see [15]). Another unpleasant fact is that strength functions estimated from resolved resonances have large statistical errors caused by the large variance of the Porter-Thomas distribution, and thus may have only local significance. Even if samples of several hundred resonances are available, as e. g. for ^{238}U, the strength function uncertainty is of the order of 10% . In general, total cross sections predicted from level statistics were found to agree to about 3-10% with those from our optical model, while for capture cross sections the deviations were more like 5-20% . Fig. 3 shows an example.

4. Combined Approach

If good experimental data exist the results of the two avenues outlined above can be improved, of course. The following unified approach has proven to be both convenient and efficient from the upper end of the resolved resonance region up to at least 200 keV (for total cross sections up to 500 keV). Hauser-Feshbach cross section expressions with width fluctuation corrections are fitted to all available total, capture, fission and angle-integrated inelastic scattering cross section data simultaneously. The adjustable parameters are strength functions, distant-level parameters, radiation widths (for E=0, parity dependent), for the fission channels (JΠ-dependent) fission widths (for E = 0), degrees of freedom, barrier heights and curvatures. The mean s-wave level spacing (for E = 0) is another input number, from which mean spacings for the higher partial waves are automatically generated via the Bethe formula (cf. e. g. [14])

$$D_c^{-1} \propto \exp\left[-\frac{J^2}{2\sigma^2}\right] - \exp\left[-\frac{(J+1)^2}{2\sigma^2}\right] \qquad (6)$$

The energy dependence of strength functions and distant-level parameters is neglected. Width fluctuation factors are calculated following Moldauer [16] because in contrast to [11] his prescription works also for low energies and few (down to one) particle channels. Prior information from the resolved resonance region (s-wave parameters mainly) and from global systematics (optical-model strength functions and distant-level parameters for higher partial waves, fission barrier parameters etc.) in the form of starting values and associated uncertainties is injected into the fit via Bayes' theorem as explained in [17]: The prior probabilities for the parameters are taken as normally distributed around the starting values with standard deviations equal to the input uncertainties. The resulting extended least-squares formalism [17] is implemented in the FORTRAN code FITACS (Fit Average Cross Sections). The formalised inclusion of prior knowledge constrains parameter variations to reasonable domains and has dramatically improved convergence of the fits. The code

is a convenient evaluation tool capable of refining calculations based on global recipes, finding average resonance parameters that are consistent with both resolved and unresolved data and also the optical model, and generating complete sets of average cross sections in the unresolved resonance region for the KEDAK file. Fig. 4 shows the average capture cross section of ^{241}Am obtained in a FITACS fit using prior information from resolved resonances and from our optical model. The predictive power of the method can be seen from Fig. 5. It shows the inelastic scattering cross section curve obtained in a comprehensive fit to total, capture and inelastic scattering cross section data for ^{238}U prior to the precision measurement of Winters et al. [25] (also shown).

Acknowledgment

We thank the Fast-Breeder Project (PSB) and Dr. H. Küsters for support of this work and Dr. H. Jahn for stimulating discussions.

References

[1] P.E. Hodgson and D. Wilmore, Nucl. Phys. 55(1964)673
[2] E.H. Auerbach, BNL 6562 (prelim.), Brookhaven (1964); P.A. Moldauer, C.A. Engelbrecht and G.J. Duffy, ANL-6978 (1964); E.H. Auerbach and S.O. Moore, Phys. Rev. B135(1964)895
[3] F.M. Mann, HEDL-TME 76-80, Hanford (1976)
[4] U. Fischer, KfK 2907, Karlsruhe (1980)
[5] T.W. Phillips and R.E. Howe, Nucl. Sci. Eng. 69(1979)375
[6] D.J. Hill and J.A. Wheeler, Phys. Rev. 56(1953)1102
[7] J.E. Lynn, "Theoretical Methods for Calculating the Cross-Sections of Fissionable Nuclei" in "Nuclear Fission and Neutron-Induced Fission Cross-Sections", A. Michaudon (ed.), Oxford etc.(1981) p. 157
[8] A.V. Ignatyuk, G.N. Smirenkin and A.S. Tishin, Sov. J. Nucl. Phys. 21(1975)255
[9] J.E. Lynn, AERE-R-7468, UKAEA Harwell (1974)
[10] J.A. Holmes, S.E. Woosley, W.A. Fowler and B.A. Zimmermann, At. and Nucl. Data Tables 18(1976)306
[11] J.W. Tepel, H.M. Hoffman and H.A. Weidenmüller, Phys. Letters 49B(1974)1
[12] W.P. Poenitz, J.F. Whalen and A.B. Smith, Nucl. Sci. Eng. 78(1981)333
[13] A.M. Lane and R.G. Thomas, Rev. Mod. Phys. 30(1958)257
[14] A. Gilbert and A.G.W. Cameron, Can. J. Phys. 43(1965)1446
[15] F.H. Fröhner, Proc. Meeting on Uranium and Plutonium Isotope Resonance Parameters, INDC(NDS)-129/GJ, IAEA Vienna (1981), p. 102
[16] P. Moldauer, Nucl. Phys. A344(1980)185
[17] F.H. Fröhner, Proc. Conf. on Nuclear Data Evaluation Methods and Procedures 1981, BNL-NCS-51363, Brookhaven (1981), vol. I, p. 375
[18] R. Batchelor and J. Towle, Nucl. Phys. 65(1965)236
[19] L.W. Weston and J.H. Todd, Nucl. Sci. Eng. 61(1976)356
[20] D.B. Gayther and B.W. Thomas, Proc. Kiev Conf. on Neutron Physics, Moscow (1977), vol. 3, p. 3
[21] K. Wisshak and F. Käppeler, Nucl. Sci. Eng. 78(1980)148

[22] L.G. Strömberg and S. Schwarz, Nucl. Phys. 71(1956)511
[23] E. Barnard, A.T.G. Ferguson, W.R. McMurray and I.J. Heerden, Nucl. Phys. 80(1966)46
[24] F.Y. Tsang and R.M. Brugger, Nucl. Sci. Eng. 65(1978)70
[25] R.R. Winters, N.W. Hill, R.L. Macklin, J.A. Harvey and G.L. Morgan, Nucl. Sci. Eng. 78(1981)147
[26] M.R. Bhat (assembler), ENDF/B-V, MAT 1390, Brookhaven (1980)
[27] J.Jary, Ch. Lagrange and P. Thomet, INDC(FR)9/L, Bruyeres-le-Chatel (1977)

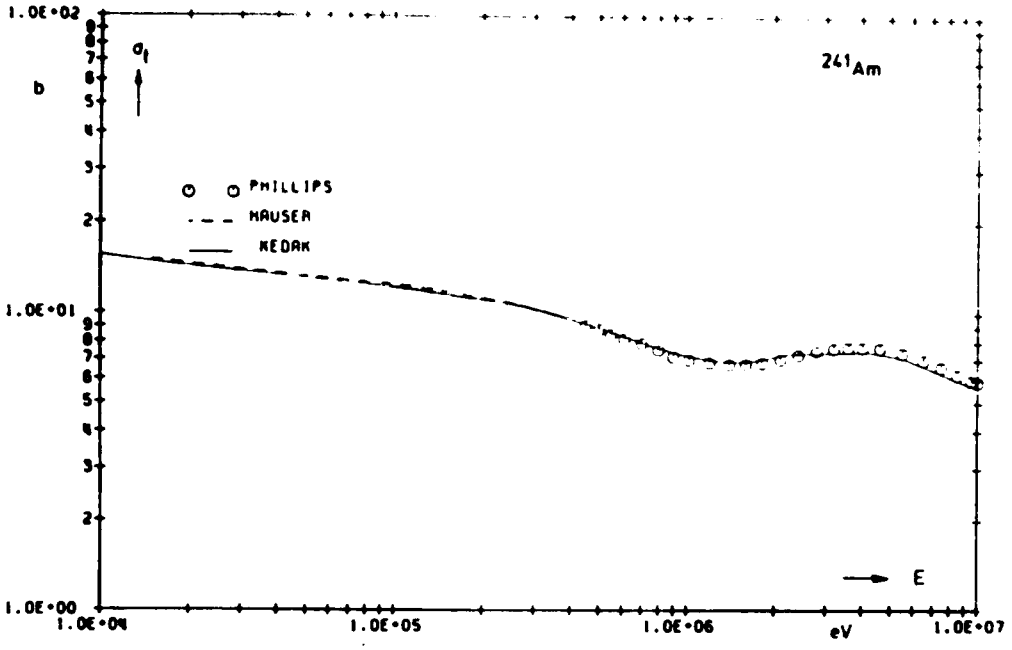

Fig. 1 - Predicted and measured [5] total cross sections for ^{241}Am+n. Above 200 keV the global HAUSER calculation was adopted for KEDAK, below it was replaced by a FITACS fit which includes information from resolved resonances and from unresolved fission and capture data (see Fig. 4).

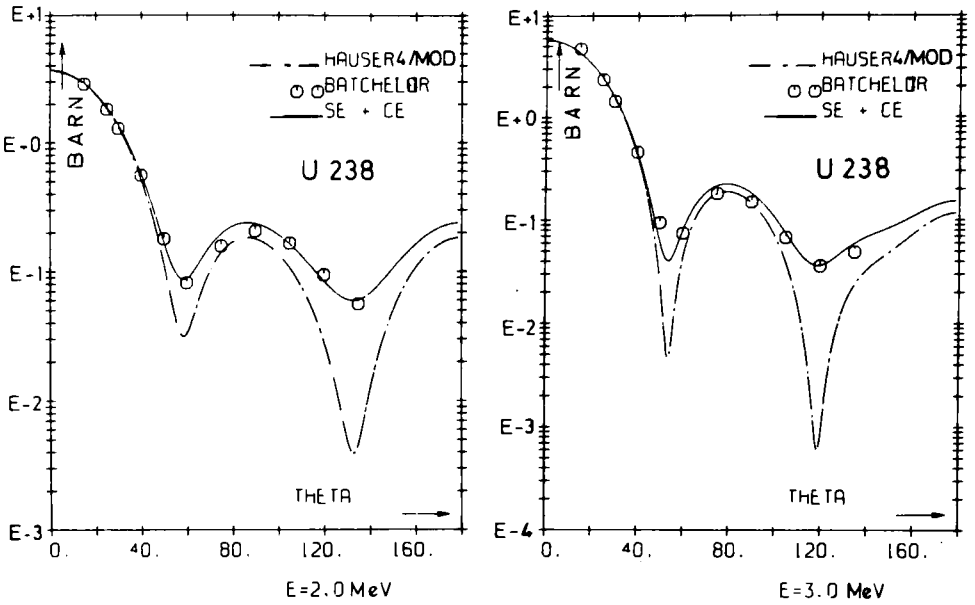

Fig. 2 - Calculated and measured [18] differential elastic scattering cross sections for ^{238}U. Curves labeled HAUSER4/MOD show shape elastic component alone, curves labeled SE + CE include compound elastic cross section (see [4]).

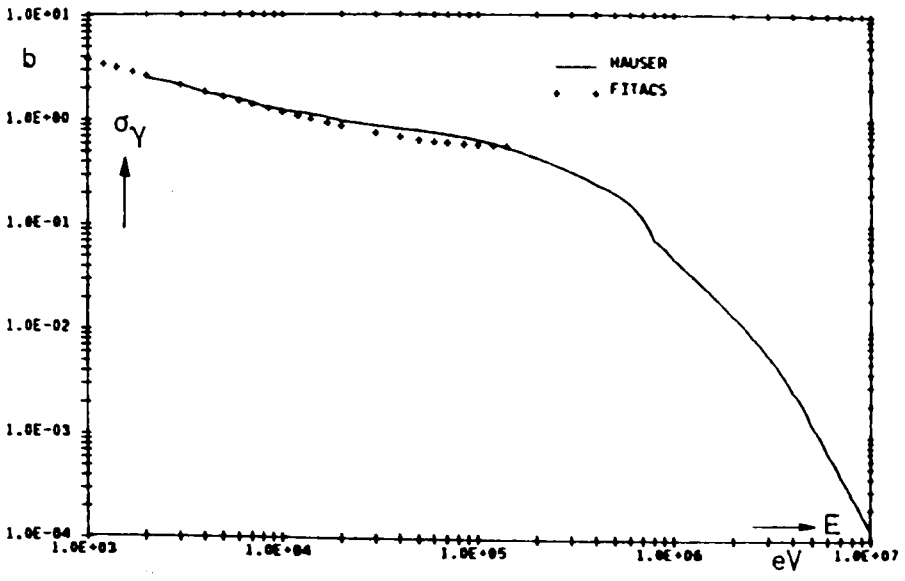

Fig. 3 - Calculated capture cross sections for $^{242m}Am+n$. HAUSER curve represents global prediction, FITACS points represent extrapolation from resolved resonance region which is also consistent with fission cross section data up to 100 keV.

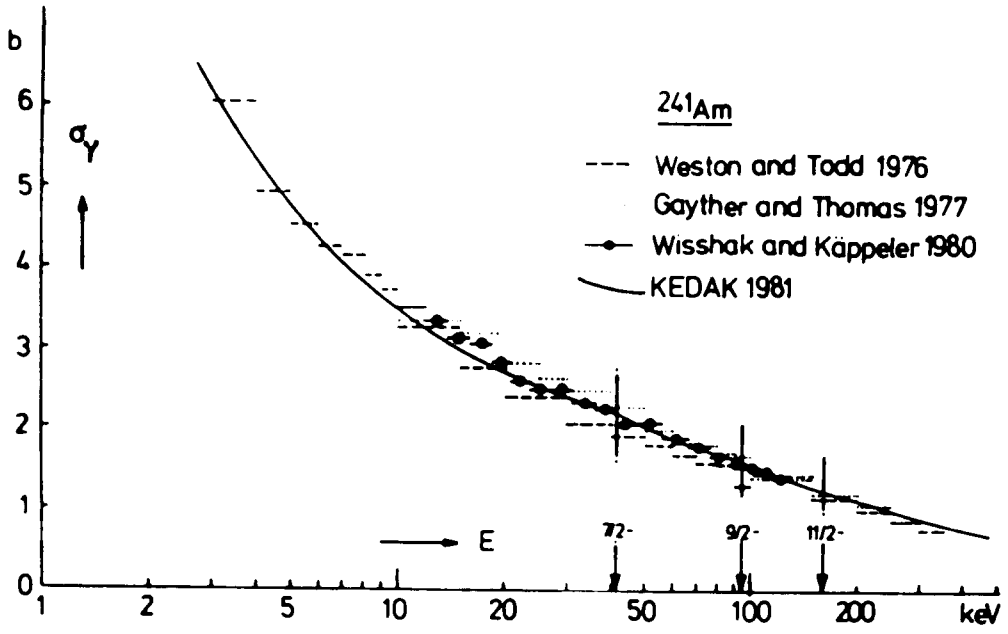

Fig. 4 - Measured capture cross sections for ^{241}Am+n [19-21] and FITACS fit. Note discontinuities of FITACS curve (labeled KEDAK81) at inelastic thresholds indicated by characteristics of residual excited levels.

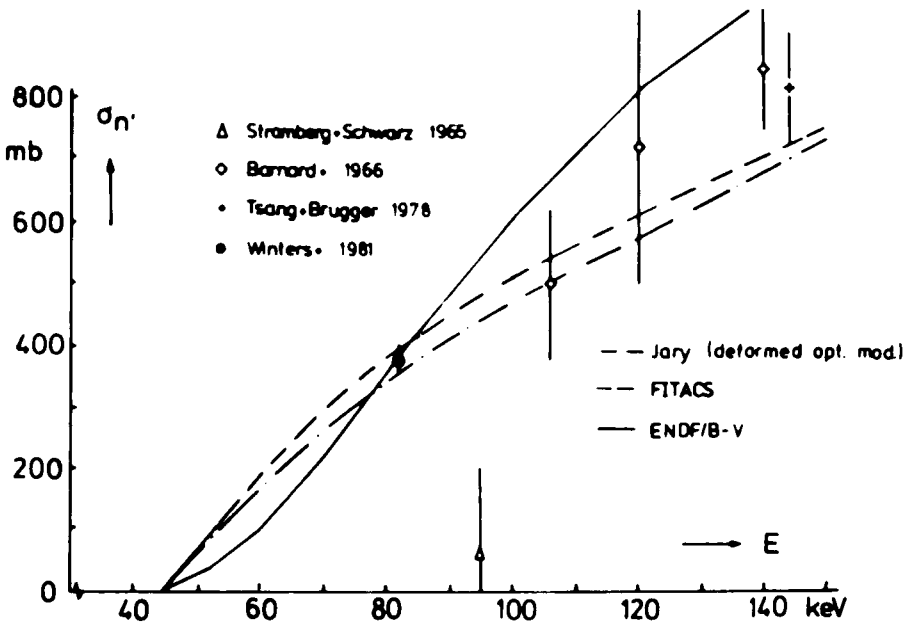

Fig. 5 - Measured [22-25], evaluated [26] and calculated [27] inelastic scattering cross sections of ^{238}U+n. FITACS curve representing fit to resolved resonance data and to unresolved total, capture and inelastic scattering data was calculated before result of Winters et al. became known.

Discussion

QUESTION: F. Corvi
Did I understand right that in your FITACS code the values of the strength functions are kept constant?

ANSWER: F. Froehner
They are adjusted, but their energy dependence is neglected - which is justified below ~ 200 keV as the figure with the ^{238}U strength functions illustrates.

QUESTION: E. Menapace
What governs the adjustment of mean parameters in the unresolved region by the FITACS code? Physical constraints should be taken such as of reproducing, within the error limits, the average parameters from resolved resonance statistics. Are these constraints included in the fitting algorithm?

ANSWER: F. Froehner
Yes, they are. The prior probabilities are taken as Gaussians with standard deviations equal to the uncertainties (1 σ) of the level-statistical parameters, e.g., $\bar{\Gamma}_\gamma$, extracted from the resolved resonance parameters (or obtained from optical-model calculations, if the prior knowledge comes from those).

QUESTION: A. B. Smith
A. Can you calculate the observed anisotropy of U-238 (n,n') at $\approx$ 82 keV as observed?

B. At 500-600 keV the U-238 (nn') cross section is $\approx$ 1.6 - 1.75. What is the result of your calculation at comparable energies?

ANSWER: F. Froehner
A. The FITACS code can calculate only angle-integrated elastic and inelastic scattering cross sections.

B. We did not calculate above 250 keV but, if I remember correctly, extrapolation to 500 keV of the curve below 250 keV indicates a value about 30% lower than those quoted by you.

THE USE OF ABAREX FOR NEUTRON CAPTURE CALCULATIONS

by

P. A. Moldauer
Argonne National Laboratory
Argonne, Illinois, USA

I. Introduction

ABAREX is an optical-statistical model program for the calculation of energy averaged neutron induced nuclear reaction cross sections. The program uses the optical model algorithm of ABACUS[1] and the statistical model method of NEARREX[2] with many improvements and modifications. The input and output are designed to be convenient for the user and the program utilizes dynamic storage allocation which avoids fixed limits on the sizes of the various arrays. The program requires 250K storage in the IBM 370 system in its present configuration. Additional storage can easily be made available. For optical model parameter fitting, the program uses the subroutine LMDIF1 of the MINPACK-1 package of subroutines for the solution of nonlinear least square problems.[3] No detailed description of the program will be attempted here. The capabilities and uses of the program will be outlined with special reference to neutron capture cross sections.

II. ABAREX INPUT

The input is arranged on uniform format card images. Meanings of the entries on each card are identified by keywords. All entries are defaulted and only those keyword cards whose entries change default values need to be entered. Information in the following categories can be entered.

1. Optical Model. Up to 15 parameters can be entered.

2. Discrete Target Levels. Energies, spins and parties.

3. Continuum Level Density. Temperature, energy shift and spin cut-off parameters.

4. Gamma Ray Channels. Can be described by transmission factors, by the strong coupling Weisskopf formula, or by specifying one giant dipole resonance energy and width. The latter two methods are normalized to slow s-wave $\Gamma\gamma/D$.

5. Fission or Other Competing Channels. Must be specified by transmission factors.

6. Statistical Model. Channel width fluctuation degrees of freedom can be entered or, for neutron channels, calculated from transmission factors by formula.[4]

III. ABAREX OUTPUT

The following cross sections and other measurable parameters can be calculated in ABAREX. A weighted chi-squared or least squares fit to data can be performed for any or all of the underlined quantities simultaneously and simultaneously at many energies by searching out some or all of the optical model parameters.

1. Total Cross Section.
2. Absorption Cross Section.
3. s and p Wave Strength Functions and R'.
4. Integrated and Differential Shape Elastic Cross Section.
5. Integrated and Differential Compound Elastic Cross Section.
6. Integrated and Differential Elastic Cross Sections.
7. Integrated and Differential Inelastic Cross Section to Individual or to Desired Combinations of Discrete Levels.
8. Integrated Inelastic Cross Section to Continuum Levels.
9. Gamma-ray Production.
10. Radiative Capture.
11. Fission and Other Cross Sections for which Transmission Factors are Supplied.

The radiative capture cross section is obtained by computing for the endpoints of the first gamma ray spectrum the probabilities of neutron remission from the compound nucleus and subtracting this from the gamma-ray production cross section.[5]

IV. A SAMPLE NEUTRON CAPTURE CALCULATION

The following pages reproduce a portion of the output of a capture calculation for ^{238}U from 0.02 MeV to 4 MeV which is based upon parameters used by W. Poenitz.[6] The first page reproduces the input deck. First there are two cards specifying the real and imaginary potentials, their depths, together with linear and quadratic energy dependences, radii in $rA^{-1/3}$ and diffusenessed. A 7 MeV real spin orbit potential is specified. Next is a LEVELS card that specifies 22 discrete levels and a continuum level density

starting at the highest discrete level and derived from a fermi gas temperature of 0.4 MeV, a shift of -0.25 MeV and a spin cutoff of 5.93. The energies, spins and parties of the 22 discrete levels follow. Next is a CAPTURE card whose entries are explained in the next portion of the output. The SCAN cards specify the energies at which calculations are to be made and the COMPUTE card initiates the computation.

Next on the first page of printout is a section that reproduces the input deck. Mass numbers and optical-model potential and integration parameters are printed, followed by parameters describing the radiation channels.

The next two pages reproduce the printout for the calculations at 1.0 and 2.0 MeV. In the second case parameters describing the target level continuum core printed. Among these is the total level density at the onset of the continuum, which is, useful for checking the reasonabless of the parameters. The excitation cross sections for all discrete levels are listed under a compound excitation.[9] All other integrated cross sections should be self-explanatory. Calculation and printout of angular distributions has been suppressed in this example.

In Fig. 1 the results of this calculation are compared with the data points drawn by Poenitz.[6] The solid heavy curve gives the capture cross section. The broken heavy curve gives the gamma ray production cross section. Above 1 MeV these calculations are uncertain because of the uncertainties in the gamma ray transmission strengths, the target level density, and the continuum level density which affects the difference between the gamma ray production and the capture cross section. Nevertheless it is possible that the difference in shape between the calculated and measured capture cross sections above 2 MeV indicates that the direct capture processes, which are ignored in these calculations, are beginning to be important.

REFERENCES

1. E. H. Auerbach, BNL-6562 (1962).

2. P. A. Moldauer, C. A. Engelbrecht, and G. J. Duffy, ANL-6978 (1964).

3. J. J. Mofe, B. S. Barbow, and K. E. Hillstrom, ANL-80-74 (1980).

4. P. A. Moldauer, Nucl. Phys., A344, 185 (1980).

5. P. A. Moldauer, Proc. Conf. Neutron Cross Section Technology, CONF-660303, Vol. 2, p. 613 (1966).

6. W. P. Poenitz in Nuclear Cross Sections for Technology, (U.S. Dept. of Commerce, 1980), p. 368.

ABAREX
======

INPUT DECK :

```
REAL      1   35.7920   -0.2500    0.0       1.4849    0.3368    7.0000    0.0
IMAG      4   22.9130    0.4000    0.0       1.3628    0.2087    0.0       0.0
LEVELS   22   92.0000    0.0       0.0       0.4000   -0.2500    5.9300    0.0
   0.0     0.0 1     0 1.00
   0.0449  2.0 1     0 1.00
   0.1480  4.0 1     0 1.00
   0.3080  6.0 1     0 1.00
   0.6800  1.0-1     0 1.00
   0.7320  3.0-1     0 1.00
   0.8270  5.0-1     0 1.00
   0.9270  0.0 1     0 1.00
   0.9310  1.0-1     0 1.00
   0.9500  2.0-1     0 1.00
   0.9660  7.0-1     0 1.00
   0.9660  2.0 1     0 1.00
   0.9930  0.0 1     0 1.00
   0.9980  3.0-1     0 1.00
   1.0370  2.0 1     0 1.00
   1.0550  4.0 1     0 1.00
   1.0600  2.0 1     0 1.00
   1.1060  3.0 1     0 1.00
   1.1270  4.0 1     0 1.00
   1.1290  2.0-1     0 1.00
   1.1680  4.0 1     0 1.00
   1.1690  3.0-1     0 1.00
CAPTURE 92    0.0011    4.8070   70.0000    0.0       6.6000   25.0000    4.0000
SCAN     1    0.0200    0.0200    0.1000    0.0       0.0       0.0       0.0
SCAN     1    0.2000    0.2000    2.0000    0.0       0.0       0.0       0.0
SCAN     1    2.5000    0.5000    4.0000    0.0       0.0       0.0       0.0
COMPUTE  0    0.5000  238.0510    0.0       0.0      -1.0000    0.0       0.0
```

MASS NUMBERS(TARGET/PROJECTILE) =238.051000/ 1.008665
==========

OPTICAL MODEL PARAMETERS : ASYMPTOPIA= 15.0000 FM 301 POINTS
==========

TYPE		DEPTH	(E)	(E*E)	RADIUS	DIFF.	VIVOL	C2
REAL	1	35.7920	-0.2500	0.0	1.4849	0.3368		
IMAG	4	22.9130	0.4000	0.0	1.3628	0.2087	0.0	0.0
S.O.	1	7.0000	0.0		1.4849	0.3368		

RADIATIVE CAPTURE INTO COMPOUND NUCLEUS
==========

A=239 Z= 92 N=147 4.807 MEV NEUTRON BINDING 70.00 RADIATIVE D. OF F. SIGMA= 4.000

NORMALIZED TO SLOW S-WAVE NEUTRON GAMMA WIDTHS/SPACINGS = 0.1142D-02

E1 GIANT RESONANCE AT 12.78 MEV WIDTH= 6.60 MEV EXCHANGE FRACTION=0.50

BLACK NUCLEUS SECOND CHANCE NEUTRON CHANNELS

NO.10 ENERGY(LABORATORY/C.M.) = 1.000000/ 0.995781 MEV LAMBDA-BAR = 0.45717 SQRT-BARN

NEUTRON CHANNEL WIDTH FLUCTUATION DEGREES OF FREEDOM ARE COMPUTED INTERNALLY.

TARGET LEVELS

LEVEL	GROUP	ENERGY	SPIN	PARITY	HEIGHT
1	1	0.0	0.0	1	1.00
2	2	0.0449	2.0	1	1.00
3	3	0.1450	4.0	1	1.00
4	4	0.3050	6.0	1	1.00
5	5	0.6000	1.0	-1	1.00
6	6	0.7320	3.0	-1	1.00
7	7	0.8270	5.0	-1	1.00
8	8	0.9270	0.0	1	1.00
9	9	0.9310	1.0	-1	1.00
10	10	0.9500	2.0	-1	1.00
11	11	0.9660	7.0	-1	1.00
12	12	0.9650	2.0	1	1.00
13	13	0.9930	0.0	1	1.00

MAXIMUM NEUTRON L VALUE,(RANGE OF TOTAL J VALUES) = 6, (0.5, 5.5)

INTEGRATED CROSS SECTIONS IN BARNS

TOTAL =	7.13709									
ABSORPTION =	3.60153									
SHAPE ELASTIC =	3.53556									
TOTAL ELASTIC =	4.47024									
COMPOUND EXCITATIONS =	0.93468	1.14024	0.56430	0.05430	0.32461	0.20578	0.00791	0.04172	0.03770	0.06193
	0.00000	0.04152	0.00438							
N-GAMMA =	0.13197									
RADIATIVE CAPTURE =	0.12382									
TOTAL COMPOUND =	3.60152									

NO.15 ENERGY(LABORATORY/C.M.) = 2.000000/ 1.991561 MEV LAMBDA-BAR = 0.32327 SQRT-BARN
==========

NO WIDTH FLUCTUATION CORRECTION

TARGET LEVELS
==========

LEVEL	GROUP	ENERGY	SPIN	PARITY	WEIGHT
1	1	0.0	0.0	1	1.00
2	2	0.0449	2.0	1	1.00
3	3	0.1480	4.0	1	1.00
4	4	0.3080	6.0	1	1.00
5	5	0.6800	1.0	-1	1.00
6	6	0.7320	3.0	-1	1.00
7	7	0.8270	5.0	-1	1.00
8	8	0.9270	0.0	1	1.00
9	9	0.9310	1.0	-1	1.00
10	10	0.9500	2.0	-1	1.00
11	11	0.9660	7.0	-1	1.00
12	12	0.9660	2.0	1	1.00
13	13	0.9930	0.0	1	1.00
14	14	0.9980	3.0	-1	1.00
15	15	1.0370	2.0	1	1.00
16	16	1.0550	4.0	1	1.00
17	17	1.0600	2.0	1	1.00
18	18	1.1060	3.0	1	1.00
19	19	1.1270	4.0	1	1.00
20	20	1.1290	2.0	-1	1.00
21	21	1.1680	4.0	1	1.00
22	22	1.1690	3.0	-1	1.00

TARGET LEVEL CONTINUUM STARTS AT 1.17 MEV

LEVEL DENSITY PARAMETERS: TEMP. = 0.400 MEV E0 = -0.250 MEV SIGMA = 5.930

AT 1.17 MEV, COMPUTED TOTAL LEVEL DENSITY = 86.82/MEV

OPTICAL MODEL CONTINUUM CHANNELS

MAXIMUM NEUTRON L VALUE,(RANGE OF TOTAL J VALUES) = 7, (0.5, 6.5)

INTEGRATED CROSS SECTIONS IN BARNS
==========

TOTAL =	7.30618									
ABSORPTION =	3.25889									
SHAPE ELASTIC =	4.04729									
TOTAL ELASTIC =	4.11952									
COMPOUND EXCITATIONS =	0.07223	0.11363	0.07508	0.01847	0.05009	0.04971	0.01449	0.02495	0.04343	0.04905
	0.00112	0.07348	0.02377	0.04019	0.06919	0.04039	0.06777	0.05631	0.03692	0.04188
	0.03494	0.03355								
CONTINUUM LEVELS =	2.17426									
N-GAMMA =	0.05398									
RADIATIVE CAPTURE =	0.03171									
TOTAL COMPOUND =	3.25889									

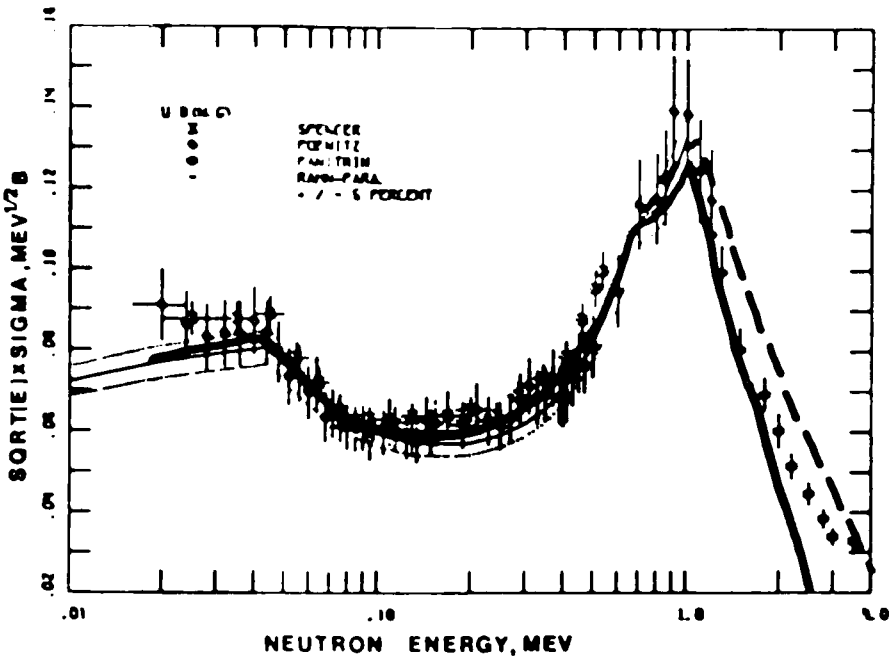

Fig. 1. ^{238}U Neutron Capture Data from Ref. 6. Heavy solid curve is calculated capture cross section. Dashed curve is gamma ray production cross section.

Discussion

QUESTION: D. Gardner
I have two questions concerning the (n;γ,x) correction to the capture cross section. First, does your latest code make the correction as it was done in your NEARREX code where for each Jπ compound state you determined the excitation energy at which

$$\Gamma_n^{J\pi} = \Gamma_\gamma^{J\pi}? \quad .$$

The second question is, do you include the (n;γ, fission) correction to the capture cross section in fissile nuclei?

ANSWER: P. Moldauer
ABAREX calculates the ratio of the probabilities for neutron and photon emission in 200 keV bins of the calculated first gamma ray spectrum. The answer to the second question is no.

QUESTION: F. Froehner
Is the optical potential used in ABAREX always taken as spherical?

ANSWER: P. Moldauer
Yes.

TOTAL γ-RAY SPECTRA AND ISOMERIC RATIO CALCULATIONS IN FAST NEUTRON RADIATIVE CAPTURE

by

Gianni Reffo
CSR "E.Clementel" E N E A Via Mazzini 2 Bologna
Italy

Abstract

Estimates of total γ-ray spectra and isomeric ratios have been attempted in the framework of the optical and statistical models for neutron radiative capture. The role of optical model, of Brink-Axel and Weisskopf assumptions as well as of the most important parameters have been investigated.
The results of these calculations satisfactorily agree with experimental information in all cases considered.
Spectra calculations were used in relative neutron capture measurements for correction of systematic uncertainties due to non-linear efficiency of the Moxon-Rae detector. Data on the calculated total γ-ray spectra and the corresponding integrated cross sections are shown for the isotopes investigated. The impact of parameters involved is discussed.

I. Introduction

Total spectrum of γ-ray emissions and total cross section for excitation of discrete levels via γ-decay is expensive information from the experimental as it is complex from the calculation view point. It is, however, required for: several fusion cross sections, where σ_m e σ_g are needed for various reactions; to solve branching problems in build-up chains in reactors and in nucleosynthesis studies in stars; for resonance and low-level spin assignments; etc.

Recently [1-3] spectra calculations have been used to correct systematic uncertainties due to the non linear efficiency of Moxon-Rae detectors.

One of the earliest attempts to give a detailed description of the γ-cascade process was made with the CASCADE code by Poenitz [4] in 1966. Renewed interest, in view of the increasing importance of this information has led to careful studies of model parameterization and the energy dependence of γ-ray intensities [5-8].

In this paper results of recent calculations [1-3] are summarized and spectra analyses for different parameter and model assumptions are briefly discussed.

II. The model and the code

The cascade model adopted has been illustrated in detail in ref. 1,2 and will be described here only briefly. Continuum bands are treated like discrete levels. For each band spin and parity dependent branching ratios are calculated allowing for the competition between E1,M1,E2 transition probabilities which are estimated according to Lorentz curve approximations to the respective giant resonances(GR)and using a Gilbert-Cameron [9](GC) level density formula,as parameterized in ref. (5).

A split GR model is used for E1 photon absorption, the Lorentzian parameters being taken from the systematics of ref.(5). Parameters for M1 and E2 Lorentz formulae are also taken from systematics (see ref. 3).

The experimental branching ratios are used for discrete levels. Missing ones are estimated assuming single particle state transitions (with E1,M1 transitions dominating) for spherical nuclei and assuming collective transitions (with E2 transitions dominating) for collective nuclei.

These calculations were performed with our modular master code the IDA MODULAR SYSTEM. It is capable of calculating integrated and differential cross sections for all reactions possible up to $\sim$ 50 MeV incident energies including most reaction mechanisms, whatever the projectile. As a particular option γ-ray cascades may be started at any step of the multiple particle cascading emission.

The main effort of the code is on organization. Cascade events are simultaneously ordered in as many different ways as there are purposes of the code i.e. according to a) stories with the same number of steps in the cascade (which allows for calculating cross sections of each γ-ray multiplicity and the corresponding partial spectra); b) cascades feeding levels a priori marked (for calculating excitation cross sections of marked levels, corresponding spectra and isomeric ratios, IR); c) emitted γ energy bands, where single-step contributions are lumped according to the respective γ-ray energies (for total γ-ray spectra calculations); d) initially a),b),c) are given for any $J\Pi$ couple of the initial decaying level (this can be useful in several investigations e.g. either to isolate a),b),c) for given incident angular momentum,l, when the initial level is a compound nucleus one; or to estimate a),b),c) for a given $J\Pi$ couple; etc.).

III. Some results

In the frame of a cooperation with the Van de Graaff group of KFK Karlsruhe an attempt has been made to correct systematic errors of fast neutron capture measurements due to the efficiency of Moxon-Rae detectors used, which is not exactly proportional to γ-ray energy.

The isotopes investigated were ^{93}Nb, ^{103}Rh, ^{181}Ta, with respect to ^{197}Au standard, and ^{241}Am, ^{240}Pu, ^{242}Pu with respect to both ^{197}Au and ^{238}U standards. (Detailed description of experimental conditions and of calculation methods and results are given in ref. 1-3 and in other contributions to this meeting [10-11]). To this end spectra calculations were performed for all target and standard isotopes.

In order to achieve best calculation accuracy much care was devoted to the involved model parametrization. In particular, optical model parameters were determined by fitting experimental data for: strength functions S_o, S_1, S_2; scattering radius R; σ_T and neutron inelastic excitation of discrete levels. Level density parameters were deduced from mean spacing, D_{obs}, of neutron resonances and from the distributions of discrete levels according to their quantum characteristics. Finally, partial calculation results, like total radiative width $\Gamma_\gamma(Bn,J,\Pi)$ at the neutron binding Bn, total $\sigma_{n,\gamma}$, σ_T, $\sigma_{n,n'}$ and IR, where possible, were compared to the corresponding experimental quantities, in order to verify the validity of adopted parameters. Calculations were tested in the whole energy range where experimental data were available.

In fig. 1,2 calculated neutron captures, total γ-ray spectra and isomeric ratios are compared to the experimental data.

In all cases calculated neutron capture compares satisfactorily with the experimental data. In ^{93}Nb a 5% valence contribution must be added at 10 KeV, which vanishes at 50 KeV. The calculated spectrum for ^{198}Au also compares reasonably well with experiment, particularly in the softer part; in the case of ^{182}Ta the comparison appears better in the harder part of the spectrum. The calculated isomeric ratio vs En for $^{241}Am(n,\gamma)$ compares well with the measurements, in absolute values, but fails with the experimental energy trend. This may be due to large deficiencies in the discrete level scheme (a large number of discrete levels are missing and branching ratios are not known).

In the case of U and Pu spectra, dashed lines give the contribution of E1 transitions which prove a large M_1+E_2 contribution.

On the whole it was found that when ^{238}U is used as a standard the correction arising from systematic errors is negligible in the case of ^{240}Pu, ^{242}Pu targets. On the contrary a correction factor of 3% has to be applied for Pu, ^{241}Am and ^{181}Ta targets when ^{197}Au standard is used.

Negligible correction was found for ^{93}Nb, ^{103}Rh targets with ^{197}Au standard.

IV. Role of relevant parameters

a) Optical model parameters

The optical model affects especially those calculations (like for IR determination) where the population probability of initial levels of given spin plays an important role and may be strongly influenced by the relative magnitude of strength functions (see ref. 2).

b) Giant resonance parameters (GRP)

GRP are involved only in the decay of continuum levels, where in most

cases only one type (among E1,M1,E2) of transition dominates in each branching ratio. M1 or E2 transitions play their role when the other two types are forbidden. As a consequence Lorentzian curve parameters do not greatly influence these calculations because they all tend to cancel out in the branching ratios, whenever γ-ray energies are smaller than the giant resonance peak energy.

For higher emitted γ-ray energies only peak energy (which is the best known) is expected to affect calculations.

c) Level density parameters

The result of γ-ray cascade calculations greatly depends on the level density and level schemes adopted.

In spite of the encouraging success of recent investigations (especially BCS), the corresponding model parametrizations do not yet offer the same confidence level as the systematics for the GC [9] level density here adopted.

A theoretical support for the last mentioned approach comes from BCS studies [12], according to which use of two different formulae becomes necessary, neglecting the energy dependence of parameter a. As an example the typical two-slope trend predicted by BCS for a vs E is shown for ^{135}Ba in fig. 3.

One observes a fast linear energy increase of a vs E below the neutron binding, B_n. This roughly corresponds to excitation energy range of the constant nuclear temperature level density GC approach, which is characterized by an exponential increase with energy.

Above B_n, after a fast change of slope,the energy trend of "a" becomes asymptotic. This range corresponds to the one where the Fermi gas formula of GC is applied (which is also characterized by a slower increase with energy). In addition the flat behaviour of a vs E above B_n gives credit to the practice of extrapolating the validity of the a-parameter (as determined from D_{obs}) to the whole energy range above B_n.

The effect of the spin distribution of level density was tested on ^{241}Am calculations , by reduction of the spin cut off factor by a factor of 2. This produced only slight effects with a shift of the spectrum toward the soft part. In addition an increase in IR of 5% was observed.

As far as the low energy region is concerned large difficulties arise where discrete level information is missing (like energy levels, their quantum characteristics or branching ratios).

In the case of the spectrum for gold we have investigated the impact of the following assumptions: (i) all known levels (28,in all, up to .571 MeV) are neglected, and replaced by the level density treatment ; (ii) all discrete levels have been included but experimental branching ratios are replaced by theoretical estimates according to sec. II.

The resulting spectra, dashed and dotted histograms, respectively, are given in fig. 4 together with the result of the standard calculation, full line.

As can be observed from the figure,hypothesis i) is much too crude and introduced severe changes in the energy trend of the spectrum. On the contrary hypothesis ii) does not appreciably influence the final result.

In the case of Americium the influence of the discrete level scheme on IR (here=$\sigma_g(n,\gamma)/\sigma(n,\gamma)$) calculations has been investigated at 30 KeV, where a

value IR=.75 is obtained from standard calculations.

Skipping half of the discrete level we got IR=.69, while, by skipping the complete level scheme we obtained IR=.5.

No significant difference was observed through replacing E2 collective transition probabilities by E1,M1 single particle transition probabilities.

d) Effect of width fluctuations

It was assumed that width fluctuations effects influence only the primary γ-ray spectrum. An investigation of the width fluctuation correction on the primary γ-ray spectrum leads the conclusion that (exception made for very weak transitions which are strongly enhanced) single transition probabilities are affected by correction factors very close to that of the corresponding integral cross section.

Thus the whole spectrum is uniformly shifted by width fluctuation correction factor.

e) Energy dependence of γ-ray intensities

Essentially one has three types of energy dependence for E1 transitions: i) E_γ^3 according to Blatt-Weisskopf single particle transitions, ii) E_γ^5 according to Axel, iii) E_γ^7 according to Dover et al.[13], Arenhovel et al.[14], Gardner et al.[8].

Recently McCullagh et al.[7] found experimental evidence for an $\sim E_\gamma^{5.5}$ energy dependence, while Raman [6] verified that validity of the Brink-Axel hypothesis has only a few exceptions.

The impact of the above three assumptions has been investigated in the total spectrum calculation of gold where measurements are available from ref.[15]. To this end fig. 20 of ref.(8) is here reproduced as fig.(5) where we have plotted, for comparison, our results (hystograms). The data in fig. 5 correspond to the following incident neutron energies: experimental ones are measured in the interval .2 ÷ .6 MeV, the two full line curves have been calculated [8] at .2 and .6 MeV, while the hystograms at .4 MeV. (It should be noted that the spread of neutron energies ΔE=.4 MeV may affect the comparison of present calculations especially in the last hystogram step).

One observes that the spectrum from our E_γ^5 -calculation ,full line hystogram, well agrees with the Gardner et al.[8] spectrum except for the hard part. This seems in contradiction with the wrong trend of the E_γ^7 - calculation (dotted hystogram) which clearly favours the hard tail against the soft one, as expected.

Except for the hard tail of the spectrum,no remarkable difference is observed between E_γ^5 - and E_γ^3 - calculations (dashed hystogram).

On the whole, one may conclude on the better results of the E_γ^5 - law, in agreement with the mentioned experimental investigations.

As far as M1 and E2 transitions are concerned, there is not sufficient information for a more than tentative treatment.

Finally it must be noted that only the Brink-Axel approach allows for absolute calculations of $\Gamma_\gamma(B_n,J,\Pi)$, as shown in ref. (16),(17), provided correct parametrization is adopted for both the level density and Lorentz-curve.

Conclusions

Spectra and IR calculations are valuable in view of the need for them in a number of applications and of the measurement difficulty in the fast neutron energy region.

Recently, spectra calculations offered appreciable help in correcting systematic errors of relative neutron radiative capture measurements made with Moxon-Rae detectors.

A number of recent experiments proves the validity of basic assumptions adopted for the energy dependence of γ-ray intensities.

A weak point of these calculations remains however the determination of reliable level schemes and inherent γ-ray branchings when these are not measured. In fact, the considerable theoretical efforts in these directions proved very useful in understanding nuclear structure, but cannot yet replace all cases where experimental information is missing. A possible improvement of present calculations may be obtained by the introduction of considerations of rotational bands in order to fill the gaps in level schemes and introducing K-selection rules in the γ-ray transitions [18].

In view of these difficulties,stress should be laid on the need for experts to provide cross section evaluators with appropriate level schemes, at least for the cases of recognized interest.

References

1) Wisshak K., Wickenhauser J., Käppeler F., Reffo G., Fabbri F., accepted by Nucl.Sc.Eng.
2) Reffo G., Fabbri F., Wisshak K., Käppeler F., accepted by Nucl.Sc.Eng.
3) Reffo G., Fabbri F., Wisshak K., Käppeler F., submitted to Nucl.Sc.Eng.
4) Poenitz W.P., Z.Phys. 197(1966)262.
5) Reffo G., IAEA Report SMR-43(1980) p.205. Lecture held at the "Winter Course on Nuclear Physics and Reactors" at ITCP Trieste, 17 Jan.- 10 Mar. 1978.
6) Raman S., invited paper at IV Int. Symposium on Neutron Capture Gamma-Ray Spectroscopy and Related Topics, Sept.7-11, 1981, Grenoble.
7) McCullagh C.M., Stelts M.L., Chrien R.E., Phys. Rev. 23, 1394, (1981).
8) Gardner D.G., Gardner M.A., Dietrich F.S., Report UCID-18759, August 7, 1980 and in Nuclear Cross Sections for Technology, edited by J.L. Fowler, C.H. Johnson and C.D. Bowman (NBS (Special Publication No.594), Washington,D.C.,1980).
9) Gilbert A., Cameron A.G.W., Can.Journ. of Phys., 43 (1965)1446.
10),11) Wisshak K., Käppeler F., Reffo G., Fabbri F., contributions to this meeting.
12) Maino G., p.c. 1982.
13) Dover C.B., Lemmer R.H., Halme F.J.W., Ann. Phys. (N.Y.) 70 (1972) 458.
14) Arenhovel H., Grainer W., Danos M., Phys. Rev. 157 (1967) 109.
15) Morgan G., Newman E., Report ORNL-TM-4973, August 1975.

16) Benzi V., Reffo G., Vaccari M., IAEA Report 169, 123 (1974).
17) Johnson C.H., Phys.Rev. C16,2238 (1977).
18) Lynn J.E., "Current Perspective on Statistical Models of Nuclear Reactions", invited review paper presented at IV Int. Symposium on Neutron Capture Gamma-Ray Spectroscopy and Related Topics, Grenoble, Sept. 7-11, 1981.

Figure Captions

Fig. 1 Calculated total neutron capture cross sections and total γ-ray spectrum at .1 MeV for ^{93}Nb, ^{103}Rh, ^{181}Ta are compared with experimental data and with previous evaluation. Total γ-ray spectrum for gold is also given.

Fig. 2 Like fig. 1 for ^{240}Pu, ^{242}Pu, ^{241}Am. Total γ-ray spectrum for ^{238}U is also given.

Fig. 3 Energy trend of level density parameter a vs excitation energy E_c as predicted by BCS approach. Dashed curve is obtained with an empirical fit $a=\tilde{a}\{1-\exp-(\gamma E_c)\}$ where $\tilde{a}$ is asymptotic value and γ is a free parameter.

Fig. 4 Standard calculation of total γ-ray spectrum of gold at 1 KeV is compared with calculations obtained skipping all discrete levels (dashed) and skipping only all experimental branching ratios (dotted).

Fig. 5 Comparison of the capture γ-rays spectrum of gold with neutrons from .2 to .6 MeV [15] with calculations of Gardner et al.[8] at these two energies, full curve, and with present calculations (hystograms) according to an E^{3}- (dashed), E_{γ}^{5}- (full line), E_{γ}^{7}- (dotted) laws for γ-ray intensities.

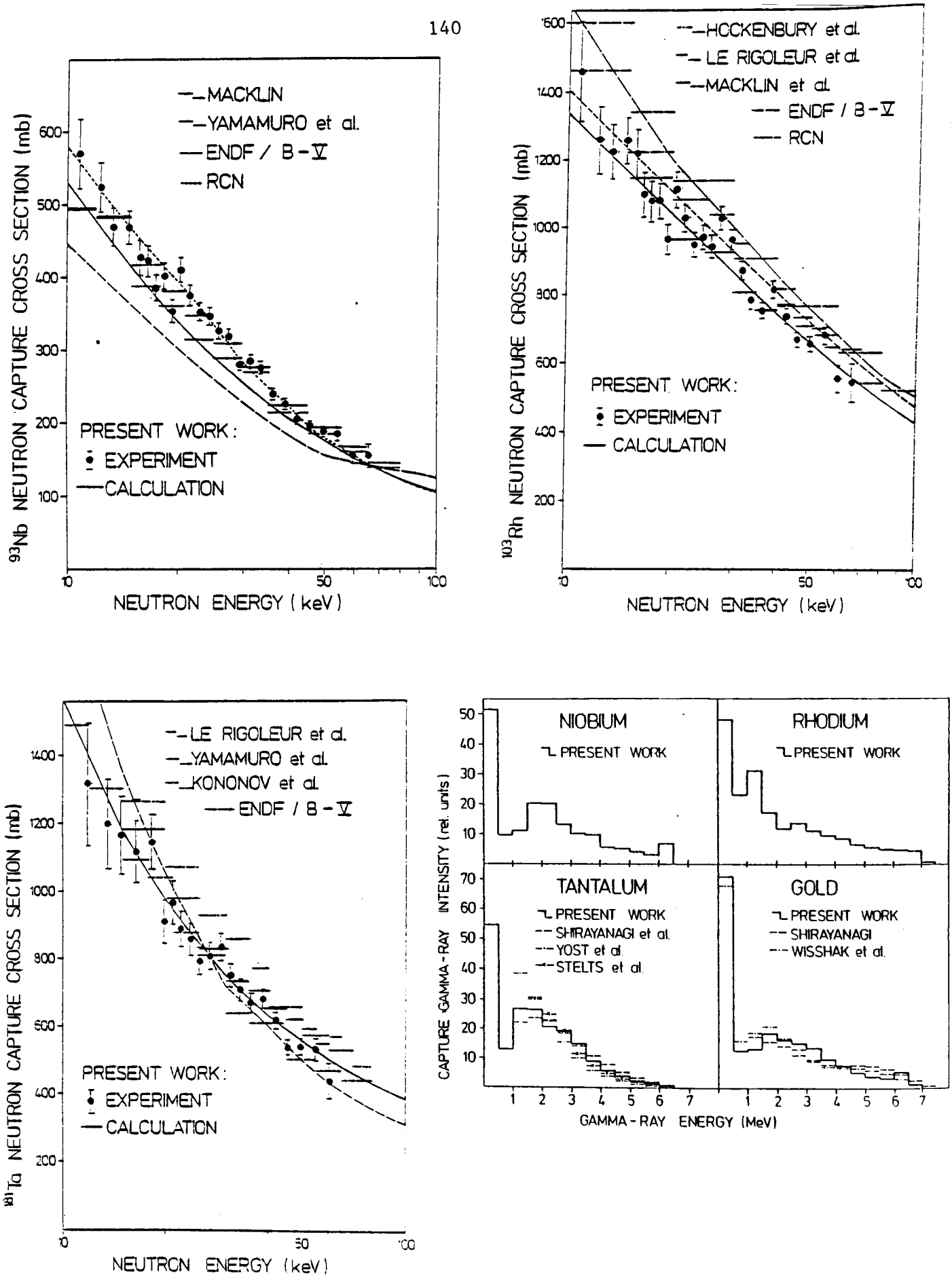
MACKLIN
YAMAMURO et al.
ENDF / B-V
RCN
PRESENT WORK:
EXPERIMENT
CALCULATION
93Nb NEUTRON CAPTURE CROSS SECTION (mb)
NEUTRON ENERGY (keV)
HOCKENBURY et al.
LE RIGOLEUR et al.
MACKLIN et al.
ENDF / B-V
RCN
PRESENT WORK:
EXPERIMENT
CALCULATION
103Rh NEUTRON CAPTURE CROSS SECTION (mb)
NEUTRON ENERGY (keV)
LE RIGOLEUR et al.
YAMAMURO et al.
KONONOV et al.
ENDF / B-V
PRESENT WORK:
EXPERIMENT
CALCULATION
181Ta NEUTRON CAPTURE CROSS SECTION (mb)
NEUTRON ENERGY (keV)
NIOBIUM
PRESENT WORK
RHODIUM
PRESENT WORK
TANTALUM
PRESENT WORK
SHIRAYANAGI et al.
YOST et al.
STELTS et al.
GOLD
PRESENT WORK
SHIRAYANAGI
WISSHAK et al.
CAPTURE GAMMA-RAY INTENSITY (rel. units)
GAMMA-RAY ENERGY (MeV)

Fig. 1

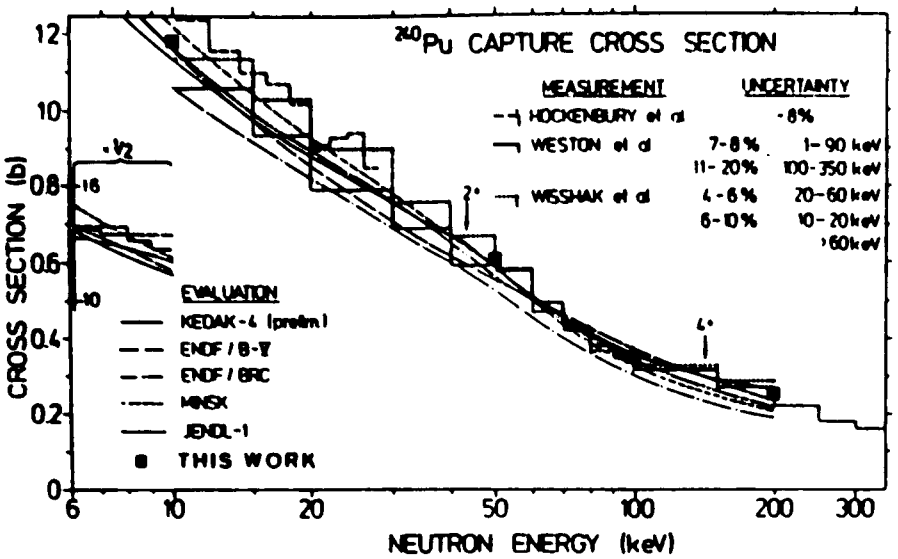
240Pu CAPTURE CROSS SECTION
MEASUREMENT
UNCERTAINTY
HOCKENBURY et al
-8%
WESTON et al
7-8% 1-90 keV
11-20% 100-350 keV
WISSHAK et al
4-6% 20-60 keV
6-10% 10-20 keV
>60 keV
EVALUATION
KEDAK-4 (prelim)
ENDF/B-V
ENDF/BRC
MINSK
JENDL-1
THIS WORK
CROSS SECTION (b)
NEUTRON ENERGY (keV)

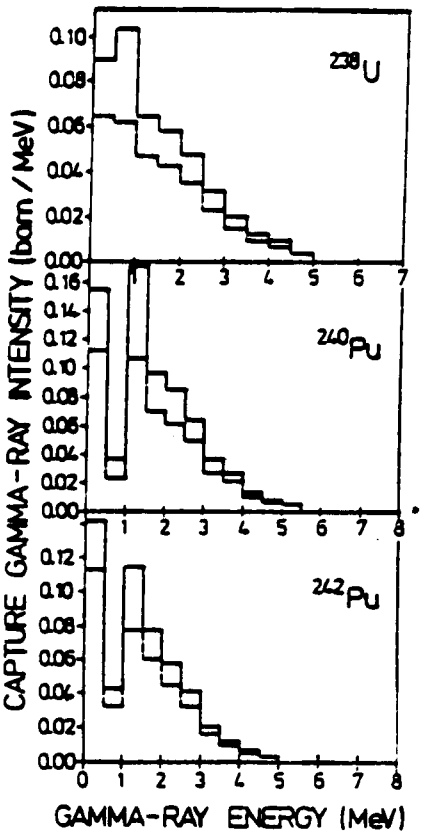
238U
240Pu
242Pu
CAPTURE GAMMA-RAY INTENSITY (barn/MeV)
GAMMA-RAY ENERGY (MeV)

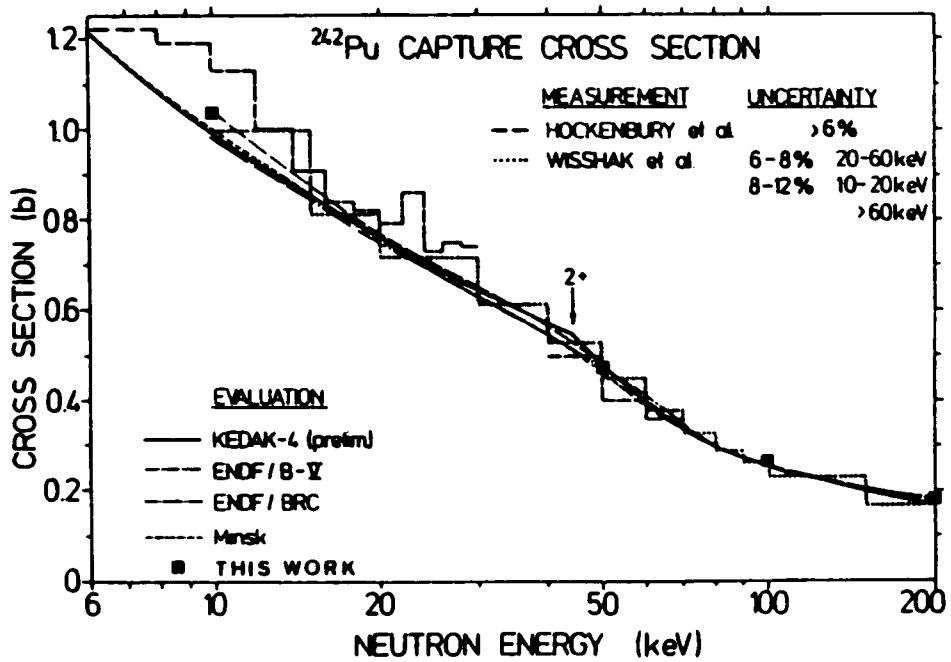
242Pu CAPTURE CROSS SECTION
MEASUREMENT
UNCERTAINTY
HOCKENBURY et al
>6%
WISSHAK et al
6-8% 20-60keV
8-12% 10-20keV
>60keV
EVALUATION
KEDAK-4 (prelim)
ENDF/B-V
ENDF/BRC
Minsk
THIS WORK
CROSS SECTION (b)
NEUTRON ENERGY (keV)

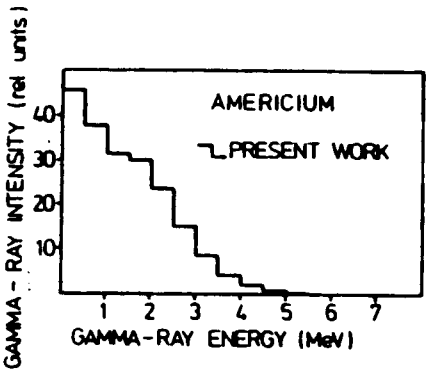
AMERICIUM
PRESENT WORK
GAMMA-RAY INTENSITY (rel units)
GAMMA-RAY ENERGY (MeV)

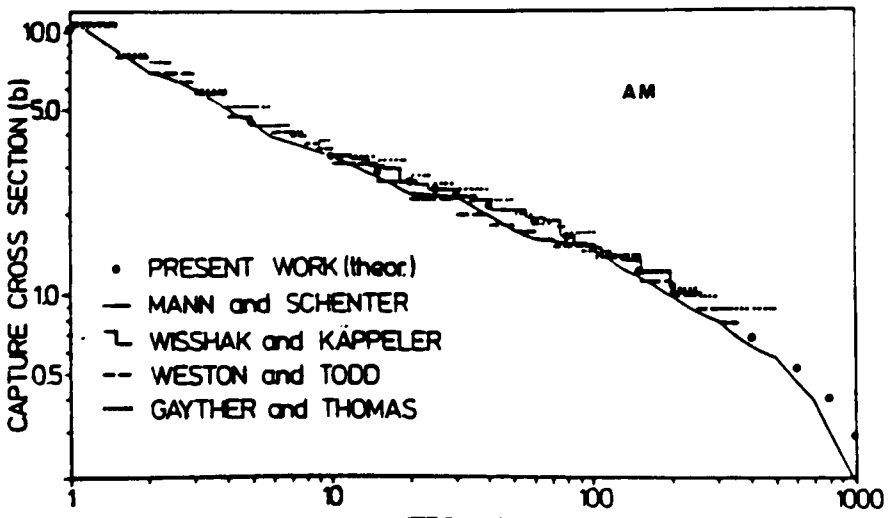
AM
PRESENT WORK (theor.)
MANN and SCHENTER
WISSHAK and KÄPPELER
WESTON and TODD
GAYTHER and THOMAS
CAPTURE CROSS SECTION (b)

Fig. 2

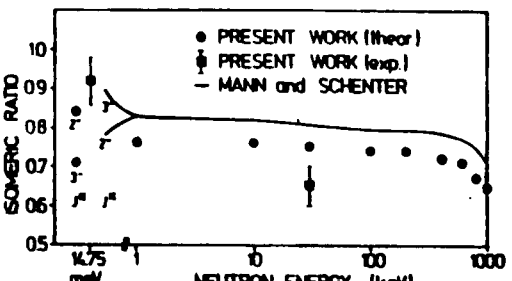
PRESENT WORK (theor.)
PRESENT WORK (exp.)
MANN and SCHENTER
ISOMERIC RATIO

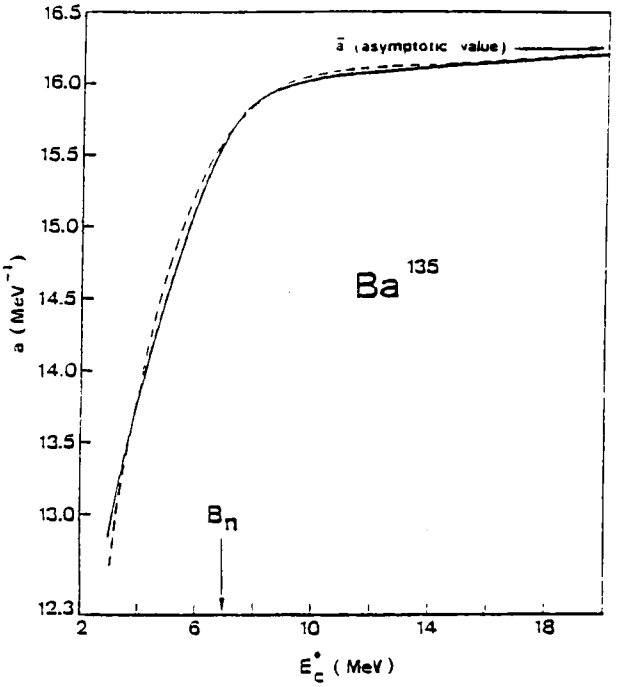
ā (asymptotic value)
Ba 135
Bn
a (MeV⁻¹)
E*c (MeV)

Fig. 3

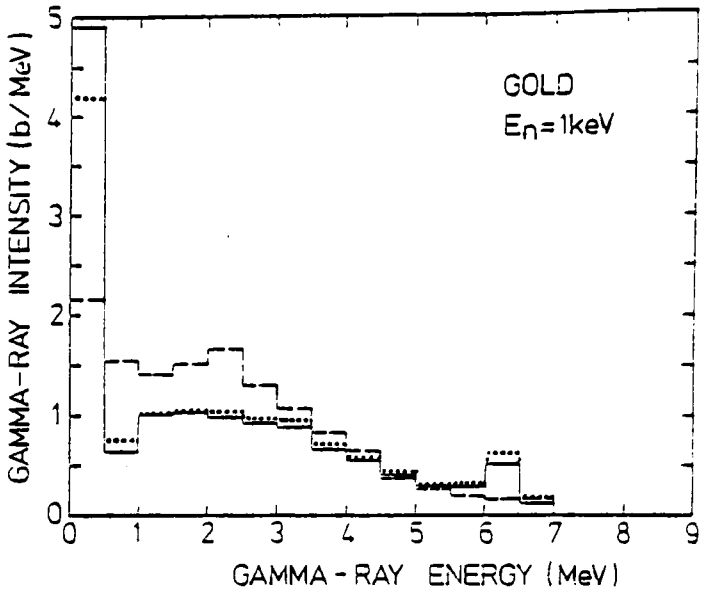
GOLD
En = 1keV
GAMMA-RAY INTENSITY (b/MeV)
GAMMA - RAY ENERGY (MeV)

Fig. 4

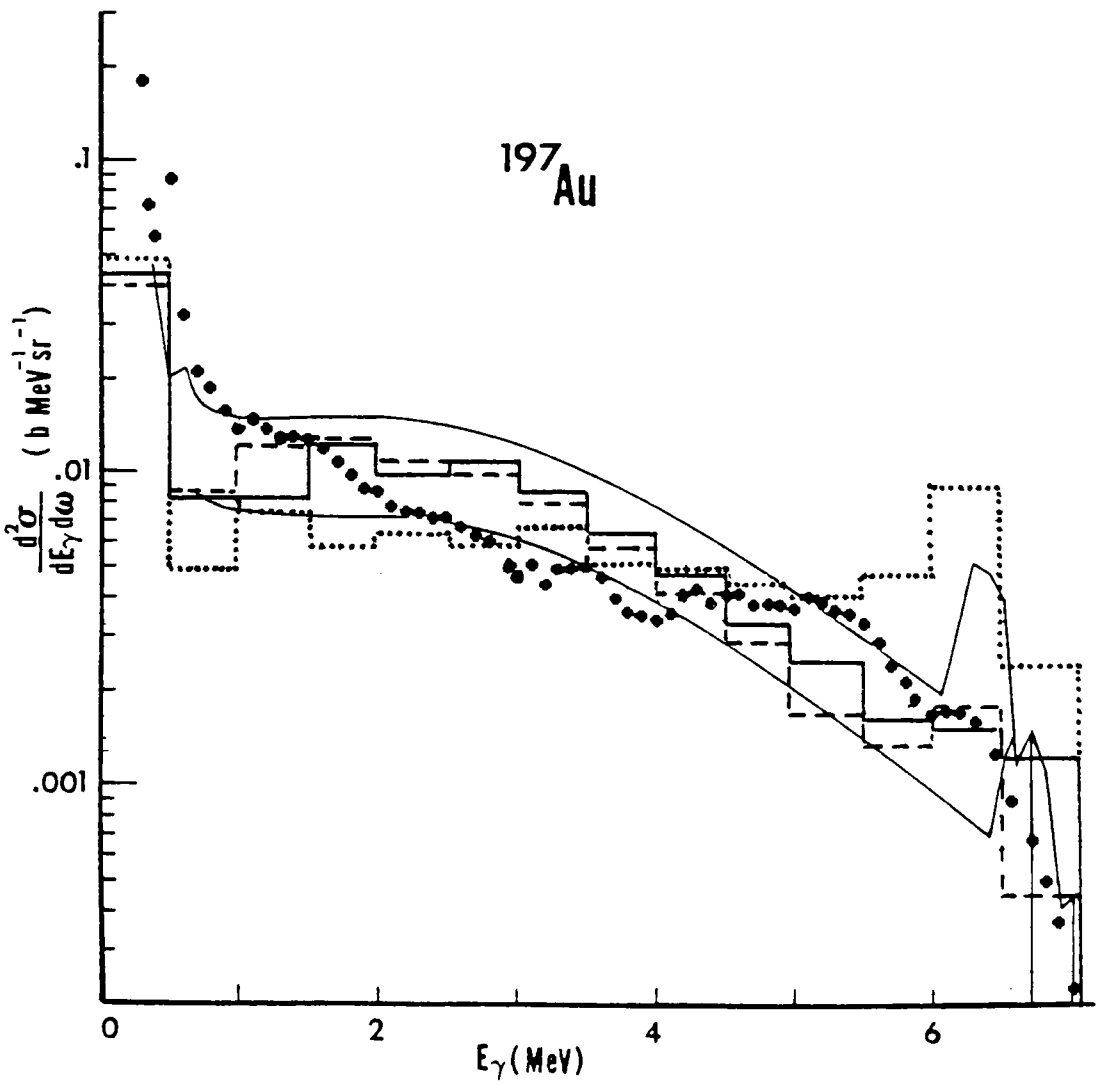
197Au
d²σ/dEγdω (b MeV⁻¹ sr⁻¹)
Eγ (MeV)

Discussion

QUESTION: S. Mughabghab
What is the sensitivity of the isomeric-cross-section calculations to the level density parameter?

ANSWER: G. Reffo
Lowering the spin cutoff by a factor of 2 in the whole excitation energy range, increases the ^{241}Am results by $\approx$ 5%. More details are given in the text.

QUESTION: R. Schenter
Did you calculate Isomeric Ratio Capture for ^{241}Am?

ANSWER: G. Reffo
Yes - See text.

QUESTION: D. Gardner
How do you parameterize the E2 strength in your gamma-ray model? Do you use the systematics for the isoscalar giant-quadrupole resonance?

ANSWER: G. Reffo
I use the systematics of Bertrand (reference in the Text). In any case, far from the peak energy the giant-resonance parameters do not play an important role. This is also discussed in the text.

THE GOLD STANDARD CAPTURE CROSS SECTION FROM 100 keV to 15 MeV

T B Ryves
National Physical Laboratory
Teddington, Middlesex, UK

Abstract

The capture cross section of gold is now generally accepted as the principal reference standard, and therefore in this review only gold is considered. Recent measurements of the gold capture cross section in the unresolved region are discussed and compared with the ENDF/B-V evaluation. It is concluded that in the energy interval 100-2000 keV the present uncertainty in the evaluation is ±8%, in the interval 2-3.5 MeV the uncertainty is ±4%, in the interval 3.5-14 MeV more measurements are needed before a realistic error can be assigned, and from 14 to 15 MeV the uncertainty is ±10%. Several recommendations for future work have been made.

I. Introduction

No other capture cross section more suitable as a standard than that of gold has been found, and none is better known, and so in this review only that of gold will be considered. The capture cross section of gold has become one of the basic standards because of its monoisotopic nature, its chemical stability and the simple decay scheme of the product nucleus formed by neutron capture, which permits accurate β and γ detection.

Numerous measurements up to 1975 have been included in the ENDF/B-V evaluation. Since then the most significant set of data to appear is by Macklin[1], covering the continuous energy range 100-2000 keV. In addition several other sets of data have been published, and are discussed by Mughabghab[2], and the position at 14 MeV has been clarified.

The ENDF/B-V evaluation is here considered as the 'yard-stick', and compared with some recent accurate measurements in various energy intervals (100-1000 keV, 1-5 MeV, 14-15 MeV) in order to estimate the present status.

Comments are made on some of the published experimental data and significant discrepancies noted, especially between 100 and 1000 keV. Also this opportunity has been taken to make several small corrections to the old NPL photoneutron measurements, which still carry the highest quoted precision of any measurements.

II. Comparison between ENDF/B-V and recent measurements

(a) 100-1000 keV

Several data sets are compared with ENDF/B-V in Fig. 1(a)-(e).

The fine structure is of course unresolved, but the high resolution time-of-flight data of Macklin[1] indicate significant intermediate structure, which will clearly be most important to the future more detailed evaluation of the gold capture cross section. For example, see Fig.1(d), he shows a substantial structure ('cusp') at 279 keV, corresponding to a threshold for an inelastic channel. In the energy interval between 130 and 279 keV the gold cross section decreases more slowly than $E^{-1/2}$ and then very suddenly drops 15%. The prompt capture-γ data of Le Rigoleur et al[3] in the same figure and of Fricke et al[41] and Kononov et al[42] in Fig.1(e) indicate a similar behaviour, bearing in mind their poorer resolution. It is interesting also to speculate that the fine-resolution activation measurements of Fort and Brunet[4] shown in Fig.1(c) exhibit the same sudden drop in the gold capture cross section, especially if one can ignore their 'high' reading at 342 keV. The other activation measurements unfortunately have insufficient energy resolution to show any sudden changes in gold capture, and are all higher than ENDF/B-V in this energy interval.

In energy intervals where no significant intermediate structure has been resolved, there is an evident irreconcilable discrepancy between different supposedly accurate data sets. Thus the reliable activation data of Paulsen et al[5] in Fig.1(a) (uncertainty ± 4%) mostly lie 10% above ENDF/B-V. Their results agree very well with the capture-γ measurements of Fricke et al[41] (uncertainty mostly 4-5%) shown in Fig.1(e). The high precision (± 2%) measurement of Robertson et al[6] using a photoneutron source at 966 keV is 13% higher! The new Macklin data (uncertainty ± 3-4%) generally fall 6-12% below. At 1000 keV, there is a difference of nearly 20% between Paulsen et al and Macklin, although the quadratically combined uncertainty of the two data sets is ± 5%. Much other less accurate data lie close to the evaluation. We shall further consider the situation in the discussion at the end of this paper.

The recent activation data of Davletshin et al[7] are not likely to clarify the situation because they have a markedly different shape to ENDF/B-V (ranging from 20% above at 350 keV to 2% below at 1200 keV), the individual data points have a large spread (± 5%), and the total uncertainty has not been given.

In Table 1 are listed nine activation measurements at energies close to 1 MeV. Assuming that the shape of the unresolved gold cross section in this region is closely proportional to $E^{-1/2}$, all the results have been adjusted to an energy of 1 MeV, and one can then take a simple weighted mean (without including correlations), which may be compared with the ENDF/B-V value of 83 mb.

As may be seen from Table 1, the Robertson et al measurement carries more weight than all the other results combined. Because it lies near the average value, it does not much affect the weighted mean except in the error. This measurement will be discussed in the next section. In taking the weighted mean C the very high result of Miskel et al, and the result of Barry, all of whose data lie much above the evaluation over a wide energy range, were also excluded. The average of the activation results is about 10% above ENDF/B-V. (See discussion).

(b) 1-5 MeV

Refering to Fig.2, the behaviour of the gold capture cross section between 1 and 2 MeV is not very well established. However from 2 to 3.5 MeV there is good agreement between Poenitz[32], Lindner et al[8], Joly et al[31] and Paulsen et al[5], and ENDF/B-V. Above 3.5 MeV there exist only some old data[10,11], although fresh activation measurements are expected from Lund University (Bergqvist[45]) from 2 to 4 MeV.Their preliminary results appear to lie above the evaluation between 2 and 2.4 MeV and then fall considerably (~10-20%) below it from 2.4 to 4.2 MeV, with uncertainties of ±7%.

The experiment of Gupta et al[39] around 2 MeV appears to be exploratory, testing a new method, and is normalised to Lindner et al. It is not an absolute measurement.

(c) 14-15 MeV

Until recently there was a considerable discrepancy (100%) between the prompt capture-γ and activation cross section measurements (see Table 2), due to the contribution to the latter from low-energy neutrons emanating from the target materials and room scatter. However several recent activation results[19,20] are much lower, and there is now agreement within the errors.

The value of the accurate activation measurement made in 1975 by Peto et al[17] is double that of the prompt-γ measurement of Drake et al[15], and this huge discrepancy is outside the experimental uncertainties. Two possible explanations might be that Peto et al

(a) included the near-by ^{196}Au (γ+X-Ray) sum peak in the 411 keV γ-peak from ^{198}Au,[20].

(b) underestimated the contribution of background neutrons from the

accelerator target, by assuming a linear extrapolation in the variation of apparent activation cross section with target thickness (see their Fig. 3), contrary to the experience of Ponnert et al[21].

No records are known of any measurements of the gold capture cross section above 15 MeV. Activation measurements here would be extremely difficult to make, and likely to carry very large errors.

III. Photoneutron source activation measurements

Several of the most accurate activation measurements have been made at NPL[6,22] making use of the standards there available. In this type of experiment the spherical photoneutron source was surrounded by several accurately spherical, concentric, very thin shells of gold. The neutron fluence was measured to <1% using the manganese-bath technique, the average gold activity was assayed to about the same accuracy, (calibrated by $4\pi\beta\gamma$ coincidence counting), and a Monte-Carlo calculation gave the spectrum and effective track-length of neutrons through the gold sample, knowing the energy of the primary photoneutrons precisely from the Q value and γ-ray energy. Other important advantages in these measurements are the low background contribution from room-scattered neutrons, and the very small scattering in the foils. The experimental uncertainty is 2 or 3%, but interpretation of the results may be difficult, due to the cross section fluctuations (fine structure). From the calculations of Liskien and Weigmann[23] a deviation from the average smooth cross section curve of $\pm$ 4% could be expected for Sb-Be photoneutrons (22.8 keV), but $<\pm$ 1% for the Na-Be photoneutrons (966 keV).

This opportunity is taken to make several small corrections to the previous NPL results. The gold cross section averaged over the Sb-Be source spectrum[24] should now be reduced by 1.5% to (674 $\pm$ 20) mb. This correction consists of 0.5% for the re-calibration of the NPL manganese bath to account for a small amount of impurities in the solution[25], and of 1.0% for a revised estimate of the fraction of higher energy (380 keV) photoneutrons, from 4.4% to about 3.0%[26]. Using the gold cross section data of ENDF/B-V, and averaging over the Sb-Be spectrum[24], the average gold cross section was 657 mb. The agreement is quite as good as can be expected[23] and supports both the evaluation and the validity of the photoneutron source activation method.

The Na-Be photoneutron source measurement[6] at 966 keV should also be reduced by 0.5%[25], becoming (95.7 $\pm$ 2.0)mb. Over 60% of the source neutrons lie in a rectangular energy distribution of 28 keV total width, (952-980 keV), in a region where there is no threshold for inelastic neutron excitation of levels in ^{197}Au. Hence one can expect a very accurate 'spot' value for the gold capture cross-section, and is placed in the almost embarassing position of having produced a result with more weight than all the other activation measurements combined.

IV. Discussion

Above 500 keV up to 1500 keV the ENDF/B-V evaluation lies about half-way between the most accurate data, the activation measurements of Paulsen et al[5] and time-of-flight capture-γ measurements of Macklin[1], but the discrepancy between these two data sets is well outside the limits of error.

Following a suggestion by Moxon[27] it was ascertained that the Paulsen et al data was not in fact corrected for the additional capture from multiple neutron scatter in the gold target foil[28]. However the thickness of the gold foils used was only 0.5 mm, and an approximate calculation shows that the necessary correction is small, decreasing from less than 4% at the lowest energy of 200 keV to less than 2% at 1000 keV. The overall effect is to significantly improve the agreement with the evaluation between 200 and 500 keV, but at higher energies to pull down the results only slightly, so that at 1000 keV, the difference is still about 8%. Paulsen et al were especially careful to apply corrections for the extra activity due to low energy neutrons from the target and room-scatter. Below 1 MeV they used a hydrogen proportional counter to measure the absolute neutron fluence, and at higher energies a proton recoil telescope. Jackson[34] has suggested that there might have been a systematic error associated with the determination of the fluence using the proportional counter, but this seems unlikely because

(a) the proportional counter was compared with the telescope over an energy-overlap region,

(b) their measurements in the International Neutron Fluence Intercomparison organised by BIPM agreed well with most other laboratories[40] at 2.2 and 2.5 MeV. Although at 250 keV they were at least 10% lower than several laboratories (NPL,PTB,NBS,CEN), this intercomparison was misleading due to the faulty technique associated with the fluence transfer device used by the earlier participating laboratories (no shadow cone was used to determine the background). If one considers the available information from laboratories who used shadow cones with the transfer instrument (Table 15 in Huynh's report) one can deduce that their fluence measurement is probably in good agreement with, and in any case unlikely to be more than 5% lower than, the mean value of the other laboratories[46].

The new Macklin data is well below the evaluation over most of the range from 100 to 2000 keV. We note that the fluence monitor efficiency depended on the $^{235}U(n,f)$ cross section, which is in doubt. According to Bhat[29] this cross section could be somewhat higher around 700 keV, and the shape around 950 keV is not well established. Thus it is at least possible that the Macklin data could be raised ~ 5% between 500 and 900 keV. One also wonders whether systematic errors can creep into the complex time-of-flight measurements, which span many decades of energy. For

example, the use of any neutron beam colliminators or restrictive apertures introduce uncertainty into the 'effective neck' and hence area of the neutron beam which will vary with neutron energy. An interesting discussion of collimators has been given by Gabbard[30]. There will also certainly be a small varying component of lower energy scattered neutrons. It is also usually assumed that the angular distribution of capture-γ rays is isotropic for all neutron energies[31].

The Robertson et al[6] photoneutron source measurement at 966 keV is 13% above ENDF/B-V, with an uncertainty of only $\pm$ 2%. A careful examination of the data for this experiment reveals no reason for the large discrepancy. Certainly this measurement supports the Paulsen et al results, and also agrees well with the activation results gathered together in Table 1, although these latter results are not all considered to be as accurate as some of their authors would claim. Table 1 has only been introduced here to indicate the activation results, and so no account has been taken of the many correlations which exist between the data which will of course affect their average value. It is at least possible that the Na-Be photoneutron spectrum might contain a few more lower energy neutrons, originating either from more inelastic scattering in the source than calculated, or from the energetically possible $^{9}Be(\gamma, \alpha + n)^{4}He$ (Q = - 1.57 MeV) and $^{9}Be(\gamma, \alpha)^{5}He$ (Q = - 2.53 MeV) reactions, which could explain the high result. However there is no information on this possibility, although it is believed that the consequent reduction in the cross section would be small.

The activation measurements of Lindner et al[8] agree reasonably well with ENDF/B-V but here one has reservations because:

(a) the fluctuations of individual data points are much greater than the statistical uncertainties, as noted by the authors themselves without explanation,

(b) the absolute uncertainty is not stated,

(c) the neutron fluence was measured relative to the $^{235}U(n,f)$ cross section,

(d) no corrections were made for neutron scatter in the gold or uranium foils (assumed equal).

In view of (a) and (b) an uncertainty of $\pm$ 7% has been assigned to their measurements, and (c) might raise their results 5% (as discussed above) between 500 and 900 keV, making for reasonable agreement with Paulsen et al.

The capture-γ results of Pöenitz[32] lie almost on the ENDF/B-V evaulation, and depend for their normalisation on the <u>calculated</u> efficiency of the 'Black Neutron Detector' at 1 MeV[38]. There were several collimators or apertures used in the experiments which might cause

normalisation problems. It is noted that their measurements of gold capture and ^{235}U fission are highly correlated, and the latter results also lie on the ENDF/B-V evaluation, so that any increase made in this cross section between 500 and 900 keV would automatically raise their gold capture results towards the Paulsen et al data.

The accurate capture-γ results of Fricke et al[41] show remarkably good agreement with Paulsen et al over the whole range of energy.

V. Conclusion

The unresolved shape of the gold capture cross section from 100 keV to 5 MeV and 14-15 MeV is reasonably well established. The recent Macklin data reveal some intermediate structure, which should be incorporated in a new evaluation. The ENDF/B-V evaluation gives a very good mean value for the experimental data, but unfortunately some of the best recent experimental data show considerable divergence, the activation results of Paulsen et al and capture-γ results of Fricke et al being about 10% high while the capture-γ results of Macklin lie 10% low, at least over part of the energy range.

With possible increases in the Macklin values, and also in the $^{235}U(n,f)$ cross section, as discussed in the last section, all the experimental data considered in this review would tend to converge. In this event the evaluation might be raised slightly, up by about 4% at 1 MeV, and would then approach the Paulsen et al data and the Robertson et al spot value, with a reduced uncertainty.

Alternatively the Paulsen et al data below 1 MeV could possibly be lowered, but not by more than about 5% (as discussed in the previous section in relation to their contribution to the International Neutron Fluence Intercomparison), making them consistent with most of the other measurements and producing convergence towards the ENDF/B-V evaluation.

Consequently it seems that the ENDF/B-V evaluation is a very reasonable representation of the gold capture cross section, but really only accurate to $\pm 8\%$ between 100 and 2000 keV until this discrepancy is understood. Thereafter to 3500 keV the evaluation is probably good to $\pm 4\%$. Above this energy up to 14 MeV there is a lack of data, so that no realistic uncertainty can be given. Finally from 14 to 15 MeV the uncertainty must be $\pm 10\%$. This estimate is more pessimistic than those of several other reviews[33-36], where an uncertainty of $\pm 4\%$ is quoted.

It has been suggested[43] that a discrepancy between activation and capture-γ measurements might be expected, due to γ-ray de-excitation through unbound states. Although there is no real evidence for this, many of the activation measurements for gold do lie above the capture-γ data, and this possibility should be further investigated. However the excellent agreement between two of the most accurate measurements, Fricke et al

(capture-γ) and Paulsen et al (activation), tend to negate this hypothesis.

There is clearly a lot of highly correlated data here, and a simultaneous evaluation of cross sections is required, including especially the $^{235}U(n,f)$ cross section. The assessment of absolute uncertainties by some authors is obviously far too small, since the discrepancies between some results are not adequately covered. This reviewer agrees completely with Smith[37], that the requirement now is for more accurate measurements, with genuine uncertainties of 2-3%, by activation and capture-γ techniques. Measurements to lesser accuracies, eg 5%, will probably have little impact. The apparently high result of the very accurate photoneutron activation measurement should be explained, and the experiment repeated. In addition any fresh data between 3.5 and 14 MeV would be useful.

The choice of gold as a neutron capture cross section standard is clearly favoured because of its excellent nuclear and physical properties, as discussed for example in detail by Carlson[44], who also lists other possible candidates. From the activation point of view gold has a few minor disadvantages:

(a) rather a large thermal capture cross section, making it sensitive to low-energy neutrons,

(b) rather a long half-life (2.7 d), so that long irradiations are required to produce reasonable activity,

(c) an isomeric state at 812 keV excitation energy with a 2.3d half-life, which fortunately is not appreciably populated by neutron capture.

However these disadvantages are not too serious, and no better standard has yet been demonstrated.

Acknowledgement

The author is very grateful to NEA Data Bank, Gif-sur-Yvette, France for supplying much ENDF/B-V data so promptly and efficiently.

References

1. Macklin R L (1981) Nucl Sci Eng 79 265
2. Mughabghab S F (1979) ENDF-300
3. Le Rigoleur C, Arnaud A and Taste J (1976) CEA-R-4788
4. Fort E and Brunet J P (1975) NBS SP425 958
5. Paulsen A, Widera R and Liskien H (1975) Atomkernen 26 80
6. Robertson J C, Ryves T B, Axton E J, Goodier I and Williams A (1969) J Nucl Energy 23 205
7. Davletshin A N, Tikhonov S V, Tipunkov A O and Tolstikov V A (1980) Sov Atomic Energy 48 97
8. Lindner M, Nagle R J and Landrum J H (1976) Nucl Sci Eng 59 381
9. Ferguson A T G and Paul E B (1959) J Nucl Energy A10 19
10. Johnsrud A E, Silbert M G and Barschall H H (1959) Phys Rev 116 927
11. Miskel J A, Marsh K V, Lindner M and Nagle R J (1962) Phys Rev 128 2717
12. Grench H A, Vaughn F J, Coop K L and Menlove H O (1965) EANDC(US)79 72
13. Cox S A (1966) WASH-1068,5,6605
14. Barry J F (1964) J Nucl Energy A/B18 491
15. Drake D, Bergqvist I and McDaniels D K (1971) Phys Lett 36B 557
16. Leithner D (1970) Anz Ost Akad Wiss 7 121
17. Peto G, Csikai J, Long V, Mukherjee S, Banhalmi J and Miligy Z(1975) Acta Phys Slav 25 185
18. Schwerer O, Winkler-Rohatsch M, Warhanek H and Winkler G (1976) Nucl Phys A264 105
19. Magnusson G, Andersson P and Bergqvist I (1980) Phys Scr 21 21
20. Ryves T B and Kolkowski P (1981) J Appl Phys G7 115
21. Ponnert K, Magnusson G and Bergqvist I (1974) Phys Scr 10 35
22. Ryves T B, Robertson J C, Axton E J, Goodier I and Williams A (1966) J Nucl Energy A/B20 249
23. Liskien H and Weigmann H (1977) Ann Nucl Energy 4 38
24. Ryves T B and Robertson J C (1971) J Nucl Energy 25 557
25. Axton E J and Bardell A G (1981) Metrologia to be published
26. Hunt J B (1981) Nucl Instr Methods to be published
27. Moxon M C (1981) Private communication
28. Liskien H (1981) Private communication
29. Bhat M R (1979) ENDF-300
30. Gabbard F (1977) NBS SP493 212
31. Joly S, Voignier J, Grenier G, Drake D and Nilsson L(1979) Nucl Sci Eng 70 53
32. Poenitz W P (1975) Nucl Sci Eng 57 300
33. Mughabghub S F (1976) BNL-NCS-21774
34. Jackson H E (1976) INDC-24/G
35. Paulsen A (1977) NBS SP493 165
36. Wasson O A (1980) NBS SP594 720
37. Smith A B (1980) INDC-30/L+Sp
38. Poenitz W P (19772) ANL-7915
39. Gupta S K, Frehaut J and Bois R (1978) Nucl Instr Methods 148 77
40. Huynh V D (1980) Metrologia 16 31

41. Fricke M P, Lopez W M, Friesenhahn S J, Carlson A D and Costello D (1970) GA-10194
42. Kononov V N, Yurlov B D, Poletaev E D and Timokhov V M (1977) Sov J Nucl Phys 26 500
43. Quaim S M (1975) AERE-R 8082, p.20
44. Carlson A D (1971) Proc of Neutron Standards and Flux Normalization Conf-701002, p.285
45. Bergqvist I (1982) Private communication
46. Hunt J B (1982) Private communication

Table 1. Activation measurements around 1 MeV

Reference	E keV	σ mb	σ at 1 MeV mb	Uncertainty (1σ) %
Paulsen et al[5]	985	92.7	92.0	4[b]
Robertson et al[6]	966	95.7[a]	94.0	2[b]
Lindner et al[8]	{1010	{ 77	82.6	7[c]
	{1070	{ 85		
Ferguson and Paul[9]	1000	97	97.0	13
Johnsrud et al[10]	1000	90	90.0	10
Miskel et al[11]	{ 990	{128	117.6	10
	{1000	{108		
Grench et al[12]	{ 926	{ 94	87.1	5
	{1027	{ 82.6		
Cox[13]	1000	92	92.0	10
Barry[14]	1014	99	99.7	5

WEIGHTED MEAN A (including all measurements) (93.5 ± 1.4)[d] mb
B (excluding ref 6) (92.9 ± 2.1) mb
C (excluding ref 6,11,14) (89.5 ± 2.3) mb

a result reduced 0.5% (see next section)
b uncertainties are probably >1σ
c estimated (see discussion)
d internal error

Table 2. Cross section measurements, 14-15 MeV

Reference	E MeV	σ mb	Fluence det.	Method
Drake et al[15]	14	0.94 ± 0.09[a]		capture-γ
Leithner[16]	14.7	< 2.3		activation
Peto et al[17]	14.7	2.0 ± 0.18	Au(n,2n)	activation
Schwerer et al[18]	14.7	2.1 ± 1.2	Al(n,α)	activation
Magnusson et al[19]	14.7	1.09 ± 0.23	Al(n,α)	activation
Ryves and Kolkowski[20]	14.3	1.09 ± 0.10	Au(n,2n)	activation

a Estimated

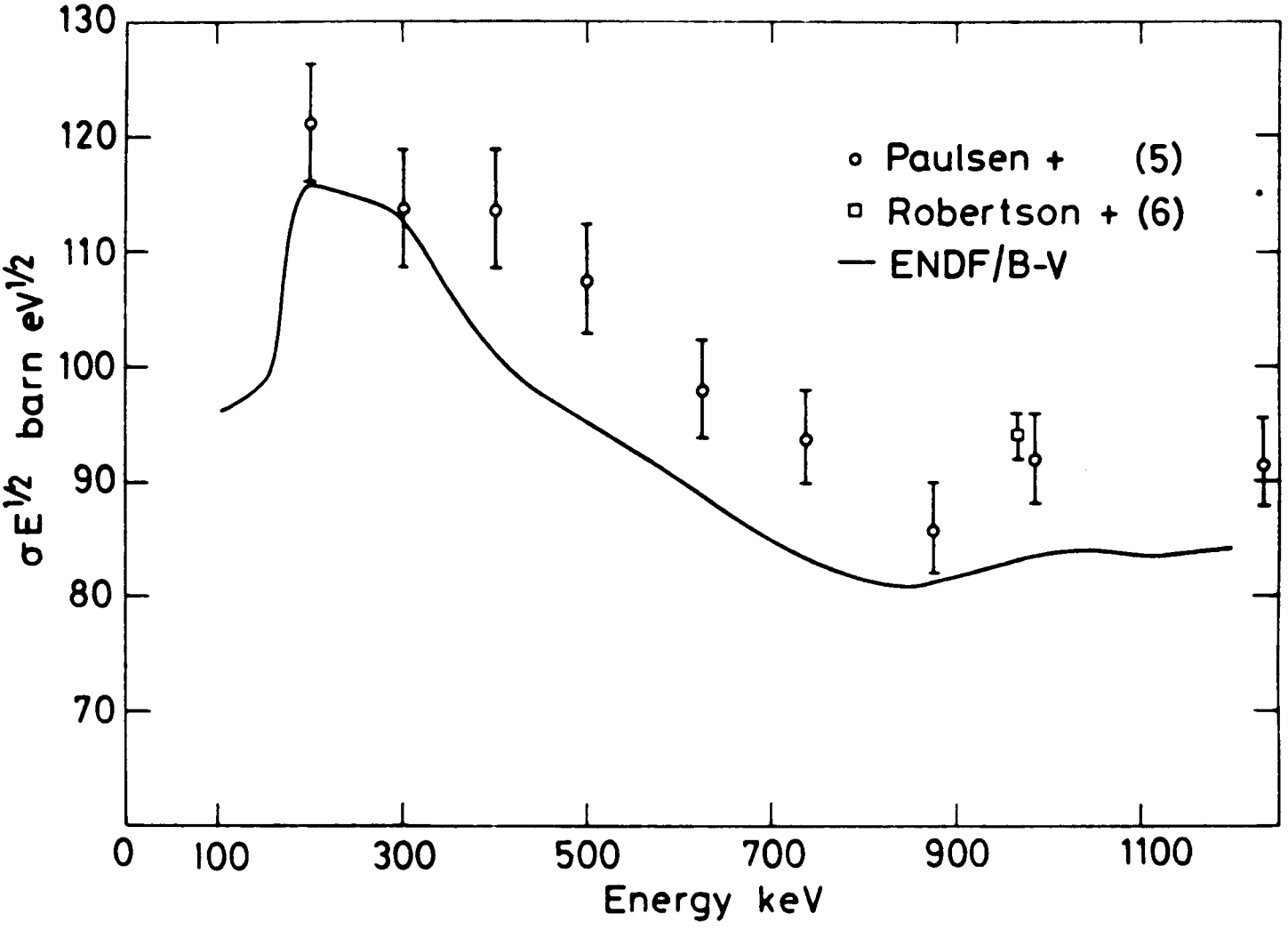

Fig.1(a) Comparison of the ENDF/B-V evaluation of the capture cross section of gold with experimental data, 100-1100 keV.

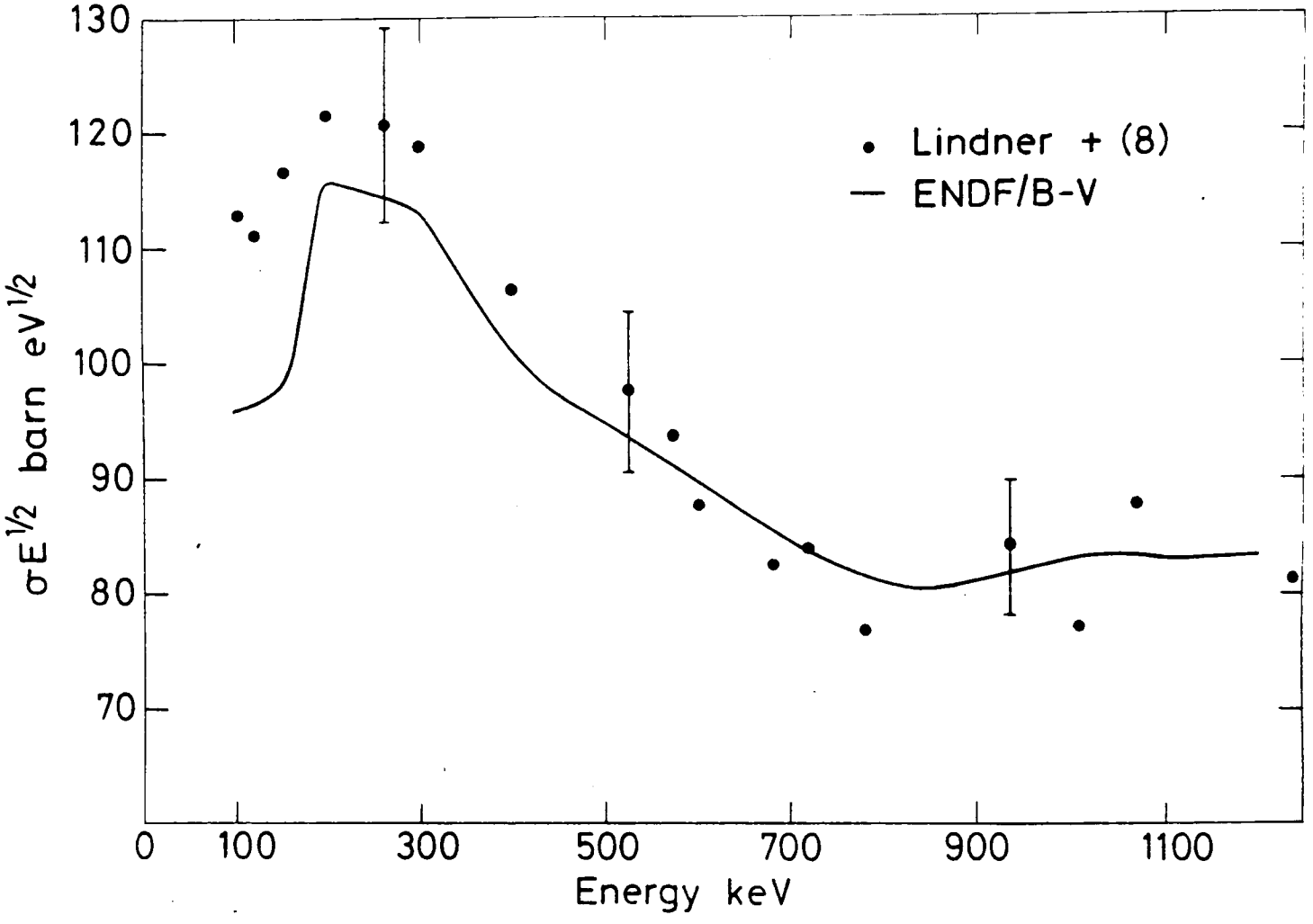

Fig.1(b) Comparison of the ENDF/B-V evaluation of the capture cross section of gold with experimental data, 100-1100 keV.

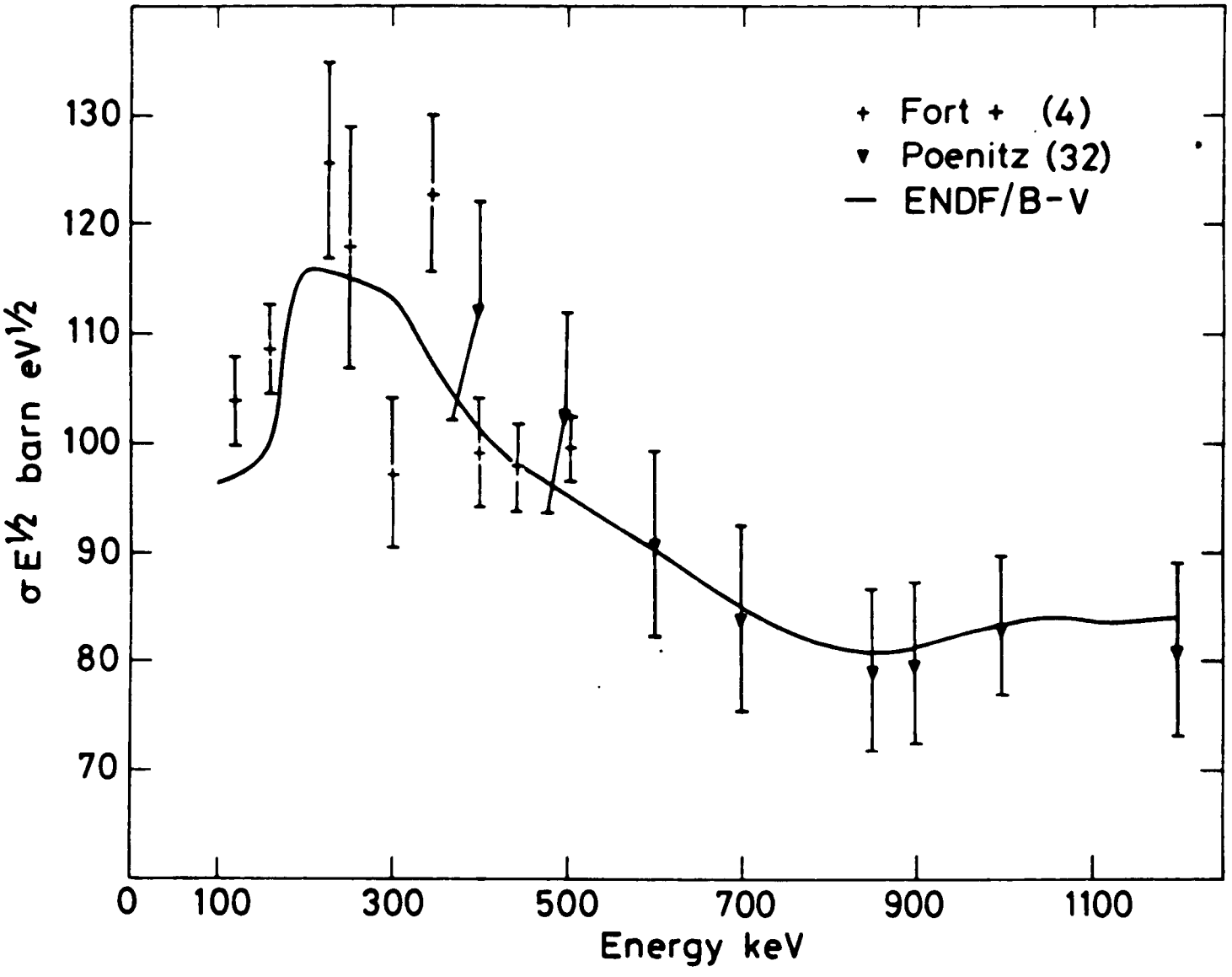

Fig.1(c) Comparison of the ENDF/B-V evaluation of the capture cross section of gold with experimental data, 100-1100 keV.

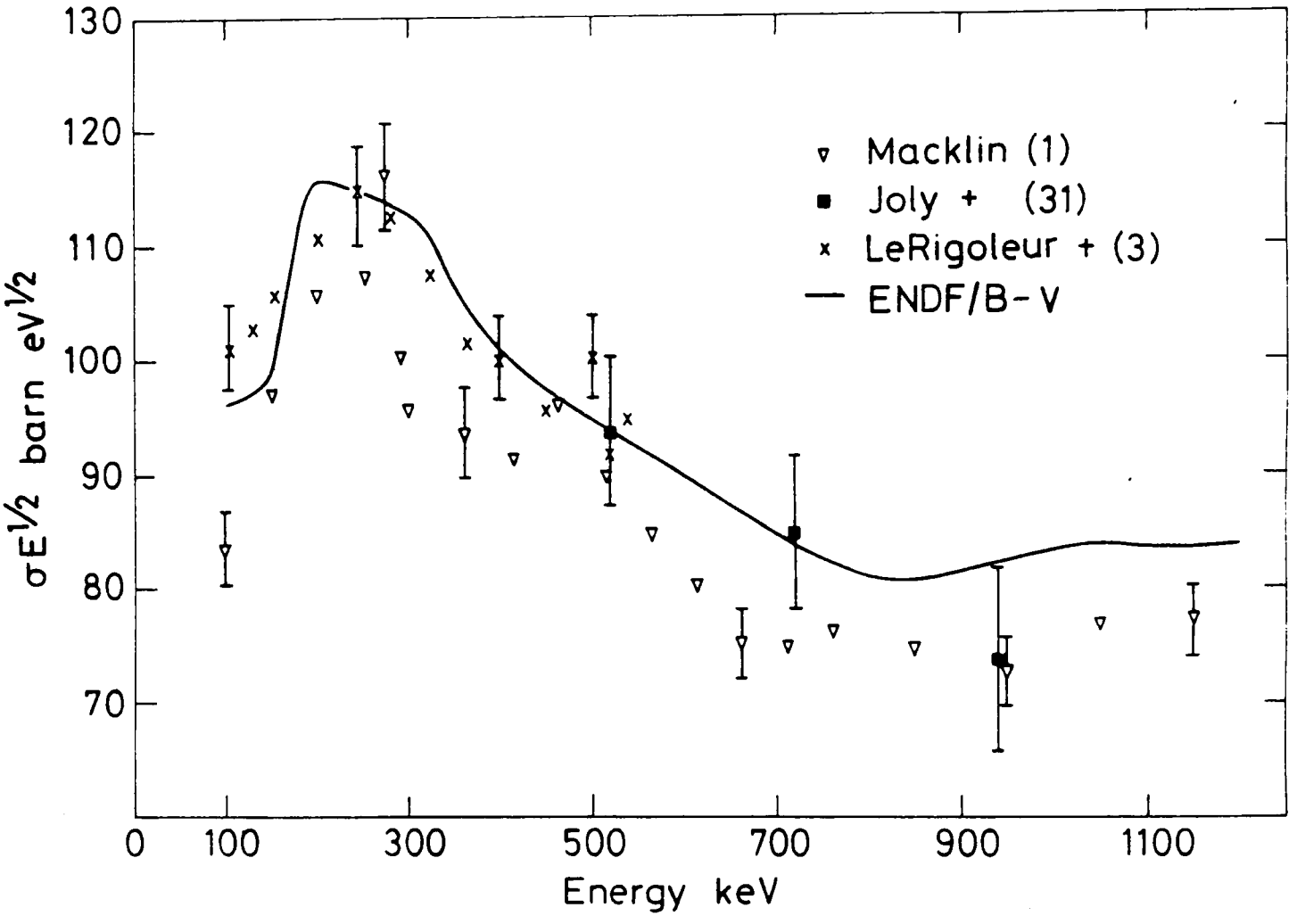

Fig.1(d) Comparison of the ENDF/B-V evaluation of the capture cross section of gold with experimental data, 100-1100 keV.

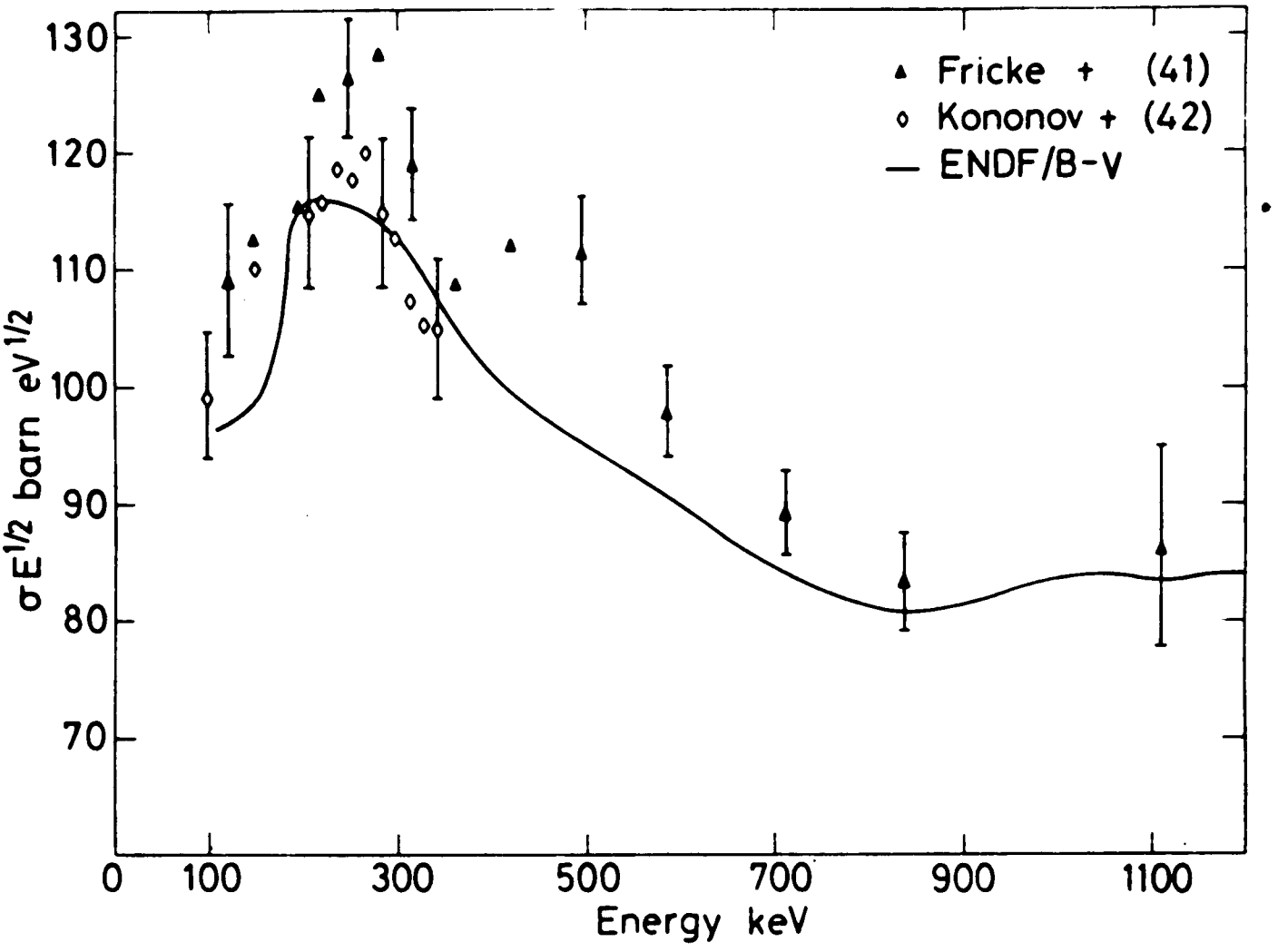

Fig.1(e) Comparison of the ENDF/B-V evaluation of the capture cross section of gold with experimental data, 100-1100 keV.

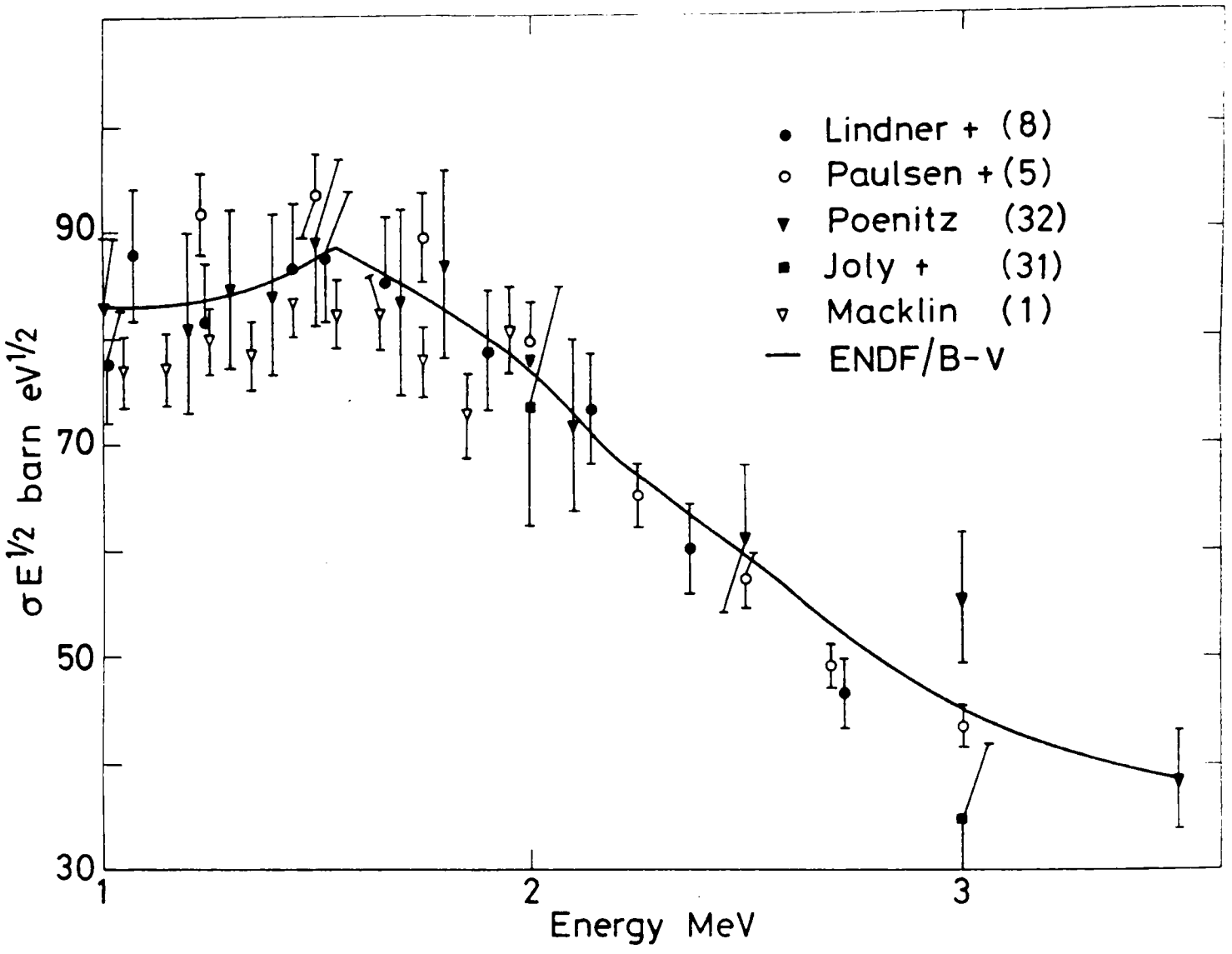

Fig.2 Comparison of the ENDF/B-V evaluation of the capture cross section of gold with experimental data, 1-3.5 MeV.

Discussion

QUESTION: R. Howerton
I would like to ask W. Poenitz what the ^{235}U (n;f) cross-section uncertainty is in the neighborhood of 700-900 keV.

ANSWER: W. Poenitz
I would not expect the ^{235}U (n,f) cross section to change over the whole energy range by more than 2%, but around 900 keV there is a step of $\approx$ 10% in the cross section and there is some uncertainty there, though it is a very local problem. It does not explain the imbalance between some of the measurements.

COMMENT: A. B. Smith
There is a paper from Geel which specifies what resolution one must have in order to avoid uncertainties caused by the fluctuation of the cross section.

COMMENT: W. Poenitz
Yes, but this applies only to the lower energy range, it does not bear on the problems in the higher energy range.

ABSORPTION AND ACTIVATION TECHNIQUES IN MEASUREMENTS OF FAST-NEUTRON CAPTURE CROSS SECTIONS

by

Ingvar Bergqvist
Department of Physics, University of Lund
Lund, Sweden

Abstract

The absorption and activation methods have been applied for a long time to systematic studies of fast neutron capture cross sections. Both methods are simple in principle but difficult in practice. The simplicity should ensure a wider use of the methods in particular for problems which may be complicated to approach with other methods. The difficulties encountered in absorption measurements are related to multiple scattering and resonance shielding effects. In activation experiments the influence of secondary low-energy neutrons causes the main problems.

I. Introduction

The purpose of the present paper is to review the two methods - absorption and activation methods - applied to measurements of fast neutron capture cross sections. Both methods have been used for a very long time and they are generally considered to be "simple in principle but difficult in practice".

The methods have obvious limitations. The absorption technique cannot be used in capture measurements when other reactions than elastic scattering and capture are possible. In general, the threshold of (n,n') reactions to the first excited state gives the upper limit on the neutron energy for which the technique should be applied. The activation method is restricted to about one third of the stable nuclei which will become radioactive after neutron capture. This number is further reduced when, in practice, one has to consider half-lives and decay modes of radioactive nuclei.

However, the methods have important merits which deserve proper attention in applications of fast-neutron capture.

II. Absorption techniques

When elastic scattering and capture are the only open reaction channels, then any absorption method can be used to determine the capture cross section. The best known method is the spherical-shell transition method, which was used as early as 1936 (1). The transmission, T, is measured for a spherical sample either by placing an isotropic neutron source inside the sphere and the neutron detector outside or vice versa (Fig. 1). The relationship between the transmission and the absorption cross section has been discussed in detail by Bethe et al. (2) and Beyster et al. (3). The physical idea is simple. The transmission is defined by

$$T = \frac{\text{count rate (sphere on)}}{\text{count rate (sphere off)}} \tag{1}$$

With only elastic scattering in the shell, T will be unity because of the spherical symmetry. In the presence of absorption, σ_a, the transmission for thin shells is given by

$$T_o = e^{-n\sigma_a(r_2-r_1)} \tag{2}$$

since elastic scattering again would have no effect. Here, n is the number of atoms/cm^3 in the shell, r_1 is the inside and r_2 the outside radius of the shell. However, for thicker shells one must consider multiple scattering events in the shell. If P_1, P_2 and P_m are the probabilities that a neutron will enter the detector after one, two or more elastic collisions then

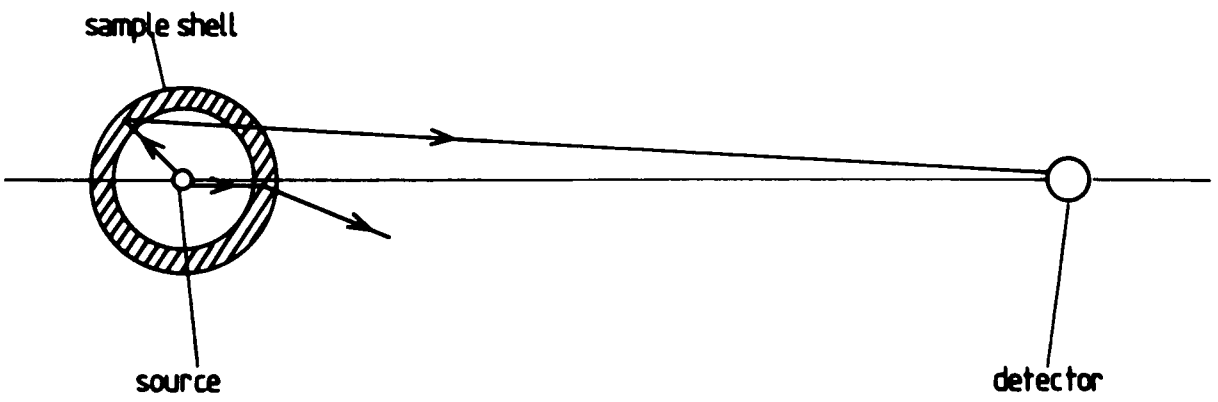

Fig. 1. Schematic arrangement in a spherical-shell transmission measurement.

$$(1-T) = (1-T_o)\frac{\sigma_a}{\sigma_t}\{1+\frac{\sigma_s}{\sigma_t}(1-P_1)+\frac{(1-P_1)(1-P_2)\sigma_s^2}{\sigma_t(\sigma_a+\sigma_s P_m)}\} \quad (3)$$

where σ_s and σ_t are the elastic and total cross sections, respectively. The probabilities, P_i, are general functions and have been evaluated (2) as functions of r_1/r_2 and $n\sigma_t(r_2-r_1)$.

The great advantage of the shell-transmission method is that absolute values of σ_a are obtained from neutron transmission measurements into which enter neither the neutron flux nor the detector efficiency. The method is limited to energies below the threshold of inelastic scattering, because, in general, the lower-energy secondary neutrons will significantly disturb the measurements. Early applications to capture cross section used a Sb-Be photoneutron source which yields 24 keV neutrons.

The drawback of the method is that rather thick samples must be used in order to determine the transmissions with sufficient accuracy. For example, Schmitt and Cook (4) in their early experiments at 24 keV used two gold spheres of shell thicknesses 1.7 and 2.5 cm. The dominating contributions to the uncertainties in the observed value of σ_a come from the corrections due to multiple scattering and resonance self-shielding effects. The contributions are relatively large (about 10%) and roughly equal for the two samples which means that rather little information on the magnitude of the corrections can be obtained from the measurements.

The original results of the measurements have later been reanalyzed with Monte Carlo-techniques. Some of the results are summarized in fig. 2, taken from a review paper by Poenitz (5). The figure shows that the results are quite sensitive to the analysis of multiple scattering and resonance self-shielding effects. We notice, for instance, that the results of the Monte Carlo-analyses(D-J) are somewhat higher than the original results (A,B) and significantly higher than the value (C) obtained by Schmitt in a later analysis of the data. Nevertheless, it seems that Schmitt and Cook (4) have quite well estimated the uncertainties of the original values. The agreement with more recent activation results (K,L) is also reasonably good.

The difficulties related to multiple scattering and resonance self-shielding have discouraged a more general application of the spherical-shell transmission method. We must recognize, however, that the original measurements by Macklin et al. (11), Schmitt and Cook (4) and by Belanova et al. (12,13) have been very important in establishing the absolute cross section at 24 keV for a number of nuclei. To my knowledge the only recent work that has been reported is the very extensive study by Dietze (14) on the capture cross section of ^{238}U in the energy range 215 eV to 100 keV. The experiment was performed at Dubna with neutrons from the pulsed fast reactor IBR-30 and with a battery of ^{3}He-detectors inside spherical shells of enriched ^{238}U. The time-of-flight technique was employed with a 1000 m flight path. A very thorough investigation was made to experimentally determine various sources of systematical errors. For example, the transmissions were measured for five shells ranging in thickness from 7.5 mm to 18.5 mm and of various inner and outer diameters up to 330 mm. The cross sections were determined at 24 and

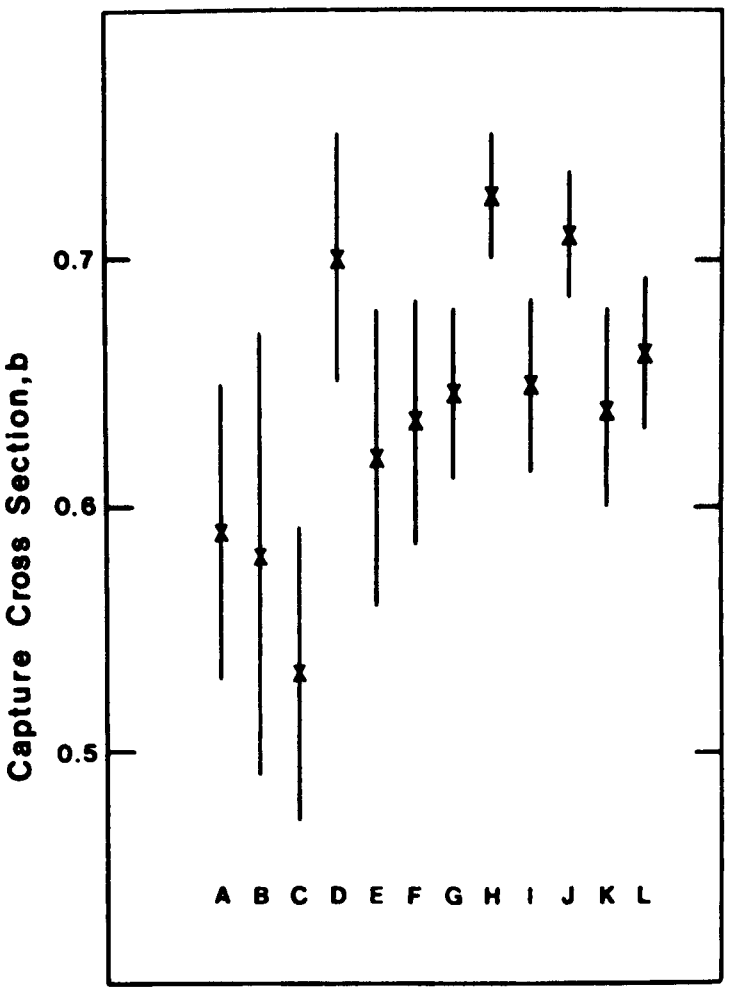

Fig. 2. Results for the capture cross section of ^{197}Au at 24 keV as reviewed by Poenitz (5). The original spherical-shell transmission results (4) are denoted A (for the 1.7 cm thick sample) and B (for the 2.5 cm sample), C represents a recalculated value by Schmitt (6), D-J are values from Monte Carlo-analyses by Bogart, Semler (7) and Froehner (8). Also shown are the results (K,L) of activation measurements by Ryves et al. (9) and Pauw (10).

and 30 keV as well as average group cross sections. The values at 24 and 30 keV are 505 ± 30 mb and 475 ± 30 mb, respectively, i.e. the relative uncertainty is about ±6%. The group cross sections are obtained with an accuracy of about 5%. Dietze concludes that improvements of the experimental method may be made and an accuracy of about 3% might be achieved.

Recently, Pavlenko and Gnidak (15) have proposed a new method for neutron absorption cross sections. The method was applied to measurements with 2 keV neutrons obtained from a Sc-filtered beam from a reactor. The experimental arrangement is illustrated in fig.3. The collimated beam falls onto a scatterer with negligible absorption and a sample for which the absorption cross section is to be determined. In the present case a disk of teflon with

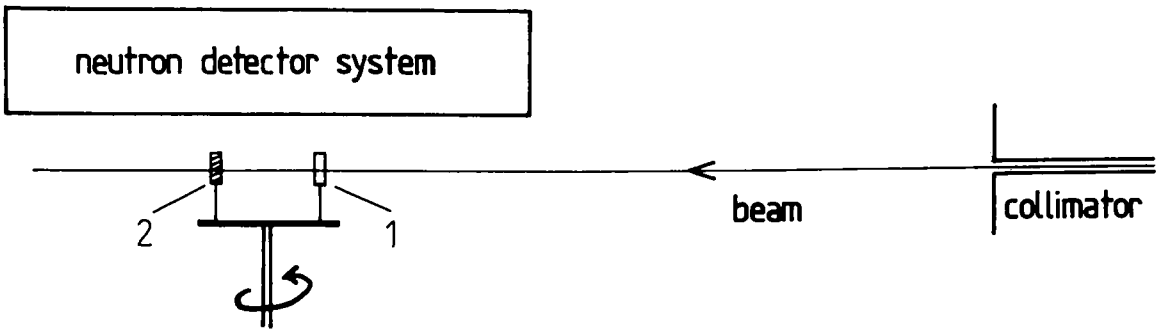

Fig. 3. Experimental arrangement for measurements of 2 keV absorption cross sections (15).

a transmission $T_3 \cong 0.75$ was utilized. The neutron detector system consisted of a battery of ^{3}He-counters (45 detectors). The length of the detector system was 50 cm, the distance from the detectors to the sample and scatterer is 5 cm and between the sample and the scatterer 7 cm. Thus, the detector geometry is nearly 2 π. The measurements consist of a number of short runs and after each run the target holder is rotated 180° in order to interchange the position of the scatterer and sample. Measurements were also made with either the scatterer or the sample in the two positions as well as with an empty target frame to determine the background. The absorption cross section can then be expressed in terms of measured quantities except for a term which is proportional to the relative difference $\delta(\varepsilon)/\varepsilon$, of the neutron detection efficiency, ε, for neutrons scattered from the scatterer and the sample, i.e.

$$\frac{\delta(\varepsilon)}{\varepsilon} = \frac{\varepsilon(\text{scatterer})-\varepsilon(\text{sample})}{\varepsilon(\text{scatterer})} \tag{4}$$

It is stated that this term may be determined with an accuracy of about 1%. A larger uncertainty, about 5%, is estimated for the contribution of neutrons above 2 keV. The influence of these neutrons was determined by placing a Mn disk in the neutron beam. Further studies will be carried out to verify whether this estimate is correct or not. Moreover, corrections have to be made for multiple scattering and resonance self-shielding.

In conclusion, the independence of the spherical-shell transmission technique or of other transmission methods from the neutron flux and detection efficiency warrant future usage in particular to cases where absolute cross sections are difficult to measure with other methods. The principle problems are the effects of multiple scattering and resonance self-shielding. The state of the art seems presently to be that absorption cross sections may be determined with an accuracy of about 5%.

III. Activation techniques

The experiment consists of the irradiation of a sample and a subsequent measurement of the induced activity. Some of the early experiments with fast neutrons were performed with unmoderated fission neutrons like the very well-known systematic studies by Hughes et al. (16,17) performed more than 30 years ago here at Argonne at the heavy-water moderated reactor. In later measurements monoenergetic neutrons have mainly been used, produced by the $^{7}Li(p,n)^{7}Be$ reaction for energies up to 650 keV and by reactions among the hydrogen isotopes, e.g. $T(p,n)^{3}He$, $D(d,n)^{3}He$ and $T(d,n)^{4}He$, for energies up to 20 MeV.

The irradiation geometry varies considerably from one experiment to another. This may be illustrated by the arrangements used in three of the most important activation measurements up to now. In the first extensive measurements with monoenergetic neutrons by Johnsrud et al. (18) the samples were made in the form of cylinders, 2.5 cm long and 3.2 cm inside diameter and placed about 8 cm from the neutron source. The samples were fitted onto a cylindrical fission chamber. In a later experiment, Menlove et al. (19) irradiated a stack of four samples (^{23}Na, ^{55}Mn, ^{115}In and ^{165}Ho) sandwiched between Al-foils. The whole batch was mounted inside a fission chamber about 3 cm from the neutron source. In a more recent experiment conducted by Lindner et al. (20) sample foils were attached to spherical Styrafoam shells surrounding the neutron source. One shell had a radius of 10 cm and another 20 cm. The foils were placed at selected angles to achieve a selection of neutron energies from the $T(p,n)^{3}He$ reaction for each incident proton energy.

The measurements of the induced activities can generally be made with good precision. In some favourable cases (see for example ref. 5) high-resolution Ge(Li) spectrometers and $4\pi\beta$-γ coincidence techniques are capable of achieving an accuracy of better than 1%. In the early measurements (see ref. 18) the activity from thermal neutron capture was frequently measured in addition to the measurements at higher energies. Likewise, the fast and thermal neutron fluxes could be measured with the same neutron counter e.g. ^{235}U fission counter (18,19). In these cases the cross section results are independent of the absolute neutron flux and detection efficiency. The results depend on the ratio of the ^{235}U fission cross section at the two energies and on the thermal capture cross section.

The principle difficulty in activation measurements of fast neutron capture cross sections is the presence of low-energy neutrons. The contamination is particularly serious in measurements at higher neutron energies because of a combination of different effects. The low-energy neutrons are produced in processes like (n,n'), (n,2n), (n,pn) in the sample itself, in structural material near the target-sample vicinity and in the room walls, etcetera. The cross sections for the production of these secondary neutrons tend to increase with the energy of the primary neutrons. These processes strongly degrade the high-energy neutrons into an energy region where the capture cross section is much higher.

This problem was recognized (21,22) more than ten years ago when the 14 - 15 MeV cross sections deduced from measurements of the prompt γ-rays were found to disagree badly with the activation results. Since then, the

influence of the secondary neutrons has been experimentally established, first by Valkonen and Kantele (23) and later by others (24-26). It has been found that the activation yield strongly depends on the geometrical conditions. With reasonable improvements of the irradiation geometry it is possible to greatly reduce the influence of secondary neutrons. It has also been observed that the corrections may be determined by systematically varying the experimental parameters. Two of the most important parameters are the distance between the neutron source (target) and the sample and the sample thickness. The influence of secondary neutrons is illustrated below by discussing in some detail the dependence of the activation yield on these two parameters.

III.1 Distance dependence

Let us first consider room-scattered neutrons and secondary neutrons from sources outside the sample itself. These neutrons cause an induced activity in the sample which can be expressed by

$$I \sim \sigma \phi + \sigma_1 \phi_1 + \sigma_2 \phi_2 \tag{5}$$

where σ is the capture cross section to be measured, σ_1 and σ_2 are effective cross sections for room-scattered and other secondary neutrons, respectively. ϕ, ϕ_1 and ϕ_2 are the corresponding neutron fluxes.

We define the activation yield, Y, as the intensity normalized to unit incident flux

$$Y = \frac{I}{\phi} \sim \sigma + \sigma_1 \frac{\phi_1}{\phi} + \sigma_2 \frac{\phi_2}{\phi} \tag{6}$$

Following refs. (23,26) we may define an apparent cross section by

$$\sigma_{app} = \sigma + \sigma_1 \frac{\phi_1}{\phi} + \sigma_2 \frac{\phi_2}{\phi} \tag{7}$$

The capture cross section for ^{197}Au, for example, at 14 MeV is about 1 mb and we estimate $\sigma_1 \cong 100$ b (thermal neutrons) and $\sigma_2 \cong 100$ mb (1 MeV neutrons), which implies that the three terms in eq. (7) are about equal for $\phi_1/\phi \cong 10^{-5}$ and $\phi_2/\phi \cong 10^{-2}$. Hence, relatively weak contaminations of room-scattered and secondary neutrons can seriously disturb the measurements at 14 MeV. The influence of these secondary sources is, of course, less at lower energies, where the cross section is higher. At 3 MeV for example, the contributions are about equal for $\phi_1/\phi \cong 2 \cdot 10^{-4}$, $\phi_2/\phi \cong 10^{-1}$. In any case, the contributions must be determined experimentally.

In general, the second and third terms will depend on the distance between the neutron source and the sample. For simplicity, let us assume

that the primary neutrons come from a point source, i.e.

$$\phi(r) \sim \frac{1}{r^2} \tag{8}$$

The room-scattered neutrons are usually rather uniformly distributed in the room and we may assume that

$$\phi_1(r) = \text{constant} \tag{9}$$

is valid in the vicinity of neutron source.

The secondary neutrons arising mainly from (n,2n) and (n,n') reactions in the target backing and structural material in the target-sample vicinity, will have a distance dependence between the two extremes. One may tentatively assume that

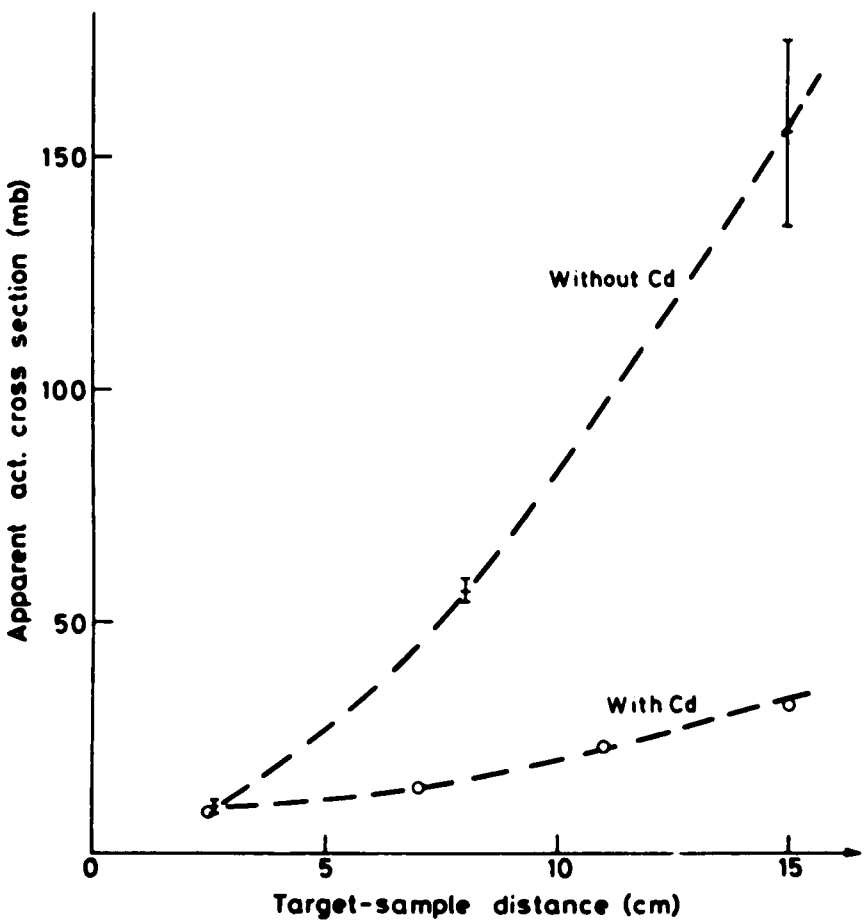

Fig. 4. Dependence of the activation yield on target-sample distance for the reaction $^{115}In(n,\gamma)^{116}In$ at 14 - 15 MeV (24).

$$\phi_2(r) \sim \frac{1}{r} \tag{10}$$

With these assumptions eqs. (6,7) can be written

$$Y(r) \sim \sigma + c_1 r^2 + c_2 r \tag{6a}$$

$$\sigma_{app} = \sigma + c_1 r^2 + c_2 r \tag{7a}$$

where c_1 and c_2 are constants. Hence the contributions of the second and third terms may be determined by measuring the dependence of Y(r) - or σ_{app} - on the distance between the neutron target and the sample. Measurements of distance dependence have shown that the contributions from room-scattered and secondary neutrons are indeed large. The results are illustrated in figs. 4 and 5 taken from the first systematic studies (23,24) with 14 - 15 MeV neutrons and in fig. 6 from work in progress in Lund (27) with neutrons in the MeV range.

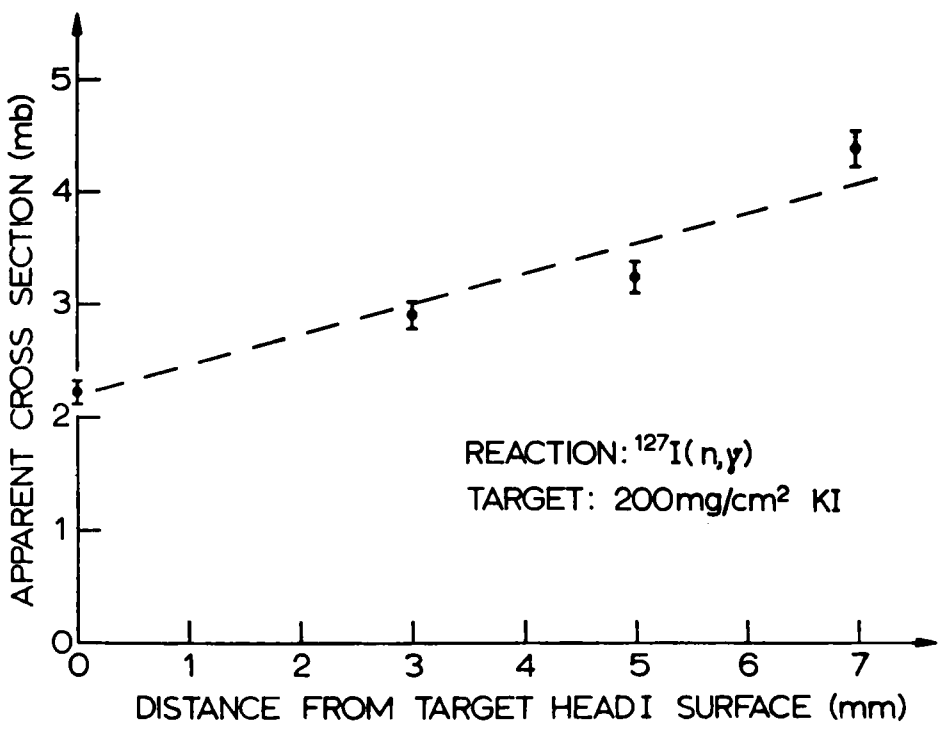

Fig. 5. Dependence of the activation yield at 14.5 MeV on target-sample distance (23).

Fig. 4 shows the activation results for rather large target-sample distances. In other respects the experimental arrangement was quite conventional at that time. Measurements were made for indium samples with an without cadmium foils to demonstrate the importance of thermal neutrons. In early experiments with 14 - 15 MeV neutrons it was customary to wrap the samples in cadmium foils to reduce the influence of room-scattered neutrons. However, the influence of secondary neutrons produced in the sample packet increased, but this influence was usually neglected. The apparent cross section observed at large distances is more than one order of magnitude larger than the true capture cross section, which implies that the contribution of the room-scattered neutrons dominates.

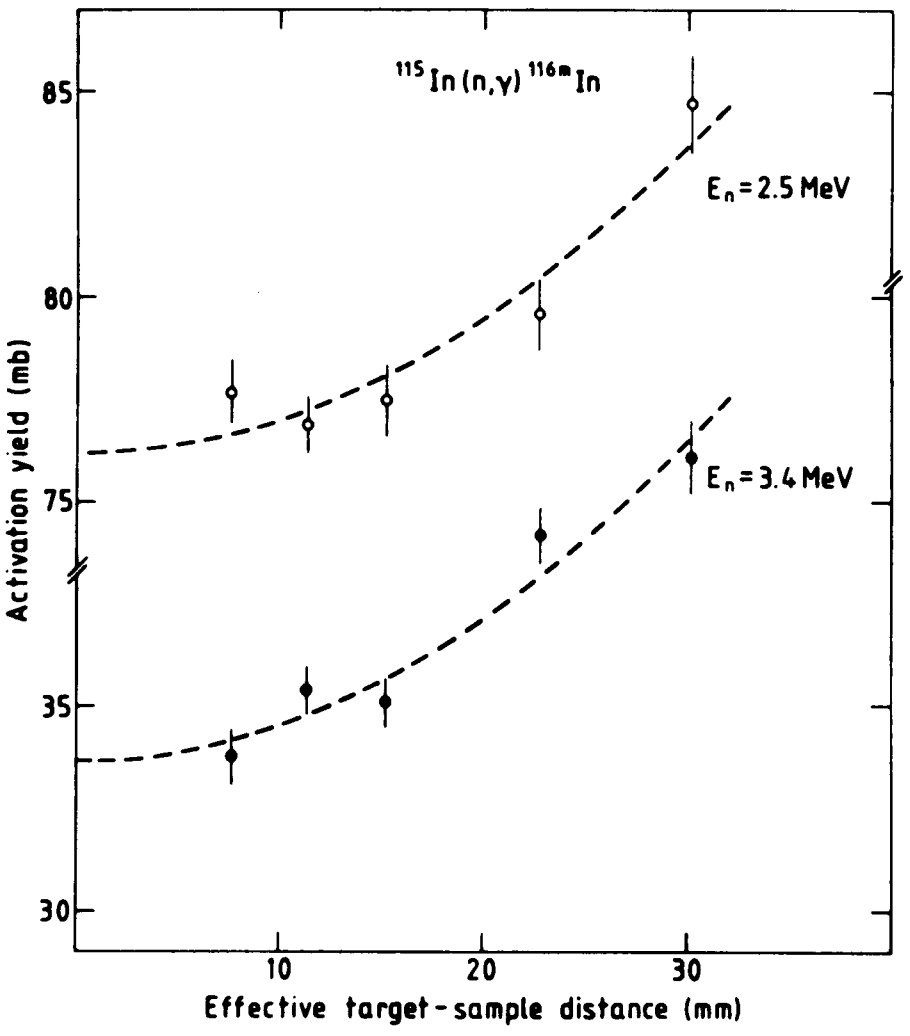

Fig. 6. Dependence of the activation yield at 2.5 MeV and 3.4 MeV on target-sample distance (27).

The results for shorter distances are displayed in fig. 5. "Target head I" is of a conventional water-cooled type made of aluminium. The dashed line was drawn to guide the eye, not to imply a linear dependence. The fact is, however, that all observed dependences at such short distances reported so far may be represented by straight lines like the dashed line in the figure.

For comparison the results at lower neutron energies are shown in fig. 6. The results indicate a contribution from the r^2 term, which seems to be roughly equal in magnitude at the two neutron energies. It would be difficult for several reasons to explore whether or not there is a contribution of a linear term in this case. With the target-sample arrangement designed for this experiment we expect that this contribution will be small compared with the room-scattered background.

The conclusion is that the influence of room-scattered and secondary neutrons from structural material in the target-sample vicinity can be studied by investigating the distance dependence. Provided the diameter of the beam spot is small relative to other linear dimensions the dependences can be analyzed with relationships like those of eqs. 6a, 7a.

III.2 Dependence on sample thickness

Secondary neutrons produced in the sample itself may give rise to a substantial contribution in measurements with MeV neutrons. The contribution varies roughly linearly with thickness for the disk samples which are generally utilized in activation measurements. There are several methods available for numerical estimates of the contribution. The Monte Carlo technique is an obvious method but there are also analytical methods, which are useful.

About ten years ago, Devany (28) derived a simple recursion formula for the contribution of secondary, tertiary etc. neutrons in a sample. In applications to some typically cases the applied formula for escape probabilities is valid for an infinitely wide, thin slab. Tertiary and higher order groups were described by a single group. The corrections to the capture corss sections for 1.3 mm slabs of ^{93}Nb, W and ^{238}W were evaluated to be 2 - 6% of the true cross section at 1 MeV and of the order of 100% at 6 - 7 MeV. The correction was also shown to vary regularly with sample thickness.

The experimental results are exemplified by measurements at 14.5 MeV on ^{127}I samples, fig. 7, by Valkonen and Kantele (23) and at 3.4 MeV on ^{115}In, fig. 8 (27). The measurements on ^{127}I were made with "target head II", which was specifically designed as a low-mass head for the experiment. It was estimated that this target head contributed about 0.1 mb to the cross-section values. The results obtained at 3.4 MeV are compared with calculations similar to those of Devany (28). The diameter of the sample was 1.0 cm, which is small compared with the mean-free-path, and the expression for the escape probability for an infinitely wide slab is not valid. Instead, formulae derived by Carlvik (29) were used in the estimation of the average probability

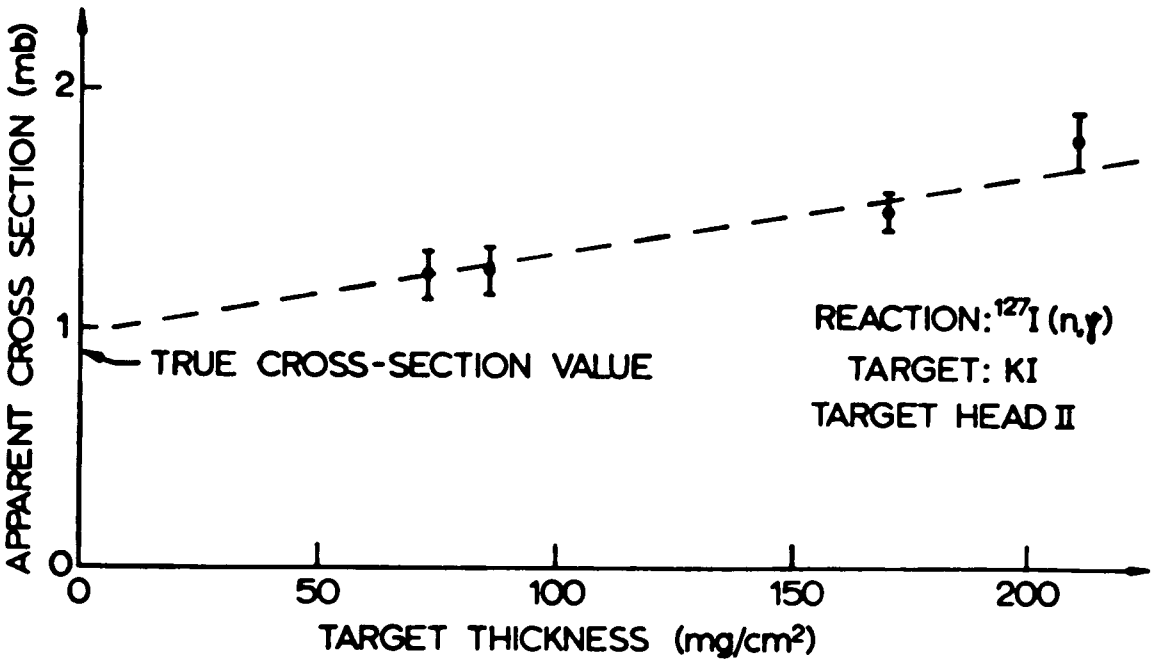

Fig. 7. Dependence of the activation yield at 14.5 MeV on sample thickness (23).

that neutrons produced uniformly and isotropically in the sample will make collisions on their way out of the sample.

The results show a rather strong thickness dependence even for very thin samples. In general, the experimental results may be well fitted by a straight line, but the calculations indicate that the thickness dependence should not be precisely linear.

III.3 Systematics of 14 - 15 MeV capture cross sections

The results from 14 - 15 MeV neutron capture experiments may give us an idea of how well we can correct for secondary, low-energy neutrons. Fig. 9 reviews the present situation. The general trend of the data seems to be that the cross section increases with mass number up to about 1 mb at A ≅ 60 and stays constant for higher mass numbers. There is no obvious difference between spectrum results obtained from measurements of prompt γ-ray spectra and from activation results.

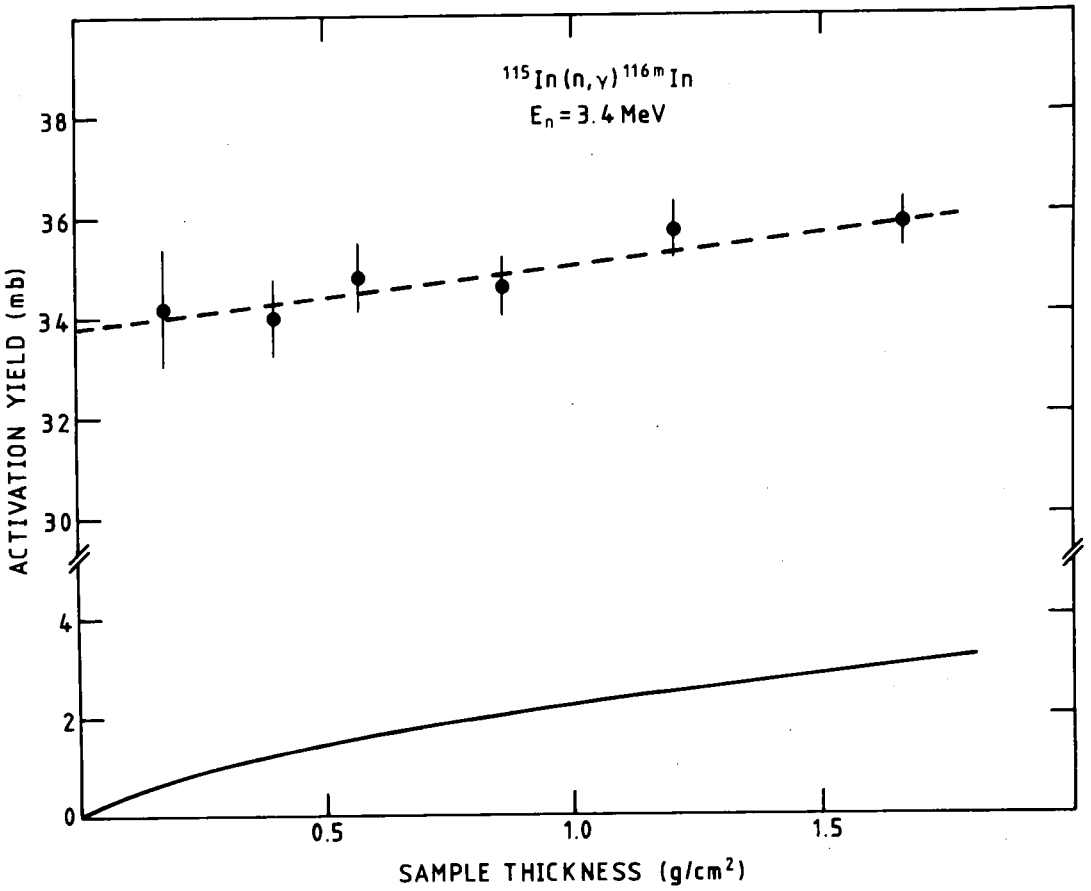

Fig. 8. Dependence of the activation yield on sample thickness for the reaction $^{115}In(n,\gamma)^{116}In$ at 3.4 MeV (27). The solid line indicates the calculated contribution of secondary neutrons.

The review of the 14 - 15 MeV data made ten years ago would show quite another picture. The activation results appeared to fluctuate very much with peaks in deformed mass regions and valleys for spherical nuclei. The highest cross sections were well above 10 mb, i.e. well outside the frame of fig. 9.

The present activation results are taken from a compilation of Wagner and Warhanek (30) and some more recent data, meeting the same requirements, have been added. Cross section data were accepted in the compilation only if necessary corrections for secondary neutrons were made or if it is likely that the influence of these neutrons is negligible. The requirements eliminates the majority of the activation results measured before 1972.

The spectrum results are mainly from measurements performed at Ljubljana, compiled in ref. 31. A geometrical arrangement was used in these measurements that effectively integrates over the γ-ray emission angle. The cross sections were obtained by integrating over the spectrum corresponding to γ-rays to bound final states.

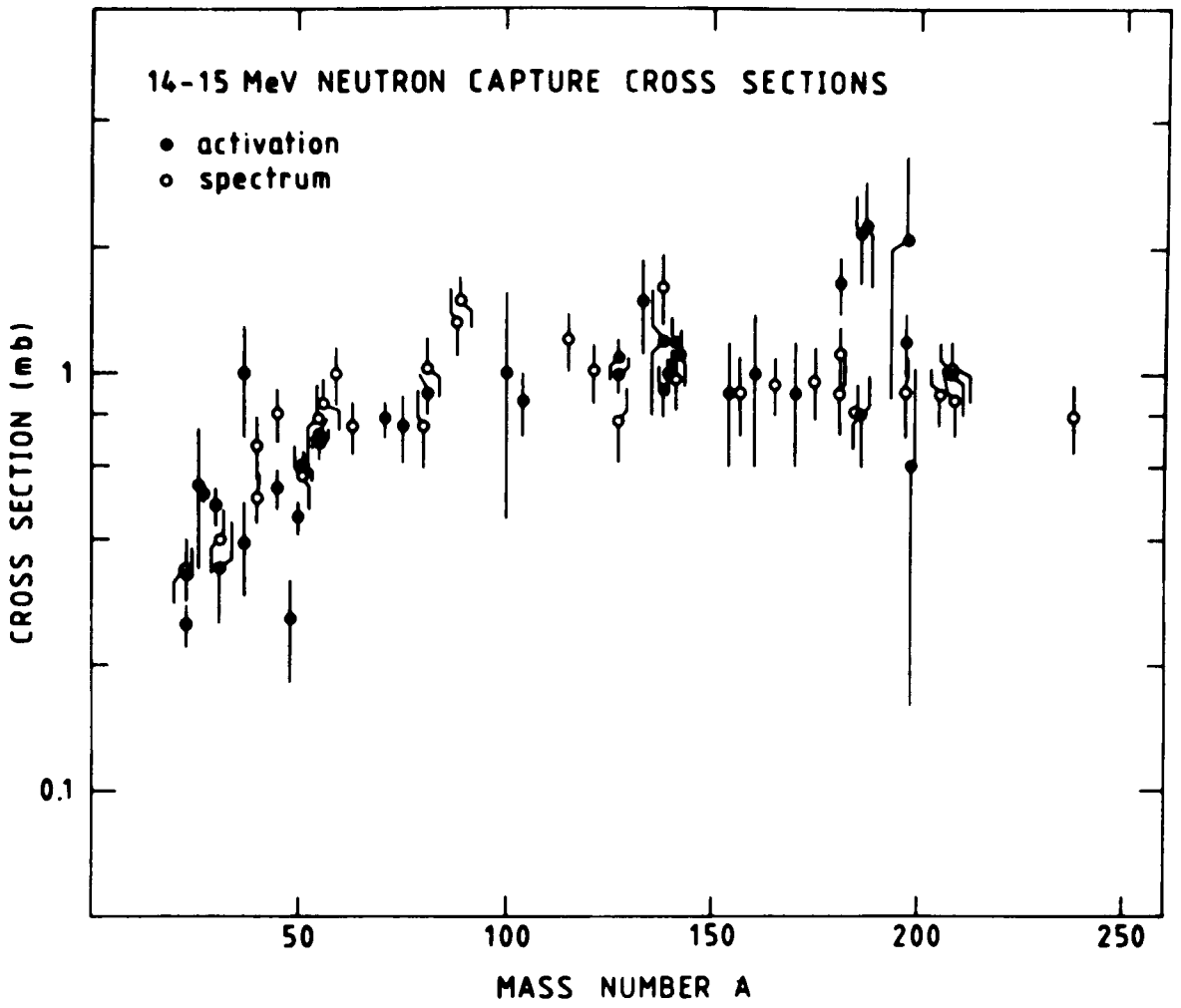

Fig. 9. Experimental capture cross sections obtained from activation and prompt γ-ray measurements.

In view of the difficulties encountered in the activation measurements one must conclude that the agreement is satisfactory between the activation and spectrum results. There are still some inconsistencies in the activation results, e.g. for A = 180 - 200, which should be further investigated. It should be noted that the agreement between activation and spectrum results indicates that γ-ray cascades through unbound levels play a rather insignificant role in 14 - 15 MeV capture. These γ-ray cascades would contribute in the activation but not in the spectrum cross section.

References

1) C.H. Collie and J.H.E. Griffiths, Proc. Roy. Soc. A155 (1936) 434

2) H.A. Bethe, J.R. Beyster and R.E. Carter, J. Nuclear Energy 3 (1956) 207,273; 4(1957) 3

3) J.R. Beyster, R.L. Henkel, R.A. Nobles and J.M. Kister, Phys. Rev. 98 (1955) 1216

4) H.W. Schmitt and C.W. Cook, Nucl. Phys. 20 (1960) 202

5) W.P. Poenitz, Argonne National Laboratory Report, ANL/NDM-58 (1981)

6) H.W. Schmitt, Private Communication (1966)

7) D. Bogart and T.T. Semler, Conf. on Neutron Cross Section Technology, Washington, CONF-66030, Vol. 1 (1966) 502

8) F. Froehner, Int. Conf. Nuclear Data for Reactors, Helsinki, Vol. 1 (1970) 197

9) T.B. Ryves, J.C. Robertson, E.Y. Axton, I. Godier and A. Williams, J. Nuclear Energy A/B 20 (1966) 249

10) H. Pauw, Energy Spectra of Radioactive Neutron Sources, Thesis, University Amsterdam (1971)

11) R.L. Macklin, H.W. Schmitt and J.H. Gibbons, Oak Ridge National Laboratory, Report ORNL-2022 (1956)

12) T.S. Belanova, JETP 34 (1958) 574

13) T.S. Belanova, A.A. Vankov, F.F. Mikhailus and Yu.Ya. Stavisskii, J. Nucl. Energy A/B 20 (1966) 411

14) K. Dietze, Zentralinstitut für Kernforschung, Rossendorf, DDR, ZFK-341 (1977)

15) Je.A. Pavlenko and N.L. Gnidak, Conf. on Neutron Physics, Kiev, Vol. 2 (1977) 248

16) D.J. Hughes, W D B Spatz and N. Goldstein, Phys. Rev. 75 (1949) 178

17) D.J. Hughes, R.C. Garth and J.S. Levin, Phys. Rev. 91 (1953) 1423

18) A.E. Johnsrud, M.G. Silbert and H.H. Barschall, Phys. Rev. 116 (1959) 927

19) H.O. Menlove, K.L. Coop, H.A. Grench and R. Sher, Phys. Rev. 163 (1967) 1299

20) M. Lindner, R.J. Nagle and J.H. Landrum, Nucl. Sci. Eng. 59 (1976) 381

21) I. Halpern, Proc. Nuclear Structure Symp. of the Thousand Lakes, Part I, p. 85, University of Jyväskylä, Finland (1970)

22) D.M. Drake, I. Bergqvist and D.K. McDaniels, Phys. Letters 36B (1971) 557

23) M. Valkonen and J. Kantele, Nucl. Instr. Meth. 103 (1972) 549

24) K. Ponnert, G. Magnusson and I. Bergqvist, Physica Scripta 10 (1974) 35

25) F. Rigaud, M.G. Desthuilliers, G.Y. Petit, J.L. Irigary, G. Longo and F. Saporetti, Nucl. Sci. Eng. 55 (1974) 17

26) G. Magnusson and I. Bergqvist, Nucl. Technology 34 (1977) 114

27) P. Andersson, R. Zorro and I. Bergqvist, University of Lund, Report LUNFD6/NFFR-3043 (1982)

28) J.J. Devany, Nucl. Sci. Eng. 51 (1973) 272

29) I. Carlvik, Nucl. Sci. Eng. 30 (1967) 150

30) M. Wagner and H. Warhanek, Private Communication (1978); Acta Phys. Austriaca 52 (1980) 23

31) M. Budnar et al, IAEA-report INDC (YUG)-6/L, 1979

Discussion

COMMENT: W. Poenitz
I would like to make a comment concerning activation measurements. In reporting cross-section data, usually half-lifes and branching ratios are reported. However, in utilizing the data at a later time, say by an evaluator, what really is needed is the sensitivity of the derived quantity to the half-life(s). The reported data are usually an average from several measurements and not directly proportional to the half-life.

ABSOLUTE MEASUREMENTS OF THE FAST NEUTRON CAPTURE CROSS SECTION OF ^{115}In+

by

D.J. Grady,* G.F. Knoll & J.C. Robertson**
Department of Nuclear Engineering
University of Michigan
Ann Arbor, Michigan 48109

Abstract

The $^{115}In(n,\gamma)^{116m1}In$ cross section has been absolutely determined at neutron energies of 23, 265 and 964 keV. These energies are the median neutron energies of the three photoneutron sources. Sb-Be, Na-CD_2 and Na-Be, utilized in this work. The measurements are independent of other cross section data except for corrections amounting to less than 10%. Independent determinations of the reaction rate, detector efficiency, neutron source strength, scalar flux and target masses were performed. Reaction rates were determined by beta counting of the $^{116m1}In$ decay activity using a 4π gas flow proportional counter. Detector efficiency was measured using $4\pi\beta$-γ coincidence counting techniques and the foil absorber method of efficiency extrapolation for correction of complex decay scheme effects. Photoneutron source emission rates were determined by intercomparison with the NBS-II calibrated ^{252}Cf spontaneous fission neutron source in the University of Michigan Manganese Bath. The normalized scalar flux was calculated from the neutron emission angular distribution results of the Monte Carlo computer program used to model neutron and gamma transport in the source. Target mass determinations were made with a microbalance. Correction factors were applied for competing reaction activities, neutron scattering from experiment components, room-return induced activities, spectral effects in the manganese bath and the neutron energy spectra of the photoneutron sources. Experimental cross section results were normalized to the source median energy using energy spectra and cross section shape data. The absolute cross sections obtained for the $^{115}In(n,\gamma)^{116m1}In$ reaction were 588±12, 196±4 and 200±3 millibarns at 23, 265 and 964 keV, respectively.

+Work supported by Division of Research, USDOE

*Present Address:
TRW
One Space Park, R1/1170
Redondo Beach, CA 90278

**Present Address:
Chemical & Nuclear Engineering Dept.
University of New Mexico
Albuquerque, New Mexico

I. Introduction

The measurement and intercomparison of neutron fluxes in the keV energy region requires standard neutron cross section data. Traditionally, the $^{197}Au(n,\gamma)$ reaction has been utilized as a standard for neutron capture reactions. An alternative is available in the ^{115}In neutron capture cross section. This isotope exhibits a cross section that is generally higher and less energy dependent. The reaction produces an activity ($^{116m1}In$) with a half life of 54.12 minutes which compares favorably with the often inconviently long ^{198}Au half life of 2.695 days. The target isotope is nearly as abundant as ^{197}Au (95.7% versus 100%) and has in general, small of short lived competing reactions to consider.

Past cross section measurements have been performed with the indium as a standard. These measurements have suffered from a lack of absolute cross section data in the keV neutron energy range. Where the data base does exist, discrepancies in evaluated data and experimental results exceed 10% over much of the energy region. In order to effectively use this reaction as a standard, more absolute measurements at discrete neutron energies, using independent experimental techniques are required. This paper discusses the efforts of the Universith of Michigan to contribute to this capture cross section data base need.

II. Experimental Technique

Nearly monoenergetic neutrons at 23, 265 and 964 keV were obtained from three spherical, photoneutron sources for use in the absolute cross section measurements of the $^{115}In(n,\gamma)^{116m1}In$ reaction. The Sb-Be, Na-CD_2 and Na-Be neutron sources consisted of spherically concentric layers of gamma emitting core, structure and neutron source material (beryllium or deuterated polyethylene). Uniform activation of these sources was accomplished by continuous rotation at the axial mid-plane of the Ford Nuclear Research Reactor in a thermal neutron flux of approximately 10^{13} neutrons/cm^2-s. Table 1 contains a summary of major photoneutron source characteristics.

Activated sources were transferred via a wheeled, lead shield to the low-albedo laboratory where both the indium foil activation measurements and the maganese bath source calibrations were performed. The laboratory was equipped with a closed circuit television system and vacuum remote manipulators for neutron source handling. One meter thick concrete walls provided personnel shielding and a 5 cm thick layer of anhydrous borax lined the interior of the 4.2 meter (mean inside diameter) laboratory to reduce the return of moderated, room-return neutrons into the experiment package. Additional room-return neutron shielding was provided by a 0.076 cm lining of cadmium inside the sealed 55 gallon drum which housed the indium foil activation assembly and photoneutron source. During activation experiments the drum was suspended at the center of the laboratory to take advantage of the fact that any remaining room-return flux would be spatially flat over the range of neutron source-indium target spacings. This positioning strategy provided the experimental determination of the room-return flux required in the indium activity correction factor.

Indium target foils were manufactured from 99.999% pure indium ribbon. Eight disks with a mean radius of 0.961 cm, a mean thickness of 0.007 cm and a mean mass of 0.144g were prepared for these capture cross section measurements. Masses were obtained from microbalance weighings before and after each foil activation experiment. Seven source-target spacings ranging from 2.1 cm to 9.73 cm (2.43 to 10.04 cm for the larger Sb-Be source) were used for each of the measurements to provide the required room-return correction data. Figure 1 diagrams the indium foil holder assembly and its means of attachment to the neutron source well which itself was fastened to the 55 gallon drum. Flux calculation sensitivity to the source-target spacing uncertainty mandated a precision source positioning device and foil holder assembly design. Fabrication of this design was accomplished with a special jig which assured proper alignment of all of the critical components. In addition, source-target measurements were performed at 18 radial locations using a precision dial gauge and gauge blocks. Spacing uncertainties of 0.002 cm were nominal.

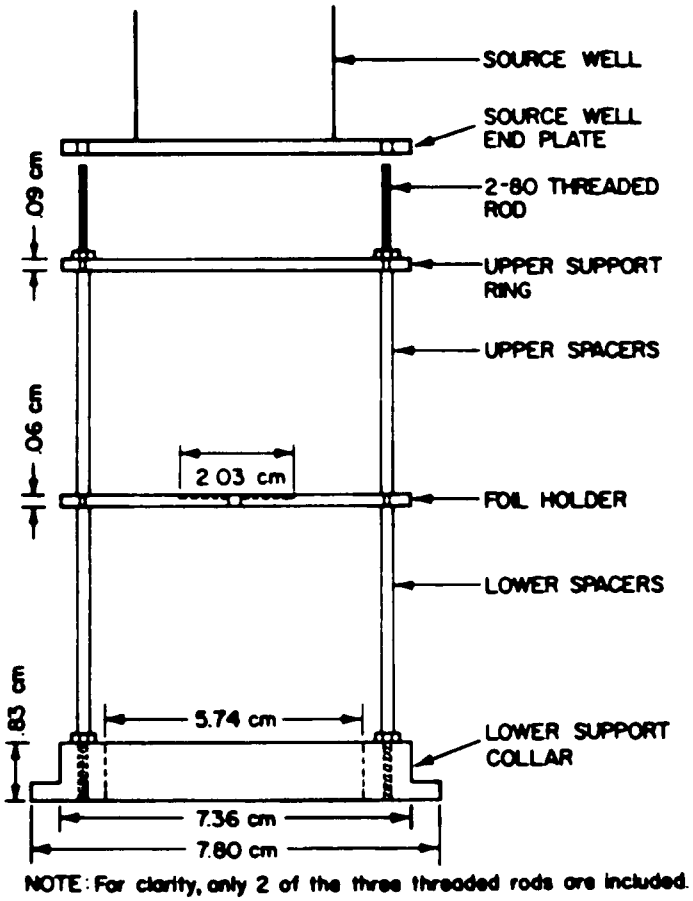

Figure 1. Indium Foil Holder Assembly

Once activated, the indium foils were transferred to a 4π gas flow proportional counter for beta counting. The detector consisted of two identical halves with about 60 cm^3 of active volume each. Phosphor-bronze anode wires of 0.005 cm diameter were operated at 2000 V and the P-10 flow gas pressure was just slightly over atmospheric. Counting durations equaled activation lengths (1-2 hours).

Detector efficiency was obtained using $4\pi\beta$-γ coincidence counting techniques. A 2" x 2" NaI(Tl) crystal was added to the beta counting system. A gamma window set on the predominant 1.293 MeV gamma photopeak was used for the coincidence counting. Each of the eight indium foils was in turn activated in a thermal neutron flux and counted in the coincidence counting configuration to obtain the apparent beta detector efficiency (N_c/N_γ). Correction for non-ideal detector behavior and the complex indium decay scheme was accomplished with the foil absorber method of the efficiency extrapolation technique described by Baerg(1). In this technique, the apparent beta detector efficiency for an activated indium foil is computed as a series of aluminum foil absorbers (20 μm) are placed above and below the indium foil. The resulting "K" correction factor of 0.974±.008 was applied to the apparent efficiency results to obtain the final beta detector efficiency for the decay of ^{116m1}In. A nominal value of 0.554±.007 was obtained.

After completion of the indium foil activation experiments, each photoneutron source was placed in the manganese bath. In the one meter diameter bath, the manganous sulfate solution (1.3 g/cm^3) was continuously recirculated and a small sample stream was drawn off and the ^{56}Mn activity was counted in a NaI(Tl) counting system operated in multiscaling mode. Comparison of the bath saturated activity with that induced by a calibrated ^{252}Cf spontaneous fission source resulted in the neutron emission rate of the photoneutron source. The ^{252}Cf source had been previously calibrated in the same fashion against the secondary national neutron standard, NBS-II. The ^{252}Cf source strength during this work was 3.1 x 10^6 n/s.

A Monte Carlo computer program was used to model gamma and neutron transport in the photoneutron sources. An analytic expression for the scalar neutron flux averaged over the indium target surface was derived based upon the neutron emission angular distribution results of the computer program. Flux results normalized to a source neutron emission rate of 1 n/s ranged from 0.021 for the narrowest spacing to 0.00084 for the widest spacing (0.015 to 0.0008 respectively for Sb-Be).

III. Corrections and Uncertainties

Five major correction factors were required for this work. The first two resulted in adjustments to the scalar flux calculations. Neutron scattering from the various support structures of the experiment were calculated using point scatter approximations. A computer program capable of modeling the various surface geometries was written to perform these corrections. Neutron backscattering from the holder upon which the indium foil was placed was modeled separately because of the inability of the point approximation to accurately handle the potentially long path lengths of backscattered neutrons through the indium foil. A Monte Carlo program was written to determine the average path length through the foil of backscattered neutrons. Typical corrections to the scalar flux as a result of these two scattering corrections were about 4% with uncertainties taken to be 20% of the correction.

Several competing reaction activities are possible. Inelastic scattering events (except for Sb-Be) give rise to ^{113m}In and ^{115m}In and an additional capture event in the 4.28% abundant ^{113}In give rise to ^{114m}In and ^{114}In activities. Abundance, neutron energy threshold, beta detector

efficiency and half life considerations reduce all but the ^{115m}In activities to corrections of less than 0.2%. The ^{115m}In activity contribution to the total detected activity was computed from cross section data and an absolute calibration of the beta counter efficiency for this decay. The maximum percentage of total detected activity attributable to the ^{115m}In activity was 2% and 7% for the Na-CD_2 and Na-Be cases, respectively. Uncertainties were taken as 8% of the correction due to propagation of parameter uncertainties.

Once all of the counting data had been reduced to saturated ^{116m1}In activity per gram of target, the room-return correction was computed. A plot of the saturated activity/target atom versus scalar flux for the seven spacings (Figure 2 is for the Sb-Be source) results in a y-axis offset which is equal to the room-return component of the activity. The fraction of the total activity due to room-return activity ranged from about 1% to 20% (±15% fo the correction) for the narrowest to the widest spacings. The correlation coefficient (r^2=.999) for the fit of Figure 2 is strong evidence that the room-return flux is spatially flat in the physical region in which these experiments were performed.

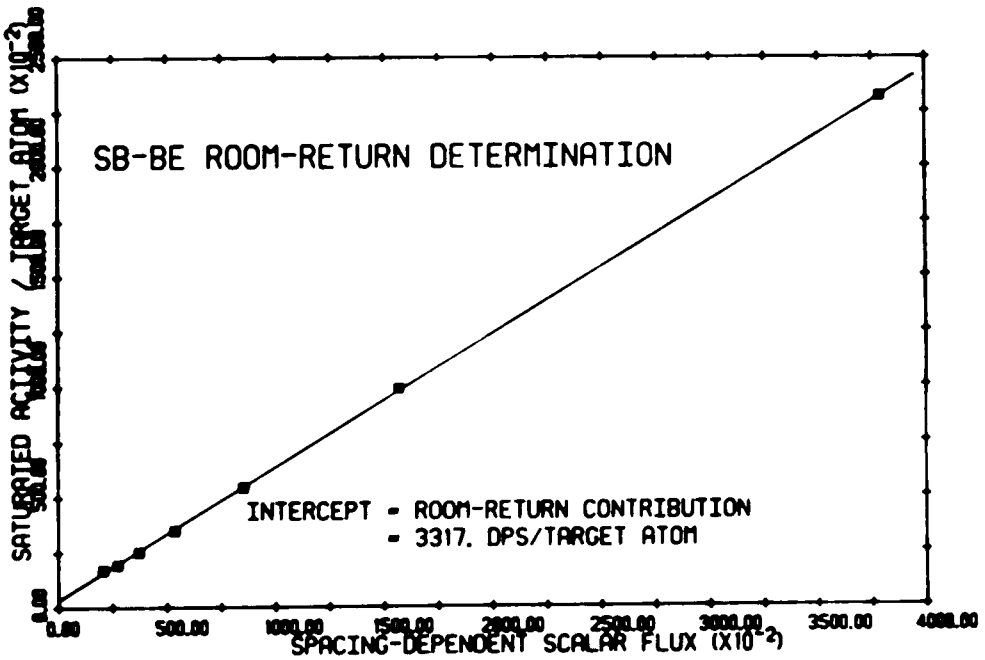

Figure 2. Sb-Be Room-Return Determination

A final correction to reduce the measured cross section to the median energy of the photoneutron sources was calculated based upon the ENDF/B-IV capture cross section shape and the neutron energy distribution. The latter was obtained from the same computer program which computed the photoneutron source emission angular distributions. These energy distributions are plotted in Figure 3. Corrections were computed as 0.6%, 5.5% and 0.1% for the Sb-Be, Na-CD_2 and Na-Be cases, respectively.

The major uncertainties were associated with counting statistics and in particular with the indium foil counting and the "K" spectrum correction analyses (~1%). Additional uncertainties related to counting statistics included half lives (0.1%), foil masses (0.1%), correction factors like dead times, chance coincidences and background (0.35%), timing of irradiation and counting (0.1%) and isotopic abundance (0.1%).

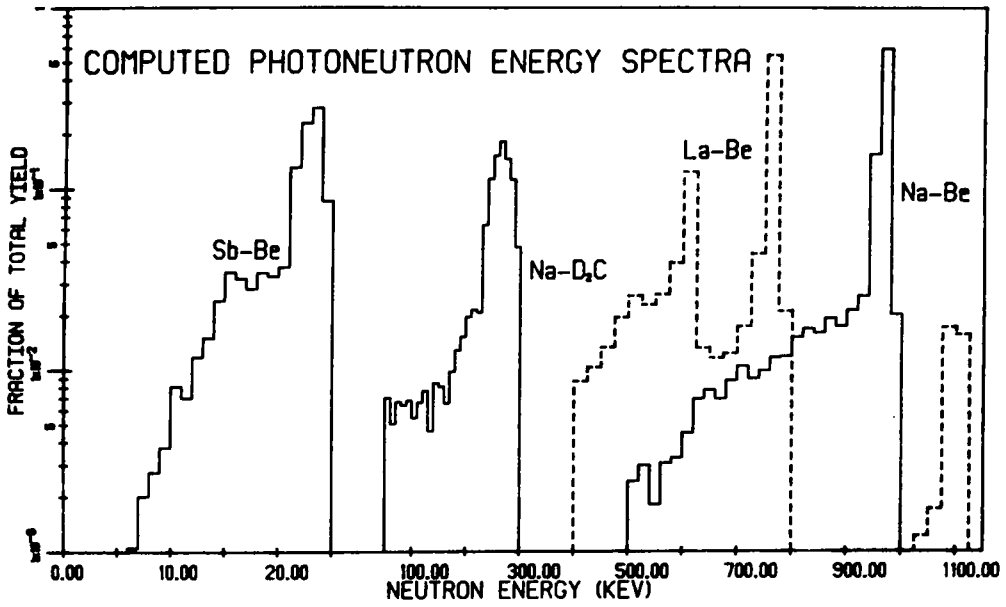

Figure 3. Photoneutron Energy Spectra

Uncertainties associated with the scalar flux calculations included source-target spacing (max=0.4%), target foil diameter (max=0.23%), target foil misalignment (max=0.18%) and Monte Carlo modeling related uncertainties associated with the scattering corrections discussed earlier.

Neutron source calibration uncertainties were driven by several factors. The first was the 0.5% uncertainty in the neutron yield of NBS-II, the primary standard upon which all of the calibrations were based. The second major uncertainty was associated with the ^{252}Cf half life. A three year delay between the cross calibration of NBS-II and ^{252}Cf resulted in an additional 0.5% uncertainty in the ^{252}Cf neutron strength. Additional uncertainties included correction factors (0.15%), counting statistics (0.1%), counting system electronics (0.3%) and photoneutron source half lives (0.1%). Correction factors were also applied to the manganese bath results to account for the non-uniform factors of parasitic neutron capture, bulk leakage, source well absorption, source self-absorption and photoactivation of the natural deuterium content of the bath. Final photoneutron source strength uncertainties were all 0.8%.

IV. Results and Conclusions

The cross section results for the ^{115}In(n,γ)^{116m1}In capture reaction are 588 ± 12, 196 ± 4 and 203 ± 3 millibarns at 23, 265 and 964 keV, respectively. These results are absolute in that they do not depend upon any other cross section data, except for correction factors amounting to less than 10%. The significance of these measurements is that they provide several accurate reference points to locate the absolute value of the more easily obtained relative cross section data. In addition, these results provide absolute data at neutron energies where few if any other absolute measurements have been performed.

In the energy region covered by this work, only a few other absolute data sets exist. Some of these data, the results of the present work and the ENDF/B-IV evaluation are plotted on Figure 4. The quantities in parantheses are the approximate percent errors and reflect uncertainties at the 68% confidence level of one standard deviation. In light of the present ENDF evaluation and the other two sets of absolute measurements, these results strongly suggest the need for re-evaluation of the $^{115}In(n,\gamma)^{116m1}In$ cross section data base.

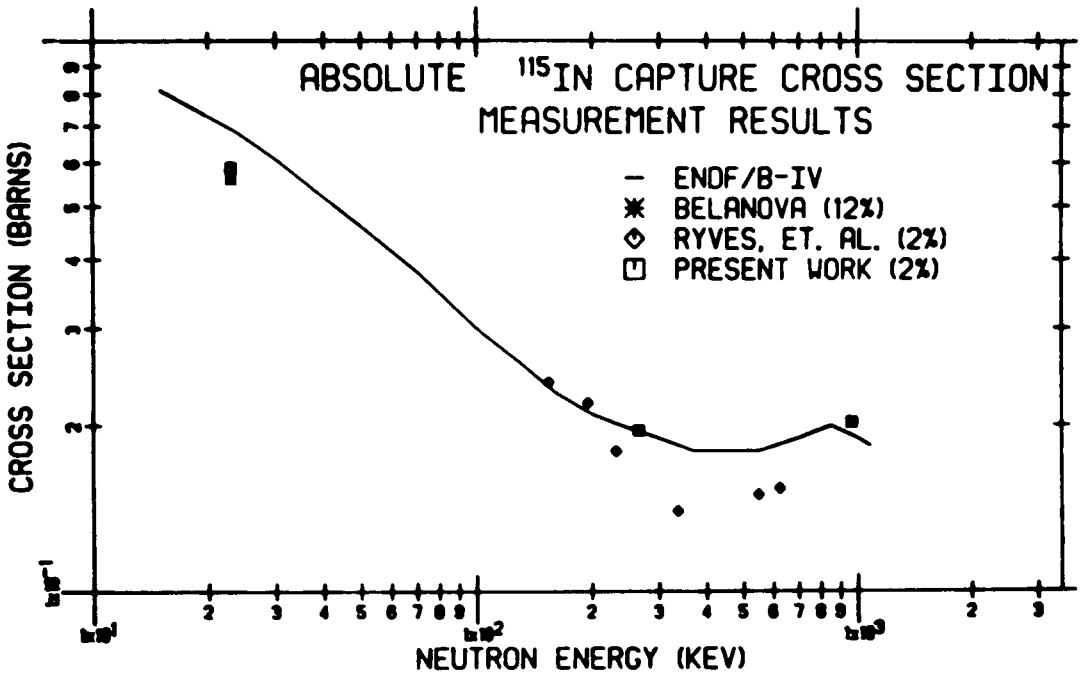

Figure 4. The Absolute $^{115}In(n,\gamma)^{116m1}In$ Cross Sections

References

1. A. P. Baerg, "The Efficiency Extrapolation Method in Coincidence Counting", Nuclear Instuments and Methods, 112, 143, (1973).

TABLE 1
PHOTONEUTRON SOURCE CHARACTERISTICS

Source	Gamma Core Diameter (cm)	Outer Shell Diameter (cm)	Gamma Emitter Half Life (hrs)	Median Energy (keV)	Initial Neutron Strength (n/s)
Sb-Be	2.90	4.20	1444.8	23	2.3×10^7
Na-CD_2	2.38	3.60	15.01	265	1.7×10^7
Na-Be	3.01	3.60	15.01	964	4.8×10^7

MEASUREMENTS AND MODEL CALCULATIONS OF THE $^{110}Cd(n,\gamma)^{111m}Cd$ CROSS SECTION

by

D. L. Smith, J. W. Meadows, P. A. Moldauer and W. P. Poenitz
Argonne National Laboratory
Argonne, Illinois, USA

Abstract

The cross section for the $^{110}Cd(n,\gamma)^{111m}Cd$ reaction has been measured in the energy 0.14 - 1.5 MeV by means of activation. Both natural cadmium and ^{110}Cd - and ^{111}Cd-enriched samples were used in the measurements in order to distinguish the capture activation reaction from the $^{111}Cd(n,n')^{111m}Cd$ reaction, which becomes involved due to the presence of ^{111}Cd in the samples. Optical, statistical and gamma-ray cascade model calculations were performed in order to explain the energy dependence of the capture activation cross section.

I. Introduction

The $^{111}Cd(n,n')^{111m}Cd$ reaction is of interest for reaction dosimetry because of its low threshold ($\approx$0.4 MeV), and convenient half life of 48.6 min[1]). However, ^{111}Cd has an abundance of only 12.8% in elemental cadmium, and a fraction of neutron capture in the 12.5%-abundant ^{110}Cd results in formation of the same isomeric state of ^{111}Cd. This makes the ^{111m}Cd activation for elemental cadmium pseudo-threshold in nature, unlike fast neutron activation of ^{115m}In[2] for elemental In, which behaves as a pure threshold reaction since inelastic scattering from ^{115}In is the only means for exciting the isomer. This distinction has important implications for dosimetry applications.

The fraction of neutron capture in ^{110}Cd resulting in activation of the isomeric state of ^{111}Cd is expected to be small because of the large spin difference between compound states of ^{111}Cd populated by s,p,d...-wave-neutron capture by the spin 0 target, ^{110}Cd, and the spin of the isomeric

state. Measurements of the ^{111m}Cd activation cross section of elemental cadmium confirmed this expectation[3] (see Fig. 1.A). Fig. 1.B indicates the response of ^{111m}Cd activation for ^{235}U fission-neutron emission spectrum. It can be concluded that the elemental Cd activation response for hard neutron spectra is predominantly ^{111}Cd(n,n')-induced, and this reflects the threshold nature of this process. However, activation in softer-spectra assemblies might have significant contributions from the neutron capture in ^{110}Cd. Thus, an investigation of ^{110}Cd capture activation of the isomer is of interest in this applied context.

The measurements on elemental cadmium have been described in detail[3]. A more detailed investigation of the ^{111}Cd(n,n')^{111}Cd and ^{110}Cd(n,γ)^{111m}Cd reactions in the energy range 0.4 - 1.5 MeV has been performed using enriched samples of ^{110}Cd and ^{111}Cd[4]. The present paper will summarize these results, emphasizing those aspects of the experiment dealing with capture.

II. Experiment

Details of the experimental procedure are reported in Refs. 3 and 4, and will only be outlined here. Two Cd metal disks 2.54-cm-dia × 0.15-cm-thick (≈12 g each), one enriched to 97.2% in ^{110}Cd and the other to 96.0% in ^{111}Cd were obtained from the Stable Isotopes Pool at Oak Ridge[5]. These samples were attached to a low-mass fission chamber (e.g., Fig. 1, Ref. 6) and then placed at zero degree on a beam line at the Argonne National Laboratory Fast-Neutron Generator Facility[7]. The fission chamber was loaded with a thin ^{235}U-enriched uranium deposit, and this device was used as a relative neutron fluence monitor. Nearly monoenergetic neutrons of variable energy were produced by the ^{7}Li(p,n)^{7}Be reaction[8], and the Cd samples were located a few cm from this near-point source. The 245-keV gamma rays occurring in the decay of ^{111m}Cd[1] were detected with a Ge(Li) detector. At least 24 hours (≈30 half lives for ^{111m}Cd decay) were allowed to elapse following irradiation of a sample before it was re-used for another measurement. This was more than adequate to insure that no run was affected by residual activity from the previous run, even in severe cases where a low-activity yield measurement followed a high-activity yield measurement.

Since the irradiation geometry was fixed, and the two cadmium samples were quite similar in shape and atom numbers, it was possible to obtain a unique value of the cross section ratio for ^{111m}Cd activation from ^{110}Cd capture and ^{111}Cd inelastic scattering at each measured energy. All that was required was a precise knowledge of the ^{110}Cd and ^{111}Cd isotopic abundances, the sample masses, and the relative neutron fluences and induced activities for the two samples. Many of the corrections normally required for cross section measurements nearly cancelled. Other corrections were smaller for this ratio measurement than they would have been for a direct cross section measurement. All the known significant corrections were calculated and applied to the ratio data. Absolute ^{111}Cd(n,n')^{111m}Cd and ^{110}Cd(n,γ)^{111m}Cd cross sections were then derived using the measured

ratios and the natural cadmium activation results reported in Ref. 3. The derived cross section values and errors are reported in Ref. 4. These cross sections are plotted in Figs. 2 and 3 of the present paper.

III. Model Calculations

The shape of the capture activation cross section for ^{110}Cd is quite interesting (see Fig. 3); thus, model calculations were performed in order to provide an explanation for this behavior. Knowledge of various properties of the compound nucleus ^{111}Cd is required in order to calculate the capture activation cross section for ^{110}Cd. Therefore, it proved beneficial to also perform inelastic scattering calculations for ^{111}Cd during this investigation.

The capture cross section for ^{110}Cd can be expressed as

$$\sigma(E) = \sum_{J,\pi} \sigma(J,\pi,E),$$

and the activation cross section is then

$$\sigma_m(E) = \sum_{J,\pi} B(J,\pi,E)\ \sigma(J,\pi,E),$$

where $J=\ell\pm 1/2$ is spin of the capture state and $B(J,\pi,E)$ is the probability that this state will ultimately decay by radiative transitions to the 0.396-MeV isomeric level.

The capture cross sections, $\sigma(J,\pi,E)$, were computed using the optical model to calculate transmission coefficients, and the Hauser-Feshbach formula with width fluctuation corrections to determine the capture cross sections, in the presence of competition from elastic and inelastic scattering[9,10]. The neutron width fluctuations were computed on the basis of chi-squared distributions with the degree of freedom parameter for each neutron channel computed according to the formula of Moldauer[11]. These calculations were performed using the code ABAREX[12].

The optical model parameter set derived by Moldauer[13] was used in the present work. Vonach and Smith[14] showed that these parameters yield reasonable agreement with experimental elastic and inelastic scattering cross sections of Ag, In and Cd for the same energy range as the present investigation. The parameters are:

Potential	Type	Depth (MeV)	Radius $\div A^{1/3}$ (fm)	Diffuseness (fm)
Real	Wood-Saxon	46	1.285	0.62
Imaginary	Gaussian	14	1.390	0.50
Real Spin-Orbit	Thomas	7	1.285	0.62

The gamma-ray transmission factors were computed on the basis of a Brink-Axel[15] giant dipole resonance at a gamma-ray energy of 16.8 MeV, with a width of 5 MeV. The factor Γ_γ/D was adjusted so that the calculated capture cross section below 0.1 MeV agreed with the values reported by Musgrove et al.[16]. The value $\Gamma_\gamma/D = 0.00046$ yielded the best results. ABAREX was modified so that it would print out not only the total capture cross section, $\sigma(E)$, but also the components, $\sigma(J,\pi,E)$. The calculated capture cross section curve is plotted in Fig. 3.

Inelastic scattering calculations were performed for ^{111}Cd using the same optical model parameters. ^{111}Cd(n,γ)^{112}Cd competition was included, with the factor Γ_γ/D set equal to 0.008 so that the calculated capture cross sections below 0.1 MeV agreed with values reported by Musgrove et al.[16]. The calculated inelastic scattering cross sections for the low-lying levels are plotted in Fig. 2. The ^{111}Cd(n,n')^{111}Cd data are well described by the model below 1 MeV if it is assumed that the isomer is fed by excitation of the 0.396-MeV (100%), 0.700-MeV (67%), 0.754-MeV (5%) and 0.867-MeV (5%) states only, with the indicated branching ratios.

The factors $B(J,\pi,E)$ were calculated using the code CASCADE which is based upon the gamma-ray cascade model of Poenitz[17]. The compound nucleus ^{111}Cd was assumed to consist of a combination of the known discrete levels below 1.1 MeV[1], and a continuum of levels described by a level density formalism at higher excitations. The level density parameters were obtained from the literature[18-20], as described in Ref. 4. The gamma-ray transitions between various states in the continuum and between the continuum and the discrete low-lying levels were calculated using the Weisskopf formula. The maximum cascade multiplicity was limited to eight. Lacking specific guidance from the literature, it was assumed that all the transitions were electric dipole (E1). It was further assumed that the only discrete levels below 1.1 MeV which feed the isomer are the 0.700-, 0.754- and 0.867-MeV levels, consistent with the observed results for ^{111}Cd(n,n')^{111m}Cd. The calculated ^{110}Cd(n,γ)^{111}Cd cross sections are shown in Fig. 3. The calculated results are quite sensitive to several aspects of the model. If, e.g., the E2/E1 gamma transition strength ratio is taken to be 0.1 instead of zero, σ_m increases by $\approx$30% at 0.5 MeV. If it is assumed that the isomeric level is populated only by transitions from continuum levels above 1.1 MeV, σ_m decreases by $\approx$60% at 0.25 MeV. The results are less sensitive to other model parameters, and these are reasonably well established [18-20].

IV. Conclusions

As seen in Fig. 3, the model calculations described in Section III provide a good description of neutron capture and neutron capture activation for ^{110}Cd. The cusps at 0.66 and 1.48 MeV indicate the onset of new levels in ^{110}Cd, and hence inelastic scattering competition to the capture process. Above 0.25 MeV, the capture and activation cross sections tend to increase with energy, due to the dominant influence of ℓ=2 and higher-order partial wave capture, until the trend is interrupted by the onset of inelastic scattering competition, first from the 0.658-MeV level and then from the 1.476-MeV level. The capture of ℓ=0 and ℓ=1 neutrons is dominant only below 0.25 MeV, and the ℓ=0 component is responsible for the increase in the cross section below $\approx$0.1 MeV.

Acknowledgements

The authors are indebted to A. B. Smith for his valuable suggestions. This work was supported by the U.S. Department of Energy.

References

1. Table of the Isotopes, Seventh Edition, eds. C. Michael Lederer and Virginia S. Shirley, John Wiley and Sons, Inc., New York (1978).

2. Donald L. Smith and James W. Meadows, "Fast-Neutron Excitation of Isomeric States in Indium," Nucl. Sci. Eng. 60, 319 (1976).

3. Donald L. Smith and James W. Meadows," Fast-Neutron Activation of 48.6-min Cd-111m for Natural Cadmium," to be published in Nuclear Science and Engineering.

4. D. L. Smith, J. W. Meadows, P. A. Moldauer and W. P. Poenitz, "Fast-Neutron Activation of 48.6-min Cd-111m," submitted to Nuclear Physics A for publication.

5. Stable Isotopes Division, Oak Ridge National Laboratory, Oak Ridge, Tennessee 37830.

6. Donald L. Smith and James W. Meadows, Nucl. Sci, Eng. 60, 319 (1976).

7. S. A. Cox and P. R. Hanley, IEEE Trans. Nucl. Sci. 18, 108 (1971).

8. J. W. Meadows and D. L. Smith, "Neutrons from Proton Bombardment of Natural Lithium," ANL-7938, Argonne National Laboratory (1972).

9. P. A. Moldauer, Phys. Rev. C11, 426 (1975).

10. P. A. Moldauer, Phys. Rev. C13, 2093 (1976).

11. P. A. Moldauer, Nucl. Phys. A244, 185 (1980).

12. P. A. Moldauer, Argonne National Laboratory, Argonne, Illinois 60439, U.S.A. (unpublished).

13. P. A. Moldauer, Nucl. Phys. 47, 65 (1963).

14. W. G. Vonach and A. B. Smith, Nucl. Phys, 78, 389 (1966).

15. P. Axel, Phys. Rev. 126, 671 (1962).

16. A. R. de L. Musgrove, B. J. Allen, J. W. Boldeman and R. L. Macklin, "Recent Measurements of Neutron Capture Cross Sections in the Fission Product Mass Region," Proc. Int. Conf. on Neutron Physics and Nuclear Data for Reactors and Other Applied Purposes, Harwell, U.K., 25-29 September 1978, p. 449 (1978).

17. W. P. Poenitz, Zeit. fuer Physik 197, 262 (1966); also paper is reprinted as "A Gamma-Ray Cascade Model for the Calculation of Average Gamma-Ray Multiplicities and Isomeric Cross Section Ratios," KFK-523, Kernforschungszentrum Karlsruhe, Karlsruhe, Fed. Rep. of Germany (1966).

18. N. N. Abdelmalek and V. S. Stavinsky, Nucl. Phys. 58, 601 (1964).

19. A. V. Malyshev, Soviet Phys. JETP 18, 221 (1964).

20. P. E. Nemirovsky and Yu. V. Adamchuk, Nucl. Phys. 39, 551 (1962).

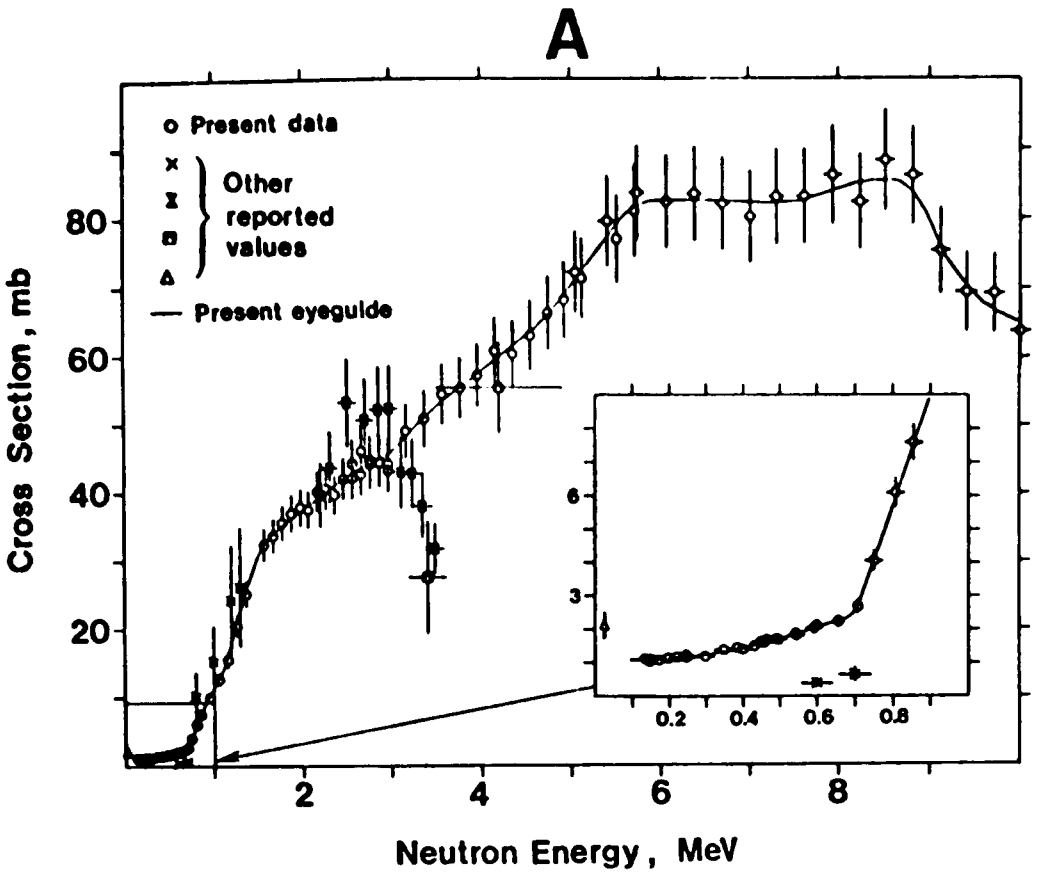

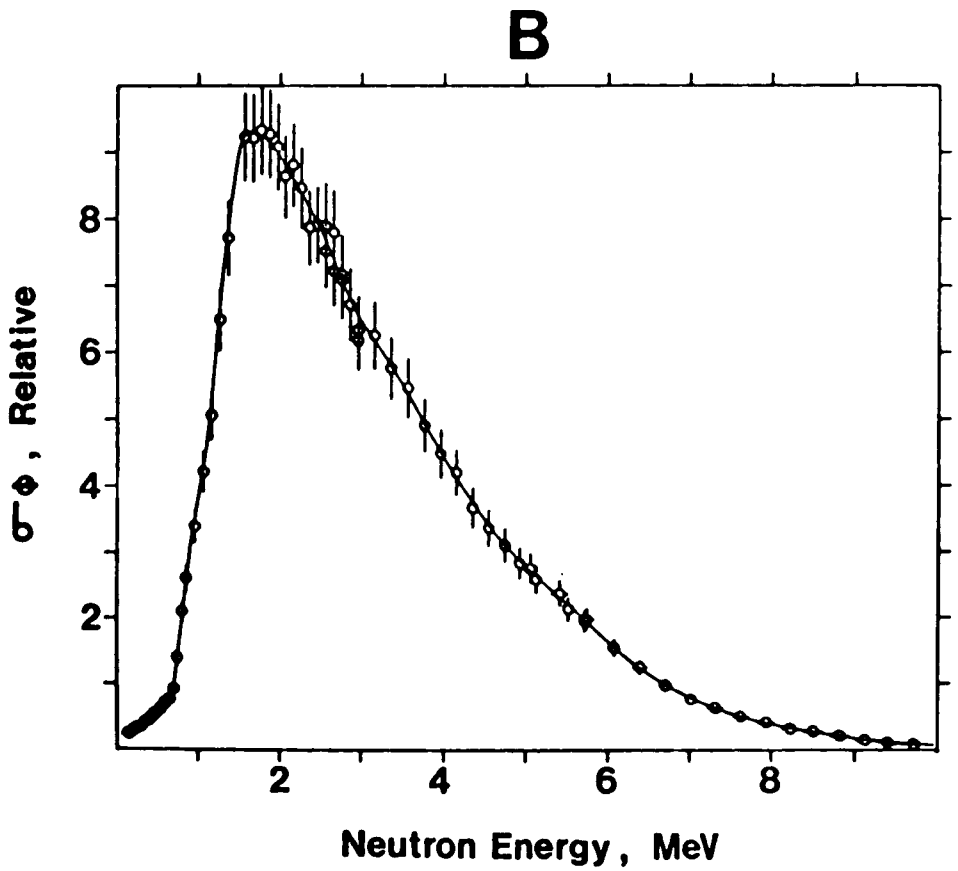

Figure 1. A: measured cross sections for fast-neutron activation of ^{111m}Cd in natural Cd (Ref. 3). B: Response of experimental cross section data from this laboratory in a ^{235}U thermal-

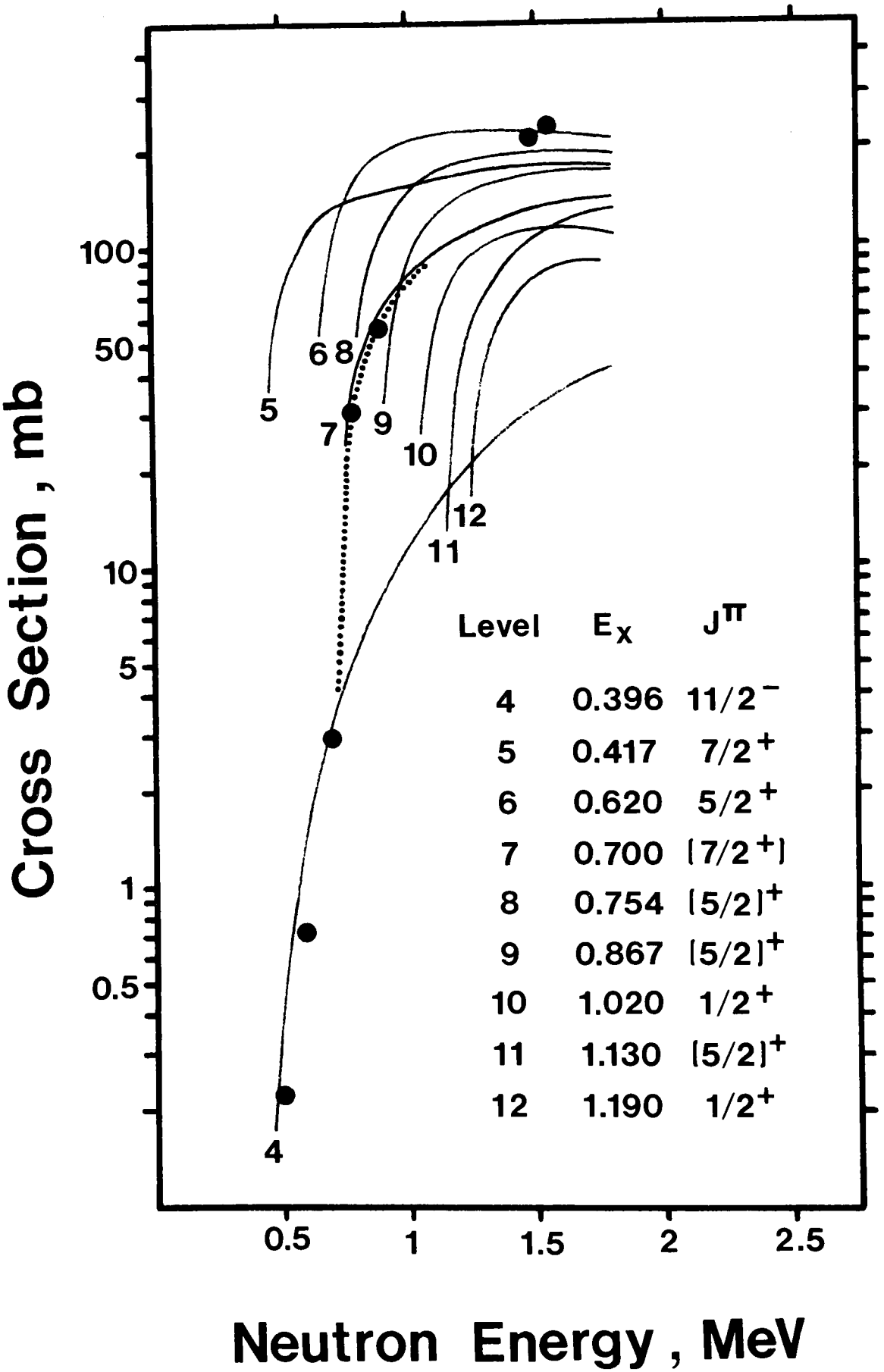

Figure 2. Measured and calculated inelastic scattering cross sections for ^{111}Cd. Solid curves apply to excitation of specific levels.

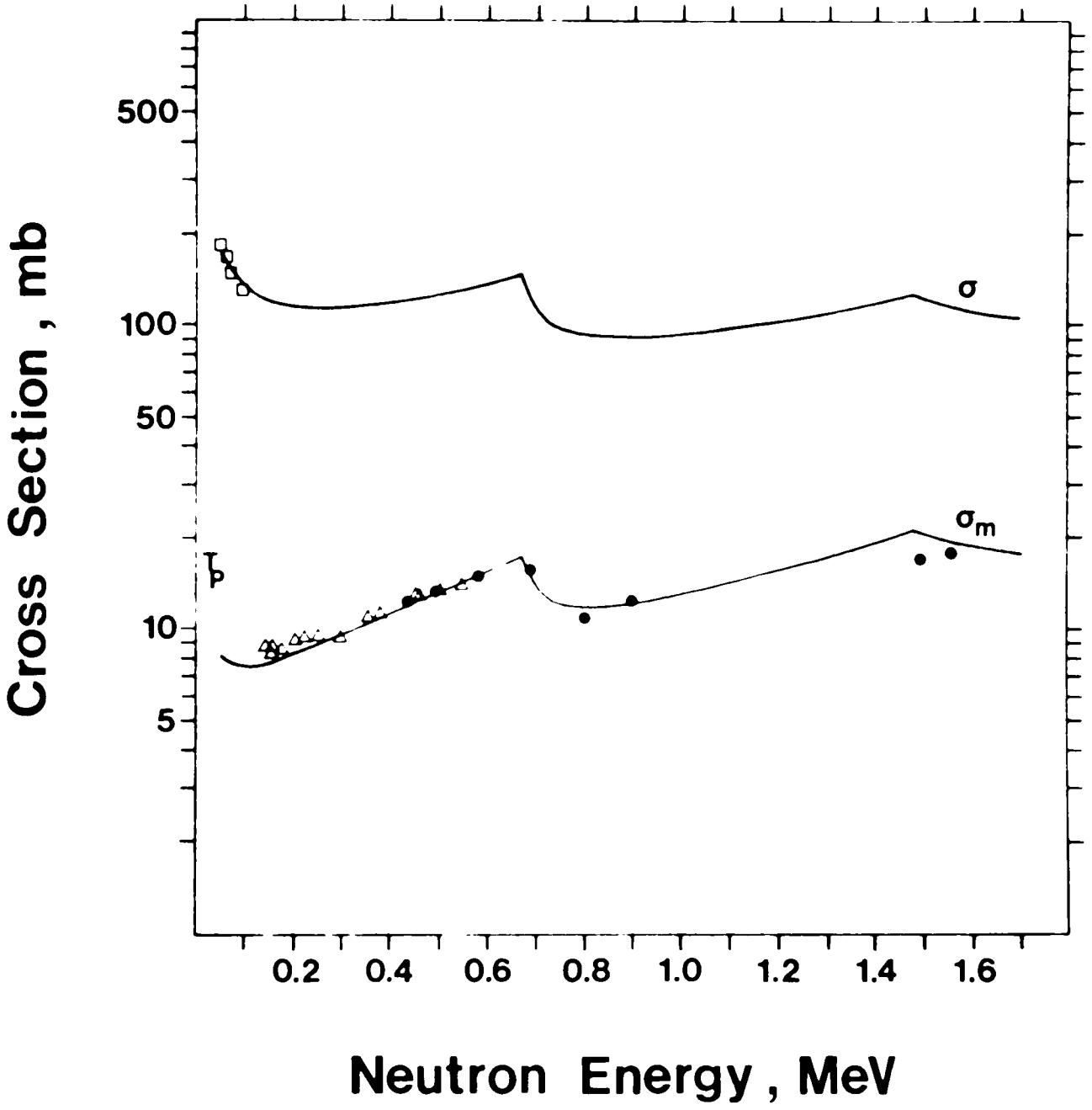

Figure 3. Measured and calculated capture (σ) and capture activation (σ_m) cross sections for ^{110}Cd. Present work (Δ and O). Other symbols refer to values reported in the literature as described in Ref. 4.

NEUTRON-CAPTURE-ACTIVATION CROSS SECTIONS OF $^{94,96}Zr$ and $^{98,100}Mo$ AT THERMAL AND 30 keV ENERGY*

by

J. M. Wyrick** and W. P. Poenitz
Argonne National Laboratory
Argonne, Illinois, USA

Abstract

Neutron-capture cross sections of $^{94,96}Zr$ and $^{98,100}Mo$ were measured relative to the standard-capture cross section of gold at thermal and 30 keV neutron energies using the activation technique. The reported values are based upon available decay-scheme information.

I. Introduction

Fast neutron-radiative-capture cross sections play a significant role in many aspects of reactor design and development. Though of importance in the applied area, they are often poorly known with significant discrepancies and a lack of experimental data. Fast neutron-capture cross sections can be calculated in terms of the optical- and statistical-nuclear models. Unfortunately, such calculations have lead to results which differ substantially[1] (by factors of 2, 5 and even 10) due to the uncertainties of model parameters and shortcomings of the models themselves. A study of model-parameter sensitivities[2-4] has shown that the lower keV range--which is of greatest importance for fast reactor applications--is to some extent an exception:

---

*This work was supported by the U.S. Department of Energy
**Summer Research Participant, Permanent Address: Department of Physical Science, Harris-Stove State College, St. Louis, MO

The shape of the cross section can be reasonably well calculated, but uncertainty exists regarding the normalization. Thus, rather reliable fast-neutron-capture cross sections could be calculated if experimental data of sufficient accuracy were available at one or two energies in the 10-100-keV energy range.

There are several neutron sources available in this energy range which have been frequently used in the past. The forward neutron cone obtained for proton energies slightly above the threshold of the $^7Li(p,n)^7Be$ reaction has an average energy of ≈30 keV, and an energy spread of ≈ ± 7 keV (for ≈1 keV primary energy above the threshold). This source has several advantageous features[5] which were considered important for the present measurements.

Neutron-capture events can be measured with a variety of methods, one of which is the activation technique. Though not generally applicable, it has several advantageous features; e.g. isotopic selectivity, the possibility of using small samples, and high accuracy in some cases. Sample activity might be measured absolutely, but more conveniently a γ-ray occurring in the decay is detected. In the latter case, the derived cross section depends on decay-scheme information. By also measuring at thermal energy, utilizing the well known thermal cross section of gold for the neutron-flux determination, one can make the fast-neutron cross-section measurement relative to the thermal cross section, and thus independent of decay-scheme information[5].

The present measurements are the first of a series intended to provide capture cross-section data at 30 keV for normalization of nuclear-model-calculated cross sections. The activation technique was used, and measurements were made relative to the standard capture cross section of gold (576 mb at 30 keV, and 98.65 b at 0.0253 eV).

II. Experimental Technique and Analysis

The experimental set-up and procedures were described on previous occasions[5]. Thus, only a brief description will be given here. The 30-keV-neutron source was the kinematically collimated forward cone obtained above and close to the threshold energy of the $^7Li(p,n)Be^7$ reaction. The primary energy was controlled by monitoring the opening angle of the neutron cone with Long Counters. The samples were metallic discs of 1.59 cm diameter of elemental zirconium, molybdenum, and gold of 99.9% or better chemical purity. The thicknesses were 0.102 cm for zirconium, 0.0254 and 0.0762 cm for molybdenum and 0.00127 and 0.0254 cm for gold. The thin gold foils were used in the thermal irradiations.

One of the gold samples, and one or two of the other samples, were placed as a sandwich at a distance of ~1 cm from the neutron source, such that the entire neutron cone passed through the samples. The irradiations at thermal energies were carried out in the thermal column of a 10 kW reactor, with the samples mounted on a rotating disc.

After irradiation, the samples were mounted ≈1.5 cm from the front surface of a 4-cm-diameter × 4.4-cm-long Ge(Li) detector and the γ-ray spectra were recorded with a multichannel analyzer. The photopeak-detection efficiency of the Ge(Li) detector was determined with absolutely calibrated γ-ray emitters (^{198}Au, see Ref. 7; ^{243}Am, see Ref. 5) and a multiline γ source.

Several gamma rays occurring in the decay-chains of the activated samples were utilized. Decay-scheme information (half lives, branching ratios, and conversion coefficients) were derived from Ref. 8, and detailed values used in the present work will be reported elsewhere[9].

III. Experimental Results and Discussion

The present results for the thermal-neutron-capture cross sections are given in Tables 1 and 2. The present data for the zirconium isotopes are in best agreement with the values reported by Fulmer et al.[10] Agreement with the results by Santry et al.[11] is reasonable, however, disagreement exists between the present results and those reported by Ricabarra et al.[12], specifically for ^{96}Zr. The present data for the molybdenum isotopes agree with most of the more recently reported values (see Table 2).

Tables 1 and 2 also list the evaluated thermal cross sections by Mughabghab et al.[23] Comparison with the present values suggests that there is no incentive to renormalize the present values at 30 keV with the thermal cross sections for ^{94}Zr and ^{98}Mo. A renormalization would result in a change for ^{100}Mo and ^{96}Zr, of 5% and 10% respectively. However, the present value for ^{96}Zr agrees rather well with the result by Fulmer et al.[10], and has a lower uncertainty than the evaluated value. The renormalized value of ^{100}Mo at 30 keV would be well within the quoted uncertainty. Thus, we choose not to utilize the thermal cross section results for the normalization of the 30 keV values, but to quote them as independent data based upon presently available decay-scheme information.

The present results for the zirconium isotopes at 30 keV are shown in Fig. 1. Previously reported values in the energy range from 20-40 keV are shown for comparison. Also shown are cross sections calculated in terms of the statistical and optical models. Optical model parameters were obtained by fitting total and inelastic cross sections and strength functions of Y and Zr with the code ABAREX[38]. Values of Γ_γ/D were adjusted (but not fitted) to yield capture cross section values in reasonable agreement with the present data. Neutron-capture cross sections were also calculated for ^{90}Zr, ^{91}Zr, and ^{92}Zr. The derived elemental capture cross section compares well with experimental data (see Ref. 39).

Agreement between the present values and previously reported data is reasonable for ^{94}Zr. A substantial discrepancy (factor of 3) exists between the present value of $\sigma_{n,\gamma}(^{96}\mathrm{Zr})$ and a measurement by Macklin et al.[22] The present result is less discrepant with an earlier measurement by Macklin et al.[24].

The present results at 30 keV for the molybdenum isotopes are shown in Fig. 2. Several of the previously reported values in the 20-40 keV energy range were obtained with Sb-Be(γ,n) sources. These data vary over a range of a factor of two for ^{98}Mo and a factor of 4 for ^{100}Mo. Our result for ^{98}Mo agrees with the more recent measurement by Rimawi and Chrien[33] but disagrees with the data by Musgrove et al.[26]; however, agreement with the latter is better for ^{100}Mo.

It is believed that the present series of experiments will help to resolve existing capture cross section data discrepancies in the keV-energy range by simultaneously measuring at thermal energy.

Table I. Present Results for the ^{94}Zr(n,γ) and ^{96}Zr(n,γ) Thermal Maxwellian Average Cross Sections and Comparison with Previously Reported Data.

Nuclei	Reference	Value/mb
^{94}Zr	Fulmer et al (10)	52 ± 3
	Santry et al. (11)	47.5 ± 2.4
	Ricabarra et al. (12)	63 ± 8
	Lyon (16)	~60
	Present Result	49.4 ± 1.7
	BNL-325 (Mughabghab et al.[23])	49.9 ± 2.4
^{96}Zr	Fulmer et al. (10)	20 ± 3
	Santry et al. (11)	22.9 ± 1.0
	Ricabarra et al. (12)	5.7 ± 1
	Lyon (16)	$\lesssim$54
	Present result	20.3 ± 0.6
	BNL-325 (Mughabghab et al.[23])	22.9 ± 1.0

Table II. Present Results for the ^{98}Mo(n,γ) and ^{100}Mo(n,γ) Thermal Maxwellian Average Cross Sections and Comparison with Previously Reported Data.

Nuclei	Reference	Value/mb
^{98}Mo	Gleason (13)	145 ± 15
	Dahlberg et al. (14)	180 ± 20
	Cabell (15)	136 ± 3
	Lyon (16)	580 ± 58
	Sims and Jahnke (17)	137 ± 6
	Hughes (18)	130 ± 50
	Pommerance (19)	400 ± 400
	Seren (20)	415 ± 83
	Fabry (21)	120
	Present Result	131.7 ± 5.3
	BNL-325 (Mughabghab et al.[23])	130 ± 6

Table II. Continued

Nuclei	Reference	Value/mb
^{100}Mo	Cabell (15)	199 ± 5
	Gleason (13)	195 ± 10
	Seren et al. (20)	475 ± 95
	Pommerance (19)	500 ± 500
	Present Result	188.8 ± 6.9
	BNL-325 (Mughabghab et al.[23])	199 ± 3

References

1. S. Iijima et al., J. Nuclear Sci. Technology 14, 161 (1977).
2. W. P. Poenitz, Proc. Specialists Meeting on Neutron Cross Sections of Fission Product Nuclei, Bologna 1979, p. 85.
3. W. P. Poenitz, Conf. on Nuclear Cross Sections for Technology, NBS Special Publication 594, 297, Knoxville (1979).
4. P. T. Guenther et al., Proc. Conf. on Nuclear Data Evaluation Methods and Procedures, DOE-NDC-23 NEANDC(US)-209, p. 567 (1981).
5. W. P. Poenitz et al., Nuclear Sci. and Engineering 78, 239 (1981).
6. A. E. Johnsrud et al., Phys. Rev. 116, 927 (1959).
7. W. P. Poenitz, Nuclear Research Center Karlsruhe Report KIK 180 (1963).
8. E. Browne et al., "Table of Isotopes", John Wiley and Sons Inc. (1978).
9. J. M. Wyrick and W. P. Poenitz, Argonne National Laboratory Report ANL/NDM 60, to be published (1982).
10. R. H. Fulmer et al., Nucl. Sci. Eng. 46, 314 (1971).
11. H. Santry, Canad, J. Physics 51, 2441 (1973).
12. M. D. Ricabarra et al., Amad J. Physics 48, 2362 (1970).
13. D. Gleason, private communication to S. F. Mughabghab (see ref. 23).
14. D. A. Dahlberg et al., J. Nucl. Energy 14, 53 (1961).
15. M. J. Cabell, J. of Inorganic and Nuclear Chemistry 12, 172 (1960).
16. W. S. Lyon, Nucl. Sci. Eng. 8, 378 (1960).
17. M. Sims et al., J. of Inorganic and Nuclear Chemistry 29, 2853 (1967).
18. D. J. Hughes, Phys. Rev. 91, 1423 (1953).
19. H. Pommerance, Phys. Rev. 88, 412 (1952).
20. L. Seren et al., Phys. Rev. 72, 888 (1947).
21. A. M. Fabry, private communication to S. F. Mughabghab (see Ref. 23).
22. R. L. Macklin, T. Inada, and J. H. Gibbons, Bull. Am. Phys. Soc. 8, 81 (Y6) (1963).

23. S. F. Mughabghab et al., "Neutron Cross Sections", Academic Press (1981).
24. R. L. Macklin et al., Phys. Rev. 107, 504 (1957).
25. J. W. Boldeman et al., Nucl. Phys. A269, 31 (1976).
26. A. R. Del. Musgrove et al., Nucl. Phys. A270, 108 (1976).
27. S. P. Kapchigashev and Yu. P. Popov, 64 Dubna, 104 (1964).
28. R. Booth et al., Phys. Rev. 112, 226 (1958).
29. D. C. Stupegia et al., J. Nucl. Energy 22, 267 (1968).
30. R. P. Anand et al., 74 Bombay, 2, 101 (1974).
31. S. N. Chaturvedi et al., 70 Madurai, 2, 615 (1970).
32. J. F. Vervier, Nucl. Physics 9, 569 (1959).
33. K. Rimawi and R. E. Chrien, Phys. Rev. C15, 1271 (1977).
34. V. N. Kononov et al., J. Nucl. Energy 11, 46 (1959).
35. M. Smiramachandra Murty et al., J Phys. Soc. Japan 35, 8 (1973).
36. S. S. Hasan et al., Nuovo Cimento B58, 402 (1969).
37. K. Furr, Duke University Report TID-16059 (1962).
38. P. Moldauer, Argonne National Laboratory, private communication (1980).
39. W. P. Poenitz, this meeting (1982).

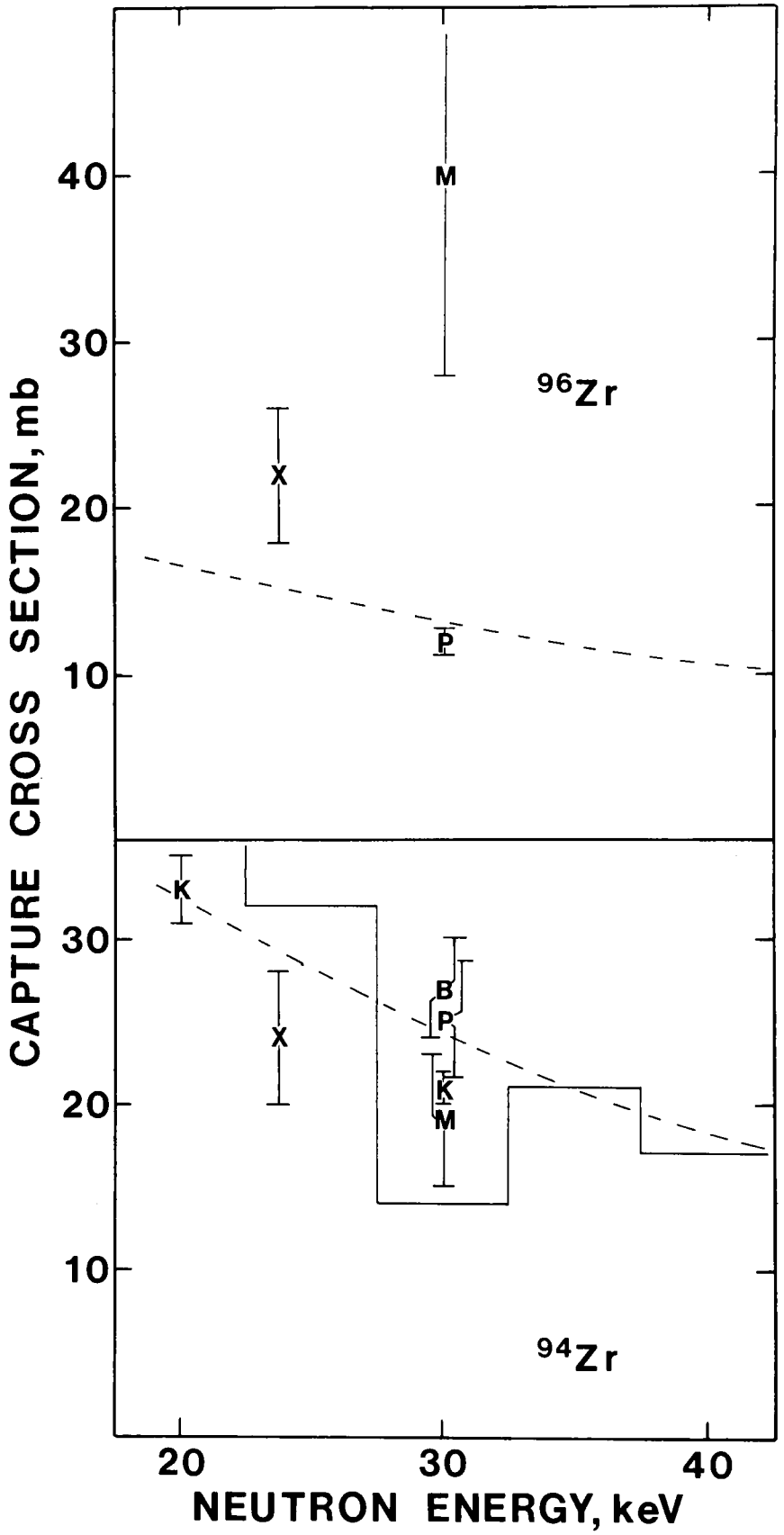

Fig. 1. Comparison of the present results for $^{94,96}Zr(n,\gamma)$ and previously reported data. The letters refer to: M Ref. 22, X Ref. 24, K Ref. 27, B Ref. 25. The histogram are also the data of Ref. 25. The present data are labeled with P. The dashed lines are model calculations (see text).

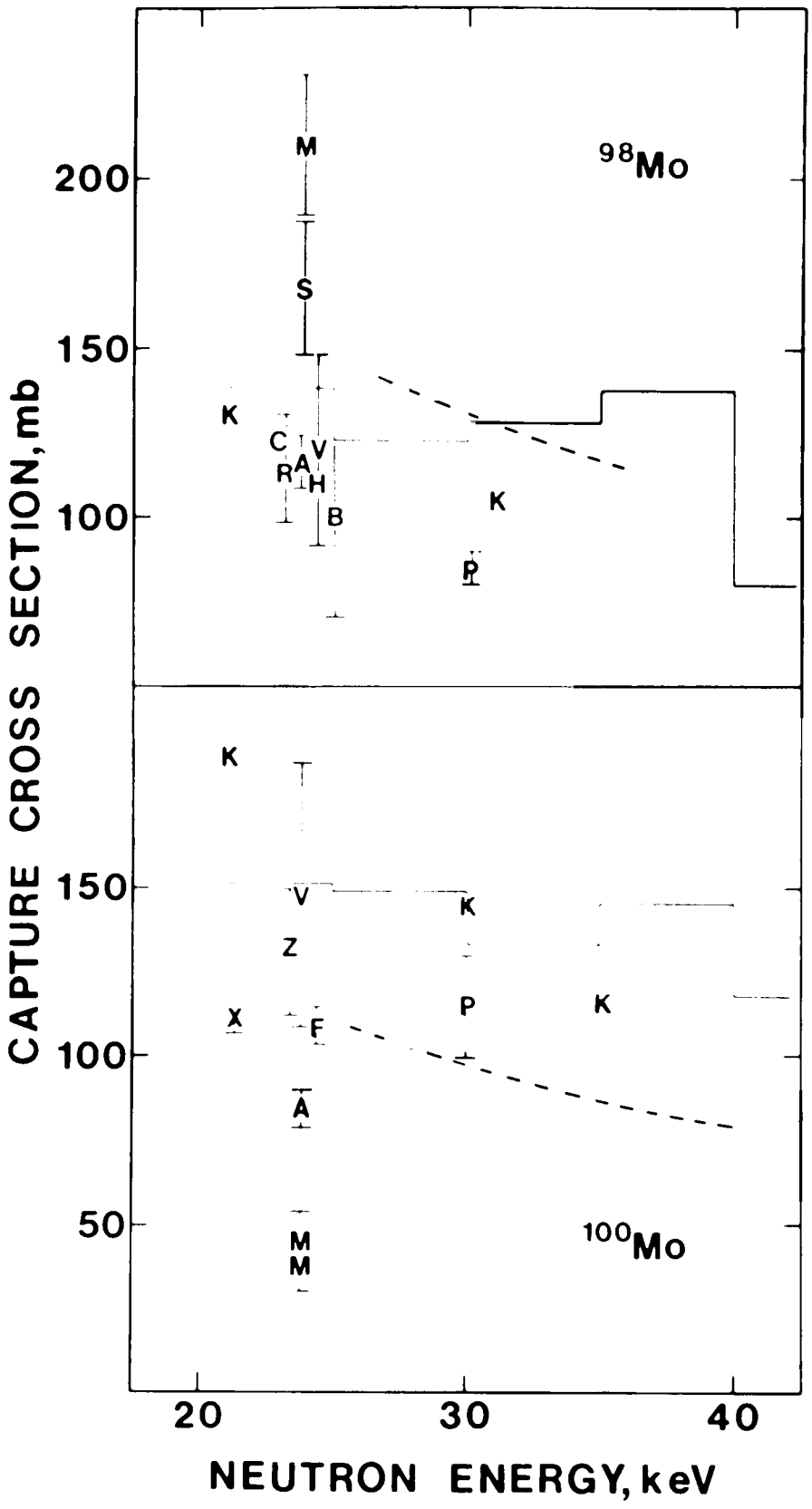

Fig. 2. Comparison of the present results for $^{98,100}Mo(n,\gamma)$ and previously reported data. The letters refer to: M Ref. 24, A Ref. 30, K Ref. 27, X Ref. 34, Z Ref. 35, V Ref. 32, H Ref. 36, C Ref. 31, F Ref. 37, B Ref. 28, R Ref. 33, S Ref. 29. The present data are labeled with P. The histogram are data of Ref. 26. ENDF/B-V values are indicated with dashed lines.

Discussion

QUESTION: K. Wisshak
How many keV above the threshold of the Li(p,n) reaction were the activations performed?

ANSWER: W. Poenitz
About 1-2 keV. That gives you a spread of about 7 keV in neutron energy.

PROMPT GAMMA-RAY DETECTORS FOR THE MEASUREMENT OF NEUTRON CAPTURE CROSS-SECTIONS.

D. B. Gayther & R. B. Thom*
Nuclear Physics Division, A.E.R.E., Harwell, Oxon, U.K.

ABSTRACT

A review is given of current techniques for detecting prompt gamma-radiation as a means of measuring total capture cross-sections. The discussion is generally restricted to systems with low or moderate gamma-ray energy resolution. Three classes of detector are considered; (i) the total absorption type (ii) detectors with efficiency proportional to gamma-ray energy, and (iii) detectors of low efficiency and known gamma-ray response. Particular attention is given to the problems of background from reactions which compete with neutron capture, and the sensitivity of capture detectors to scattered neutrons. The extraction of capture yields from observed data is briefly considered.

1. INTRODUCTION

In this review we shall discuss techniques for measuring fast neutron radiative capture cross-sections which rely on observation of the emitted prompt gamma-radiation. Developments which have taken place since the review by Chrien /1/ at the 1975 Washington Conference will be emphasized. Although we shall be mainly concerned with measurements in the kilovolt region and above, most of the detectors described are equally suitable for lower energies. Indeed, a system which can be used at thermal neutron energy provides a convenient point for the absolute normalization of the cross-section.

The discussion will be limited to the measurement of the total capture cross-section, that is the cross-section for all transitions which de-excite the compound nucleus. The use of high resolution spectroscopy to measure the partial capture cross-sections for particular transitions will not in general concern us.

Neutron sources available for measuring fast neutron capture cross-sections include Van de Graaff generators, pulsed 'white' neutron sources such as linacs, and reactor filtered beams.

* Imperial College of Science and Technology, London, attached to A.E.R.E.

Prompt gamma-ray detectors are particularly suited to the time-of-flight technique on a pulsed neutron source, and most of the measurements we shall consider are of this type.

In the following section, Section 2, the general features of detector design will be considered and subsequent sections will be devoted to more detailed discussions of particular systems. For convenience we have chosen to classify the detectors in the following way; (i) Total Absorption Detectors, whose principal feature is a high efficiency, (ii) Detectors which give a response proportional to total energy released, and (iii) Detectors whose efficiency is known either through measurement or calculation. These three types are discussed in Sections 3, 4 and 5. In Section 6 we consider the particular problem of the sensitivity of capture detectors to neutrons. Section 7 outlines the steps involved in the reduction of raw capture data to capture yields and in Section 8 we make some concluding remarks.

2. THE DESIGN OF CAPTURE GAMMA-RAY DETECTORS.

In a capture gamma-ray detection system, a sample of the material to be studied is placed at some distance from a neutron source and the prompt gamma-radiation emitted by the sample is observed in a detector which is protected from radiation coming directly from the source. With a monoenergetic source this protection can be in the form of gamma-ray and neutron shielding material, but when a 'white' source is used, the sample is placed in a collimated neutron beam and the protection from direct source radiation simply requires the detector to be placed outside the beam. Common factors which affect the design of such a system, and the influences of which we shall now discuss in turn, include;

(i) relevant properties of capture gamma-ray spectra,
(ii) discrimination against sources of prompt gamma-rays other than capture in the sample, and
(iii) relevant properties of available gamma-ray scintillators.

2.1 The nature of the capture gamma-ray spectrum.

When a neutron is captured by a nucleus, a state is formed whose initial excitation Ex is :

$$Ex = En + Es$$

where En is the centre of mass energy of the incident neutron and Es is the neutron separation energy. In a capture reaction the nucleus de-excites by emitting one or more gamma-rays, called the cascade, the energies of the individual members of which sum to Ex. Figure 1, which is taken from a review by Bollinger /2/, shows a representative capture gamma-ray spectrum for a heavy nucleus. The spectrum consists of discrete high energy lines arising from primary transitions from the initial to low-lying

final states, a statistical continuum at intermediate energies which emerges as the final state level spacing approaches the detector resolution, and discrete lines at low energy due to secondary gamma-rays from low-lying states. For less complex nuclei with a wide level spacing near the ground state the discrete nature of the spectrum is enhanced at the expense of the statistical component.

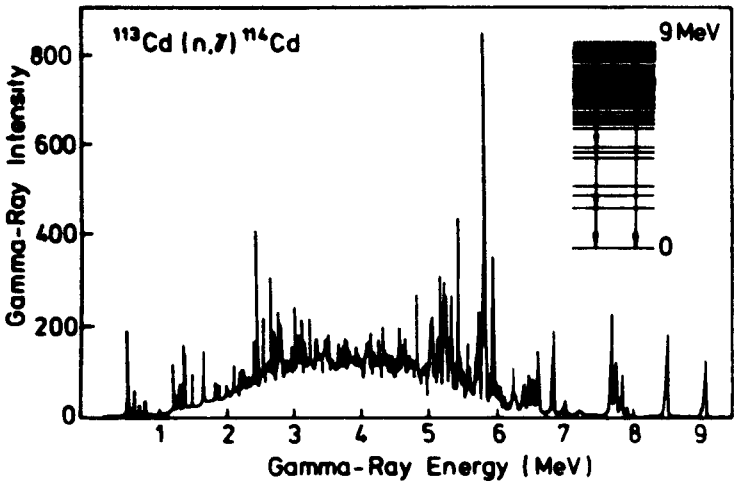

Figure 1. Representative thermal neutron capture gamma-ray spectrum observed with a Compton spectrometer (Groshev et al.,1960).

The example given is for thermal neutron capture. In the resonance region and above the spectra have a broad overall similarity of shape, however the intensities of particular transitions fluctuate and for compound nuclear reactions follow the well known Porter-Thomas distribution. This has the effect that in medium mass nuclei, such as occur in reactor structural materials, the gamma-ray spectra show pronounced differences between one resonance of the compound nucleus and the next. Even when averaged over many resonances, angular momentum selection rules impose a dependence of the spectrum on incident neutron energy. This is illustrated in Fig. 2 where spectra obtained with reactor filtered neutron beams of different energies are shown. In going from an average neutron energy of 2 keV to 24 keV the ratio of p-wave to s-wave capture is calculated to increase from 0.14 to 2.10 with a resultant change in the primary gamma-ray spectrum. Neutron capture mechanisms other than compound nucleus formation introduce an additional dependence of the spectrum on excitation energy. For a detailed discussion of capture mechanisms see for example Lynn /4/.

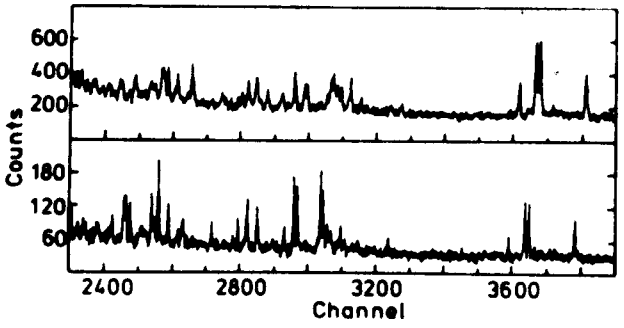

Figure 2. Spectrum of primary capture gamma-rays from resonance averaged capture of 2 keV (upper) and 24 keV (lower) neutrons in U-238 (C.W.Reich /3/).

An important consequence of these effects is that a central problem in the design of prompt gamma-ray detectors for the measurement of total capture cross-sections is the attainment of detection efficiencies which are independent of the changes in the gamma-ray spectra. This requirement leads to three broad classifications of detector type according to their response to gamma-rays, as follows:

(i) Total Absorption Detectors.

In this type of detector, usually a liquid scintillator of large volume, independence of the cascade mode is attained by making the detection efficiency approach 100% for all capture gamma-rays. Ideally, the detector surrounds the sample (4π - geometry) and absorbs all the emmitted gamma-radiation. This ideal is seldom achieved in practice since single capture gamma-rays of energy 8 MeV or more are not uncommon, and a device capable of detecting all such events would be so large that the environmental background would be overwhelming.

Total absorption detectors lend themselves to multi-segment arrangements which can yield information on gamma-ray multiplicities. The multiplicity may be of fundamental interest, but it can also be used to discriminate against unwanted events.

(ii) Total Energy Detectors

Suppose that we devise a system whose gamma-ray detection efficiency, ε_γ , is proportional to gamma-ray energy, E_γ ,

$$\varepsilon_\gamma = kE_\gamma$$

If we observe capture gamma-rays with such a system and further arrange that ε_γ is small so that the chance of observing more than one gamma-ray from a particular decay is negligible, then in a cascade of gamma-rays,

$$\sum_{i=1}^{\nu} E_{\gamma i} = E_x$$

and the probability of detecting an event, $\varepsilon_{\gamma T}$ can be written,

$$\varepsilon_{\gamma T} = \sum_{i=1}^{\nu} \varepsilon_{\gamma i} = k\sum_{i=1}^{\nu} E_{\gamma i} = kE_x$$

which depends only on the excitation energy of the capturing nucleus and is therefore independent of the mode of decay.

This is the principle of the Moxon-Rae detector which achieves this type of response through its design /5/. An alternative means of producing the same result is by appropriately weighting the pulse amplitude response of an arbitrary detector. Based on a suggestion by H.Maier-Leibnitz /6/, the first detector of this type was built by Macklin and Gibbons /7/.

(iii) Low efficiency detectors of known gamma-ray response.

Any system which detects only one cascade gamma-ray for each capture event can be used to determine the cross-section if the complete gamma-ray spectrum can be deduced. This requires a detector with adequate resolution and a measurement of a substantial portion of the spectrum. The usual pulse amplitude bias which is required to remove background events should, if possible, correspond to a low gamma-ray energy. The detector gamma-ray response function must be accurately known, and preferably it should be of simple shape. This will allow the true gamma-ray spectrum to be obtained above the discriminator bias level by unfolding the response function from the observed spectrum. The complete spectrum is obtained by some form of extrapolation. With this type of system, the extrapolation below a given bias will in general be considerably larger than for the Total Absorption Detector where the amplitude spectrum tends to peak near the total excitation energy. The arrangement suggested by Maier-Leibnitz can be regarded as a special case of this type of detector, but we discuss it in the section on Total Energy Detectors. The use of low efficiency sodium iodide detectors for measuring total capture cross-sections is described in Section 5.

2.2 Discrimination against other sources of prompt gamma-radiation.

Any neutron reaction in the sample or surrounding material which produces prompt gamma-radiation may give rise to unwanted events. The two main sources of this type of background will now be considered briefly.

(i) Reactions other than capture in the sample.

These include $(n,n'\gamma)$, fission, $(n,\alpha\gamma)$, and $(n,p\gamma)$. There is no simple way of discriminating against the last two reactions, and we shall not discuss them any further here other than to comment that they are only significant above a few MeV.

Inelastic scattering can only be detected when the incident neutron energy exceeds the gamma-ray energy corresponding to the discriminator level of the system (below which pulses are rejected). With large liquid scintillators, for example, this level is approximately 2.5 MeV and for neutron energies below this value the $(n,n'\gamma)$ reaction will not be observed. However,when there is a need to extrapolate the pulse height spectrum to zero energy to determine the capture cross-section it may be necessary to make some correction to allow for the contribution of inelastic gamma-rays. Section 5 treats this problem for a sodium iodide detector. A method of allowing for the $(n,n'\gamma)$ events which relies on observation of the inelastically scattered neutron in a large liquid scintillator loaded with a material which has a large capture cross-section is described in Section 3.2. In Moxon-Rae detectors discriminator settings corresponding to a gamma-ray energy of 100 keV or less are usual, and

the (n,n'γ) events will restrict the upper energy at which it can be used.

When a fissile sample is used, discrimination against the prompt gamma-rays is necessary. Use can be made of the property that more gamma-ray energy is released in fission than in capture. Thus, if a bias is imposed on the pulses from a large liquid scintillator at an energy greater than that corresponding to the excitation energy of the compound nucleus, only fission events will be observed. At lower biases both capture and fission will be detected. A combination of measurements at high and low bias will allow the capture and fission cross-sections to be derived. The technique is discussed further in Section 3.2. Fission, like inelastic scattering, can also be distinguished from capture by detecting the neutrons in a scintillator loaded with material which has a large neutron capture cross-section (Section 3.2).

With detectors in a multi-segment arrangement it is possible to use the different gamma-ray multiplicities of capture and fission to discriminate between the two processes. This is discussed in Section 3.3.

(ii) Capture of secondary neutrons in the detector environment.

Secondary neutrons produced in reactions like (n,n), (n,n'γ), (n,2n) and (n,pn) in the sample will create a problem if they are subsequently captured in nearby material. The gamma-rays so produced may be indistinguishable from the sample capture gamma-rays when detectors with moderate energy resolution are used. With monoenergetic neutron sources, secondary neutron production in the target backing and in the structure of the detector and shielding materials can also be troublesome. If the secondary capture takes place some way from the sample, or after some moderation of the neutron has occurred, it may be possible to discriminate against it by timing. A particularly serious background problem of this nature occurs when measuring the s-wave resonance parameters of medium mass nuclei such as the reactor structural materials. Here neutron scattering in the resonance is often several orders of magnitude greater than capture, and if accurate capture measurements are to be made, the response of the detector to scattered neutrons should ideally be lower than its response to the capture gamma-rays by a factor of about 10^5. This subject is further discussed in Section 6 where the neutron sensitivities of several contemporary detectors are compared.

These considerations show the need to construct gamma-ray detectors sparingly with materials of low neutron capture cross-section. Detector and constructional materials which minimize neutron moderation are preferable. Good detector timing resolution is also desirable.

This discussion has so far been limited to measurements with thin samples. At the higher neutron energies, it will not in general be possible to use such samples because of the small capture cross-section, in which case capture of secondary neutrons within

the sample itself can occur. This type of secondary capture is, of course, indistinguishable from the required primary capture, and to correct for it resort has to be made to calculation. The estimation of this contribution to the observed capture yield is beyond the scope of this review.

2.3 Properties of gamma-ray scintillators.

Some of the properties of a selection of scintillators suitable for measuring total capture cross-sections are given in Table 1. It will be seen that only solid and liquid scintillators have been listed. Other detector types have been excluded because their response to gamma-radiation is low or difficult to account for when considering the complete capture gamma-ray cascade.

TABLE 1 SCINTILLATOR PROPERTIES

Scintillator	Density (g/cm^3)	Linear Attenuation Coefficient+ For 2.5 MeV γ-ray (cm^{-1})	Thermal Neutron Absorption Mean Free Path* (cm)	Light Output Relative To NaI(Tl) (%)	Decay Constant Main Component (ns)
Sodium Iodide NaI(Tl)	3.67	0.145	10	100	230
Bismuth Germanate $Bi_4Ge_3O_{12}$	7.13	0.310	41	10	300
Liquid $C_xH_{1.25x}$	0.87	0.036	61	33	3
Hexafluorobenzene C_6F_6	1.61	0.060	2200/	9	3
Deuterated Benzene C_6D_6	0.95	0.036	2900/	26	3
Plastic $C_xH_{1.1x}$	1.03	0.043	57	28	2

+ Defined as μ in the expression exp(-μd) for the transmission of γ-rays through a layer d cm in thickness.

* Defined as 1/[(Nuclei per unit volume)(neutron absorption cross-section)].

/ Using hydrogen content quoted by Nuclear Enterprises Ltd. for scintillators NE 226 and NE 230.

The linear attenuation coefficient is shown for a typical gamma-ray energy of 2.5 MeV to give an indication of the size of detector required for a given purpose. A scintillator with high density and atomic number has an advantage in this respect since its volume can be small and the cosmic ray background rate will be correspondingly low.

In evaluating the response of a detector to neutrons, as discussed in the previous section, an important quantity to consider is the ratio of its gamma-ray to neutron sensitivity, which should be as high as possible. The absorption mean free path for thermal neutrons is given in the table to give some indication of the rate of secondary capture in the scintillator itself. If we use the above criterion to assess the importance of neutron sensitivity, sodium iodide and hydrogenous scintillators show the worst performance because of neutron capture in iodine and hydrogen, fluorobenzene and deuterated benzene being much superior. It must be pointed out, however, that fluorine has strong capture

resonances at energies above 27 keV, and for measurements in the keV-region the fluorobenzene scintillator will not be as insensitive to neutrons as the Table suggests.

The emission of light by recoiling atoms as a neutron passes through a scintillator will produce an additional source of neutron sensitivity if the neutron energy is large enough. This is most serious for proton recoils in hydrogenous scintillators, but the light emitted by deuteron and carbon recoils may not be trivial. Fortunately, protons and heavier particles produce a much smaller light output in organic materials than electrons of the same energy. For example, in a Moxon-Rae detector with a hydrogenous plastic scintillator and a bias equivalent to a gamma-ray energy of 60 keV, only protons of energy above approximately 500 keV will create enough light to exceed the bias. Such a detector would therefore only be subject to events of this type for neutron energies greater than approximately 500 keV. In practice, because of the low energy resolution of the system, proton recoils are likely to be detected from neutrons of energy as low as several hundred keV. For the liquid scintillators in the Table, pulse shape discrimination is a means of distinguishing between pulses from gamma-rays and recoiling atoms.

In measuring capture cross-sections with detectors other than those of the large total absorption type, a prime requirement is the ability to measure or calculate the detector response to gamma-radiation for a wide range of energies. A response which has a simple energy dependence is preferable. Good gamma-ray energy resolution, although of less fundamental value, nevertheless may help to distinguish background from genuine capture events.

Sodium iodide having the highest light output is capable of giving the best energy resolution of the detectors in Table 1. With its high density and atomic number the detector needs to be of modest dimensions and the environmental background will be much reduced compared to that for the large liquid scintillators. Against these advantages must be offset its high neutron sensitivity, which has already been mentioned, and also the long-lived decay components of its light emmission (>230ns) which can be troublesome when it is subjected to the intense 'gamma-flash' from a pulsed electron linac.

The response of bismuth germanate (BGO) to gamma-rays with energies up to 8.3 MeV has been studied by Evans /8/ and its use in the detection of gamma-rays up to 22 MeV has been described by Drake et al. /9/. Crystals of this material are commercially available with volumes of up to approximately 0.5l. In comparison with sodium iodide, BGO has several attractive properties. The volume required to achieve a given gamma-ray detection efficiency is smaller, and the ratio of gamma-ray to neutron sensitivity is greater. Because of its lower light output the energy resolution of the full energy peak of a BGO detector is usually about half that of an equivalent sodium iodide detector, a typical value being 9% at 2.5 MeV. However, because of its higher atomic number the fraction of the response in the full energy peak is greater for BGO which helps to fulfil the need for simplicity of response. Another advantage is the absence of significant long-lived components in the light emission of BGO.

All the scintillators considered here are capable of giving a time resolution of two to three nanoseconds when coupled to a suitable fast photomultiplier. This is generally adequate for the pulsed accelerators in use today.

In considering the construction of practical detectors, mention has already been made of the need to use materials with low capture cross-sections. Beryllium or thin-walled aluminium, for example, make suitable canning materials, and quartz is superior to borosilicate glass for photomultiplier cathodes.

3. TOTAL ABSORPTION DETECTORS

3.1 Large Liquid Scintillators

Large liquid scintillators have been used for the detection of prompt capture gamma-rays for many years and the literature covering their design and operation is extensive (refs. 10-20). Consequently only a brief outline will be given of their principal features with the Harwell 2701 tank serving as an example. This sub-section will be concerned in the main with the deduction of the energy dependent detector efficiency by studying the gross features of the pulse amplitude spectrum.

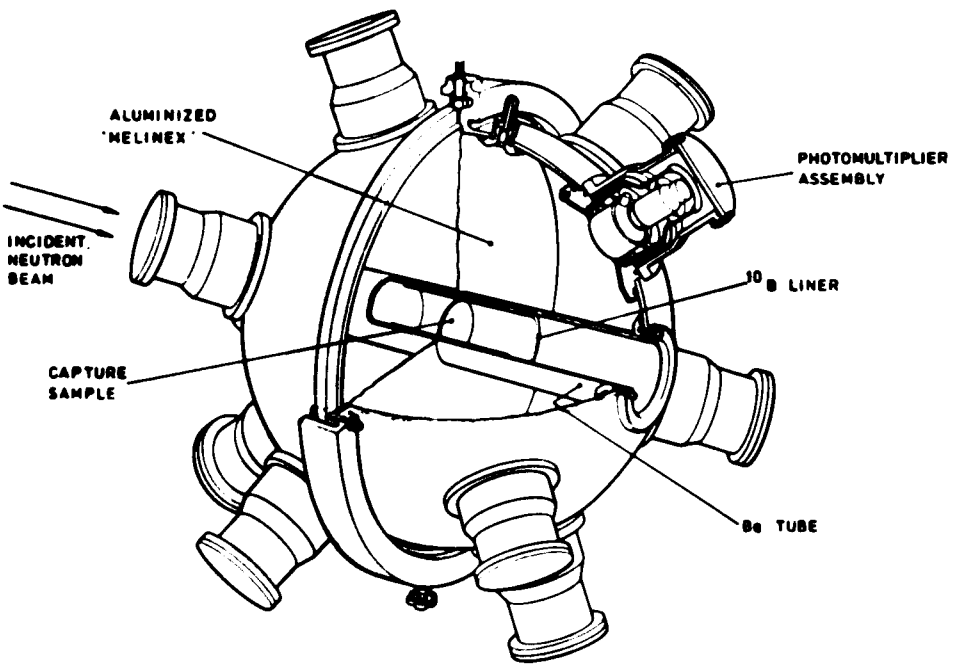

Figure 3. The main design features of the Harwell 2701 liquid scintillator.

Large liquid scintillators vary in size from the 2701 tank in use at Harwell to the 4000l log assembly built by Haddad et al. /13/. Figure 3 shows the Harwell detector. It consists of a spherical iron shell containing 2701 of NE211 scintillator viewed by 12 photomultipliers. The scintillator contains 10% by volume

of methyl borate in order to absorb neutrons in preference to their capture by hydrogen which yields a troublesome 2.2 MeV gamma-ray. The through-tube is of beryllium of 6.4mm wall thickness, chosen for its particularly low capture cross section. The capture sample at the centre of the tank is protected from return neutrons by a 12.7mm thick B-10 sleeve. The tank is optically divided by an aluminised Melinex curtain to allow coincidence operation, a feature which reduces the natural background by a factor of around 7.

As mentioned in Section 1 it is not feasible to build a detector large enough to contain all of the gamma-radiation emitted in the neutron capture reaction. The pulse which registers a capture event is the sum of the partial or complete energy depositions of the individual gamma-rays in the cascade and hence the pulse amplitude response of the detector depends in a complex way on the number of gamma-rays emitted and on their component energies. If, as often happens, the nature of the gamma-ray cascade changes as the incoming neutron energy is increased it then becomes necessary to correct for the differing response of the detector system to the different combinations of gamma-rays.

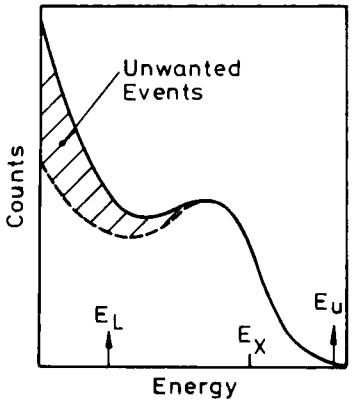

Figure 4. A schematic pulse amplitude response from a large scintillation tank. The energies E_L and E_u are the lower and upper discriminator levels imposed to reject unwanted events. E_X is the total energy released in the reaction.

A schematic representation of a typical pulse amplitude response in a large liquid scintillator is shown in Fig.4. The tendency for the spectrum to be peaked near the excitation energy corresponding to the total energy released in the capture reaction allows the operation of the detector with a high lower bias threshold, typically 2.5 MeV. This is considered necessary because despite the presence of methyl borate in the scintillator solution an unacceptable number of hydrogen captures still occur. An upper bias level is also imposed by the system to reject large energy depositions by high energy cosmic rays passing through the tank. While the rather high lower threshold is convenient for the supression of low energy background and unwanted gamma-rays from competing reactions such as inelastic scattering, a significant fraction of legitimate capture events are rejected and account must somehow be taken of these 'missed' events. This problem is particularly severe in the important case of U-238 for which the separation energy is a mere 4.8 MeV (see Poenitz/21/) The 'spectrum fraction' is defined to be the number of detector counts above the bias divided by the total count rate. The tank effi-

ciency, here called the 'fractional' efficiency is expressed as the product of two factors:

$$\varepsilon_f = \varepsilon_i f_s$$

where, ε_i is the 'intrinsic' efficiency or efficiency in the absence of any bias and f_s is the above mentioned spectrum fraction. A major problem in the use of large liquid scintillators is the determination of ε_f as a function of incident neutron energy, the variation being more marked the smaller the detector. It should also be pointed out in this connection that due to the 'summed' nature of the detector response a weighting function of the Maier-Leibnitz type, which depends for its correct application on the detection of a pulse from one gamma-ray per cascade only, is inappropriate here.

To help determine tank efficiencies in time-of-flight experiments the pulse amplitude response is usually recorded for each event as well as the neutron flight time. A strongly peaked spectrum indicates a large fraction of high energy gamma-rays present in the cascade and hence a low efficiency. On the other hand a flattish spectrum indicates that the available energy is distributed amongst several gamma-rays and that the efficiency is high. Figure 5 illustrates these differences for neighbouring narrow resonances in the cross-section of Fe-56 from Harwell capture data and (inset) Karlsruhe data /19/.

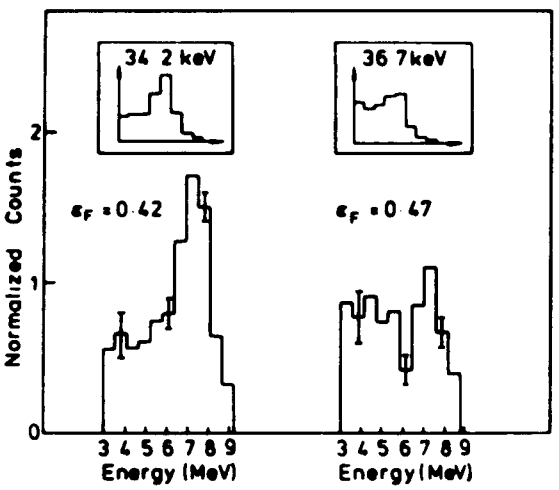

Figure 5. Pulse amplitude spectra for two narrow resonances in Fe-56 from Harwell data. Inset are the spectra as measured with the Karlsruhe 800l tank /19/.

Many tanks being optically halved or quartered are capable of coincidence operation. The coincidence count rate when considered in relation to the total count rate gives important information about gamma-ray multiplicity at the expense of increasing still further the dependence of the efficiency on cascade characteristics (see Fig.6).

It is common practice to make an extrapolation of the observed pulse height spectrum to zero bias with the aid of a separately recorded 'low bias' pulse height distribution which is usually some average over a wide energy region. In this way the spectrum fraction is obtained. The intrinsic efficiency calculation is based on the known thermal capture spectrum with modifications to the single gamma-ray component dependent upon the 'hard', 'soft'

or 'intermediate' appearance of the amplitude spectrum (see, for example, /16/). Froehner /22/ has estimated the overall uncertainty in the capture yield using this technique to be about 15%.

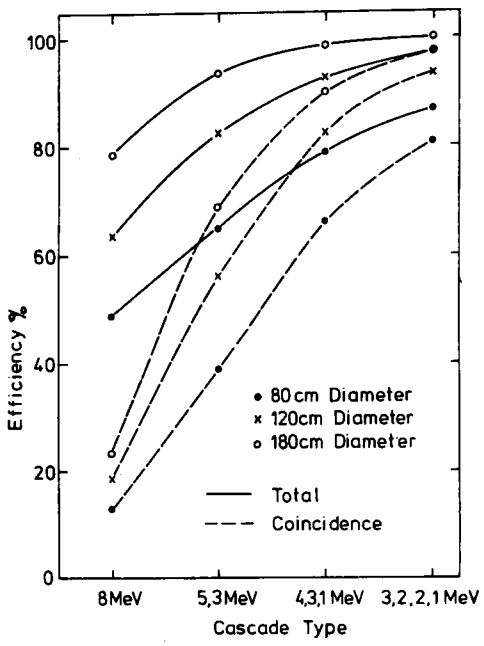

Figure 6. Variation in tank efficiency with increasing gamma-ray multiplicity for three sizes of spherical liquid scintillator. Coincidences are observed between two optically separated sections of the tanks.

The Harwell 2701 tank, because of its size is particularly sensitive to the type of efficiency variation being discussed and so it is vitally important for accurate cross-section determination that the response of the system to capture gamma-rays be well understood. For this reason a Monte Carlo code, GAMOC /23/, which simulates the response of the detector to gamma-rays was developed. A direct calculation of the tank efficiency is, of course, only possible when the gamma-ray cascade is either known or can be generated from a reliable model calculation. In practice this is not possible for individual resonances and so recourse has to be made to a semi-empirical approach based on the shape of that portion of the pulse amplitude spectrum which appears above the detector bias.

The quantity E_f defined as:

$$E_f = \sum_{I=L}^{U} A_I E_I \Big/ \sum_{I=L}^{U} A_I$$

which we call the fractional energy, is used to characterise the amplitude spectrum shape. In this expression A_I corresponds to the number of pulses observed in channel I when the energy E_I is deposited in the detector. L and U are the amplitude channels corresponding to E_L and E_U as defined in Fig.4. A wide variety of amplitude spectrum types generated by the Monte Carlo code have been investigated and a strong correlation is found to exist between E_f and the efficiency ε_f.

Figure 7 shows the correlation between the fractional energy and the detector efficiency. The curve is a polynomial fit to the

points. The points marked Au and Fe on the figure apply to the more realistic spectra calculated from cascade schemes generated by a model description of de-excitation from a statistical and a non-statistical nucleus respectively. The successful application of the method to these more complex spectra reinforces the belief that the method is valid. The foregoing description applies to the total tank efficiency, that is with no coincidence condition imposed. The required coincidence efficiency is obtained by multiplying by the appropriate coincidence to total count rate ratio. It is worth pointing out that since the method is applied to the sample under study and to the reference sample, in this case gold, any systematic error involved tends to cancel rather than to sum. The overall uncertainty in estimating the detection efficiency with this method depends on the quality of the amplitude information available and generally lies within the range 5-10%.

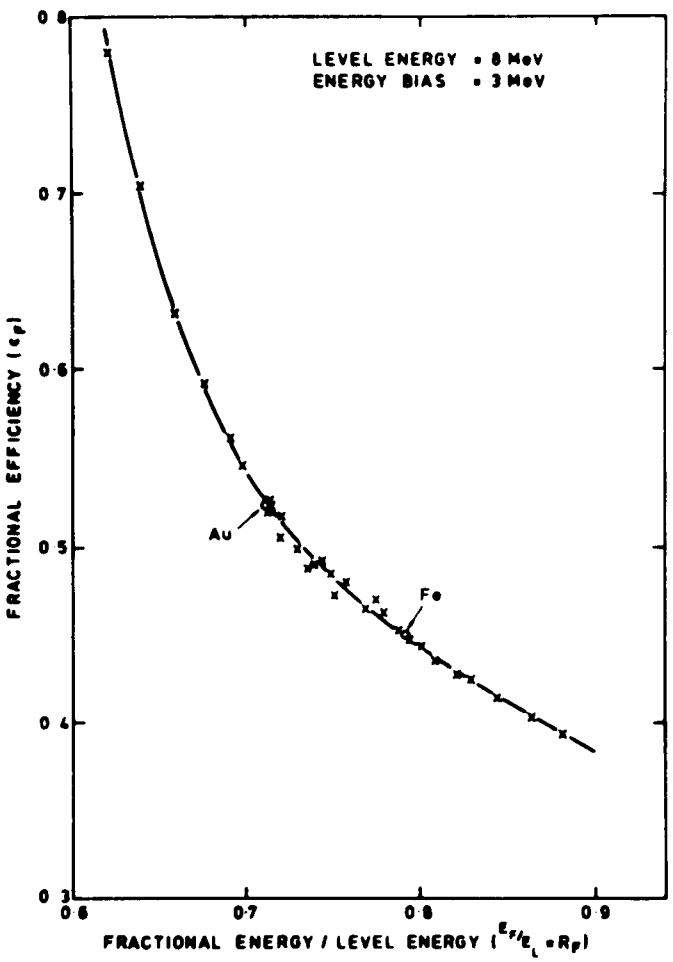

Figure 7. Correlation observed between detector efficiency and fractional energy at 8 MeV excitation. See text for an explanation of the curve and points marked Fe and Au. E_L in the figure corresponds to E_X in the text.

When estimating detector efficiencies by whatever method it is necessary to correct for the attenuation of gamma-rays in the sample. For the Harwell data these corrections are based on Monte Carlo calculations which assume isotropy of the emitted gamma-radiation. For a thick sample the correction can be substantial, for example the Harwell measurements used three thicknesses of natural iron, 0.5, 2.0 and 6.4mm, and the average

correction factors which had to be applied to the data were, respectively 3.2, 7 and 15 %.

3.2 The use of large liquid scintillators when other reactions are present.

The most important reactions, other than capture, which produce prompt gamma-radiation are fission and inelastic neutron scattering. The effect of these on capture measurements was discussed in general terms in Section 2.2. In this sub-section we consider separately measurements with large liquid scintillators according to whether the sample is fissionable or not.

(i) Non-fissionable samples.

For all but the lighest nuclei, the only background reaction we need to consider at incident neutron energies below about 5 MeV is inelastic scattering. At higher energies, other types of reaction may occur which cannot be readily distinguished from capture by experimental means. In any detector, inelastic scattering levels capable of producing observed events only become accessible when the incident neutron energy exceeds the discriminator bias. For the spectrum from a large liquid scintillator a bias setting of 2.5 to 3 MeV would be typical. Inelastic scattering for this type of detector thus presents no background problem for incident neutron energies below about 3 MeV.

At energies above approximately 3 MeV the rejection of inelastic or fission events, can be accomplished by observing the neutrons in a scintillator loaded with material which has a large capture cross-section. This technique was first used by Hopkins and Diven /24/ for fissionable samples. Gupta et al. /25/ have discussed the suitability of a system of this type for energies up to 10 MeV. As in the measurements of Hopkins and Diven discussed below, a pulsed monoenergetic source of neutrons was used together with the time-of-flight technique to reduce the effect of general background. The scintillator was loaded with 0.5% by weight of Gd so that more than 98% of the neutrons originating in the sample were captured within 50 microseconds. The effectiveness of the system was demonstrated by measuring the capture cross-sections of gold and the capture to fission ratio for U-238 at energies around 2 MeV. Since the technique relies on registering as capture those events that are not accompanied by a neutron, other reactions such as $(n,\alpha\gamma)$ and $(n,p\gamma)$ cause ambiguity of interpretation at incident energies above 10 MeV. Additional ambiguity occurs at high energies because neutrons from the sample can undergo C-12$(n,\alpha\gamma)$ and C-12$(n,p\gamma)$ reactions in the scintillator. These reactions can produce prompt pulses with the disappearance of the neutron and so be confused with genuine capture events.

(ii) Fissionable samples.

The presence of fission can be detected by observing the frag-

ments, the prompt fission gamma-rays, or the prompt fission neutrons. If fragment detection is used, the fissionable material is contained in a fission chamber (usually of the ionization type) placed at the centre of the large liquid scintillator. A pulsed neutron source is used and, in principle, a fission or capture event is recognized according to whether or not a scintillator pulse is accompanied by a coincident pulse from the fission chamber. To obtain good counting rates it is usually necessary to have as large a quantity of fissionable material in the chamber as alpha-particle pile-up will allow. The fissionable deposits will often be of moderate thickness, therefore, and because of loss of fragments in the deposits it is unlikely that every fission event will be detected in the chamber. In practice this would mean that fissions not seen in the chamber would be registered as capture events and a correction for this effect would be required. This technique has been used by Gwin et al. /26/ to measure the neutron absorption and fission cross-sections of Pu-239 and U-235 up to an incident neutron energy of 200 keV. In this measurement a considerable improvement in the signal to background ratio was achieved by operating the two optically separated halves of the large liquid scintillator in coincidence.

If circumstances dictate the use of an amount of fissionable material greater than can be contained in a fission chamber (about 1g) it will be necessary to detect the fission neutrons or gamma-rays. Gamma-ray detection is used in the 'high bias' technique, the principle of which was described in Section 2.2. This method has been used by Gwin et al. /27/ to measure the fission and absorption cross-sections of Pu-239 up to 30 keV incident neutron energy with metal samples ranging in mass from 5g to 21g. A problem of interpretation in this type of measurement arises from possible variation in the total energy release as fission gamma-radiation if a wide range of incident neutron energies is covered.

Neutron detection as a means of identifying fission events when measuring the capture cross-sections of fissionable nuclei was used by Hopkins and Diven /24/. They used a Van de Graaff generator to produce a pulsed monoenergetic source of neutrons which was collimated and passed through a sample placed at the centre of a large liquid scintillator. Sufficient Cd was loaded into the scintillator to ensure that 95% of the neutrons were captured, with the production of a 9 MeV pulse within 32 microseconds of a fission event. When capture or fission occurred in the sample the accompanying gamma-radiation was detected in coincidence with the beam pulse. This radiation was detected with a high efficiency, and produced a prompt pulse which was used to open a delayed 32 microsecond gate. Neglecting the effect of background and missed fission events, if a 9 MeV pulse occurred during the gate the prompt pulse must have been caused by a fission event, otherwise it must have been caused by a capture event. Measurements were taken up to an incident neutron energy of 1 MeV. The small pulses produced by inelastic and elastic scattering events were discarded by discriminating against pulses below an amplitude corresponding to 1 MeV gamma-ray energy. With this type of measurement, corrections have to be made for the small number of fission neutrons that produce no 9 MeV pulse

within the gate, and for the loss of capture events below the discriminator bias. In addition, a correction should be applied for those fission events in which no neutron is emitted using the known neutron multiplicity distribution.

3.3 Multi-sectional Detectors.

If the sample is placed at the centre of a totally absorbing detector which is divided into a number of individual sections the multiplicity of the secondary radiation can be observed with coincidence techniques and used as a means of determining the type of reaction which has occurred. Neutron scattering, for example, can be separated from capture by the detection of one secondary neutron rather than several capture gamma-rays. Fission can be distinguished from capture by the greater multiplicity of the emitted radiation. This idea has been exploited by Muradyan et al. /28,29/ with the DAISY detector which is a multi-sectional arrangement of NaI crystals. Although large liquid scintillators are often divided into two or more optically isolated compartments, this is generally used to enable a reduction in the environmental background rate to be achieved, rather than to identify reactions.

(i) The DAISY detector.

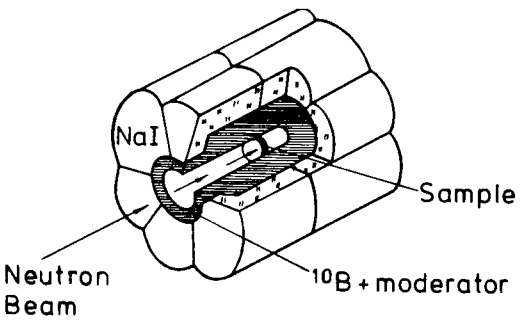

Figure 8. The main features of the DAISY detector.

This detector, so named because of its cross-sectional appearance, has undergone several stages of development. Figure 8 shows DAISY-1 which is comprised of 12 optically isolated NaI(Tl) crystals occupying a total volume of 16 litres. The sample is surrounded by a sleeve of B-10 and moderator to convert neutrons into gamma-rays and so enable them to be included in the measurement of multipicity. The sleeve has the additional function of protecting the NaI crystals from scattered neutrons which can give rise to troublesome background with this type of scintillator (Section 2.3). DAISY-2 is similar to DAISY-1 but with the volume of NaI increased to 26 litres. Figure 9 shows multiplicity spectra obtained with DAISY-2 for the spontaneous fission of Cf-252 and neutron radiative capture in Cd-113. The clear separation of the two types of event is apparent.

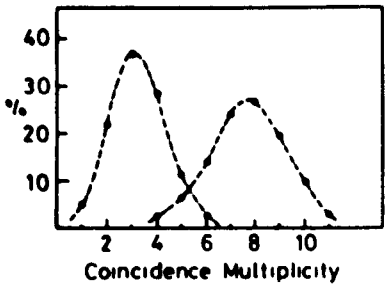

Figure 9. Multiplicity spectra observed with the DAISY detector for capture (low multiplicity) and fission (high multiplicity) events.

The fission and capture cross-sections of U-235 and U-238 have been measured in the energy range 0.1 to 30 keV using versions of the DAISY detector containing up to 100l of NaI divided into 46 sections. The spins of neutron resonances have been determined in favourable cases where the different multiplicities of the two states of the compound nucleus can be clearly distinguished. The system offers also the possibility of separating the s- and p-wave neutron cross-sections in the unresolved region. The multiplicity spectrum in this region is averaged over many levels and is therefore less affected by Porter-Thomas fluctuations than the spectrum from separate resonances.

(ii) Recent developments in multi-sectional detectors.

The principal disadvantage of the DAISY system when used in capture measurements above a few keV is its sensitivity to scattered neutrons. This problem could be reduced considerably by replacing the sodium iodide with bismuth germanate crystals. Alternatively, a separation of scattered neutrons from capture gamma-rays can be achieved by time-of-flight if the detector is large enough. This property is exploited in the spin spectrometers described by Sarantites et al. /30/ and Simon /31/. Designed for the study of the high multiplicity cascades from heavy ion reactions, these are detectors in which, for each event comprehensive information is obtained on properties of the emitted radiation such as individual transition energies, the total gamma-ray decay energy, the mutiplicity of the emitted gamma-rays and their angular distributions. In the Darmstadt-Heidelberg Crystal Ball described by Simon there are 162 individual NaI modules each 20cm in radial thickness, the whole forming a spherical shell with a free inner radius of 25cm and surrounding the sample in 4π-geometry. With these dimensions, a scattered neutron of energy 1 MeV, say, would arrive about 18ns later than the prompt gamma-rays, and those modules which were triggered by a neutron alone could be resolved from the rest in the shell. Because of their very high cost it seems unlikely that the use of such complex systems could be justified for precision capture cross-section measurements.

4. TOTAL ENERGY DETECTORS

The essential feature of the Moxon-Rae detector, as discussed in Section 2.1(ii), is an efficiency which is proportional to

gamma-ray energy and low enough in magnitude to ensure that no more than one gamma-ray is detected for each capture event. In its original form the required efficiency characteristic was achieved by the physical arrangement of the system, and this will be described in Section 4.1. The generalization of the principle to higher efficiency devices through the use of a weighting function is dealt with in Section 4.2.

4.1 The Moxon-Rae detector.

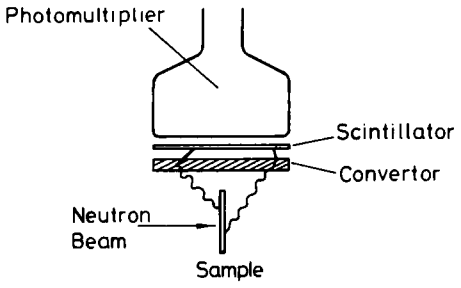

Figure 10. Schematic view of the Moxon-Rae detector.

The arrangement of Moxon and Rae /5/ (Fig.10) is derived from the thick-walled Geiger or proportional counter /32,33/. The capture gamma-rays eject electrons from a layer of graphite or aluminium placed to one side of the sample. Secondary electrons which emerge from the converter produce light signals in a thin layer of plastic scintillator which is attached to a photomultiplier cathode. Provided the converter thickness is greater than the maximum range of the secondary electrons, the approximate linear relationship which exists between detection efficiency and gamma-ray energy derives from the combined effect of electron production and transmission in the converter (Malik/34/). In the original detector, Moxon and Rae considered a maximum gamma-ray energy of 12 MeV which required a thickness of graphite of 3.2cm. A scintillator thickness of about 1mm is sufficient for the system to produce pulses well above the photomultiplier noise and yet detect very few gamma-rays directly.

For a graphite converter, k, the detection efficiency per unit gamma-ray energy is only approximately constant. The value of k rises rapidly with gamma-ray energy below 1 MeV, reaches a peak at about 2 MeV and thereafter falls off with increasing energy to a value at 12 MeV of around 70% of the maximum. For high Z elements, k reaches a plateau well below 1 MeV and thereafter increases slowly with energy. Converters with a Z of about 50 show a more constant behaviour, k deviating from the mean by no more than about 0.5% in the energy range 1-12 MeV. The same effect can be achieved by mixing high and low Z materials. An important consideration in designing a converter is the neutron sensitivity of the detector. Carbon is a suitable material because of its low capture cross-section. Macklin et al. /35/ considered graphite-lead and graphite-bismuth oxide mixtures and showed that these can give reasonably constant k above 1 MeV, but still exhibit a rapid fall below 0.5 MeV. Iyengar et al. /36/ investigated a number of converters using a Monte Carlo simulation and concluded that a mixture composed of 50 atoms of carbon and 10 molecules of bismuth oxide gives a response which

approaches the ideal in the range 1-12 MeV. The addition of bismuth will unfortunately introduce resonant structure in the neutron sensitivity above 800 eV. The use of pulse amplitude weighting as a means of achieving constancy of k for an arbitrary detector is dealt with in the following section. If it can be shown that, at least for the lower energy gamma-rays, the amplitude response varies in a systematic way with gamma-ray energy then there is no reason why this technique should not be applied to a Moxon-Rae detector. The ideal response would be obtained at the expense of having to record the pulse amplitude however, and its basic simplicity would be lost.

The detector is operated with a bias level corresponding to a gamma-ray energy of about 60 keV, and it was seen in Section 2.3 that, as a result, the system will become sensitive to proton recoils resulting from scattered neutrons when their energy exceeds a few hundred keV. This then defines the upper energy at which the Moxon-Rae detector in its standard form can be used. The low bias also makes the system sensitive to gamma-rays from inelastic neutron scattering which may further limit the upper energy of use.

Because of its smaller size, shielding against background poses less of a problem than for a large liquid scintillator. The detection efficiency is usually about 4%, but for measurements below a few hundred keV it is generally capable of giving a higher signal to background ratio than the large liquid scintillator. Its simplicity of construction and ease of use has led to its adoption in many laboratories for capture cross-section measurements. It must be remembered, however, that by its very nature it should be used with monoisotopic samples. Unlike the total absorption systems this detector is not used in 4π-geometry, which could lead to errors if the angular distribution of the cascade gamma-rays changes with incident neutron energy.

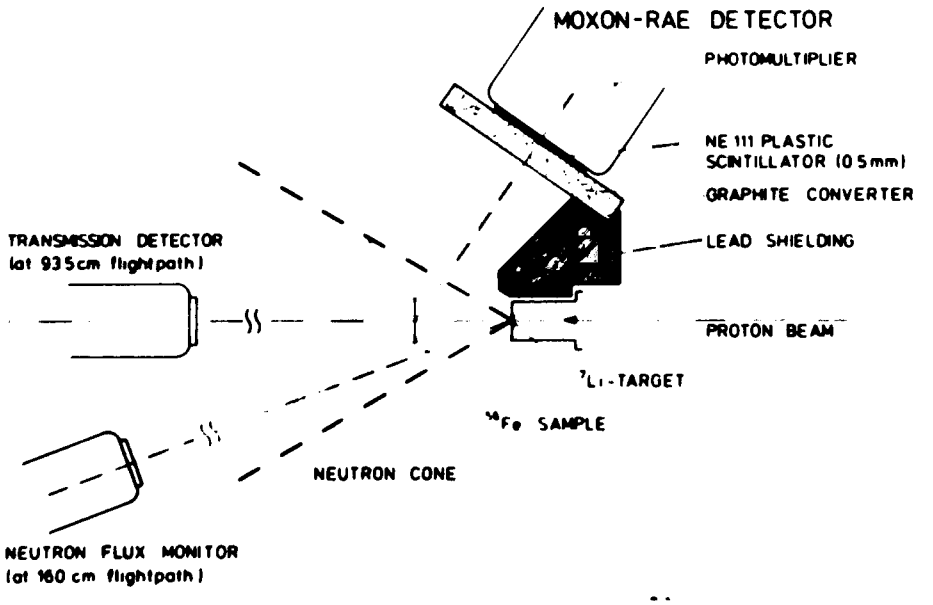

Figure 11. General arrangement of the Moxon-Rae detector used on the Karlsruhe Van de Graaff.

Figure 11 shows the arrangement recently used by Wisshak and Kaeppler /37/ at Karlsruhe to measure the radiation width of the 27.7 keV s-wave resonance in Fe-56. In this instance the sample was only a short distance (8cm) from the pulsed neutron source and the low efficiency of the detector was not a disadvantage. The overall time resolution was 1.2ns allowing a clear separation by time-of-flight of the 27.7 keV resonance from its p-wave neighbours. A cone of neutrons was defined by kinematic collimation as shown in the Figure. A unique feature of this Moxon-Rae system is the use of time-of-flight to discriminate against the detection of neutrons scattered by the sample or surrounding materials.

Moxon has recently re-designed the Harwell detector to have a very low neutron sensitivity. The arrangement is shown in Fig.16 in Section 6.

4.2 Total Energy Detectors which use a Weighting Function

It can be shown (e.g. Czirr /38/) that in the case of the Moxon-Rae detector the proportionality of its efficiency to gamma-ray energy arises from the converter properties, while the detection of the secondary electrons introduces no further dependence on gamma-ray energy. It is also possible in certain circumstances to achieve a detector response proportional to gamma-ray energy by transforming the pulse height spectrum through the operation of a weighting function. The generality of the concept allows the optimisation of other desirable features in the design of the detector, such as insensitivity to scattered neutrons.

Since the original work by Macklin and Gibbons, who applied the idea to small volume liquid scintillators, many laboratories have followed suit, although there has been a general preference for deuterated benzene rather than the more neutron sensitive fluorobenzene as the liquid scintillator solution.

We consider here the case of a small volume of liquid scintillator for which the probability of detecting more than one gamma-ray from the cascade is negligible* (<1%). The detector response matrix W is assumed to be known and can be expressed as the product of two factors:

$$W_j(I) = P_j S_j(I)$$

where P_j is the interaction probability of a gamma-ray of energy E_j and $S_j(I)$ is the probability that it will produce a pulse of height, I, in the detector. It follows that:

$$\sum_{I=1}^{I_m} S_j(I) = 1$$

* In practice the detection of more than one gamma-ray per cascade can be corrected for by using the coincidences observed between two identical detectors (see e.g. Macklin et al. /6/).

where the sum extends to the maximum pulse height recorded. We next suppose that a function G(I) of pulse height only exists that satisfies the condition:

$$\sum_{I=1}^{I_m} G(I)W_j(I) = E_j$$

The series of equations obtained by varying the energies E_j define the values G(I) provided that the detector response changes in a systematic way with increasing gamma-ray energy E_j.

Calculation of the Weighting Function G(I)

The predominance of the Compton interaction process allied with the poor resolution of organic liquid scintillators ensures the absence of structure in the detector response function and for this reason G(I) can be expected to have a smooth dependence on pulse height. Following the prescription of Le Rigoleur /39/ we express G(I) as a polynomial function of order N:

$$G(I) = \sum_{k=0}^{N} \alpha_k I^k$$

Substituting this form of G(I) into the previous equation, yields:

$$\sum_{I=1}^{I_m} \sum_{k=0}^{N} \alpha_k I^k W_j(I) = E_j$$

$$\rightarrow \sum_{k=0}^{N} \alpha_k \sum_{I=1}^{I_m} W_j(I).I^k = E_j$$

introducing:

$$a_{jk} = \sum_{I=1}^{I_m} W_j(I)\, I^k$$

gives finally:

$$\sum_{k=0}^{N} \alpha_k a_{jk} = E_j.$$

and the problem has reduced to finding the coefficients α_k from a series of equations, one for each gamma energy E_j. The first few coefficients only are required to define G(I) and so by choosing the number of gamma-ray spectra M to be greater than the number of coefficients N we have an overdetermined system of equations and by minimising the expression:

$$\sum_{j=1}^{M} \left[\sum_{k=0}^{N-} \alpha_k a_{jk} - E_j \right]^2$$

we can converge on the best set of coefficients α_k , k=1, N.

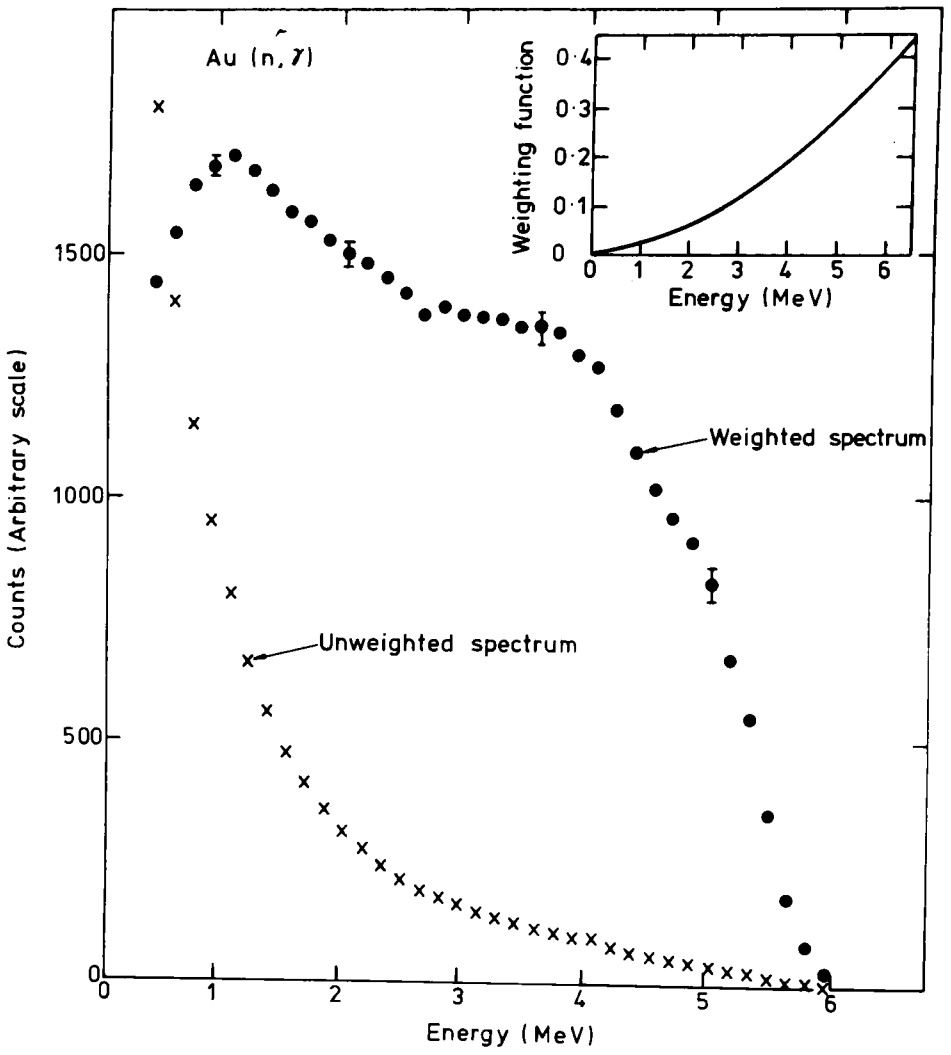

Figure 12. The unweighted and weighted pulse height response of a 400cc volume of C6D6 liquid scintillator to gamma-rays emitted in the Au(n,γ) reaction at thermal energies. The weighting function used is also shown.

A weighting function was calculated in this way for a 400cc cell of deuterated benzene scintillator at Harwell. The response matrix W was found by application of the Monte Carlo method to the interaction of monoenergetic gamma-rays in the detector. This is considered to be an acceptable procedure since good agreement is observed between calculated and experimental spectra for low energy gamma-ray sources. The result of applying the weighting function to the thermal capture gamma-ray spectrum of gold is shown in Figure 12. An advantage of using the weighted rather

than the unweighted spectrum is in the extrapolation to zero bias where in this example less than 5% of the weighted count rate is below the bias of 400 keV. The penalty for this convenience is not just the reliance placed on the accuracy of the weighting function calculation but of more fundamental importance is the loss of statistical accuracy incurred by heavily weighting the high energy end of the gamma-ray spectrum. Worthy of consideration also is the important role played by secondary electrons in determining the shape of the weighting function at high energies. By allowing for the escape of secondary electrons we found a 50% increase in the weight to be applied to events depositing 8 MeV in the detector. The effect of using electron range/energy data from different sources has been considered in detail by Brusegan et al. /40/ in relation to the deuterated benzene detector developed at the Geel Laboratory. To test their weighting function the Geel group observed capture gamma-rays from a variety of samples exposed to a thermal neutron beam. There is evidence to suggest a residual dependence of the weighted detector response on the nature of the gamma-ray cascade. The Harwell detector was similarly tested and exhibited no serious dependence on cascade type /41/ although it should be said that the cascade types chosen were not as widely varying as those used by the Geel group.

5. LOW EFFICIENCY DETECTORS OF KNOWN GAMMA-RAY RESPONSE

This is the third and final classification of detector which we shall discuss. The general principle of measuring the cross-section from a determination of the complete gamma-ray spectrum was considered in Section 2.1(iii). If the discriminator bias is sufficiently low in value an empirical method of extrapolating the observed spectrum to zero energy will be adequate. In fast neutron measurements however, the bias often removes a considerable portion of the spectrum because of the need to reject inelastically scattered neutron events. Some form of theoretical basis for making the extrapolation is therefore necessary. For example, if the parameters of a theoretical calculation can be adjusted to reproduce the observed spectrum, this same calculation can provide the extrapolation. This is the method used by Joly and co-workers which is discussed below. The method requires the detector gamma-ray response function to be known and preferably it should have a simple energy dependence to assist the unfolding of the spectrum.

Bartholomew et al. /42/ have reviewed theoretical spectrum fitting techniques. The calculations require information on the energy dependence of the average gamma-ray transition probability and the nuclear level density distribution. It is usually assumed that in the heavier nuclei transitions are predominantly dipole in character and have a transition probability which is proportional to the cube of the gamma-ray energy. The assumption that all the radiation is of the dipole type is likely to introduce errors in some nuclei. In the collective region, for example, the predominant mode of decay between low-lying excited states is by quadrupole radiation.

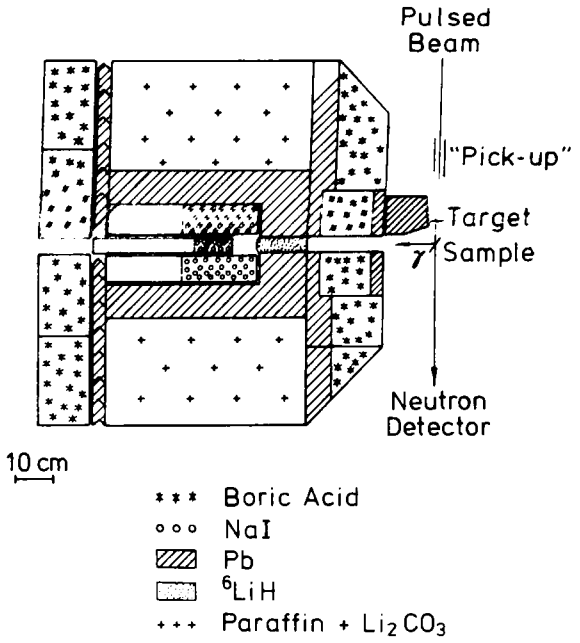

Figure 13. The sodium iodide detector at Bruyeres-le-Chatel.

The spectrum fitting technique has been used extensively by the Bruyeres-le-Chatel group (Joly et al. /43/) for measurements on heavy nuclei between 0.5 and 3 MeV. Figure 13 shows their experimental arrangement, which is similar to that used by Bergqvist et al. /44/ to measure partial capture cross-sections for fast neutrons. The gamma-rays were detected by a NaI detector 7.6cm in diameter and 15.2cm long surrounded by an annular NaI crystal. The system was used in the anti-Compton and first-escape modes to obtain response functions of simple shape. The detector was of moderate size to keep the background from thermal neutron capture in the detector itself and its surroundings to a reasonable level. A nanosecond pulsed beam of 'monoenergetic' neutrons was used. The measurements were made by the time-of-flight technique to further improve the signal to background ratio. Implicit in the method is a spread in energy of the incident beam sufficient to cover a large number of initial states so that Porter-Thomas fluctuations in the observed spectrum are smoothed out.

The response functions of the spectrometer were measured experimentally using monoenergetic gamma-rays from radioactive sources and $(p,\alpha\gamma)$ and (p,γ) reactions in light nuclei. A response matrix for each of the two modes of detection for gamma-ray energies between 1 and 12 MeV was then obtained by interpolation. The absolute detection efficiencies were determined by using calibrated radioactive sources.

The experimental pulse-height distributions for a particular capture measurement were converted to gamma-ray energy spectra by means of the above response matrices. Figure 14 (upper) shows a typical spectrum before and after the unfolding of the response function. The theoretical spectrum was determined from a statistical model calculation using a method described by Starfelt /45/. A level density expression of the form suggested by Gilbert and Cameron /46/ was used. The nuclear temperature in this

expression was determined separately for each nucleus using available data. Near the neutron threshold, information on levels was obtained from neutron resonance spectroscopy, while at 1 to 2 MeV above the ground state it was obtained from (n, γ) and particle reactions. The spectrum calculated for gold at a neutron energy of 0.72 MeV is shown in Fig.14 (lower). After the unfolded experimental spectrum had been corrected for the spectrometer efficiency and for gamma-ray absorption in the sample it was compared with the calculated spectrum. The two spectra were normalized one to the other above a minimum gamma-ray energy E_{min}, allowing the experimental data to be extrapolated between 0 and E_{min} and the cross-section to be derived. For low incident neutron energies E_{min} was approximately 1.5 MeV and corresponded to the discriminator bias, while at $E_n > 1.5$ MeV, $E_{min} = E_n$ to eliminate the detection of inelastic neutron scattering events.

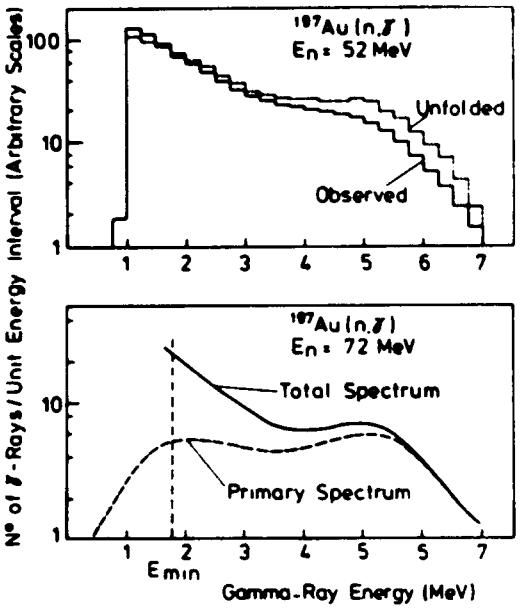

Figure 14. Observed (anti-Compton mode) and calculated spectra for gold capture for the Bruyeres-le-Chatel detector.

In a given measurement the two modes of detector operation were used simultaneously. Comparison between the final results improved confidence that the data were analyzed correctly, and in addition the two sets of data could be considered to be statistically independent. The final cross-section was given as the weighted mean obtained from the two modes of acquisition. The principal sources of systematic uncertainty in the measured capture cross-sections were the detector efficiency determination (6-8% contribution for the anti-Compton mode), the level density distribution (5-10% contribution), and the spectrum extrapolation (2-4% contribution).

An advantage of this method is that, since it relies on obtaining the spectrum of the capture gamma-radiation, gamma-ray strength functions can be studied over a wide energy range. The experimental arrangement also makes it possible to investigate the angular distribution of the capture gamma-rays.

6. PROMPT DETECTION OF SCATTERED NEUTRONS.

The problem of the detection of secondary neutrons in capture gamma-ray detectors was considered briefly in Section 2.2(ii). In this section we shall make a few comments on the importance of neutron sensitivity and compare some detectors recently engaged in capture cross-section measurements.

The detectors we consider are used in the time-of-flight mode with pulsed neutron sources. We are, therefore, only concerned with secondary neutrons detected within the time resolution of the system which are thus indistinguishable from the required capture events. Secondary neutrons which are moderated before capture and detected at later times form part of the measurable background.

At the lower incident energies only elastically scattered neutrons contribute to the neutron sensitivity. Although prompt detection of scattered neutrons has been recognized as a problem for some time the inconsistencies which persist especially in structural material data ($45<A<65$) can be attributed at least in part to the underestimation of this effect. The recent drop in value of the radiation width of the important 27.7 keV s-wave resonance in Fe-56 can be largely attributed to the attention given to detector neutron sensitivity as a result of the 1977 Structural Materials Meeting at Geel /47/. The ratio of neutron width to radiation width for this resonance is in the range 1400-1500:1, which is typical for an s-wave resonance in the structural materials. The measured radiation width therefore provides a stringent test for claimed insensitivity to promptly scattered neutrons. In the early seventies the radiation width was thought to be in the region of 1.4 eV. More recent values /48/, however, either from re-analysis of old data /49/ or from new measurements with particular emphasis on the reduction of prompt neutron detection /37/ tend to favour a value of 1 eV or less. To achieve consistency in the measurement of capture cross-sections a case can certainly be made for the adoption of a resonance of this type as a standard.

Detector neutron sensitivity also has an important bearing on the correlations which have been observed between the reduced neutron widths and the capture widths of s-wave resonances in the stuctural materials. These correlations indicate the presence of non-statistical processes in neutron capture, but before a quantitative assessment of this component can be made it is important to ensure that any contribution from scattered neutrons to the measured capture width has been correctly determined.

Macklin and collaborators, notably those from Lucas Heights, have made an extensive series of capture measurements on the Oak Ridge linear accelerator, ORELA, with a fluorobenzene detector. Allen et al. /50/ have reviewed methods of determining the neutron sensitivity of capture detectors and show how measurements on scattering samples with few capture resonances such as Pb-208 can be used for this purpose. Figure 15 shows the result of their analysis on the Oak Ridge detector. The large peaks in the curve correspond to fluorine resonances in the scintillator and aluminium resonances in the detector structure. It can be seen

that the neutron sensitivity is much greater than the value of 10^{-5} to 10^{-4} recommended for accurate capture measurements on the structural materials. The Karlsruhe group have also made a substantial contribution to capture data using an 800l liquid scintillator. The neutron sensitivity of this detector is also shown in Fig.15, the peaks in the sensitivity come from the aluminium through-tube in the tank and the rather massive bronze sample holders.

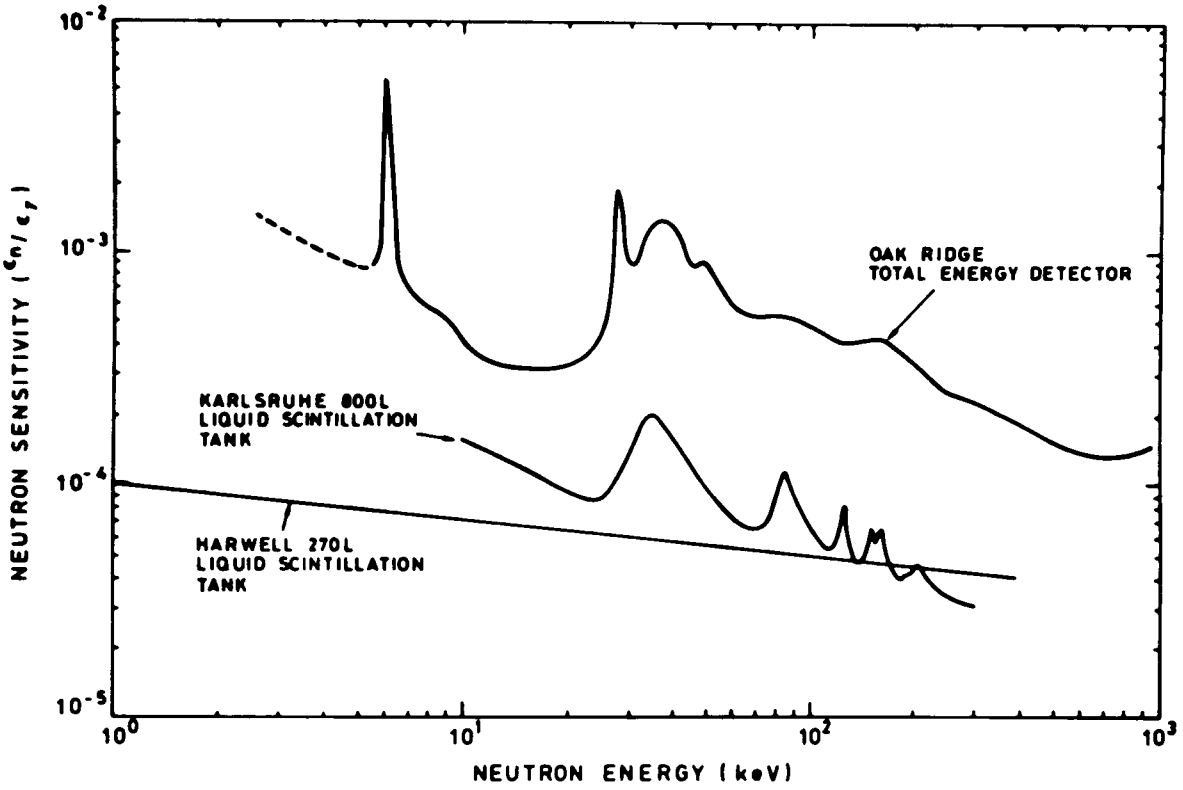

Figure 15. Neutron sensitivity (probability of detection per neutron scattered divided by an assumed average capture probability) of the Harwell scintillator compared with two other published calculations.

The experience of the Oak Ridge and Karlsruhe groups was invaluable in building the Harwell 270l liquid scintillator. The sensitivity of this detector was kept to a minimum by using a through-tube of beryllium and using a light Melinex sample holder. For the Harwell detector, the neutron sensitivity, defined as the ratio of prompt neutron events to capture events, was found experimentally from the observation of detector response to a purely scattering sample, to be of the order 10^{-4} for incident neutron energies between 25-150 keV. To substantiate this result and understand more fully the response of the detector to neutrons the time-dependent neutron transport code MORSE /51/ has been used. The code applies the Monte Carlo method to the tracking of individual neutrons and has been adapted to record the absorption rate in the detector materials and environment. The response of the system to gamma-rays from a particular

nucleus is then determined with the gamma-ray Monte Carlo code GAMOC /23/. This type of analysis was performed for several neutron energies and the resulting curve of neutron sensitivity is shown in Fig.15. The approximate experimental value of 10^{-4} is somewhat higher but not in disagreement with the calculated sensitivity.

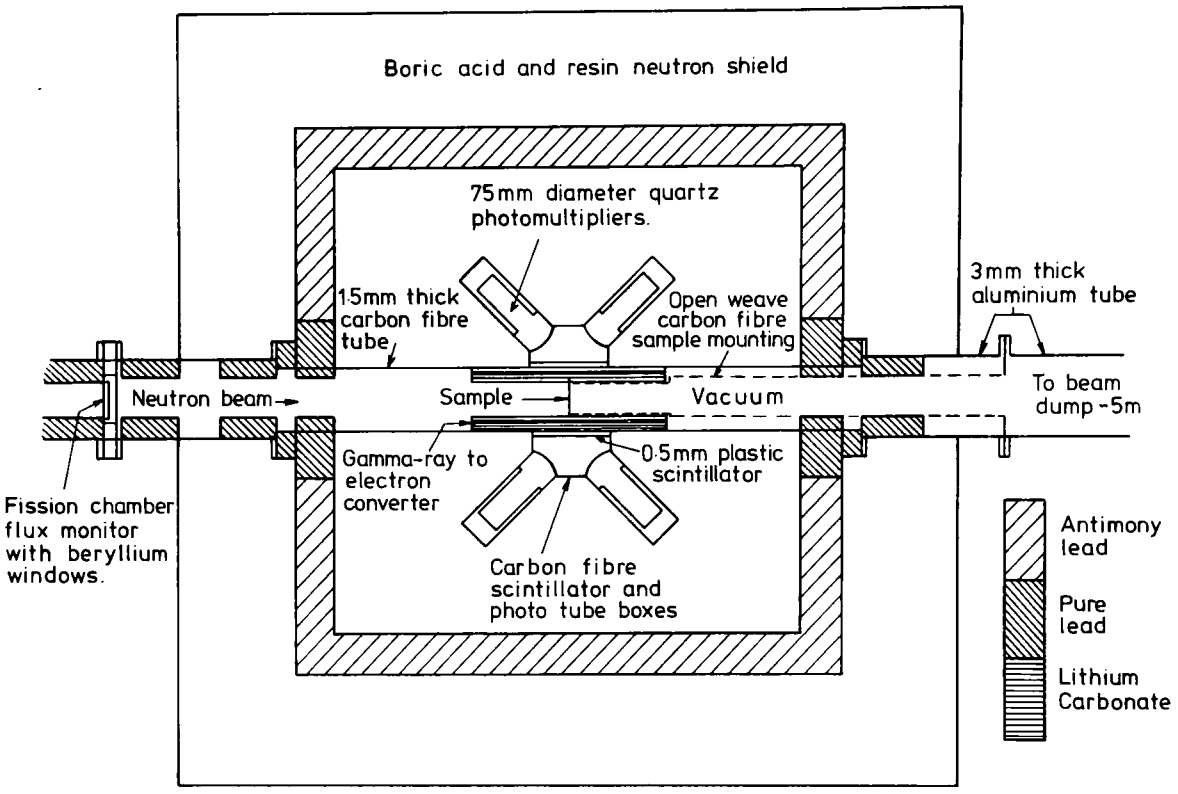

Figure 16. The Moxon-Rae detector at Harwell.

Figure 16 shows the constructional materials used in the latest Moxon-Rae detector at Harwell /52/ to achieve a very low neutron sensitivity. The lithium carbonate converter has the additional role in this system of shielding the materials surrounding the sample from scattered neutrons.

In measurements where the detector sensitivity to scattered neutrons is an important factor it will be necessary to assess its value as a function of energy. An attractive experimental method, which is suitable for small detectors, is to observe the neutrons directly by the time-of-flight method on a pulsed Van de Graaff. For 4π-detectors, the same effect can be produced by using a 'pure' scatterer at the sample position. A detailed calculation, using either analytical or Monte Carlo techniques, will aid interpolation between experimental points and extrapolation beyond the measured region.

7. DETERMINATION OF THE CAPTURE YIELD.

In a cross-section measurement the capture yield, Y, which is defined as the number of capture events per neutron incident on the sample is related to the observed counting rate, C, through the expression,

$$C - B = Y \varepsilon \emptyset$$

where B is the background in the measurement, ε is the detector efficiency for capture events, and $\emptyset$ is the incident neutron flux. In a time-of-flight measurement, the time interval is taken to be small enough to remove any energy-dependence of the terms in the expression. The yield can be related to the required capture cross-section, σ_γ, as follows,

$$Y = f\, n\, \sigma_\gamma$$

where n is the number of sample atoms per unit area normal to the incident beam, and f is a correction factor which allows for self-shielding and multiple reactions of the neutrons in a sample of finite thickness. For a thin sample, f->1 and the cross-section is readily obtained from the capture yield. The determination of the thickness correction factor is beyond the scope of this review, but a few comments will be made on the other factors which contribute to the yield.

The problems of background from promptly scattered neutrons and reactions which compete with capture have been discussed in previous sections. Background which occurs after the initial capture event can be recognized by timing if a pulsed source of neutrons is used. With Van de Graaffs, pulse lengths are about 1ns and it is possible to account for a substantial portion of the scattered neutron background in this way. For pulsed 'white' neutron sources it is usual to determine the background which falls outside the time resolution of the system by using 'black resonances' or 'notch' filters. The technique employs filters which have negligible neutron transmission at energies corresponding to isolated strong resonances, and the background is assumed to be the observed count rate in these regions. Measurements are made with filters of different thickness and a suitable extrapolation is made to obtain the background with no filter present. It can be shown that this method is only strictly applicable when there is a single component in the background field. Syme /53/ has proposed a new method of background determination which uses black resonance filter data both on and off resonance. It is valid when there are several components in the background field, and can be used at higher energies than the conventional black resonance method. The absence of suitable resonances still limits the upper energy at which the method is applicable to 1 MeV. If the background is small an adequate value at higher energies may be obtained by extrapolation.

The capture detectors we have considered can be classified according to whether or not the detector efficiency is known absolutely. When only the neutron-energy variation, or shape, of

the efficiency is known, the absolute capture yield will have to be obtained from some form of normalization. If the energy-variation of the incident neutron flux is also known the shape of the capture yield can be obtained and normalized to an absolute value at some energy. When a 'white' neutron source is used it may be possible to make the normalization at thermal energy where the capture cross-section is usually known accurately. This may, however, entail a drastic alteration in the experimental conditions, such as a change in flight path, and it is more usual to normalize at some higher energy to a standard reference capture cross-section. Gold provides such a cross-section and a convenient normalization energy is 30 keV. It is important to choose a wide enough energy interval in making the normalization to ensure that any structure in the gold cross-section is smoothed out.

An alternative method of normalization which is available on 'white' neutron sources is the 'saturated resonance' technique. A sample is used of an element which has an isolated low energy resonance for which the radiation width greatly exceeds the neutron width. If the sample is thick, the counting rate will be seen to saturate near the peak of the resonance where every neutron is captured (Y=1). The product $\varepsilon\emptyset$ is then simply given by the saturated counting rate.

The shape of the neutron flux can be determined by any of the standard methods (see for example ref.53). It will usually be convenient, however, to use the gold capture cross-section and this may have the added advantage that systematic uncertainties in detecting the capture process may cancel to some extent. A suitable standard can be provided by the B-10(n,$\alpha\gamma$) reaction if the 480 keV gamma-ray can be detected.

8. CONCLUDING REMARKS.

In this review we have tried to assess the performance of prompt gamma-ray detectors currently being used in the measurement of capture cross-sections in the neutron energy range from thermal to a few MeV. Beyond this energy range a limiting factor becomes the lack of clear distinction between the prompt gamma-rays of capture and those of competing reactions. Above 10 MeV or so the detection of prompt gamma-rays is not a good method for measuring total capture cross-sections.

Below a few hundred keV, for its cheapness and simplicity, the Moxon-Rae detector may still be the best choice if count rate is not the prime consideration. At higher energies the Maier-Leibnitz technique as applied to moderate efficiency liquid scintillators will give increased efficiency but may introduce hidden systematic errors. Both types of detector having an efficiency proportional to total energy released ideally require the use of mono-isotopic samples, however, the sophisticated resonance analysis programmes currently available /55,56/ can to some extent remove this restriction. The fast timing resolution and small size of Moxon-Rae detectors make them particularly suitable for short flight paths on pulsed Van de Graaffs.

Large liquid scintillators possess a high intrinsic efficiency but because of their high background are not particularly well suited to the measurement of small cross-sections. The high bias permissible with this detector effectively suppresses competing reactions but makes the determination of the efficiency a complicated and inaccurate procedure. In terms of time resolution the large scintillator is only slightly inferior to the other detectors. Because of its extended size, however, particularly when surrounded by shielding material, it may be most suited for use at the long flight path lengths associated with 'white' sources.

The spectrum fitting method has been shown by the Bruyeres-le-Chatel group to be a useful technique for measuring the total capture cross-section in the energy range 0.5-3 MeV. Count rate considerations may limit its application at higher energies.

The high cost of building the complex multi-sectional sodium iodide detectors which are used in heavy ion research hardly justifies their use for capture measurements. The simpler multiplicity spectrometer used by the Russians are worthy of consideration, but because of their high neutron sensitivity are only useful in the lower keV range.

The recently introduced bismuth germanate scintillator offers the interesting possibility of making a multi-sectional 4π-detector of modest neutron sensitivity and high efficiency. The high stopping power of this material also makes it useful for those interesting nuclei which have strong components in their gamma-ray spectra.

It is apparent that no one prompt gamma-ray detector is suited to the measurement of capture cross-sections over the entire range of nuclei and energy. Neither is it necessarily desirable that there should be, for it is only by the repeated measurements by different techniques that some idea can be obtained of the systematic errors involved.

ACKNOWLEDGEMENTS.

It is a pleasure to thank Mr.M.C.Moxon, Dr.M.G.Sowerby, and Dr.B.H.Patrick for helpful discussions during the preparation of this paper. We are also grateful to Dr.M.S.Coates for critically reading the original manuscript. Dr.W.P.Poenitz kindly let us have a draft of a chapter on neutron capture detectors which he has written for a Monograph /57/. Mr.P.D.Robinson was responsible for preparing the text.

References

1. R.E.Chrien, Nuclear Cross-sections and Technology, NBS Spec.Publ.425 Vol.1 p.139, Washington (1975)

2. L.M.Bollinger, Proceedings of the Conference on Nuclear Structure Study with Neutrons, Budapest 1972, p.347
3. C.W.Reich, Proceedings of the Third International Symposium on Neutron Capture Gamma-Ray Spectroscopy and Related Topics, Brookhaven, Plenum Press, 105 (1979)
4. J.E.Lynn, "The Theory of Neutron Resonance Reactions", Clarendon Press, Oxford (1967)
5. M.C.Moxon and E.R.Rae, Nucl.Instr.Methods, Vol.24 p.445 (1963)
6. H.Maier-Leibnitz, private communication to R.L.Macklin and J.H.Gibbons (see ref.7)
7. R.L.Macklin and J.H.Gibbons, Phys.Rev., Vol.159 p.1007 (1967)
8. A.E.Evans,Jnr, IEEE Transcript on Nuclear Science, NS-27, No.1, 172 (1980)
9. D.M.Drake, L.R.Nilsson and J.Faucett, Nucl.Instr.Methods, Vol.188 p.313 (1981)
10. B.C.Diven, J.Terrell and A.Hemmendinger, Phys.Rev., Vol.120 p.556 (1960)
11. J.H.Gibbons, R.L.Macklin, P.D.Miller and J.H.Neiler, Phys.Rev. Vol.122 p.182 (1961)
12. D.Kompe, Nucl.Phys., Vol.A133 p.513 (1969)
13. E.Haddad, R.B.Walton, S.J.Friesenhahn and W.M.Lopez, Nucl.Instr.Methods, Vol.31 p.125 (1964)
14. E.G.Silver, J.Lewin, and J.Todd, Oak Ridge reports, ORNL-4280, p.135 and ORNL-4433, p.11 (1969)
15. G.de Saussure, E.G.Silver, R.B.Perez, R.Ingle, and H.Weaver, Nucl.Sci.Eng., Vol.51 p.385 (1973)
16. R.W.Hockenbury, Z.M.Bartolome, J.R.Tatarczuk, W.R.Moyer and R.C.Block, Phys.Rev., Vol.178 p.1746 (1969)
17. R.G.Stieglitz, R.W.Hockenbury and R.C.Block, Nuclear Physics, Vol.A163 p.1592 (1971)
18. W.P.Poenitz, Nucl.Sci.Eng., Vol.57 p.300 (1975)
19. A.Ernst, F.H.Froehner and D.Kompe, Proceedings of the 2nd International Conference on Nuclear Data for Reactors, Helsinki, Vol.1 p.633 (1970)
20. D.B.Gayther, M.S.Coates, G.D.James, M.C.Moxon, D.B.Syme, B.W.Thomas and R.B.Thom, Harwell report AERE-R.9058 (1978)
21. W.P.Poenitz, Proceedings of International Conference on Nuclear Cross-sections for Technology, Knoxville 1979, NBS Spec.Publ.368 Washington (1980)
22. F.H.Froehner, Specialists Meeting on Structural Materials, Karlsruhe 1973,report KFK 2046
23. R.B.Thom. Ph.D thesis, to be published
24. J.C.Hopkins and B.C.Diven, Nucl.Sci.Eng. Vol.12 p.169 (1962)
25. S.K.Gupta, J.Frehaut and R.Boss, Nucl.Instr.Methods, Vol.148 p.77 (1978)
26. R.Gwin, E.G.Silver, R.W.Ingle and H.Weaver, Nucl.Sci.Eng., Vol.59 No. 2, p.79 (1976)
27. R.Gwin, L.W.Weston, G.de Saussure, R.W.Ingle, J.H.Todd, F.E.Gillespie, R.W.Hockenbury and R.C.Block, Oak Ridge report ORNL-TM-2598 (1969)
28. G.V.Muradyan, Yu.G.Shcepkin, Yu.V.Adamchuk, G.I.Ustroev, report IEA-2634, Moscow (1976)

29. G.V.Muradyan, Yu.G.Shcepkin, Yu.V.Adamchuk, M.A.Voskanyan, Nuclear Cross-sections for Technology, NBS Spec.Publ.594, p.488, Washington. (1980)
30. D.G.Sarantites, M.Jaaskelainen, J.T.Hood, R.Woodward, J.H.Barker, D.C.Hensley, M.L.Halbert and Y.D.Chan, Journal de Physique, Colloque C10, supplement 12, Vol.41 p.269 (1980)
31. R.S.Simon, as ref.29, p.281 (1980)
32. W.A.Fowler, C.C.Lauritsen and T.Lauritsen, Rev.Mod.Phys., Vol.20 p.265 (1948)
33. N.T.Kashukeev, Yu.P.Popov and F.L.Shapiro, J.Nucl.Energy A/B Vol.14 p.76 (1961)
34. S.S.Malik, Nucl.Instr.Methods, Vol.125 p.45 (1975)
35. R.L.Macklin, J.H.Gibbons and T.Inada, Nucl.Phys., Vol.43 p.353 (1963)
36. K.V.K.Iyengar, B.Lal and M.L.Jhingan, Nucl.Instr.Methods, Vol.121 p.33 (1974)
37. K.Wisshak and F.Kaeppler, Nuclear Cross-sections for Technology, NBS Spec.Publ.594 p.155, Washington (1980)
38. J.B.Czirr, Nucl.Instr.Methods, Vol.72 p.23 (1969)
39. C.Le Rigoleur, Cadarache report CEA-N-1905 (1976)
40. A.Brusegan, F.Corvi, G.Rohr, R.Shelley and T.van der Veen, Nuclear Cross-sections for Technology, NBS Spec.Publ.594 p.163, Washington (1980)
41. R.B.Thom, D.B.Gayther and T.M.Horscroft, Harwell report AERE-PR/NP28 p.14 (1981)
42. G.A.Bartholomew, E.D.Earle, A.J.Ferguson, J.W.Knowles, M.A.Lone, Advances in Nuclear Physics, Vol.7 p.229 (1973)
43. S.Joly, J.Voignier, G.Grenier, D.M.Drake and L.Nilsson, Nucl.Instr.Methods, Vol.153 p.493 (1978)
44. I.Bergqvist, D.M.Drake, and D.K.McDaniels, Nucl.Phys., Vol.A191 p.641 (1972)
45. N.Starfelt, Nucl.Phys., Vol.53 p.397 (1964)
46. A.Gilbert and A.C.W.Cameron, Can.J.Phys., Vol.43 p.1446 (1965)
47. Neutron Data of Structural Materials for Fast Reactors, Pergamon Press (1979)
48. D.B.Gayther, B.W.Thomas, R.B.Thom and M.C.Moxon (1977), contribution to ref.46 (p.547)
49. M.C.Moxon, private communication (1979)
50. B.J.Allen, A.R.de L.Musgrove, R.L.Macklin, R.R.Winters (1977), contribution to ref.46 (p.506)
51. MORSE-CG, RSIC Computer Code Collection - 203
52. M.C.Moxon, private communication. (1981)
52. D.B.Syme, Harwell report AERE-R10244 (1981)
54. Neutron Standards and Applications, NBS Spec.Publ.493, Washington (1977)
55. F.H.Froehner, 'FANAC', Karlsruhe report KFK.2145 (1977)
56. M.C.Moxon, 'REFIT', Harwell report AERE-R10520, to be published.
57. Neutron Physics and Nuclear Data in Science and Technology, Pergamon Press, Volume to be published.

Discussion

QUESTION: F. Corvi
You said that Bismuth Germanate has a much lower neutron sensitivity than Sodium Iodide. Could you give a figure on that, not only for thermal neutrons?

ANSWER: D. Gayther
No, all I can give you are the values from Table I. I did not make any calculations, but it does not show any resonance structure in the same way flourine does. It is very much more favorable, though not as much so C_6D_6.

QUESTION: A. B. Smith
If you are faced with the problem of measuring the $^{238}U(n,\gamma)$ cross section, what would you do?

ANSWER: D. Gayther
What energy range?

A. B. Smith:
Say 100 keV to 2 MeV.

D. Gayther:
I would be tempted to try the spectrum weighting technique. There may be some different opinions at Karlsruhe.

A. B. Smith:
The feeling that I get is that prompt detection techniques are bottoming out over a 10 year period at something like 5-10%. If you try ^{238}U with a requested 3% you have a problem.

D. Gayther:
Yes, that's right. With the large tank and the semiempirical methods to determine its efficiencies we felt that it might be possible to achieve 5%. ^{238}U might be more favorable because the spectrum does not change that much, not as much as the structural materials.

FAST-NEUTRON CAPTURE-CROSS-SECTION MEASUREMENTS WITH THE ARGONNE NATIONAL LABORATORY LARGE-LIQUID-SCINTILLATOR TANK*

W. P. Poenitz
Argonne National Laboratory
Argonne, Illinois, USA

ABSTRACT

Measurements of the neutron-radioactive-capture cross sections of Y, Zr, Mo, Ag, Cd, In, Sb, La, Eu, Gd, Tb, Dy, Er, Yb, Hf, W, Re, and Pt in the 0.5 - 4.0-MeV-energy range are presented. A large-liquid-scintillator detector was used for detecting the capture events. A grey neutron detector was used as neutron monitor. The reported cross sections are relative to the capture cross section of gold at 0.5 MeV. Where prior data exist the present data are lower for most elements. However, good agreement was obtained with very recent results reported by the group from Bruyères-le-Châtel.

I. Introduction

Fast-neutron-capture cross sections were unavailable for many elements above a few hundred keV until recently when some data from the present program and from the group at Bruyères-le-Châtel became available.[1,2] Data requirements were filled with theoretically calculated cross sections using the optical and statistical models. A comparison of such calculated cross sections at 2 MeV showed differences with factors of 2 to 5 occurring frequently, and even factors of 10 being present.[3] One might consider, as an example, the neutron-capture cross sections of important fission products, which are required to be known with 5-7% uncertainty.[4] Using the sensitivity of reactor parameters to changes of the capture cross sections, one can roughly estimate that the capture cross sections of fission-product nuclei should be known with 25-35% in the 1-2 MeV energy range.

The measurements of capture cross sections with a large-liquid-scintillator detector (LLST) at an accelerator, which permits the production of monoenergetic neutrons, has substantial advantages for the MeV-neutron-energy range: gamma rays originating in inelastic neutron scattering events can be discriminated against without compromising the basic detector principle, and background can be suppressed by the time-of-flight technique. The capture-event-detection efficiency is about 70-80%, due to the requirement to set a threshold corresponding to a γ-ray energy of 2-3 MeV. The uncertainty of the required extrapolation to zero-pulse height is estimated to be in the range of

*This work was supported by the U.S. Department of Energy.

5-10%. With the addition of other uncertainties (5% for the reference cross section, 2-5% for the correction for capture of scattered neutrons) one should obtain cross-section data with 7-13% uncertainties. Compared with experimental-data discrepancies of up to 100%, and nuclear-model-prediction discrepancies of up to 1000%, this should be a substantial improvement.

The elements measured in the present program and the status of the data are listed in Table I. Capture cross sections for 18 elements (out of 32) are presented here. Measurements were typically made in the energy range from 0.5 to 4.0 MeV. The data are presently considered preliminary as scattering corrections will be reconsidered.

II. Experimental Procedure

The experimental set-up and procedure were described at various occasions in detail,[1] and only a brief description will be given here. The $^{7}Li(p,n)^{7}Be$ reaction with a pulsed- and bunched-proton beam (1-2 nsec width and a 2-MHz-repetition rate) was used as a neutron source. Metallic-lithium targets were chosen to provide neutron-energy resolutions of ± 20 - 40 keV. The neutron source was shielded in 4π geometry, with a conical opening providing a collimated-neutron beam which passed through the sample, and was finally captured in a grey neutron detector. The samples were placed in the center of a channel through the 1300 liter LLST at a flight path of 2.5 m from the source. The LLST has a time resolution of 3 nsec. The samples were metallic discs with 8.9 cm diameter and typical thickness corresponding to 0.006 - 0.015 nuclei/barn. Exceptions were La, Y, and Re with 0.041, 0.048, and 0.034 nuclei/barn, respectively.

Measurements of the capture yields of all samples were made relative to the shape of the grey-neutron-detector efficiency. The ratio relative to the capture cross section of gold was measured at 0.5 MeV; for many samples repeatedly with a typical reproducability of 2-4%. The cross section of some samples were measured relative to the capture cross section of gold over the entire energy range (e.g. Zr and Eu). The γ-energy-detection fraction was determined by extrapolating the measured spectrum or by extrapolating the integrated spectrum to zero-pulse height.

Corrections were applied for neutron transmission through the sample and the air between the sample and the neutron detector, for neutron-capture events due to elastic and inelastic scattering, for total γ-cascade-energy loss due to γ-absorption in the sample and escape from the tank, and the second neutron group of the $^{7}Li(p,n)$-source reaction. Background was measured with carbon samples, without samples and with the collimator aperture plugged. It proved to be insignificant below 2-3 MeV.

III. Results and Discussions

The present data are shown in Figs. 1-4. A complete comparison with

previously reported data has not been made at this time. However, the present results are compared with other very recently reported data. The present data for Dy, Yb, Er, Hf, Cd, and In are shown in Fig. 1. Recent data are not available for these cross sections. The present data for Tb, Pt, Gd, Re, W and Sb and recent data from Bruyères-le-Châtel (BRC) are compared in Fig. 2. The generally good agreement is an encouraging indication of the present state of the art for capture cross section measurements. The data sets were obtained with different measurement techniques. The data differences indicate that estimated uncertainties of 8-12% for the ANL measurements and 15% for the BRC measurements are certainly realistic and probably conservative. Results for Y, Zr, and La are shown in Fig. 3. The cross sections for these elements are small ($\approx$ 10 mb) throughout the energy range and thus more difficult to measure. Thick samples were used for Y and La. Again, the agreement with the BRC results is very good, excepting a value at 2.5 MeV for Zr. The results of nuclear model calculations with the code ABAREX[5] are shown for Y and Zr. Finally, Fig. 4 shows the present results for Mo, Ag, and Eu. These elements include important fission products. Of specific interest is Ag, for which other results became available also at this time. The present data agree within 5% with the sum of the ^{107}Ag and ^{109}Ag cross sections measured by Macklin,[6] however, disagreement exists with the data by Mizumoto et al.[7] The ENDF/B-V evaluation (sum of ^{107}Ag and ^{109}Ag) is also shown in this figure. The present data suggest a different shape in this region.

The good agreement between the present data and the measurements from BRC was also observed for data previously reported (Au, Nb, Rh). Agreement with data measured by Macklin is also good after revision of some of these data[8] (Rh, Pd, Th). This situation suggests that substantial improvements have been made in fast-neutron-capture cross section measurements.

References

1. W. P. Poenitz, Argonne National Laboratory Reports ANL/NDM-8 (1974), ANL/NDM-15 (1975), ANL/NDM-42 (1978); Nucl. Sci. and Eng. 57, 300 (1975); Proc. Conf. Nucl. Cross Sections and Technology, Wash. 1975, p. 901; Proc. Spec. Meet. on Neutron Cross Sections of Fission Product Nuclei, Bologna 1979, p. 85.

2. J. Voignier et al., Bruyères-le-Châtel report CEA-R-5089; Proc. Spec. Meet. on Neutron Cross Sections of Fission Product Nuclei, Bologna 1979, p. 63; S. Joly et al., Nucl. Inst. Methods 153, 493 (1978), Fourth Intl. Symp. on Neutron-Capture Gamma Ray Spectr., Grenoble (1981).

3. S. Iijima et al., J. Nucl. Sci. Technology 14, 161 (1977).

4. Proc. Specialists Meeting on Neutron Cross Sections of Fission Product Nuclei, Status reported by Working Groups, Bologna (1979).

5. P. Moldauer, this meeting (1982).

6. R. L. Macklin, private communication (1982).

7. M. Mizumoto et al., priv. communication to R. Block (1982), to be contributed to Conf. on Nucl. Data for Science and Technology (Antwerp 1982).

8. R. L. Macklin and R. R. Winters, Nucl. Sci. Eng. 78, 110 (1981).

Table I
Elements Measured in the Present
Program and the Status of the Data

Element	Data Reported	Presently Reported Data	Comment
Cr			Data may be derived
Zn	75 Wash.		Add. Data
Ni	75 Wash.		Add. Data
Cu	75 Wash.		Add. Data
Y		Present ✓	
Zr		Present	
Nb	ANL/NDM 8		
Mo		Present	
Rh	79 Bologna		
Pd	79 Bologna		
Ag		Present	
Cd		Present ✓	
In		Present ✓	
Sb		Present ✓	
La		Present	
Nd	79 Bologna		
Sm	79 Bologna		
Eu		Present	
Gd		Present ✓	
Tb		Present ✓	
Dy		Present ✓	
Ho	ANL/NDM 15		
Er		Present ✓	
Yb		Present ✓	
Hf		Present ✓	
Ta	ANL/NDM 15		
W		Present ✓	
Re		Present ✓	
Pt		Present ✓	
Au	NSE 57 (75)		
Th	ANL/NDM 42		
U8	NSE 57 (75)		

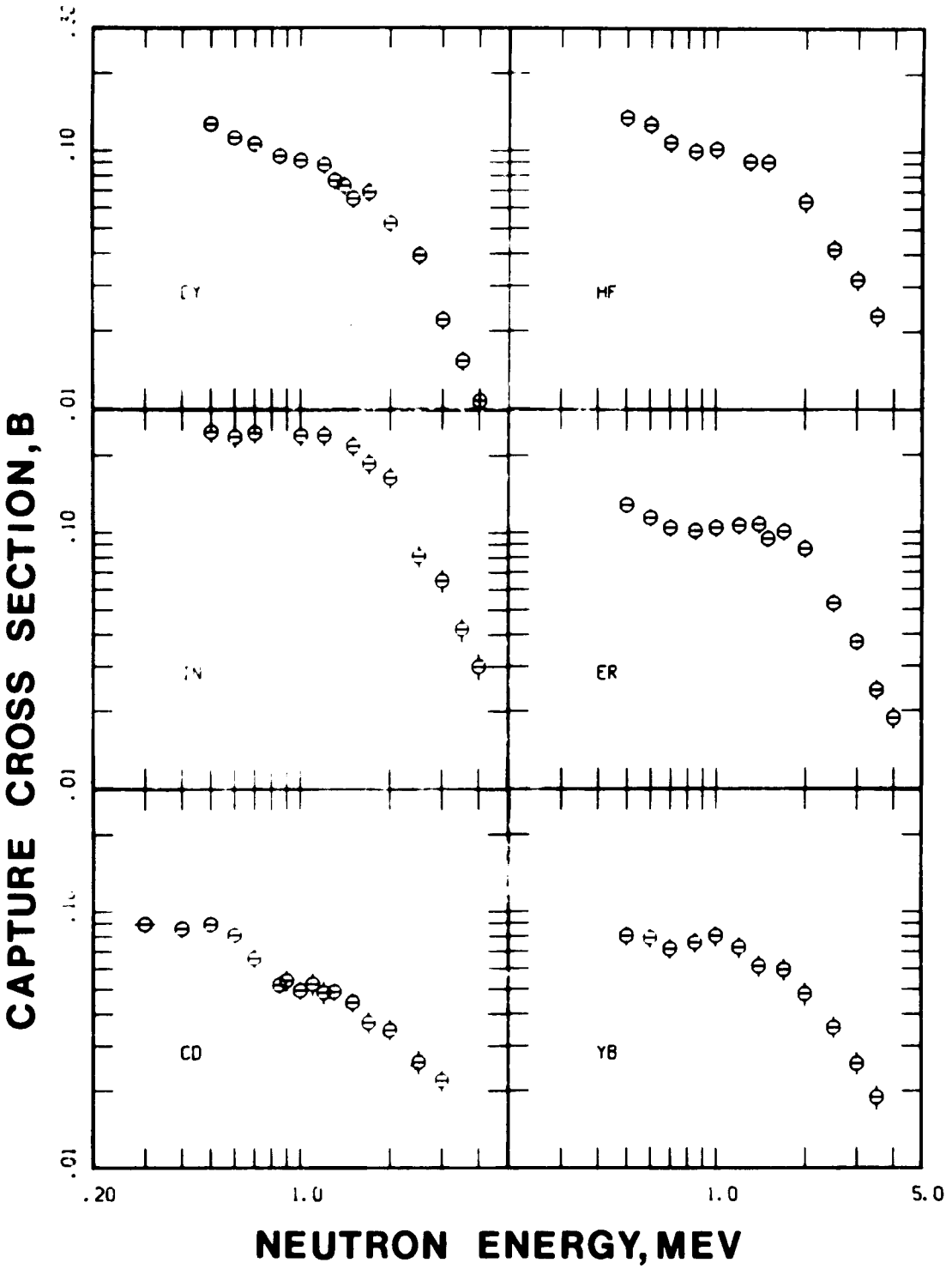

Figure 1. Present Results for the Neutron-Capture Cross Sections of Cd, In, Dy, Yb, Er, and Hf.

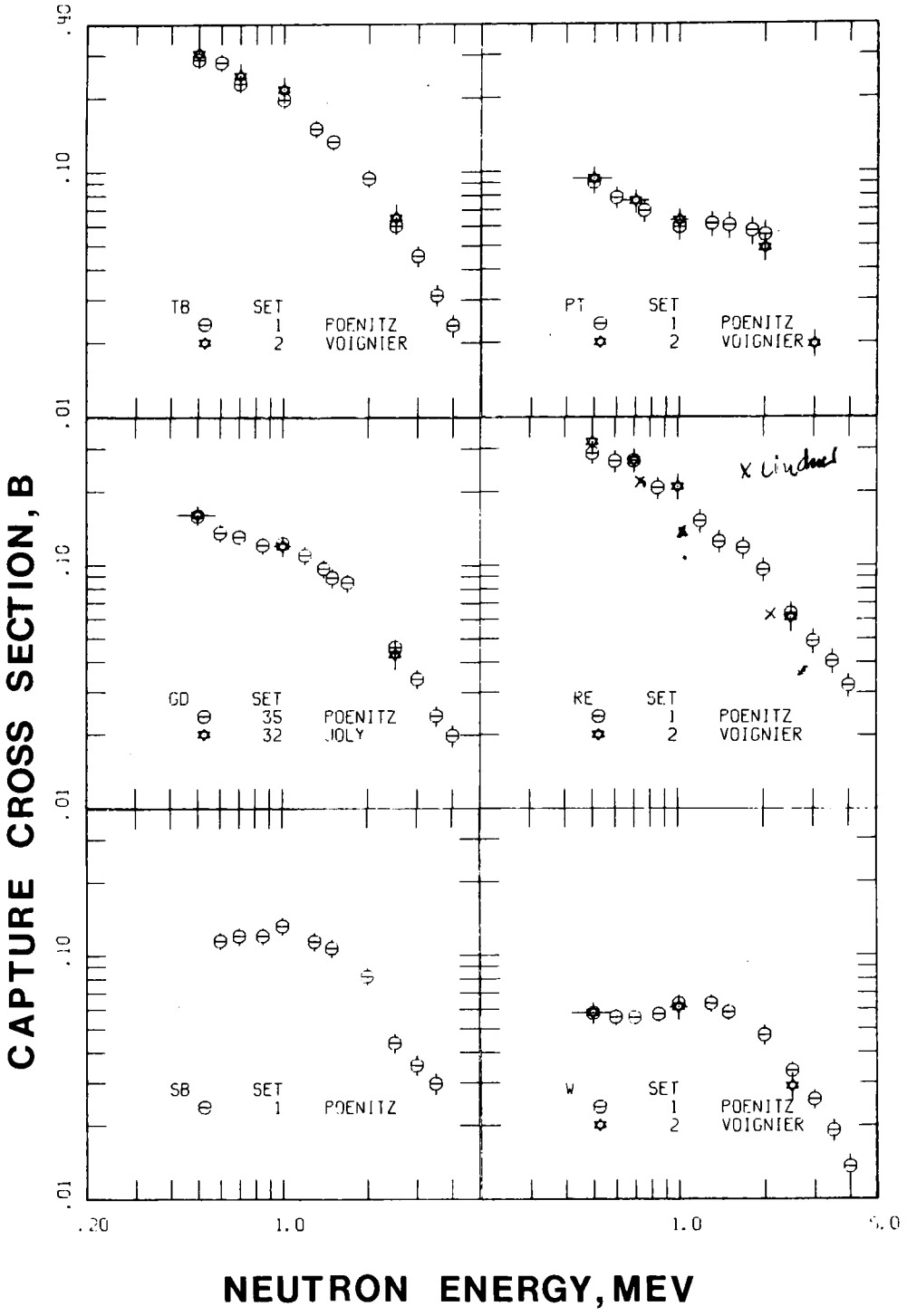

Figure 2. Comparison of the Present Results for Sb, Gd, Tb, W, Re, and Pt with Recent Data from Bruyères-le-Châtel.

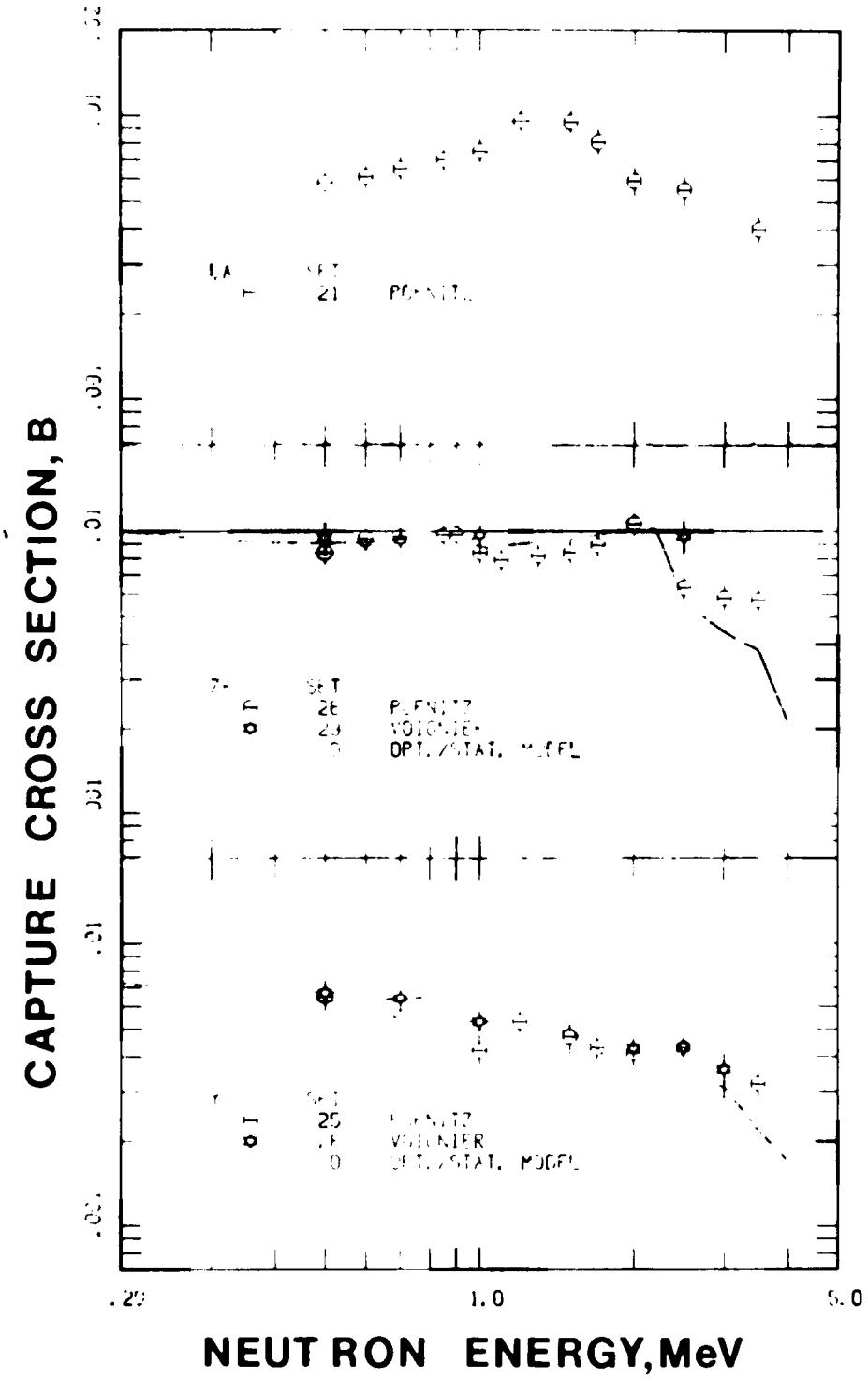

Figure 3. Present Results for Y, Zr, and La. Data by Voignier et al. and Optical/Statistical Model Calculations are also shown.

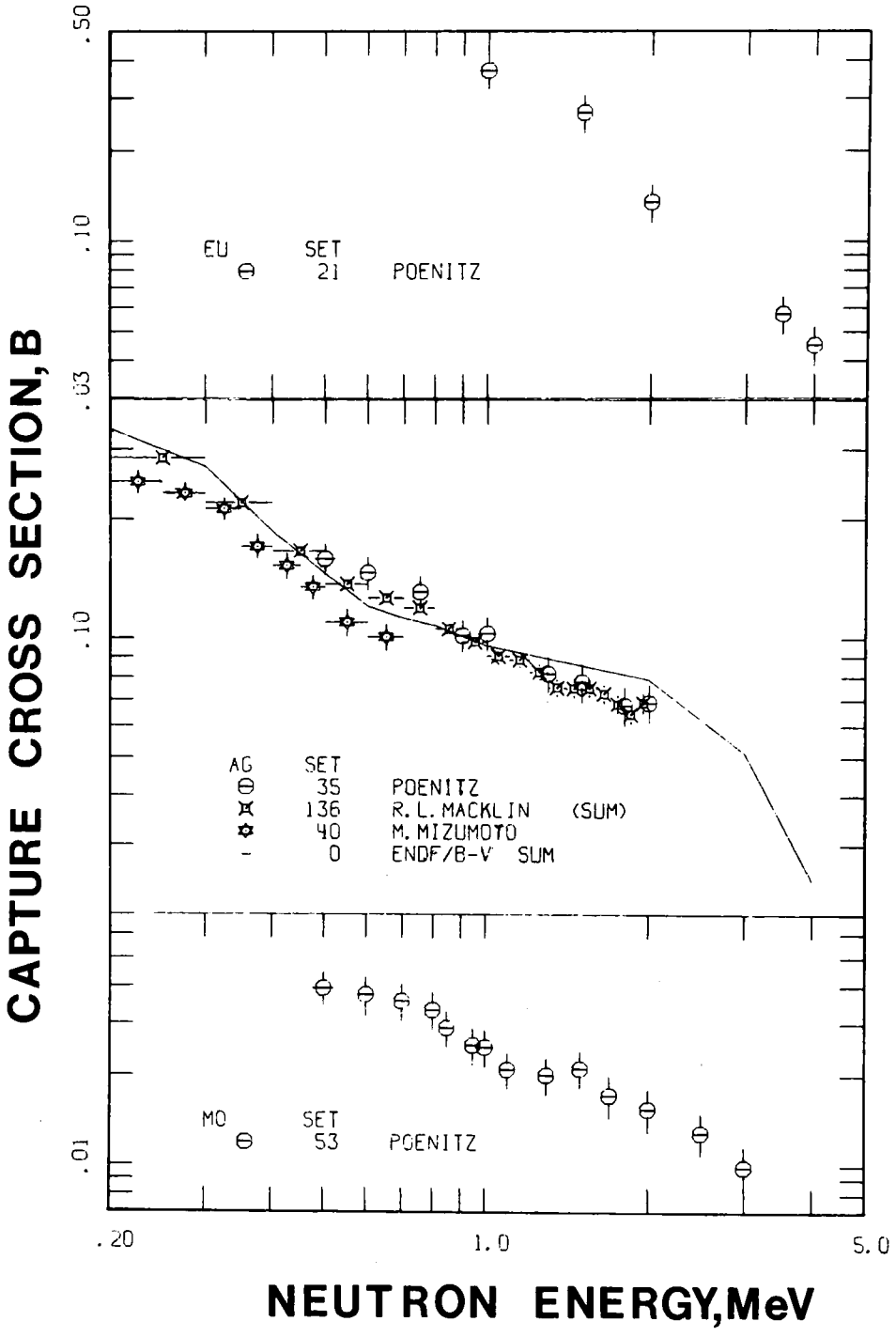

Figure 4. Present Results for the Neutron-Capture Cross Sections of Mo, Ag, and Eu. Recent Data by Macklin[6], by Mizumoto et al.[7], and the ENDF/B-V Evaluation are shown for Silver.

Discussion

QUESTION: R. Peelle
Did you make the detector-efficiency γ-ray cascade calculations for each target and for capture from the various partial waves and neutron energies? How large were these efficiency corrections?

ANSWER: W. Poenitz
Yes. The correction was made for the total loss of the cascade energy due to absorption in the sample and escape from the tank. Due to the partial compensation with the standard Au sample, the correction was usually small (a few percent).

QUESTION: R. Howerton
Which gold cross section did you use for your normalization, and at what energies?

ANSWER: W. Poenitz
The measurements were made relative to the ENDF/B-V standard at 500 keV.

QUESTION: R. Schenter
Did you perform the optical model calculations described for the elements in a single calculations or were calculations made on individual isotopes.

ANSWER: W. Poenitz
The calculations were carried out for the isotopes and added up for the elements.

FAST NEUTRON CAPTURE CROSS SECTION MEASUREMENTS USING A NaI DETECTOR

by

S. Joly, G. Grenier and J. Voignier
Service de Physique Neutronique et Nucléaire
Centre d'Etudes de Bruyères-le-Châtel
B.P. N° 561
92542 MONTROUGE CEDEX, France

Abstract

We present the different ways the total capture cross section is determined starting from the pulse-height distribution as given by a NaI detector surrounded by an annulus. The time-of-flight technique associated with an improved shielding of the system is used to reduce background making capture cross sections as low as 1 mb measurable. The extrapolation of the capture γ-ray energy distribution in the (n,n'γ) region is made using a simple statistical model calculation. The principle of energy conservation is also used. The unfolding stage can be avoided by applying the pulse-height weighting technique to the NaI pulse-height spectrum. The present method has also the advantage of giving the (n,γn') cross section as a byproduct.

I. Introduction

The technique developed at Bruyères-le-Châtel is based on the detection of prompt γ-rays emitted by the sample and was first applied to the capture of neutrons between 0.5 and 3.2 MeV. The lowest limit corresponds roughly to the energy of the first excited state of the target nucleus thus avoiding the contribution of the (n,n'γ) reaction which is otherwise difficult to estimate with the conventional techniques of measuring capture cross sections (Moxon-Rae or Maier-Leibnitz detectors, large liquid scintillator tanks). This inelastic contribution is not taken into account with the activation technique but the main problem concerns the effect of low-energy secondary neutrons. Moreover, this technique can be used only for radioactive residual nuclei. Our method allows the contribution of the (n,γ) reaction to be estimated in the region containing mostly γ-rays from inelastic scattering.

II. Experimental and data processing techniques

The technique has been described in details [1] and is summarized briefly here. Depending on the desired neutron energy, the $^7Li(p,n)^7Be$ ($E_n < 0.7$ MeV) and $^3H(p,n)^3He$ ($E_n < 3.2$ MeV) reactions have been used as sources of monoenergetic neutrons. The pulsed and bunched proton beam is delivered by the 4 MV Van de Graaff accelerator at Bruyères-le-Châtel. The pulse width is about 1 ns and the average beam intensity of 8 μA. Targets consist of metallic lithium or tritium adsorbed in titanium on tantalum backings. Samples (cylinders or disks) are located at 8 cm from the target. The neutron flux is measured through the sample by a BF_3 detector located at 0° and at about 2 m from the target.

Gamma-rays are detected by a 3" x 6" NaI crystal surrounded by a NaI annulus. The spectrometer is used in the anti-Compton and first-escape modes simultaneously. The γ-ray detector efficiency and the response functions are determined by calibrated radioactive sources and nuclear reactions for γ-ray energies between 1.0 and 12.5 MeV.

The spectrometer is shielded with special neutron and γ-ray absorbing materials. The sample to detector distance is about 80 cm and the energy distribution of the γ-rays can thus be deduced. This distance is also necessary for using the TOF technique and for shielding the γ-ray detector efficiently. The detector is protected further from direct target radiations by a shadow bar and from the sample scattered neutrons by 20 cm of LiH.

The net pulse-height spectra are converted to γ-ray distributions using a least-squares unfolding method and the response functions of the spectrometer. The unfolded spectra are corrected for the detector γ-ray efficiency and for the γ-ray attenuation in the sample thus giving the capture γ-ray spectrum emitted by the sample. This is done for the two detection modes and the weighted average of these two distributions is taken thus improving the statistical accuracy of the energy distribution $S(E_\gamma)$.

III. Gamma-ray energy distribution technique

Capture and inelastic γ-rays emitted by the sample are detected by the spectrometer. For the neutron energies of interest ($0.5 \leq E_n \leq 3.2$ MeV), the contribution of the (n,n'γ) reaction is very important in the low-energy region ($E_\gamma < E_n$) of the measured distribution and we have to estimate the (n,γ) contribution in this region. The first method we developed combines the technique used to study γ-ray strength functions and the spectrum method of measuring partial capture cross sections. As γ-rays are detected at one angle (generally 90°), we deduce angle-integrated capture cross sections assuming isotropy for capture γ-rays but this is a good approximation for these neutron energies.

The unknown part of the capture spectrum is estimated by means of a simple statistical model calculation. The shape of this spectrum is known [2] to depend on two factors : the γ-ray strength function $f(E_\gamma)$ and the level-density distribution $\rho(U)$. The level density of the residual nucleus

has to be determined from other sources but is not of crucial importance here. Given a γ-ray strength function to start with, we calculate the energy distribution of primary γ-rays emitted by the capture states and the total spectrum which is the sum of the primary distribution and the cascade γ-rays. This total calculated spectrum is then compared to the measured distribution in the region containing only capture γ-rays, i.e. for $E_\gamma > E_n$. The level density being fixed, the $f(E_\gamma)$ function is changed accordingly up to a good agreement is obtained between the measured and calculated shapes in the region of the fit. The γ-ray strength function is extrapolated down to $E_\gamma = 0$ to obtain the entire capture spectrum. The extrapolation of the capture spectrum is thus replaced by the extrapolation of the $f(E_\gamma)$ function. A different $\rho(U)$ distribution would give another energy dependence for $f(E_\gamma)$ in the region of the fit and a different extrapolation to zero but this effect introduces a small additional uncertainty on the deduced cross sections. Anyway this extrapolation is minimized because determined for the spectrum obtained at the lowest neutron energy (E_n = 0.5 MeV) and then used for the other energies as well. To get the number R_c of capture reactions having occured in the sample, the primary energy distribution ν_p is defined with the following normalization :

$$\int_{E_n}^{U_{max}} \nu_p(E_\gamma)\, dE_\gamma = 1 \qquad (1)$$

i.e. we consider only those transitions to bound states and to states within a narrow range above B_n where $\Gamma_\gamma > \Gamma_n$. The number of reactions is then given by the ratio between the observed γ-ray spectrum $S(E_\gamma)$ and the calculated total spectrum per capture $\nu_t(E_\gamma)$:

$$R_c = \int_{E_n}^{U_{max}} S(E_\gamma)\, dE_\gamma \Big/ \int_{E_n}^{U_{max}} \nu_t(E_\gamma)\, dE_\gamma \qquad (2)$$

with $U_{max} = E_n + B_n$ where B_n is the neutron separation energy. So we use the shape of the measured distribution to get the energy distribution of primary and total capture γ-rays emitted per capture reaction and its absolute value to determine the number of capture reactions. Combined with the neutron fluence Φ and the number of nuclei N in the sample, we deduce the capture cross section :

$$\sigma_{n\gamma} = 4\pi(d\sigma/d\Omega)_{90°} = 4\pi\, R_c\, / \Phi\, N \qquad (3)$$

The calculation of the total capture distribution is necessary with this method because the contribution of cascade γ-rays is important and adds to the primary γ-rays so the common integrated spectrum technique cannot be used. This is only possible when the incident neutron energy E_n is larger than the neutron separation energy B_n because the capture distribution

contains then only primary γ-rays.

Another way of deducing the number of capture reactions when starting with the energy distribution of γ-rays emitted by the sample is to use the principle of energy conservation. The number of reactions R'_c is then given by :

$$R'_c = \int_0^{U_{max}} E_\gamma \, S(E_\gamma) \, dE_\gamma \Big/ U_{max} \qquad (4)$$

However, the observed spectrum $S(E_\gamma)$ has also to be extrapolated from $E_\gamma = E_n$ down to zero energy. For this extrapolation, we assume first that the spectrum has the following energy dependence :

$$S(E_\gamma) \, dE_\gamma \sim \exp(-\alpha E_\gamma) \, dE_\gamma \qquad (5)$$

where α is a constant. Sometimes, the γ-ray spectrum deviates considerably from this behaviour (bumps in spectra) and this extrapolation is very uncertain. As a second possibility, we assume a constant value for $E_\gamma < E_n$, i.e. $S(E_\gamma) = S(E_n)$ in this region. At low neutron energy, this method of deducing capture cross sections is easy to apply as the extrapolation range is pretty small and also weighted by the E_γ-factor (eq. 4) and statistical model calculations are avoided. However, for larger neutron energies, this energy conservation method is less accurate because of the difficulties of extrapolating a spectrum having relatively poor statistics. Consequently, the distribution ratio method is preferred for neutron energies above 1.0 MeV. It has been observed that the result obtained with the distribution ratio method was between the too values deduced using the energy conservation principle.

IV. Pulse-height weighting technique

Recently, we have applied the weighting technique to our NaI pulse-height spectra to determine capture cross sections [3]. In principle, this technique could be applied to any kind of γ-ray detector to measure neutron capture cross sections. In this technique, a weighting function W(I) is introduced so that the total energy emitted by the sample can be directly obtained from the observed pulse-height distribution C(I) :

$$E_t = \int_0^{I_{max}} C(I) \, W(I) \, dI \qquad (6)$$

Dividing this total energy, corrected for the energy loss in the sample, by U_{max} gives the total number of capture reactions. The weighting function W(I) was easily obtained as the efficiency and the response functions were

known from 1.0 to 12.5 MeV and was extended down to zero energy. But the pulse-height distribution C(I) has also to be extrapolated in the region of the $(n,n'\gamma)$ contribution and different extrapolations have been used : constant,linear and exponential. For this purpose, the extrapolation of the pulse-height spectrum is preferred to the extrapolation of the weighted spectrum for it is easier to use the smooth dependence of the pulse-height spectrum for $E_\gamma > E_n$. The extrapolated part of the total capture spectrum is very important for high neutron energies ($E_n > 2$ MeV) and the deduced cross section is very uncertain . Consequently, it was observed that this technique was difficult to apply for $E_n > 1.5$ MeV.

V. $(n,\gamma n')$ cross sections

A radiative cross section σ_{rad} can be defined when using the following normalization for the primary spectrum :

$$\int_0^{U_{max}} \nu_p(E_\gamma)\, dE_\gamma = 1 \qquad (7)$$

This corresponds to the deexcitation of capture states to bound and unbound states, i.e. to (n,γ) and $(n,\gamma n')$ processes, respectively. The $(n,\gamma n')$ cross section can thus be deduced by difference :

$$\sigma(n,\gamma n') = \sigma_{rad} - \sigma(n,\gamma) \qquad (8)$$

This cross section is very small at 0.5 MeV but increases with neutron energy.

VI. Conclusion

From the results obtained with the different ways of deducing the capture cross section when starting with the pulse-height spectrum given by the NaI spectrometer, we saw that the different solutions can be applied for neutron energies below 1.0 MeV, or so. However, for higher neutron energies, the distribution ratio method is the only one we can rely on because we have there a possibility of calculating the extrapolation of the capture spectrum in the low-energy region. Apart from the activation technique, which is restricted to radioactive nuclei, this method can be applied for any neutron energies thus filling the gap with the application of the integrated spectrum technique. As an example, we present in table I the cap-

ture cross section of natural Pt for neutron energies of 0.5 and 3.0 MeV as obtained with the gamma-ray energy distribution and pulse-height weighting techniques. As far as the (n,γn') cross sections are concerned, we found $\sigma(n,\gamma n') \approx 0$ at 0.5 MeV and $\sigma(n,\gamma n') \approx 24$ mb at 3.0 MeV, i.e. a larger cross section than for the capture process.

Table I - Neutron capture cross sections of ^{nat}Pt at 0.5 and 3.0 MeV. Comparison between the different techniques.

method	extrapolation	$\sigma_{n\gamma}$(mb)	
		E_n = 0.5 MeV	E_n = 3.0 MeV
Gamma-ray energy distribution	distribution ratio (Method I)	93.5	20.0
	Constant (method II)	91.0	16.0
	Exponential (method II)	93.5	18.5
Pulse-height weighting	Constant	82.5	16.0
	Exponential	92.0	18.5

References

[1] - S. Joly et al., Nucl. Instr. Meth. 153 (1978) 493.

[2] - N. Starfelt, Nucl. Phys. 53 (1964) 397.

[3] - S. Joly, Nucl. Sci. Eng. 79 (1981) 315.

Discussion

QUESTION: R. Chrien
Do your calculated curves include (n;n',γ).

ANSWER: S. Joly
No, the statistical calculations we make are only for the capture contribution in the low energy part of the measured energy distribution and do not include (n;n',γ) estimates.

QUESTION: F. Corvi
I was struck by the fact that the weighting function which you have calculated for your NaI(Tℓ) detector increases rather steeply with energy. The shape of the response function in NaI(Tℓ) should favor an increase of the slope of W(Eγ) less important than that for liquid scintillators of the C_6D_6 or C_6F_6 type. Can you comment on that?

ANSWER: S. Joly
The figure presents the weighting function when using the NaI spectrometer in the anti-compton mode so that a large part of the compton component is rejected and this is responsible for the non-linearity of weighting function.

FAST NEUTRON CAPTURE CROSS SECTION MEASUREMENT WITH PULSE-HEIGHT WEIGHTING TECHNIQUE

N. Yamamuro, M. Igashira and M. Shimizu

Research Laboratory for Nuclear Reactors
Tokyo Institute of Technology

ABSTRACT

Neutron capture cross section measurement has been performed in the energy range from 200 to 610 keV with the pulse-height weighting technique. Monoenergetic neutrons were generated by $^{7}Li(p,n)$ reaction, and capture gamma-rays emitted from a sample were detected with a hollow cylindrical NE-213 scintillation detector. The volume of the scintillator is about 10 liter. An annular graphite gamma-ray absorber was inserted into the center of the detector as to make the weighting function straight as possible. To reduce the background, a cube of 40-cm boric-acid and paraffin surrounded the neutron source, and a hollow cylindrical shield consisting of 10-cm thick lead and 35-cm thick boric-acid and paraffin surrounded the detector. The capture cross sections of ^{165}Ho at the neutron energies of 200, 300, 460, and 610 keV were obtained from the relative values to the $^{197}Au(n,\gamma)$ cross sections which were quoted from the ENDF/B-V file. The uncertainty of the data was 8 ~10 %.

I. INTRODUCTION

The pulse-height weighting technique[1)] is a useful method for the capture cross section measurement, because it can in principle be applied to any gamma-ray detector that is insensitive to the neutron. The C_6F_6[2-4)] and the C_6D_6 scintillators[5-7)] are widely used for the capture cross section measurement with the pulse-height weighting technique. These detectors are cylindrical and have the small solid angle to avoid the detection of more than one gamma-ray from the same capture event, since the excess weight is in general imposed in that case. However, a detector with large solid angle can be used when the weighting function of the detector is represented by a linear function of the energy. In a case of the linear weighting function, the weight for two gamma-rays count simultaneously is the same as that for these two gamma-rays count nonsimultaneously[8)].

The 10-liter NE-213 liquid scintillation detector with the shape of hollow cylinder was designed to measure the capture cross section in the neutron energy above 100 keV. An annular graphite absorber was inserted into the center of the detector as to make the weighting function linear as possible. To study the performance of the detector, the capture cross sections of ^{165}Ho and ^{197}Au at the neutron energies of 200, 300, 460, and 610 keV were measured with the pulse-height weighting method, in which $^{197}Au(n,\gamma)$ cross sections were used as the reference. The detector and the response to the gamma-ray detection are described in Section II , and an experiment of the capture cross section measurement in Section III. In Section IV , the result and discussions of the present study are given.

II. HOLLOW CYLINDRICAL DETECTOR AND RESPONSE TO GAMMA-RAY DETECTION

The NE-213 liquid scintillator is sealed in an aluminum container of the half of the hollow cylinder with 17-cm inner-diam 37-cm outer-diam and 13-cm thick. The detector is composed of these two halves, and each has two glass windows, on which photomultipliers RCA-8575 are mounted. The annular graphite gamma-ray absorber of 7 cm in the inner-diameter and 19.5 cm in the length is inserted into the center of the detector.

The light collection efficiency depends on the position that scintillation occurs, since the windows are small compared with the scintillator volume. To obtain the distribution of the light collection efficiency, an experiment was carried out with a collimated gamma-ray beam from ^{60}Co source. The gamma-ray beam impinged perpendicularly on the surface of the detector from several positions on the circle through the center of window, and the pulse-height spectrum was measured at each position. The distribution of the light collection was calculated from the probability of direct incidence of the light to the window, which is proportional to the solid angle subtended by the window at the scintillation point, and from that of indirect incidence after many times reflection on the wall of the container. The fraction of the contribution of the indirect incidence was derived from the experiment mentioned above as a function of the position on the circle. The distribution of the light collection efficiency is shown in Fig. 1, obtained when the radiation occurs at the same rate in the cells of the scintillator which are defined by dividing the radial direction by the equal distance and the direction of azimuth by the equal angle.

The responses of the detector to the monoenergetic gamma-rays were measured using several gamma-ray sources placed on the center of the detector from 1.25 MeV (mean of 1.17 and 1.33 MeV gamma-rays from ^{60}Co) to 7.48 MeV ($^{9}Be(p,\gamma)$ reaction). On the other hand, responses were calculated with a Monte-Carlo method, which can consider the gamma-ray interactions in the absorber and the scintillator, and were broadened by the distribution of the light collection efficiency. As the result of comparing the calculated spectrum with the experimental one, the energy resolution of the detector was determined. Fig. 2 shows experimental and calculated pulse height spectra for ^{60}Co.

The weighting function of the detector was calculated for 1 to 7 MeV gamma-rays assuming the formula, $W(E) = aE + bE^2 + cE^3$. While the present weighting function obtained by inserting the 5-cm thick carbon absorber between the sample and the scintillator was not linear, the uncertainty produced from the excess weight was calculated to be less than 2 % in the case of a typical simultaneous two gamma-rays detection.

III. EXPERIMENT

Monoenergetic neutrons were generated by $^{7}Li(p,n)$ reaction induced by pulsed proton-beam from the Tokyo Institute of Technology 3 MV Pelletron accelerator. The neutron energies used in this study were 200, 300, 460, and 610 keV with the spread of ± 20 keV. A sample was placed at 185 cm from the neutron source, and capture gamma-rays emitted from the sample were detected with the hollow cylindrical scintillation detector, described in Section II. The neutron source was surrounded by a cube of 40-cm boric-acid and paraffin, and neutrons were led to 0° direction with respect to the proton-beam by pre-collimators. The detector was mounted in the shield consisting of 10-cm thick lead and 35-cm thick boric-acid and paraffin. By these shields for

during the accelerator running increased only about twice what it was without running. The neutron flux impinging on the sample was measured by a 1-mm thick ^{6}Li-glass scintillator. Since the ^{6}Li(n,α) reaction has a large resonance at 250-keV neutron energy, an auxiliary ^{10}B slab-NaI neutron monitor was used in the present experiment.

The capture gamma-ray spectrum was measured by means of the time-of-flight (TOF) method. In the TOF spectrum, the channels corresponding to the capture event and both sides of these were selected and signals over these channels are recorded in the pulse-height analyzer. After background subtraction and extrapolation of the pulse-height spectrum to the lower energy, the weighted spectrum was produced multiplied by the weight. The spectrum was extrapolated from the channel corresponding with the incident neutron energy to the zero channel, so that the contribution of gamma-rays from the inelastic scattering was eliminated. The error introduced by the extrapolation was estimated to be less that 1 %, because the weight was small at the lower energy region.

The corrections of the neutron resonance self-shielding and multiple scattering in the sample were estimated by the Dresner-Macklin method[9,10] and that of the gamma-ray self-absorption by a Monte-Carlo method.

IV. RESULT AND DISCUSSIONS

The capture cross sections of ^{165}Ho were obtained using the ^{197}Au(n,γ) cross sections from ENDF/B-V file as the reference. The result is shown in Fig. 3 with the other data. The uncertainty of the present data is 8∼10 %, but that at 300 keV is 15 % due to the lower neutron yield of ^{7}Li(p,n) reaction at that energy. The present results agree well with the recent data of Macklin and Winters[11] and with the activation cross section measured by Johnsrud et al.[12]. Czirr and Stelts's[13] and Brazosko et al.'s[14] measured data, and the ENDF/B-IV evaluated value are also shown in Fig. 3.

The ^{10}B slab used as the neutron flux monitor in the present experiment is small, and the shield for the detector has the long size because it was designed for a large annular NaI-crystal used in an anti-Compton or a pair spectrometer. The experimental arrangement, in which the small ^{10}B slab was placed at behind the long shield, should be adopted, so that the diameter of incident neutron beam at the sample was limited to 30 mm, while the diameter of sample is 55 mm. To increase the counting rate of the detector, a 3-mm thick gold and a 2-mm thick holmium samples were used. Therefore, the corrections of gamma-ray self-absorption in the samples, especially in the gold reference sample, became large, resulting in the about 5 % uncertainty of the capture cross section. Another main source of the uncertainty is the statistical errors of the area of the weighted spectrum, which are 3∼6 % except at the 300-keV data.

First of all, a large boron slab neutron monitor must be prepared. And if non-hydrogenous liquid scintillator can be used in the hollow cylindrical detector, the shield for the detector might be much more simple. Then, the accurate fast neutron capture cross section can be measured with the 10-liter liquid scintillation detector using the pulse-height weighting technique.

REFERENCES

1. R.L. Macklin and J.H. Gibbons, Phys. Rev. 159, 1007 (1967).

2. R.L. Macklin and B.J. Allen, Nucl. Instrum. Methods 91, 565 (1971).

3. N. Yamamuro, T. Hayase, T. Doi, Y. Fujita, K. Kobayashi, and R.C. Block, Nucl. Instrum. Methods 133, 531 (1976).

4. N. Yamamuro, T. Doi, T. Miyagawa, Y. Fujita, K. Kobayashi, and R.C. Block, J. Nucl. Sci. Technol. 15, 637 (1978).

5. N. Yamamuro, K. Saito, T. Emoto, T. Wada, Y. Fujita, and K. Kobayashi, J. Ncul. Sci. Technol. 17, 582 (1980).

6. A. Brusegan, F. Corvi, G. Rohr, R. Shelley, and T. Van der Veen, Proc. Int. Conf. Nucl. Cross Sections and Technol., NBS SP 594, 163 (1980).

7. P. Staveloz, E. Cornelis, L. Mewissen, F. Poortmans, G. Rohr, R. Shelley, and T. Van der Veen, Proc. Int. Conf. Nucl. Cross Sections and Technol., NBS SP 594, 315 (1980).

8. J.B. Czirr, Nucl. Instrum. Methods 72, 23 (1969).

9. L. Dresner, Nucl. Instrum. Methods 16, 176 (1962).

10. R.L. Macklin, Nucl. Instrum. Methods 26, 213 (1964).

11. R.L. Macklin and R.R. Winters, Nucl. Sci. Eng. 78, 110 (1981).

12. A.E. Johnsrud, M.G. Silbert, and H.H. Barschall, Phys. Rev. 116, 927 (1959).

13. J.B. Czirr and M.L. Stelts, Nucl. Sci. Eng. 52, 299 (1973).

14. J.S. Brzosko, E. Gierlik, A. Soltan JR., Z. Szeflinski, and Z. Wilhelmi, Acta Phys. Polonica B2, 489 (1971).

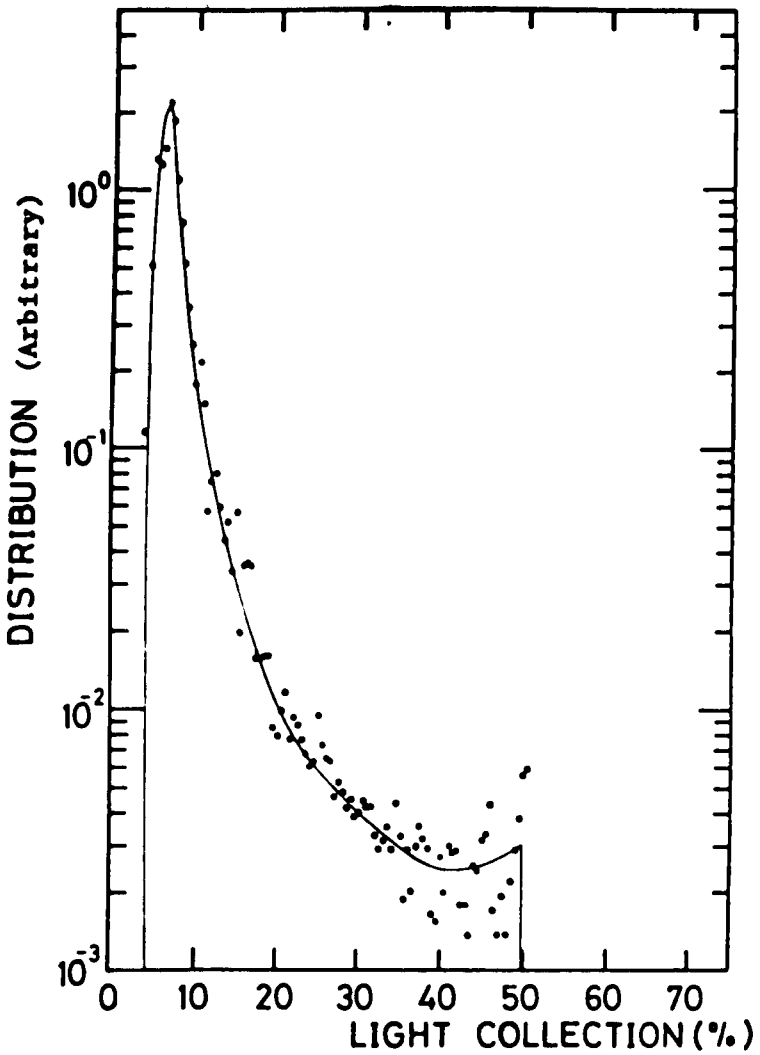

Fig.1 The distribution of the light collection efficiency of the detector

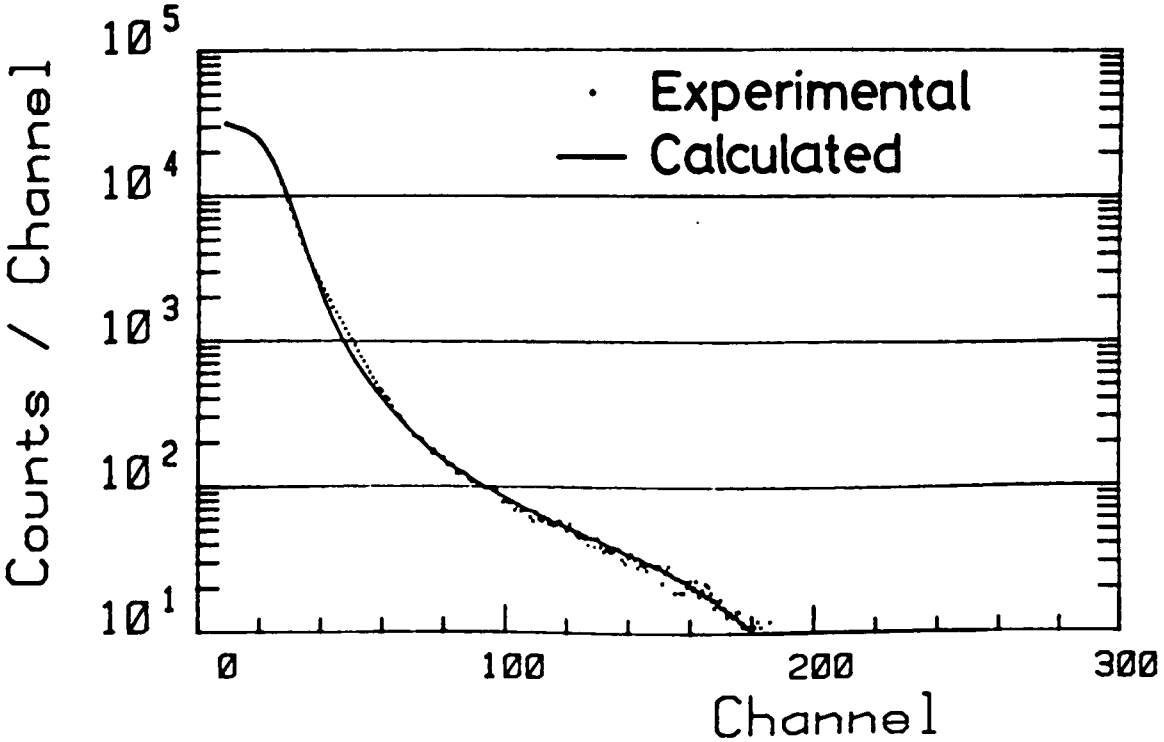

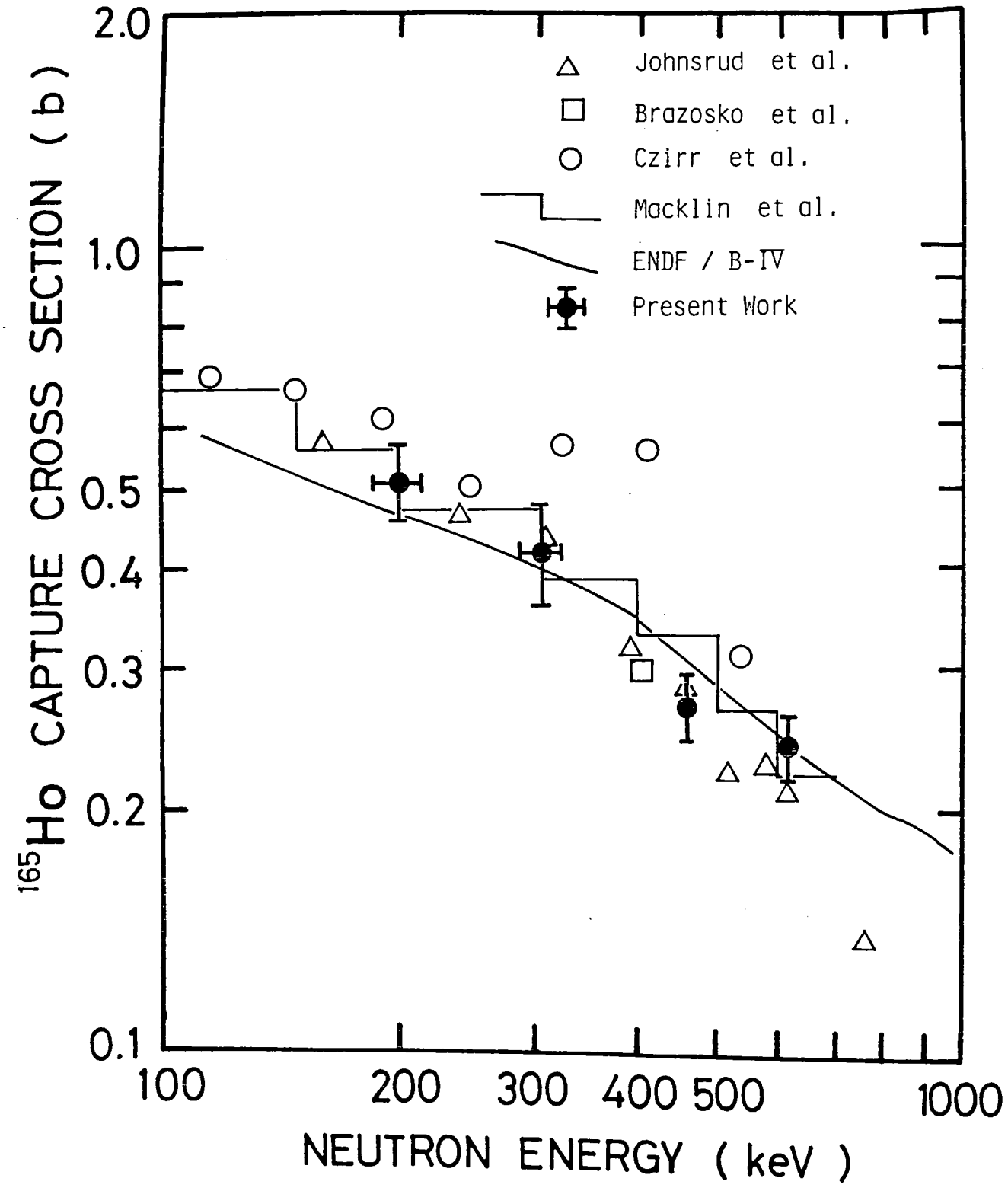

Fig.3 Neutron capture cross sections of ^{165}Ho

Discussion

QUESTION: R. Block
How does the efficiency of the 10-liter pulse-height-weighting detector compare to the efficiency of the C_6D_6 detector?

ANSWER: Y. Fujita
The efficiency of the 10-liter detector installed with the graphite sleeve is 5 to 6 times higher than that of a pair of the C_6D_6 detectors for a typical capture gamma ray.

QUESTION: S. Mughabghab
May I have the viewgraph representing the capture cross section of ^{165}Ho as derived by you on the basis of ENDF/B-V Au evaluation? Examining the figure, I note that your ^{165}Ho capture cross section in the energy range 200 to 610 keV is neither systematically low or high when compared with other measurements. One can then conclude that the ENDF/B-V capture cross section of Au is consistent with that of Ho, within the error limits, in the energy range 200-610 keV.

ANSWER: Y. Fujita
I think one cannot judge the adequacy of the standard cross section used in this experiment by using this experimental result. He can only conclude this data for ^{165}Ho agrees with other measurements.

COMMENT: W. Poenitz
I should insert here a remark. According to the CSISRS file, Czirr has withdrawn his data at higher energies, which are still shown in the figure. I also do not know, whether the data by Macklin which are shown in the figure are the revised data. There is a factor of 1.07 involved.

GAMMA-RAYS FROM RADIATIVE CAPTURE REACTIONS IN ^{133}Cs, ^{181}Ta AND ^{197}Au

N. Yamamuro, M. Igashira, H. Shirayanagi,

Research Laboratory for Nuclear Reactors
Tokyo Institute of Technology

Y. Fujita and K. Kobayashi

Research Reactor Institute, Kyoto University

ABSTRACT

Gamma-ray spectra following neutron capture in ^{133}Cs, ^{181}Ta and ^{197}Au have been measured at the neutron energy from 1.5 to 75 keV using linac-TOF method. A sample was located at 12 m from the neutron source, and a pair of deuterated benzen (C_6D_6)liquid scintillation detectors with 11 cm diam by 5 cm thick was set at the both sides of sample. Response functions of the detector were calculated by a Monte-Carlo method, and the energy resolution of the detector was determined by comparing the calculated energy deposit spectra with the measured spectra. To unfold the gamma-ray spectrum from the observed one, a 93×256 gamma-ray response matrix was generated by interpolation from the response functions. The capture gamma-ray spectra for cesium, tantalum and gold were obtained by means of the unfolding code FERDOR. The spectra in gold and cesium show the 5.5 MeV anomaly, as expected from other experiments. The gamma-ray strength functions were calculated by the spectrum-fitting method. As the result of this calculation in gold, it was found that the better spectrum fitting was obtained if the two pigmy resonances were assumed to exist at 5 MeV and 6 MeV.

I. INTRODUCTION

A gamma-ray spectrum following neutron capture is observed in a capture cross section measurement with the pulse-height weighting technique to calculate a weighted spectrum[1]. The emitted gamma-ray spectrum can be derived from the measured pulse-height spectrum, whenever we have precise response functions of the detector. In many measurements of gamma-ray spectrum for neutron induced reaction, an NaI scintillator was used. Although the liquid scintillator, used in our capture cross section measurements, has poorer energy resolution than that of NaI scintillator, it can be expected that the capture gamma-ray spectrum is obtained, from which a gamma-ray strength function is derived using the spectrum-fitting method[2].

The energy dependence of gamma-ray strength function is often represented by a Lorentzian function which describes the giant-dipole resonance photo-absorption cross section. However, there is a definitive fact that the anomalous bump at about 5.5 MeV was found for some nucleus near closed shells. For cesium and gold, several authors measured gamma-ray spectra at keV- and MeV-

spectra[3-8]. Because of the small number of the gamma-ray spectrum data at keV-region, the gamma-ray pulse-height spectra following keV-neutron capture are measured by means of Linac-TOF method and are unfolded using the response functions of the detector for Cs and Au, with Ta which is expected to have no bump in the spectrum.

In the present paper, the experimental procedure for gamma-ray spectrum measurement is described in Sec. II , the spectrum unfolding and the gamma-ray strength function extracted are discussed in Sec. III.

II . EXPERIMENTAL PROCEDURE

The pulsed white neutron beam was generated from a tantalum photo-neutron reaction induced by irradiation of 30-MeV electron beam from the KUR linear accelerator. The collimated beam of 46-mm diam impinged on a sample, mounted at 11.7 m from the neutron source. A pair of deuterated benzen (C_6D_6)liquid scintillation counters with 11-cm diam by 5-cm thick was placed at the both sides of sample and the capture gamma-rays emitted from the sample were detected by these counters. The experimental arrangement and the electronics system were almost the same as that shown in the previous papers[1,9].

A sample of ^{133}Cs is cesium-oxide (Cs_2O) powder with 0.0099 cesium atoms per barn in thickness, which is encapsulated in an aluminum cap. Gold and tantalum samples are metal plates of 2.0-mm thick. The signal of counters was fed to a pulse-height analyzer gated with timing signal, which is generated by delay and gate generator. Since the capture gamma-ray spectrum hardly changed in the keV-neutron region, the signals corresponding to from 1.5- to 75-keV neutron capture were summed to reduce the statistical uncertainty of data. An open beam run and a lead run were carried out for background determination. The total background count in the pulse-height spectrum was 13 % for tantalum and 20 % for cesium and gold. Since the spectrum of background was composed of low energy gamma-rays and 2-MeV gamma-rays, which were probably emitted from neutron capture with hydrogen, the signal-to-noise ratio in the region above 2 MeV is better than the value mentioned above.

The response functions of the detector are necessary to unfold the measured spectrum. Because monoenergetic gamma-ray sources in the wide energy range are difficult to obtain, we calculated the response functions of the detector using a Monte-Carlo method, and determined the energy resolution of the detector by comparing the calculated energy deposit spectra with the measured pulse-height spectra. Gamma-ray sources used are ^{137}Cs(0.662 MeV), ^{24}Na(1.37 and 2.75 MeV), Am-Be(4.44 MeV), and ^{16}N(6.13 MeV). The standard deviation $\sigma(E)$ in the Gaussian resolution function, which is a function of the energy E, is given by the relation[10]

$$\left(\frac{\sigma(E)}{E}\right)^2 = P + Q/E \ , \qquad (1)$$

and the most probable values of parameters P and Q are determined by the least square method.

Because ^{16}N has half-life of ~7 sec, the spectrum measurement should be carried on as producing the source with the $^{16}O(n,p)^{16}N$ reaction. The neutron producing target of the linear accelerator was placed in a water tank [illegible]d by neutrons was circulated by a pump through a vinyl

pipe. The 6.13-MeV gamma-rays emitted from ^{16}N after β-decay were detected by two C_6D_6 scintillation counters mounted on the both sides of an aluminum chamber at the 12-m station.

A 93 × 256 gamma-ray response matrix for the C_6D_6 scintillation counter was generated by interpolation from the response functions, determined as mentioned above.

III. GAMMA-RAY SPECTRUM AND STRENGTH FUNCTION

The gamma-ray spectrum was derived with a unfolding code, FERDOR[11]. Figures 1, 3 and 5 show the capture gamma-ray spectra for $^{197}Au(n,\gamma)$, $^{133}Cs(n,\gamma)$, and $^{181}Ta(n,\gamma)$ reactions, respectively. The gamma-ray intensity $\nu(E_\gamma)$ is normalized to satisfy the equation

$$\int_0^{E_B+E_n} E_\gamma \cdot \nu(E_\gamma)dE_\gamma = E_B + E_n , \qquad (2)$$

because the inelastic-scattering is negligible in the present experiments, where the E_B and E_n are the neutron separation energy and the mean incident neutron energy, respectively. Also the gamma-ray self absorption in the sample was assumed to be negligible.

Gamma-rays from the $^{197}Au(n,\gamma)$ reaction show the enhanced high energy gamma-ray transition around 5.5 MeV. This fact was found by many authors[3-8] in the wide energy range of neutrons from thermal to MeV-region. In those studies, experimental spectra with thermal and 15-keV neutrons showed two pigmy resonances at about 5- and 6-MeV gamma-ray energies[3]. In the present result for the $^{197}Au(n,\gamma)$ reaction, it can be expected that two bumps exist in the higher energy region, as shown in Fig. 1.

The average gamma-ray spectral distribution $\nu(E_\gamma)$ are represented by the average gamma-ray transition probability, or gamma-ray strength function $f(E_\gamma)$, and by the level-density distribution $\rho(U)$. Therefore, if we make the assumption that only dipole gamma-ray emission is important at all energies, we may be possible to calculate the dipole gamma-ray strength function from the spectral distribution with the assumed level-density distribution by means of the spectrum-fitting method[2]. In the calculation, the profile of the gamma-ray strength function is assumed to be

$$f(E_\gamma) = \frac{\Gamma_G E_\gamma}{(E_\gamma^2 - E_G^2)^2 + (\Gamma_G E_\gamma)^2} \exp\left\{ L_G(E_\gamma - E_G)\right\}$$
$$+ \sum_i C_i \frac{\Gamma_i E_\gamma}{(E_\gamma^2 - E_i^2)^2 + (\Gamma_i E_\gamma)^2} \exp\left\{ L_i(E_\gamma - E_i)\right\} . \qquad (3)$$

The first term of the right side of eq. (3) has the shape of the Lorentzian, multiplied by a exponential reduction factor in below the peak energy E_G of the giant-dipole resonance, where Γ_G is the width of this resonance. The second term corresponds to the pigmy resonance of energy E_i and width Γ_i. The parameter C_i is the relative contribution of the pigmy resonance with respect to the giant resonance. The data of giant resonance were

from the photoneutron cross sections edited by Berman[12]. As the level-density distribution, Gilbert and Cameron's formula[13] was employed, and parameter a used in the calculation is shown in Table I.

The gamma-ray strength function for ^{198}Au has been obtained in two cases of one pigmy resonance and two pigmy resonances. From Fig. 1, it is clear that we can obtain the better fitting to the experimental spectrum with two pigmy resonances, the width of which is about 1 MeV. The values of parameters obtained are shown in Table I. The strength function in absolute unit was calculated using the total averaged radiative width, which was determined from the resonance data, near the neutron separation energy of the compound nucleus.

The present gamma-ray strength function for ^{198}Au agrees with that of Lundberg and Starfert[5] and both functions exceed that for the Lorentzian tail of the giant-dipole resonance between 4.5 MeV and 6.5 MeV. While, Joly et al.'s strength function[8], shown in Fig. 2 by the dot-dashed line, shows a lack of strength compared to the Lorentzian extrapolation. Earle et al.[7] also show a lack of strength from the Lorentzian, especially below 6 MeV gamma-ray energy. The reason of these discrepancies is not clear, but a part of it may be depend on the difference of the methods determining the absolute unit and of the utilized level density distribution.

The capture gamma-ray spectrum for ^{133}Cs also showed that the higher energy gamma-rays were enhanced, as shown in Fig. 3. Bergqvist et al.[4] and Brzosko et al.[6] also show the bump around 5.5 MeV in the gamma-ray spectrum for the $^{133}Cs(n,\gamma)$ reactions at the neutron energy of 20 keV and 400 keV, respectively. We extracted the gamma-ray strength function from the experimental spectrum, assuming one pigmy resonance exists. The result is shown in Fig. 4 with the strength function, which is the extrapolation to the lower energy region of the Lorentzian shape of the giant-dipole resonance. The relative contribution of the pigmy resonance with respect to the giant resonance cannot be exactly determined.

The gamma-ray spectrum and the gamma-ray strength function deduced for tantalum are shown in Figs. 5 and 6, respectivery. Many experimental studies [3-7] showed that the gamma-ray from the $^{181}Ta(n,\gamma)$ reaction have no bump at the higher energy region. However, the experimental spectrum does not agree with the calculated one, shown in Fig. 5 by the dotted line, in which the Lorentzian shape of the giant resonance is used as the gamma-ray strength function and the discrete transitions from the higher excited level to the level near ground state are neglected. Considering the reduction factor of $\exp\{L_G(E_\gamma - E_G)\}$, we can obtain the better fitting to the experimental spectrum, as shown in Fig. 5 by the solid line. The value of L_G is about 0.3 in the present case. The corresponding strength functions obtained are shown in Fig. 6 by the dotted and the solid lines, respectively. The present result of the gamma-ray strength function for ^{182}Ta agrees fairly well with the Earle et al.'s data at the neutron energy of 2.6 MeV[7], and the Joly's recent result at the neutron energies between 0.5 and 3.0 MeV[14], though the level density distribution used is different each other.

IV. CONCLUSION

The gamma-ray pulse-height spectra for $^{197}Au(n,\gamma)$, $^{133}Cs(n,\gamma)$, and

liquid scintillation detectors at the neutron energies between 1.5 and 75 keV. The spectra were unfolded with the response functions of the detector and the unfolding code FERDOR. The emitted gamma-ray spectra following the neutron capture in ^{197}Au and ^{133}Cs showed the enhanced gamma-ray transition around 5.5 MeV, while the spectrum for ^{181}Ta showed no bump. The gamma-ray strength functions were derived from the emitted spectra using the spectrum-fitting method. The best fitting are obtained assuming two pigmy resonances at 5 MeV and 6 MeV for gold, one pigmy resonance at 6 MeV for cesium. In the case of tantalum, including the reduction factor in the profile of the strength function approaches the calculated spectrum to the experimental one.

REFERENCES

1. N. Yamamuro, T. Doi, T. Miyagawa, Y. Fujita, K. Kobayashi, and R.C. Block, J. Nucl. Sci. Technol. 15, 637 (1978).

2. G.A. Bartholomew, E.D. Earle, A.J. Ferguson, J.W. Knowles, and M.A. Lone, Adv. Nucl. Phys. 7, 229 (1973).

3. I. Bergqvist and N. Starfelt, Nucl. Phys. 39, 353 (1962).

4. I. Bergqvist and N. Starfelt, Nucl. Phys. 39, 529 (1962).

5. B. Lundberg and N. Starfelt, Nucl. Phys. 67, 321 (1965).

6. J.S. Brzosko, E. Gierlik, A. Soltan JR., Z. Szeflinski, and Z. Wilhelmi, Acta Phys. Polonica B2, 489 (1971).

7. E.D. Earle, M.A. Lone, and G.A. Bartholomew, Can. J. Phys. 52, 989 (1974).

8. S. Joly, D.M. Drake, and L. Nilsson, Phys. Rev. C20 2072 (1979).

9. N. Yamamuro, K. Saito, T. Emoto, T. Wada, Y. Fujita, and K. Kobayashi, J. Nucl. Sci. Technol. 17, 582 (1980).

10. E. Nardi, Nucl. Instr. Method 95, 229 (1971).

11. H. Kendrick and S.M. Sperling, " An Introduction to the Principles and Use of the FERDOR Unfolding Code ", GA-9882 (1970).

12. B.L. Berman, " Atlas of Photoneutron Cross Sections Obtained with Monoenergetic Photons ", UCRL-78482 (1976).

13, A. Gilbert and A.G.W. Cameron, Can. J. Phys. 43, 1446 (1965).

14. S. Joly, " Photon Strength Functions for ^{90}Y, ^{94}Nb, ^{160}Tb and ^{182}Ta ", Fourth International Symposium on Neutron Capture Gamma-ray Spectroscopy and Related Topics, Grenoble, September 1981.

Table I. Parameters used in the calculation of the spectrum-fitting and parameters of the gamma-ray strength function derived.

Nuclei		^{198}Au		^{134}Cs	^{182}Ta
Total radiation width	(meV)	125		118	56.6
Level density parameter a	$(MeV)^{-1}$	18.765		14.85	21.14
Reduction factor L_G	$(MeV)^{-1}$	0.21		0.15	0.28
Parameters of pigmy resonance					
C_i		0.01	0.05	0.01~ 0.02	
E_i	(MeV)	5.0	5.8	5.8	
Γ_i	(MeV)	1.1	1.1	2.0	
L_i	$(MeV)^{-1}$	0.24	0.24	0.15	

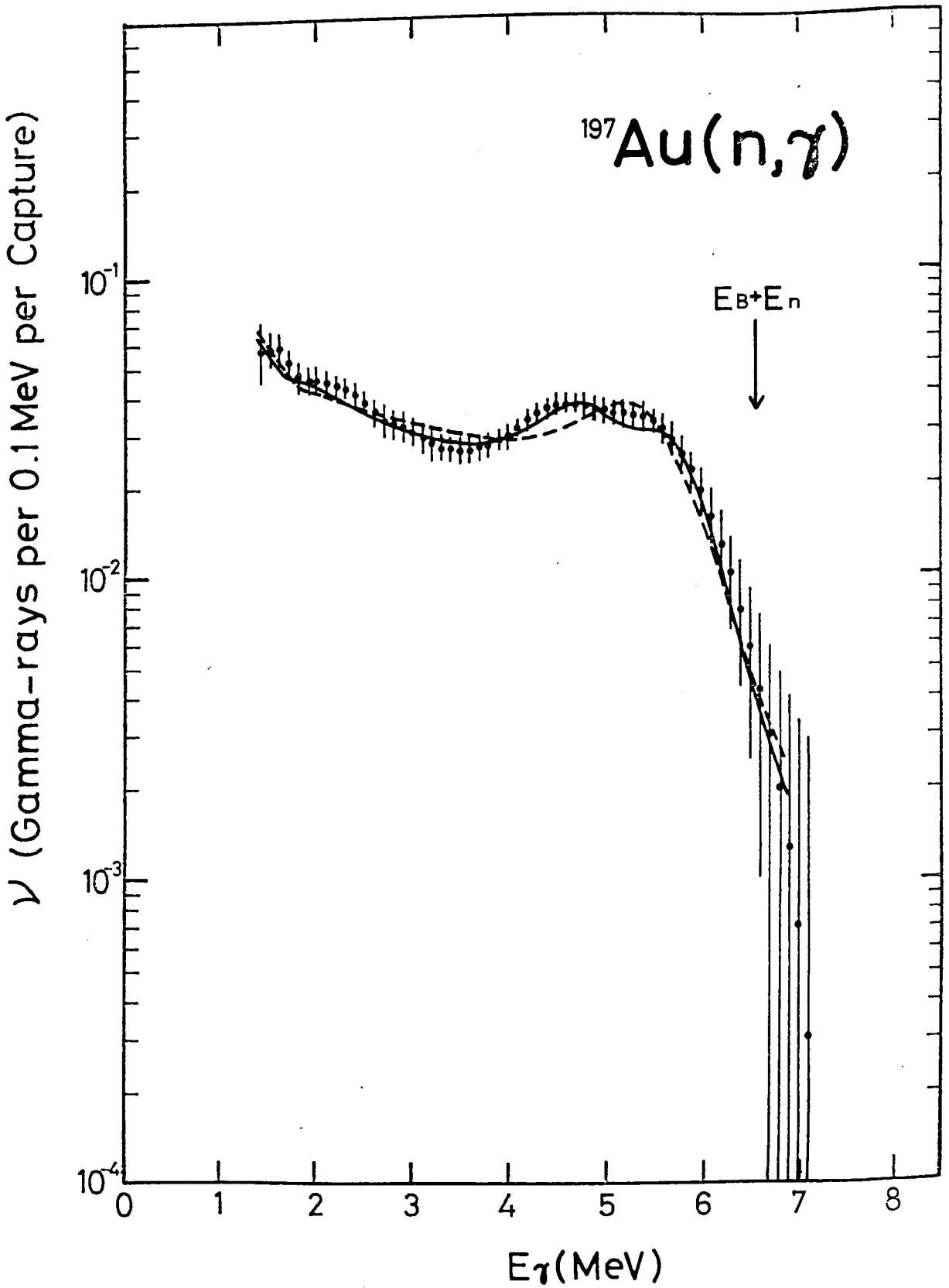

Fig. 1 Capture gamma-ray spectrum and fitting curves with one pigmy resonance (dotted line) and two pigmy resonances (solid line) for the ^{197}Au(n,γ) reaction.

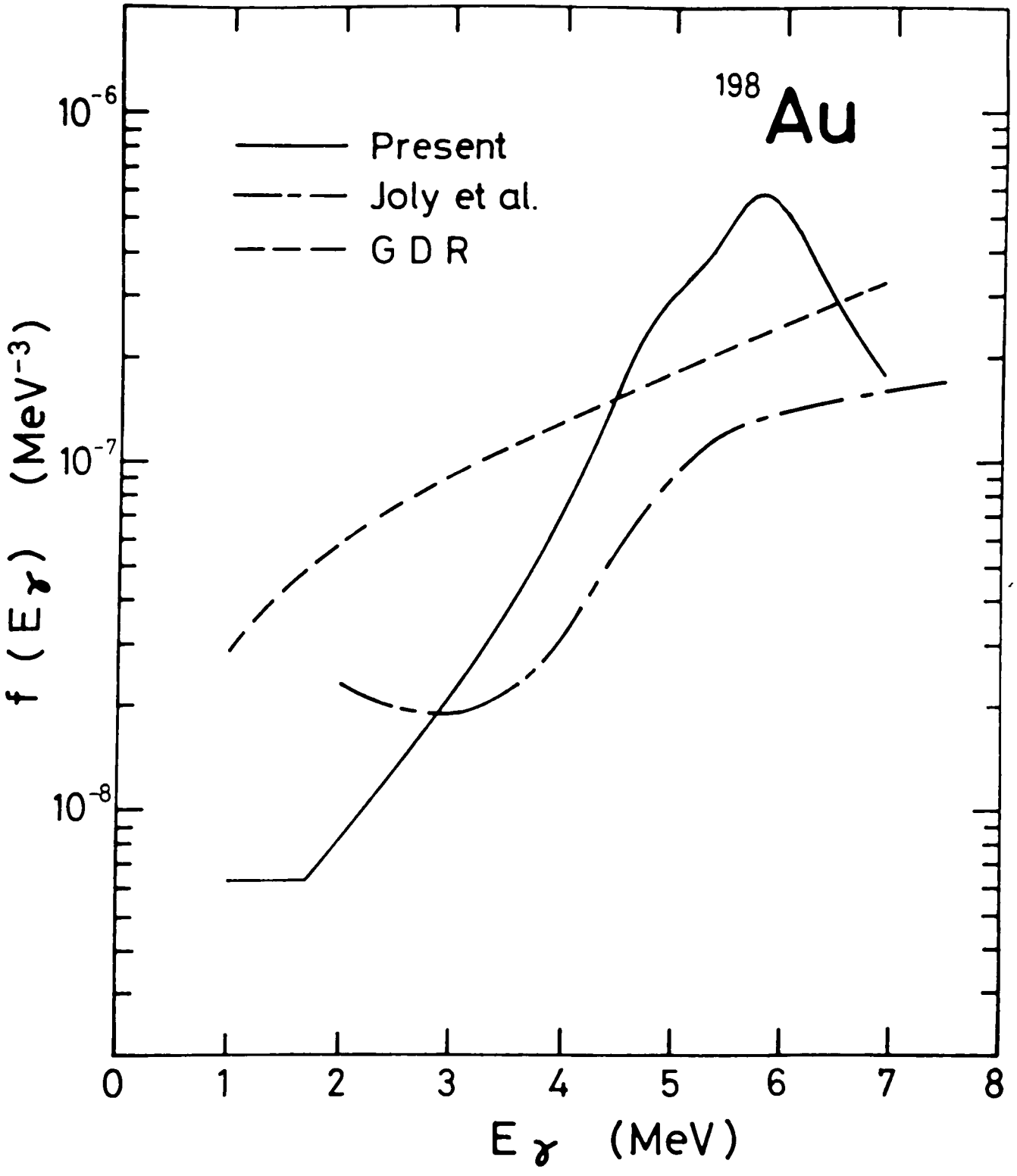

Fig. 2 Gamma-ray strength functions for ^{198}Au. The present, Joly et al.'s and the Lorentzian tail are shown by the solid, dot-dashed, and dotted lines, respectively.

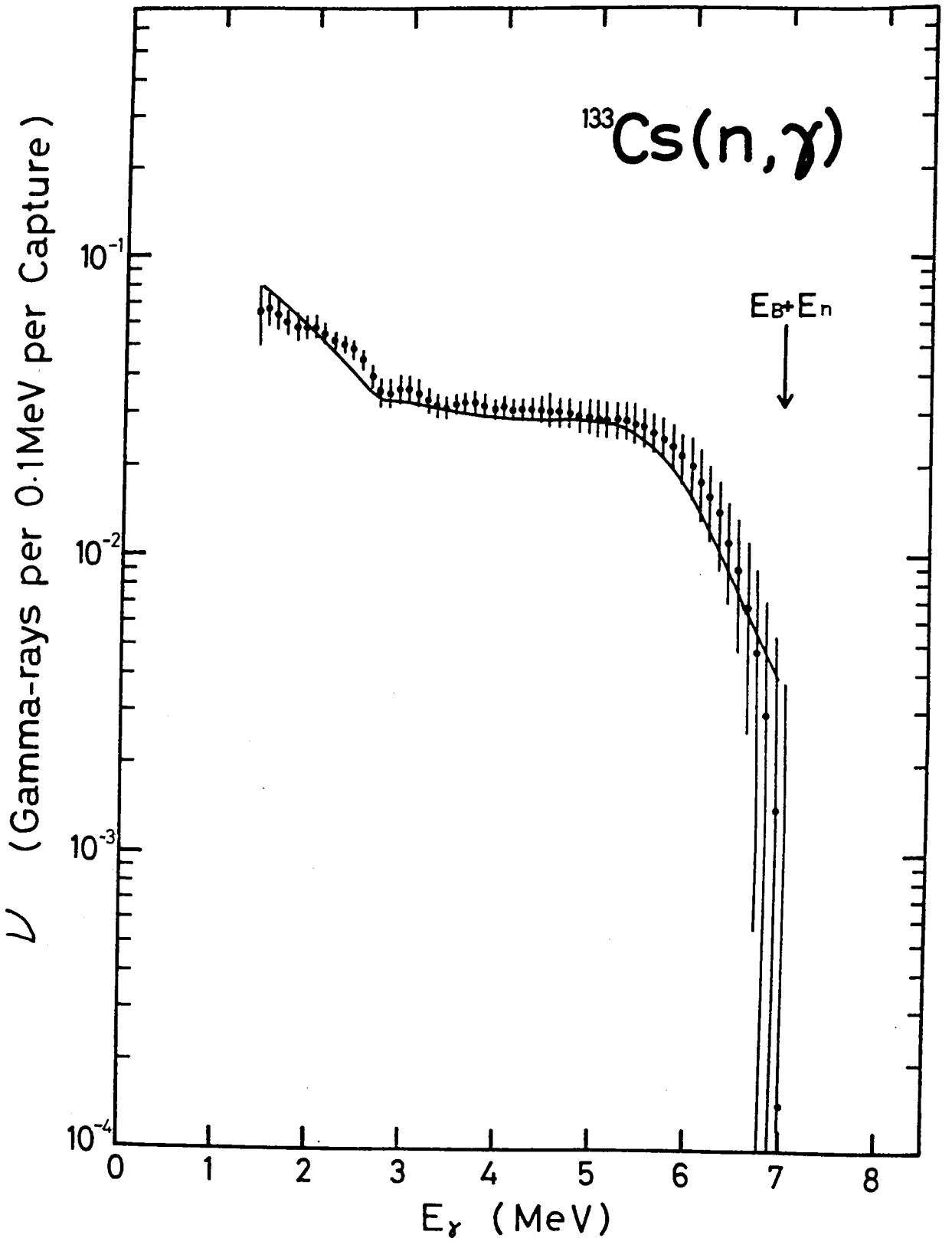

Fig. 3 Capture gamma-ray spectrum and fitting curve with one pigmy resonance for the ^{133}Cs(n,γ) reaction.

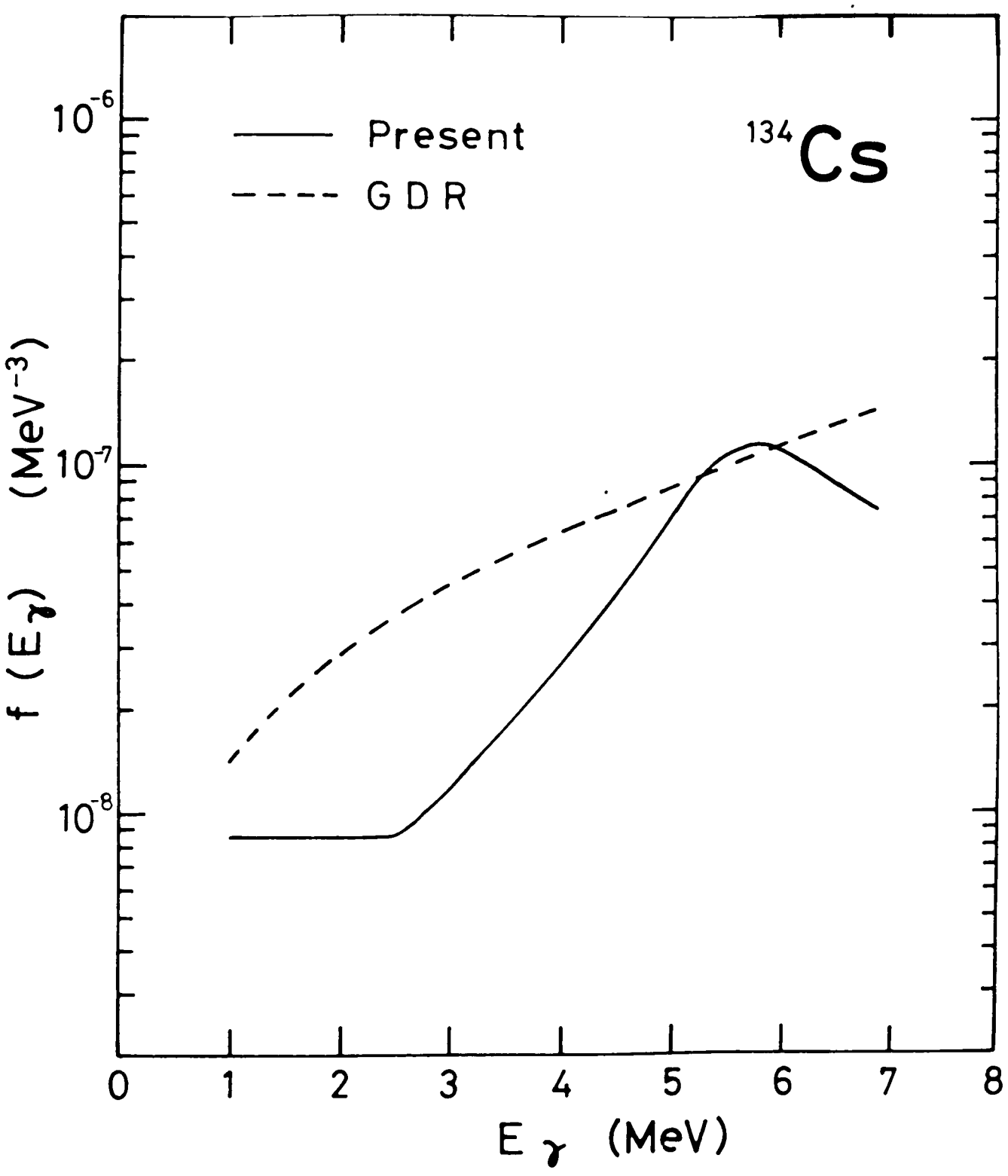

Fig. 4 Gamma-ray strength functions for ^{134}Cs. The present and the Lorentzian tail are shown by the solid and dotted lines, respectively.

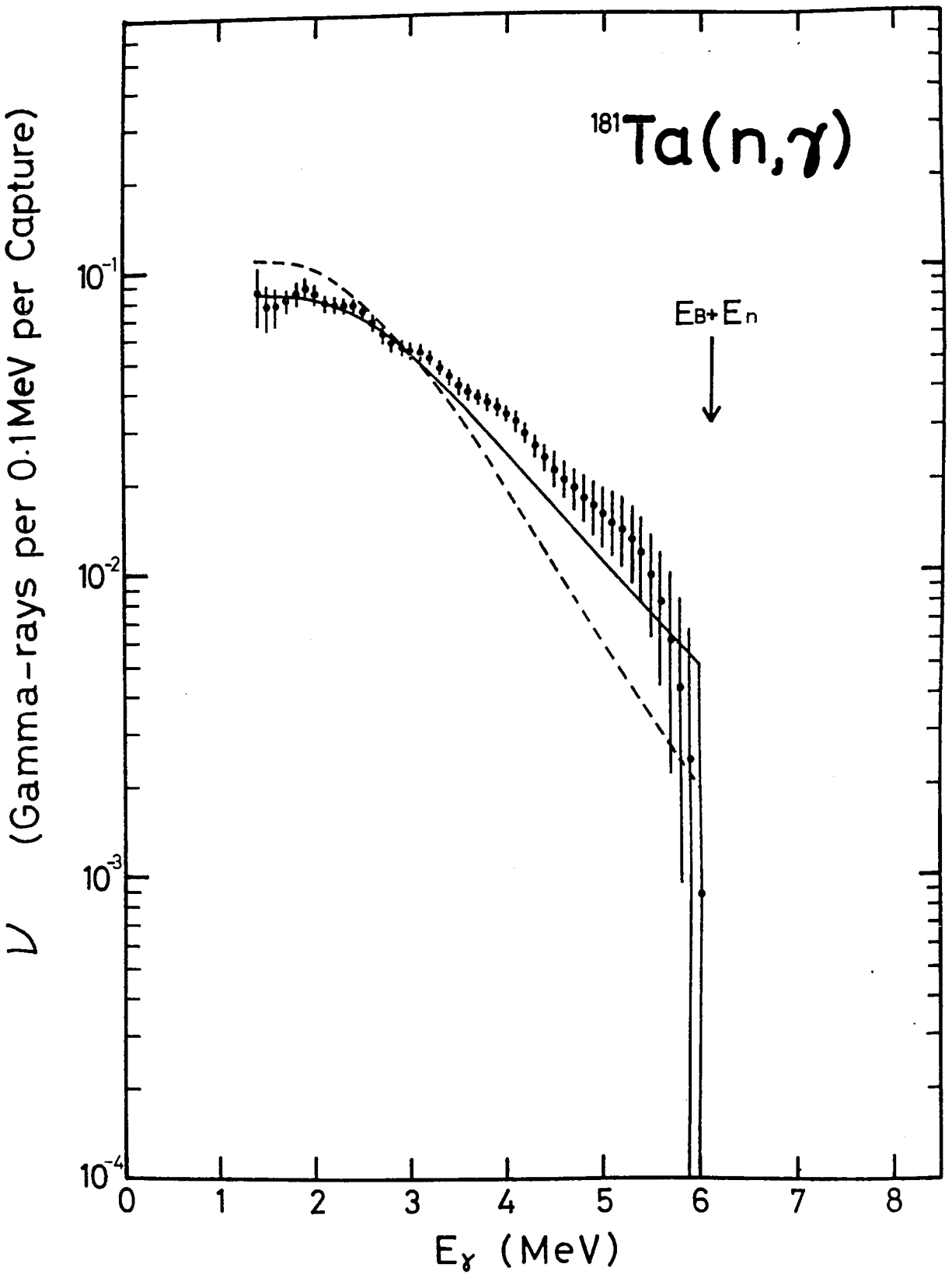

Fig. 5 Capture gamma-ray spectrum and fitting curves with and without the reduction factor in the profile function of the strength function.

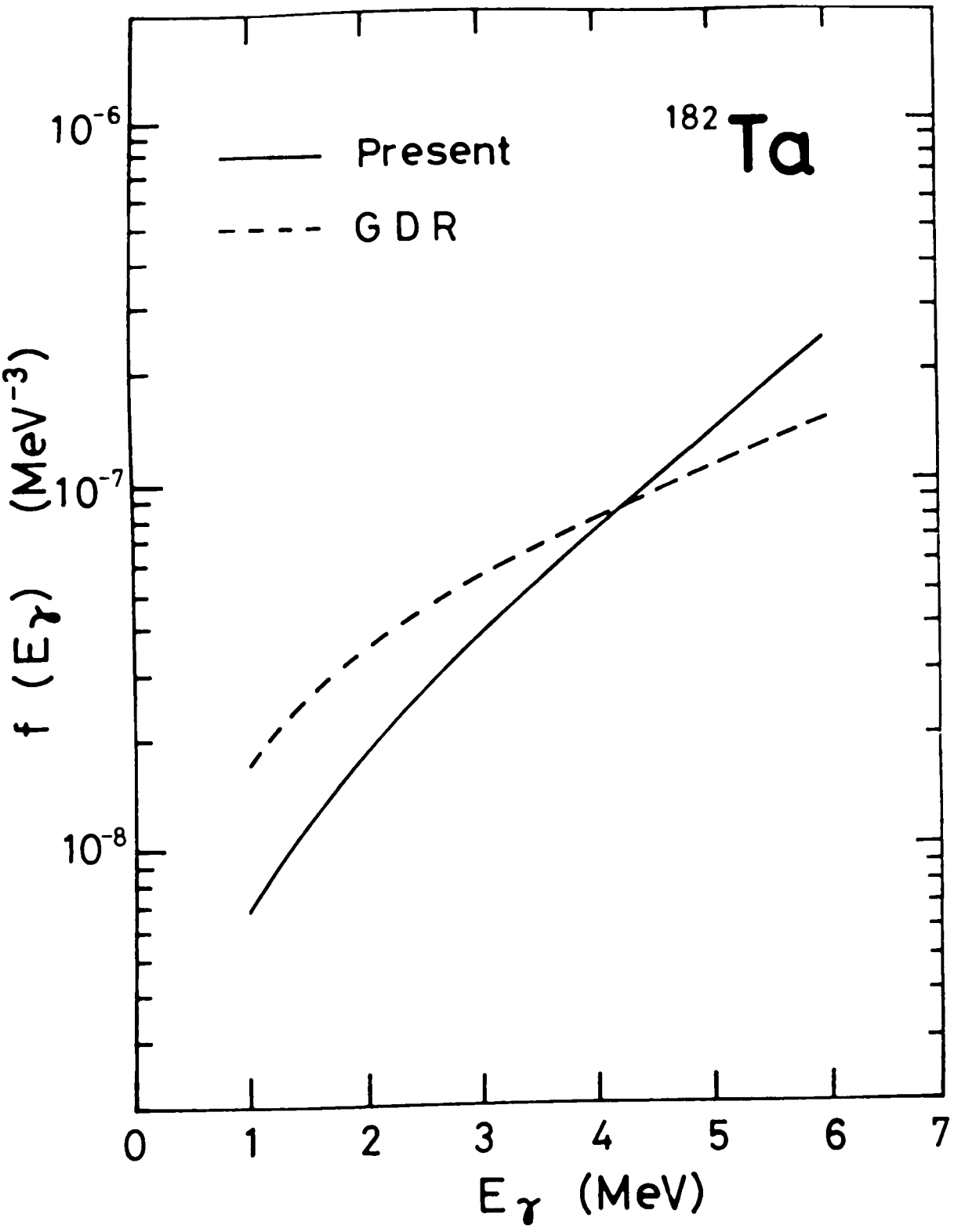

Fig. 6 Gamma-ray strength functions for ^{182}Ta. The present and the Lorentzian tail are shown by the solid and dotted lines, respectively.

Discussion

COMMENT: R. Chrien
Just a comment. Your photon strength function obtained for Ta is in excellent agreement with the studies by Bartholomew and his collaborators, who studied (d,p) and (n,γ) reactions.

AVERAGING $\sigma(n,\gamma)$ IN THE TRANSITION REGION E_n = 1-150 keV

by

R. L. Macklin
Oak Ridge National Laboratory,
Oak Ridge, Tennessee 37830 USA

Abstract

The technique of determining a smooth average neutron capture cross section by least squares adjustment of strength functions is illustrated for ^{179}Hf(n,γ) high resolution data from ORELA. The s-, p- and d-wave neutron strength functions and $\overline{\Gamma_\gamma}/\langle D_{\ell=0}\rangle$ found agree well with systematics, model calculations and other experimental information despite their strong correlation when determined solely from the capture data.

For many isotopes, such as the fission products, the measured capture cross sections exhibit clearly defined resonances up to a few keV but a nearly smooth energy dependence beyond 150 keV. Techniques for representing average capture between these extremes include histograms for chosen energy intervals and linear eye-guides to the data on double logarithmic plots. Plots of cross section times velocity are often used to remove much of the slow energy dependence.

A more informative approach uses the optical and statistical models to describe average capture with adjustments of model parameters to fit measured data. Capture cross sections below ~ 120 keV are not equally sensitive to the dozen or more available parameters and a usable subset can be expressed as four energy independent strength functions S_0, S_1, S_2 and S_γ. Imposing a further relation

$$D_J = D_{\ell=0}/g_J \qquad , \; g_J = (2J+1)/2(2I+1) \tag{1}$$

where D is an average level spacing, J a resonance spin, I the target spin, ℓ the relative orbital angular momentum or impact parameter and g the statistical weight factor, introduces the scaling factor or renormalization property of $D_{\ell=0}$, the average s-wave spacing. Each strength function is defined as a ratio of the average width to the average spacing and the absolute cross section (fully correlated over energy) can be viewed as inversely proportional to the spacing parameter with the average (reduced) widths sensitive only to the energy dependence of the cross section. To effect this factorization for the neutron strength functions one needs width fluctuation corrections, for both one and two channel population of the resonances.

A recent example using this technique is the $^{179}Hf(n,\gamma)$ cross section.[1] Thirteen thousand data points covered the energy range from 2.6 to 150 keV, giving about five points per resolution width (full width at half maximum). For strength function fitting these were first averaged into several hundred 250-eV bins. The experimental resolution and counting statistics are then negligible in comparison to the nuclear structure.

An average capture cross section is calculated as[2,3]

$$\langle\sigma_c\rangle = \frac{2\pi^2}{k^2} \sum_{\ell} \sum_{J} g_J \sum_{j} \frac{\langle\Gamma_J(n,\ell,j)\rangle\langle\Gamma_J(\gamma)\rangle}{D_J \langle\Gamma_J\rangle} F \qquad (2)$$

where j is a neutron channel spin and F is a correction factor dependent on the ratio of average radiation width to average neutron width .

The average neutron widths vary smoothly with energy for each ℓ value and are conveniently related to the nearly energy independent neutron strength functions by

$$\langle g\Gamma_n^{\ell}\rangle = S_{\ell}D_{\ell}(2\ell+1) \qquad (4)$$

and

$$\Gamma_J(n,\ell) = \Gamma_J^{\ell}(n,\ell)\ V_{\ell}\ \sqrt{E_n/1\ \text{eV}} \qquad (3)$$

The square root, evaluated at 1 eV is a traditional method of avoiding the arbitrary assumption of a square well radius (e.g., $R = 1.35\ A^{1/3}$ fm) for the s-wave strength function where $V_{\ell} = 1$. For the p-wave and d-wave penetrabilities it is traditional to report data using the square well formulas

$$V_1 = k^2R^2/(1+k^2R^2)$$

$$V_2 = k^4R^4/(9+3k^2R^2 + k^4R^4)$$

where k is the neutron wave number, proportional to the neutron velocity.

Clearly further simplifying assumptions about the distribution of average reduced neutron width and radiation width over resonance spin (and channel) for each partial wave are needed to implement the formulation. Independent evidence from other experiments can readily be incorporated to modify any of these assumptions, particularly the use of a single average radiation width for all resonances.

The chief modification seen directly in capture cross section data is due to competition with inelastic scattering.[3,4] In a few important cases (^{232}Th, ^{238}U) the threshold for inelastic scattering falls below ~ 100 keV and the reduction in capture through <u>some</u> of the (ℓ,J^{π}) channels must be specifically allowed for.

In a few cases, particularly near closed shells, one can expect to see clusters of strength corresponding to intermediate structure. This can also be parametrized and included in the least squares data fitting.[5] One of the aims of the averaging process, however, is to develop the systematics of strength function parametrization sufficiently to permit adequate prediction of unmeasured cross sections for the broad neutron spectra of terrestrial reactors and of galactic stars.

The research was sponsored by the Division of Nuclear Sciences, U.S. Department of Energy, under Contract No. W-7405-eng-26 with the Union Carbide Corporation.

1. "^{178,179,180}Hf(n,γ) and ^{180}Ta(n,γ) Cross Sections and their Contribution to Stellar Nucleosynthesis", H. Beer and R. L. Macklin, to be published (1982).

2. A. M. Lane and J. E. Flynn, Proc. Phys. Soc. (London) A70, 557 (1957).

3. J. H. Gibbons, R. L. Macklin, P. D. Miller, and J. H. Neiler, Phys. Rev. 122, 182 (1961).

4. See for example R. L. Macklin, NSE 79, 265 (1981).

5. R. B. Perez et al. Phys. Rev. C 20, 528 (1979).

Discussion

QUESTION: P. Moldauer
I am surprised by the large correlation between, say, S- and P-wave strength-function values, since these are expected to dominate the determination of the cross section in different energy regions.

ANSWER: R. Macklin
Several answers were proposed; many from the audience but no full understanding was reached. Some are:
1. The Fluctuation Correction introduces S_n vs. S_γ correlation.

2. The assumption that $\bar{\Gamma}_\gamma(\ell=0)$ is proportional to $\bar{\Gamma}_\gamma(\ell=1)$ (equal in the example shown) used in fitting by least squares intercorrelates the resulting neutron strength function.

3. Systematic uncertainties (such as sample mass and detector efficiency) correlate the data "points" but effect all four strengths equally. Including this 100% correlation was avoided for the least squares adjustment.

QUESTION: W. Poenitz
The correlations you showed for the parameters, are they based on a simple χ^2 fit?

ANSWER: R. Macklin
Yes.

COMMENT: W. Poenitz
You might get quite different correlations between the parameters if the correlation of the input data would be taken into account. The input data are, of course, correlated. Some errors apply to all energies, etc. Not taking this into account might make the results and their correlation somewhat arbitrary.

QUESTION: R. Schenter
Do you have correlation matrices for your Pd and Ru strength function fits?

ANSWER: R. Macklin
The fitting code produced them. They may not have been filed with the working papers retained indefinitely but they could be regenerated fairly readily.

Discussion Continued

QUESTION: R. Block
I do not understand why the S_0 and S_1 correlation is so large, especially when the $\ell=0$ component of the capture cross section is dominated by the data below 5 keV where $\ell=1$ capture is at least an order of magnitude smaller.

ANSWER: R. Macklin
See Moldauer's question which is closely related.

QUESTION: R. Peelle
Am I correct in thinking that your fit in terms of strength functions differs from that discussed this morning by Froehner (FITACS) in that he would also input data from the resolved resonance region and total, etc., cross sections when they are available?

ANSWER: R. Macklin
Yes. For many even isotopes with low level density I also use an S_0 value from other sources and only adjust S_1, S_2 and S_γ to the capture data.

QUESTION: S. Mughabghab
I would like to make a comment that, in capture measurements, it is customary to find the value derived from the resolved neutron resonances and then extract the other parameters: p- and d-wave neutron strength functions and s-and p-wave gamma ray strength functions. This reduces the uncertainty of the derived parameters (i.e. dependence on S_0) providing of course there is no energy dependence of the S-wave neutron strength function. Such an approach was followed by Macklin in his studies of Pd and Ru isotopes and Konskov et al. in the studies of the rare earth region.

ANSWER: R. Macklin
Caution; the revised (corrected) Pd(n,γ) data (CSIRS Files) should be refitted with strength functions if they are desired. F. Froehner's FITACS code should be useful.

COMMENT: F. Froehner
I would like to make a comment in this context. One of the things we learned in using FITACS was that you should not use the strength functions from low-energy resonances. The reason is that these are usually local values. You want something which is valid over a larger energy range. This is the reason why we put in this information as a-priori but with a certain margin for adjustment, and then we go to the full energy range and see what comes out. It is usually 20 or 50% different.

Discussion Continued

COMMENT: S. Mughabghab
That is not bad. Considering the expected statistical error.

COMMENT: P. Moldauer
There is another comment to be made here. If you use the strength function in this way the strength function can really be an energy dependent quantity. The optical model gives the energy dependence of the neutron strength function.

COMMENT: F. Froehner
What we determine in this approach is something which could be called an effective strength function which is a weighted average over the region where, say the p-wave strength function is important.

COMMENT: P. Moldauer
I think it is true that if you are sitting in the vicinity of an s-wave strength function, in the space of a few hundred keV from neutron threshold, you can have a considerable variation in the value of the strength function.

COMMENT: F. Froehner:
Let me show you here the strength functions from the spherical optical model in the range up to 15 MeV. You can see that in a slice of a few hundred keV the variation is small.

COMMENT: P. Moldauer
This is in a vicinity of a p-wave resonance, if you would have done it in a s-wave peak, say for Fe, you would get something different.

CORRECTION TECHNIQUES FOR CROSS SECTION AND ANGULAR DISTRIBUTION MEASUREMENTS IN FAST NEUTRON CAPTURE

by

S. Joly, G. Grenier and J. Voignier
Service de Physique Neutronique et Nucléaire
Centre d'Etudes de Bruyères-le-Châtel
B.P. N° 561
92542 MONTROUGE CEDEX, France

Abstract

In order to have a good statistics, fast neutron capture measurements are usually performed with a pretty big sample. However, corrections for finite geometry, for neutron and γ-ray absorption and for neutron multiple scattering can be very important and, consequently, have to be calculated accurately. Depending on the size of the sample, simple and fast analytical expressions or more accurate but time consuming Monte-Carlo techniques must be used. We show that for angular distribution measurements, especially for small asymmetry factors, the Day approximation cannot be used but the Monte-Carlo technique instead. These techniques are applied to the $^{197}Au(n,\gamma)$ total and $^{208}Pb(n,\gamma_0)$ partial cross section measurements.

I. Introduction

In the technique we use to determine total capture cross sections, the detection solid angle is very small (of the order of 10^{-2} sr) and long runs are necessary to get a good statistics. Generally, the mass of the sample is chosen so that the total correction effect is less than 20%. However, in the study of the neutron capture mechanism by measuring the excitation function of a particular transition as a function of neutron energy, we are restricted to nuclei having a high-lying first excited state because of the relatively poor energy resolution of NaI detectors, i.e. to closed shell nuclei like ^{89}Y, ^{140}Ce and ^{208}Pb. These nuclei have very low capture cross sections and the easiest way to overcome these difficulties is to use a large sample, for which the corrections will be very important and should be estimated as accurately as possible.

II. Corrections in fast neutron capture measurements

The different corrections to be applied in fast neutron capture cross section or angular distribution measurements are :

- the anisotropy of the neutron producing reaction (A_S) over the solid angle subtended by the sample. The neutron flux is measured at 0° and with this correction, the total number of neutrons having interacted with the sample is known.

- the neutron attenuation in the sample which is determined by measurements with sample in and sample out ; the deduced attenuation factor is generally in good agreement with the calculated value using the total cross section and the sample thickness.

- the neutron attenuation in the air between the sample and the neutron detector over a distance of about 2 m. This attenuation is computed according to the air chemical composition and the total cross sections for the elements (mainly nitrogen and oxygen).

- the neutron self-shielding (A_n) within the sample because incident neutrons are removed out of the flux and, consequently, are not contributing to the radiative capture reactions.

- the γ-ray attenuation (A_γ) within the sample. For the determination of the capture γ-ray energy distribution necessary to deduce the number of capture reactions and then the capture cross sections [1], the γ-ray attenuation is computed for γ-ray energies between 1.0 and 12.5 MeV in steps of 250 keV using analytical expressions [2] . For partial capture cross section measurements, generally with large samples, the γ-ray attenuation for the transition of interest is calculated either with a Monte Carlo technique or with analytical method where the sample is divided into a large number of elements as explained later.

- the multiple scattering effect (A_{ms}). For simple geometries and low mass samples, simple analytical methods can be used. For total capture cross section measurements, a disk shape is generally preferred with a large diameter (of the order of 6 cm) and relatively small thickness (between 1 and 5 mm) to minimize the multiple scattering effect. With this geometry, approximations can be used in the transport theory thus giving simple analytical expressions. For thin samples and low energy neutrons (E_n < 0.5 MeV) the method given by Taste [3] can be used. For higher neutron energies, the more sophisticated method proposed by Devaney [4] should be used but these calculations are complicated for thick samples for which contribution to the capture yield has to be considered up to the fourth or fifth interaction, and then we have to rely on Monte Carlo calculations.

III. Comparison between analytical and Monte Carlo techniques

To estimate the validity of the approximations made with the analytical expressions for different sample geometries, we have calculated the corrections as given before for two cases :

i) total capture cross section measurements at E_n = 0.5 and 3.0 MeV for the $^{197}Au(n,\gamma)$ reaction (geometry given in Table I),

ii) partial capture cross section measurements at E_n = 3.8 and 5.9 MeV for the $^{208}Pb(n,\gamma_0)$ reaction (geometry given in Table II).
These corrections have also been calculated using the Monte Carlo technique. To perform these calculations we used the program originally written by D. Smith [5] and modified to treat also samples in a disk shape with their axis in, or perpendicular to, the reaction plane and for neutrons of energy larger than the highest target excited state for which the inelastic cross section has been measured. The inelastically scattered neutrons are then characterized by an evaporation distribution corresponding to a nuclear temperature T associated to the level density.

For the gold sample, the neutron and γ-ray absorption corrections were determined using simple attenuation formulae. The neutron source anisotropy effect was calculated by means of $\langle d^2 \rangle$ which is the harmonic mean of the square of the distance from the neutron source to the sample weighted by the angular distribution of the neutron source. The Devaney method was used for the multiple scattering correction. We have not considered the neutron attenuations in the sample or in the air because these are independent of the method for the comparisons.

Table I - Analytical and Monte Carlo calculation corrections for the $^{197}Au(n,\gamma)$ reaction total capture cross sections.
Sample : thickness (e = 0.15 cm), radius (R = 3.0 cm), mass (M = 82 g).
Geometry : target-sample distance (d = 7.3 cm)
sample to γ-ray detector distance (D = 80 cm).
γ-ray detection angle (θ_γ = 90°) - disk plane to beam angle (θ_d = 45°).

neutron energy	0.5 MeV		3.0 MeV	
method	analytical	Monte Carlo	analytical	Monte Carlo
A_γ	1.092	1.080	1.092	1.089
A_n	1.041	1.031	1.046	1.044
A_S	1.044	1.057	1.082	1.116
A_{ms}	0.904	0.885	0.817	0.866
$C = \prod A_i$	1.073	1.043	1.010	1.099

Table I shows that apart from a difference for multiple scattering at 3.0 MeV, the results of both methods are in fairly good agreement. We deduce that for disk samples, geometry and absorption corrections can be estimated using simple analytical expressions, the difference with Monte Carlo results for these combined effects is less than 1% at 0.5 MeV but the Monte Carlo technique should be used for estimating the multiple scattering if very accurate corrections are necessary. Using the Monte Carlo code and possible uncertainties for the different cross sections, we estimated the precision for all the corrections to be about 15% and, consequently, the corresponding contribution to the gold capture cross sections amounts to about 2% and this is relatively small compared to the statistical and other uncertainties introduced in our technique.

Table II - Analytical and Monte Carlo calculation corrections for the $^{208}Pb(n,\gamma_0)$ partial capture cross sections.
Sample : height (H = 3.9 cm), radius (R = 1.7 cm), mass (M = 420 g).
Geometry : target-sample distance (d = 8.3 cm)
sample to γ-ray detector distance (D = 80 cm)
γ-ray detection angle (θ_γ = 90°)

neutron energy	3.8 MeV		5.9 MeV	
method	analytical	Monte Carlo	analytical	Monte Carlo
A_γ	1.897	1.911	1.971	1.949
A_n	1.334	1.374	1.302	1.318
A_S	1.061	1.061	1.164	1.149
A_{ms}	0.813	0.777	0.846	0.759
$C = \prod A_i$	2.183	2.165	2.526	2.240

Corrections obtained for the $^{208}Pb(n,\gamma_0)$ reaction are presented in Table II and similar conclusions can be drawn. There is a small difference concerning the geometry and absorption effects (less than 4%) and this is a good agreement due to the large amplitude for these corrections. In the analytical method, the neutron and γ-ray absorption effects are calculated by summing the contribution from various parts of the sample. The grid system is made of cubic elements in the code we used for these calculations [6]. Generally, the Day approximation [7] is used to estimate the multiple scattering effect. In this approximation, it is assumed that the effects of multiple scattering just cancel out the neutron attenuation at the first collision and this is obtained by replacing the total neutron cross section by the nonelastic cross section. This approximation is thus very easy to apply and eliminates long and complex multiple scattering calculations. This approximation gives fairly good results at 3.8 MeV but there is a 11% difference with the Monte Carlo calculations at 5.9 MeV. Moreover, with the large amplitude of the corrections for this lead sample, the correction contribution to the capture cross sections error is about 15% which is very important.

IV. Angular dependence of the corrections

To determine asymmetry factors, or angular distributions, it is necessary to calculate the corrections at each angle. These corrections are very important for small asymmetry factors where uncorrect estimates could change the final value. In Table III, we have compared the corrections obtained at three angles for the $^{208}Pb(n,\gamma_0)$ reaction using the same analytical method and experimental conditions as in Table II.

Table III - Angular dependence of the corrections at E_n = 5.9 MeV

method	analytical			Monte Carlo		
angle θ_γ	55°	90°	125°	55°	90°	125°
$A_{abs+geom.}$	3.466	2.987	2.638	3.448	2.951	2.574
A_{ms}	0.819	0.846	0.869	0.770	0.759	0.742
$C = \prod A_i$	2.839	2.526	2.292	2.655	2.240	1.910

From Table III we see that the angular dependence of the total corrections is quite different for the two techniques and is mainly due to the multiple scattering effect. The first row takes into account the geometry and the neutron and γ-ray absorption effects but the forward-to-backward correction difference is only 2 % between the two methods. The angular dependence for the multiple scattering correction is opposite so that the total forward-to-backward correction ratio is 1.24 for the analytical method using the Day approximation and 1.39 with the Monte Carlo technique thus giving larger asymmetry factors.

The 2.615 MeV line from neutron inelastic scattering on ^{208}Pb was also recorded in the experiment ; this is a $2^+ \rightarrow 0^+$ transition and, consequently, the intensity should be symmetric compared to 90°. When the intensities at 55° and 125° are corrected for the different effects it is found that the 2.615 MeV γ-ray intensities are equal within 2.5% as expected. The intensity at 55° is corrected by a factor 1.23 compared to the intensity at 125° and the symmetry of this transition after correction by such a large factor testifies of the validity of our correction technique.

V. Conclusion

This study has shown that analytical methods could be used for geometry and absorption effect corrections whatever the dimensions of the sample are. However, these simple methods can be used for the multiple scattering correction only for simple sample geometries like thin disks. In other cases we have to rely on the Monte Carlo technique to calculate the magnitude and the angular dependence of the multiple scattering correction.

References

[1] - S. Joly, G. Grenier and J. Voignier, Contribution to this meeting.

[2] - J.K. Dickens, Nucl. Instr. Meth. 98 (1972) 451.

[3] - J. Taste, CEA-Report-N-18771 (1976).

[4] - J.J. Devaney, Nucl. Sci. Eng. 51 (1973) 272.

[5] - D.L. Smith, Argonne Report, ANL/NDM-17 (1975).

[6] - A. Lindholm, private communication.

[7] - R.B. Day, Phys. Rev. 102 (1956) 767.

Discussion

QUESTION: W. Poenitz
You may have said it and I missed it. Do you take into account the angular distribution of elastic and inelastically scattered neutrons?

ANSWER: G. Grenier
In the Monte Carlo calculations, yes; but not for the inelastic.

COMMENT: W. Poenitz
That is something I am worried about. Measurements of the inelastic angular distributions show quite some anisotropy above a few MeV. I also used so far isotropic distributions for the inelastics, but this might be something one has to look at.

FAST-NEUTRON CAPTURE IN ^{238}U AND ^{232}Th

by

W. P. Poenitz
Argonne National Laboratory
Argonne, Illinois, USA

Abstract

Experimental detection techniques employed in the measurements of the $^{238}U(n,\gamma)$ and $^{232}Th(n,\gamma)$ cross sections are discussed. The experimental data base is considered and it is concluded that these cross sections are presently known with ±5% in the energy range of greatest importance for LMFBR applications. New measurements will have an insignificant impact on the $^{238}U(n,\gamma)$ cross sections if they do not achieve an uncertainty of ≈2% or less.

I. Introduction

The $^{238}U(n,\gamma)$ cross section is one of the most important quantities in fast-breeder-reactor design and calculations. Based upon sensitivity coefficients,[1,2] it ranks among the three quantities of highest importance which influence the reactor-design parameter k_{eff} and the economically important breeding ratio. Sensitivity to uncertainties of other capture cross sections (fissile materials, structural materials, and fission products) is typically a factor of 5 lower. The $^{232}Th(n,\gamma)$ cross section is of similar importance if one considers a ^{233}U-^{232}Th-fuel cycle. However, though the latter recently received some attention, the result of the INFCE study[3] reestablished the ^{239}Pu-^{238}U-fuel cycle as the one of primary interest.

The $^{238}U(n,\gamma)$ and $^{232}Th(n,\gamma)$ cross sections were reviewed at the Knoxville Conference in 1979.[4] The emphasis of the present review will be on new developments and an update of the previous considerations with the energy range restricted to above 10 keV.

II. Measurement Techniques for ^{238}U and ^{232}Th

The need to measure the $^{238}U(n,\gamma)$ and $^{232}Th(n,\gamma)$ cross sections with 1-2% uncertainties makes it inevitable to consider measurement techniques which have been applied in the experiments but have shortcomings, specfically for these two nuclei. The various experimental techniques applicable to the determination of capture events were reviewed in the preceeding session of this meeting[5] as well as in a recent monograph.[6] However, the application of these techniques to ^{238}U and ^{232}Th warrents some additional considerations.

Specific problems are:

i. The low neutron-binding energy (<5 MeV),

ii. The high background due to the radioactive decay-chain daughters,

iii. Identical parity (positive) of most low-energy states of the compound nucleus,

iv. The long half-life of one of the low-energy states (780nsec) in ^{239}U.

II.1 Prompt-Detection Technique with a Large-Liquid-Scintillator Tank (LLST)

The low neutron-binding energy and high background result in a low spectrum fraction (~60%) compared with 75-85% for most of the other nuclei. As a result, the detection efficiency becomes conceivably sensitive to γ-spectrum changes which might occur with changing energy and angular momentum of the captured neutron. The required extrapolation to zero-pulse height makes absolute capture-rate determinations uncertain by 5-10%, with the lower limit being extremely optimistic. Measurements, in which the black-resonance technique was used for normalization, do not require this extrapolation, however, the sensitivity to γ-spectrum changes might cause an errors of a similar size. An estimate of a possible spectrum effect could be made if the spectra obtained at various energies and in the black resonance could be compared. Such information was, unfortunately, never published. Another uncertainty in context with the black-resonance technique might be the predominant surface absorption versus volume absorption of the neutrons in the sample at other energies.

Figure 1 shows the ratio between the $^{238}U(n,\gamma)$ cross sections measured by DeSaussure et al.[7] and by Fricke et al.[8] Both data sets were obtained with (rather large) LLST's, both were normalized with the black-resonance technique, and both were measured relative to the $^{10}B(n,\alpha)$ cross section. The approximately 25% change of this ratio over the energy range of 1-100 keV shows some similarity to the change from s- to p-wave neutron capture with increasing energy. Thus, one might suspect that possible gamma-spectrum changes are the cause for the observed variation of the ratio shown in Fig. 1. The effect could come from changes of the spectral fractions of the detectors. DeSaussure et al.[7] measured with two differently thick samples

(0.0004 and 0.0028 at/b) and obtained agreement of the two data sets within ≈1-2%. Fricke et al.[8] measured with samples of 0.0047 at/b (or possibly with 0.0117 at/b). Because the agreement obtained by DeSaussure et al. for the two different samples, effects due to γ-absorption in the sample seem to be insufficient to explain the 25% data difference. Because both detectors were very large (2400 and 3000 liters), and the ^{238}U spectrum is rather soft, one would not expect that the spectrum fraction changes sufficiently to account for the 25% difference either. DeSaussure et al.[7] operated their detector in coincidence mode (between two optically separated halves) which might make the result more sensitive to spectral changes. However, a measurement without the coincidence mode was also made and resulted in agreement within ≈7%, again insufficient to explain the 25% data difference (in shape) with spectral sensitivity.

Spencer et al.[9] and Poenitz[10] measured the ratio of the $^{238}U(n,\gamma)$ cross section relative to the $^{197}Au(n,\gamma)$ cross section. Large liquid scintillators were used in both experiments (800 and 1300 liters) and normalization was obtained by extrapolation to zero-pulse height. The ratio between these data sets is also shown in Fig. 1. It does not show an energy dependence as pronounced as the data sets discussed above, but a bias of ≈5% is obvious. The latter can be understood with the substantial uncertainty of the extrapolation to zero-pulse height.

Above considerations suggest that the detection technique cannot be the major cause for data differences in the measurements by DeSaussure et al.[7] and Fricke et al.[8] The problem which results in the 25% shape difference is more likely related to other aspects of the experiments.

II.2 Prompt-Detection Technique with γ-Energy-Proportional Counters

Two types of γ-energy-proportional detectors are in use: the thick-walled proportional counters and the Moxon-Rae detector. Measurements of the $^{238}U(n,\gamma)$ cross section were carried out by Stavisskii et al.[11] using the former, and by Moxon[12] using the latter detector. The $^{10}B(n,\alpha)$ cross section was used in both experiments for the determination of the neutron flux. The measurements by Moxon[12] were carried out at a LINAC, and the black-resonance technique was used for the normalization of the data. The measurements by Staisskii et al.[11] were carried out with a lead-slowing-down spectrometer and resonance parameters were used for the normalization. The ratio of the two data sets changes by 20% between 1 and 30 keV (see Fig. 1). It is not clear whether the data by Stavisskii et al. were corrected for resonance self shielding and capture of scattered neutrons.

The possible effect of γ-spectrum changes on the detection efficiency of the Moxon-Rae detector has been considered by Wisshak et al.[13] utilizing γ-cascade calculations by Reffo.[14] It was concluded that any effect would be only a few percent. Thus, the observed shape difference, again, appears to be unrelated to the detection technique.

II.3 Prompt-Detection Technique with Pulse-Height Weighting

The pulse-height-spectrum weighting technique has the inherent advantage of acknowledging the spectral sensitivity of the detector and to correct for it. Using this technique, measurements of the $^{238}U(n,\gamma)$ cross section have been made by Macklin and Halperin[17] for the $^{232}Th(n,\gamma)$ cross section and corresponding data are available from Kobayashi et al.[18] The ratio from these two data sets is shown in Fig. 1. It does not show an energy dependence outside of the ≈5% range the values scatter, but a bias of ≈5% exists.

II.4 Activation Technique

The above considerations of the prompt detection techniques and the uncertainties and inconsistencies of the results obtained with the various detector types make it highly unlikely that the $^{238}U(n,\gamma)$ cross section can be determined with less than ≈5% without major and costly efforts. However, the $^{238}U(n,\gamma)$ as well as the $^{232}Th(n,\gamma)$ reaction permit the use of the activation technique. A special calibration method is applicable, which nature appears to have provided for us as a way out of the predicament caused by the low neutron-binding energy and high radioactive background.

Both, the ^{239}U, formed in the ^{238}U neutron capture, and the α-emitter ^{243}Am, decay to ^{239}Np which decays with a half-life of ~2.35 days to ^{239}Pu. Thus, the absolute measurement of ^{238}U-capture events is possible by detecting a γ transition of ^{239}Pu and calibrating with an ^{243}Am sample. The calibration factor contains the detection efficiency as well as the frequency with which the γ transition occurs in the ^{239}Np decay. The absolute ^{243}Am-decay rate can easily be measured with ≈0.1% accuracy by using low-geometry α-counting. The same technique can be applied for ^{232}Th-capture-rate measurements.

These favorable conditions led to the recommendation, made at the Knoxville Conference,[3] that the $^{238}U(n,\gamma)$ cross section should be measured at some energies using the activation technique. However, there are a variety of effects which must be considered if measurements with an accuracy of 1-2% are required. It is indeed in this area that some progress has been made since 1979.

i. γ-ray sum-coincidence effects and oblique angle γ-absorption are different for the metallic ^{238}U samples used in the experiment and the thin, non-absorbing, ^{243}Am sample. These effects have been studied in detail[19] using three different experimental techniques. Good agreement was obtained for the results from the three methods (<1%).

ii. Extensive intercomparisons were carried out in order to establish the confidence level at which the ^{238}U-capture rate can be determined with the activation technique. Results from these intercomparisons are shown in Fig. 2. The intercomparisons are pair-wise shown in chronological order.[19-21] The various techniques

included: the ^{243}Am-calibration technique, use of the well-known thermal capture cross section of ^{238}U, radiochemical separation of the ^{239}Np with a ^{237}Np tracer, and mass spectroscopic determination of ^{239}Pu with a ^{241}Pu tracer added before chemical separation. The agreement in most intercomparisons is quite good, the exception being the mass-spectroscopy technique. However, the problem is at a completely different level of discrepancy than it is the case for the prompt-γ-detection technique. One can conclude from Fig. 2 that at present the ^{238}U-capture rate can be determined with $\approx$1.0% uncertainty using the activation technique.

III. The Status of the Cross Sections

III.1 The ^{238}U(n,γ) Cross Section

The more recent data for the ^{238}U(n,γ) cross section are shown in Fig. 3. Also shown in the figure is a optical/statistical model calculation of the cross section using the $\Gamma\gamma/D$ obtained from low-energy resolved-resonance measurements by Rahn et al.[22] The dotted lines indicate a ±5% range around the calculated cross section. New measurements have not been made since the Knoxville Conference, however, final data were published for the measurements by Davletchin et al.[23] and by Poenitz et al.[24]

It was concluded at the Knoxville Conference that the present uncertainty of the ^{238}U(n,γ) cross section between 10 keV and 500 keV is $\approx$5%. This remains the present status. ENDF/B-V (the evaluation is described in Ref. 25) is well within this range. Several newer data sets were not available for the evaluation of ENDF/B-V. However, a simultaneous evaluation of several cross sections ((H(n,n), ^{6}Li(n,n), ^{6}Li(n,α), ^{10}B(n,α), ^{10}B(n,n), ^{10}B(n,$\alpha\gamma$), Au(n,γ), ^{235}U(n,f), and ^{238}U(n,γ)) included these newer data sets[26], and the result is compared in Fig. 3 with ENDF/B-V. It is obvious that substantial changes cannot be expectd for this cross section, though a future version of ENDF/B will involve nuclear model calculations in order to improve on the shape of the cross section by giving it more physical significance.

III.2 The ^{232}Th(n,γ) Cross Section

New measurements of the ^{232}Th(n,γ) cross sections were reported by Kobayashi et al.[18] and by Baldwin and Knoll.[27] The data by Macklin and Halperin[17] were revised,[28] thus removing the major discrepancy which existed at the time of the Knoxville Conference. The data consistency of the newer measurements is now such that a similar uncertainty as for ^{238}U(n,γ) can be concluded (see Fig. 4): $\approx$5% between 10 keV and 500 keV and $\approx\pm$10% above 1 MeV. However, an approximately 10% discrepancy appears to be indicated by the new measurement by Baldwin and Knoll on the one hand and the data by Chrien et al.,[29] Yamamuro et al.,[16,18] Macklin and Halperin,[17] and Poenitz and Smith[30] (which are all in good agreement) on the other hand. The ENDF/B-V evaluation is in good agreement with the consensus from these newer data above 40 keV (evaluation as described in Ref. 31), but somewhat low below 40 keV (evaluation as described in Ref. 32).

IV. Conclusions and Recommendations

It is concluded that the $^{238}U(n,\gamma)$ and $^{232}Th(n,\gamma)$ cross sections are known with ±5% between 10 keV and 500 keV and with ±10% above 1 MeV. In the case of the $^{238}U(n,\gamma)$ cross section, a large number of measurements is available in which many different experimental techniques were employed (absorption technique, activation technique, various prompt detection techniques), that systematic uncertainties in individual measurements can be expected to be partially compensated if all the measurements are considered. The present situation is such that new measurements with similar uncertainties than previous data sets (≈5-10%) will have an insignificant impact and not improve our knowledge of the cross section. It is recommended that measurements should be carried out with uncertainties of 2% or less at some selected energies, the 10-100 keV range being the most important for LMFBR applications. The activation technique is recommended to be used based upon the considerations in Section II. The kinematically-collimated forward neutron cone obtained slightly above the threshold of the $^{7}Li(p,n)^{7}Be$ reaction is recommended as a neutron source because the associated ^{7}Be activity can be utilized for the neutron-flux determination with an uncertainty of less than 1%. The neutron source also provides for a low background experiment.

References

1. E. M. Bohn et al., Argonne National Laboratory Report, private communication (1976).

2. C. R. Weisbin et al., ENDF-265 (1978).

3. C. E. Till, Proc. Conf. on Nuclear Cross Sections for Technology, NBS Sp. Publ. 594, 115 (1979), C. E. Till et al., Argonne National Laboratory Report, ANL-80-40 (1980).

4. W. P. Poenitz, Proc. Conf. on Nuclear Cross Sections for Technology, NBS Sp. Publ. 594, 368 (1979).

5. D. Gayther and T. Thom, Atomic Energy Research Establishment, Harwell, these proceedings (1982).

6. W. P. Poenitz, Argonne National Laboratory Report, ANL/NDM-58 (1981).

7. G. de Saussure et al., Nucl. Sci. Eng. 51, 385 (1973).

8. M. P. Fricke et al., Conf. on Nucl. Data for Reactors, Helsinki, Vol. II, 265 (1970).

9. R. Spencer and F. Kaeppeler, Conf. on Neutron Cross Sections for Technology, Washington 1975, NBS Spec. Publ. 425, 620 (1975).

10. W. P. Poenitz, Nucl. Sci. Eng. 57, 300 (1975).

11. Yu. Ya. Stavisskii et al., Conf. Nuclear Data for Reactors, Helsinki, Vol. II, 51 (1970).

12. M. C. Moxon, Atomic Energy Research Establishment Report AERE-R-6074 (1969).

13. K. Wisshak et al., Karlsruhe Research Center, this meeting (1982).

14. G. Reffo, Centro di Calcolo del (CNEN, this meeting (1982).

15. See R. B. Perez et al., Phys. Rev. 20, 528 (1979).

16. N. Yamamuro et al., Nucl. Sci. Technol. 15, 637 (1978).

17. R. L. Macklin and J. Halperin, Nucl. Sci. Eng. 64, 849 (1977).

18. K. Kobayashi et al., Nucl. Sci. Technol. 18, 823 (1981).

19. G. J. DiIorio and W. P. Poenitz, Nucl. Instr. Meth., to be published (1982).

20. J. A. Morman and R. J. Armani, Argonne National Laboratory Report, ZPR-TM (1982).

21. D. W. Maddison, Argonne National Laboratory, private communications 1981-1982.

22. F. Rahn et al., Phys. Rev. C6, 1854 (1972).

23. A. N. Davletchin et al., Atom Energia 48, 87 (1980).

24. W. P. Poenitz et al., Nucl. Sci. Eng. 78, 239 (1981).

25. W. P. Poenitz et al., Argonne National Laboratory Report, ANL/NDM-32 (1977).

26. W. P. Poenitz, Proc. Conf. Nucl. Data Evaluation Methods and Procedures, Brookhaven National Laboratory, Reports DOE-NDC-23, NEANDC(US)-209, Vol. 1, 249 (1981).

27. G. Baldwin and G. Knoll, University of Michigan, this meeting (1982).

28. R. L. Macklin and R. R. Winters, Nucl. Sci. Eng. 78, 110 (1981).

29. R. E. Chrien et al., Nucl. Sci. Eng. 72, 202 (1979).

30. W. P. Poenitz and D. L. Smith, Argonne National Laboratory Report, ANL/NDM-42 (1978).

31. J. Meadows et al., Argonne National Laboratory Report, ANL/NDM-35 (1978).

32. M. R. Bhat, ENDF-268 (1981).

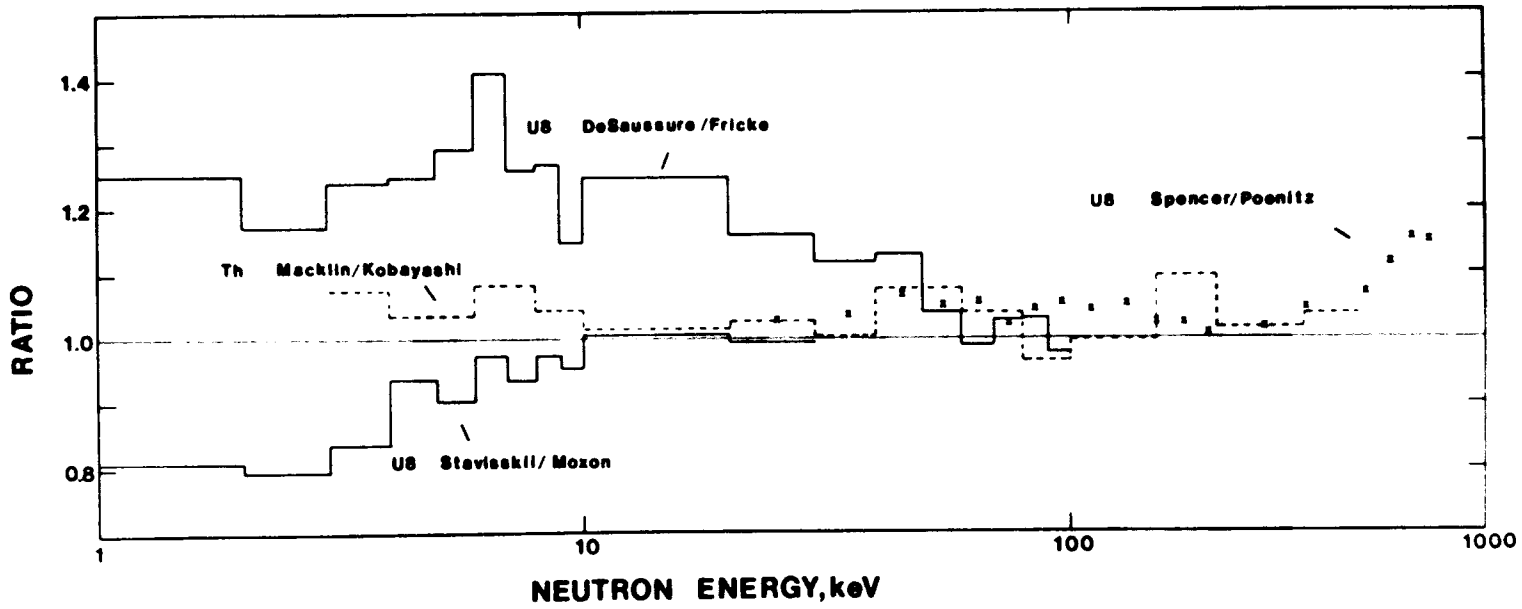

Fig. 1. Ratios of Experimental Data Obtained with Different Prompt-Detection Techniques (see Text).

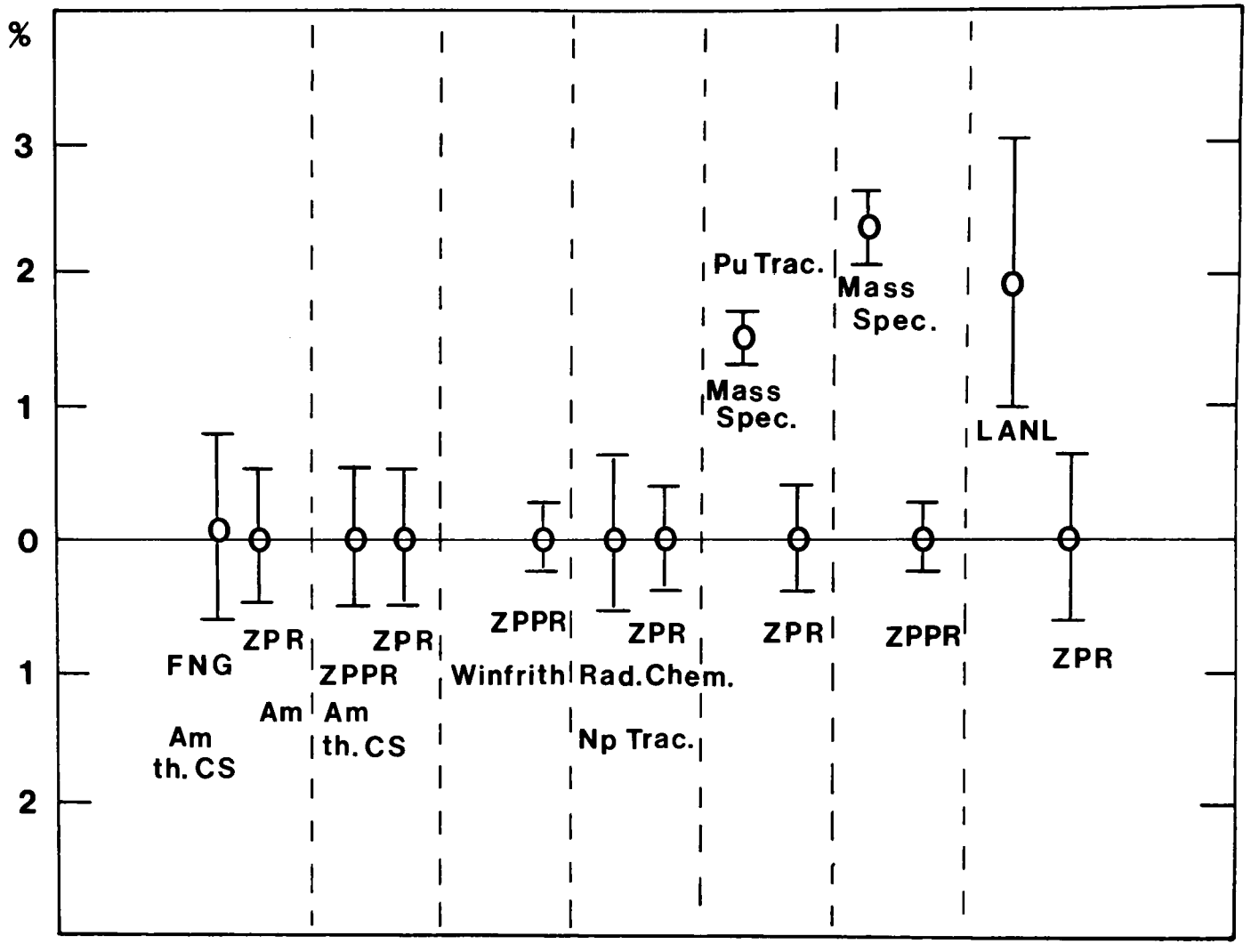

Fig. 2. Various Intercomparisons of $^{238}U(n,\gamma)$ Capture Rate Measurements Based upon the Activation Technique (see Text).

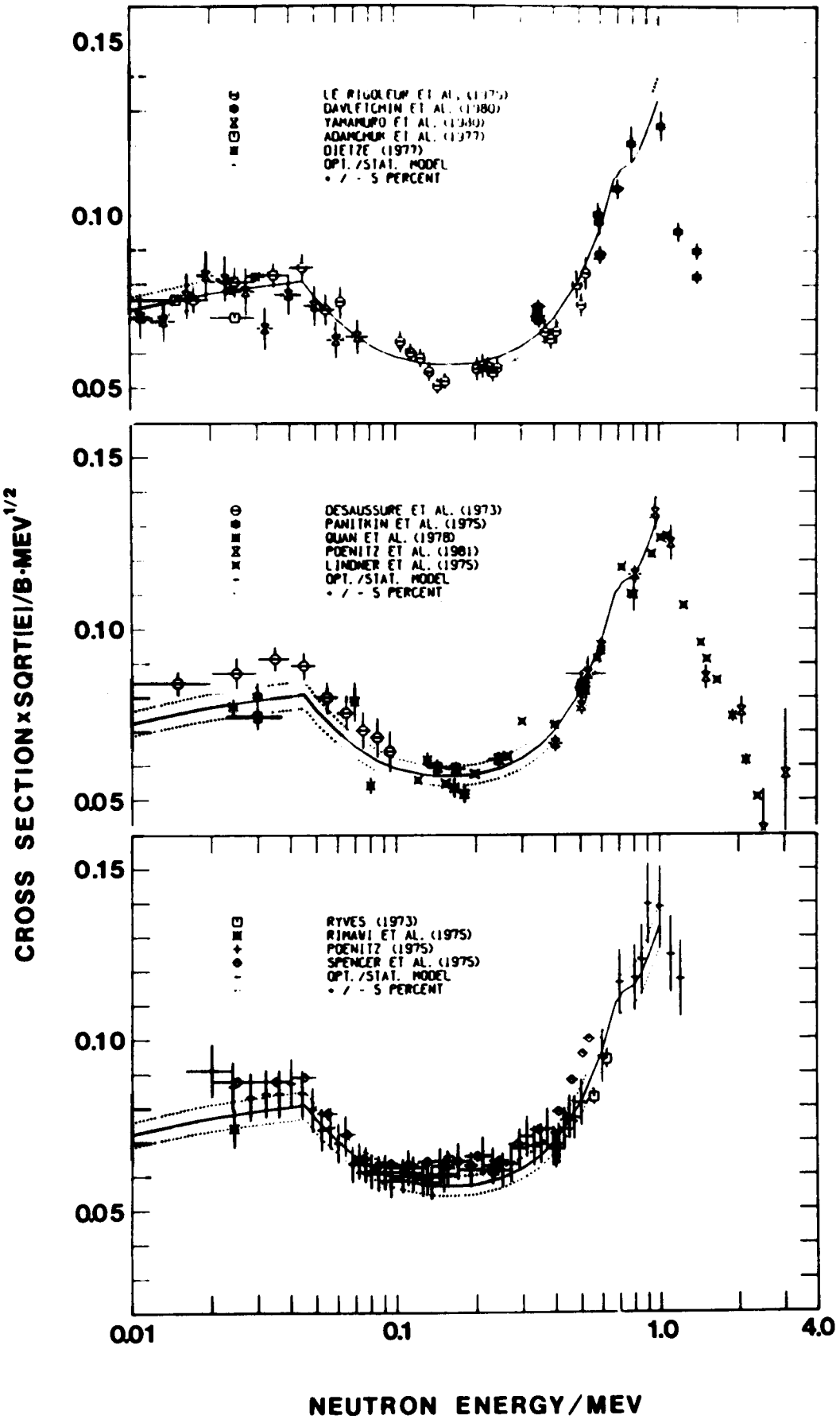

Fig. 3. Recent Experimental Data of the $^{238}U(n,\gamma)$ Cross Section. The solid line represents an optical/statistical nuclear model calculation[4]

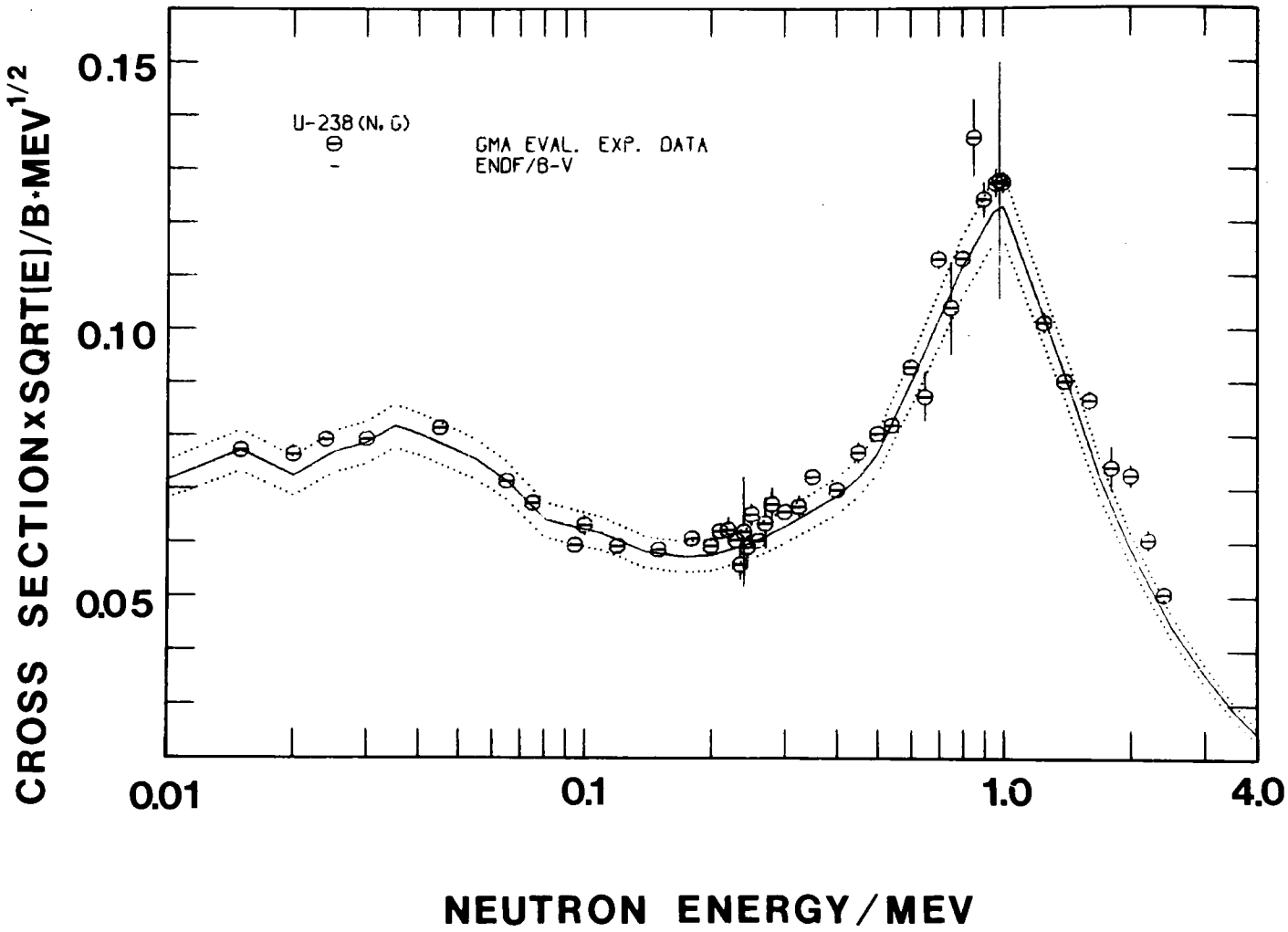

Fig. 4. Comparison of the $^{238}U(n,\gamma)$ Cross Section Obtained in a Simultaneous Evaluation of Several Cross Sections[26] with ENDF/B-V.

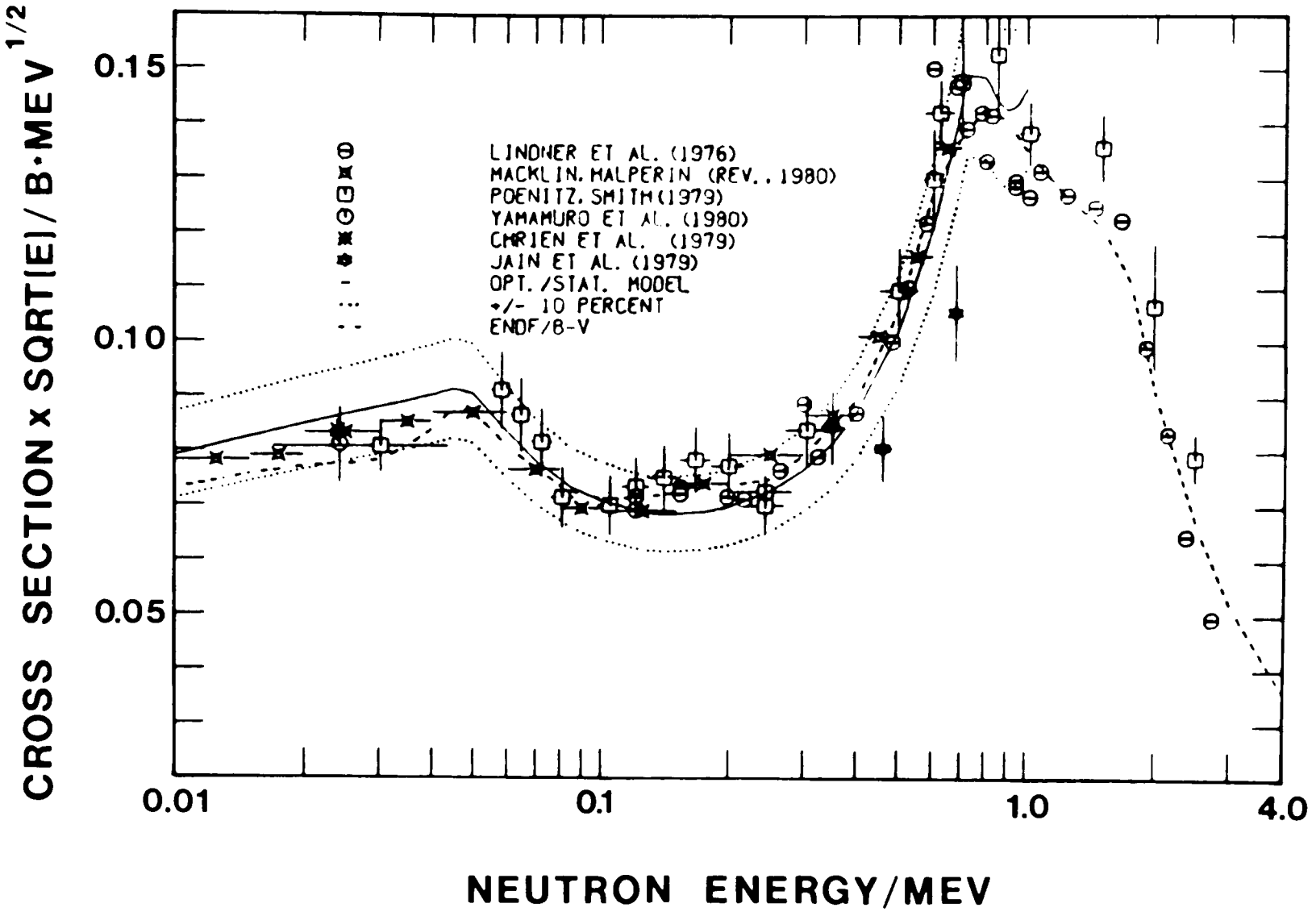

Fig. 5. Recent Experimental Data of the $^{232}Th(n,\gamma)$ Cross Section. The solid line represents an optical/statistical nuclear model calculation[4] and the dashed line is ENDF/B-V.

Discussion

COMMENT: R. Block
You said that there might be a problem in ^{238}U with a ~ 1 μsec decay time of one of the low-energy states of ^{239}U. That could easily be checked with a monoenergetic beam at a Van de Graaff by looking at the dispersion.

COMMENT: W. Poenitz
Yes, one would look at the tail in the time-of-flight distribution. The only detector where it might be a problem would be the Moxon-Rae detector with a very low threshold. How much of a problem it is, I do not know. I wanted to make a calculation of the occupation probability for this state with my KASKADE code, but did not get to it.

COMMENT: R. Chrien
If one would do a high-resolution time-of-flight experiment, that is, high-resolution in both, γ-energy and TOF, then one could see whether the shape of a resonance would be different for a γ-ray coming from that level.

COMMENT: A. B. Smith
The statement was made that nuclear model calculations would be involved in a future evaluation. I pointed out yesterday that apparently nobody has succeeded so far in finding a model which describes the excitation of the first inelastic level correctly. I have trouble with that. If you cannot describe the other pieces of the cross sections, how can you use it for an evaluation.

COMMENT: W. Poenitz
There are two issues involved here. First, one could use Γ_γ/D values to obtain additional information for the normalization of the cross section. Whether one should do this might be an open question, it was several times discussed at this meeting. The second approach is to use the model just for smoothing of the result from the least-squares consistency fit. This latter approach should definitely be used. Asides from these questions, you can see from the figure that the calculated capture cross section agrees quite well over the inelastic competition cusp with the experimental data. How much that says about the inelastic cross section, I do not know, one would have to get the sensitivity by artifically forcing the inelastic cross section up. I might be interested in doing that some day.

COMMENT: A. B. Smith
I am not against models, but one has to use them with care. Another aspect of this persistent problem of not being able to calculate that inelastic cross section is whether the compound nucleus concept is here sufficient, is there another physical mechanism which could explain this?

COMMENT: F. Froehner
Below the inelastic threshold things are very simple as far as model calculations are concerned. The interpretation is more unique, and (as W. Poenitz just said) one may have help from the model calculation. Let me make a second remark. I could think of a reason why the inelastic scattering cross section is not well calculated. We always use the same strength function or transmissin coefficients, but they might be different for the excited state.

COMMENT: P. Moldauer
You mean the potential.

COMMENT: W. Poenitz
There is some work on that, I remember a Russian paper where a different potential was derived for the excited state.

COMMENT: A. B. Smith
There you would open up another ball of wax, another slew of parameters.

QUESTION: R. Pellee
Am I correct in understanding that the uncertainty bands in your figures apply to the uncertainty over rather local energy regions, perhaps a lethargy unit, while the data requirements given yesterday were in terms of one-group spectrum averages? (The 5% uncertainty band in your plots might correspond to ~ 2% uncertainty averaged over a typical fast reactor k-sensitivity functions?)

ANSWER: W. Poenitz
No, this includes the correlated error, a substantial part might be normalization uncertainty.

ABSOLUTE MEASUREMENT OF THE CROSS SECTION FOR 23-keV NEUTRON ACTIVATION OF THORIUM*

by

George T. Baldwin† and Glenn F. Knoll

University of Michigan, Department of Nuclear Engineering, Ann Arbor, Michigan 48109

Absolute measurement of the thorium radiative capture cross section has been made using antimony-beryllium photoneutrons and an activation method. The average of two determinations is 606 mb near 23 keV neutron energy with a 3.2% estimated error from all sources. This value is about 10% higher than those reported from recent measurements employing iron-filtered neutron beams.

INTRODUCTION

Radiative neutron capture in thorium results in eventual formation of the fissile isotope ^{233}U. For this reason, the associated reaction cross section is of key importance in fast reactor design calculations based upon a Th/^{233}U fuel cycle. This alternative (thorium) fuel cycle has been of interest lately in response to concerns about nuclear fuel cycle safeguards and uranium availability, and has motivated recent reevaluations of nuclear cross section data for thorium.[1–3] The conclusions reported in these evaluations have indicated a high-priority need for additional measurements of the thorium capture cross section for fast neutrons.

Facilities have been developed at the University of Michigan for making absolute measurements of actinide fission cross sections using five photoneutron sources.[4] Of these sources, only antimony-beryllium can generate sufficient neutron fluence to be feasible for a thorium capture measurement.

The conceptual basis for absolute measurement derives from the defining equation for the reaction cross section, viz,

$$\sigma = \frac{R}{N\Phi}.$$

*Text of paper submitted to *Nuclear Science and Engineering* for publication.

†Present address: Sandia National Laboratories, Division 1232, Albuquerque, N.M. 87185.

Here R is the capture reaction rate (s^{-1}), N is the total number of ^{232}Th target nuclei, and Φ is the scalar neutron flux ($cm^{-2}s^{-1}$). The value of each quantity is measured absolutely; the cross section σ (cm^{2}) then follows directly.

The reaction rate R is determined indirectly by measuring the amount of the ^{233}Pa daughter isotope activity present in a thorium target after a prescribed irradiation period. From the differential equations associated with the decay sequence

$$^{232}Th(n,\gamma)^{233}Th \xrightarrow[t_{1/2}=22\,min]{\beta^-} {}^{233}Pa \xrightarrow[t_{1/2}=27\,days]{\beta^-} {}^{233}U$$

one obtains the solution:

$$\sigma = \frac{1}{N\Phi_0}\left[\frac{n_p(t_1,t_2)\,(\lambda_p-\lambda_s)\,\exp(\lambda_p t_2)}{\exp(-\lambda_s t_1)-\exp(-\lambda_p t_1)}\right].$$

Here the expression in brackets is just the reaction rate, quantitatively related to the number n_p of ^{233}Pa nuclei present at time t_2 after an irradiation of duration t_1. λ_p is the ^{233}Pa decay constant. A photoneutron flux of the form $\Phi(t) = \Phi_0 \exp(-\lambda_s t)$ is assumed.

EXPERIMENTAL METHOD

Neutron Source

The spherical source consisted of a core of metallic antimony, 1.5 cm in radius, surrounded by a 3 mm-thick beryllium shell and a 3 mm-thick aluminum outer casing. It was activated by irradiation for 20 days in a flat flux approximately 10^{13} $cm^{-2}s^{-1}$ in the 2 MW pool-type Ford Nuclear Reactor. The source strength was calibrated by the manganese bath method; i.e., by comparing the saturated ^{55}Mn activity induced by the Sb-Be source with that induced by a laboratory-reference ^{252}Cf source. The ^{252}Cf source had been previously calibrated against the NBS-II secondary neutron standard.[5] Small corrections ($<2\%$) were made to account for detector counting losses, source decay, solution mixing, and neutron losses (including source self-absorption). Manganese bath calibration runs were made once before and once following two target exposure runs. Interpolation of the source strength during the target exposures assumed a photoneutron source half-life of 60.20 ($\pm 0.1\%$) days.[6] Results are given in Table I.

Thorium Target

Samples of natural thorium metal were obtained from the Oak Ridge National Laboratory in the form of flat sheets measuring 25.13 × 12.00 × 0.05 cm and weighing approximately 170 g. The number of ^{232}Th nuclei in each sample was determined to within an uncertainty of 0.5%, by weighing and using the supplier's value for the sample purity (98.5±0.5 mass percent Th, measured by chemical analysis[7]).

For each target activation, a single thorium sheet was bent into a cylinder 8 cm I.D. × 12 cm high, enclosed by an outer 1 mm-thick aluminum casing. The Sb-Be source sphere was positioned at the center of the target cylinder (see Figure 1). A cadmium-lined 55-gallon steel drum isolated the assembly from room-scattered (thermal) neutrons.

Table I
Sb-Be Source Strength

A. Measured

Time of Calibration	Extrapolated Cf-252 Reference Strength*	Saturated Activity Ratio	Sb-Be Source Strength*
2/11/81 (17:12)	2.729×10^6 ($\pm$0.73%)	7.803	2.129×10^7 ($\pm$0.84%)
4/11/81 (13:00)	2.616×10^6 ($\pm$0.75%)	4.106	1.074×10^7 ($\pm$0.88%)

B. Extrapolated

	Sb-Be Source Strength*		
Time of Run Start	Based on First Calibration	Based on Second Calibration	Weighted Average
2/17/81 (00:16)	2.003×10^7 ($\pm$0.84%)	1.989×10^7 ($\pm$0.88%)	1.997×10^7 ($\pm$0.9%)
3/10/81 (08:34)	1.567×10^7 ($\pm$0.84%)	1.556×10^7 ($\pm$0.88%)	1.562×10^7 ($\pm$0.9%)

*All source strengths are in (n/s).

Flux Determination

The neutron flux was obtained as the product of the (time-dependent) source strength, measured by the manganese bath technique, and the (time-independent) scalar flux at the target per unit source strength, determined by calculation. Only the spatial average of the flux per unit source strength is of interest, because the method that is used after the irradiation to measure the induced ^{233}Pa activity depends only on its total amount, not its spatial distribution.

A Monte Carlo method[8] was used for the flux-per-unit-source-strength calculation in order to represent accurately the source/target geometry, the complex polar angle distribution of emitted source neutrons, and the effects of scattering within the source, target and structural materials. One energy group and isotropic scattering were assumed in the model. No energy loss in scattering was treated. The flux per unit source strength was derived as the accumulated total track length of neutrons within the target divided by the target volume and by the number of neutrons started. The net effect of scattering was observed to increase the flux by almost 6% over that obtained when no scattering was assumed. Most of the flux increase resulted from scattering within the thorium sheet itself (4% effect). A value of 3.61×10^{-3} cm^{-2}($\pm$0.9%) was obtained for the average scalar flux per unit source strength.

Isolation of ^{233}Pa

Two thorium targets were irradiated in succession, each for about two weeks. A

chemical procedure[8] was used after irradiation to isolate ^{233}Pa. First the thorium was dissolved in approximately 1 liter of hydrochloric acid containing a trace amount of HF. Following dissolution, the fluoride ion was complexed by adding $AlCl_3$. A carrier-free solvent extraction with undiluted diisobutylcarbinol was then carried out, using a succession of extraction/back extraction steps to concentrate the volume of solution containing ^{233}Pa. Protactinium was obtained finally in approximately 3 ml of 2M HCl/trace HF solution, sealed in a small polyethylene counting vial. Excellent decontamination from natural thorium radioactivity was achieved.

Loss of ^{233}Pa during the chemistry was measured by isotopic tracing with ^{232}Pa, which decays with a 1.3 day half-life. Details of the tracer isotope production by means of the ^{232}Th$(p,n)^{232}$Pa reaction are presented elsewhere.[8,9] ^{232}Pa in 2M HCl/trace HF was added to the irradiated thorium as it was being dissolved in acid. An equal amount of ^{232}Pa tracer solution was delivered directly to a counting vial and set aside as a control sample. Volumetric sampling by micropipette was verified by weighing. After performing the chemical separation, the spiked target solution and the control sample were each counted under identical conditions using a Ge(Li) spectrometer. Using the photopeaks for two ^{232}Pa decay gamma rays, at 894- and 969-keV, the ratio of the corrected counting rate for the target sample to the corrected counting rate for the control gave a direct measure of the fractional recovery of protactinium. A 90% yield was obtained for both target separations.

Absolute Gamma Counting

The prominent 312-keV gamma ray from ^{233}Pa decay was counted using a Ge(Li) detector, after allowing time for the relatively short-lived ^{232}Pa tracer isotope activity to decay. As depicted schematically in Figure 2, the measured counting rate for the separated target sample was compared indirectly with that for a $^{237}NpO_2$ deposit, used as a steady-state reference of ^{233}Pa activity. The intermediate ^{233}Pa samples shown in Figure 2 were prepared from equal-weight micropipette aliquots of a stock solution of ^{233}Pa (*i.e.*, protactinium chemically separated from reactor-activated thorium).

The ^{237}Np alpha activity of the $^{237}NpO_2$ deposit was calibrated by the National Bureau of Standards, using good-geometry surface-barrier-detector counting, to be 6039 Bq ($\pm$0.25%).[10] This is assumed to be equal to the disintegration rate of the ^{237}Np daughter, ^{233}Pa. The NBS alpha counting measurement was checked by a direct determination of ^{233}Pa activity at the University of Michigan, by counting the 312-keV gamma activity and using 38.6 gammas per 100 decays for the branching ratio.[11] However, the latter method was limited by the accuracy to which the absolute Ge(Li) detector efficiency was measured.

All gamma counting made use of a 55 cm^3 closed-end coaxial Ge(Li) detector in the presence of low ambient background. Samples were counted in a reproducible geometry, both at 6- and 11-cm from the face of the detector cryostat. Counting rates were sufficiently low so that corrections for pulse pileup, random summing and dead time were negligible. Effects of coincidence summing were compensated in all cases by using only *ratios* of photopeaks of the same isotope, each counted with the same

efficiency. Spectra were accumulated with a multichannel analyzer resolution of 0.5 keV per channel. Photopeak fitting and area determination by numerical integration were done with the SKEWGAUS computer code.[12]

Results

The average of two measurements of the thorium capture cross section for Sb-Be photoneutrons was 606 mb $\pm 3.2\%$. Errors are one standard deviation and are combined in quadrature.

DISCUSSION

In order to compare this result with other measurements near 23 keV, we need to take into account the effect of scattered neutrons comprising the "tail" of the photoneutron energy spectrum, as well as those Sb-Be photoneutrons in a second, low-intensity group near 375 keV. We attribute 4.4% of the neutrons to the 375 keV group,[14] and calculate the energy distribution of primary-group photoneutrons by Monte Carlo simulation[8](see Figure 3). For the relative shape of the cross section as a function of energy, we used both ENDF/B-V and the measurements of Macklin and Halperin[13]. In either case, the resulting spectrum correction was negligible; we conclude that the cross section is 606 mb near 23 keV (*e.g.*, as measured with an approximately Gaussian-shaped distribution with 2 keV FWHM). This result further appears to be relatively insensitive to uncertainties in the exact energy distribution and centroid energy of the neutron source.

Our measurement of the thorium capture cross section is plotted in Figure 4, compared with the results of Macklin and Halperin[13] and ENDF/B-V. The variation of the capture cross section with energy in this resonance region is appreciable, as seen in Figure 4, arising due to fluctuations in the nuclear level spacing. However, these fluctuations are not resolved by the 2-keV-broad primary Sb-Be neutron group.

We also note that our measurement is about 10% higher than the iron-filtered neutron beam measurements reported by Chrien, *et al*, at Brookhaven[15], and Yamamuro, *et al*, in Japan[16]. However, our value is in close agreement with a 1966 measurement by Belanova, which was a transmission experiment using an Sb-Be photoneutron source. Additional measurements would therefore seem to be appropriate in order to confirm an absolute normalization of the evaluated thorium capture cross section in this energy range.

ACKNOWLEDGMENT

This work has been supported by the U.S. Department of Energy under contract number C-EY-76-S-02-2025.

REFERENCES

1. J. Meadows, W. Poenitz, A. Smith, D. Smith, J. Whalen and R. Howerton, *Evaluated Nuclear Data File of Th-232*, ANL/NDM-35 (1978).

2. G. Vasiliu, *et al*, *Nuclear Data Evaluation for Th-232*, INDC(RUM)-10 (1980).

3. W.P. Poenitz, "Fast Neutron Capture in U-238 and Th-232", *Standard Reference and Other Important Nuclear Data*, BNL-NCS-51123, ENDF-300 (1980).

4. G.F. Knoll, "Absolute Fission Cross Section Measurements Using Fixed Energy Neutron Sources", NBS Special Publication 493, *Proceedings of the International Specialists Symposium on Neutron Standards and Applications*, held at the National Bureau of Standards, Gaithersburg, MD, March 28-31, 1977.

5. M.C. Davis, PhD Dissertation, University of Michigan (1976).

6. C.M. Lederer and V.S. Shirley, *ed.*, *Table of Isotopes*, 7th ed., 1978.

7. W.R. Laing, private communication, 1980.

8. G.T. Baldwin, PhD Dissertation, University of Michigan (1981).

9. G.T. Baldwin, H.C. Griffin and G.F. Knoll, "Production of Protactinium-232 from Thorium", *Radiochemical and Radioanalytical Letters*, to be published.

10. D.M. Gilliam, private communication, 1981.

11. R.J. Gehrke, R.G. Helmer and C.W. Reich, "Emission Probability of the 312-keV Gamma Ray from the Decay of Protactinium-233", *Nuclear Science and Engineering*, **70**, 298 (1979).

12. W.C. Schick, Jr., "SKEWGAUS: A Fortran Program for Fitting Peaks in Semiconductor Detector Spectra". IS-3460, Oct. 1974.

13. R.L. Macklin and J. Halperin, "^{232}Th(n,γ) Cross Section from 2.6 to 800 keV", *Nuclear Science and Engineering*, **64**, 849 (1977), (as revised, *Nucl. Sci. & Eng.*, **78**, 110 (1978)).

14. T.B. Ryves and J.C. Robertson, *Journal of Nuclear Energy*, **25**, 557 (1971).

15. R.E. Chrien, H.I. Liou, M.J. Kenny and M.L. Stelts, "Neutron Cross Sections of Thorium-232", *Nuclear Science and Engineering*, **72**, 202 (1979).

16. N. Yamamuro, T. Doi, T. Miyagawa, Y. Fujita, K. Kobayashi and R.C. Block, "Measurement of Neutron Capture Cross Sections with Fe-Filtered Beam", *Journal of Nuclear Science and Technology*, **15**, 637 (1978).

Figure 1
Assembly of Cylindrical Thorium Target onto Neutron Source Support Well

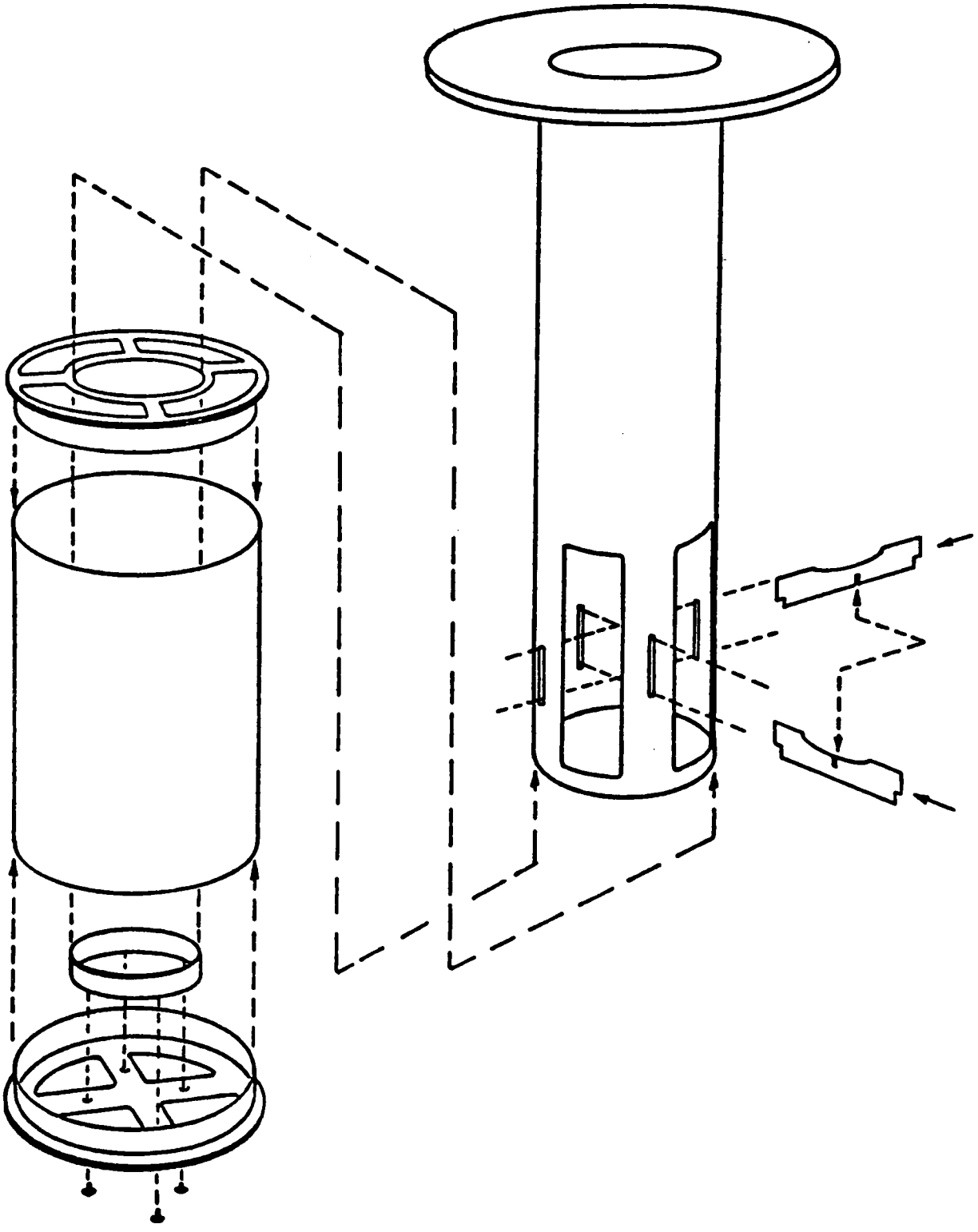

Figure 2
Indirect Measurement of ^{233}Pa Activity

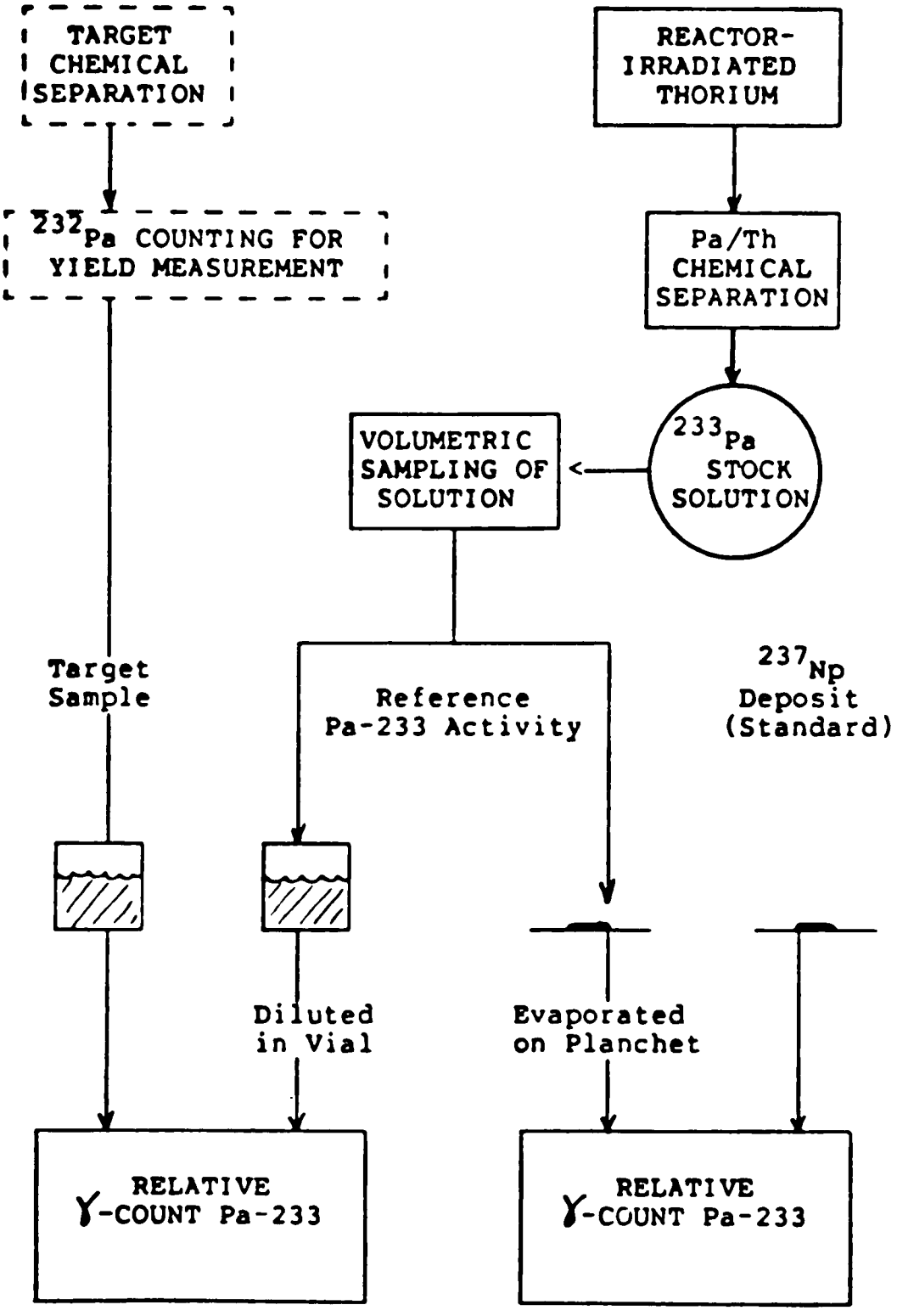

Figure 3
Sb-Be Photoneutron Energy Distribution
Calculated by Monte Carlo Simulation

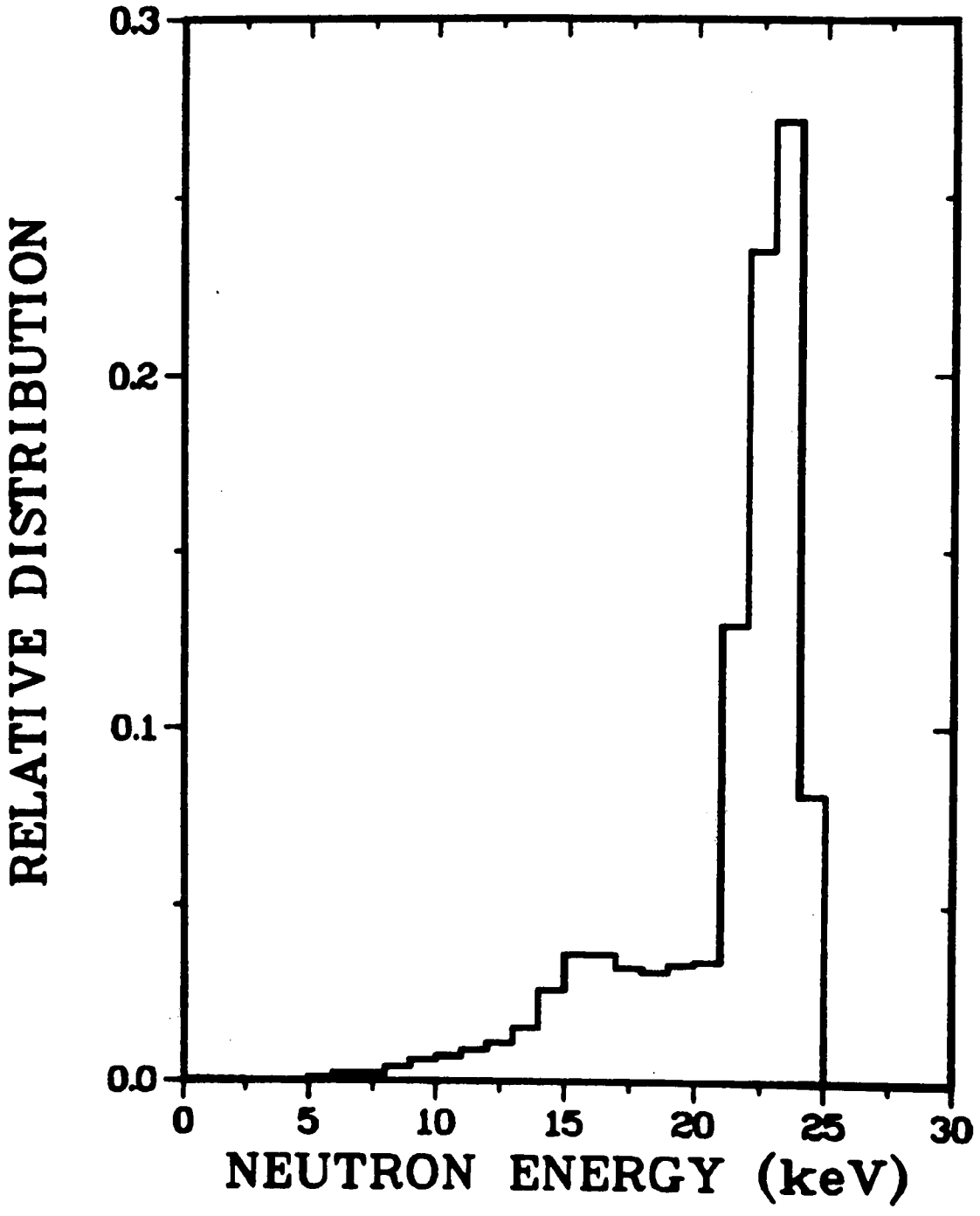

Figure 4
Neutron Capture Cross Section of ^{232}Th

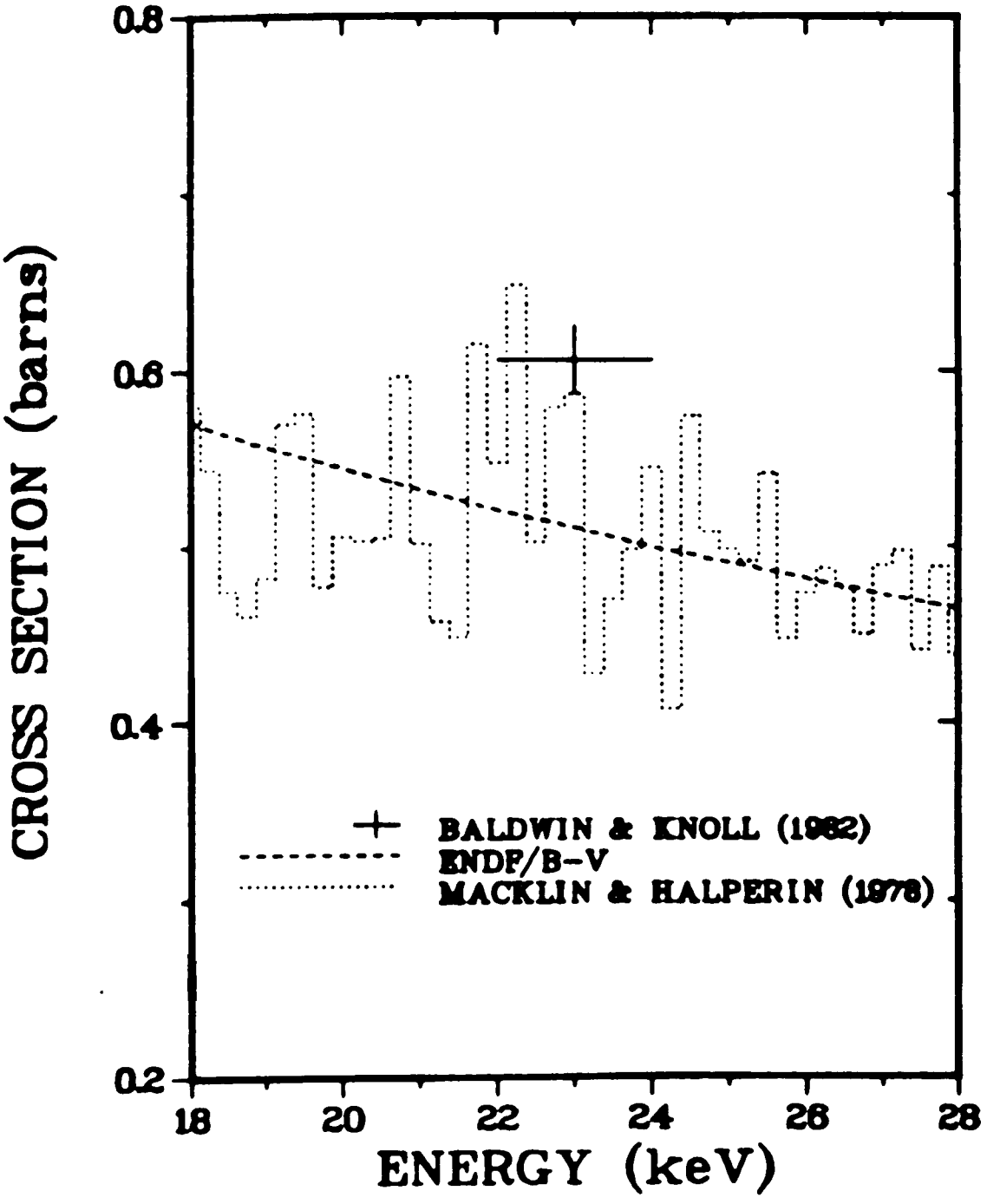

Discussion

QUESTION: A. B. Smith
There are two issues:
1) Flux determination
2) Reaction-rate determination
Could you carry out step #2 at the BNL filtered beam?

ANSWER: G. Knoll
Because the radiochemical separation of the Pa-233 activity from the large thorium background is unique to our work, it would be very interesting to apply the same methods to filtered beam irradiations. However, the technique does involve destructive processing of the target.

COMMENT: R. Anderl
I would like to comment on integral measurements for $^{232}Th(n,\gamma)$ made at the CFRMF and their implications on adjusting the ENDF/B-V capture cross section. Our work indicates that the present capture cross section for $^{232}Th(n,\gamma)$ is inconsistent with CFRF integral data. The ratio of calculated-to-measured spectrum-averaged cross sections is 0.87 ± 4%. Least squares adjustment analysis indicate that the cross section should be adjusted upward by as much as 10% over the response range (1 keV - 1 MeV) in the CFRMF central spectrum. This is consistent with your measurement at 23 keV.

QUESTION: R. Peelle
Is the result you quote for the average of the source spectrum?

ANSWER: G. Knoll
Yes. An adjustment of -0.3% resulted from converting the apparent cross section over the source spectrum to the quoted value at 23 keV, using the cross section shape data of Macklin and Halperin.

QUESTION: R. Block
You have made several Sb-Be measurements, so you have some idea of how these results compare over a range of nuclei, and cross sections. Is there any systematic effect observed, such as would indicate a common bias in flux determination, detector efficiency, etc.

ANSWER: G. Knoll
There is no obvious systematic departure from our previously published fission and capture cross sections that used the same source and calibration system.

QUESTION: R. Chrien
What fraction of the total activity you observed is due to the low energy tail in your photoneutron-source spectrum?

ANSWER: G. Knoll
38% of the emitted neutrons lie in this scattered tail. Since the cross section average is rather flat across this energy range, about the same fraction of activations are due to these neutrons.

STATUS OF NEUTRON CAPTURE DATA OF ^{233}U, ^{235}U AND ^{239}Pu IN THE UNRESOLVED RESONANCE REGION

by

F. Corvi
CEC - JRC, Geel Establishment
Central Bureau for Nuclear Measurements, B-2440 Geel, Belgium

Abstract

First, the outstanding requests for σ_γ and α data of the three main fissile nuclei are briefly summarized. Then the methods employed in the last twenty years of differential α-measurements are critically discussed. They can be classified into three groups: a) systems measuring simultaneously absorption radiation and fissions with two separate detectors; b) systems in which a large fraction of fission and capture γ-rays are identified by means of prompt or delayed coincidences with a high efficiency fission detecting apparatus; c) systems consisting of a γ-ray detector only, in which capture and fissions are distinguished by some special feature of the radiation emitted. Advantages and drawbacks of the various techniques are discussed, particularly in connection with all sources of systematic errors. Measurements of alpha in the unresolved resonance region are separately reviewed for each of the three fissile isotopes.

I. Introduction

An accurate knowledge of the fast neutron capture cross section and/or alpha for the fissile isotope burned in a fast breeder reactor is needed for calculating many quantities. Between them most important is the breeding ratio and then the effective multiplication factor, the build-up of higher actinides, the Doppler temperature coefficients, the reactor fuel inventory and the flux distribution across the reactor.

The isotope ^{239}Pu plays of course a leading role because of the advanced stage of development of the fast breeder based on the ^{238}U-^{239}Pu cycle. Bobkov et al.[1] have calculate for example that, for a target accuracy of $\pm$ 2% in the breeding ratio, the required accuracy on α of ^{239}Pu is $\pm$ 2.5% below 100 keV, $\pm$ 6.5% between 100 and 800 keV and $\pm$ 41% above.

A similar level of accuracy will be needed for ^{233}U should a reactor based on the ^{232}Th-^{233}U cycle be seriously considered. Finally, ^{236}U could have an increased importance if it were chosen as a fuel for a first generation of breeders.

It is perhaps appropriate for the scope of this meeting to summarize the existing requirements relevant to our subject. This is done in Table I, where on the left the requests from the WRENDA 81/82 issue[2] are quoted and on the right those of the new NEANDC/NEACRP High Priority List[3].

Only data needs above 100 eV have been considered. The WRENDA entries have been condensed by merging capture and alpha and by considering only Priority 1 requests. Moreover, if several entries exist for equal or largely overlapping energy ranges, only one request is listed, extended to the largest range and with the highest required accuracy.

One of the tasks of the present meeting, and more particularly of the concerned working groups, is probably to get an idea of the accuracies attained so far and of the work which is left to be done.

Already ten years ago, Sowerby and Konshin[4] in the conclusions of their review on α-data for ^{239}Pu have stated that although the required accuracy was not achieved, further measurements should not be performed unless the techniques to be used are either new or significantly improved. Similar statements were repeated more recently by other evaluators[5,6]. Therefore, in this paper the emphasis has been put on a critical review of the experimental methods used so far. The present analysis will be restricted to differential measurements in the energy region above 100 eV.

II. Review of the experimental methods

Although the quantity normally required by the users is the neutron capture cross section σ_γ, experimental difficulties usually prevent its direct determination with reasonable accuracy. It has therefore become customary to refer to $\alpha = \sigma_\gamma / \sigma_f$, the capture-to-fission ratio, since this quantity can be directly measured. The capture cross section, which is derived from the product of α and σ_f, has very much the same uncertainty as α since σ_f is usually known with higher precision. It should be noted here that, when reference is made to an average over a given neutron energy interval, the quantity α is defined as $\alpha = \langle\sigma_\gamma\rangle / \langle\sigma_f\rangle$ rather than average α.

In the present review we shall restrict ourselves to direct α determinations, i.e. methods involving the measurement of both absorption γ-rays and fissions, since they constitute the main bulk of the experimental data. Other methods, such as α determination from η measurements and σ_γ determination by subtracting from the total all other partial cross sections, have provided useful results only at rather low energy, say up to 100 eV or at most 1000 eV. Shell transmission techniques, in which the problem consists of distinguishing between transmitted and fission neutrons, have produced rather inaccurate data. Finally, the activation technique cannot be applied to differential measurements because in all three cases the product nuclei have extremely long half lives.

Looking back over the last 20 years of α-measurements, one is impressed by the amount of activity which has taken place since the early

days, activity which had its peak at the time of the Helsinki Conference in 1970, when six papers on this subject were presented.

The pressing needs of the reactor community, and more particularly those of the fast breeder project, hastened the development of a number of techniques to cope with what is one of the hardest experimental problems of the whole neutron cross sections field. However, because of the difficulty of the task and because the development took place even before some of the present capture measurement techniques were firmly established, not all results are equally reliable. Therefore the large discrepancies of some data sets should not be a matter of surprise. Now the time is ripe to critically re-examine the past experience in order to select the most reliable methods both in view of evaluating the existing data and of setting the characteristics of future measurements.

II A - Absorption methods

Most methods consist of measuring simultaneously absorption radiation and fissions with two separate detectors. These systems have in common the lack of any attempt to distinguish between capture and fission γ-rays in the absorption channel. With the assumption of negligible multiple scattering and self-screening corrections, as is the case for thin samples (typically samples of thickness 10^{-3} atoms/barn or less in the region above 100 eV), the quantity α for a given neutron energy can be expressed as:

$$\alpha = \frac{\sigma_\gamma}{\sigma_f} = \frac{a(N_\gamma/N_f)-1}{b - c\,(N_\gamma/N_f)} \qquad (1)$$

where N_γ and N_f are the number of counts at that energy in the absorption detector and in the fission detector, respectively, and a, b, c are instrumental constants. A nice property of α is that Eq. (1) still holds at low neutron energies, where samples are usually no longer thin, provided the ratio σ_n/σ_T between the scattering and the total cross-section is small or α is constant. This allows normalization of the data at thermal neutron energy or in the region immediately above, where α is well known, or in well-resolved resonances. These normalizing procedures are currently used for determining the instrumental constants. If the fission detector is insensitive to γ-rays, as is true in the majority of cases, then c = 0 and Eq. (1) can be written:

$$\alpha + B = A \cdot (N_\gamma/N_f) \qquad (2)$$

It can be shown that $B = \epsilon_{\gamma f}/\epsilon_{\gamma c}$, where $\epsilon_{\gamma f}$ and $\epsilon_{\gamma c}$ are the efficiencies of the absorption apparatus for detecting fission and capture events, respectively. The absolute value of the constant B which varies between 0.6 and 2.5 in this kind of experiment acts as a figure of merit since the relative error in α is proportional to $(\alpha + B)/\alpha$. In fact, without considering the uncertainties in A and B, we have

$$\frac{\delta\alpha}{\alpha} = \frac{\alpha + B}{\alpha} \cdot \frac{N_f}{N_\gamma}\,\delta\left(\frac{N_\gamma}{N_f}\right) \qquad (3)$$

The larger the value of B, the less accurate is the α-determination; Eq.(3) shows also that the error in measuring α increases as its absolute value decreases. Another factor influencing the precision of the measurement is the accuracy with which B, and of course also A, are determined: that's why the normalization of the data is so important.

The γ-ray detector. The characteristics of the γ-ray detectors to be used in α measurements do not differ from those employed in the determination of radiative capture in non-fissile nuclei. Also here an absolute must is that the detector efficiency be independent of the shape of the γ-ray spectrum, i.e. of the mode in which the compound nucleus decays to its ground state. This is important for two reasons: first, the spin and parity distribution of the compound states formed after neutron interaction changes with energy, since the role of p-wave (and eventually also d-wave) capture increases with energy. Second, α-data are often normalized to resonances of a given spin or to the thermal or low energy region, where the spin distribution is different. It has been known[7] for a long time that both the shape of the capture γ-ray spectrum and its multiplicity depend to some extent on the initial spin and parity. On the contrary, little is known about prompt fission γ-rays and their possible variation with neutron energy, spin, parity or even K quantum number. However, a detector insensitive to spectrum shape is also in this case a guarantee of reliable data.

Three types of detectors have an efficiency which is to a large extent spectrum independent: they are large liquid scintillators, Moxon-Rae detectors and total energy detectors. A description of them can be found for example in ref.[8] In the following only their use in α-measurements and some special problems are treated.

Large liquid scintillators [9-13] with volumes ranging from 400 l to 3000 l have been used. The lowest limit of the volume would generally speaking be too small to ensure 100% efficiency for capture detection, because an 8 MeV γ-ray has an absorption mean length of about 41 cm in a liquid scintillator. However, they are probably adequate for measurements in the actinide region where capture γ-ray spectra are soft. What is more worrying is the fact that some authors[11,12] measure the coincidence rate between the two halves of the tank, which are optically separated, in order to reduce the background. This procedure can give rise to a systematic error since the efficiency for detecting coincidences depends on the multiplicity of the capture cascade. In fact, neglecting angular correlation and assuming 100% detection efficiency for any γ-ray, the probability $C(J,\pi)$ of not detecting a capture when working in a coincidence mode can be expressed as:

$$C(J,\pi) = \sum_{n=1}^{\infty} \frac{1}{2^{n-1}} P_n(J,\pi) \qquad (4)$$

where $P_n(J,\pi)$ is the frequency distribution of n-step cascades from an initial state of spin J and parity π. To obtain an estimate of $C(J,\pi)$, the values of P_n could be deduced from simulations of the γ-decay. Alternatively, $C(J,\pi)$ could be obtained by comparing coincidences to single rates in isolated resonances of known spin. The effect just mentioned will decrease with the increasing number of the optically separated sections. For example, Beer and Käppeler[13] count all coincidences between at least two of the four quarters of their 800 l tank: in this case, $C(J,\pi)$ will be half the value given by Eq. (4).

Different types of Moxon-Rae detectors[14-16] have been used, but they have gradually been replaced by the so-called "total energy detectors"[17,19]. These are liquid scintillators in which the proportionality of the efficiency to the total γ-ray energy is achieved by convenient weighting of the pulses according to their amplitude. A compromise between these two different detector concepts is the system developed by Czirr[20, 21], consisting of a 1 l deuterated hexabenzene based liquid scintillator having a 10 g/cm^2 graphite absorber in front, in order to obtain a linear weighting function. Linear weighting eliminates the need for corrections for pulse summing in the detector and greatly simplifies the data acquisition procedure. When applying Moxon-Rae or total energy detectors to α measurements, it should be realized that it is not known whether the average prompt fission γ-ray energy stays constant with neutron energy. The only possible way of checking it is to also measure α_γ by comparing the fissile capture rate to that of a known standard, e.g. gold. This has been done in ref.[19] and the result was found in agreement within 2% with the normalization to the thermal α value. We can then conclude that the fission γ-ray energy is reasonably constant in the region below 100 keV.

Detectors other than the three types just mentioned, such as NaI(Tl)[22] or stilbene crystals,[23-26] have also been extensively employed in α-measurements. These detectors are small, thus improving signal-to-background ratio, and by a proper choice of the amplitude window they can minimize the constant B. Bolotskii et al.[25] have measured α from the resonance region up to 10 keV using stilbene crystals and two different windows, one from 0.4 to 0.7 MeV and the other from 0.7 to 2.5 MeV. They have shown that the two data sets corresponding to the two windows agree within the errors. However, these errors are rather large, typically 10 to 15%, and moreover the 10 keV upper limit corresponds only to aboutone third p-wave contribution.

The systematic errors due to the sensitivity of these detectors to changes in spectrum shape are probably not large but they are very difficult to assess. In fact, we don't see any serious experimental justification for using such detectors in place of those previously described. We therefore suggest that these measurements should either be disregarded or given a low weight.

The fission detector. All three main products of a fission reaction, i.e. fission fragments, fast neutrons and prompt gamma radiation, have been used to detect fission. Fast neutrons have usually been detected by an organic liquid scintillator[14,17] in which pulses from recoil protons are selected by pulse shape discrimination (PSD). A gamma ray-to-neutron suppression ratio of 10^{-3} or better can normally be achieved, thus satisfying the condition required by Eq. (2). In a number of cases the same apparatus is used to detect absorption γ-rays and fast neutrons which are separated by PSD: this technique has been applied by some Russian groups[22-26] to stilbene crystals and by Czirr[20,21] to a C_6D_6 scintillator. In this case the detector is hydrogen-free in order to reduce the sensitivity of the gamma channel to scattered and fission neutrons, and pulses from deuteron recoils are observed.

An uncertainty associated with the use of fast neutron detectors is the possible variation of $\bar{\nu}$ with neutron energy. Moreover, if the detectors subtend a small solid angle at the sample, their efficiency can change with fission fragment angular distribution.

A large liquid scintillator[27,28] has also been used to separate absorption from fission by means of a two-bias technique: a low bias, typically 2 to 3 MeV, allows detection of fission and capture events, while a high bias, typically 11 MeV, selects only a certain fraction of fission events with very high γ-ray energy emission. Beer and Käppeler[13] have used the same technique but with a more sophisticated procedure which allowed a considerable decrease of the high bias in order to reduce statistical uncertainties.

In all these cases Eq.(1) to Eq. (3) remain valid, the only difference being that N_γ and N_f are now the counts in the absorption channel and in the fission channel, respectively, of the same detector. Fission fragment detection by semiconductors has been used by Farrell et al.[15] in an underground nuclear explosion. The case of fission chambers will be treated in the next sub-section.

II B - Coincidence methods

The only effective way of separating fission and capture γ-rays measured in the absorption detector consists of operating it in coincidence with a high efficiency fission detector. As the efficiency approaches unity, all fission events are detected and capture is directly obtained by measuring the anticoincidence rate. In practice, experimental difficulties have kept the efficiency well below one, so that corrections due to the undetected fissions must be applied to the data. The Eq.(2) is still valid but is more conveniently rewritten in the following way:

$$a = \frac{\epsilon_{\gamma f}}{\epsilon_{\gamma c}} \cdot \left[\epsilon_f \cdot \frac{AC}{CO} - (1 - \epsilon_f) \right] \qquad (5)$$

where AC and CO are the anticoincidence and the coincidence rates (background subtracted) and ϵ_f is the efficiency for detecting fission. The figure of merit B, which is now expressed as $B = (1-\epsilon_f)(\epsilon_{\gamma f}/\epsilon_{\gamma c})$ shows explicitly the advantage of reaching a high fission efficiency. Basically two kinds of experimental set-up have been used to implement the method:

1) Large liquid scintillators loaded with gadolinium or cadmium.

This technique has been first applied by Hopkins and Diven[29] and later on by Weston et al.[30,31] and Kononov et al.[32,33] It consists essentially of a delayed coincidence technique, where capture and fission events are identified by detecting fission neutrons after their moderation and absorption in the poisoning element, typically gadolinium or cadmium. More specifically, each detected γ-ray starts a gate which stays open for several μs, waiting for a fission pulse to be detected.

In Kononov's set-up the absorber-converter was not dissolved in the whole tank but rather concentrated in a central cavity filled with an aqueous solution of cadmium nitrate. This type of construction allowed the use of a high concentration of Cd nuclei (H : Cd = 100 : 1) thereby decreasing the lifetime of neutrons. In this way the length of the gate could be reduced from 32 to 6 μs.

The expression for a is more complicated than Eq. (5) because of the

need to correct for random delayed coincidences due to background pulses. The problem of random coincidences limits the use of such an apparatus to neutron sources with not too high instantaneous rates, i.e. typically pulsed Van de Graaff accelerators. With this type of system , a value of B = 0.14 has been achieved by Weston et al.[30] and B = 0.3 by Kononov et al.[32]

2) Fission chambers. Parallel plate fission chambers containing gram quantities of fissile material have been used in conjunction with a large liquid scintillator tank. Weston et al.[30] have used a chamber containing 5 g of ^{235}U as a 1 mg/cm^2 coating on both sides of 10 cm diameter magnesium plates. It consisted of 29 plates spaced about 1 mm, and had an internal pressure of 5 atm. The chamber had a 70% efficiency for detecting fission fragments, which corresponds to a figure of merit B ~ 0.30. The Oak Ridge group has applied this technique first to measurements with a Van de Graaff accelerator and later to Linac measurements, since it does not suffer the limitations of the previous method. The most complete and recent of these experiments is the work of Gwin et al.[11], covering the energy range from thermal to 200 keV for ^{235}U and ^{239}Pu. Having a chamber with a high content of fissile material is a much harder problem for ^{239}Pu than for ^{235}U because of the higher specific α-activity. Gwin et al. were able to fit 1.4 g of ^{239}Pu in the chamber with a detection efficiency ϵ_f = [0.425.] Since the ratio $\epsilon_{\gamma f}/\epsilon_{\gamma c}$ was [1.27], the figure of merit was B = 0.73, a value which is not much better than that of the experiments under II A. Recently, Corvi et al.[19] have used a fission chamber containing 2.5 g of ^{235}U in conjunction with four fluorocarbon based liquid scintillators with pulse height weighting. The average thickness of coatings was 1.16 mg/cm^2 and the chamber efficiency was found to be ϵ_f ~ 0.84 yielding a constant B ~ 0.14. A peculiar feature of this experiment was that data were normalized to gold neutron capture as well as to thermal and resonance α-values, and all normalizations agreed within 3%.

Very recently, Weston et al.[34] have tried to measure α in ^{233}U using a high efficiency fission chamber and total energy detectors of C_6F_6 type. The parallel plate chamber had fissile deposits 300 μg/cm^2 thick for a total of 0.24 g of ^{233}U. The data have not yet been analyzed but they appear to suffer from a very high background.

To summarize, this technique of α-measurement seems to us the cleanest one and most free from systematic errors. Values of B as low as 0.14 have been obtained in the case of ^{235}U. It has also been shown[18] that using total energy detectors the signal-to-background ratio is a factor of 2 to 10 better than in the case of a large tank, when this is not operated in a coincidence mode. However, with such small quantities of material the background is a problem and extreme care should be taken in its determination. Moreover a fission chamber for ^{233}U and ^{239}Pu having high efficiency and containing gram quantities of fissile isotope has still to be built.

II C - Gamma-ray based methods

Under this heading are included methods which exploit some particular feature of the capture and fission γ-ray spectra in order to discriminate between the two reactions. In such cases B can become negligible.

1) Method based on low-energy γ-rays. An attempt was made in Geel[35] to extend the low-level population method of spin assignment to α-measurements.

In fact a high resolution Ge(Li) spectrum of low energy γ-rays following neutron absorption in ^{235}U exhibits many resolved transitions, a few belonging to capture and the majority to fission. A ratio between the intensities of the two types of transitions can be a measure of α provided one can reasonably assume that these intensities are proportional to the average capture or fission rate. This is generally not the case, at least for capture, if the spin distribution of the compound states changes. For the same reason, normalization of the data is a problem. The capture transition at 642 keV de-exciting a $J^{\pi} = 2^{-}$ level in ^{236}U, and two fission γ-rays at 352 and 1280 keV were used to derive relative α-values in the range 86 eV to 31.6 keV. Calculations show that the uncertainty associated with the different initial spin distributions is ± 4% at 30 keV and less than ± 2% below 10 keV.

2) Multiplicity method. The average number of prompt γ-rays emitted per fission in ^{235}U is approximately [36,37] 6 - 7 as compared to 3 - 4 emitted in radiative capture. Muradyan et al.[38,39] have exploited such a difference to separate capture from fission by using a multiplicity spectrometer. Their detector[39], which is called Romashka-3 (romashka in Russian means daisy) consists of a 4π assembly of NaI(Tl) crystals divided into 46 sections giving a total volume of 100 ℓ: one-, two-, n-fold coincidences between detector sections are counted as a function of neutron energy. To increase the fission multiplicity, a ^{10}B + wax mixture having the double function of converter and shielding is placed around the sample so that scattered and fission neutrons are moderated and then absorbed in boron. Plotting the frequency distribution as a function of the coincidence level n, two peaks are apparent, the lowest one belonging to capture and the other to fission. The two peaks are not completely separated; for example in the "capture" channel, which covers the range $2 \leq n \leq 5$, the ratio of the efficiencies for detecting fission and capture is B = 0.22. However, the fission contribution in the overlapping region can be accurately measured by making use of the ^{10}B pulses which are delayed compared to those of prompt γ-rays, thus allowing another way of distinguishing a certain fraction of fissions from capture events. The method is absolute, since the detection efficiency for both reactions is almost 100% and Muradyan was able to reproduce the thermal α value within 1%. Background is also small, typically 9% at 10 keV, so that the authors claim a 5% accuracy in the α-values obtained for ^{235}U in the range 0.1 to 30 keV. In the last two years the detector has been improved, particularly with regard to the separation between capture and fission events.[40]

This method undoubtedly constitutes a major breakthrough in the field of α-measurements and should be applied to other isotopes. Also, the feasibility of extending such a multisection idea to a large liquid scintillator tank should be investigated, since this has a prompt neutron background which is much less than that of a NaI(Tl) assembly.[41] However, the possible dependence of the efficiency in the capture channel on the initial spin should be investigated in detail.

Table II summarises the various experimental methods used, which are ordered for increasing values of the figure of merit B. The experiments are classified with ABS, CO or GAM according to whether they belong to the types described in IIA, IIB or IIC, respectively.

III. Review of the Data

III A - The ^{233}U data

Basically only two data sets exist for the energy region above 100 eV:

1) the data of Weston et al.[9], based on an ORNL-RPI collaboration, covering the energy range up to 2000 eV. The experimental arrangement used consisted of a multiplate fission chamber containing about 1 g of fissile material placed inside a large scintillator tank. Capture and fission cross sections were normalized to low energy total cross section data of Pattenden and Harvey[44], assuming a constant value of 12.5 b for the scattering cross section. In ref.[9] data are presented under the form of resonance integrals over 0.25 lethargy intervals up to 1223 eV. Point values up to 2000 eV are given in the corresponding EXFOR library[45];

2) the data of Hopkins and Diven[29], obtained with the gadolinium loaded scintillator tank. The measurement is absolute and nine points covering the range from 30 to 1000 keV are given.

It is clear that the available data are obviously insufficient, in particular no experimental values exist in the very important (for a fast breeder) energy region between 2 and 30 keV. A measurement in a range encompassing this region and providing a good overlap with the two previous data sets is highly desirable. It should be noted that, due to the low value of α for ^{233}U (typically $\alpha \sim 0.1$ in the 30 to 100 keV region), it is particularly important in this case to apply methods with low values of the figure of merit B.

III B - The ^{235}U data

A rather extensive bibliography on α of ^{235}U including 17 papers published before 1977 can be found in the evaluation of Konshin et al.[6] After that date, three works have appeared, namely those of Beer et al.[13], Muradyan et al.[38] and Corvi et al.[19] From this material, eight works have been selected to give the best picture of the present status of α data for ^{235}U in the unresolved region. Although this kind of selection is never completely objective, it has been carried out with the following criteria:

1) A group of papers published at different dates and reporting on similar measurements performed in the same laboratory are represented by the last published paper, having checked that the methods used are the same throughout and that the data sets supersede or include the previous ones;

2) following the arguments developed in Section 2, priority has been given to measurements of the coincidence type (CO) and of the γ-ray type (GAM). These experiments are rather numerous in the case of ^{235}U, mainly because of the much lower specific activity of this isotope compared to the other two.

3) the only experiments not belonging to the previous types are those of Czirr et al.[21], and Beer et al.[13] The measurement of Czirr[21] was done with a hydrogen-free detector insensitive to changes in spectrum shape and having a constant B not too high. The measurement of Beer et al.[13] which utilizes a large liquid scintillato

and a low-high bias technique, has the advantage of being absolute, though the extrapolation of the pulse height spectra to the low energy end contributes the main systematic uncertainty.

The main parameters of the eight selected experiments are listed in Table III: they include information on the type of measurement, the γ-ray and fission detector, the sample thickness, the time-of-flight resolution, the energy range investigated, the region where data are normalized, the constant B and the total estimated uncertainty at about 30 keV. For those measurements which are not absolute, normalization of the data may be a problem in the case of ^{235}U. In fact, in order to determine the two constants of Eq. (2), or Eq. (5), two different α values are needed. Now, in the energy region below 1 eV, α has a low and rather constant value, contrary to what happens in ^{239}Pu. On the other hand, normalizing the data in the region of isolated resonances is also subject to uncertainties because different evaluations[50-53] give quite discrepant values for resonance parameters.

In ref. [19] some of these difficulties were avoided by independently measuring the efficiency ϵ_f of the fission chamber so that only one constant remained to be determined.

Using the data available in 1978 Konshin et al.[6] have produced an evaluation based on a method which allows for correlations between the partial errors of different experiments. To do so, the total experimental error on α was divided into 13 independent partial errors. Their conclusion was that, if the correlations are correctly taken into account, the relative error on α in the region up to 80 keV ranges from 5 to 8.5% increasing to 12% at 1 MeV. However, the recent measurement of Muradyan et al.[38] contradicts this finding, their data being on average about 16% lower than those of Gwin et al.[11], a work which plays an outstanding role in any evaluation of α below 100 keV. Similarly, the data of Corvi et al.[19] are about 10% lower than those of ref.[11] These three experiments use the most up-to-date techniques, in particular the work of Muradyan is based on an original method which is largely uncorrelated with previous ones. Whatever the true values are, it seems reasonable to conclude that the errors given by Konshin et al.[6] are too optimistic. This is probably due to the fact that even the most sophisticated techniques of error analysis cannot cope with a situation in which many systematic errors exist whose magnitude is difficult to assess.

In Fig. 1 six data sets of works quoted in Table III are plotted: also the maximum relative spread of these values $\Delta\alpha_{max}/\bar{\alpha}$ is plotted in the lower part of the figure. This is not intended to be an error value but rather an indicator of the level of agreement of the data.

III C - The ^{239}Pu data

A very accurate and comprehensive review of α measurements for ^{239}Pu in the range 100 eV to 1 MeV was published ten years ago by Sowerby and Konshin[4]. All the measurements performed up to that date were critically examined and a thorough discussion of all possible sources of systematic errors was given. Most of the points raised are still valid today and the review is recommended to those who want to get a more complete picture of the problems connected with α measurements.

The paper also included an evaluation providing recommended values with an estimated accuracy of ± 10% below 30 keV, increasing to ± 20% at 100 keV and ± 30% at 1 MeV. For the purpose of the present review, such an evaluation will be considered the summary of all data published prior to December 1971, which will not be examined here again. The main parameters of the experiments which were performed later are summarized in Table IV.

The works have been grouped according to the laboratory and the neutron facility used. The first two measurements listed were performed at ORELA with different detector arrangements. In ref.[18] the two techniques were discussed and compared and the results were found to agree within a few per cent over the whole energy range, in spite of the fact that the estimated errors for both data sets ranged from 10 to 25% above 10 keV. According to the authors, the close agreement above 40 keV could be fortuitous.

The next three works were performed by Kononov and his co-workers at the pulsed Van de Graaff accelerator of the Obninsk Institute. The measurements were carried out using the time-of-flight technique and a continuous spectrum of neutrons from thick targets in the energy range 10-80 keV, and using monoenergetic neutrons with a resolution between 10 and 30 keV in the region 100 keV - 1 MeV. The data are summarized in ref.[46] where 52 data points covering the range from 9.4 keV to 1 MeV are given. Also listed are the $\bar{\sigma}_f$ and $\bar{\sigma}_\gamma$ values averaged over decade energy intervals between 10 and 80 keV, from which $\alpha = \bar{\sigma}_\gamma / \bar{\sigma}_f$ can be deduced. The estimated total uncertainty, resulting from a composition of statistical and systematic errors, is 21.5% in the 10 - 20 keV interval and 12% between 20 and 80 keV increasing to 20% at 500 keV and 36% at 1 MeV.

With the exception of the work of Bergman et al.[16], all other measurements listed in Table IV were performed with a stilbene crystal as a γ-ray detector. Therefore, for the reasons explained in subsection IIA, such measurements should receive limited attention. The experiment of Bergman et al.[16] on the other hand was performed with a lead slowing down spectrometer, a technique which is apparently not very reliable as it has often produced discrepant results.

The data of Weston et al.[17], Gwin et al.[11], Poletaev et al.[46] and the evaluated values of Sowerby and Konshin[4] are plotted in Fig. 2 over the range 100 eV to 1 MeV. Also, the maximum relative spread of these values $\Delta\alpha_{max}/\alpha$ is plotted in the lower part of the figure for the region up to 100 keV.

Several evaluations of α for ^{239}Pu have been performed in recent years[5,6,47-48]. One is that of Kononov and Poletaev[5], giving values of α in the format of decade energy intervals from 0.1 keV to 1 MeV with an estimated accuracy of 8 - 12%. More recently, Konshin et al.[6] have evaluated α of ^{239}Pu with the same method used for ^{235}U. They concluded that α is known with an accuracy of 6% in the region from 0.1 to 20 keV, 8 - 10% from 20 to 100 keV, 13 - 17% from 100 to 800 keV and 25% from 0.8 to 1 MeV. For the reasons discussed in sub-section III B, these accuracies should be taken with some caution.

IV. Conclusions and Recommendations

The present status of the α data for the three main fissile nuclei, as described in Section III, shows clearly the need for more measurements. First of all, in the case of ^{233}U there is absence of data in the important

region from 2 keV to 30 keV. Moreover no new measurement has been performed since 1968.

Contrarily, three new measurements[13,19,38] of α for ^{235}U have been performed in the last 3 - 4 years. The surprising thing about them is that two[19,38] give α values which are on the average 10% to 16% lower than those of Gwin[11], work which was generally recognized as the best measurement in the region below 100 keV. This finding should warn the evaluators to be more conservative in estimating the attained accuracy level. These considerations should also apply to the more important case of ^{239}Pu, for which no new measurement has been performed in the last five years. In fact, new measurements are needed in order to make sure that the discrepancies which recently appeared in α of ^{235}U do not show up for ^{239}Pu as well.

As to the techniques which should be employed in future measurements, it is suggested here that the use of absorption methods as defined and described in Sub-section II A should be discontinued. Conversely, effort should be concentrated on coincidence methods (Sub-section II B) and γ-ray based methods (Sub-section II C). In particular the multiplicity method recently proposed by Muradyan[38] seems to yield great promise.

Acknowledgements

The author is indebted to Mr. R. Buyl for preparing the graphs.

References

1. Y.G. Bobkov, L.T. Pyatnitskaya, L.N. Usachev, Nuclear Constants, Vol. 10, Obninsk (INDC (CCP)-33L).

2. WRENDA 81/82, N. Dayday Editor, INDC(SEC)-78/URSF.

3. Revised NEANDC/NEACRP High Priority List, to be published, and J.L. Rowlands, private communication.

4. M.G. Sowerby and V.A. Konshin, At. Energy Rev. 10, 453 (1972).

5. V.N. Kononov and E.D. Poletaev, Atomn. Energ., 45, 3, 187 (1978).

6. V.A. Konshin, E.S. Sukhovitskij and V.F. Zharkov, INDC (CCP)-132/LV (1979).

7. C. Coceva, F. Corvi, P. Giacobbe and G. Carraro, Nucl. Phys. A117, 586 (1968).

8. R.E. Chrien, Proc. Int. Conf. on Nuclear Cross Sections and Technology, Washington, 1975, Vol. I, 139.

9. L.W. Weston, R. Gwin and G. de Saussure, R.R. Fullwood and R.W. Hockenbury, Nucl. Sci. Eng. 34, 1 (1968).

10. R.B. Perez, G. de Saussure, E.G. Silver, R.W. Ingle and H. Weaver, Nucl. Sci. Eng. 52, 46 (1973).

11. R. Gwin, E.G. Silver, R.W. Ingle and H. Weaver, Nucl. Sci. Eng. 59, 79 (1976).

12. V.N. Kononov et al., Atomn. Energ. 30, 362 (1971).

13. H. Beer and F. Käppeler, Phys. Rev. C, 20, 1, 201 (1979).

14. M.G. Schomberg, M.G. Sowerby, D.A. Boyce, K.J. Murray and D.L. Sutton, Proc. Int. Conf. on Nuclear Data for Reactors, Helsinki, 1970, IAEA 1, 315.

15. J.A. Farrell, G.F. Auchampaugh, M.S. Moore and P.A. Seeger, ibidem, 1, 543.

16. A.A. Bergman, A.N. Medvedev, A.E. Samsonov and V.A. Tolstikov, Atomn.Energ. 39, 4, 291 (1975).

17. L.W. Weston and J.H. Todd, ORNL-4800, p. 4 (1972).

18. R. Gwin, L.W. Weston, J.H. Todd, R.W. Ingle and H. Weaver, Proc. Int. Conf. on Nuclear Cross Sections and Technology, Washington, 1975, vol. 2, p. 627.

19. F. Corvi, L. Calabretta, M. Merla, T. van der Veen and M.S. Moore, contribution to the present meeting.

20. J.B. Czirr, Nucl. Instr. Meth. 72, 23 (1969).

21. J.B. Czirr and J.S. Lindsey, Nucl. Sci. Eng. 41, 56 (1970).

22. F.N. Belyaev, K.G. Ignat'ev, S.I. Sukhoruchkin, S.P. Borovlev, V.V. Pavlov, M.V. Polozov and A.N. Soldatov, Proc. Int. Conf. on Nuclear Data for Reactors, Helsinki, 1970, IAEA, vol. 1, 339.

23. V.G. Dvukhsherstnov, Y.A. Kazanskii, V.M. Furmanov, and V.L. Petrov, Atomn. Energ. 37, 2, 131 (1974).

24. P.E. Vorotnikov, V.A. Vukolov, E.A. Koltypin, Y.D.Molchanov, G.B. Yankov, Proc. Second All-Union Conf. on Neutron Physics (1974), part 4, 42.

25. Y.V. Ryabov, Atomn. Energ. 41, 1, 45 (1976).

26. V.P. Bolotskii, M.V. Polozov, A.N. Soldatov and S.J. Sukhoruchkin, Atomn. Energ. 42, 3, 218 (1977).

27. R. Gwin, L.W. Weston, G. de Saussure, R.W. Ingle, J.H. Todd, F.E. Gillespie, R.W. Hockenbury and R.C. Block, Nucl. Sci. Eng. 40, 306 (1970).

28. E.G. Silver, G. de Saussure, R.B. Perez and R.W. Ingle, Proc. Third Conf. on Neutron Cross Sections and Technology, Oak Ridge, 1971, vol.II, p. 728.

29. J.C. Hopkins and B.C. Diven, Nucl. Sci. Eng. 12, 169 (1962).

30. L.W. Weston, G. de Saussure and R. Gwin, Nucl. Sci. Eng. 20, 80 (1964).

31. A. Lottin, L.W. Weston, G. de Saussure and J.H. Todd, Rep. ANL 7320,22 (1966).

32. V.N. Kononov, E.D. Poletaev, Y.S. Prokopoets, A.A. Metlev and Y.Y. Staviss-kii, Atomn. Energ. 32, 1, 85 (1972).

33. V.N. Kononov, E.D. Poletaev and B.D. Yurlov, Atomn. Energ. 38, 2, 82 (1975).

34. L.W. Weston, private communication.

35. F. Corvi and P. Giacobbe, Proc. Int. Conf. on Nuclear Cross Sections and Technology, Washington, 1975, NBS SP 425, Vol. II, p. 599.

36. V.V. Verbinski, H. Weber and R.E. Sund, Physics and Chemistry of Fission (IAEA, Vienna, 1969), p. 929.

37. F. Pleasonton, R.L. Ferguson and H.W. Schmitt, Phys. Rev. C6, 1023.

38. G.V. Muradyan, Y.G. Schepkin, Y.V. Adamchuk, M.A. Voskanyan, Proc. Int. Conf. on Nuclear Cross Sections for Technology, Knoxville, 1979 (NBS SP 594), p. 488.

39. G.V. Muradyan, Proc. Int. Conf. on Nuclear Cross Sections for Technology, Knoxville, 1979 (NBS SP 594), p. 488.

40. G.V. Muradyan, private communication.

41. F.H. Froehner, Proc. Int. Conf. on Neutron Physics and Nuclear Data, Harwell, 1978, p. 268, Fig. 7.

42. J.C. Hopkins and B.C. Diven, Nucl. Sci. Eng. 12, 169 (1962).

43. M.G. Schomberg, M.G. Sowerby, F.W. Evans, Fast Reactor Physics (Proc. Symp. Karlsruhe, 1967) 1, IAEA, Vienna 289 (1968).

44. N.J. Pattenden and J.A. Harvey, Nucl. Sci. Eng. 17, 404 (1963)

45. EXFOR Library, Entry 12336, Sub-entry 005 (1976)

46. E.D. Poletaev, Candidate's Dissertation, Dimitrovgrad, NIIAR (1976); EXFOR Library, Entry 40412, Sub-entry 001-008 (1977)

47. B. Goel, Report KFK-2386 (1977)

48. S. Igarasi, Report JAERI-1261 (1979)

49. A. Lottin et al., Proc. Conf. Fast Critical Experiments and their analysis, ANL-7320, p. 22, Argonne National Laboratory (1966)

50. J. Krebs, G. Le Cocq, J.P. L'Heriteau and P. Ribon, Proc. 3rd Conf. on Neutron Cross Sections and Technology, Knoxville, Vol. 1, p. 410 (1971)

51. G. de Saussure, R.B. Perez and W. Kolar, Report ORNL-TM-3707 (1972)

52. J.R. Smith and R.C. Young, Report ANCR-1044 (1971)

53. Y. Kikuchi, A. Asami and T. Koshida, Proc. Cons. Meeting on Uranium and Plutonium Resonance Parameters, IAEA, Vienna, 1981, to be published.

Table I - Summary of Requests for σ_γ or α Measurements above 100 eV for ^{233}U, ^{235}U and ^{239}Pu

Isotope	WRENDA 81/82 LIST - 1st PRIORITY ONLY				NEANDC/NEACRP HIGH-PRIORITY LIST 1982			
	Energy Range		Accuracy	Requestors	Energy Range		Accuracy	Requestors
	LL	UL			LL	UL		
^{233}U	100 eV	1.50 MeV	5 % to 8 %	USA, GER	100 eV	1 MeV	20 %	GER
	1 MeV	20 MeV	10 %	JAP	1 MeV	10 MeV	10 %	JAP
^{235}U	100 eV	1.0 MeV	5 %	FR, CCP				
	1 MeV	10 MeV	5 % to 10 %	JAP, FR	1 MeV	20 MeV	5 % to 10 %	JAP
^{239}Pu	100 eV	1.0 KeV	7 %	USA, CCP	100 eV	600 KeV	6 %	USA
	1.0 KeV	50 KeV	4 %	USA, CCP, FR				
	50 KeV	3 MeV	5 %	USA, CCP, FR				
	3 MeV	10 MeV	10 %	USA				

Table II - Comparison of experimental arrangements, listed for increasing value of the figure of merit B

r.	Authors	Year	Exp. Type	Gamma-ray Detector	Fission Detector	Sample	ϵ_f	B
1	Hopkins et al.[42]	1962	CO	Large Liquid Scint.	Loaded with Cd	^{233}U, ^{235}U, ^{239}Pu	0.90	0.10
2	Weston et al.[30]	1964	CO	Large Liquid Scint.	Loaded with Gd	^{235}U	0.875 ± 0.007	0.145 ± 0.013
3	Corvi et al.[19]	1982	CO	C_6F_6 weighted	Fission Chamber	^{235}U	0.836 ± 0.008	0.145 ± 0.010
4	Muradyan et al.[38]	1979	GAM	NaI(Tl) assembly with 46 sections		^{235}U		0.22
5	Weston et al.[9]	1968	CO	Large Liquid Scint.	Fission Chamber	^{235}U	0.78	0.25
6	Kononov et al.[32]	1972	CO	400 l liquid scint. loaded with Cd		^{233}U, ^{239}Pu	0.704 ± 0.007	0.3
7	Weston et al.[30]	1964	CO	Large Liquid Scint.	Fission Chamber	^{235}U	0.70	0.34
8	Gwin et al.[11]	1976	CO	Large Liquid Scint.	Fission Chamber	^{235}U, ^{239}Pu	0.43 - 0.49	0.58 - 0.73
9	Bolotskii et al.[26]	1977	ABS	Stilbene crystals with PSD		^{239}Pu	-	0.62
10	Czirr et al.[21]	1970	ABS	C_6D_6 lin. weighted with PSD		^{239}Pu	-	0.86
11	Beer et al.[13]	1979	ABS	800 l. liquid scint. high-low bias		^{235}U	-	~ 1
12	Farrell et al. [15]	1970	ABS	Solid state Moxon-Rae	Solid state	^{239}Pu	-	1.27 ± 0.08
13	Ryabov[25]	1976	ABS	Stilbene crystal with PSD		^{239}Pu	-	1.5
14	Schomberg et al.[14]	1970	ABS	Moxon-Rae	Liquid Scint. with PSD	^{239}Pu	-	1.5 ± 0.2
15	Schomberg et al.[43]	1968	ABS	Moxon-Rae	Liquid Scint. with PSD	^{239}Pu	-	2.5

Table III: A selection of measurements of α for ^{235}U in the fast energy region.

Nb	Authors	Year	Meas. Type	Gamma-ray Detector	Fission Detector	Sample Thick. (at/b)	ToF resol.	Energy Range	Normal. Region	B	Total Error at ~ 30 keV (%)
1	Hopkins et al.[29]	1962	CO	Gd Loaded Large Liquid Scintill.		~ 0.024	-	30keV-1MeV	absolute	0.10	9.6
2	Lottin et al.[49]	1966	CO	Gd Loaded Large Liquid Scintill.		~ 0.022	0.2 ns/m	17keV-600keV	absolute	0.14	8.6
3	Czirr et al. [21]	1970	ABS	C_6D_6 linear. weighted with PSD		$0.4 \cdot 10^{-3}$	50 ns/m	48eV-28keV	resonance	0.86	11.6
4	Gwin et al. [11]	1976	CO	3000ℓ Liqu.Scint.	Fission chamber	$1.4 \cdot 10^{-4}$	1 ns/m	0.02-200keV	0.02-0.4eV	0.58	7.3
5	Poletaev et al.[46]	1976	CO	Cd Loaded Large Liquid Scintill.		$3.6 \cdot 10^{-3}$	18 ns/m	10keV-1MeV	absolute	0.3	10.3
6	Beer et al. [13]	1979	ABS	Large Liq. Scintill. with Low and High Bias		$0.6 \cdot 10^{-3}$	2 ns/m	10keV-500keV	absolute	1	8.0
7	Muradyan et al.[38]	1979	GAM	46 Section NaI(Tl)		$0.8 \cdot 10^{-3}$	2 ns/m	100eV-30keV	absolute	0.22	5.0
8	Corvi et al. [19]	1982	CO	$4xC_6F_6$ weighted	Fission chamber	$1.0 \cdot 10^{-4}$	0.5 ns/m	2keV-85keV	thermal and keV	0.14	7.0

Table IV - Summary of experimental parameters for recent measurements of α in ^{239}Pu

Nr.	Authors	Year	Exp. Type	Gamma-ray Detector	Fission Detector	Sample Thickness (at/b)	ToF resol.	Energy Range	Normal.Region	B
1	Weston et al.[17]	1972	ABS	C_6F_6 weighted	Liquid Scint. with PSD	$6.0 \cdot 10^{-4}$	~ 2 ns/m	0.02eV-200keV	0.02eV-0.4eV	
2	Gwin et al.[11]	1976	CO	30001 liquid Scint.	Fission Chamber	$0.8 \cdot 10^{-4}$	1 ns/m	0.02eV-200keV	0.02eV-0.4eV	0.73
3	Kononov et al.[32]	1972	CO	400 l Cd loaded Liq. Scintillator		$2.9 \cdot 10^{-3}$	18 ns/m	10keV-1MeV	Absolute	0.3
4	Kononov et al.[33]	1975	CO	" " " " "		" "	"	10keV-80keV	"	"
5	Poletaev et al.[46]	1976	CO	" " " " "		" "	"	10keV-1MeV	"	"
6	Dvukhsherstnov et al.[23]	1974	ABS	Stilbene Crystal with PSD		$5 \cdot 10^{-3}$	-	2, 24.5, 140keV	Thermal	
7	Bergman et al.[16]	1976	ABS	Moxon-Rae prop. counter	Fission Chamber	$1.7 \cdot 10^{-4}$	Lead slowing down	0.2keV-30keV	Thermal	
8	Ryabov[25]	1976	ABS	Stilbene Crystal with PSD		$2.1 \cdot 10^{-3}$	230 ns/m	0.007eV-12keV	Resonance	1.5
9	Bolotskii et al.[26]	1977	ABS	Stilbene Crystals with PSD		$\sim 1.6 \cdot 10^{-3}$	16 ns/m	0.1keV-30keV	Resonance	0.62

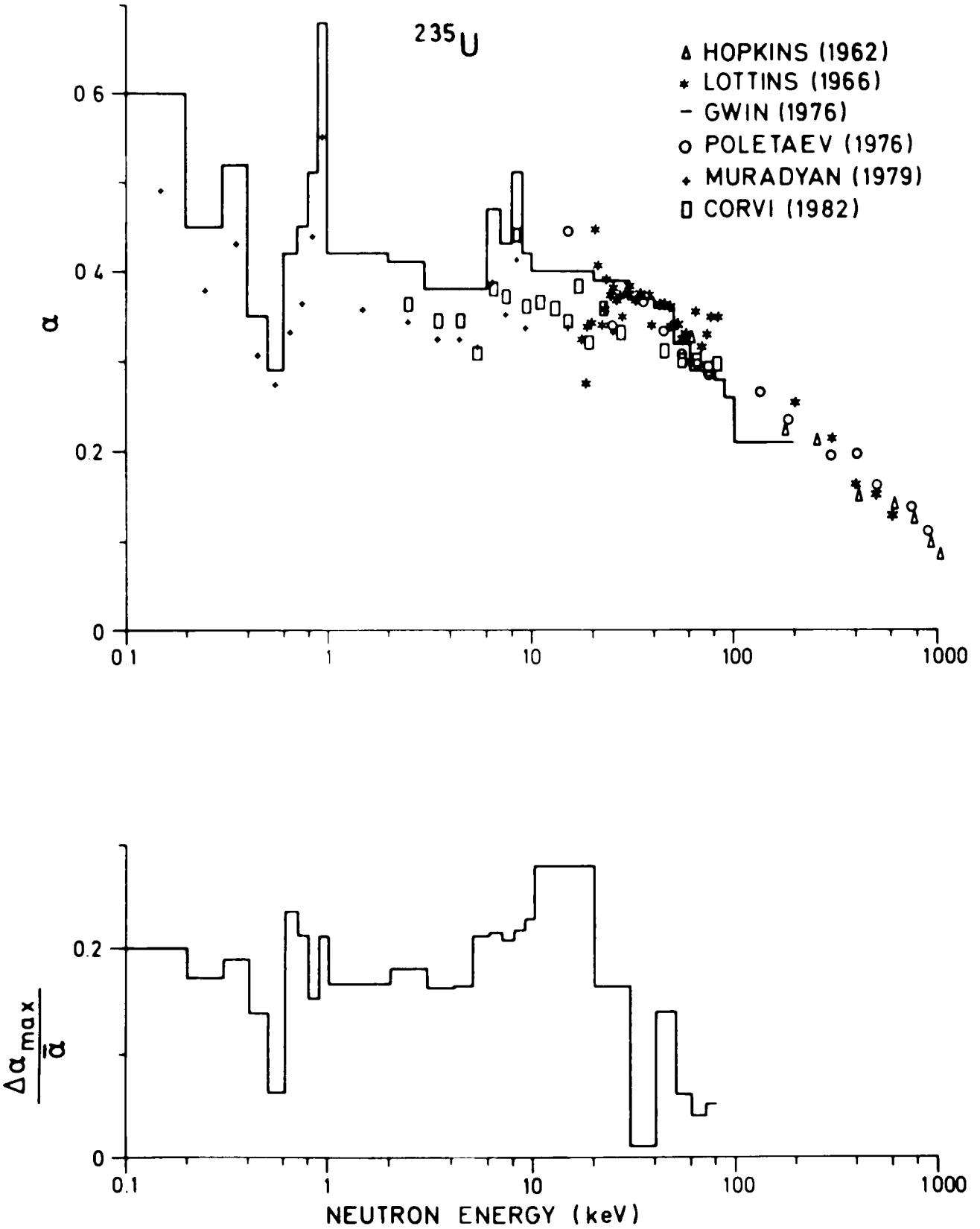

Fig. 1 - Comparison of six selected measurements of α for ^{235}U. In the lower part of the graph the maximum relative spread $\Delta\alpha_{max}/\bar{\alpha}$ is given.

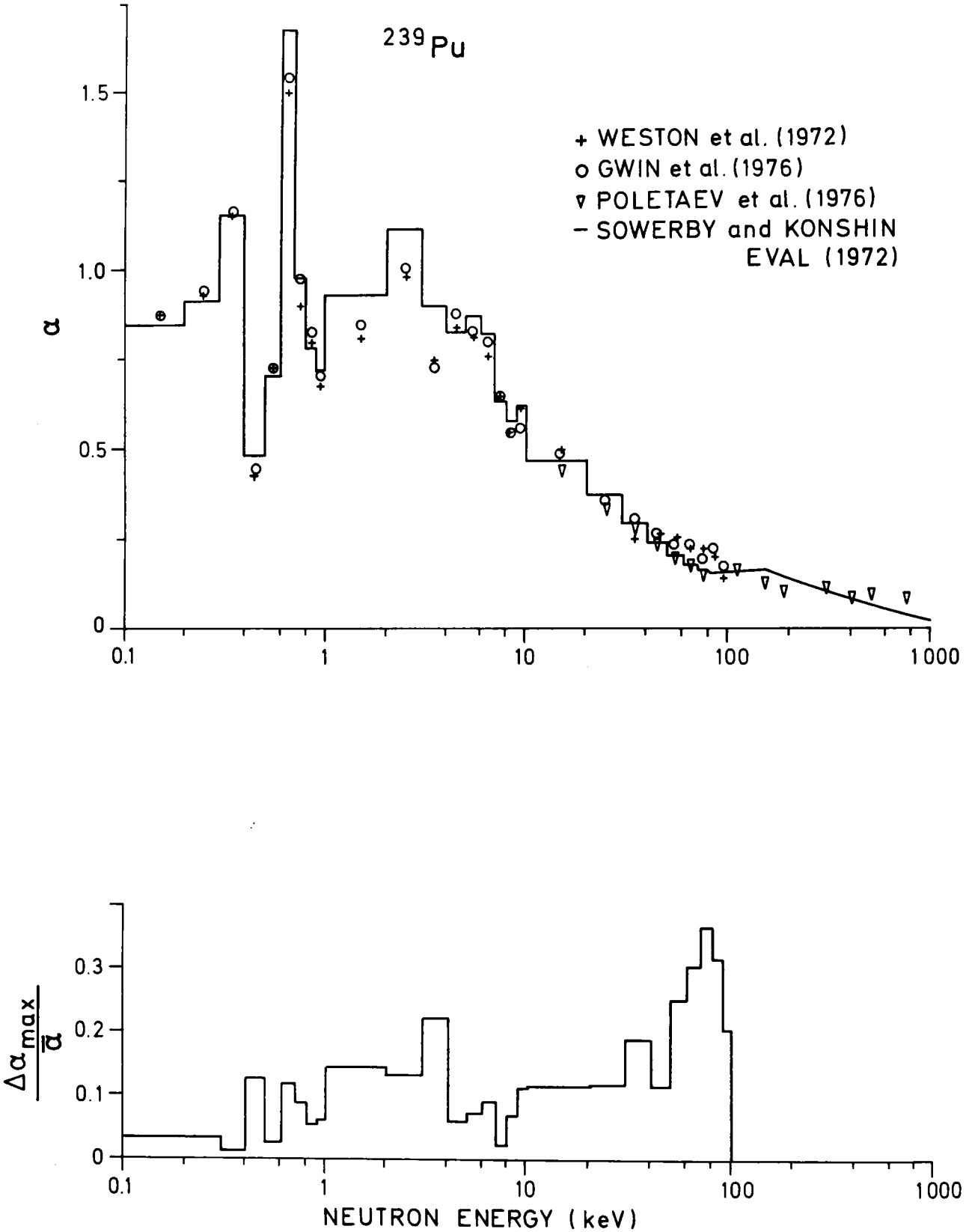

Fig. 2 - Comparison of three selected data sets appeared after 1972 with the evaluation of Sowerby and Kowshin of α for ^{239}Pu. In the lower part of the graph the maximum relative spread of the data $\Delta\alpha_{max}/\bar{\alpha}$ is plotted for the "interval" region up to 100 keV.

Discussion

QUESTION: R. Block
I was impressed with Muradyan's Romashlea multiplicity detector when I saw it in 1976. It should be very useful for cross section measurements. Is anyone (in the 'Western' world) planning on using such a detector for cross section measurements?

ANSWER: F. Corvi
I don't believe there is any new detector of this type under construction for neutron work. However, large multi-sectional detectors based always on NaI(Tl) (crystal balls) have been built for heavy-ion physics (e. g. at Heidelberg and ORNL).

FAST NEUTRON CAPTURE IN ACTINIDE ISOTOPES: RECENT RESULTS FROM KARLSRUHE

K. Wisshak, F. Käppeler, G. Reffo[+], and F. Fabbri[+]

Kernforschungszentrum Karlsruhe GmbH
Institut für Angewandte Kernphysik
P.O.B. 3640, D-7500 Karlsruhe
Federal Republic of Germany

ABSTRACT

Capture gamma-ray spectra of ^{241}Am, ^{240}Pu, ^{242}Pu ^{238}U and ^{197}Au were calculated in the framework of the spherical optical model and the statistical model. These spectra were used to correct experimental data for the capture cross sections of ^{240,242}Pu and ^{241}Am from relative measurements using a Moxon Rae-detector with graphite converter and ^{197}Au as well as ^{238}U as standards. This correction is required to take into account that the detector efficiency is not exactly proportional to gamma-ray energy. The resulting correction factors proved to be negligible for measurements relative to ^{238}U, whereas they are ∿3 % if gold is used as a standard.

The capture cross section of ^{243}Am has been measured in the energy range 10-250 keV using kinematically collimated neutrons from the ^{7}Li(p,n) and T(p,n) reaction. The samples are positioned at flight paths of 5-7 cm and gold was used as a standard. Capture events were detected by two Moxon-Rae detectors with graphite and bismuth-graphite converters shielded by 0.5 - 2 cm of lead. Fission events were detected by a NE213 liquid scintillator. The present status of the experiment and some preliminary results will be presented.

INTRODUCTION

Moxon Rae detectors in connection with kinematically collimated neutrons from (p,n) reactions and the use of very short flight paths proved to be a suited method to measure capture cross sections of highly radioactive actinides in the keV range.

[+]Comitato Nazionale per l'Energia Nucleare, Bologna, Italy

Measurements have been performed for ^{240,242}Pu and ^{241}Am using ^{197}Au and ^{238}U as standards[1,2,3]. Very recently, this series has been completed by investigating a sample of ^{243}Am. One of the largest systematic uncertainties in these measurements is due to the fact that the efficiency of a Moxon-Rae detector deviates slightly from the ideal shape (which increases linearly with gamma-ray energy). In the first part of the present paper we describe the evaluation of the respective correction factors which turned out to be of the order of 3 % if gold is used as a standard. In the second part we report on a measurement of the capture cross section of ^{243}Am which is presently underway. The strong radiation background up to ∿350 keV gamma-ray energy from the decay of ^{239}Np makes this experiment rather difficult and up to now no data are published for this isotope in the keV range.

EFFICIENCY CORRECTION OF PREVIOUS CAPTURE CROSS SECTION MEASUREMENTS ON ^{240,242} Pu AND ^{241}Am.

Correction of deviations of the Moxon-Rae efficiency from the ideal shape requires knowledge of two quantities: (i) the shape of the capture gamma-ray spectrum of sample and reference sample and (ii) the shape of the efficiency curve for the particular converter material. Then the respective correction factors can be calculated according to the formula given in Ref. 4 (this conference).

The capture gamma-ray spectra were calculated in the framework of the statistical model and the optical model. A detailed description of the method is given in Refs. 5,6,7 and the present results will be published in Ref. 8. The model parameters have been determined from model-guided systematics and from analyses of available experimental information on total, elastic and inelastic cross sections and on neutron resonances. In the calculation of capture gamma-ray spectra each gamma-ray story is followed starting from the decay of the compound system down to the ground state. A maximum multiplicity of 7 was sufficient to account for more than 99 % of the total capture cross section. All experimental information on level schemes and gamma-ray branchings was explicitely used as input in the calculations. In addition to the capture gamma-ray spectra the capture- and total cross sections as well as gamma-ray strength functions and total radiation widths were calculated for all isotopes to check the reliability of input parameters. The spectra obtained are shown in Fig. 1. As they vary slightly with neutron energy, only averages over the results at 10, 40 and 100 keV are given.

In the lower left corner of Fig. 1 two possible shapes for the efficiency of a Moxon-Rae detector with graphite converter are plotted. The dashed one is an eye guide curve to the experi-

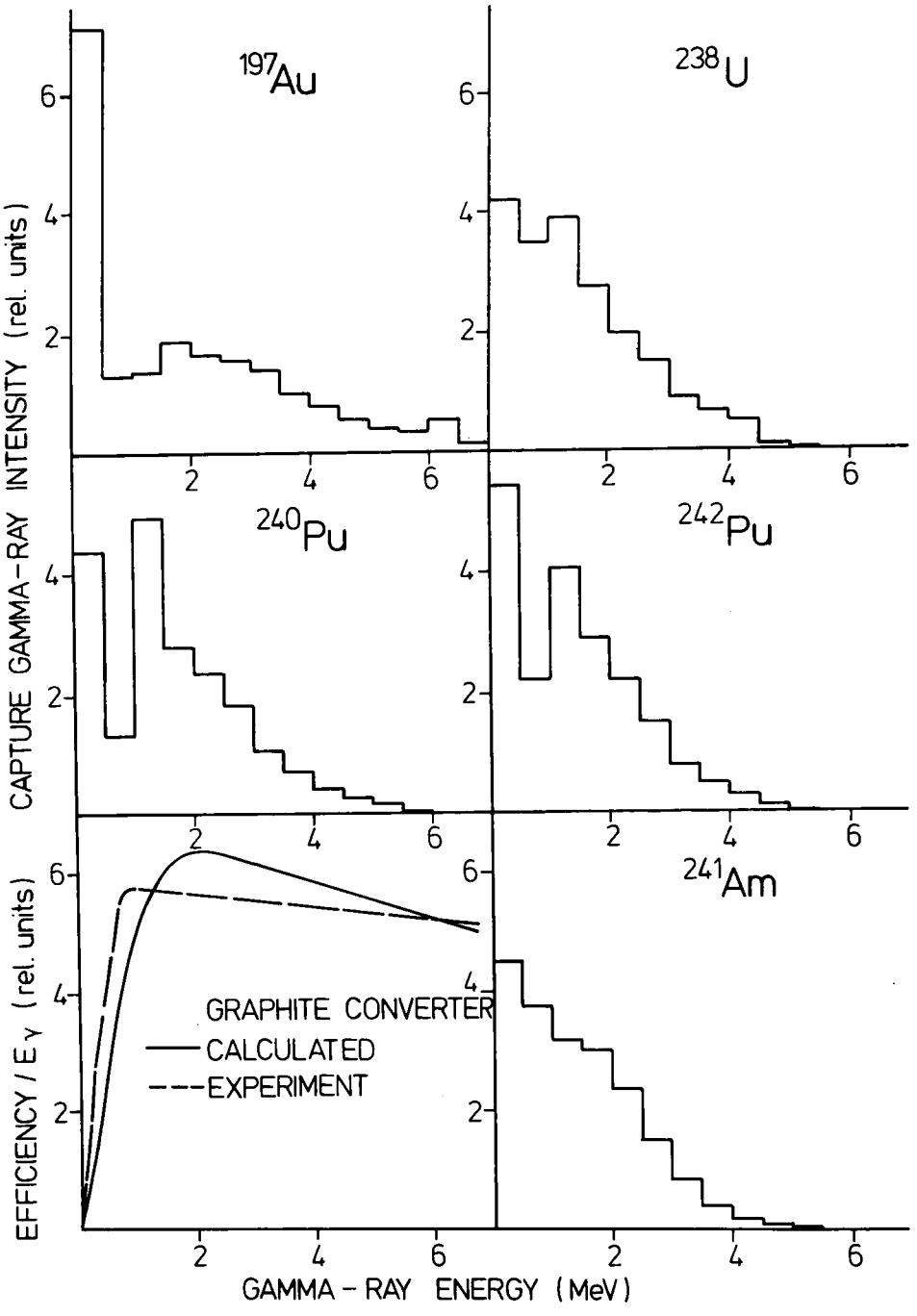

Fig. 1 Capture gamma-ray spectra for keV neutron capture in ^{197}Au, ^{238}U ^{240}Pu, ^{242} Pu and ^{241}Am. In the lower left corner relative shapes of the efficiency of a Moxon Rae detector with graphite converter are given (for details see text).

mental results of Macklin et al. [9], Moxon and Rae [10] and our own measurements as discussed in Ref. 11. The solid curve was calculated theoretically by Malik and Majkrzak[12]. With the information of Fig. 1 the correction factors were calculated in the same way as discussed for ^{56}Fe and ^{58,60}Ni in Ref. 4. The results are given in Table I. On the average, cross section ratios measured relative to a ^{197}Au standard have to be corrected by 3 % whereas no correction is required for measurements using the ^{238}U standard.

TABLE I Correction factors K for our previous capture cross section ratios ^{240,242}Pu and ^{241}Am versus ^{197}Au and ^{238}U

Cross section ratio	Correction factor K
^{240}Pu/^{197}Au	0.966
^{240}Pu/^{238}U	0.994
^{242}Pu/^{197}Au	0.973
^{242}Pu/^{238}U	1.002
^{238}U/^{197}Au	0.972
^{241}Am/^{197}Au	0.973

In Table II averaged and corrected values for the capture cross sections of ^{240,242}Pu and ^{241}Am are given. They were obtained by correcting the experimental ratios of Refs. 1,2,3 according to Table I and by converting them to absolute values using the evaluated cross sections for gold from ENDF/B-V and for ^{238}U from KEDAK-4. The results of five complementary measurements for each isotope using different neutron spectra, flight paths or cross section standards are finally averaged by weighting each data point according to its uncertainty. The uncertainties of the averaged cross sections are dominated by systematic effects which are slightly larger for ^{242}Pu because of the sizeable correction for isotopic impurities in this particular sample. The values given in Table II are estimated from the systematic uncertainties of individual runs and are not evaluated by a covariance analysis. They are determined from the experimental ratios and do not include the uncertainty of the standard cross section.

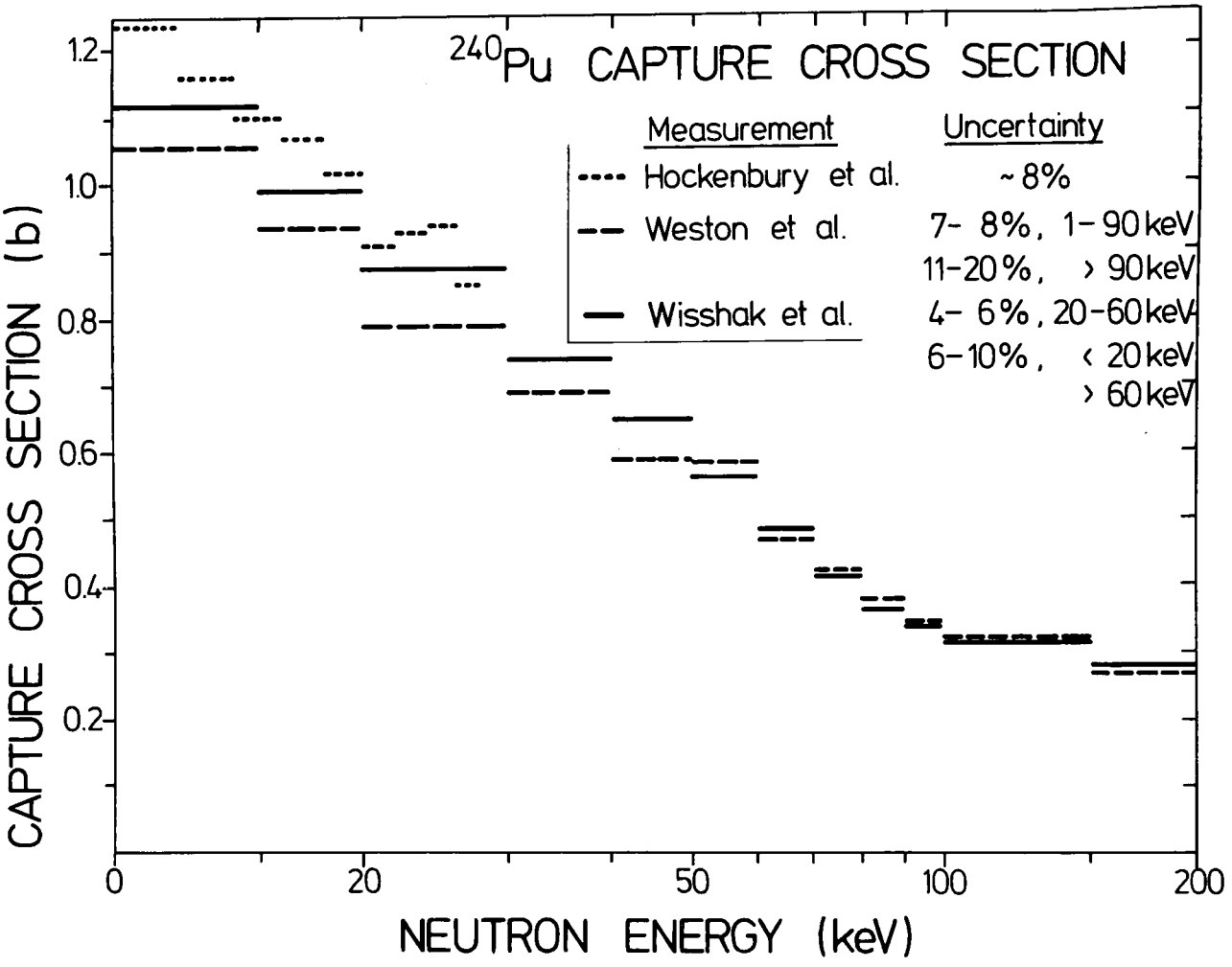

Fig. 2 Corrected and averaged values for the capture cross section of ^{240}Pu, previously published in Refs. 1 and 2. Comparison is made to the results of other authors.

In Fig. 2 a comparison is made for the capture cross section of ^{240}Pu with the two other data sets available in literature[13,14], which both agree quite well within the quoted uncertainties.

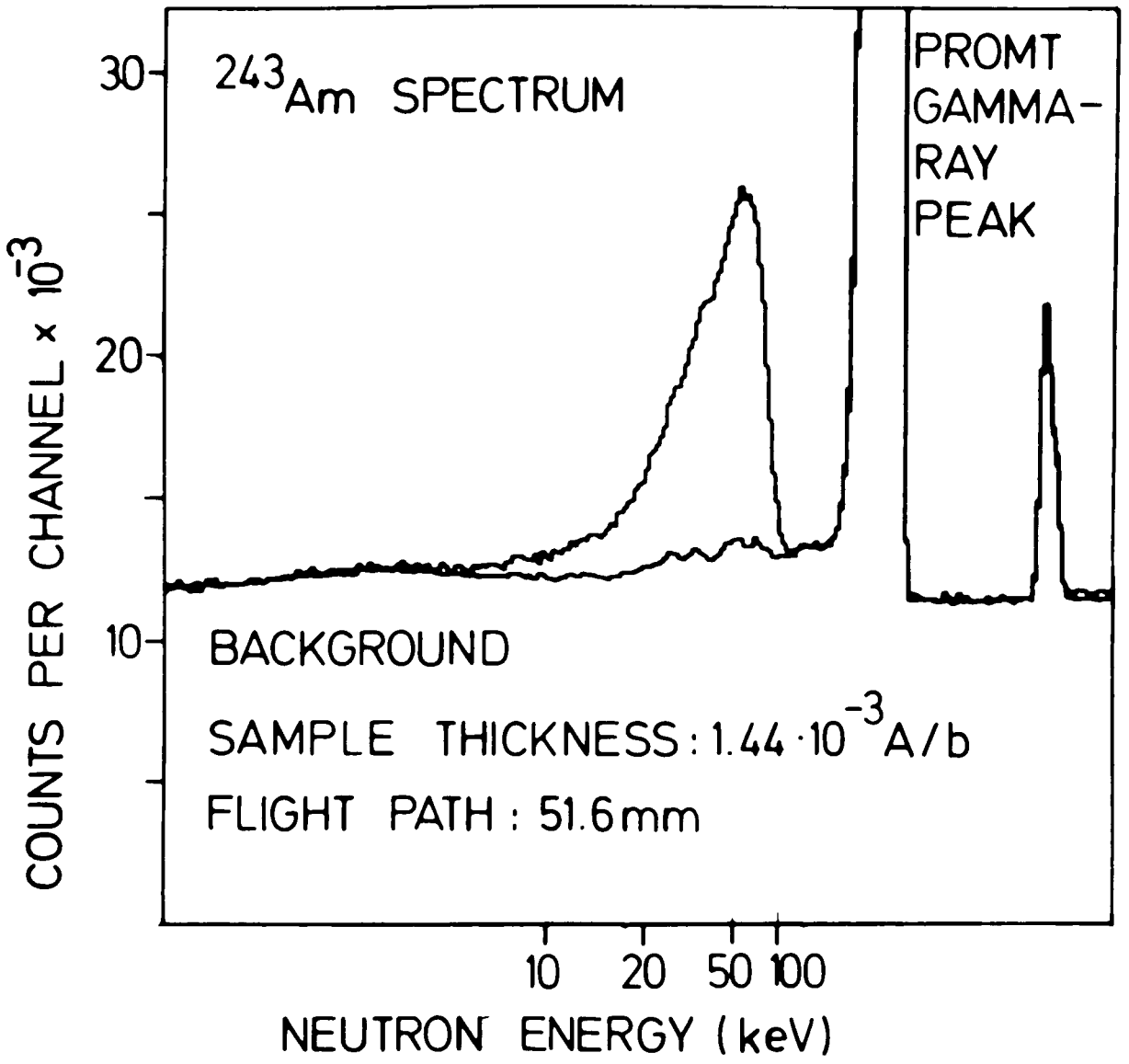

Fig. 3 Experimental TOF spectrum of the ^{243}Am sample measured by a Moxon-Rae detector with bismuth-graphite converter and with a lead shielding of 0.7 cm. A constant value has been added to the background spectrum measured with the graphite sample to account for the time-independent background from the ^{243}Am decay (the peak right of the gamma peak is caused by a diaphragm in front of the Li-target).

TABLE III Parameters for the Individual Measurements of the Neutron Capture Cross Section Ratio $\sigma_\gamma(^{243}Am)/\sigma_\gamma(^{197}Au)$

Run	Lead Shielding of Moxon-Rae Detectors (cm)	Flight Path (mm)	Neutron Energy Range (keV)
1	2.0	52	10-90
2	1.0	52	10-90
3	0.7	52	10-90
4	0.5	52	10-90
5	2.0	71	10-90
6	1.0	71	10-90
7	2.0	65	50-250
8	1.0	65	50-250

capture gamma-ray spectra as discussed above. A preliminary estimate of the capture cross section shows that it is about 20 % lower than for ^{241}Am. The fission cross section appears to be very small in the energy range from 40-80 keV, the observed effect is compatible with a cross section of the order of 10 mb.

REFERENCES

1) K. WISSHAK and F. KÄPPELER, Nucl. Sci. Eng. 66, 363 (1978).
2) K. WISSHAK and F. KÄPPELER, Nucl. Sci. Eng. 69, 39 (1979).
3) K. WISSHAK and F. KÄPPELER, Nucl. Sci. Eng. 76, 148 (1980).
4) K. WISSHAK, F. KÄPPELER, G. REFFO and F. FABBRI, contribution to this conference.
5) G. REFFO, F. FABBRI, K. WISSHAK and F. KÄPPELER, accepted for publication in Nucl. Sci. Eng.
6) K. WISSHAK, J. WICKENHAUSER, F. KÄPPELER, G. REFFO and F. FABBRI, accepted for publication in Nucl. Sci. Eng.
7) G. REFFO and F. FABBRI, contribution to this conference.
8) G. REFFO, F. FABBRI, K. WISSHAK and F. KÄPPELER, submitted for publication to Nucl. Sci. Eng.
9) R.L. MACKLIN, J.H. GIBBONS and T. INADA, Nucl. Phys. 43, (1963) 353.
10) M.C. MOXON and E.R. RAE, Nucl. Instr. Meth. 24 (1963) 445.
11) K. WISSHAK and F. KÄPPELER, Nucl. Sci. Eng. 77 (1981) 58.

12) S.S. MALIK and C.F. MAJKRZAK, Nucl. Instr. Meth. 130 (1975) 443
13) R.W. HOCKENBURY, W.R. MOYER, and R.C. BLOCK, Nucl. Sci. Eng. 49 (1972) 153
14) L.W. WESTON and J.H. TODD, Nucl. Sci. Eng. 63 (1977) 143.

Discussion

QUESTION: R. Anderl
How do your recent measurements for $^{243}Am(n,\gamma)$ compare with ENDF/B-V?

ANSWER: K. Wisshak
The capture cross section of ^{243}Am given in ENDF/B-V is about a factor of two smaller than the cross section of ^{241}Am in the KeV range. We find only a difference of ~ 20-30% between both cross sections, so there is a large discrepancy between ENDF/B-V based on very preliminary results.

NOTE: A. B. Smith made the comment after the question/answer time that for ENDF/B-V the $^{243}Am(n,\gamma)$ cross section is $\approx$ 50% smaller than that for $^{241}Am(n,\gamma)$ at 100 keV and 200 keV.

QUESTION: R. Peelle
How do you confirm the energy scale in these experiments? Do you use absorbers (e.g. Al) and look for resonance dips?

ANSWER: K. Wissak
We have measured resolved resonances from structural materials with the same short flight path and could reproduce the energies to ~ 1-2% around ~ 30 keV. The uncertainty in flight path measurements is converted into an uncertainty in the energy scale of all the measurements.

MEASUREMENT OF NEUTRON CAPTURE CROSS SECTION AND ALPHA OF ^{235}U FROM 2 TO 85 keV

by

F. Corvi, L. Calabretta *, M. Merla, T. van der Veen
and M.S. Moore **

CEC - JRC, Geel Establishment
Central Bureau for Nuclear Measurements, B-2440 Geel, Belgium

Abstract

The measurement was performed at the Geel linac, using a multi-plate fission chamber of known efficiency and four C_6F_6 scintillators. Two different normalizations, one based on the Au(n,γ) cross section in the keV region and the other on the thermal α value were compared and found to agree within 3%.

I. Introduction

The neutron capture cross section and alpha of ^{235}U have been extensively measured in the past with a large variety of techniques. However, in view of the inherent difficulties of such measurements, it is doubtful that the required precision of about ± 5% had been reached. Recently, Muradyan et al. [1] have measured α in the range 0.1 to 50 keV with an original technique [2], claiming a high accuracy. Their results are on average about 15% lower than the values of Gwin et al. [3].
In an effort to resolve this discrepancy a new experiment has been carried out in Geel. Although the technique used follows the main lines of those previously developed [3,4,5] in Oak Ridge, there is an important new approach: it consists of directly comparing the ^{235}U capture rate with that of Au in the keV region. This is made possible by the use of total energy detectors coupled to a fission chamber. Another important improvement is the accurate determination of the efficiency of the fission chamber performed in preliminary experiments.

II. Description of the Experiment

II.A. General lay-out. The experiment was carried out at the Geel 140 MeV electron linac equipped with the rotary target [6] for maximum power dissipation. This target consists of a mercury cooled uranium annulus which slowly rotates in a horizontal plane. Neutrons produced in uranium are moderated by the water contained in two rectangular beryllium cans 4 cm thick, placed above and below the target which is itself shielded by a copper and lead shadow bar.
In the present experiment, the linac was operated at 14 ns burst width and 800 Hz repetition frequency, yielding an average beam power of 10 kW.

---

* Bursary of the European Community

** Present address: Los Alamos National Laboratory, Los Alamos, New Mexico USA

The detector system was placed at 28.8 m from the target, on a flight path perpendicular to the moderator plane, yielding a nominal resolution of 0.5 ns/m. A vertical section of the experimental set up together with the associated electronics scheme is shown in Fig. 1: after appropriate definition with copper and lead collimators, a neutron beam of 9 cm diameter impinges on a multiplate fission chamber containing deposits of U_3O_8 enriched in ^{235}U. The γ-rays resulting from neutron absorption in the sample are detected by four C_6F_6 liquid scintillators of 10.2 cm diameter and 7.6 cm height. The whole detector system which is supported by a light aluminium frame, is kept completely unshielded. Pulses from C_6F_6 detectors were first divided into two parts according to whether in coincidence or not with fission chamber pulses. The coincident ones are due to prompt fission γ-rays while the others are associated to capture γ-rays or to γ-rays from undetected fissions or simply to background radiation. After this partition, the data were subdivided in 22 pulse height intervals covering the energy range from 0.3 to 7.7 MeV. The usual weighting procedure according to the detected pulse height was then applied to gamma pulses in order to achieve a response proportional only to the total γ-ray energy emitted. Finally, weighted time-of-flight spectra were built for coincidences and for anti-coincidences respectively. A short description of the acquisition system is given in Ref. [7].

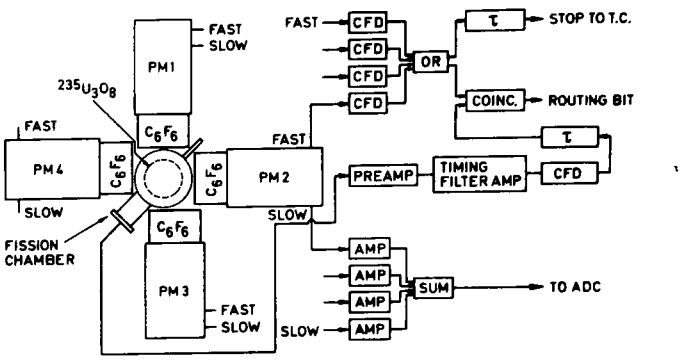

Fig. 1. Experimental set up.

II.B. The fission chamber. To achieve good discrimination between capture and fission events, the efficiency of the fission chamber should obviously be as high as possible. On the other hand, to obtain a reasonable signal-to-background ratio, a maximum amount of ^{235}U should be used. Moreover the chamber thickness should be minimized both because of time-of-flight resolution requirements and because of the small size of the γ-ray detectors. Finally, the structure of the chamber should be as light as possible to minimize γ-ray background. Our multiplate fission chamber is the result of a compromise between these largely conflicting requirements. It consists essentially of a cylindrical aluminium container of 14 cm external diameter and 10 cm height, inside which is located a stack of parallel aluminium plates with back-to-back coatings of uranium oxide prepared by electro-spraying. The chamber is operated with continuous methane flow at atmospheric pressure and its main physical characteristics are listed in Table I.
A special wiring of the plates similar to that suggested in ref. [8] was adopted in order to reduce its large electrical capacitance. Pulses from the chamber were sent via a charge sensitive pre-amplifier to a filter amplifier with differentiation and integration constants set equal to 20 ns and then to a constant fraction discriminator. Because of the small inter-plate spacing, there was no valley between alpha and fission pulses. In fact, when the chamber was working in a coincidence mode, the threshold was kept so low as to accept some 10^4 α counts/s. in order to maximize the efficiency for detection of fission fragments. When the chamber was used alone, as in the separate measurement of the fission cross

of the coincidence between pulses from the fission chamber and those from the C_6F_6 scintillators was set at 36 ns, a value which was largely sufficient since the FWHM timing resolution of the chamber was found to be about 10 ns.

II.C. Efficiency of the fission chamber. The data analysis procedure requires to know the efficiency ϵ of the chamber with high precision. For this reason, a special effort was deployed to determine this fundamental parameter as accurately as possible. For checking purposes, two independent methods were used:

1) the coincidence rate was measured between the fission chamber exposed to a thermal neutron flux, and a fast neutron detector consisting of a NE 213 liquid scintillator coupled to a pulse shape discrimination circuit. If the fast neutrons present are only produced by fissions in the chamber, then the ratio of coincidences to singles rate in the neutron detector is a measure of the efficiency of the chamber. Because of the strong angular correlation between fission neutrons and fragments, the measured efficiency depends on the angle θ between the axis of the chamber and that of the neutron detector. By simply rotating the chamber, ϵ could be measured for different values of θ: in the limiting cases $\theta = 0°$ and $\theta = 90°$ it was found $\epsilon = 0.892$ and $\epsilon = 0.791$, respectively. These data were first fitted with a function of the type $\epsilon(\theta) = a + b \cdot \cos\theta$, which was then integrated over the whole solid angle, yielding a value $\epsilon = 0.839$;

2) using the set up of Fig. 1, a run was performed at thermal neutron energy. To do so, the apparatus was brought to a 13 m flight path and appropriately shielded with lead and borated wax. As said before, the anti-coincidence counting rate consists of capture γ-rays, fission γ-rays and background. This last component is the sum of a constant background, mainly due to the activity of fission fragments, plus that produced by scattered neutrons. While the first one was measured at flight-times much longer than those of the Maxwellian peak, the second was deduced from a mock chamber run. In the range 0.02 - 0.1 eV the ^{235}U capture counting rate was estimated from a run with a gold sample and from the known thermal cross sections of ^{235}U and Au. Using the data of ref. [3], a correction was introduced which accounts for the deviation of the ^{235}U (n,γ) cross section from the 1/v behaviour. After subtraction of these contributions, the ratio r between what is left of the anti-coincidences and the coincidences can be expressed as $r = (1-\epsilon)/\epsilon$. The parameter r was calculated in the eight 10 meV intervals between 0.02 and 0.10 eV. Its average value and associated standard deviation were found to be $\bar{r} = 0.2005 \pm 0.0103$ from which an efficiency $\epsilon = 0.833 \pm 0.007$ was deduced. Since the results of the two methods are in excellent agreement, their average $\epsilon = 0.836$ was adopted with a relative standard deviation equal to 1%.

II.D. Measurement method. In order to deduce σ_γ and α, five different runs with the following experimental conditions had to be performed:

1) Main run. Sample: ^{235}U fission chamber. Detectors: C_6F_6.
2) Background run. Sample: Mock chamber. Detectors: C_6F_6.
3) Normalization run. Sample: Au. Detectors: C_6F_6.
4) Neutron flux run. Detector: ^6Li-glass.
5) Fission normalization run. Detector: ^{235}U chamber.

Runs 1 to 4 were all performed with a 2.4 cm thick aluminium filter permanently kept in the beam, in order to monitor the background in the region of the 34.8 keV "black" resonance. The most significant points of measurements and analysis are discussed in the following.

III. Background Determination

About 50% of the total measuring time was devoted to the determination of background since this is perhaps the hardest problem to be faced in this kind

of experiments. In fact the signal-to-background ratio of the anti-coincidences is typically 1 : 1 above 30 keV and becomes worse at lower energy. An absolute necessity in these cases is a measurement with a mock chamber (M.C.) i.e. an ionization chamber of identical construction as the fission chamber (F.C.) containing exactly the same amount of aluminium but no fissile isotopes on its plates. A second important point is keeping a "black resonance" filter permanently in the beam, to monitor the background at least at a given energy. Aluminium was chosen as a filter on the basis that the amount of this material present in the chamber would in any case prevent and accurate determination of α around the 5.9, 34.8 and 87.4 keV resonances. The F.C., the M.C. and the Au runs were repeated with different filter combinations, namely with an additional 2.4 cm thick slab of aluminium or with a 1 cm thick sodium metal filter in order to have "black" resonances at 87.4 and 2.85 keV, i.e. at energies encompassing the zone which we intended to cover.

The following conclusions are drawned:

i) the counting rates of the M.C. run at 87.4, 34.8 and 2.85 keV are proportional, within about 2%, to the corresponding ones of the F.C. run;

ii) the background, expressed in counts/TOF unit, varies very slowly with energy, at 2.85 keV being 84% of that at 87.4 and 34.8 keV;

iii) when normalizing at the same integrated neutron flux, the counting rate of the M.C. at 34.8 keV is 93% of that of the F.C.;

iiii) the background finally subtracted from the F.C. run consists of the M.C. spectrum, normalized to the same neutron flux, plus a constant contribution to make up for the remaining 7%;

iiiii) the uncertainties in the background determination are estimated to be ± 3.1% at 87.4 keV, ± 1% at 34.8 keV and ± 2.1% at 2.85 keV.

These correspond to uncertainties in σ_γ or α of about 6%, 3% and 10%, respectively.

Plots of the F.C. anti-coincidence spectrum and its associated background are given in Fig. 2.

As far as the coincidences are concerned, the background, which is at most 2% of the signal, has been fitted with a simple exponential function going through the black resonance points.

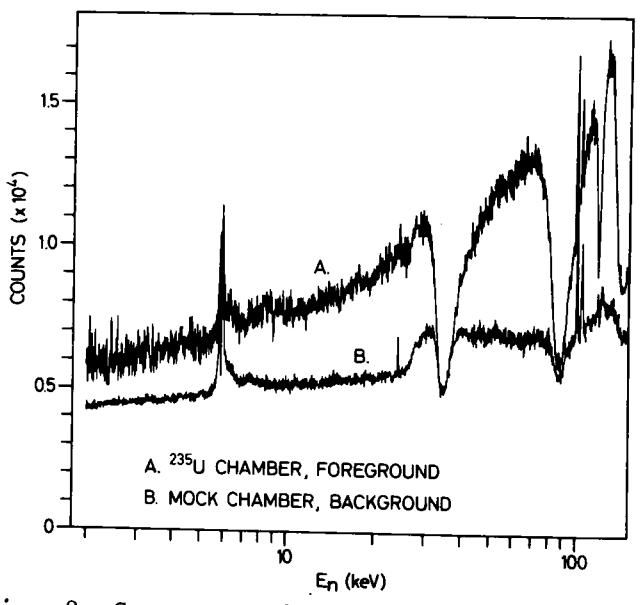

Fig. 2. Spectrum of γ-ray pulses not in coincidence with fission chamber pulses, and associated background.

IV. Normalization Procedure

The cross sections σ_γ and σ_f, and α of ^{235}U are related to the actual counts by the following expressions:

$$\sigma_\gamma = \frac{K_\gamma C_\gamma}{\Phi} = \frac{K_\gamma}{\Phi} \cdot \left[AC - \frac{1-\epsilon}{\epsilon} CO \right]; \quad \sigma_f = \frac{K_f C_F}{\Phi} = \frac{K_f}{\Phi} \frac{CO}{\epsilon} \quad ;$$

$$\alpha = \frac{K_\gamma C_\gamma}{K_f C_f} = \frac{K_\gamma}{K_f} \left[\epsilon \cdot \frac{AC}{CO} - (1-\epsilon) \right];$$

where AC and CO are the anti-coincidences and the coincidences, respectively, after removing the detector backgrounds; Φ is the neutron flux as derived from a ^{6}Li-glass run, C_γ are the counts due to capture only and C_f those due to fissions normalized to 100% efficiency. The normalization procedure described in the following consists of estimating the constants K_γ, K_f and/or their ratio.

IV.A. Normalization to the Au(n,γ) cross section. A normalization run was performed by replacing the stack of aluminium foils of the M.C. with three gold discs of 9 cm diameter and 0.2 mm thickness, spaced to reproduce the geometry of the ^{235}U deposits. The normalization constant K_γ can then be derived from the following expression:

$$K_\gamma = \mu \cdot \frac{N(Au) \cdot S_n(Au)}{N(U\ 35) \cdot S_n(U\ 35)} \cdot \left[\frac{\sigma_\gamma(Au) \cdot \Phi}{C_\gamma(Au)} \right]$$

where N indicates the nb. of atoms/cm^2 of the samples, S_n the neutron separation energy, C_γ(Au) the counts in the Au run normalized to the same integrated flux as the ^{235}U run and μ = 1.052 is a factor cumulating all calculated correction terms of Au relative to ^{235}U. It includes corrections for self-shielding, multiple scattering, extrapolation to zero bias and summing in the scintillators. Assuming a 50% error for each correction, the error on μ is 3.3%. The term in square brackets, which should be independent of neutron energy, was calculated in 2 keV intervals from 6 to 32 keV using the σ_γ(Au) values from ENDF/B-V, and its average value was taken. Since it is believed that in this way most of the uncertainty due to the strong cross section fluctuations is eliminated, a 4% uncertainty equal to that estimated [9] above 100 keV is assumed for σ_γ(Au). Finally, the error due to the weighting method is estimated to be 3%. The total error of the normalization, obtained by quadratic composition, is then 6%.

IV.B. Fission normalization. An independent measurement of σ_f from a few eV up to 100 keV was performed in a separate run using the multi-plate fission chamber in conjunction with a ^{6}Li-glass run. The data were normalized to the ENDF/B-V value [10] of the low energy fission integral $I_{7.8}^{1\,eV}$ = 241.2 b.eV after correcting for a 2% self-shielding effect. With such normalization , we get a value of the other fission integral $I_{0.1\ keV}^{1.0\ keV}$ = 1.1891·10^4 b.eV, in excellent agreement with the ENDF/B-V average: 1.1924 x 10^4. In fact, over the whole range, our average σ_f values fall within ± 2.5% of the ENDF/B-V values. The error associated with σ_f, mainly due to flux uncertainty, is estimated as 1% at 1 keV and 3% at 100 keV with logarithmic interpolation in between.

IV.C. Normalization of alpha. 1) The constant K_f was derived from the known values of σ_f, C_f and Φ by averaging in the zone from 2 to 30 keV. The normalization constant for α could then be calculated and it was found that $\kappa = K_\gamma/K_f$ = 0.876.

Neglecting the uncertainty on σ_f, the error of such a normalization is taken as equal to that of σ_γ, i.e. 6%.
2) Alpha was also normalized to the thermal value α = 0.169, using the same run employed to determine the efficiency ϵ of the F.C. The value obtained was κ = 0.895. The error of κ depends in this case on the uncertainties in ϵ and the background which are estimated to be 1% and 2% respectively. These errors produce a relative uncertainty in κ of 6.4% and 3.9%, respectively. Combining them quadratically, we get a total error of 7.5%.
3) Finally, κ could be determined also in the resonance region by comparing the values or C_γ/C_f in some rather isolated resonances to the ratios Γ_γ/Γ_f. These data are listed in Table II.: the errors given for C_γ/C_f include statistics and background uncertainties. The resonance parameters used were evaluated by Smith and Young [11], for ENDF/B-III and are still included in Version V. The value of κ was calculated for six resonances, its average and standard deviation being $\bar{\kappa}$ = 0.866 ± 0.037. The error associated to $\Delta\epsilon/\epsilon$ = 1% is in this case only 2.1% so that the total relative error is 4.8%.

IV.D. Summary. We have three different α normalizations all lying within 3.3%, i.e. in excellent agreement. We discard the third normalization because the resonance parameters used cannot be regarded as standard since they widely differ from one evaluation to the other. Then we take as a final value of κ the average of the first two: κ = 0.885 ± 0.042. The final data averaged over given intervals are listed in Table III: the $\bar{\sigma}_f$ values were taken directly from the run described in IV.B., the α values were independently calculated using the κ value given above,while $\bar{\sigma}_\gamma$ was simply derived from the product of $\bar{\sigma}_f$ and α. Although $\bar{\sigma}_\gamma$ could be directly obtained from IV.A., it was felt that the adopted procedure gives the most consistent and accurate set of data. The given errors for $\bar{\sigma}_\gamma$ and α include the uncertainty in background and F.C. efficiency plus, in the case of $\bar{\sigma}_\gamma$, a 1 to 3% flux uncertainty.The normalization error is not included.

V. Conclusion

The present α data are compared to those of Muradyan et al. [2] and Gwin et al. [3] in Fig. 3: though falling in between the two previous data sets, they are nearer to the russian values, being on average 10% lower than Gwin's data. However, on the high energy side, the present data and those of Gwin agree very well.

Acknowledgements

We are indebted to Messrs. Verdingh, Van Audenhove and Tjoonk for providing the fissile deposits and to Mr. De Bièvre for the mass spectrometry analysis of the samples.

References

1. G.V. Muradyan, Y.G. Schepkin, Y.V. Adamchuk, M.A. Voskanyan, Proc. Int. Conf. on Neutron Cross Sections for Technology, Knoxville 1979, NBS-594, p. 488.
2. G.V. Muradyan, Y.G. Schepkin, Y.V. Adamchuk, G.V. Ustroev, IAE-2634 (1976).
3. R. Gwin, E.G. Silver, R.W. Ingle and H. Weaver, Nucl. Sci. Eng. 59, 79 (1976).
4. R.B. Perez, G. de Saussure, E.G. Silver, R.W. Ingle and G.H. Weaver, Nucl. Sci. Eng. 52, 46 (1973).
5. R. Gwin, L.W. Weston, G. de Saussure, R.W. Ingle, J.H. Todd and F.E. Gillespie, Nucl. Sci. Eng. 45, 25 (1971).
6. J.M. Salomé and R. Cools, Nucl. Instr. Methods 179, 1, 13 (1981).
7. A. Brusegan, F. Corvi, G. Rohr, R. Shelley and T. van der Veen, Proc. Int. Conf. on Neutron Cross Sections for Technology, Knoxville 1979, NBS-594, p. 163.
8. L.W. Weston, G. de Saussure and R. Gwin, Nucl. Sci. Eng. 20, 80 (1964).

References (continued)

9. G.A. Wagner, Proc. Int. Conf. on Neutron Cross Sections for Technology, Knoxville 1979, NBS-594, p. 720.
10. M.F. Chat, [illegible] (NNDC-[illegible]) (1980). 11. J.R. Smith and R.C. Young, ANCR-1044 (1971).

Table I: Description of the fission chamber

Number of aluminium plates	21
Thickness of aluminium plates	30 μ
Thickness of end windows	50 μ
Filling gas	methane
Diameter of back-to-back U_3O_8 coatings	9.0 cm
Average thickness of coatings	1.18 mg/cm^2
^{235}U enrichment	99.508%
Impurities: ^{234}U	0.169%
^{236}U	0.026%
^{238}U	0.301%
Total mass of ^{235}U	2.549 g
Average plate spacing	0.2 cm

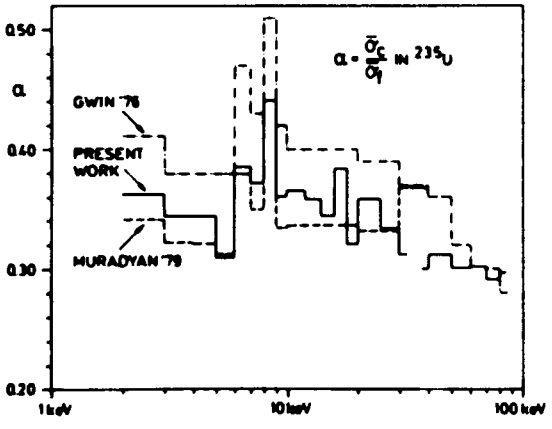

Fig.1 Comparison of α-values for different experiments.

Table II: Normalization of α in the resonance region

E_n(eV)	C_γ/C_f	relative error %	$\alpha = \Gamma_\gamma/\Gamma_f$ (ENDF/B-V)	$k = \alpha \frac{C_f}{C_\gamma}$
39.4	0.685	3.57	0.589	0.860 ± 0.031
33.5	1.489	3.07	1.377	0.925 ± 0.028
32.1	0.701	4.12	0.626	0.893 ± 0.037
21.1	1.490	3.10	1.274	0.855 ± 0.027
19.3	0.690	2.06	0.579	0.839 ± 0.017
12.4	1.521	3.51	1.255	0.825 ± 0.029

Table III : ^{235}U average neutron cross sections

ΔE_n(keV)	$\bar{\sigma}_f$ (b)	$\bar{\sigma}_\gamma$ (b)	$\alpha = \bar{\sigma}_\gamma/\sigma_f$
2.0 - 3.0	5.231 ± 0.073	1.898 ± 0.23	0.363 ± 0.045
3.0 - 4.0	4.684 ± 0.072	1.615 ± 0.16	0.345 ± 0.035
4.0 - 5.0	4.157 ± 0.069	1.435 ± 0.13	0.345 ± 0.031
5.0 - 5.8	3.772 ± 0.065	1.166 ± 0.12	0.309 ± 0.033
6.0 - 7.0	3.235 ± 0.059	1.234 ± 0.12	0.381 ± 0.036
7.0 - 8.0	3.148 ± 0.059	1.171 ± 0.09	0.372 ± 0.028
8.0 - 9.0	2.937 ± 0.057	1.296 ± 0.08	0.441 ± 0.026
9.0 - 10	3.080 ± 0.061	1.111 ± 0.070	0.361 ± 0.022
10 - 12	2.645 ± 0.054	0.967 ± 0.060	0.366 ± 0.021
12 - 14	2.581 ± 0.055	0.926 ± 0.054	0.359 ± 0.020
14 - 16	2.451 ± 0.053	0.846 ± 0.049	0.345 ± 0.018
16 - 18	2.297 ± 0.051	0.883 ± 0.045	0.384 ± 0.018
18 - 20	2.325 ± 0.053	0.745 ± 0.041	0.321 ± 0.016
20 - 25	2.148 ± 0.050	0.770 ± 0.038	0.359 ± 0.016
25 - 30	2.060 ± 0.050	0.683 ± 0.035	0.332 ± 0.015
30 - 33	2.016 ± 0.050	0.630 ± 0.045	0.312 ± 0.021
38 - 40	1.870 ± 0.049	0.561 ± 0.049	0.300 ± 0.025
40 - 50	1.835 ± 0.049	0.572 ± 0.042	0.312 ± 0.021
50 - 60	1.781 ± 0.049	0.537 ± 0.036	0.301 ± 0.018
60 - 70	1.727 ± 0.049	0.523 ± 0.034	0.302 ± 0.018
70 - 80	1.652 ± 0.048	0.482 ± 0.038	0.291 ± 0.021
80 - 85	1.580 ± 0.046	0.468 ± 0.048	0.297 ± 0.029

Discussion

QUESTION: S. Mughabghab
I am surprised that you adopted the Au capture cross section as a standard in the energy range 6-32 keV because of the presence of structure in the cross section as indicated in Macklin's data. It is precisely for this reason that the capture cross section of Au was not emphasized as a standard below 100 keV excluding, of course, the thermal region. Which Au capture cross sections did you use?

ANSWER: F. Corvi
I used the ENDF/B-V values which are given point-wise above 5 keV. I think these data are mainly based on the old Macklin measurements. As far as fluctuations are concerned, may I suggest that future experimenters working with white neutron sources give, besides point values, also cross sections averaged in decade energy intervals, as it is above for ^{235}U fission. This could substantially improve the accuracy of the data in the "fluctuation" region.

I would like to make a point. People often say you can't use this Au cross section as a standard because of the fluctuations. But if you take averages and if you have accurately determined the neutron flux, you can get these averages rather accurately. It would be good to make comparisons in order to define systematic problems.

COMMENT: W. Poenitz
I strongly support this statement.

REVIEW OF FAST-NEUTRON CAPTURE CROSS SECTIONS OF THE HIGHER PLUTONIUM ISOTOPES AND Am-241*

by

L. W. Weston
Oak Ridge National Laboratory
Oak Ridge, Tennessee 37830

Abstract

The fast-neutron capture cross sections of Pu-240, 241, 242 and Am-241 are reviewed. These nuclides are important to core physics of reactors that contain Pu-239. There have been several significant measurements of these cross sections in recent years. These measurements were instigated by the need for these cross sections for reactor calculations involving high burn-up and build-up of the higher actinides. These recent measurements have satisfied the urgent need for these cross sections in the context of the accuracy needed relative to those of the major fissile isotopes. Problems that exist in the experimental measurements and their evaluation are discussed.

I. Introduction

In recent years there has been emphasis on improved measurement and evaluation[1,2,3] of the capture cross sections of the higher plutonium isotopes and Am-241. This emphasis was brought about because of the production of these nuclides in both thermal and fast reactors. Reactor core physics as well as waste management planning are affected by these nuclides. Core physics at high burn-up is affected by the build-up of these actinides. The build-up of Pu-240,242 and Am-241 brings about parasitic neutron loss because these nuclides have relatively low fission cross sections. The Pu-241 has a high fission cross section and tends to compensate for the neutron loss to the other nuclides.[4] Waste management is affected because these nuclides are the paths to the buildup of the even higher mass actinides which have high rates of spontaneous fission.

There have been experimental measurements with LINACS as well as Van de Graaff accelerators as neutron sources for the capture cross sections of concern except for Pu-241 where there is only one LINAC measurement.[5] The experimental measurements are in reasonable agreement and their evaluations are

*Research sponsored by the Division of Research and Technology U. S. Department of Energy, under contract W-7405-eng-26 with the Union Carbide Corporation.

converging towards consistency. The capture cross sections of these nuclides in the keV region of neutron energies is no longer a major problem. The foremost problems[6] in these nuclides are (1) the discrepancy between integral and differential measurements of capture in the 1-eV resonance of Pu-240, and (2) the shape of the capture and fission cross sections of Pu-241 in the thermal region of neutron energies.

The status of fast neutron capture in Pu-240,241,242, and Am-241 will be reviewed. The experimental and evaluation problems will be discussed. Emphasis will be given to the remaining difficulties in the evaluation of these cross sections.

II. Pu-240

Figure 1 illustrates the three experimental measurements of the fast neutron capture cross section for Pu-240. The data are plotted on an expanded scale and multiplied by the square root of the neutron energy so that the data can be compared in detail. The three measurements on Pu-240 used quite different techniques and they agree within the experimental uncertainties. Hockenbury, Moyer, and Block[7] used a large liquid scintillator tank to detect capture and fission events and a LINAC as a neutron source. Weston and Todd[8] used "total energy detectors" which are small liquid scintillators with pulse-height weighting to detect capture and fission events and a LINAC as a neutron source. Wisshak and Käppeler[9] used Moxon-Rae detectors to detect capture and fission events and a Van de Graaff accelerator as a neutron source. The Wisshak and Käppeler data have been normalized downward by 3.4% from the published results in accordance with recent normalization calculations by Reffo el al.[10] The Wisshak and Käppeler data[9] were measured relative to Au-197 with a calculated absolute efficiency ratio. Part of the Wisshak and Käppeler data[9] was averaged and not all of the data are presented in Fig. 1. The ENDF/B-V evaluation of Au-197 capture,[11] which has structure in this neutron energy region, was used to convert the data to capture cross sections, so the Wisshak and Käppeler data[9] of Fig. 1 should only be considered as representative. The Hockenbury et al. data were normalized to their total cross section measurement in the resonance region and the neutron flux measured with a ^{10}B-NaI detector. The Weston and Todd data[8] were normalized at thermal and at the 1-eV resonance and the flux was measured with a parallel plate BF_3 ion chamber.

The evaluation of the fast capture data on Pu-240 presents the major challenge since the experimental measurements are in reasonable agreement. The ENDF/B-V evaluation[12] is also illustrated in Fig. 1. This evaluation gave most weight to the Weston and Todd data since these data were in agreement with the average resonance parameters from the resonance region and the data of Wisshak and Käppeler[9] were preliminary at the time. The resolved resonance region extended to 3.9 keV and the shape from 1 to 3.9 keV was an attempt to reconcile the resonance parameters with the average capture cross section measurements.

Table 1 gives the average resonance parameters evaluated by Weigmann et al.[13] and recent unpublished results by Gwin.[14] The average resonance parameters of ENDF/B-V are essentially those of Weigmann et al.[13] The unpublished results of Gwin[14] are from thick sample transmission measurements. The higher s-wave strength function of Gwin is in better agreement with the Weston and Todd[8] and Hockenbury et al.[7] capture measurements in the 1- to 10-keV neutron

energy region (see the dotted line in Fig. 1), however, the difference is within the uncertainties of the capture measurements.

An evaluation problem is that the high measured values of the capture cross sections at around 30 keV are difficult to reproduce with the evaluated average resonance parameters from the resonance region and with the normal accepted assumptions. It is usually assumed in fitting capture cross sections that the radiation width divided by the spacing, $\langle\Gamma_\gamma/D\rangle$, is the same for p-wave neutrons as for s-wave neutrons. The dotted line in Fig. 1 is a good representation of the experimental data, however, to achieve this fit it had to be assumed that $\langle\Gamma_\gamma/D\rangle$ was ~20% higher for p-wave neutrons than for s-wave. The other parameters used were the s-wave strength function of Gwin and $\langle\Gamma_\gamma/D\rangle_s$ and the p-wave strength function of Weigmann et al. given in Table 1. This calculation was done with the program, UR, by Pennington[15] which is frequently used in ENDF evaluations. Weigmann et al.[13] were able to achieve a somehwat better fit to the Hockenbury et al. data with $\langle\Gamma_\gamma/D\rangle$ the same for s-wave and p-wave neutrons, which is not in agreement with the above fit.

There are theoretical reasons why the average radiation width, $\langle\Gamma_\gamma\rangle$, in particular could be higher by a few percent for p-wave neutrons than for s-wave neutrons for the case of Pu-240;[16] however, there has been no clear case in the fitting of capture cross sections for other nuclides where there was a significant difference. It is unlikely that the evaluated s-wave $\langle\Gamma_\gamma/D\rangle$ could be in error by ~20% because the experimental uncertainties from the determination of this quantity in the resonance region is much smaller (~4%).[13] Because of the strong correlation in the fitting procedure, $\langle\Gamma_\gamma/D\rangle_p$ could be reduced if $\langle\Gamma_n^1/D\rangle$ were increased, which was done by Hockenbury et al.,[7] however, this would cause a discrepancy with other data.[13,14]

Both the Wisshak and Käppeler[9] and the Weston and Todd[8] data are indicating a rapid decline in the capture cross section above 50 keV which would be due to competition with inelastic scattering from the first 2+ level in Pu-240 at 42.8 keV. The ENDF/B-V evaluation did not properly take this effect into account.

III. Pu-241

There has been only one reported measurement of the differential fast capture cross section for Pu-241 by Weston and Todd.[5] This was a measurement of the ratio of capture-to-fission in Pu-241 using "total energy detectors," fast neutron detectors and a LINAC as a neutron source. The data were normalized at thermal neutron energies. These results and the ENDF/B-V evaluation[17] are illustrated in Fig. 2. Since the ENDF evaluation was based on these experimental data, the agreement yields no insight. The experimental data and evaluation are reasonable; however, it is unfortunate that there is not an additional experimental measurement. The measurement of this cross section is difficult because of the relatively short beta decay half-life of Pu-241 (14.8 y) leading to the build up of Am-241, and the associated gamma-ray activity.

Since Pu-241 has a large fission cross section and exhibits intermediate structure, describing the average capture cross section with average resonance parameters is complex. The available capture cross section data can be fitted with reasonable average resonance parameters as was done for ENDF/B-V as well

as other evaluations.[18,19] Because the average capture data can be fit with reasonable resonance parameters, because capture is small compared to fission, and because of the experimental difficulty of this capture measurement, it is doubtful that an additional measurement will be undertaken.

IV. Pu-242

Figure 3 illustrates the two experimental measurements of the fast capture cross section of Pu-242. The agreement of the Hockenbury et al.[20] and the Wisshak and Käppeler data[9,10] is well within the experimental uncertainties. The ENDF evaluation[21] by F. Mann and others was based on the average resonance parameters from the resonance region and the measurements shown in Fig. 3. Other evaluations have described the experimental data quite well.[22] Since there is consistency between the experimental measurements of the capture cross sections and with the average resonance parameters of Pu-242, there appears to be no outstanding problems in the fast capture cross section of Pu-242.

V. Am-241

The experimental measurements and the ENDF evaluation for fast neutron capture by Am-241 are illustrated in Fig. 4. The experimental measurements are in agreement within experimental uncertainties, however, the Wisshak and Käppeler measurements[23] and the Gayther and Thomas measurements[24] have a higher average cross section than the Weston and Todd measurements.[25] The Gayther and Thomas measurements[24] have a preliminary normalization to the Weston and Todd measurements[25] between 1 and 2 keV. An additional measurement has been reported by Cornelis et al.,[26] however, the results were not available to the author at the present time.

The Gayther and Thomas measurements[24] used a large liquid scintillator tank to detect capture, a Li-glass scintillator at <30 keV and a U-235 fission detector at >30 keV to measure the shape of the neutron flux, and a LINAC as a neutron source. The normalization is preliminary. The Wisshak and Käppeler measurements[23] used the same techniques as discussed for their Pu-240 measurements. Their data shown in Fig. 4 have been normalized downward by 2.7% as suggested by Reffo et al.[10] in a normalization calculation to be published. All of the Wisshak and Käppeler data is not shown in Fig. 4 and part of their data are averaged so that the plot should be regarded as only indicative of the data. Also the ENDF/B-V Au-197 capture evaluation[11] which has structure in this neutron energy region was used to convert the ratio data to the capture cross section of Am-241.

The ENDF evaluation[27] by F. M. Mann et al. was based on the average resonance parameters from the resolved resonance region and the Weston and Todd[25] measurements. The other measurements were not complete at the time of the ENDF evaluation. It has been shown by Derrien et al.[28] that the higher average capture cross section indicated by the other measurements can be reproduced by evaluated average resonance parameters from the resonance region and a reasonable p-wave strength function (2.54×10^{-4}).

Recent unpublished results by Anderl, Schroeder, and Harker[29] concerning an integral capture measurement in CFRMF, which has a peak sensitivity at about 300 keV, indicate that the CFRMF spectrum-averaged Am-241 capture is

about 16% higher than that indicated by the ENDF evaluation. As can be seen in Fig. 4 the results of Gayther and Thomas[24] would be quite consistent with these results which would also be within the experimental uncertainties of the Weston and Todd measurements.[25] The recent results of Anderl, Schroeder, and Harker,[29] thus, represent no discrepancy with the previously measured results.

For reactor physics, it is important whether Am-241 capture leads to the ground state of Am-242 or the excited state, Am-242m. The ground state has a half-life for beta decay to Cm-242 of only 16 hours whereas Am-242m has a half life of 152 years. There are recent measurements and theoretical calculations of the ratio of the excited state to ground state cross sections by Wisshak, Wickenhauser, and Käppeler.[30] These theoretical calculations and those by Mann and Schenter[31] are within experimental uncertainties, however, the experimental measurement[30] indicates an appreciably stronger decline in the ratio between thermal and ~30-keV neutron energies.

The fast neutron capture cross section of Am-241 is reasonably well known in the context of the uncertainty weighted by the occurrence in fuel elements as compared to the capture cross sections of U-235 and Pu-239. The agreement of the experimental data is marginally within experimental uncertainties and the ENDF/B-V evaluation probably needs revision. These difficulties probably do not require additional experimental measurements; especially not until the time that the Cornelis et al.[26] measurements are available and evaluated.

VI. Conclusions

The status of fast neutron capture measurements for Pu-240,241,242, and Am-241 has been reviewed. There appear to be no outstanding discrepancies to warrant a strong recommendation for additional measurements at this time unless an appreciably more accurate experimental technique is developed. If such a technique is developed, it should be first applied to Pu-239 rather than the higher A nuclides.

The basis of the above statement is that for reactor applications the important quantity is the concentration of a particular nuclide multiplied by the cross section. Plutonium concentrations[32] for end-of-life fuel elements from light water reactors are about 59% Pu-239, 26% Pu-240, 12% Pu-241, and 3% Pu-242. The concentrations of the higher Pu isotopes would be less for fast reactor fuel elements. Thus, the fast neutron capture cross seciton of Pu-239 needs to be known with an uncertainty of at least a factor of 2.3 less than that for Pu-240, a factor of 5 less than that for Pu-241 (or Am-241), and a factor of 20 less than that for Pu-242. The uncertainty of the fast capture cross section for Pu-239 does not meet the above criteria so that on a relative basis the capture cross sections of the higher Pu isotopes and Am-241 are sufficiently well known at the present time.

The ENDF/B-V evaluations are not very consistent with the presently available data for Pu-240 and Am-241, however, this is an evaluation rather than an experimental measurement problem. Thus the status of the fast capture cross sections of the higher actinides of concern which are important to core physics as well as waste disposal, which were in alarmingly poor condition a decade ago, are now reasonably well known as compared to the cross sections of the major fissile nuclei.

References

1. Proceedings of the Advisory Group Meeting on Transactinium Isotope Nuclear Data, Karlsruhe, Germany, Nov. 3-7, 1975, IAEA-186, International Atomic Energy Agency (1976).

2. Proceedings of the Second Advisory Group Meeting Transactinium Isotope Nuclear Data, Cadarache, France, May 2-5, 1979, IAEA-TECDOC-232, International Atomic Energy Agency (1979).

3. Proceedings of the Specialists' Meeting on Nuclear Data of Plutonium and Americium Isotopes for Reactor Applications, Upton, New York, Nov. 20-21, 1978, BNL-50991, NEANDC L-116, Brookhaven National Laboratory (1979).

4. M. Becker et al. "The Relationship Between Basic Nuclear Data and LWR Fuel Cycle Parameters," Proc. Nuclear Data Problems for Thermal Reactor Applications, Brookhaven National Laboratory, May 22-24, 1978, EPRI NP-1098, p. 14-1, Electric Power Research Institute, Palo Alto, California.

5. L. W. Weston and J. H. Todd, Nucl. Sci. Eng. 65, 454 (1978); also Nucl. Sci. Eng. 68, 125 (1978).

6. L. W. Weston, "Review of Microscopic Neutron Cross Section Data for the Higher Plutonium Isotopes in the Resonance Region," Proc. Specialists Meeting on Nuclear Data of Plutonium and Americium Isotopes for Reactor Applications, Upton, New York, Nov. 20-21, 1978, BNL 50991, NEANDC L-116, Brookhaven National Laboratory (1979).

7. R. W. Hockenbury, W. R. Moyer, and R. C. Block, Nucl. Sci. Eng. 49, 153 (1972).

8. L. W. Weston and J. H. Todd, Nucl. Sci. Eng. 63, 143 (1977).

9. K. Wisshak and F. Käppeler, Nucl. Sci. Eng. 66, 363 (1978); also Nucl. Sci. Eng. 69, 39 (1979).

10. G. Reffo, F. Fabbri, K. Wisshak, and F. Käppeler, "Calculated Gamma-Ray Spectra for keV Neutron Capture in Pu-240, Pu-242, and U-238," submitted for publication in Nuclear Science and Engineering (1982).

11. ENDF/B-V data file for Au (MAT 1379), evaluated by S. F. Mughabghab, BNL-NCS-17541 (ENDF-201) available from the National Nuclear Data Center, Brookhaven National Laboratory (1979).

12. ENDF/B-V data file for Pu-240 (MAT 1380), evaluated by L. W. Weston et al. BNL-NCS-17541 (ENDF-201) available from the National Nuclear Data Center, Brookhaven National Laboratory (1979).

13. H. Weigmann, G. Rohr, and F. Poortmans, Proc. Conf. Resonance Parameters of Fertile Nuclei and Pu-239, Saclay, NEANDC(E) 1634, p. 219, Commissariat a l'Energia Atomique, Saclay (1974).

14. R. Gwin et al., Oak Ridge National Laboratory, private communication (1982).

15. E. Pennington, Argonne National Laboratory, Unresolved Resonance Program (UR), available from National Nuclear Data Center, Brookhaven National Laboratory (1973).

16. M. S. Moore, "Systematics of s- and p-wave Radiation Widths," Proc. Conf. on Nuclear Data Evaluation Methods and Procedures, Brookhaven National Laboratory, Upton, N. Y., September 22-25, 1980, BNL-NCS-51363, vol. 1, p. 449 (1981).

17. ENDF/B-V data file for Pu-241 (MAT 1451), evaluated by L. W. Weston et al., BNL-NCS-17541 (ENDF-201) available from the National Nuclear Data Center, Brookhaven National Laboratory (1979).

18. Y. Kikuchi, J. Nucl. Sci. Tech. 14, 467 (1977).

19. V. A. Konshin et al., "Evaluation of Nuclear Data for Pu-241 in Neutron Energy Range from 10^{-5} eV to 15 MeV," INDC(CCP)-142/GJ, International Atomic Energy Agency, Vienna (1979).

20. R. W. Hockenbury, A. J. Sanislo, and N. N. Kaushal, Proc. Conf. on Nuclear Cross Sections and Technology, Washington, D. C., March 3-7, 1975, NBS Special Publication 425, vol. II, p. 584, National Bureau of Standards (1975).

21. ENDF/B-V data file for Pu-242 (MAT 1342), evaluated by F. M. Mann et al. BNL-NCS-17541 (ENDF-201) available from the National Nuclear Data Center, Brookhaven National Laboratory (1979).

22. K. Wisshak, F. Käppeler, and F. H. Frohner, "Review of the Pu-240 and Pu-242 Unresolved Resonance Region," Proc. IAEA Consultants' Meeting on U and Pu Resonance Parameters, Sept. 28 - Oct. 2, 1981, Vienna, to be published.

23. K. Wisshak and F. Käppeler, Nucl. Sci. Eng. 76, 148 (1980).

24. D. B. Gayther and B. W. Thomas, Proc. IV National Soviet Conf. on Neutron Physics, Kiev, vol. 3, p. 3 (1977).

25. L. W. Weston and J. H. Todd, Nucl. Sci. Eng. 61, 356 (1976).

26. E. Cornelis et al., "Neutron Capture Cross Section of Am-241," Annual Progress Report on Nuclear Data, INDC (EUR) 14/G, NEANDC (E) 222 "U", CBNM, Geel, Belgium (1980).

27. ENDF/B-V data file for Am-241 (MAT 1361), evaluated by F. M. Mann et al. BNL-NCS-17541 (ENDF-201) available from the National Nuclear Data Center, Brookhaven National Laboratory (1979).

28. H. Derrien, E. Fort, and D. Lafort, "Evaluation of Am-241 Resonance Parameters and Their Consequences for the Unresolved Region," Proc. Specialist's Meeting on Nucl. Data of Plutonium and Americium Isotopes for Reactor Applications, p. 71, Brookhaven National Laboratory, November 20-21, 1978, BNL-50991, NEANDC L-116, Brookhaven National Laboratory (1979).

29. A. Anderl, N. C. Schroeder, and Y. D. Harker, "Fast Integral Cross Sections for Am-241, and Am-243," to be published; also private communication (1982).

30. K. Wisshak, J. Wickenhauser, and F. Käppeler, "The Isomeric Ratio in Thermal and Fast Neutron Capture of Am-241," to be published in Nuclear Science and Engineering (1982).

31. F. M. Mann and R. E. Schenter, Nucl. Sci. Eng. 63, 242 (1977).

32. P. Greebler, B. A. Hutchins, and C. L. Cowan, Proc. Conf. Nuclear Data for Reactors, Helsinki, vol. 1, p. 19, IAEA, Vienna (1972).

Table 1. Average Resonance Parameters for Pu-240

	Γ_n^0/D ($\times 10^{-4}$)	$\bar{D}$ (eV)	Γ_γ (meV)	Γ_n^1/D ($\times 10^{-4}$)
Weigmann *et al.*[13]	$1.04\ ^{+0.14}_{-0.12}$	12.7 ± 0.3	30.8 ± 1	2.2 ± 0.2
Gwin *et al.*[14]	1.20 ± 0.04			2.2 ± 0.11

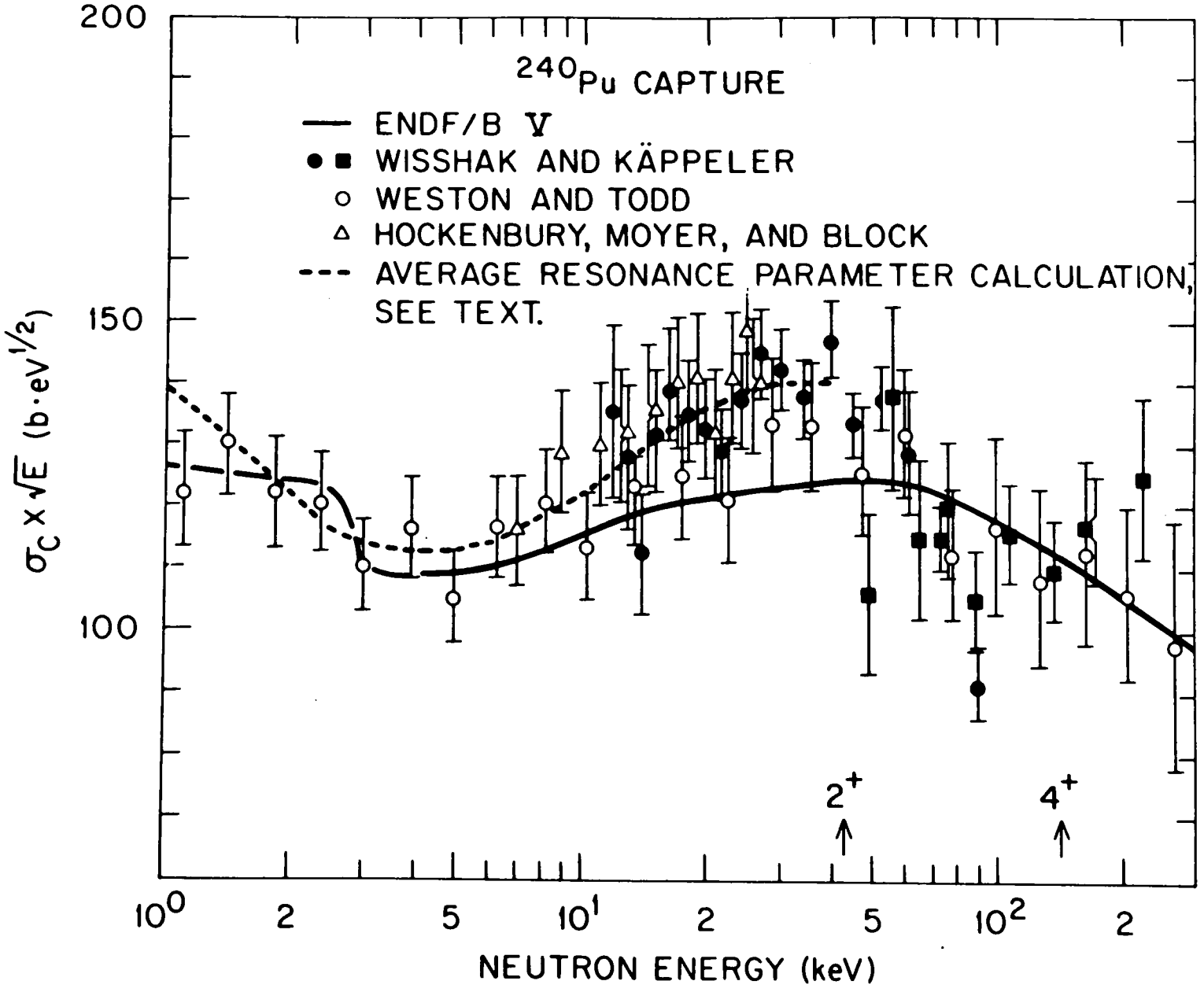

Fig. 1. The neutron capture cross section of Pu-240 multiplied by the square root of the neutron energy in the neutron energy range from 1 to 300 keV. The experimental data as well as the ENDF/B-V evaluation are illustrated.

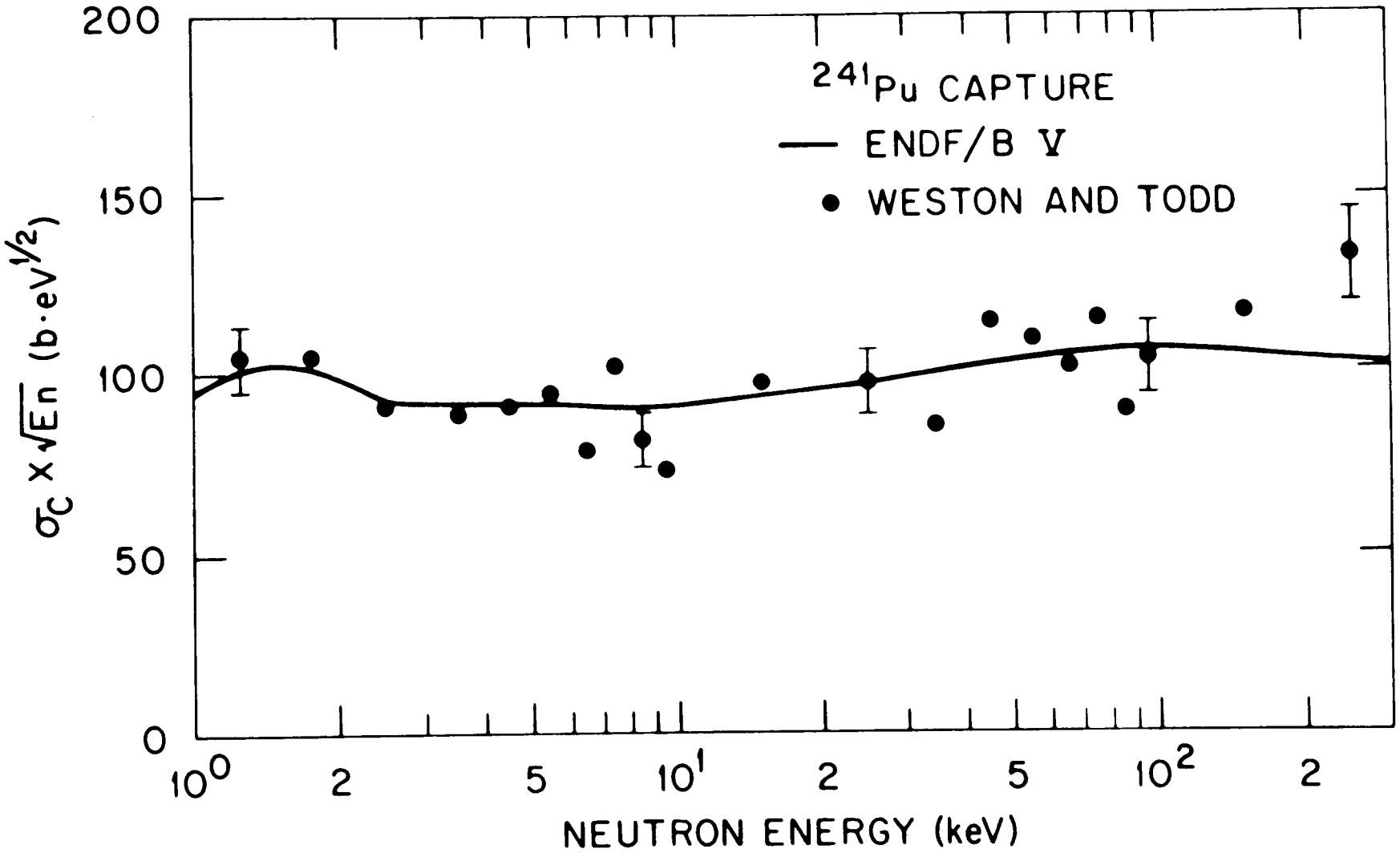

Fig. 2. The neutron capture cross section of Pu-241 multiplied by the square root of the neutron energy in the neutron energy range from 1 to 300 keV. The experimental data as well as the ENDF/B-V evaluation are illustrated.

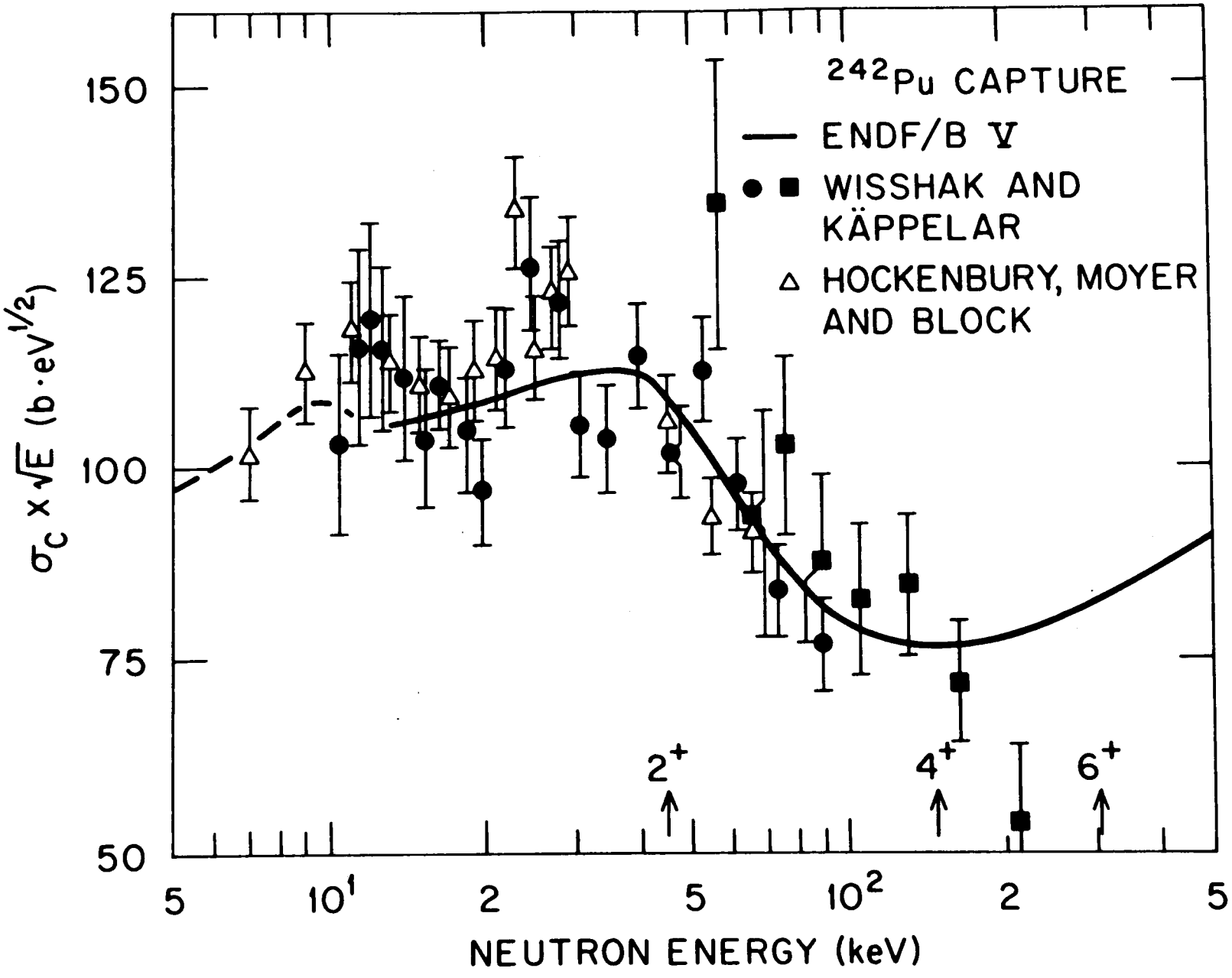

Fig. 3. The neutron capture cross section of Pu-242 multiplied by the square root of the neutron energy in the neutron energy range from 5 to 500 keV. The experimental data as well as the ENDF/B-V evaluation are illustrated.

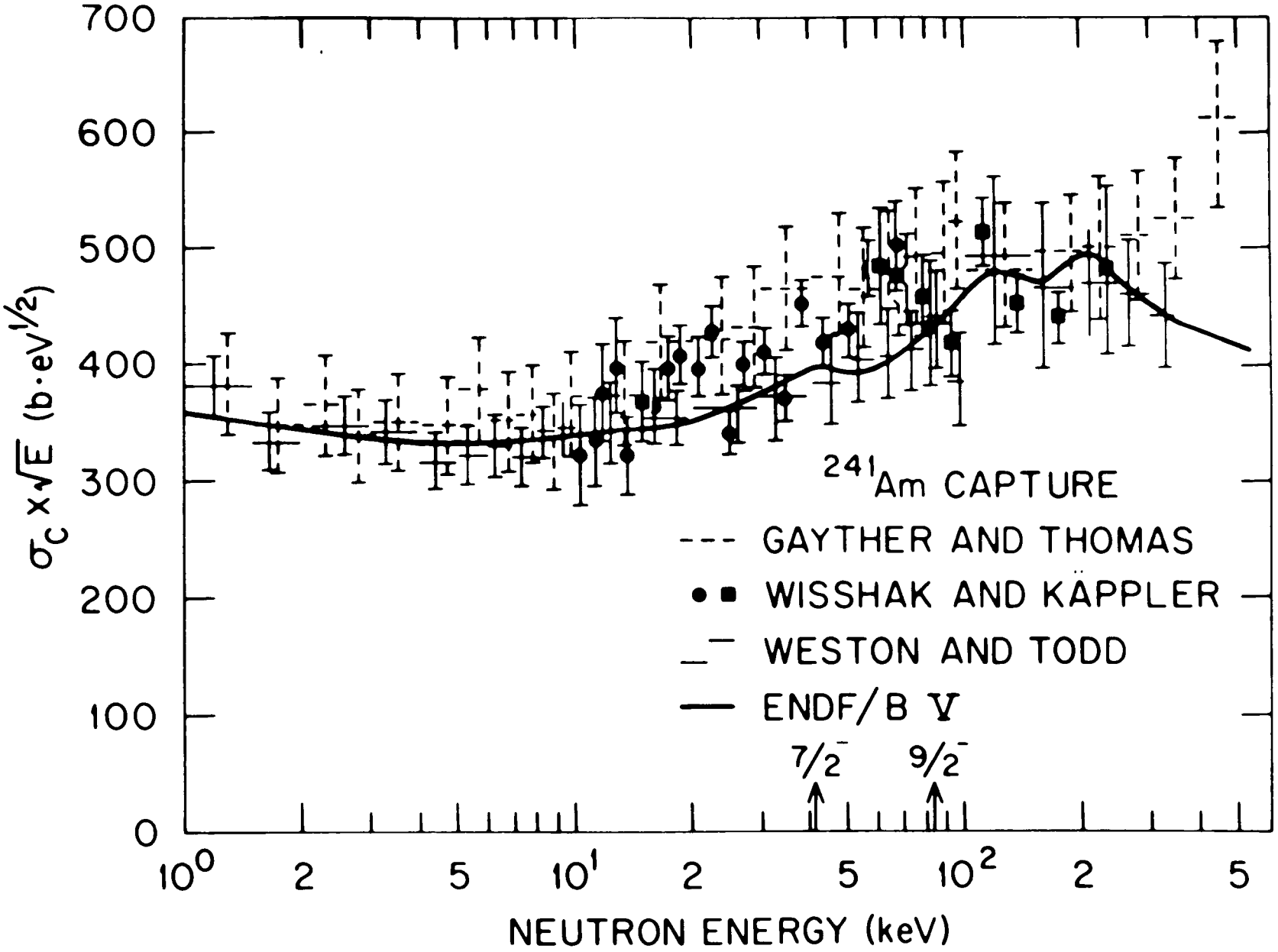

Fig. 4. The neutron capture cross section of Am-241 multiplied by the square root of the neutron energy in the neutron energy range from 1 to 600 keV. The experimental data as well as the ENDF/B-V evaluation are illustrated.

Discussion

QUESTION: S. Whetstone
How will your conclusion number one get fed into the system?

ANSWER: L. Weston
The comment that there are no outstanding discrepancies to warrant a strong recommendation for additional measurements was made to give guidance to the working groups at this meeting.

QUESTION: R. Schenter
In the ENDF/B-V evaluation for ^{241}Am a nuclear-model calculation was used with a value of Γ_γ/D picked to agree with the Weston et al. measurement. Would you recommend Γ_γ/D be readjusted to be consistent with your new recommended cross section or would you change the p-wave strength function?

ANSWER: L. Weston
For an evaluation of the capture cross section of Am-241, I would raise both $(\Gamma_\gamma/D)p$ and Γ_n/D to better agree with the average of the experimental data. There are theoretical reasons why $(\Gamma_\gamma/D)p$ may be larger than for s-waves by a few percent so this quantity could be raised by a few percent and then Γ_n/D could be raised to make up the difference.

COMMENT: R. Schenter
Recent FFTF measurements of the neutron source strength imply that if the ENDF/B-V capture cross section was raised ~ 10-15% better agreement (this assumes the branching Am^{242m}/Am^{242G} is correct) would be obtained between measurement and calculation. The FFTF result depends upon a broad spectrum response (1 keV-260 keV) with a peak at ~ 50 keV.

ACTINIDE INTEGRAL MEASUREMENTS IN THE CFRMF AND INTEGRAL TESTS FOR ENDF/B-V*

by

R. A. Anderl, Y. D. Harker, J W Rogers
EG&G Idaho, Inc.
Idaho National Engineering Laboratory
Idaho Falls, Idaho 83415

Abstract

Integral capture and/or fission rates have been reported earlier for several actinides irradiated in the fast neutron field of the Coupled Fast Reactivity Measurements Facility (CFRMF). These nuclides include ^{232}Th, ^{233}U, ^{235}U, ^{238}U, ^{237}Np, ^{239}Pu, ^{240}Pu, ^{242}Pu, ^{241}Am and ^{243}Am. This paper focuses on the utilization of these integral data for testing the respective cross sections on ENDF/B-V. Integral cross sections derived from the measured reaction rates are tabulated. Results are presented for cross-section data testing which includes integral testing based on a comparison of calculated and measured integral cross sections and testing based on least-squares-adjustment analyses.

I. Introduction

Integral reaction rates have been measured for several actinides irradiated in the fast neutron field of the Coupled Fast Reactivity Measurements Facility (CFRMF)[1,2]. The purpose of this paper is to summarize this integral data base and to present the results of using these integral data to test the respective cross sections on ENDF/B-V. The impact of this work on the radiative neutron capture reactions is highlighted. Section II of this paper includes a brief description of the CFRMF, an identification of the types of integral measurements and a tabulation of integral cross sections derived from the measured reaction rates. The utilization of the measured integral data for testing the respective cross sections on ENDF/B-V is covered in Section III. Both conventional integral testing based on a comparison of

* Work supported by the US Department of Energy under DOE contract No. DE-AC07-76ID01570.

calculated-to-measured integral cross sections and testing based on least-squares-adjustment analyses are used to assess the consistency between the measured integral data and the evaluated cross sections. Conclusions drawn from this work are presented in Section IV.

II. Integral Data Base

The irradiation facility for the actinide integral measurements is the CFRMF[1,2] which is a zoned-core critical assembly with a fast neutron spectrum zone in the center of an enriched ^{235}U, water moderated thermal driver. Approximately 95% of the neutrons in the central spectrum are between 4 keV and 4 MeV and the median and mean neutron energies are 370 keV and 1760 keV, respectively. The central neutron spectrum is a Cross-Section Evaluation Working Group (CSEWG) benchmark field for testing dosimetry, fission-product and actinide cross sections for ENDF/B-V. An update of the CFRMF central neutron spectrum characterization has been reported recently[3,4].

A variety of techniques have been used for the integral measurements. Fission rates based on absolute fission chamber (FC) measurements have been reported by Grundl et. al[5] for ^{235}U, ^{238}U, ^{237}Np and ^{239}Pu. Measurements of the fission rates of ^{232}Th, ^{233}U and ^{240}Pu relative to the fission rate of ^{235}U have been reported by Gilliam and Rogers[6]. These latter experiments employed the NBS double fission chamber (DFC). The gamma spectrometric method[7] was used in the determination of the fission rates for ^{232}Th, ^{242}Pu, ^{241}Am and ^{243}Am based on absolute measurements of the gamma emission rates of the prominent lines in the ^{140}Ba-^{140}La decay[8,9,10]. With the exception of the capture rate for ^{241}Am which was determined using isotope-dilution-alpha spectrometry (IDAS)[10], the capture rates for ^{232}Th, ^{238}U, ^{242}Pu and ^{243}Am are based on gamma spectrometric measurements[7,10]. Many of the measurements were made as part of the Interlaboratory Reaction Rate (ILRR) Program[11].

Spectrum-averaged cross sections were derived by dividing the measured integral reaction rates by absolute neutron fluxes which were determined for each measurement. The neutron flux determinations are based on the use of the $^{197}Au(n,\gamma)\,^{198}Au$ reaction as a power level monitor and on an independent determination of the neutron flux for one power level. The independent absolute flux value is based on a flux transfer[12] using measured fission rates for ^{239}Pu in the CFRMF and in the National Bureau of Standards (NBS) ^{252}Cf standard field and on a measured integral cross section for $^{239}Pu(n,f)$ in the ^{252}Cf field[7].

A tabulation of the "measured" integral cross sections is given in column 4 of Table 1. The value in parenthesis is the estimate of the total percent error in the integral cross section, at the one sigma confidence level. Columns 2 and 3 provide necessary identification of the experiment type and the reference for the integral reaction-rate measurements.

III. Cross-Section Data Testing

Integral tests of the evaluated capture and fission cross sections were made by comparing the "measured" integral cross sections to integral cross sections computed using 620-group representations of the CFRMF central spectrum[13] and of the differential data on ENDF/B-V. The calculated integral

cross sections and the ratios of calculated-to-measured integral cross section are listed in columns 5 and 6, respectively, of Table 1. Two uncertainty values, expressed as percent, are listed in parenthesis for the calculated integral cross sections. The first corresponds to the error in the calculated integral cross section due to spectrum uncertainties[4] only. The second uncertainty contribution, wherever it is given, corresponds to the error in the calculated integral cross section due to cross-section uncertainties as processed from the ENDF/B-V uncertainty files. One uncertainty value, expressed as percent, is given for each C/M ratio. That value corresponds to the quadrature sum of the error in the "measured" integral cross section and the error in the calculated integral cross section due to spectrum error contributions only.

For the radiative capture reactions, the integral test analysis indicates an inconsistency between the measured integral data and the ENDF/B-V evaluated cross sections for ^{232}Th, ^{242}Pu, ^{241}Am and ^{243}Am. The integral test indicates that the ENDF/B-V capture cross section for ^{238}U is consistent with the measured integral data. Column 7 in Table 1 lists the ratio of the integral cross section computed with ENDF/B-V differential data to that computed with ENDF/B-IV differential data. This information indicates how the changes made to the capture cross section in going from ENDF/B-IV to ENDF/B-V impact the consistency test. The last two columns in Table 1 provide a qualitative indication of the response range for each reaction in the CFRMF spectrum. Response plots as a function of energy are given in Reference 14 for these reactions.

Least-squares-adjustment analyses were made with the FERRET code[15]. The adjustment analysis was made in a 53-group energy structure and it included the following input data: (1) 23 dosimeter integral reaction rates[3], (2) six integral reaction rates for capture and fission in ^{242}Pu, ^{241}Am, ^{243}Am, (3) CFRMF spectrum and associated covariance matrix, (4) cross sections processed with CFRMF spectrum weighting from ENDF/B-V for all reactions, and (4) covariance matrices for all reactions. The measured integral data were assumed to have zero correlation in the analyses. Covariance matrices for the dosimeter reactions were a mixture of matrices processed directly from the ENDF/B-V covariance files and matrices generated by F. Schmittroth to improve upon the ENDF/B-V prescriptions[16]. Covariance matrices for the actinide reactions were generated by using a gaussian-type parametric form to describe the short-range correlations between the group wise uncertainties as obtained from ENDF/B-V and adding an additional normalization uncertainty in the unresolved and smooth energy ranges. This approach was used because of the limitations of the error files on ENDF/B-V (no error files for ^{243}Am, missing error and correlation information for some energy regions for ^{241}Am and ^{242}Pu, block-type correlation specifications.) The ^{241}Am uncertainty information on ENDF/B-V was used for ^{243}Am, however, the normalization component was doubled from 15% for ^{241}Am to 30% for ^{243}Am.

Preliminary results of the least-squares-analysis are illustrated in Figures 1-3 for the ^{232}Th, ^{241}Am and ^{243}Am radiative capture cross sections. The upper part of each figure shows a direct comparison of the 53-group cross sections over the neutron energy ranges in which the CFRMF spectrum is sensitive. The bottom part of each figure shows the ratio of adjusted-to-unadjusted cross sections for the analysis. These figures indicate the energy range and the magnitude of the adjustments required to achieve consistency

between the measured integral data and the evaluated cross sections. For $^{242}Pu(n,\gamma)$, the input covariance specification was too tight to permit sufficient cross-section adjustment to achieve consistency between the measured integral data and the adjusted cross section.

IV. Conclusions

In this paper we have summarized the actinide capture and fission integral data base for measurements in the fast neutron field of the CFRMF. An integral testing analysis in which the "measured" integral cross sections were compared to integral cross sections calculated with ENDF/B-V differential data indicated that for the fast neutron radiative capture cross sections for ^{232}Th, ^{242}Pu, ^{241}Am and ^{243}Am, the measured integral data are inconsistent with the evaluated cross sections. This same analysis indicated consistency between the measured integral data and the ENDF/B-V capture cross section for ^{238}U. A least-squares-adjustment analysis indicated that the following cross-section adjustments are required to resolve the discrepancies between the measured integral data and the ENDF/B-V capture evaluations: $^{232}Th(n,\gamma)$, ~ 5% to 10% up (1 keV to 17 MeV); $^{241}Am(n,\gamma)$, ~30% up (0.1 keV to 17 MeV), $^{243}Am(n,\gamma)$ ~ 44% up (0.1 keV to 17 MeV). This assessment for ^{232}Th is consistent with a recent measurement at 23-keV neutron energy by Baldwin and Knoll[17]. The above assessment for the ^{241}Am and ^{243}Am capture reactions is contingent on an experimental verification of the neutron-capture branching fraction data used in the analysis of the integral experiments[18]. However, the assessment of the ^{241}Am and ^{243}Am ENDF/B-V capture cross sections is consistent with other information presented at this meeting[19,20]. Although the present work indicated a significant discrepancy between the measured integral data and the ENDF/B-V capture cross section for ^{242}Pu, additional work is required to resolve questions concerning the accuracy of the measured integral data[15].

REFERENCES

1. J W Rogers, D. A. Millsap and Y. D. Harker, Nucl. Tech. 25, 330 (1975).

2. J W Rogers, D. A. Millsap and Y. D. Harker, "The Coupled Fast Reactivity Measurements Facility (CFRMF)," in Proc. of IAEA Consultants Meeting on Integral Cross-Section Measurements for Reactor Dosimetry, IAEA, Vienna, Austria, November 15-19, 1976, IAEA-208, Vol. II, 117 (1976).

3. R. A. Anderl, Y. D. Harker, D. A. Millsap, J W Rogers and J. M. Ryskamp, "CFRMF Spectrum Update and Application to Dosimeter Cross-Section Data Testing," in the Proc. for the Fourth ASTM-EURATOM Symposium on Reactor Dosimetry, National Bureau of Standards, March 22-26, 1982.

4. J. M. Ryskamp, R. A. Anderl, B. L. Broadhead, W. E. Ford III, J. L. Lucius, J. H. Marable, and J. J. Wagschal, Nucl. Tech. 57, 20 (1982).

5. J. A. Grundl, et. al, Nuc. Tech 25, 237 (1975).

6. D. M. Gilliam and J W Rogers, "Fission Cross-Section Ratios for U-233, Th-232, and Pu-240 in CFRMF and Preparation for Absolute Fission Counting at 100 kW," contribution to Interlaboratory Reaction Rate Program 12th Progress Report, HEDL-TME 79-58, pp. NBS-57 to NBS-68 (1979).

7. R. C. Greenwood, et. al, "Radiometric Reaction-Rate Measurements in CFRMF and BIG-10," in Proc. 2nd ASTM-EURATOM Symposium on Reactor Dosimetry, Palo Alto (1977), NUREG/CP-004, Vol. 3, 1207 (1978).

8. R. A. Anderl and Y. D. Harker, "Measurement of the Integral Capture and Fission Cross Sections for ^{232}Th in the CFRMF," in Proc. International Conference on Nuclear Cross Sections for Technology, Knoxville, Tennessee, October 22-26, 1979, NBS Special Publication 594, 475 (1980).

9. Y. D. Harker, R. A. Anderl, E. H. Turk, and N. C. Schroeder, "Integral Measurements for Higher Actinides in CFRMF," ibid, p 548.

10. R. A. Anderl and N. C. Schroeder, "Integral Capture and Fission Cross Sections for ^{241}Am and ^{243}Am in the CFRMF," to be published as US DOE Report EGG-PHYS-5691, Idaho National Engineering Laboratory (1982).

11. W. N. McElroy and L. S. Kellogg, Nuc. Tech 25, 180 (1975).

12. J. A. Grundl and C. M. Eisenhauer, "Fission Spectrum Neutrons for Cross-Section Validation and Neutron Flux Transfer," in Proc. Conf. on Nuclear Cross Sections and Technology, NBS Special Publication 425, Vol. I, p. 270 (1975).

13. R. A. Anderl, D. A. Millsap, J W Rogers, Y. D. Harker, "Addendum to Integral Data Testing Report for ENDF/B-V Dosimeter Cross Sections," US DOE Report EGG-PHYS-5668, Idaho National Engineering Laboratory (1982).

14. R. A. Anderl, "INEL Integral Data-Testing Report for ENDF/B-V Fission-Product and Actinide Cross Sections," US DOE Report EGG-PHYS-5406, Idaho National Engineering Laboratory (April, 1980).

15. F. Schmittroth, "FERRET Data Analysis Code," US DOE Report HEDL-TME 79-40, Hanford Engineering Development Laboratory (1971).

16. Private communication from F. Schmittroth, Hanford Engineering Development Laboratory (February, 1982).

17. G. T. Baldwin and G. F. Knoll, "Absolute Measurement of the Cross Section for 23-keV Neutron Activation of Thorium," this meeting.

18. R. A. Anderl, N. C. Schroeder and Y. D. Harker, "Fast Integral Cross Sections for ^{241}Am and ^{243}Am," contributed paper to be presented at the ANS Topical Meeting on Advances in Reactor Physics and Core Thermal Hydraulics, Kiamesha Lake, New York, September 22-24, 1982.

19. K. Wisshak, et. al, "Fast Neutron Capture in Actinide Isotopes: Recent Results from Karlsruhe," this meeting.

20. L. W. Weston, "Review of Fast-Neutron Capture Cross Sections of the Higher Plutonium Isotopes and ^{241}Am," this meeting.

Table 1. Summary of Integral Measurements and Integral Test Results for Actinide Reactions in the CFRMF

Reaction	Experiment Type	Reference	Integral Cross Section (mb) Measured	Integral Cross Section (mb) Calculated	C/M	V/IV	95% Response Range[a] E_L(MeV)	95% Response Range[a] E_u(MeV)
^{232}Th(n,f)	γ-Spec	8	19.6(5.2)	19.14(7.5,5)	0.98(9)	1.06	1.2	8.3
(n,γ)	γ-Spec	8	290.8(3.8)	252.0(1.5,11)	0.87(4.1)	0.91	6.8 E-5	1.6
^{235}U(n,f)	FC	5	1538.(3.1)	1552.(0.5,2)	1.01(3.1)	0.99	2.2 E-4	3.6
^{238}U(n,f)	FC	5	75.1(3.3)	79.59(7.4,4)	1.06(8)	1.00	1.1	7.8
(n,γ)	γ-Spec	7	217.(3.7)	216.8(1.6,5)	1.00(4)	0.99	8.7 E-5	1.4
^{237}Np(n,f)	FC	5	548.(3.3)	606.1(3.6,10)	1.11(5)	1.01	0.3	5.8
^{239}Pu(n,f)	FC	5	1792.(2.2)	1773.(0.2,2)	0.99(2.2)	1.00	2.4 E-4	4.1
^{240}Pu(n,f)	DFC	6	573.(3.8)	623.4(6,-)	1.08(7)	1.01	9.0 E-2	5.6
^{242}Pu(n,f)	γ-Spec	8	557.(10)	477.1(6,-)	0.86(12)	0.96	0.3	5.9
(n,γ)	γ-Spec	8	146.(15)	266.1(2,-)	1.82(15)	1.18	5.2 E-5	1.3
^{241}Am(n,f)	γ-Spec	9	450.(6.2)	526.4(6,-)	1.17(9)	1.07	0.3	6.2
(n,γ)	IDAS	9	1550.(3.5)	1098.(2,-)	0.71(4)	1.69	1.2 E-4	1.0
^{243}Am(n,f)	γ-Spec	9	353.(6.1)	419.8(6,-)	1.19(9)	1.21	0.4	6.6
(n,γ)	γ-Spec	9	895.(4.8)	583.6(2,-)	0.65(5)	1.30	7.8 E-5	0.7

a. Ninty-five percent of the reaction response in the CFRMF is between the lower energy, E_L, and the upper energy E_u.

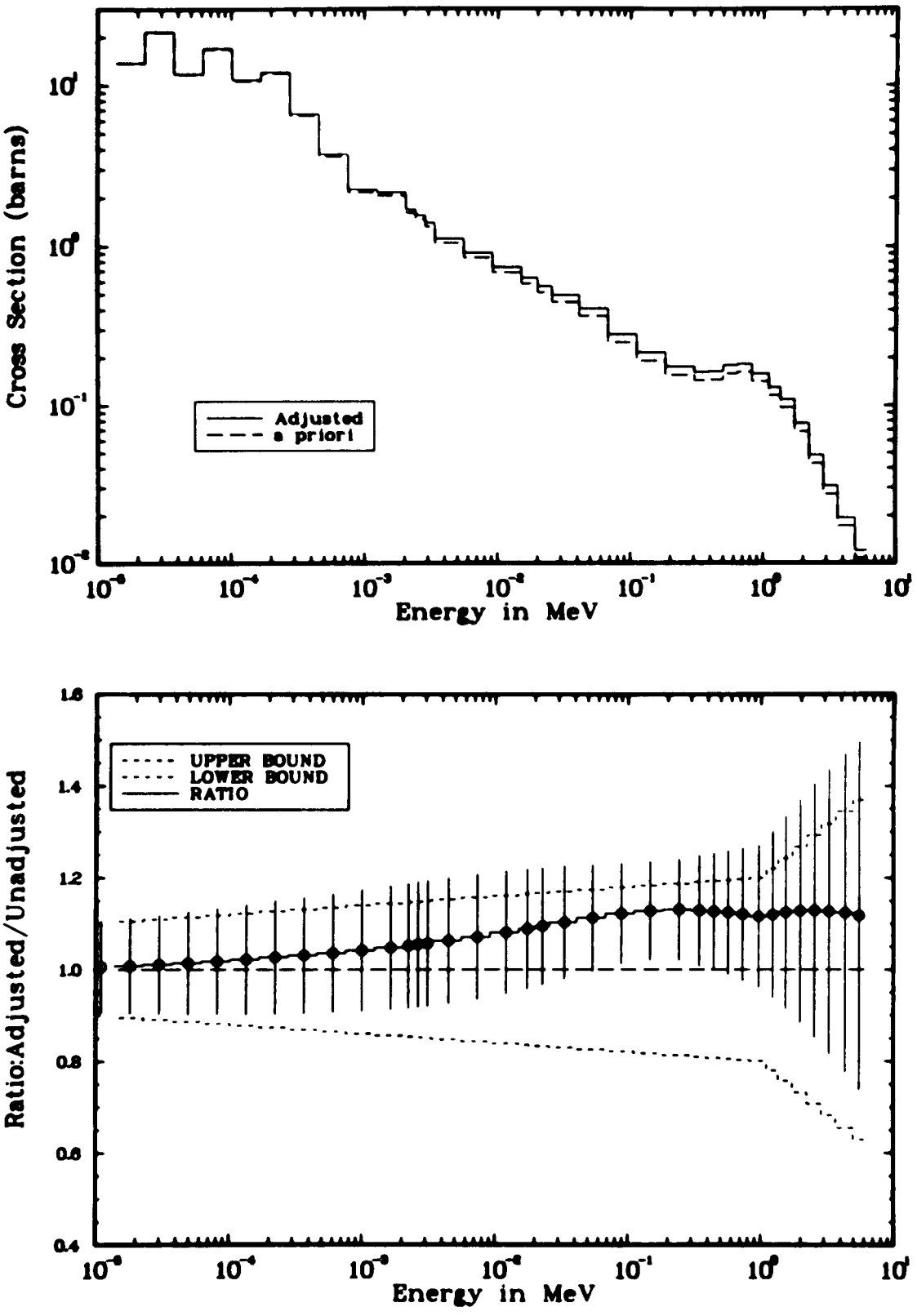

Figure 1. Comparison of adjusted and unadjusted cross sections for $^{232}Th(n,\gamma)$. In the lower half of the figure, input cross-section uncertainties are indicated by upper and lower bounds and adjusted uncertainties are indicated by vertical lines through the group mid-energy points.

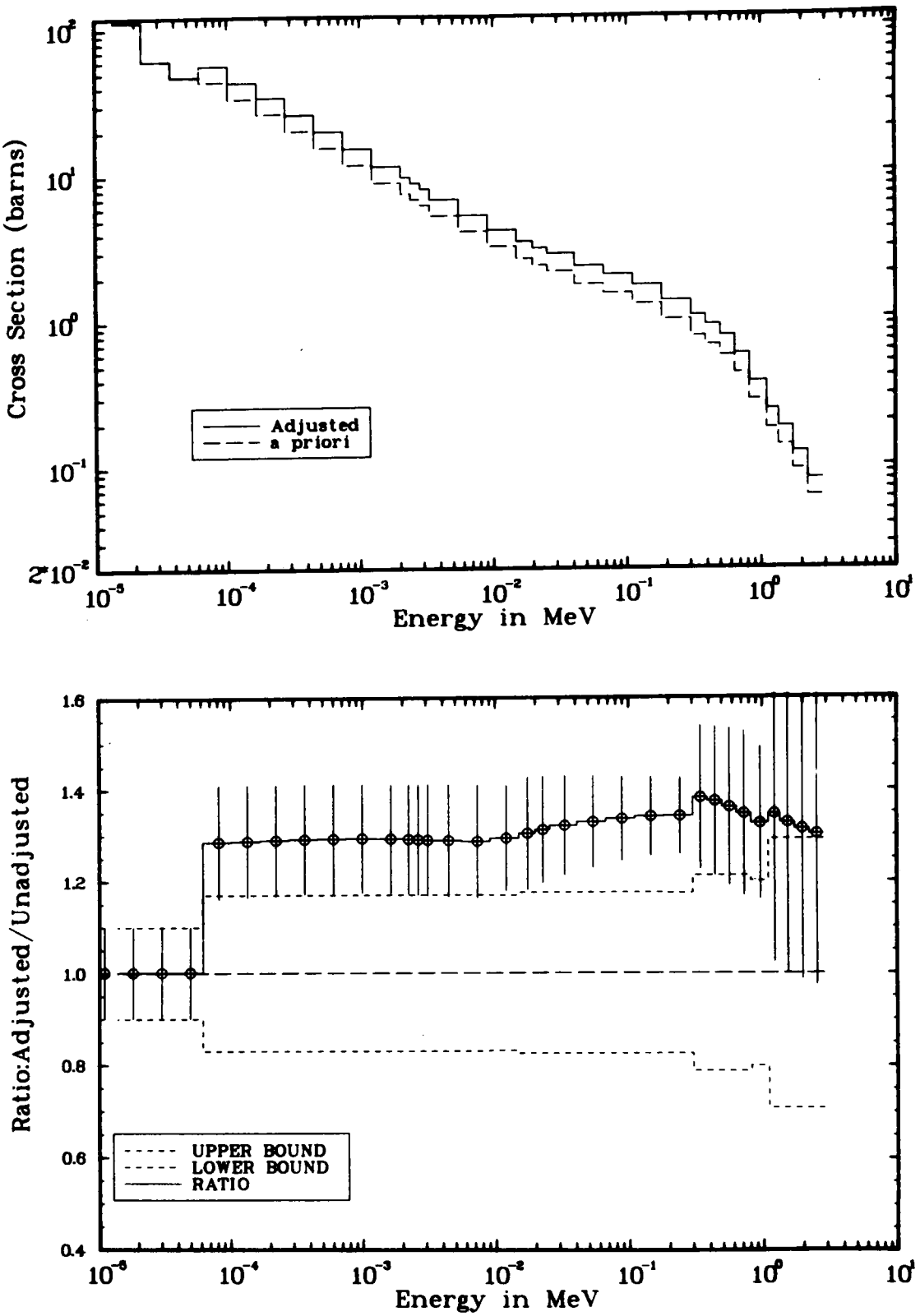

Figure 2. Comparison of adjusted and unadjusted cross sections for $^{241}Am(n,\gamma)$. In the lower half of the figure, input cross-section uncertainties are indicated by upper and lower bounds and adjusted uncertainties are indicated by vertical lines through the group mid-energy points.

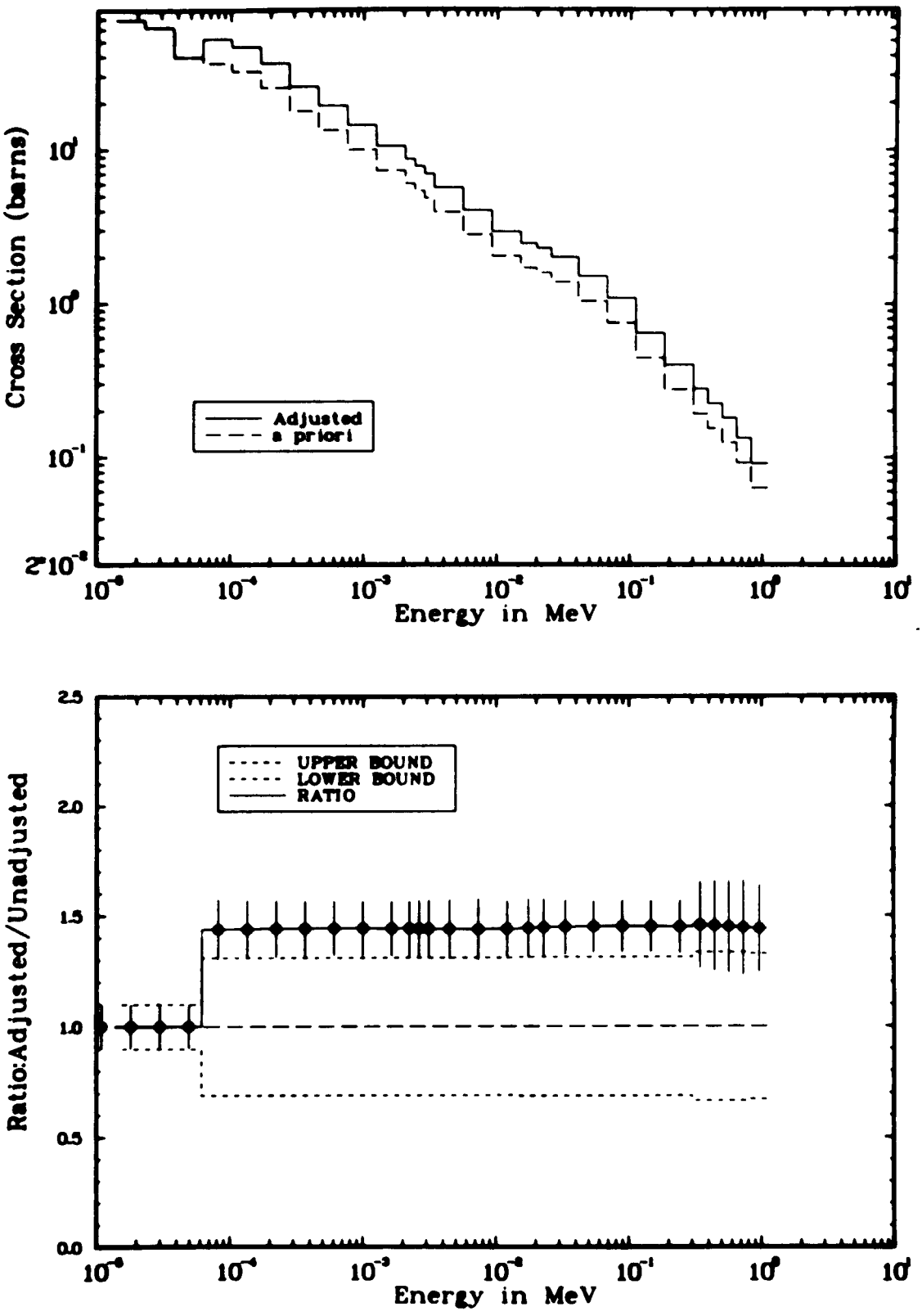

Figure 3. Comparison of adjusted and unadjusted cross sections for $^{243}Am(n,\gamma)$. In the lower half of the figure, input cross-section uncertainties are indicated by upper and lower bounds and adjusted uncertainties are indicated by vertical lines through the group mid-energy points.

Discussion

QUESTION: L. Weston
Did I understand correctly that the CFRMF results are normalized to the absolute fission cross section of Pu-239? This is of concern to me since, in my opinion, the ENDF/B-V fission cross section in this neutron energy region is too high by a few percent.

ANSWER: R. Anderl
The absolute flux determination for the CFRMF is based on the flux transfer method suggested by Grundl at NBS. This involves relating fission-rate measurements for ^{239}Pu in CFRMF to fission-rate measurements for ^{239}Pu in the NBS standard ^{252}Cf field so it does depend on the ^{239}Pu fission cross section. The transfer involves using the ratio for the ^{239}Pu(n,f) spectrum averaged cross section in CFRMF to that in the ^{252}Cf field and an independent measurement of the integral cross section in the ^{252}Cf field. The ratio is derived from calculated spectrum-averaged cross sections using ENDF/B-V data. Because of this fact, raising the cross section should not change the flux transfer. However, I would like to explore this further.

QUESTION: R. Block
Bob, you quote a C/M=0.87±11% for ^{232}Th capture. This seems to be just beyond standard deviation from unity. I cannot call this an 'outstanding' discrepancy.

ANSWER: R. Anderl
The 11% uncertainty was computed as the quadrature sum of the uncertainty in the measured integral quantity and an estimated uncertainty for the calculated integral quantity. The uncertainty in the measured integral quantity is ~ 3.8%. The spectrum uncertainty contribution to the calculated integral quantity is ~ 1.5%. The remaining uncertainty component for the calculated integral is due to estimated uncertainty in the ^{232}Th capture cross section as defined by ENDF/B-V. So the point is that ENDF/B-V has large uncertainties on the cross section over the energy response range in CFRMF. If we neglect this component, the C/M uncertainty is ~ 4%.

COMMENT: W. Poenitz
I would like to make a comment, Th(n,γ) of ENDF/B-V has been derived by matching two different evaluations around 30-40 keV. About 50% of the capture in your spectrum falls below this energy and it is there where ENDF/B-V is lower than the very well agreeing data sets which I mentioned in my talk. Thus, part of the problem would be solved by increasing ENDF in this low-energy range. Considering your uncertainty, the agreement would then be called good.

SOME ASPECTS OF THE EVALUATION OF 237Np, 238Pu AND 241Am CAPTURE CROSS-SECTIONS IN THE UNRESOLVED REGION

H. DERRIEN
CEN/CADARACHE - FRANCE

- INTRODUCTION -

The 237Np, 238Pu and 241Am neutron cross-sections have been evaluated in the energy range from 10^{-5} ev to 14 Mev /1,2,3/. Optical model and statistical model codes have been used to calculate the cross-sections in the unresolved region and at higher energy. The input parameters have been adjusted to reproduce the experimental data available in these energy ranges and particularly the capture cross-sections. The S_0 and S_1 strength functions obtained from resonance parameter analysis or from experimental capture cross-sections in the unresolved region have been compared to those deduced from the optical model calculations. In this paper, we present the different aspects of the evaluation related to the use of the experimental capture data as a basis in the determination of the statistical and optical model parameters.

- ^{241}Am -

The average parameters obtained from the analysis of the experimental resonance data are shown in Table I. The S_1 strength function is not given in this table, since all the resonances seen in the experimental cross-sections are s-wave resonances. The p-wave strength function should be obtained from the analysis of the experimental cross-sections in the unresolved region or from optical model parameters. A typical representation of the neutron cross-sections for a nucleus similar to 241Am is given in table II in the energy range from 1 kev to 40 kev where the compound nucleus formation cross-section is mainly due to the contribution of s-wave and p-wave neutrons ; the contribution of higher angular momenta is less than 0.6%. In this example, the s-wave neutron capture contri-

butes to 82% in the total compound cross-section at 1 kev and, then, is very sensitive to the S_0 strength function at this energy. At 40 kev, the contribution to the capture is about 60% from s-wave neutrons and about 40% from p-wave neutrons. These figures show that it is possible to obtain or to check the S_0 strength function from the capture data in the 1 kev region, and the S_1 strength function by fitting the capture cross-sections in the energy range below 40 kev. However, the accuracy in the determination of S_1 is limited by the fact that the p-wave capture width is not known ; that is not too important for 241Am, since the increase of the p-wave capture width by a factor of 2, results in an increase of only 6% of the total capture at 40 kev.

Three sets of measured capture or absorption cross-sections - the difference between absorption and capture is very small at low energy - are available in the unresolved region : absorption cross-sections from WESTON et al /6/ in the energy range thermal to 380 kev, capture cross-sections from GAYTHER et al /7/ between 0.1 kev and 500 kev and from WISSHAK et al /8/ between 10 kev and 220 kev. The WESTON and GAYTHER data are in good agreement below 10 kev and are well reproduced in the 1 kev region by the s-wave average parameters of table I. One can then conclude that the value $S_0 = (0.94 \pm 0.09) \times 10^{-4}$ gives a good representation of the total cross-section in the resonance region and of the capture cross-section at 1 kev. Above 10 kev WESTON data become lower than GAYTHER data and WISSHAK data, the difference being 20% at 40 kev. Fitting the GAYTHER and WISSHAK data leads to a S_1 strength function of 2.54×10^{-4}, when the fit to the WESTON data gives a value 1.82×10^{-4}, with a capture width value of 43.8 mev for both s-wave and p-wave neutrons. Using

a p-wave capture width of twice the s-wave value - as suggested by E. FORT /3,5/ - should give a S_1 value only 5% lower. Here, the lack of accuracy in the determination of S_1 is mainly due to the discrepancy among the available experimental data.

Looking now to the optical model, a set of parameters have been obtained by E. FORT /3,5/ by fitting the measured total cross-sections of PHILLIPS et al /9/ in the energy range 0.45 Mev to 16 Mev (table III). These optical model parameters correspond to a S_0 strength function of 1.225×10^{-4}, leading to a capture cross-section of 12.8 barns at 1 kev, which is about 25% larger than the experimental values. At 40 kev, the calculated capture value is then equal to 2.20 barns in agreement with GAYTHER et al. and WISSAK et al. data, i.e. 20% higher than WESTON et al. data. On the other hand, using the same parameters as those obtained by LAGRANGE /10/ for the even plutonium isotopes (table IV), one obtain a S_0 value of 0.98×10^{-4} and a good description of WESTON absorption in the energy range 1 kev to 40 kev. But at high energy, the fit to the PHILLIPS total cross-section is not as good : -8% at 0.5 Mev, -1.6% at 1 Mev, +4% at 2 Mev and -0.5% at 5 Mev which, however, is not a too bad situation. If one adopts this solution for the description of the 241Am neutron cross-sections, then the S_1 strength function should be $(1.80 \pm 0.20) \times 10^{-4}$. Figure 1 shows the results of some calculations in the unresolved region.

Considering now the integral data, the results of the measurements in RAPSODIE and PHENIX /16/ confirm the data of GAYTHER and WISSHAK. Therefore, the Cadarache evaluation /9,5/ has been performed according to the highest values.

- ^{237}NP -

As it is shown on table I, the average parameters obtained by analysing the resonance data are very similar to those of 241Am and the cross-sections calculated in the unresolved region should be very close to those shown in table II. The capture cross-section should exhibit the same sensitivity to the strength functions S_0 and S_1 between 1 kev and 40 kev.

The absorption cross-section has been measured by WESTON et al. /11/ in the energy range from thermal region to 500 kev and normalized to that obtained from the total cross-section measured at Saclay /12,1/. A statistical model calculation using the parameters of table I gives a valueof 10.65 barns at 1 kev in excellent agreement with the experimental value of 10.70 barns obtained by averaging WESTON et al. data in the energy range 0.8 kev to 1.2 kev. Below 40 kev, WESTON et al. data are well fitted by using in addition a S_1 strength function value equal to 1.82×10^{-4}, with a capture width of 40.0 mev for both s-wave and p-wave.

There is no experimental total cross-section data available at high energy to check the validity of a set of optical model parameters for 237Np. One must, at least, reproduce the strength functions obtained from the resonance parameters and from the absorption data. That has been done in our evaluation /1/. The parameters obtained, which are shown in table V, are still very similar to those used by LAGRANGE for the even Pu isotopes. They correspond to a S_0 strength function value equal to 0.98×10^{-4} and a S_1 strength function value equal to 1.76×10^{-4} at 40 kev, i.e. very close to those obtained from a pure statistical model fit to the WESTON data.

The figure 2 shows the calculated absorption cross-sections compared to WESTON et al. experimental data.

- ^{238}PU -

This nucleus does not show the same features as 241Am or 237Np in the unresolved region. The capture cross-section and the fission cross-section have the same order of magnitude in the low energy range and it is not possible to find an accurate value of the S_1 strength function by fitting only the capture cross-section in the energy range 1 kev to 40 kev. The experimental data available below 40 kev are mainly the total cross-section measured by YOUNG et al. /13/, and the fission and capture cross-sections measured by SILBERT et al. /14,15/. From the resonance parameters published by these authors, one obtain the average parameters given in table I. The value of the S_0 strength function is equal to 1.17×10^{-4} which is 24% higher than the value of 0.944×10^{-4} obtained by LAGRANGE /10/ from his optical model parameters. A better agreement is found by using the parameters given in table VI, corresponding at 1 kev to the strength functions $S_0 = 1.12 \times 10^{-4}$ and $S_1 = 1.97 \times 10^{-4}$ /2/.

One of the most severe difficulties encountered in the evaluation of 238Pu cross-sections is due to the capture cross-section. As it is shown on figure 3, it is impossible to represent the experimental capture data in the resonance region without using a large background of 4 to 7 barns. This background is too important to be explained by direct capture, negative resonances or other external effect. In our evaluation, we do not take it into account considering that it is due to some experi-

mental effect. This effect should remain at higher energy in the unresolved region where its importance could be evaluated by performing a statistical model calculation of the cross-sections in this energy range. Such a calculation has been made using the parameters of table I, the S_1 strength function corresponding to the optical model parameters of table VI and a fission barrier which reproduces the average experimental fission cross-sections between 1 kev and 40 kev. The results are shown in table VII. The correction to the SILBERT et al. capture data varies from 1.3 barns on average between 1 kev and 4 kev and 0.48 barns on average between 20 kev and 40 kev, which is more than 30% of the measured values.

The results of our evaluation is confirmed by the integral capture measurements in PHENIX /16/.

REFERENCES

/1/ H. DERRIEN et al.
INDC(FR)-42/L

/2/ H. DERRIEN
To be published

/3/ E. FORT et al.
To be published

/4/ H. DERRIEN et al.
Proceeding of the specialist's meeting on nuclear data of Pu and Am isotopes for reactor applications.
BNL, Nov. 1978, page 71.

/5/ E. FORT et al.
International conference on Nuclear cross-sections for technology.
Knoxville, Oct. 1979.

/6/ L. WESTON et al.
Nuclear Science and Engineering 61, 356 (1976).

/7/ D.B. GAYTHER et al.
Proceedings of IV National Soviet Conference on Neutron Physics.
Kiev, 1977, Vol. 3.

/8/ K. WISSHAK et al.
Proceedings of the specialist's meeting on nuclear data of Pu and Am isotopes for reactor applications.
BNL, Nov. 1978.

/9/ T.W. PHILLIPS et al.
UCRL-81176 (1978).

/10/ C. LAGRANGE
CEA-N-1970 (1977).

/11/ L. WESTON et al.
Private communication

/12/ L. WESTON et al.
DOE Progress Report (1981).

/13/ T.E. YOUNG et al.
Nuclear Science and Engineering 30, 355 (1967).

/14/ M.G. SILBERT et al.
Nuclear Science and Engineering 52, 176 (1973).

/15/ M.G. SILBERT et al.
Nuclear Science and Engineering 52, 187 (1973).

/16/ A. GIACOMETTI et al.
Colloque International sur la physique des réacteurs à neutrons rapides.
Aix-en-Provence, Septembre 1979.

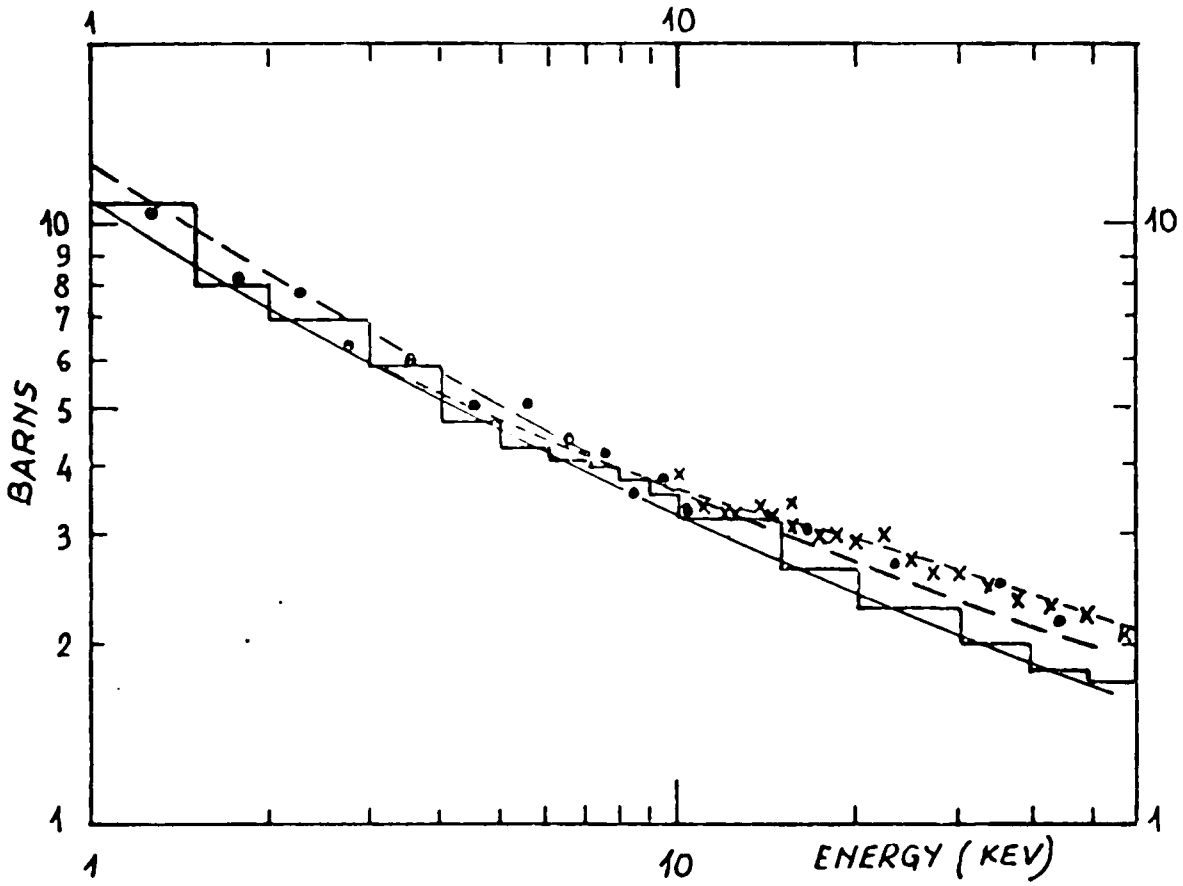

Fig. 1 : Experimental and calculated ^{241}Am capture cross-sections in the energy range 1 kev to 40 kev.

WESTON et al. data

● GAYTHER et al. data

X WISSHAK et al. data

— Statistical model calculations with the parameters of Table I and $S_1 = 1.80 \times 10^{-4}$

------ Statistical model calculations with the parameters of Table I and $S_1 = 2.54 \times 10^{-4}$

– – – – From optical model calculations with the parameters of Table III

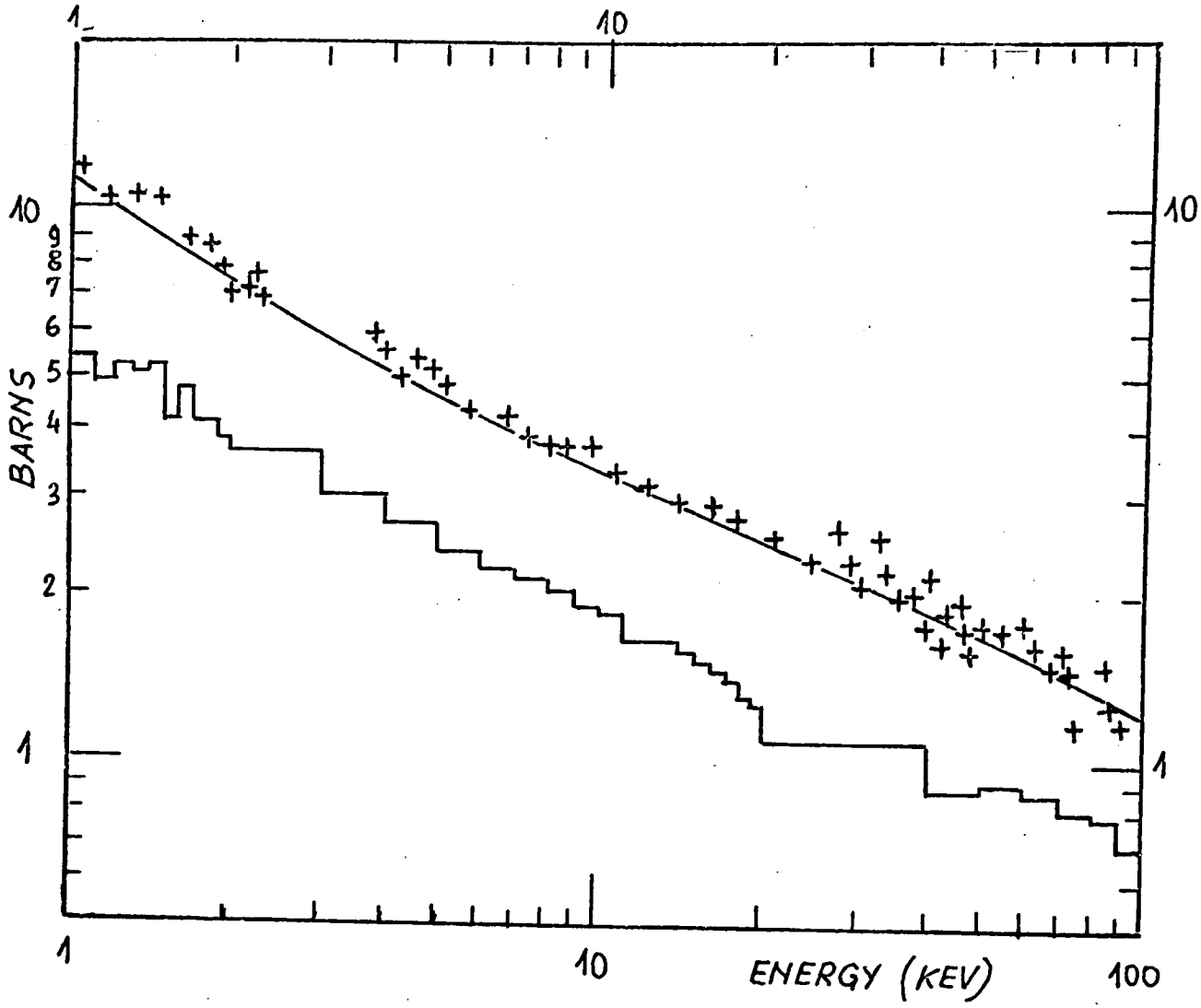

Fig. 2 : Experimental and calculated ^{237}Np capture data in the energy range 1 kev to 100 kev.

+ WESTON et al. data

HOFFMANN et al. data

— Statiscal model calculations with the parameter of Table I and $S_1 = 1.82 \times 10^{-4}$ (very similar to the results of the calculations using the optical model parameters of Table V)

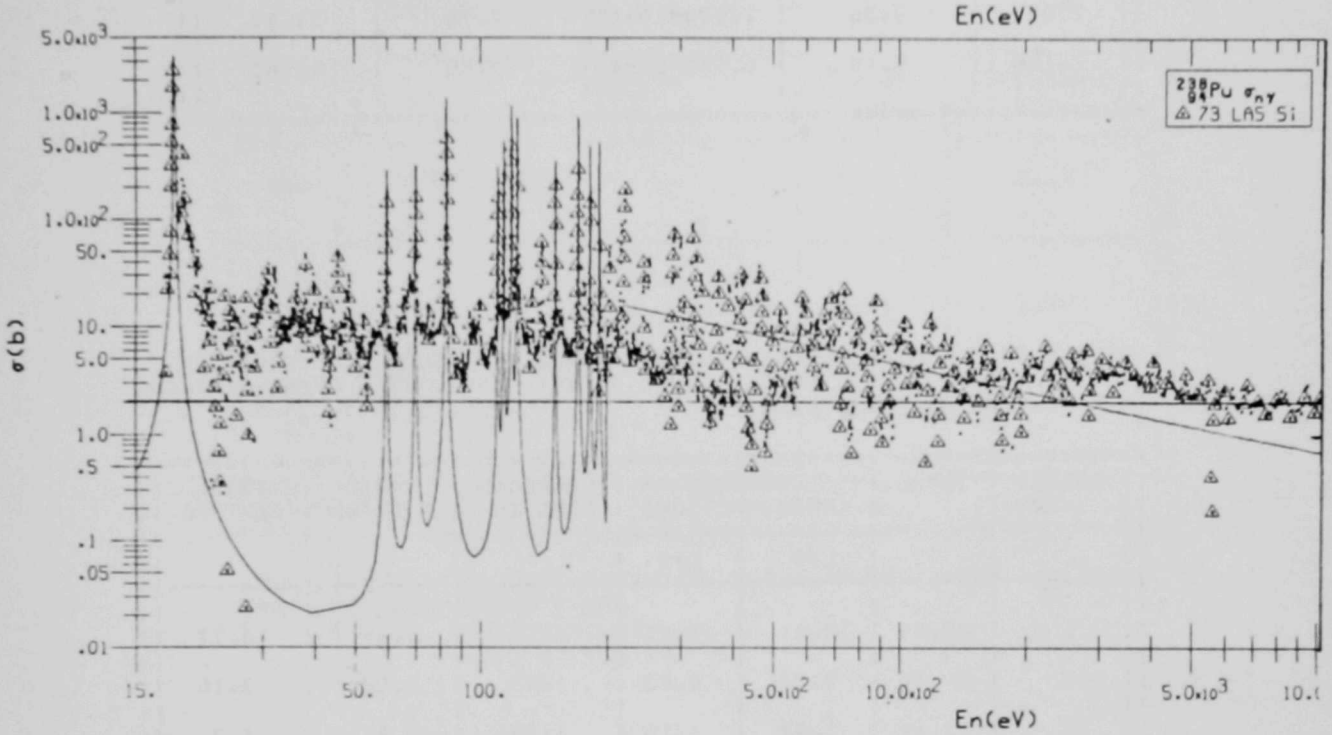

Fig. 3 : ^{238}Pu capture cross-sections in the energy range 15 ev to 10 kev (from BNL 325)

TABLE I - AVERAGE PARAMETERS OBTAINED FROM S-WAVES RESONANCE PARAMETERS ANALYSIS

NUCLEUS	EFFECTIVE SCATTERING RADIUS(FM)	STRENGTH FUNCTION	LEVEL SPACING (EV)	CAPTURE WIDTH (mev)
237NP	9.54	0.994*10-4	0.56	40.00
238PU	9.36	1.170*10-4	7.70	34.00
241AM	9.40	0.940*10-4	0.55	43.80

TABLE II - TYPICAL CROSS-SECTION VALUES OF A NUCLEUS SIMILAR TO 241AM IN THE ENERGY RANGE 1KEV TO 40KEV (THE CROSS-SECTIONS ARE GIVEN IN BARNS)

ENERGY (KEV)	TOTAL	COMPOUND CROSS-SECTIONS		COMPOUND ELASTIC	TOTAL FISSION	TOTAL CAPTURE
		L=0	L=1			
1	23.45	12.81	0.21	2.16	0.09	10.77
10	14.70	3.98	0.63	1.43	0.02	3.16
40	12.50	1.97	1.16	1.18	0.01	1.93

TABLE III - OPTICAL MODEL PARAMETERS USED BY E.FORT (3) FOR PHILLIPS ET AL. (9) 241AM TOTAL CROSS-SECTIONS

POTENTIAL	DEPTH(MEV)	RADIUS (FM)	DIFFUSENESS (FM)
REAL	47.0-03E	1.23	0.62
SURFACE IMAGINARY	2.7+0.4E FOR E <= 10MEV 6.7 FOR E >= 10MEV	1.26	0.58
REAL SPIN ORBIT	7.5	1.24	0.62

DEFORMATION PARAMETERS : β_2 = 0.220 β_4 = 0.036

THIS POTENTIAL IS EQUIVALENT TO THE FOLLOWING STRENGTH FUNCTIONS AT 1KEV

S0 = 1.225*10-4

TABLE IV - OPTICAL MODEL PARAMETERS USED BY LAGRANGE (10) FOR PU ISOTOPES

POTENTIAL	DEPTH(MEV)	RADIUS (FM)	DIFFUSENESS (FM)
REAL	47.5-03E	1.24	0.62
SURFACE IMAGINARY	2.7+0.4E FOR E <= 10MEV 6.7 FOR E >= 10MEV	1.26	0.58
REAL SPIN ORBIT	7.50	1.24	0.62
DEFORMATION PARAMETERS : β_2 = 0.216		β_4 = 0.089	

APPLIED TO 241AM, THIS POTENTIEL CORRESPONDS TO THE FOLLOWING STRENGTH FUNCTIONS AT 10KEV

S0 = 0.960*10-4
S1 = 1.850*10-4

TABLE V - OPTICAL MODEL PARAMETERS USED BY H.DERRIEN ET AL.(1) FOR 237NP. THEY ARE SIMILAR TO THOSE USED BY LAGRANGE (10) FOR PU ISOTOPES.

POTENTIAL	DEPTH(MEV)	RADIUS (FM)	DIFFUSENESS (FM)
REAL	47.57-03E	1.235	0.62
SURFACE IMAGINARY	2.7+0.4E FOR E <= 10MEV 6.7 FOR E >= 10MEV	1.235	0.62
REAL SPIN ORBIT	7.50	1.24	0.62
DEFORMATION PARAMETERS : β_2 = 0.218		β_4 = 0.055	

THIS POTENTIAL CORRESPONDS TO THE FOLLOWING STRENGTH FUNCTIONS AT 40KEV

S0 = 0.980*10-4
S1 = 1.760*10-4

TABLE VI - OPTICAL MODEL PARAMETERS USED BY H.DERRIEN ET AL.(2) FOR 238PU CROSS-SECTIONS

POTENTIAL	DEPTH(MEV)	RADIUS (FM)	DIFFUSENESS (FM)
REAL	47.20-03E	1.244	0.62
SURFACE IMAGINARY	2.7+0.4E FOR E <= 10MEV 6.7 FOR E >= 10MEV	1.280	0.58
REAL SPIN ORBIT	7.50	1.240	0.62
DEFORMATION PARAMETERS : β_2 = 0.216 β_4 = 0.089			

THE CORRESPONDING STRENGTH FUNCTIONS ARE THE FOLLOWING AT 1 KEV

S0 = 1.120*10-4

S1 = 1.970*10-4

TABLE VII

ENERGY (KEV)	AVERAGE FISSION (EXP.) REF.(14),(15)	AVERAGE CAPTURE (EXP.) REF.(14),(15)	AVERAGE CAPTURE (CALC.)	DIFFERENCE CAPTURE
0.050- 0.300		23.43	18.80 (1)	4.62
0.060- 1.000	3.98	12.11	7.75 (2)	4.86
1.00 - 4.00	1.22	3.97	2.67 (2)	1.30
4.00 -10.00	0.98	2.25	1.35 (2)	0.90
10.00 -20.00	0.752	1.744	0.950 (2)	0.79
20.00 -40.00	0.803	1.152	0.675 (2)	0.48

(1) CALCULATED FROM RESONANCE PARAMETERS

(2) STATISTICAL MODEL CALCULATIONS COHERENT WITH THE AVERAGE EXPERIMENTAL FISSION VALUES

Discussion

QUESTION: E. Menapace
$\langle\Gamma_\gamma\rangle$ values, for s- and p- waves are equal in your evaluation of ^{237}Np. Is that a consequence of model calculations or a pure assumption? Concerning the deformation parameters β_2 and β_4 in OM calculations for the same nucleus, are they obtained according to the quadrupole moment or simply adjusted for reproducing the estimated strength-function values?

ANSWER: H. Derrien
A good fit to the WESTON et al. absorption data is obtained by using the same $\langle\Gamma_\gamma\rangle$ values for s and p waves. It is not a consequence of model calculation. The deformation parameters β_2 and β_4 have been adjusted with view of reproducing the values of the strength functions. However, the β_2 are very similar to those used by LAGRANGE; only β_4 can be very different.

THE STATUS OF STRUCTURAL MATERIAL DATA IN THE RESOLVED RESONANCE REGION

by

G. Rohr
CEC-JRC, Geel Establishment
Central Bureau for Nuclear Measurements, B-2440 Geel, Belgium

Abstract

This review is mainly concerned with the accuracy aspect of neutron capture data for structural materials. As examples data sets of ^{54}Fe, ^{56}Fe and ^{57}Fe will be compared critically. The results of the investigation of the C_6D_6 detector performed at CBNM will be used to study the deviations in the different data sets. Recommendations to reduce the uncertainty of capture data and to improve the capture detectors using the weighting method will be given.

I. Introduction

Many high resolution neutron capture cross section measurements of structural materials (S.M.) have been performed over the last 15 years. In total there are now five resonance data sets available for the most important S.M., i.e. the main iron isotopes. The capture areas ($g\,\Gamma_n\Gamma_\gamma/\Gamma$) are still not accurately known. The discrepancies are typically 20% even for well isolated resonances and exceed 50% for broad s-wave resonances.

At the last specialists meeting on S.M. in Geel /1/ the neutron sensitivity of capture detectors has been made mainly responsible for the large deviation obtained in resonances with $\Gamma_n \gg \Gamma_\gamma$. In the meantime a substantial effort has been devoted to reduce this effect by using improved detectors and special techniques.

In a contribution to the Knoxville Conference /2/ special emphasis has been given to problems connected with capture detectors incorporating the weighting method and to the normalization of capture data of ^{56}Fe /3/. According to this the normalization performed with resonances of different γ-ray spectra hardness may lead to systematic errors which are reflected in weak as well as strong resonances.

This review is mainly concerned with the accuracy aspect of capture data for S.M.. As examples data sets of ^{54}Fe, ^{56}Fe and ^{57}Fe, including new results for ^{54}Fe and ^{57}Fe from CBNM, will be compared critically. The results of the investigation on the C_6D_6 detector performed at CBNM will be used to study the deviations in the different data sets. Recommendations to reduce the uncertainty of capture data and to improve the capture detectors using the weighting method will be given.

II. PROBLEMS IN MEASURING CAPTURE CROSS SECTIONS OF STRUCTURAL MATERIALS

A typical capture cross section of S.M. is shown in Figure 1, where $\sigma(n,\gamma)$ of ^{54}Fe is plotted in the energy ranges 5-12 keV and 50-60 keV. The cross section has a pronounced resonance structure represented by very broad s-wave resonances with a small peak cross section and very sharp p- and d-wave resonances. The extremely large scattering to capture ratio of 10^3-10^4 in the broad resonances makes the measurement of the capture cross section a problem. Multiple scattering of the neutrons in the sample and their subsequent capture causes corrections which exceed 100% of the first collision capture yield (indicated by a solid line in Figure 1) in practical sample thicknesses. There are three Monte Carlo codes available which can handle even larger corrections within an agreement of 3% /4/. These are the codes developed at ORNL-RPI /5/, KFK (FANAC) /6/ and at Harwell (REFIT) /7/. The second consequence is the prompt background caused by neutrons scattered in the sample and captured in the detector or its environment. Methods similar to those used for the determination of the multiple scattering effect can be employed to determine the prompt background. However these methods require rather extensive calculations or very difficult measurements of the energy dependent neutron sensitivity of the capture detectors, which depends on all materials in the detector system and its vicinity. More efficient is a reduction of this effect by using appropriate detectors with a minimum of constructional material which should, moreover, have a low capture cross section. In special cases the prompt background can be eliminated for resonances in a limited energy range (15-40 keV) by performing short-distance measurements at the Van de Graaff, where the capture yield and the scattered neutrons are separated by time of flight /8,9/. The underestimation of the prompt background leads to a correlation between the resonance parameters Γ_n and Γ_γ, which is sometimes interpreted as evidence of a valence nucleon contribution.

Another complication in measuring capture in S.M. results from the de-excitation process. The low level density of the compound system together with the Porter Thomas distribution for the partial transition strength favours high energy transitions with a strength varying substantially. A relative measure of the hardness and the fluctuation of γ-ray spectra in resonances can be obtained using one of the detectors suited for the application of the weighting method. Results of the C_6D_6-system are given in Figure 2, where the mean value of the average weight $< w >$ (ratio of weighted to unweighted resonance areas for the particular weighting function used at CBNM) is plotted against the atomic number A for various nuclei. The error

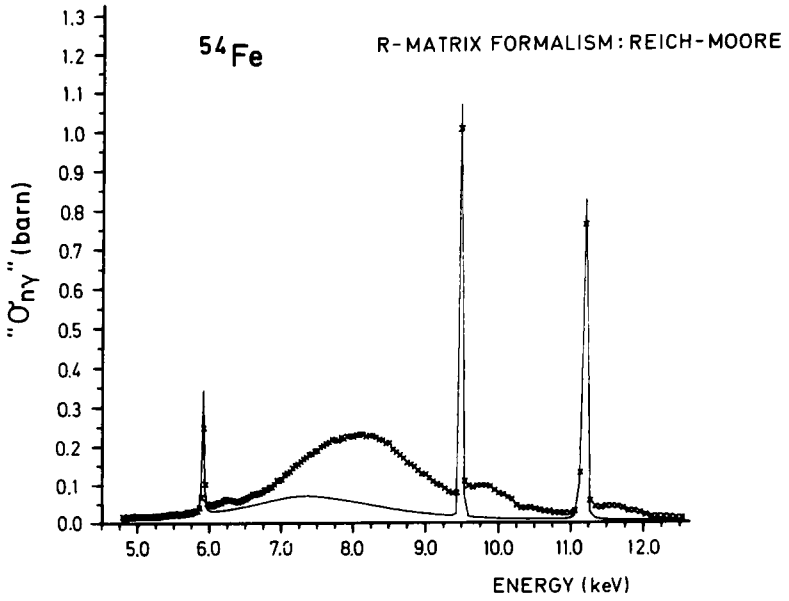

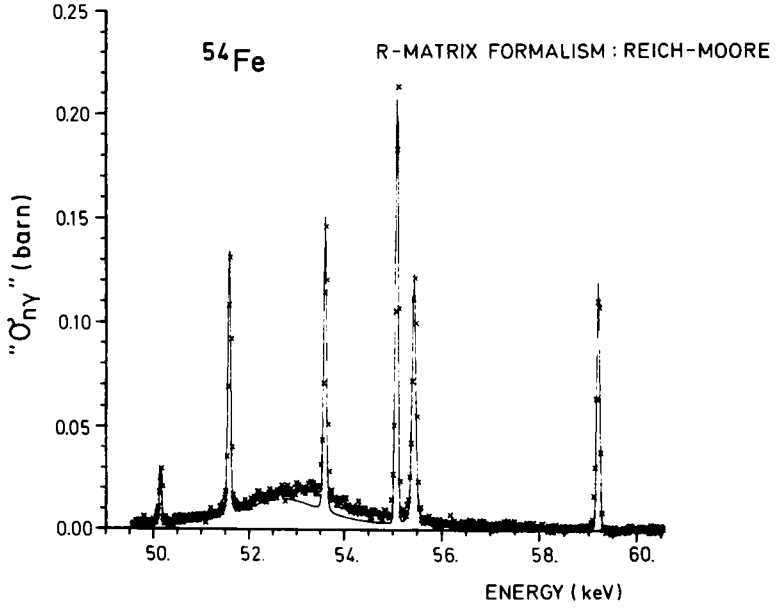

Fig. 1 Typical capture cross section of ^{54}Fe

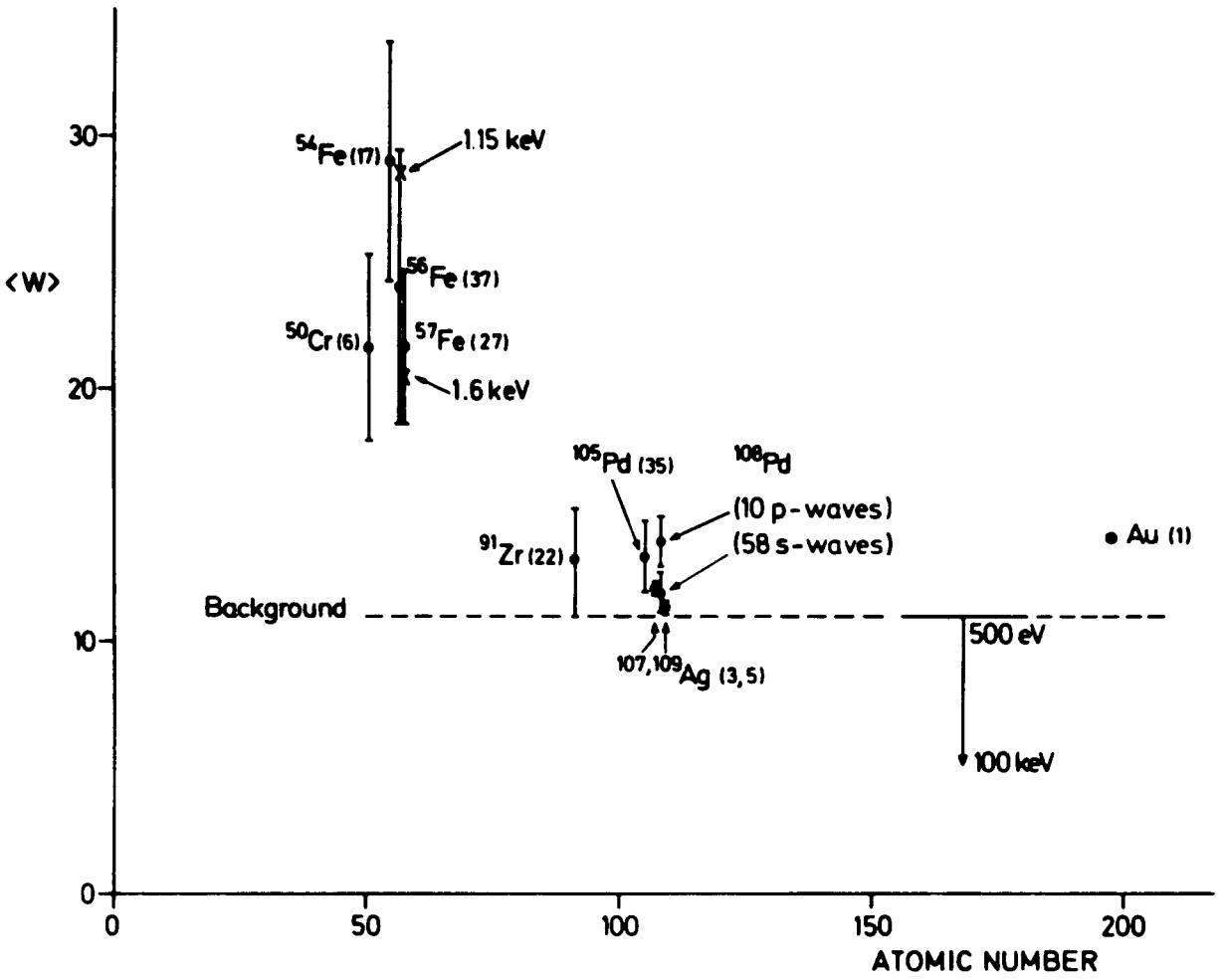

Fig. 2 Average weight w (γ-ray spectra hardness) for various isotopes (arbitary units)

bar assigned to each isotope gives the $\pm 1\sigma$ deviation of the $< w >$ value distribution calculated for the total number of resonances given in brackets near the isotopic symbol. The γ-ray spectra of S.M. ($A < 70$) are much harder and vary more widely than those elements, such as Au and Ag, which are normally used for the normalization of capture data. For example, in ^{56}Fe the 1.15 keV resonance has the same γ-ray spectra hardness as at thermal energy /3/ where the two transitions, to the ground state and to the 14 keV level in ^{57}Fe, have almost 50% of the total intensity from the capture state /10/. The "correction of the efficiency" using the weighting function for the 1.15 keV resonance in ^{56}Fe ($< w > = 28.9$) compared to that of Ag resonances ($< w > = 10.9$) is almost a factor three. Assuming that no capture detector is perfect, the normalization becomes more accurate when resonances with similar γ-ray spectra are used.

On the other hand resonances with very different spectra can be used as an excellent tool to study the independence of the detector response to the particular γ-ray decay mode.

Another consequence of these specific γ-ray spectra is the large fluctuation of the total radiation widths. The distribution function of Γ_γ can be described by a χ-square function with a low degree of freedom ν and can be calculated by means of the statistical model. For ^{56}Fe, Γ_γ = 0.92 eV (s-wave) and ν = 8 is obtained using the known level scheme of the compound nucleus up to 5 MeV /11/. The low degree of freedom can prevent a good description of the actual cross section in between resonances by means of the Reich-Moore R-Matrix formalism /12/.

III. CAPTURE SPECTROMETER USED FOR STRUCTURAL MATERIALS

In the following the capture detectors and their properties, in respect to efficiency and the prompt background, are summarized. The result of the total radiative width for the 27.7 keV resonance in ^{56}Fe has been used to check the treatment of the prompt background in different detector systems. This information is relevant to judge the deviations in the capture area discussed in the next section.

III.A. MEASUREMENTS REVIEW

RPI: The first high resolution capture cross section for S.M. was performed at the RPI linac using a large scintillator of 1100 l /13/. The efficiency correction has been divided into two parts: the first is due to the high bias setting of the discriminator corresponding to a γ-ray energy of 2.5 MeV, introduced to exclude capture events in hydrogen. The fraction of the scintillator events passed by the discriminator, the so-called "spectrum fraction", was determined from pulse-height data. A value of 0.69 $\pm$ 0.03 for all resonances in ^{56}Fe was used. The second part concerns the cascade correction, an estimation made for the photons which pass through the detector without interaction. Assuming that the capture γ-ray de-excitation scheme is the same for resonance capture as that for thermal neutron capture, a value of 0.87 $\pm$ 0.02 was obtained. The total efficiency is then the product of the spectrum fraction and the cascade correction and results for ^{56}Fe as 0.60 $\pm$ 0.035. A very low neutron sensitivity $\epsilon_n/\epsilon_\gamma \sim 10^{-5}$ has been measured and therefore no correction of the prompt background was made. A total radiative width of 1.44 eV has been obtained for the 27.7 keV resonance.

KFK: The measurement of Karlsruhe has been performed at the 1 n-sec pulsed Van de Graaff generator with a large liquid scintillator (800 l), separated into four parts, in order to get qualitative information on the γ-ray multiplicity for individual resonances /14/. In addition crude γ-ray spectra taken with a bias of 3 MeV have been measured in order to correct the spectrum fraction and the cascade correction for resonances individually. The neutron sensitivity has been measured and its correction changed the Γ_γ value of the 27.7 keV resonance from 1.4 eV to 1.25 eV /35/.

ORNL-AAEC: The first measurements of S.M. with a hydrogen free C_6F_6 detector using the weighted methods has been performed at ORELA. The low bias of 0.15 MeV γ-ray energy needed no correction for the spectral fraction. The cascade correction (escape probability) is included in the pulse-height weighting. The neutron sensitivity is rather large due to the construction of the detector and the resonance structure of fluorine in the scintillator. The very uncertain value of Γ_γ = 1.4 eV for the 27.7 keV resonance, obtained without correction of the neutron sensitivity /15/, has been even increased to Γ_γ = 1.6 eV taking into account the prompt background /16/.

A.E.R.E.: A relatively small liquid scintillator (270 l) divided into two parts has been used at the Harwell linac. All corrections, the spectrum fraction (bias 2.5 MeV) and the cascade correction are performed with a semi-empirical method using the code GAMOC. This Fortran program simulates the observed pulse-height distribution in individual resonances by a Monte Carlo routine based on typical cascade schemes. The neutron sensitivity of the detector below 100 keV neutron energy is smaller than that of the ORNL and KFK, because of a Be-tube which passes through the tank /17/. The inclusion of a prompt background correction of 10% results in Γ_γ = 0.85 eV for the 27.7 keV resonance.

CBNM: Two C_6D_6-detectors together with the weighting method have been used at GELINA /3/. The normalization of the capture data is performed with resonances which have a similar γ-ray spectrum to the resonances to be measured. The neutron sensitivity is not yet determined but care was taken to minimize the constructional material of the detector. A scintillator with no neutron resonance structure in the measured energy range was used. For the 27.7 keV resonance a total radiative width Γ_γ = 1.00 eV was obtained.

KFK and AAEC: A special technique has been applied to eliminate the prompt background in the 27.7 keV resonance at the Van de Graaff at Karlsruhe and Lucas Heights. Both laboratories produced neutrons in a limited energy range of 20-40 keV and the capture yield was measured with Moxon-Rae detectors. The distance, ^{56}Fe sample-detector, was chosen as two times larger than the distance neutron target-detector in order to separate the scattered neutrons at the sample from the prompt γ-rays by time of flight. The results of the total radiative widths are 0.78 eV and 1.0 eV for Lucas Heights and Karlsruhe respectively /8,9/. In a contribution to this meeting from Karlsruhe the same method has been applied using different versions of Moxon-Rae-detectors to improve the radiative widths of s-wave resonances /18/.

III.B. SOME TESTS WITH C_6D_6-DETECTORS

The starting point of studies in connection with the weighting method, using C_6D_6 scintillators at CBNM, was the use of the ^{56}Fe (1.15 keV)resonance for normalization /3/. The application of this resonance for structural materials should have the following advantages:

1) the 1.15 keV resonance is an almost pure capture resonance ($\Gamma_n < \Gamma_\gamma$), hence the capture area can be determined very precisely in a transmission experiment.

2) the γ-ray spectrum of this resonance is very hard, similar to those which have to be measured.
3) the ^{56}Fe-isotope is present as an impurity in all iron samples, eliminating the need for a special normalization run.
4) no extrapolation of the neutron flux from eV to keV range is needed, as would be the case for the Au and Ag resonances generally used for normalization.

With these conditions the accuracy of the capture data for the iron isotopes depends mainly on the precision of the relative flux measurement.

The problem came to light because of the widely differing results of the capture area for the ^{56}Fe (1.15 keV) resonance obtained in the transmission experiment (Γ_n = 58 meV, Γ_γ = 610 meV, A_γ = 53 meV) and the capture measurement normalized to the low energy Ag-resonances (A_γ = 70 meV).

A capture measurement for the same resonance normalized to the precise capture cross section at thermal energy yielded A_γ = 0.52 meV, which is in very good agreement with the transmission result. The normalization at thermal energy is independent of the weighting function because the hardness of the γ-ray spectra at thermal energy and for the 1.15 keV resonance is the same. We have to conclude that the Ag-normalization overestimates the capture area for resonances with a hard spectrum.

In order to test the weighting function thermal capture measurements have been performed with samples, listed in Table 1, of widely varying neutron separation energy (S_n) and spectral shape ($< w_{th} >$). The detector efficiency ϵ normalized to unity for Ag is defined as the ratio between thermal "weight" counting rate C_w and the product of S_n and the capture probability P_γ listed in column 5. The overestimation of the structural material data is reproduced, but the results are not satisfactory since the deviations of the efficiency from unity are not correlated with the average weight (hardness) of the spectra.

The ^{56}Fe data of CBNM published at Knoxville /3/ have been corrected for a deviation of 10% between Ag-normalization and the transmission result of the 1.15 keV resonance. The change in the capture area depends on the average weight $< w(E_x)>$ of the resonance E_x and has been calculated by linear interpolation according to:

$$\Delta A_\gamma/A_\gamma = 0.1 \cdot [< w(1.15)> - < w(E_x)>] / [< w(1.15)> - < w(Ag)>] .$$

Very recently the capture area of the ^{56}Fe (1.15 keV) resonance normalized to Ag has been tested at Geel using different weighting functions (WF). The WFs plotted in Figure 3 have been employed:
The 'OLD' WF is calculated with a Monte Carlo based computer code developed at Cadarache and Karlsruhe /19/. The same WF was obtained at AERE /20/ using the routine GAMOC and a Fortran program based on an analytical method developed at ORNL /21/. All three codes use a mathematical expression to calculate the most probable energy loss of the electrons in the scintillator.

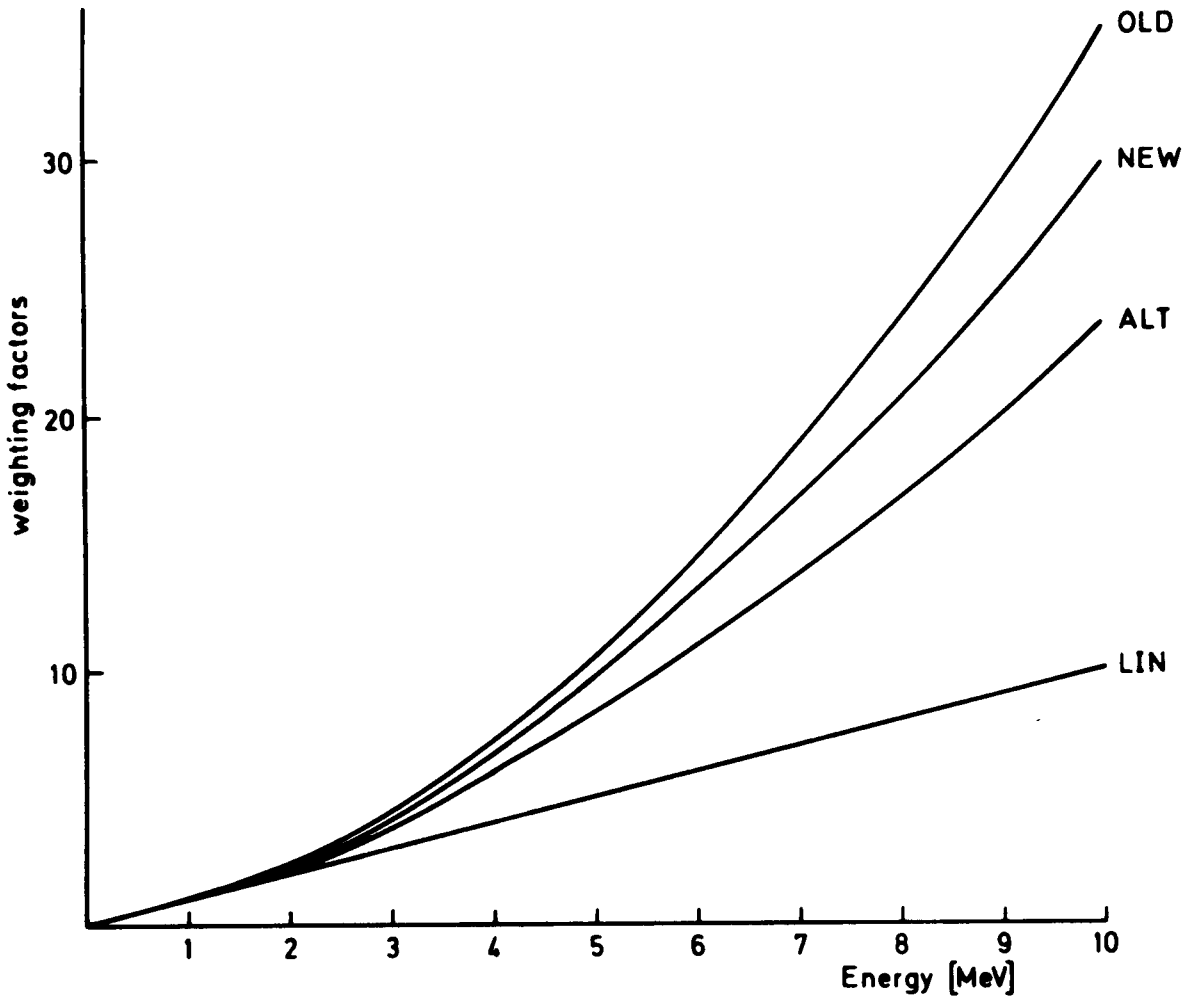

Fig. 3 C_6D_6 capture detector weighting functions

The 'NEW' WF has been calculated using an increased energy loss of electrons in the scintillator employing newly evaluated data from Atomic Data /22/. The 'ALT' WF includes γ-absorption in the sample and the scintillator containers by assuming an absorption of 40% for a γ-ray energy of 330 keV, corresponding to the absorption in 1 mm of Ag (R = 4 cm) or in the Fe oxide samples used for the measurements at CBNM. As an upper limit the linear WF (LIN) has been added for comparison.

In Table 2 the capture areas normalized to Ag obtained for the different WFs have been listed for ^{56}Fe (1.15 keV) and, in addition, ^{57}Fe (1.6 keV), a newly measured pure capture resonance with the following resonance parameters obtained in a transmission measurement /23/: Γ_n = (42.6 ± 0.4) meV and Γ_γ = (996. ± 300) meV (ℓ = 1, J = 2, g = 1.25). The transmission results for the pure capture resonances are given under TRA in the table.

In the case of ^{57}Fe excellent agreement is obtained between the transmission value and the capture result using the 'NEW' weighting function. On the other hand to get a similar agreement for ^{56}Fe it becomes necessary to utilize a WF that is nearer to the 'LIN' one. There is no WF for which transmission results for both ^{56}Fe and ^{57}Fe can be reproduced. However, we conclude that the weighting method can be used confidently at least for resonances with an average weight up to $< w > = 20.5$. As plotted in Figure 4 the method fails for the ^{56}Fe (1.15 keV) resonance with $< w > = 28.9$, where the capture area is overestimated by 22.6% using the NEW weighting function. The weighting function used in this method is only valid for a single γ-ray of a cascade. The sum of two pulses is assigned more weight than the two pulses taken separately, due to the non-linearity of the WF. The overweighting for coincidences for typical spectra has been estimated to be 25% /24/ and together with a coincidence rate of 8% gives a mean overweight of 2%. The result for the 1.15 keV resonance normalized to Ag seems also to indicate an overestimation; in this resonance the total energy of the capture process is released in γ-quanta larger than 7.5 MeV for almost half

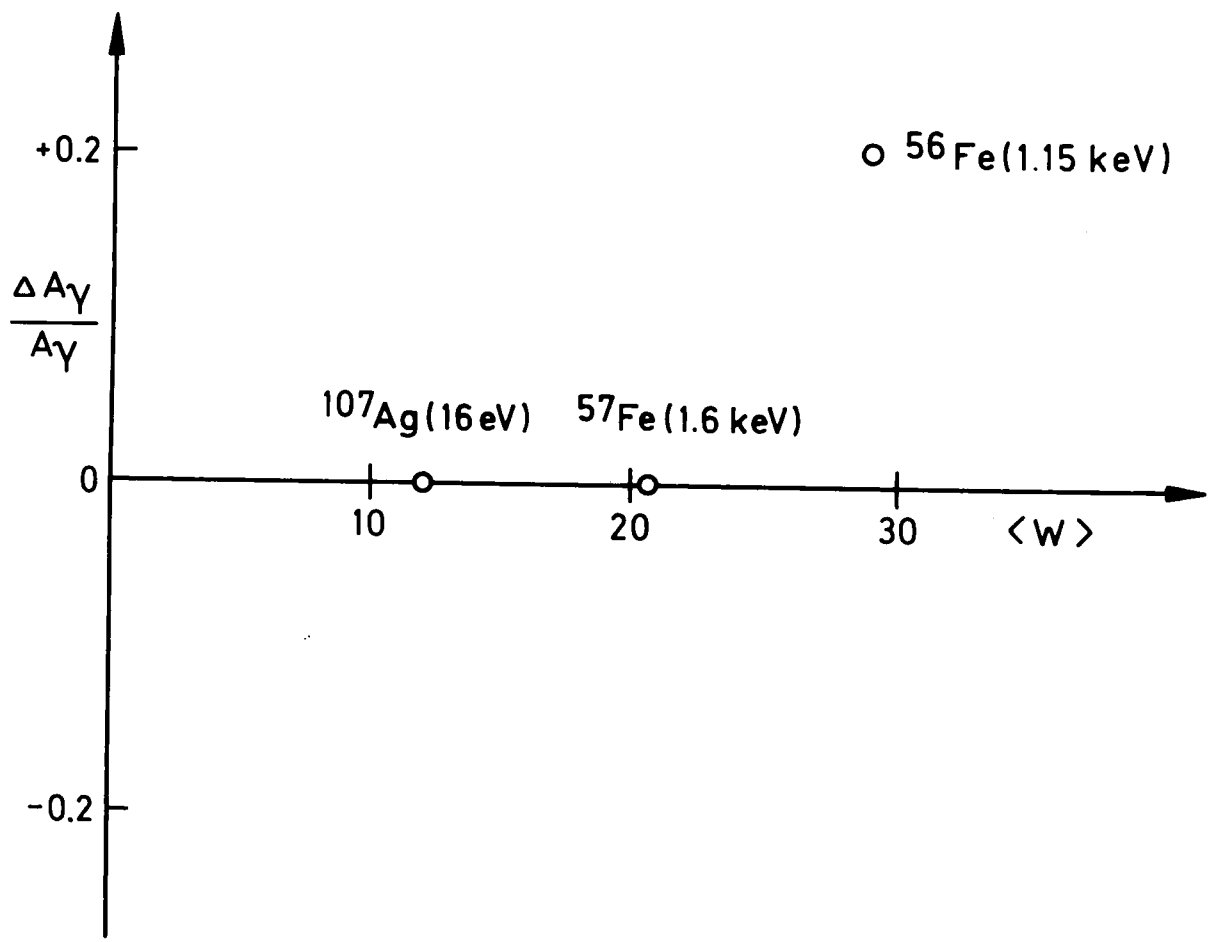

Fig. 4 Behaviour of C_6D_6 detector capture yield for resonances with different γ-ray spectrum hardnesses

of all transitions. In order to determine the upper limit of the validity of the pulse height weighting technique and to study the behaviour of the detector beyond this limit, more pure capture resonances with different $< w >$ have to be measured. But there is a possibility of getting this information by comparing results from other capture detectors which do not depend so strongly on the spectral shape.

IV. STATUS OF CAPTURE CROSS SECTION DATA FOR STRUCTURAL MATERIALS

Structural material data published since the last specialist meeting at Geel are shown in Table 3. Most of the publications are concerned with the iron isotopes, which will be taken as an example to discuss the status of the accuracy of the capture data. A more general review on resonance cross sections for structural materials has been presented by Fröhner at the Harwell Conference /34/.

^{56}Fe data: Five resonance data sets of ^{56}Fe are collected in Table 4 up to a neutron energy of 65 keV: RPI /13/, KFK /35/, ORNL-AAEC /15/, AERE /31/ and CBNM /3/. They are ordered corresponding to the date of publication from left to right and only resonances which are well separated and have a high statistical accuracy are included. In the second column $< w >$, a measure of the hardness of the resonance spectra, is added.

In Figure 5 the capture area of weak ^{56}Fe (p-wave) resonances for the four recent measurements of Table 4 have been plotted against the neutron energy. In order to emphasize the systematic deviations the data points of ORNL, AERE and CBNM are connected by eye-guide-lines. The large average, but systematic, deviation of 17% between the data sets of ORNL and CBNM is mainly explained by the use of spectra with different hardnesses for normalization, as discussed in Section III.B. The weighting function applied to the raw data overestimates the capture area of hard spectra when using a soft resonance for calibration. Since all resonances in ^{56}Fe have γ-ray spectra harder than those of Au (or Ag), the capture areas obtained at ORNL can be considered as upper limit values. The normalization by means of a resonance with a hard spectrum, as performed at CBNM, improves the results but underestimates the soft resonances (*). Whether or not the CBNM set can be considered as a low limit depends on the transmission value of ^{56}Fe (1.15 keV) resonance, which has been listed in Table 5 and taken from the literature. No conclusion can be made from these values as the deviations are as large as in the capture data. But two remarks should favour the value of Brusegan et al. The transmission data of CBNM have been analysed at Harwell yielding the same result /39/ and the data have been improved by inclusion of a recent analysis of a transmission measurement performed with a 1 mm iron sample resulting in: Γ_n = (58.9 $\pm$ 2.0) meV and Γ_γ = (665. $\pm$ 150) /40/. With this result the data sets of ORNL and CBNM define an uncertainty band, within which the true value should fall.

(*) The CBNM data in Table 4 are partly corrected for this effect as described in Section III.B. The raw (uncorrected) data from CBNM have also been analysed at Harwell using RIFIT and the results are published elsewhere /29/.

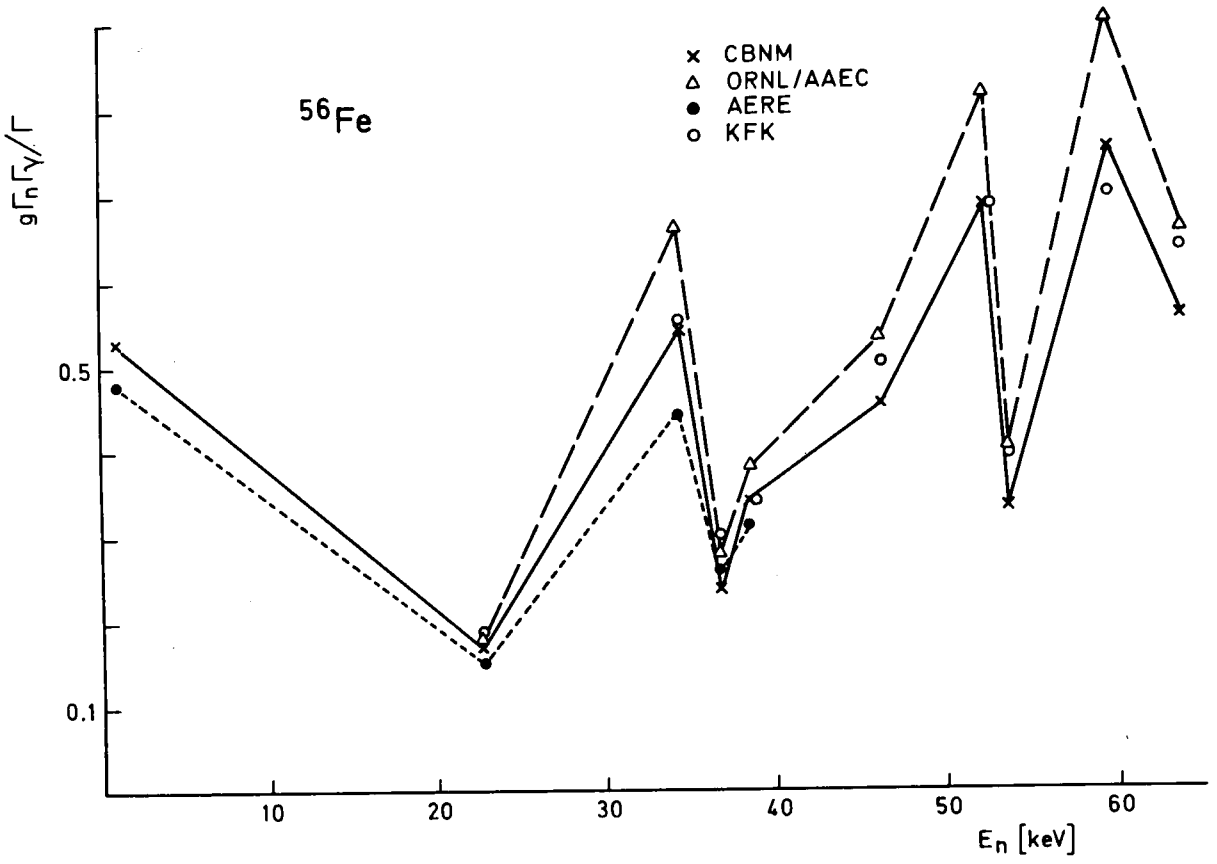

Fig. 5 Comparison of ^{56}Fe capture resonance data

The AERE data enter this uncertainty band, apart from the resonance at 34 keV, if the data are normalized to the ^{56}Fe (1.15 keV) transmission result mentioned above. All resonances with a hard spectra agree better with the CBNM data, but the result for the single soft resonance at 36 keV, which enters the uncertainty band without normalization, agrees better with the ORNL-AAEC value.

The KFK data obtained with a large liquid scintillator are all within the uncertainty band except the 59.2 keV resonance. Also here the data for soft spectra resonances agree better with the ORNL data and these for a hard spectra with the CBNM data.

To visualize this fact, the ratios of ORNL/KFK and of CBNM/KFK data expressed in percentage have been plotted against the average weight in the upper and lower part of Figure 6 respectively. As can be seen there is a good agreement between the results obtained with the large tank measurement (KFK) and those from the total energy weighting technique, when the data of the latter are combined with ORNL data normalized to Au for $< w > < 23.5$ and

with CBNM data normalized to ^{56}Fe (1.15 keV) for $< w > > 23.5$. The comparison of capture data obtained with scintillator tanks may lead to the following conclusions for the application of the weighting technique using liquid scintillators: the spectrum independence of these capture detectors is limited to an average weight of $< w > \approx 23.5$; beyond this hardness the capture data should be normalized to a resonance of similar hardness.

If we use this condition for the results of ORNL and CBNM and normalize the AERE data to the transmission value of the 1.15 keV resonance, the average deviation of the data plotted in Figure 5 reduces to 6%.

The results of the strong s-wave resonance in ^{56}Fe at 27.7 keV with a scattering to capture ratio of $1.5 \cdot 10^3$ are listed in Table 4. The total radiative widths show a tendency to decrease from left to right, with the exception of the ORNL result. The two recent values obtained at Linacs (AERE and CBNM) are in good agreement with those obtained at Van de Graaffs (KFK and AAEC - see Section III.A), where the prompt background is eliminated by a time of flight technique. This result indicates that the prompt background for the newly developed capture detectors at Linacs is not at all significant for the 27.7 keV resonance. But the problem remains for s-wave resonances, where the scattering to capture ratio appreciably exceeds 10^3. In an evaluation of the total radiative width of the 27.7 keV resonance, contributed to this meeting /41/, $\Gamma_\gamma = 1.00 \pm 0.04$ eV is recommended.

<u>^{54}Fe data</u>: The capture area of ^{54}Fe p-wave resonances up to 85 keV, which have a good statistical accuracy and which do not overlap with s-wave resonances, are listed in Table 6 and plotted in Figure 7. Data sets from ORNL-AAEC /42/, KFK /43/ and as yet unpublished capture data of CBNM /44/ are included. The latter are normalized to the ^{56}Fe (1.15 keV) resonance, for which the γ-ray spectrum hardness agrees with the average weight obtained for the ^{54}Fe resonances (see Figure 2). The deviation of the ORNL and CBNM data averaged over the resonances considered is 20%. Since all resonances, apart from those at 3.1 and 68.7 keV, have an average weight larger than 23.5, the CBNM data should be the correct values. A change in the slope of the neutron flux between ORNL and CBNM data is observed below $E_n < 30$ keV, where the capture area of both sets agree much better. This effect is also indicated in the ^{56}Fe data, where only one resonance below 30 keV is considered. The KFK results are on average 46% higher than the CBNM data and are not consistent with the normalization obtained for the KFK ^{56}Fe data.

<u>^{57}Fe data</u>: In Table 7, four resonance data sets RPI /13/, KFK /43/, ORNL-AAEC /45/ and CBNM /23/ of ^{57}Fe up to a neutron energy of 40 keV are listed, very weak resonances and the doublet at 21 keV have been excluded. Many of the p-wave resonances included in the table are superimposed on broad s-wave resonances. The normalization of the CBNM data has been performed with the capture area of the ^{57}Fe (1.6 keV) resonance. In this case the capture areas of CBNM should agree with those of ORNL normalized to the Au resonance. This is certainly true for resonances beyond 30 keV neutron energy, but in the lower energy range the systematic change in the flux shape causes even lower capture areas below 21 keV compared to CBNM data,

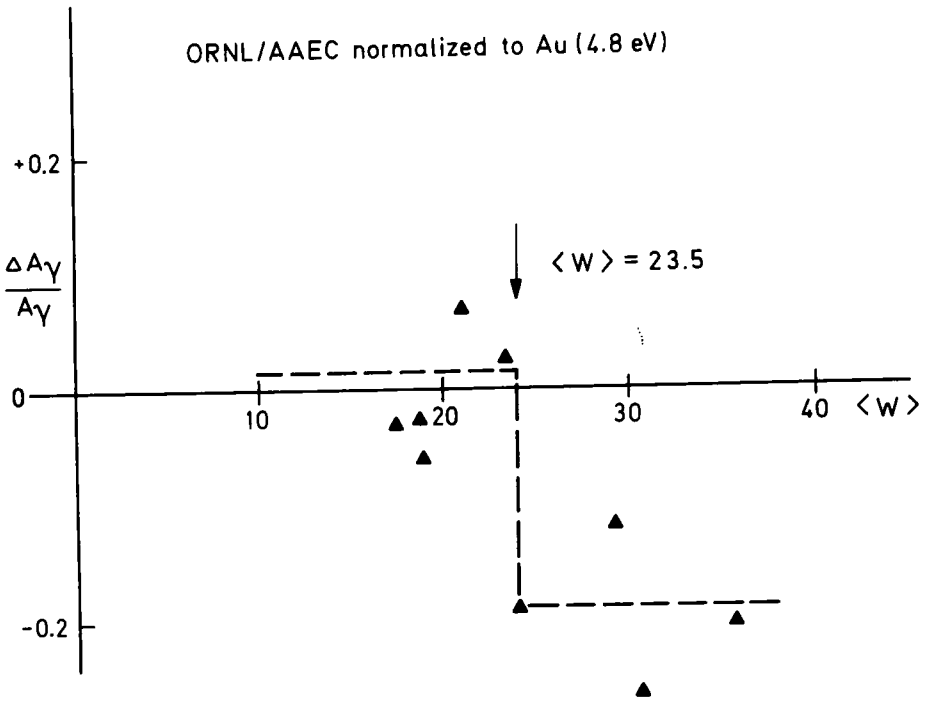

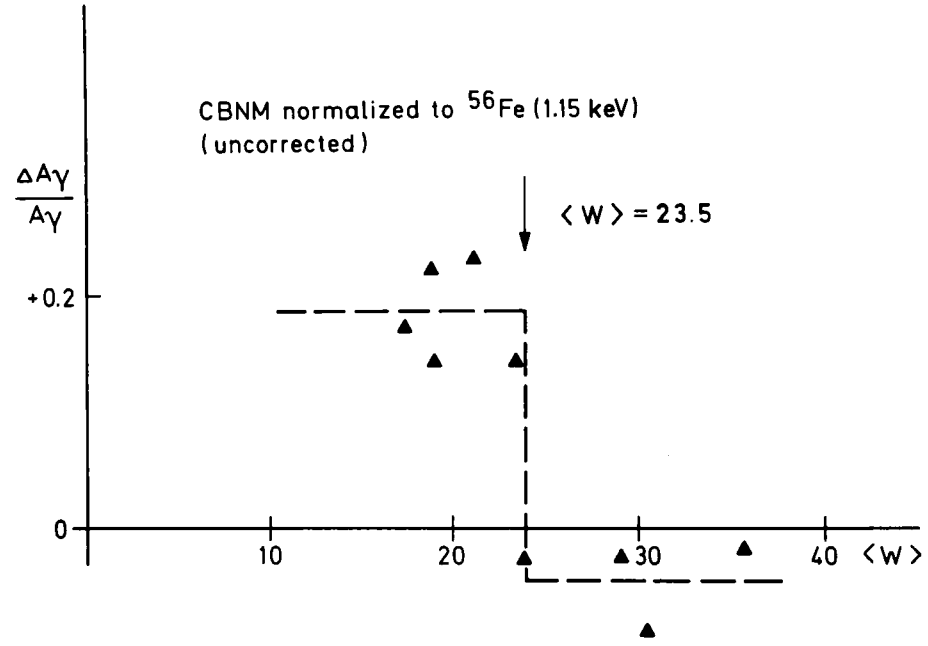

Fig. 6 ORNL-AAEC and CBNM resonance area data of ^{56}Fe normalized to KFK data

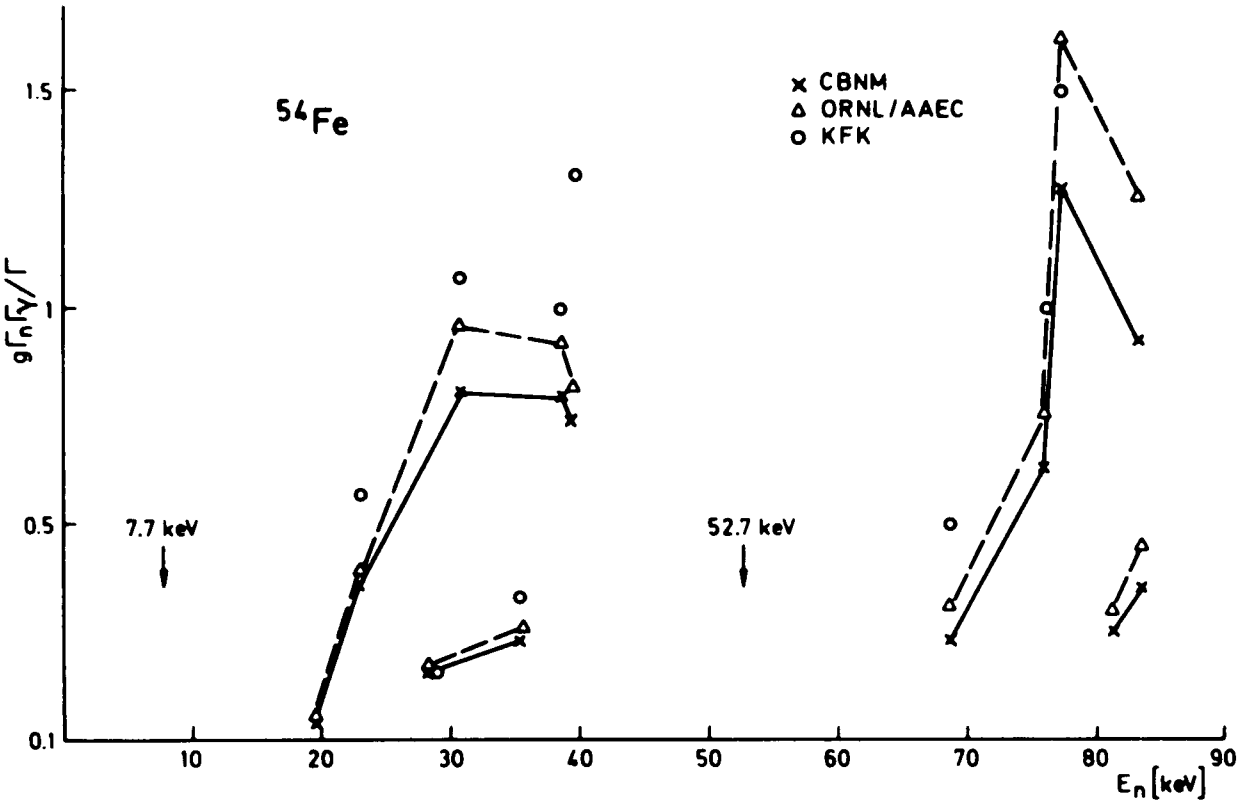

Fig. 7 Comparison of ^{54}Fe capture resonance data

resulting in a discrepancy averaged over all resonances of -10%. The best agreement below 20 keV is obtained for RPI and CBNM data, where the average deviation is +7%. The KFK data are systematically too high below 10 keV and become too low beyond this energy.

V. CONCLUSIONS AND RECOMMENDATIONS

The pulse height weighting technique applied to liquid organic scintillators has to be used with care for capture cross section measurements of structural materials. Tests of these detectors performed at CBNM and the comparison of ^{56}Fe capture areas obtained with the weighting technique (ORNL-AAEC and CBNM) on the one hand and those obtained using large liquid scintillators (KFK, AERE) on the other, may lead to the following conclusions: The capture detectors based on the pulse height weighting technique are independent of the spectral shape up to a hardness of the γ-ray spectra of $\langle w \rangle = 23.5$. Resonances with harder spectra characterized by a large partial transition strength to the ground state or a low lying excited state have to be normalized with resonances of similar properties.

The application of this condition to the ^{56}Fe data reduces the discrepancy averaged over the resonances, from initially 20% to 6%.

With this restriction the pulse height weighting technique is not applicable for average cross section measurements for structural materials.

Only the data sets of ORNL-AAEC and CBNM, although different in the results, behave similarly in all three data sets of the main iron isotopes. The different shape in the neutron flux below 30 keV in both sets should be reassessed.

The normalization of capture data for structural materials should be performed with pure capture resonances, where the capture area can be determined precisely in a transmission experiment. Therefore transmission measurements of such resonances are highly recommended.

Furthermore, the capture area of pure capture resonances with different average weight can be used to test the properties of capture detectors in general and those requiring the weighting technique in particular.

REFERENCES

/ 1/ Proc. NEANDC/NEACRP Specialist Meeting on Neutron Data of Structural Materials for Fast Reactors, Geel, 5-8 Dec. 1977.

/ 2/ Proc. of the Int. Conf. on Nuclear Cross Sections for Technology, Knoxville, Oct. 22-26, 1979.

/ 3/ A. Brusegan, F. Corvi, G. Rohr, R. Shelley and T. van der Veen, contribution to Ref. 2, p. 163.

/ 4/ M.C. Moxon and D.A.J. Endacott, U.K. Nuclear Data Progress Report (Jan.-Dec.1978), NEANDC(E)202U. Vol. 8, p. 38.

/ 5/ J.G. Sullivan, G.G. Warner, R.C. Block and R.W. Hockenbury, Rensselaer Polytechnic Institute report RPI-328-155 (1969).

/ 6/ F.H. Fröhner, Report KFK 2145 (1977).

/ 7/ M.C. Moxon, contribution to Ref. 1, p. 644.

/ 8/ B.J. Allen, D.D. Cohen, F.Z. Company, J. Phys. G6 (1980) 1173.

/ 9/ K. Wisshak and F. Käppeler, Nucl. Sci. Eng. 77 (1981) 58.

/10/ L.V. Groshev, A.M. Demidov, G.A. Kotelnikov and V.N. Lutsenko, Nucl. Phys. 58 (1964) 465.

/11/ G. Rohr, Proc. of the third Int. Symp. on Neutron Capture Gamma-Ray Spectroscopy and Related Topics, Brookhaven, Sept. 1978, p. 734.

/12/ S.H. Kim, P.R. Harris and R.C. Block, Proc. of an Int. Conf. on Neutron Physics and Nuclear Data, Harwell, Sept. 1978, p. 730.

/13/ R.W. Hockenbury, Z.M. Bartolome, J.R. Tatarczuk, W.R. Moyer and R.C. Block, Phys. Rev. Vol. 178 No. 4 (1969) p. 1746.

/14/ A. Ernst, D. Kompe and F.H. Fröhner, Proc. Int. Conf. on Nuclear Data for Reactors, Helsinki, 1970, Vol. 1, p. 633.

/15/ B.J. Allen, A.R. de L. Musgrove, J.W. Boldeman, M.J. Kenny and R.L. Macklin, Nucl. Phys. A269 (1976) 408.

/16/ B.J. Allen, A.R. de L. Musgrove, contribution to Ref. 1, p. 447.

/17/ D.B. Gayther, R.W. Thomas, B. Thom and M.C. Moxon, contribution to Ref. 1, p. 547.

/18/ K. Wisshak, F. Käppeler, G. Reffo and F. Fabri, contribution to this meeting.

/19/ C. Le Rigoleur and A. Arnaud, Proc. NEACRP/NEANDC Specialist Meeting on Neutron Capture in the keV Energy Range in Structural Materials for Fast Reactors, Karlsruhe, May 1973, Report KFK 2046 (1975).

/20/ R.B. Thom, U.K. Nuclear Data Progress Report (Jan.-Dec.1979), NEANDC(E)212 Vol. 8, p. 22.

/21/ R.L. Macklin and J.H. Gibbons, Phys. Rev. 159 (1967) 1009.

/22/ L. Pages et al., Atomic Data 4, (1972) 1.

/23/ G. Rohr et al., to be published.

/24/ R.L. Macklin and B.J. Allen, Nucl. Instr. and Methods 91 (1971) 565.

/25/ A.R. de L. Musgrove, B.J. Allen and R.L. Macklin, Proc. of an Int. Conf. on Neutron Phys. and Nucl. Data, Harwell, Sept. 1978, p. 426.

/26/ B.J. Allen et al., AAEC/E-402 (1977).

/27/ R.R. Winters, R.L. Macklin and J. Halperin, Phys. Rev. C18 (1978) 2092.

/28/ A. Brusegan, F. Corvi, G. Rohr, R. Shelley, T. van der Veen and B.J. Allen, Int. Symp. on Neutron-Capture Gamma-Ray Spectroscopy and Related Topics, Grenoble, Sept. 1981, p. 408.

/29/ M.C. Moxon, U.K. Nuclear Data Progress Report (Jan.-Dec. 1980), NEANDC(E)222, Vol. 8, p. 22.

/30/ B.J. Allen and R.L. Macklin, J. Phys. G: Nucl. Phys. 6 (1980) 381.

/31/ D.B. Gayther, M.C. Moxon, R.B. Thom and J.E. Jolly, U.K. Nuclear Data Progress Report (Jan.-Dec.1979), NEANDC(E)212, Vol. 8, p. 23.

/32/ A. Brusegan, F. Corvi, G. Rohr, C. Coceva, P. Giacobbe and M. Magnani, Proc. of an Int. Conf. on Neutron Phys. and Nuclear Data, Harwell, Sept. 1978, p. 706.

/33/ A. Brusegan, F. Corvi, G. Rohr and B.J. Allen, Int. Symp. on Neutron-Capture Gamma-Ray Spectroscopy and Related Topics, Grenoble, Sept. 1981, p. 406.

/34/ F.H. Fröhner, Proc. of an Int. Conf. on Neutron Physics and Nuclear Data, Harwell, Sept. 1978, p. 268.

/35/ F.H. Fröhner, contribution to Ref. 1, p. 138.

/36/ R.C. Block, Phys. Letters 13 (1964) 234.

/37/ J. Julien, R. Alves, S. De Barros, V.D. Huynk, J. Morgenstern and C. Samour, Nucl. Phys. A132 (1969) 129.

/38/ M.C. Moxon and J.B. Brisland, contribution to Ref. 1, p. 689.

/39/ M.C. Moxon, private communication to A. Brusegan.

/40/ A. Brusegan, private communication.

/41/ B.J. Allen, contribution to this meeting.

/42/ B.J. Allen, A.R. de L. Musgrove, J.W. Boldeman and R.L. Macklin, (1977) AAEC/E 403, Nucl. Phys. A283 (1977) 37.

/43/ H. Beer and R.R. Spencer, Nucl. Phys. A240 (1975) 29.

/44/ A. Brusegan et al., to be published.

/45/ B.J. Allen, A.R. de L. Musgrove, R. Taylor and R.L. Macklin, contribution to Ref. 1, p. 476.

/46/ B.J. Allen, private communication.

Sample	S_n [MeV]	σ_{th} (barn)	$< w_{th} >$	$\epsilon = C_w/(S_n \cdot P_\gamma)$
Ag	6.80	63.6 ± 0.6	10.9	1.00
Au	6.51	98.8 ± 0.3	13.5	1.018 ± 0.01
Fe	7.65	2.55 ± 0.03	28.9	1.082 ± 0.03
^{50}Cr	9.26	15.9 ± 0.2	23.1	1.093 ± 0.02
^{53}Cr	9.72	18.2 ± 1.5	26.1	1.24 ± 0.09

Table 1 Test of the weighting function at thermal energy /3/.

Weighting Function	^{57}Fe (1.6 keV) $g\Gamma_n\Gamma_\gamma/\Gamma$ (meV)	^{56}Fe (1.15 keV) $g\Gamma_n\Gamma_\gamma/\Gamma$ (meV)
O L D	54.	70.
N E W	51.5	65.
A L T	49.	61.
L I N	41.	49.
T R A	51.	53.
$< w >$	20.5	28.9

Table 2 Test of weighting functions for ^{56}Fe (1.15 keV) and ^{57}Fe (1.6 keV) resonances.

Isotope	Energy range (keV)	Detector	Reference	
^{23}Na	7 - 599	C_6F_6	Musgrove	/25/
$^{46-50}Ti$	3 - 292	C_6F_6	Allen	/26/
^{51}V	4 - 212	C_6F_6	Winters	/27/
^{54}Fe	1 - 100	C_6D_6	Brusegan	/3/
^{56}Fe	1 - 85	C_6D_6	Moxon	/29/
^{56}Fe	15 - 40	Moxon-Rae	Allen	/8/
^{56}Fe	15 - 40	Moxon-Rae	Wisshak	/9/
^{58}Fe	2.5 - 200	C_6F_6	Allen	/30/
Fe nat.	1 - 35	Tank	Gayther	/31/
^{91}Zr	0.15 - 14.6	C_6F_6	Brusegan	/32/
^{96}Zr	0.15 - 30	C_6F_6	Brusegan	/33/

Table 3 Published data of structural materials since the Geel Specialists meeting.

^{56}Fe RESONANCE PARAMETERS (eV)

MEASUREMENT → CBNM NORMALIZATION → ^{56}Fe			AERE Au	ORNL-AAEC Au	KFK Au	RPI Ag Au
E(keV)	⟨w⟩	$g\Gamma_n\Gamma_\gamma/\Gamma$	$g\Gamma_n\Gamma_\gamma/\Gamma$	$g\Gamma_n\Gamma_\gamma/\Gamma$	$g\Gamma_n\Gamma_\gamma/\Gamma$	$g\Gamma_n\Gamma_\gamma/\Gamma$
1.15	28.8	$\Gamma_n=0.058$ $\Gamma_\gamma=61$ 0.053	$\Gamma_n=0.053$ $\Gamma_\gamma=0.615$ 0.048			$\Gamma_n=0.086$ 0.075
22.8	23.4	0.17	0.15	0.18	0.18	0.19
27.7	24.4	$\Gamma_\gamma = 1.00$	$\Gamma_\gamma = 0.85$	$\Gamma_\gamma = 1.6$	$\Gamma_\gamma = 1.25$	$\Gamma_\gamma = 1.44$
34.2	35.8	0.54	0.44	0.66	0.55	0.59
36.7	21.2	0.23	0.26	0.28	0.30	0.30
38.4	29.3	0.34	0.31	0.38	0.34	0.46
46.0	18.9	0.45		0.53	0.50	0.32
52.1	24.0	0.68		0.81	0.68	0.51
53.5	18.8	0.33		0.40	0.39	0.54
59.2	30.5	0.74		0.87	0.69	0.54
63.5	17.5	0.55		0.65	0.63	

Table 4 Comparison of ^{56}Fe capture data obtained in different laboratories.

Author		Year	Γ_n (meV)	Γ_γ (meV)	$g\Gamma_n\Gamma_\gamma/\Gamma$ (meV)
Block	/36/	1964	68. ± 6.	530. ± 80.	60. ± 6.
Julien et al.	/37/	1969	62. ± 4.	570. ± 60.	56. ± 4.
Moxon et al.	/38/	1977	50. ± 4.	(600 assumed)	46. ± 4.
Brusegan et al.	/3/	1979	58. ± 4.	610. ± 60.	53. ± 4.

Table 5 Transmission results for the 1.15 keV resonance in ^{56}Fe.

E_n (keV)	< w >	CBNM $g\Gamma_n\Gamma_\gamma/\Gamma$ (eV)	ORNL-AAEC $g\Gamma_n\Gamma_\gamma/\Gamma$ (eV)	KFK $g\Gamma_n\Gamma_\gamma/\Gamma$ (eV)
3.1	23.0	0.0028	0.0030	
19.3	26.2	0.046	0.047	
23.0	31.5	0.36	0.39	0.57
28.2	31.3	0.16	0.17	0.16
30.6	28.7	0.81	0.96	1.07
35.3	26.1	0.23	0.26	0.33
38.4	26.5	0.80	0.92	1.0
39.1	27.7	0.74	0.82	1.31
68.7	22.8	0.23	0.31	0.5
75.8	27.9	0.63	0.76	1.0
77.2	26.5	1.27	1.62	1.5
81.3	37.5	0.25	0.30	
83.2	28.2	0.92	1.27	
83.5	24.7	0.35	0.45	

Table 6 Comparison of ^{54}Fe capture areas for weak resonances measured in different laboratories.

E_n (keV)	< w >	CBNM $g\Gamma_n\Gamma_\gamma/\Gamma$ (eV)	ORNL-AAEC* $g\Gamma_n\Gamma_\gamma/\Gamma$ (eV)	KFK $g\Gamma_n\Gamma_\gamma/\Gamma$ (eV)	RPI $g\Gamma_n\Gamma_\gamma/\Gamma$ (eV)
1.6	20.5	0.051			0.05
7.2	33.3	0.36	0.29	0.42	0.36
7.9	24.0	0.15	0.13	0.25	0.18
12.9	24.8	0.39	0.34	0.27	0.42
14.0	20.8	0.69	0.56	0.40	0.70
18.1	20.7	0.22	0.19		
18.3	24.6	0.56	0.40	0.47	0.52
18.7	20.2	0.036	0.034		
21.1	23.2	0.31	0.25		
21.4	21.7	0.11	0.11		
27.2	21.4	0.10	0.12		
28.7	18.1	0.35	0.42		
32.0	21.8	0.21	0.22		
35.2	20.7	0.47	0.44		
37.2	22.4	0.37	0.34		
38.0	18.7	0.14	0.15		
39.4	18.7	0.46	0.45		

* Correction factor 1.036 has not been applied /46/

Table 7 Comparison of ^{57}Fe-capture areas for weak resonances measured at different laboratories.

Discussion

QUESTION: W. Poenitz
Somehow the step function you proposed seems hard to accept. If one looks at that graph, one might draw a more gradually changing line through the points.

ANSWER: G. Rohr
I agree, that it is difficult to accept, but looking at the data, it seems to be very sharp. Probably I should have shown the errors.

QUESTION: K. Wisshak
From the statistical model calculations we know that, on the average, capture gamma-ray spectra of d-wave resonances are much harder than spectra of p-wave resonances. Might the step in your normalization be due to the fact that d-wave resonances have been analyzed as p-wave resonances?

ANSWER: G. Rohr
The d-wave resonances below 70 keV neutron energy are too weak to use in this inter-comparison.

NEUTRON CAPTURE WIDTHS OF s-WAVE RESONANCES IN ^{56}Fe, $^{58,60}Ni$ and ^{27}Al

K. Wisshak, F. Käppeler, G. Reffo[+], and F. Fabbri[+]

Kernforschungszentrum Karlsruhe GmbH
Institut für Angewandte Kernphysik
P.O.B. 3640, D-7500 Karlsruhe
Federal Republic of Germany

ABSTRACT

The neutron capture widths of s-wave resonances in ^{56}Fe (27.7 keV), ^{58}Ni (15.4 keV), ^{60}Ni (12.5 keV) and ^{27}Al (35.3 keV)have been determined, using a set-up completely different from LINAC experiments. A pulsed 3 MV Van de Graaff accelerator and the $^{7}Li(p,n)$ reaction served as a neutron source. The proton energy was adjusted just above the reaction threshold to obtain a kinematically collimated neutron beam. This allowed to position the samples at a flight path as short as ∿90 mm. Capture events were detected by three Moxon-Rae detectors with graphite, bismuth-graphite and pure bismuth converter, respectively. The measurements were performed relative to a gold standard . The setup allows to discriminate capture of scattered neutrons completely by time of flight and to use very thin samples (0.15 mm) in order to reduce multiple scattering. After correction for deviations of the detector efficiency from a linear increase with gamma-ray energy, the results obtained with different detectors agree within their remaining systematic uncertainty of ∿5 %. Only preliminary results are presented.

INTRODUCTION

Exact values for the capture widths of broad s-wave resonances in structural materials are important nuclear data for fast reactors, mainly because of two reasons: (i) The large capture areas contribute significantly to the reactor

---

[+]Comitato Nazionale per l'Energia Nucleare, Bologna, Italy

spectrum averaged cross sections (ii). The large ratio of $\Gamma_n/\Gamma_\gamma \sim 10^3$ caused that older measurements are severely affected by systematic uncertainties due to capture of resonance scattered neutrons and multiple scattering effects.

Part of these difficulties have been overcome in recent years in LINAC experiments by the use of arrangements with very low neutron sensitivity[1,2]. In the present experiments which were performed at a Van de Graaff accelerator, a completely different approach was made to solve these problems. Events due to capture of resonance scattered neutrons are discriminated completely by time of flight, using very short flight paths between neutron target and sample. This approach has the additional advantage of a high neutron flux at the sample position. Therefore very thin samples can be used, thus avoiding large multiple scattering corrections. With this method the following s-wave resonances have been measured: ^{56}Fe (27.7 keV), ^{58}Ni (15.4 keV), ^{60}Ni (12.5 keV) and ^{27}Al (35.3 keV).

EXPERIMENTS

The experiment is an optimized version of a setup proposed by Macklin et al.[3] already in 1964. A schematic drawing is shown in Fig. 1. The measurements were performed at the Karlsruhe 3-MV pulsed Van de Graaff accelerator. A kinematically collimated neutron beam is produced via the ^{7}Li(p,n) reaction by adjusting the proton energy just above the reaction threshold. In this case no further collimation is required and the samples can be placed at a flight path as short as 9 cm. The capture detectors are arranged at backward angles completely outside the neutron cone. Data were taken simultaneously from three Moxon-Rae detectors with graphite, bismuth-graphite and pure bismuth converters, respectively. This is an essential feature which allows to reduce systematic uncertainties due to the deviations of the detector efficiency from the ideal, linear increase with gamma-ray energy. Five samples are used in each run: two isotopes of the structural materials under investigation, a gold sample as a cross section standard, a graphite sample as a pure scatterer and an empty position in the sample changer frame for background determination. Details of the experimental method, data evaluation and systematic uncertainties are given in Ref. 4.

The main advantages of this setup are the following:

1.) The distance between samples and detectors is a factor of two larger than the flight path of the primary neutrons. Thus, events due to capture of scattered neutrons in the detector or in surrounding materials are completely discriminated by the additional time of flight.

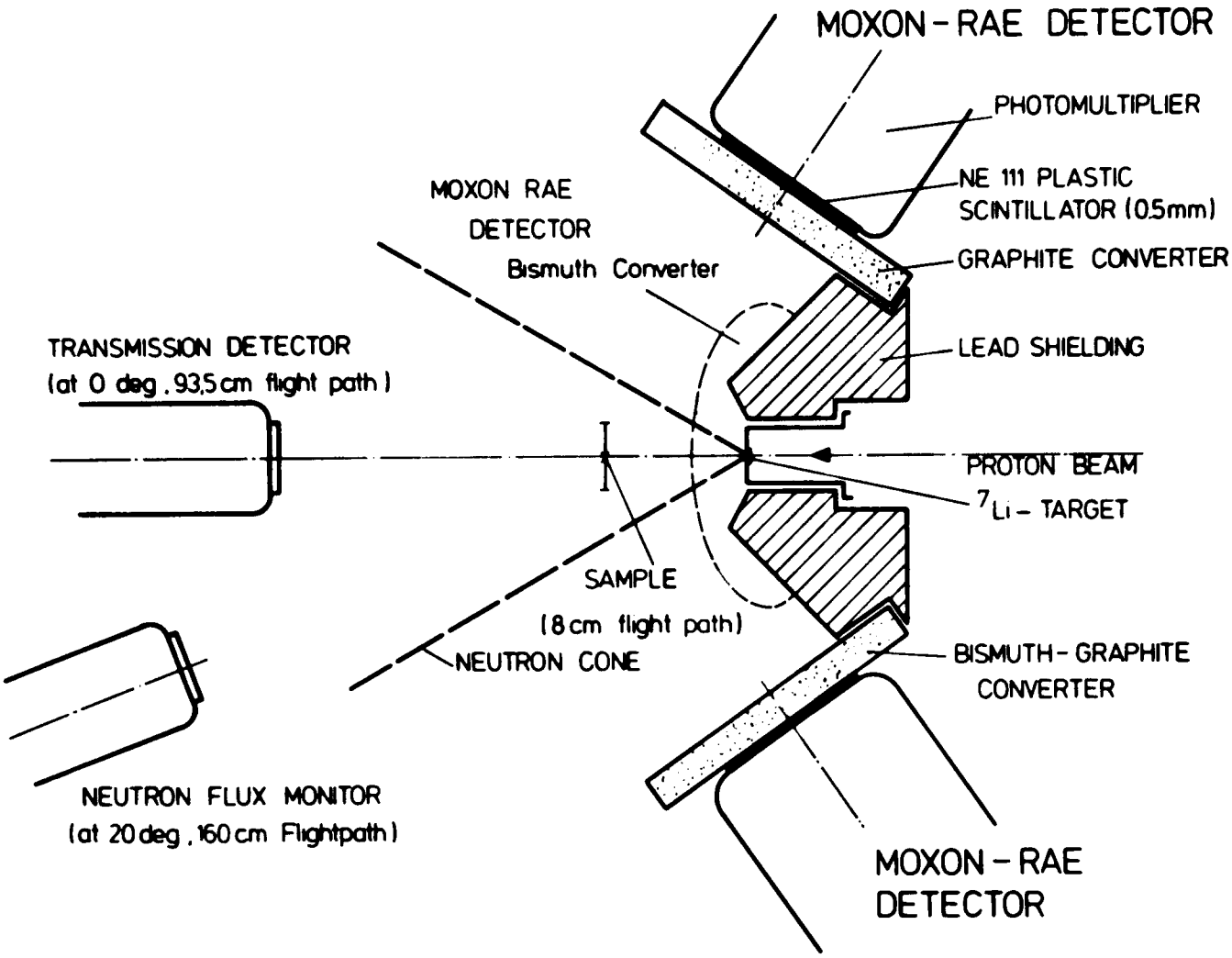

Fig. 1. Schematic view of the experimental setup for the capture cross section measurement on s-wave resonances in structural materials.

2.) The high neutron flux at the sample position allowed the use of very thin samples (e.g., 0.15 mm for $^{58/60}$Ni, the isotopes of main interest).
3.) The limited energy range of the neutron spectrum from 10 to 60 keV avoids unwanted background from scattering resonances at higher energies.
4.) The total time resolution of 1.2 ns is sufficient to separate the s-waves from neighbouring p-wave resonances (except for ^{60}Ni).

The important parameters of the individual measurements are compiled in Table I. Four measurements with different neutron spectra have been performed on $^{58/60}$Ni samples of different thickness. This allows to study in detail systematic uncertainties connected with the multiple scattering correction and with background subtraction. In case of ^{56}Fe, a detailed study has

already been published [4] using a single detector with graphite converter. Therefore, we remeasured this isotope only with two sample thicknesses. Aluminium was included in the present study as this isotope is of general interest, e.g., in connection with astrophysics. For demonstration of the experimental signal to background ratio, Fig. 2 shows time of flight spectra measured with ^{58,60}Ni samples of 0.3 mm thickness (2.7×10^{-3} A/b). Comparing the relative intensities of the resonances, one has to keep in mind that the neutron flux is strongly increasing with energy.

RESULTS

The capture width of the s-wave resonances was determined from the capture yield using the FANAC code of Fröhner[5]. Two examples of the fits for resonances in ^{58,60}Ni are shown in Fig. 3. In addition to the s-wave resonances, multiplets of unresolved p-wave resonances are also analyzed. In Table II the results for s-wave resonances are summarized. For ^{60}Ni the quoted

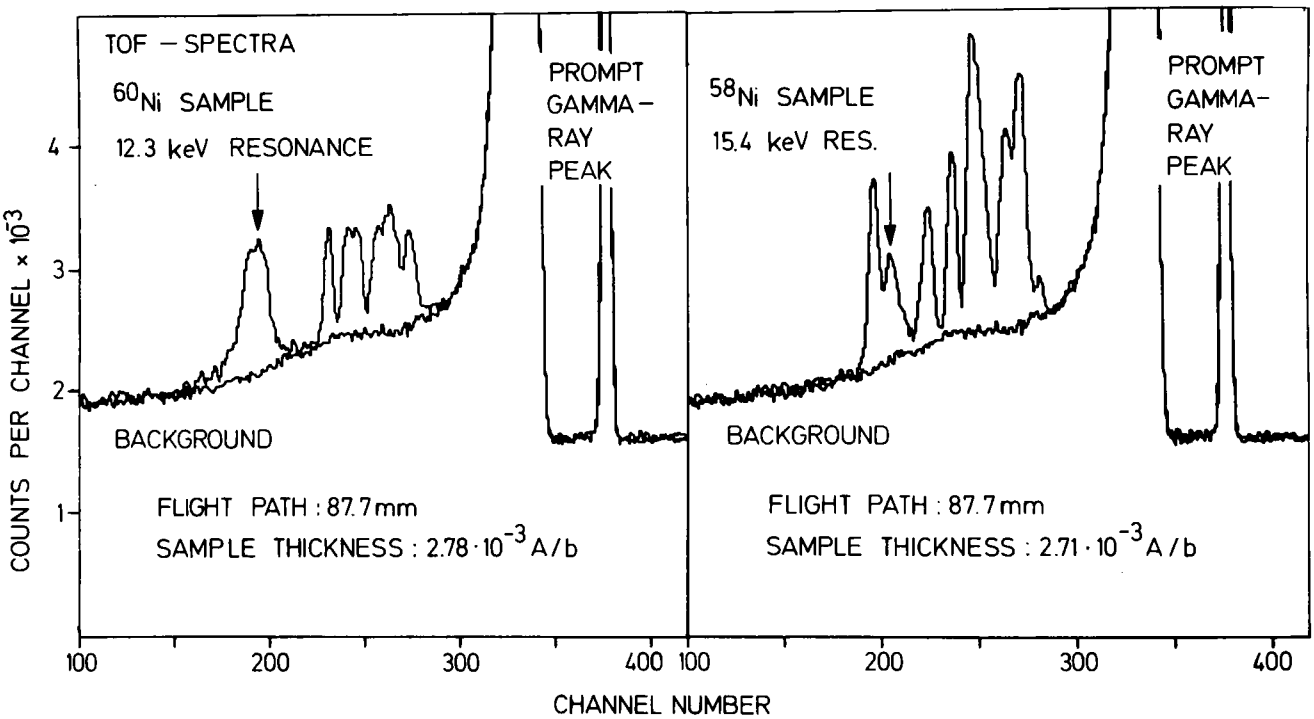

Fig. 2 Time of flight spectra measured from ^{58}Ni and ^{60}Ni samples (thickness 0.3 mm) using a Moxon Rae-detector with graphite converter. (The peak on the right hand side of the gamma-ray peak is caused by a diaphragm in front of the target).

Table I Important Parameters of the Individual Measurements

Measurement	Sample 1	Multiple Scattering in s-Wave (%)	Sample 2	Multiple Scattering in s-Wave (%)	Maximum Neutron Energy (keV)
1	$^{58}Ni(4.10 \cdot 10^{-3}$ A/b)	44	$^{60}Ni(4.12 \cdot 10^{-3}$ A/b)	53	90
2	$^{58}Ni(2.71 \cdot 10^{-3}$ A/b)	35	$^{60}Ni(2.77 \cdot 10^{-3}$ A/b)	43	75
3	$^{58}Ni(1.39 \cdot 10^{-3}$ A/b)	23	$^{60}Ni(1.35 \cdot 10^{-3}$ A/b)	29	60
4	$^{58}Ni(4.10 \cdot 10^{-3}$ A/b)	44	$^{60}Ni(4.12 \cdot 10^{-3}$ A/b)	53	60
5	$^{27}Al(6.15 \cdot 10^{-3}$ A/b)	18	$^{56}Fe(2.65 \cdot 10^{-3}$ A/b)	18	60
6	$^{56}Fe(1.62 \cdot 10^{-2}$ A/b)	47	$^{56}Fe(2.65 \cdot 10^{-3}$ A/b)	18	60

Sample Diameter: 38.2 mm

Standard: Gold ($1.36 \cdot 10^{-3}$ A/b)

Scattering Sample: Graphite ($7.57 \cdot 10^{-3}$ A/b)

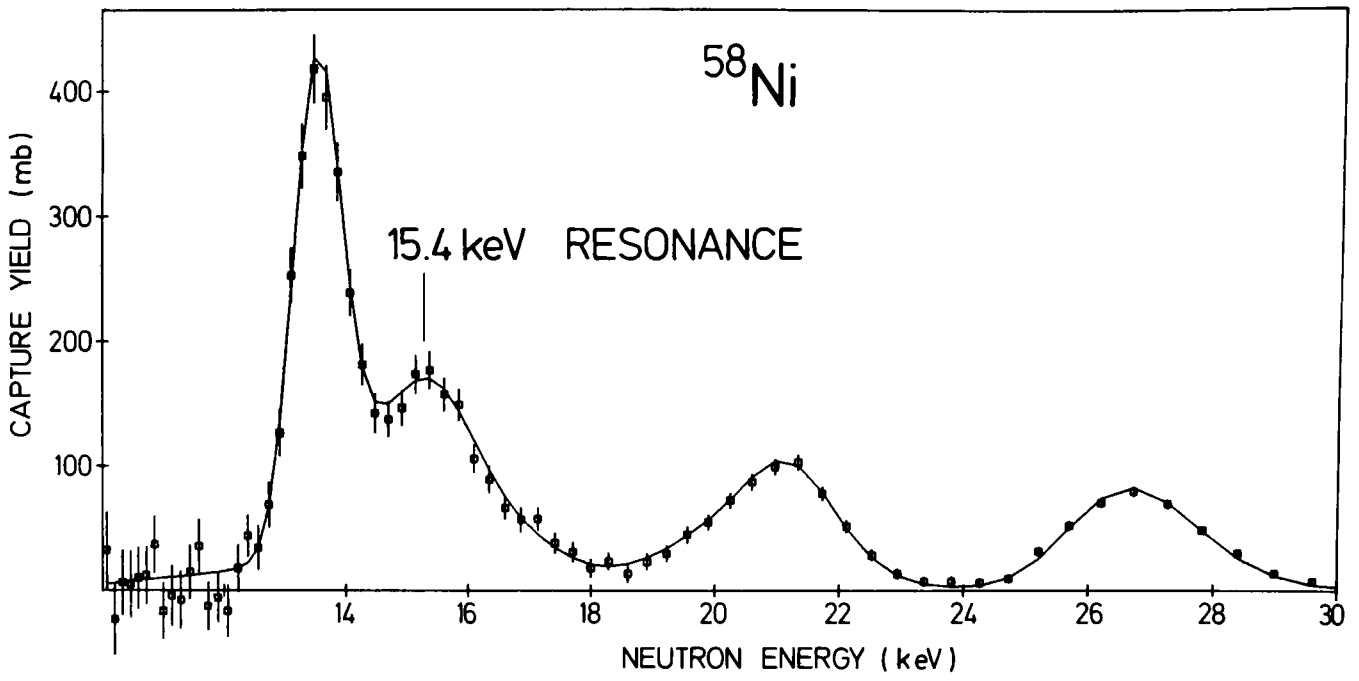

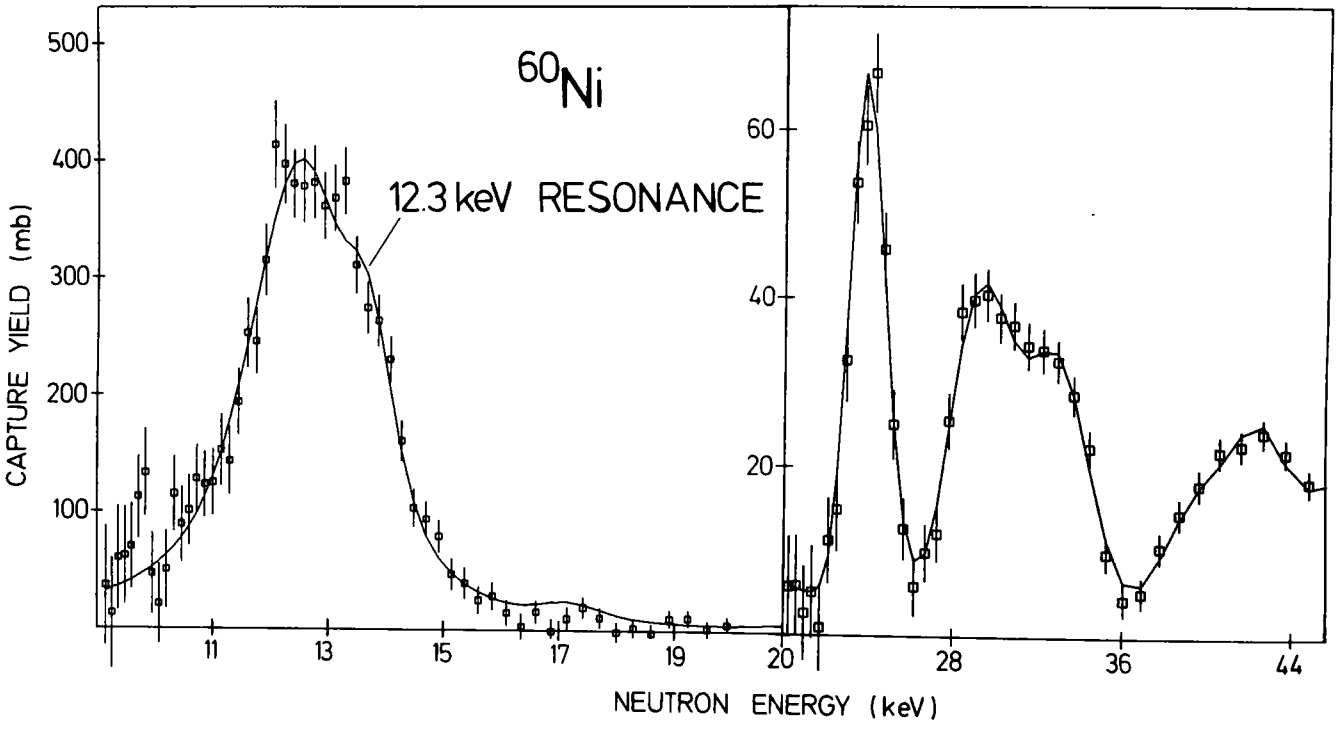

Fig. 3 FANAC fit to the capture yield of ^{58}Ni and ^{60}Ni as obtained from the spectra given in Fig. 2.

values are the sum of the s-wave resonance at 12.3 keV and the two p-wave resonances at 12.23 and 13.63 keV which could not be resolved in the present experiment. No systematic differences between individual measurements with different sample thicknesses were found thus confirming the reliability of multiple scattering corrections and of background subtraction. On the other hand strong systematic differences are observed for the results obtained with different detectors. This is to be expected as the capture gamma-ray spectra of the investigated isotopes and the gold standard are known to be quite different. This leads to systematic effects via the efficiency of the individual converters which deviates in different ways from the ideal linear increase with gamma-ray energy.

To correct for this effect, capture gamma-ray spectra of the investigated samples and of the gold standard were calculated according to the statistical and optical model as described in detail in Ref. 6. The gamma transitions to the groundstate follow a Porter-Thomas distribution and therefore the calculation cannot give exact results for these transitions in single resonances. In addition, other effects like doorway states or valence capture may contribute to the hard component in the capture gamma-ray spectra. For these reasons the capture gamma-ray spectra were corrected by experimental results for high energetic gamma transitions. In case of ^{56}Fe, ^{58,60}Ni measurements have been performed by Beer et al. [7] and for ^{27}Al by Bergqvist et al. [8]. The resulting spectra are shown in Fig. 4, where the statistical model calculation is given as a solid line and the effect of additional contributions at high energies is indicated by a dashed line. For ^{56}Fe the model calculation agrees with the experimental result for high energy transitions but for the other isotopes additional strength had to be added in this region. In the lower left corner of the figure the assumed shape of the efficiency curve is shown for the different converters. In case of the graphite converter two efficiency curves have been used, one as calculated by Malik and Majkrzak and the other as evaluated from experimental results of Macklin et al. [10], Moxon and Rae[11] and our group[4]. The efficiency for the bismuth-graphite converter was taken from Macklin et al.[10] (also the converter itself was kindly ceded to us by R.L. Macklin). For the pure bismuth converter the calculated curve by Malik and Majkrzak[9] was adopted.

With these four different efficiency curves ε_i (i=1,2,3,4) and with the capture gamma-ray spectra $I_j(E_\gamma)$ (j=^{56}Fe, ^{58,60}Ni, ^{27}Al and ^{197}Au) given in Fig. 4, an effective efficiency $\bar{\varepsilon}_{ij}$ was calculated according to:

TABLE II Preliminary results for the capture width (in eV) of s-wave resonances in ^{56}Fe, $^{58,60}Ni$ and ^{27}Al as obtained with different detectors and different sample thicknesses. The data are not yet corrected for deviations of the detector efficiency from linear increase with gamma-ray energy. Statistical uncertainties in % are given in brackets.

Resonance	Isotope	Measurement	Γ_γ Graphite Converter	Γ_γ Bi-Graphite Converter	Γ_γ Bismuth Converter
15.4 keV s-wave	^{58}Ni	1	1.31	1.73	1.80
	^{58}Ni	2	1.42	1.67	1.77
	^{58}Ni	3	1.30	1.80	1.80
	^{58}Ni	4	1.29	1.60	1.75
average			1.33 (4.2)	1.70 (4.0)	1.78 (3.7)
12.5 keV s-wave	^{60}Ni	1	3.10	3.83	3.91
	^{60}Ni	2	3.24	3.76	3.86
12.2+13.6 p-wave	^{60}Ni	3	3.20	3.87	4.06
	^{60}Ni	4	3.08	3.43	3.63
average			3.15 (2.6)	3.72 (3.4)	3.86 (2.9)
27.7 keV s-wave	^{56}Fe	5+6	1.01	1.17	1.13
	^{56}Fe	6	1.04	1.15	1.13
average			1.03 (3.8)	1.16 (4.0)	1.13 (3.8)
35.3 keV s-wave	^{27}Al	5	1.95 (3.0)	2.33 (2.9)	2.27 (2.8)

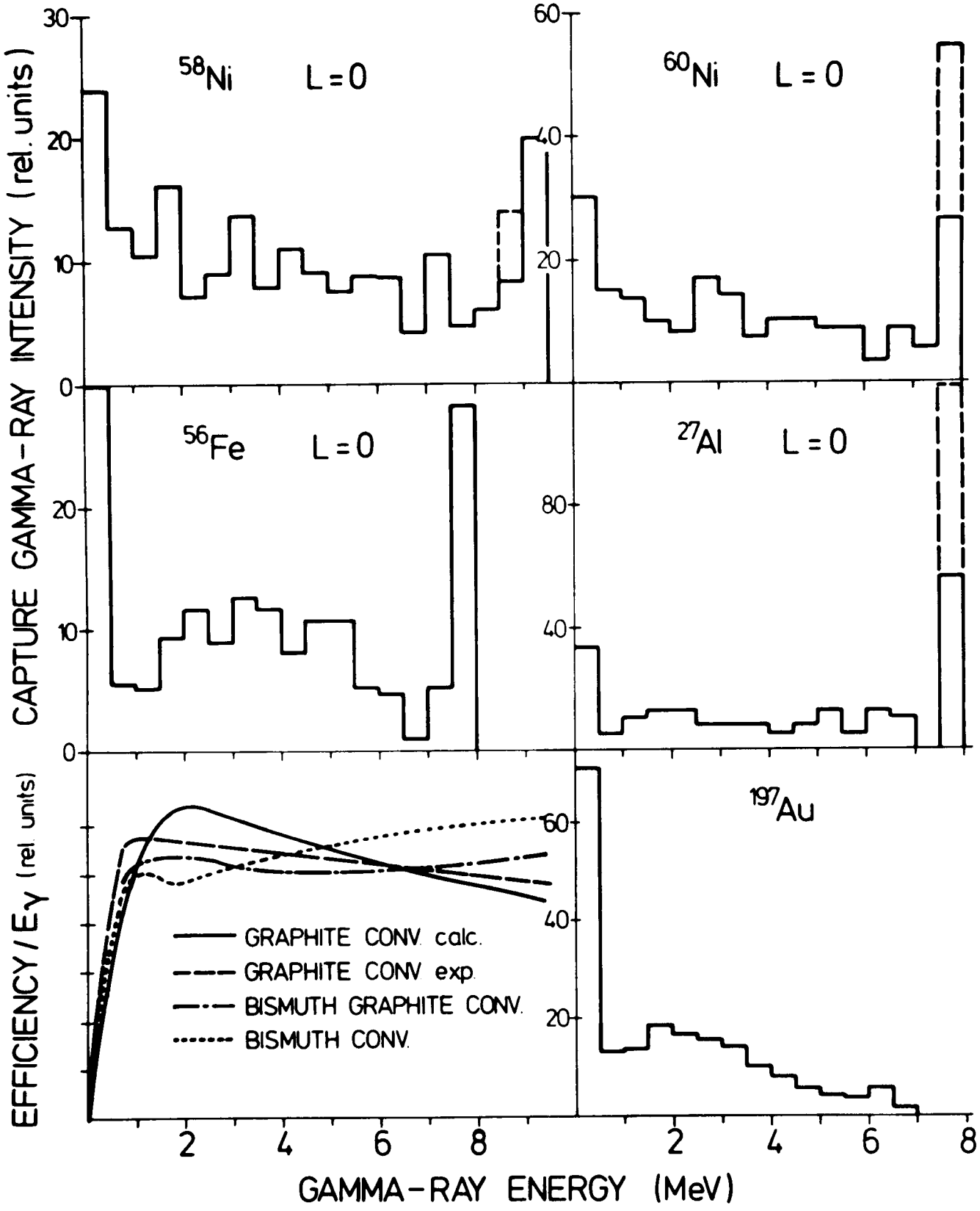

Fig. 4 Calculated capture gamma-ray spectra for s-wave resonances in ^{27}Al, ^{56}Fe $^{58/60}Ni$ and for ^{197}Au. In the lower left corner the relative shape of the detector efficiency is given for several converter materials as described in the text.

$$\bar{\varepsilon}_{ij} = \frac{\int \varepsilon_i(E_\gamma)\ I_j(E_\gamma)dE_\gamma}{\int \tilde{\varepsilon}\ (E_\gamma)\ I_j(E_\gamma)dE_\gamma}$$

where $\tilde{\varepsilon}\ (E_\gamma) = C \cdot E_\gamma$ corresponds to the ideal case. Finally, the measured capture widths had to be corrected by the efficiency ratio:

$$K_{ij} = \frac{\bar{\varepsilon}_{i,gold}}{\bar{\varepsilon}_{i,j}} \qquad j = {}^{27}Al,\ {}^{58,60}Ni,\ {}^{56}Fe$$

The values for $K_{i,j}$ are compiled in Table III. Their estimated uncertainties were derived by consideration of the uncertainties in the efficiency curve ε_i and in the capture gamma-ray spectra $I_j(E_\gamma)$. The effect of ε_i was deduced from the different results obtained with the two assumptions for the graphite converter. While the uncertainty contribution from $I_{Au}(E_\gamma)$ was taken from Ref. 4, the corresponding value for $I_j(E_\gamma)$ of the investigated isotopes was determined by the variation of K_{ij} if we skipped the experimental correction to the higher energy part of $I_j(E_\gamma)$. In Table IV preliminary results for the corrected capture widths are compiled together with the respective statistical uncertainties. The total remaining systematic uncertainty, which has been evaluated in detail for the ^{56}Fe measurement in Ref. 4 is of the order of 5 %. On the average the results show good agreement between the data measured with graphite and bismuth converter, while in all cases the results obtained with the bismuth-graphite converter is slightly larger. This may

TABLE III Efficiency ratios $K_{i,j}$ for the measurement of s-wave resonances in ^{27}Al, $^{58,60}Ni$ and ^{56}Fe relative to a gold standard using Moxon-Rae detectors with different converter materials

	Converter Material			
	Graphite	Bismuth-Graphite	Bismuth	Uncertainty(%)
^{58}Ni	1.072	0.964	0.897	3.2
^{60}Ni	1.056	0.974	0.901	2.7
^{56}Fe	1.048	0.983	0.924	2.0
^{27}Al	1.083	0.965	0.882	3.5

TABLE IV Preliminary results for the capture width of s-wave resonances in ^{27}Al, ^{56}Fe and $^{58,60}Ni$ (statistical uncertainties in % are given in brackets).

	Converter Material		
	Graphite	Bismuth-Graphite	Bismuth
^{58}Ni	1.42(4.2)	1.64 (4.0)	1.60(3.7)
average	Γ_γ (15.4 keV) = 1.55 (2.3) eV		
^{60}Ni	3.33(2.6)	3.63(3.4)	3.48(2.9)
average	Γ_γ(12.5 + 12.2 + 13.6 keV) = 3.45 (1.7) eV		
adopted	Γ_γ(12.2 + 13.6 keV) = 0.56		
	Γ_γ(12.5 keV) = 2.89 (1.7) eV		
^{56}Fe	1.07(3.8)	1.14(4.0)	1.04(3.8)
average	Γ_γ(27.7 keV) = 1.08 (2.2) eV		
^{27}Al	2.11(3.0)	2.25(2.9)	2.00(2.8)
average	Γ_γ(35.5 keV) = 2.11 (1.7) eV		

indicate that the respective efficiency curve has to be modified. However, such a step requires at best an experimental determination of the efficiency curve.

As a preliminary result we obtain a capture width Γ_γ=1.55 eV for the 15.4 keV resonance in ^{58}Ni. If we correct for the p-wave resonances at 12.23 and 13.62 keV in ^{60}Ni, using Γ_γ(12.23 + 13.62) = 0.56 eV for the sum of their widths according to Ref. 12, we end up with a value Γ_γ = 2.89 eV for the 12.3 keV resonance in ^{60}Ni. In case of ^{56}Fe the value Γ_γ = 1.08 eV for the 27.7 keV resonance is in good agreement with our first (more accurate) measurement[4] since our first result Γ_γ=1.01 has to be corrected by a factor 1.048 according to Table III. For the resonance at 35.3 keV in aluminium a value of Γ_γ=2.11 eV is obtained.

If we compare the present results with data from literature we find the following situation:
^{56}Fe, 27.7 keV - The present value is significantly lower than all results published before 1980 (Refs. 3,13,14), except the value of Fröhner[9] who quoted Γ_γ = 1.25 ± 0.2 eV. Among the recent measurements good agreement is found with Brusegan et al.[15] while the values given by Gayther et al.[16] and by Allen et al.[17] are lower by 15-20 %. It should be noted, that the latter experiment used a technique similar like the one that was applied in this work. We have complemented our Moxon-Rae measurements by one using C_6D_6 detectors with better energy resolution, and we get a preliminary value of Γ_γ = 1.04 eV.

^{58}Ni, 15.4 keV - In this case we agree well with the refined evaluation of Fröhner[12] whereas the value given in BNL 325 (Ref. 18) and the preliminary value of Perey[19] are ∿30 % higher.

^{60}Ni, 12.3 keV - For this resonance we again obtained good agreement with Fröhner[12], the earlier value in BNL 325 (Ref. 18) being some 15 % higher.

^{27}Al, 35.4 keV - Our result confirms the value quoted in BNL 325 (Ref. 18) but is significantly lower than the width of Γ_γ = 3.1 ± 0.6 eV reported by Musgrove et al.[20].

CONCLUSION

We have used an experimental method to determine s-wave resonances in structural materials which is completely independent from LINAC experiments. Capture of scattered neutrons is discriminated by time of flight and multiple scattering is reduced to ∿20 % by the use of thin samples.
The results obtained for ^{27}Al, ^{56}Fe and ^{58,60}Ni have a statistical accuracy of ∿2 % and a remaining systematic uncertainty of the order of 5 %.

REFERENCES

1) D.B. GAYTHER, B.W. THOMAS, B. THOM, and M.C. MOXON, Proc. Specialists' Meeting Neutron Data of Structural Materials for Fast Reactors, Geel, Belgium, December 5-8, 1977, p. 547, Pergamon Press, Oxford (1979).
2) A. BRUSEGAN, F. CORVI, G. ROHR, R. SHELLY, and T. VAN DER VEEN, Proc. Conf. Nuclear Cross Sections and Technology, Knoxville, Tenn., October 22-26, 1979, NBS Spec. Publ. 594, National Bureau of Standards.
3) R.L. MACKLIN, P.J. PASMA, and J.H. GIBBONS, Phys. Rev. B136, (1964) 695

4) K. WISSHAK and F. KÄPPELER, Nucl. Sci. Eng. 77 (1981) 58.
5) F.H. FRÖHNER, "FANAC-A Shape Analysis Program for Resonance Parameter Extraction from Neutron Capture Data for Light and Medium-Weight Nuclei", KfK-2145 (Kernforschungszentrum Karlsruhe, 1977).
6) G. REFFO and F. FABBRI, contribution to this conference.
7) H. BEER, R.R. SPENCER, and F. KÄPPELER, Z. Physik A284, (1978) 173.
8) I. BERGQVIST, J.A. BIGGERSTAFF, J.H. GIBBONS, and W.M. GOOD, Phys. Rev. 158 (1967) 1049.
9) S.S. MALIK and C.F. MAJKRZAK, Nucl. Instr. Meth. 130 (1975) 443.
10) R.L. MACKLIN, J.H. GIBBONS, and T. INADA, Nucl. Phys. 43 (1963) 353.
11) M.C. MOXON and E.R. RAE, Nucl. Instr. Meth. 24 (1963) 445.
12) F.H. FRÖHNER, Proc. Conf. on Neutron Data of Structural Materials for Fast Reactors, Geel, Belgium, December 5-8, 1977, p. 138, Pergamon Press, Oxford (1979).
13) R.W. HOCKENBURY, Z.M. BARTOLOME, J.R. TATARCZUK, W.R. MOYER, and R.C. BLOCK, Phys. Rev. 178 (1969) 1746.
14) B.J. ALLEN, A.R. de L. MUSGROVE, J.W. BOLDEMAN, and M.J. KENNY, Nucl. Phys. A 269 (1976) 408.
15) A. BRUSEGAN, F. CORVI, G. ROHR, private communications.
16) D.B. GAYTHER, M.C. MOXON, R.B. THOM, and J.E. JOLLY, "U.K. Nuclear Data Progress Report", UKNDC (80)P96, NEANDC(E) 212, Vol. 8, AERE Harwell, 1980.
17) B.J. ALLEN, D.D. COHEN, and F.Z. COMPANY, J. Phys. G: Nucl. Phys. 6 (1980) 1173.
18) S.F. MUGHABGHAB and D.I. GARBER, "Neutron Cross Sections Vol. I Resonance Parameters", BNL 325, Third Edition Brookhaven National Laboratory.
19) F.G. PEREY, G.T. CHAPMAN, W.E. KINNEY, and C.M. PEREY, Proc. Conf. on Neutron Data of Structural Materials for Fast Reactors, Geel, Belgium, December 5-8, 1977, p. 530 Pergamon Press, Oxford (1979).
20) A.R. de L. MUSGROVE, B.J. ALLEN, and R.L. MACKLIN, Proc. Conf. on Neutron Physics and Nuclear Data, Harwell, Sept. 1978, OECD Nuclear Energy Agency 1978.

Discussion

QUESTION: F. Corvi
I was a bit surprised that you could fit the high energy part of the ^{56}Fe capture spectrum. Do you include a valence contribution?

ANSWER: K. Wisshak
No, this is strictly a statistical calculation, no valence contribution. It is known that the 27.7 keV resonance has a relatively soft spectrum. Only 15% is going to the ground state.

QUESTION: R. Block
How does your radiation width for the 12 keV resonance in ^{60}Ni compare to the RPI result (as published in Nuclear Physics)?

ANSWER: K. Wisshak
The value quoted by Stieglitz et al. for the 12.5 keV resonance in ^{60}Ni is 3.3 ± 0.3 eV, this is the value quoted in BNL 325. This is slightly larger than the value of 2.9 eV obtained in the present work.

EVALUATION OF THE RADIATION WIDTH OF THE 27.7 keV RESONANCE IN ^{56}Fe*

by

B.J. Allen
AAEC Research Establishment,
Lucas Heights Research Laboratories
Private Mail Bag
Sutherland, NSW, 2232, Australia

Abstract

A critical review is given of measurements of the radiation width of the 27.7 keV resonance in ^{56}Fe. An evaluation of results yields a recommended value of $\Gamma_\gamma = 1.00 \pm 0.04$ eV for this resonance.

I. Introduction

The status of resonance capture data for ^{56}Fe was reviewed by Fröhner[1] at the conclusion of the 1977 Specialist Meeting on Neutron Data of Structural Materials for Fast Reactors at Geel, Belgium. Large uncertainties in the parameters of the 1.15 and 27.7 keV resonances were noted, with consequent effects on the fast reactor temperature coefficient and the transmission window produced by resonance-potential interference of the 27.7 keV s-wave resonance. This resonance alone is estimated to contribute ~ 14% to the total absorption of neutrons in iron in a fast reactor spectrum.

Since the Geel meeting two Linac measurements have been finalised, and a new Linac and two Van de Graaff measurements have been reported. A wide range of detection and accelerator techniques have been applied to the measurement of ^{56}Fe capture, particularly at the 27.7 keV resonance. In this paper both recent and early measurements of this resonance are critically reviewed in an endeavour to resolve the variation by up to a factor of two in reported radiation widths.

The 27.7 keV resonance has a neutron width of ~ 1.5 keV, and a capture to scatter ratio of only ~ 6.10^{-4}. Consequently, careful corrections are needed to allow for the sensitivity of the capture detectors to resonance scattered neutrons[2]. In Linac measurements, the resonance scattered neutron events are unresolved in time from the capture γ-rays, and cause a prompt background (PBG). This may not be the case in Van de Graaff measurements[3], where the scattered neutrons are readily resolved by time of flight discrimination.

Three types of γ-ray detectors have been used in the Linac and Van de Graaff measurements. Liquid scintillator tanks[4,5,6] operate at a high bias of 2-3 MeV, and the pulse height spectrum has to be extrapolated to zero energy. Spectral data and γ-ray decay models are therefore needed to allow

appropriate corrections for soft (e.g. Ag, Au) and hard (e.g. Fe) capture spectra. These corrections were applied in all the scintillator tank measurements reported in this paper. Pulse height weighting methods are also used with small solid angle, liquid scintillators (e.g. C_6F_6, C_6D_6)[7,8] to achieve an efficiency proportional to the total energy of the capture reaction. These detectors operate at a threshold of a few hundred keV and are therefore independent of spectrum variation. In principle the Moxon-Rae detector[3,9,10,11,12] is also a total energy detector but departures from the required linearity of efficiency per MeV are found for carbon converters[9,13,14] and, to a much lesser extent, for the carbon-bismuth converter[9]. Corrections for this non-linearity depend on the capture spectrum and calculated and experimental efficiency curves.

A considerable variance in the Moxon-Rae spectrum correction for a graphite converter is found for the 27.7 keV Fe resonance measured relative to gold. A 4% variation in the efficiency can arise from uncertainty in the Fe spectrum, particularly for the intensity of transitions to the ground and first excited states. However, the evidence now points to $\Gamma_{\gamma_0} = 0.14 \pm 0.03$ eV (Allen et al.[11] and references therein for (n,γ_0) and (γ_0,n) data), reducing the above uncertainty.

Allen et al.[11] used the average efficiency per MeV from Iyengar et al.[13] and Macklin et al.[9] whereas Wisshak & Kappeler[12] estimated their correction with the efficiency of Malik & Majkrzak[14]. When the 30 keV Au spectrum of Bergquist & Starfelt[15] is used, the correction factor of ~ 4% for the Malik efficiency[14] increases to ~ 9% for the Iyengar-Macklin average. Clearly this situation is most unsatisfactory and further efficiency studies are needed. For the present evaluation, a correction factor of 1.06 ± 0.03 is applied to the Fe/Au results from Moxon-Rae measurements with a graphite converter.

II. Measurements

(a) R.L. Macklin et al.(1964) [ref. 3]. This Van de Graaff measurement, although free from PBG, had poor timing resolution and the 22.7 keV resonance was not resolved from the 27.7 keV resonance.

The cross section measurement used Moxon-Rae detectors with C-Bi converters[9], and was insensitive to the hardness of the γ-ray spectra of the Fe resonance relative to that of the Ta standard. The Ta cross section at 30 keV was calculated to be 803 mb, and is in agreement with current expectations. Average path length and resonance self shielding corrections were applied to the data, but a Monte Carlo analysis of the 27.7 keV capture yield was not undertaken.

The next three measurements (see b, c, d below) were in good agreement with the 27.7 keV radiation width as measured by Macklin et al., but the p-wave group at 34.2, 36.6, 38.4 keV appears to have been over-estimated in relation to all subsequent measurements by a factor of 1.59.

Accepting then that the p-wave group at 34.38 keV was over-estimated, the data can be renormalised by this factor to obtain $\Gamma_\gamma(27.7) = 0.95 \pm 0.27$ eV, assuming a 20% systematic error in the normalisation procedure.

(b) R.W. Hockenbury et al. (1969) [ref. 4]. In principle, this liquid scintillator tank measurement was subject to PBG. However a measurement at 88 keV gave a very low value of 10^{-5} for the scattered neutron sensitivity. The 27.7 keV resonance was measured for three sample thicknesses and shape fitted with a Monte Carlo code, using a rather large value of Γ_n = 1670 eV.

(c) A. Ernst et al. (1970) [ref. 5]. A PBG component can also be present in this liquid scintillator tank measurement with a Van de Graaff accelerator. No correction was made for this but the resonance area was analysed by Monte Carlo code and included a 59% correction for multiple scattering.

F.H. Fröhner (1979) [ref. 16]. A re-evaluation of these data included multi-level shape analysis and a 6% correction for the PBG. The neutron width used was Γ_n = 1400 ± 200 eV.

(d) B.J. Allen et al. (1976) [Al - ref. 7,17]. The C_6F_6 detectors (with pulse height weighting) used in this Linac measurement are known to be quite sensitive to resonance scattered neutrons which can capture in the 27.06 keV resonance in fluorine, although 90° single scatters will fall below this resonance. The s-wave data of ref. 7 were re-analysed[17] using the Monte Carlo PBG method[2] and a slightly modified value is given here. The PBG component of the observed resonance yield was estimated to be 37% and the multiple scattering correction was 18%.

(e) D.B. Gayther et al. (1979) [ref. 6]. The liquid scintillator tank used in this Linac measurement featured a Be through-tube lined with ^{10}B, and the addition of 10% by volume of methyl borate to the liquid scintillator. The tank was operated at a bias of 2.5 MeV to eliminate capture γ-rays in the tank. These measures should reduce the scattered neutron sensitivity of the detectors, which was estimated to be 10^{-4}. Measurements were made for two target thicknesses of an elemental sample, with Monte Carlo shape analysis. A final, modified value is also given in table 1 (priv. comm. - M.C. Moxon).

(f) M.C. Moxon (1965) [ref. 10]. The upper limit reported in this Moxon-Rae measurement has been corrected for p-wave resonances and the PBG. However the carbon converter used in the detectors requires a further correction for the difference in response for the Au/Ag and Fe γ-ray spectra (see preceding discussion) and increases the radiation width by a factor of 1.06 ± 0.03. Note however that the uncorrected value for the ^{Nat}Fe thermal capture cross section was in good agreement with the recommended value, casting doubt on the validity of the spectral correction.

(g) B.J. Allen et al (1980) [ref. 11]. As part of a study of the radiation widths of neutron scattering resonances, the 27.7 keV resonance was measured with Moxon-Rae detectors relative to Au with a Van de Graaff. Both C and C-Bi converters were used in simultaneous measurements but were not separately analysed. The capture yield was fitted in a Monte Carlo analysis which accounted for large self shielding and multiple scattering corrections. A correction was also made for the difference in detector response to the Fe and Au γ-ray spectra but a revised value is given here which is consistent with the discussion in the preceding section. Time-of-flight discrimination eliminated the PBG problem.

(h) K. Wisshak & F. Kappeler (1981) [ref. 12]. A similar but more accurate measurement than that in ref. 11 was made on three thin samples with improved timing to permit a shorter flight path and higher γ-ray yield. Corrections for the non-linear efficiency of the carbon converter were calculated but considered to be insignificant. A correction of 1.06 ± 0.03 has been applied in line with the preceding discussion.

(i) A. Brusegan et al. (1980) [ref. 8]. C_6D_6 detectors (with pulse height weighting) in an open beam geometry were used in this Linac measurement. A PBG correction was not made but is expected to be much smaller than that for ref. 7. Normalisation was made via the 1.15 keV resonance for Γ_n = 58 MeV. A final value[18] is given after reanalyses with REFIT and FANAC programs, and assuming a 5% systematic error in the normalisation.

III. Discussion

The first four measurements[3,4,5,17] appeared to define the radiation width quite well with only a 6% SD, i.e. Γ_γ = 1.49 ± 0.09. This happy situation crumbled at the Geel meeting in 1977, with the new results of Gayther (1979)[6]. Subsequent measurements contributed to a much reduced average of Γ_γ = 0.84 ± 0.09, and it is necessary to reconcile the wide range of values. This is achieved by first noting the high consistency of the 34-38 keV group of ℓ>0 resonances. With the exception of Macklin (1964)[3], the standard deviation of the sum of $g\Gamma_\gamma\ \Gamma_n/\Gamma$ for these resonances is 8.3%, and implies that there is not a significant normalisation problem.

The next problem is the PBG correction. The Moxon-Rae Van de Graaff measurements[3,11,12] are not subject to this effect and from these (using the modified values) the weighted average and standard deviation is Γ_γ = 1.00 ± 0.09 eV. The Moxon-Rae average is 25-60 per cent lower than the early corrected Linac measurements[4,16,17] which were all experiments subject to a prompt background in s-wave resonances which had, in all likelihood, been underestimated. These results are therefore excluded from further consideration.

Whereas a PBG will be present in the later Linac results[6,8,10] there is no evidence to indicate that it is at all significant. On the contrary, using the modified and/or final values, the weighted mean of Γ_γ = 1.01 ± 0.05 eV for this group is in good agreement with the Van de Graaff set. There is no a priori reason for further discrimination and the weighted mean and standard deviation for both groups is Γ_γ = 1.00 ± 0.04 eV. This new determination is more consistent with relative and absolute γ-ray spectrum measurements of the 27.7 keV resonance, and with results for the inverse photoneutron reaction $^{57}Fe\ (\gamma_o,\ n)\ ^{56}Fe$, as discussed in ref. 11.

The radiation width of the 27.7 keV resonance in ^{56}Fe represents the state of the art for capture in neutron scattering resonances, and, as such, could be taken as a secondary standard or bench mark for both linac and Van de Graaff measurements of this kind. The lack of such a standard has undoubtedly caused considerable uncertainty in s-wave radiation widths, particularly in the structural materials, over the past decade.

IV. References

(1) F.H. Fröhner. Specialist Meeting on Neutron Data of Structural Materials for Fast Reactors, Geel, Belgium, (1977) Ed. K.H. Bockhoff, Pergamon Press (1979) 795.

(2) B.J. Allen, A.R. Musgrove, R.L. Macklin, R.R. Winters. See ref. 1, p. 506.

(3) R.L. Macklin, P.J. Pasma, J.H. Gibbons. Phys. Rev. 136B (1964) 695.

(4) R.W. Hockenbury, Z.M. Bartolome, J.R. Tartarczuk, W.R. Moyer, R.C. Block. Phys. Rev. 178 (1969) 1746.

(5) A. Ernst, D. Kompe, F.H. Fröhner. Proc. Int. Conf. in Nuclear Data for Reactors, Helsinki (1970), vol. 1, p. 619 IAEA.

(6) D.B. Gayther, B.W. Thomas, B. Thom, M.C. Moxon. See ref. 1, p. 547.

(7) B.J. Allen, A.R. Musgrove, J.W. Boldeman, M.J. Kenny, R.L. Macklin. Nucl. Phys. 269 (1976) 408.

(8) A. Brusegan, F. Corvi, G. Rohr, R. Shelley, T. Van de Veen. Proc. Conf. Nuclear Cross Sections and Technology, Knoxville (1979). NBS Spec. Pub. 594 (1980) 163.

(9) R.L. Macklin, J.H. Gibbons, T. Inada. Nucl. Phys. 43 (1963) 353.

(10) M.C. Moxon. Int. Conf. on the Study of Nuclear Structure with Neutrons, Antwerp (1965), and private communication based on these data (1981).

(11) B.J. Allen, D.D. Cohen, F.Z. Company. J. Phys. G 6 (1980) 1173.

(12) K. Wisshak and F. Kappeler. Nucl. Sci. Eng. 77 (1981)58.

(13) K.V.K. Iyengar, B. Lal, M.L. Jhingan. Nucl. Instrum. Methods 121 (1974) 33.

(14) S.S. Malik & C.F. Majkrzak. Nucl. Instrum. Methods 130 (1975) 443.

(15) I. Bergquist & N. Starfelt. Nucl. Phys. 39 (1962) 353.

(16) F.H. Fröhner. See ref. 1, p. 138.

(17) B.J. Allen and A.R. Musgrove. See ref. 1, p. 447.

(18) F. Corvi. Priv. comm. (also this conference).

* This paper was not presented orally.

TABLE 1

CAPTURE MEASUREMENTS AT 27.7 keV

For errors 1.50 (30) ≡ 1.50 ± 0.30

Expt.	ref.	det. / accel.	10^3 atom b^{-1}	PBG	Γ_γ eV		$g\Gamma_\gamma\ \Gamma_n/\Gamma$ eV		
					27.7	34.2	36.7	38.4	(34-38)
a) Macklin(64)	3	MR VdG	6.54	No	1.50(30)				1.9(3)
m					0.95(27)				
b) Hockenbury(69)	4	LST Linac	54.0 6.8 6.3	Yes	1.44(14)	0.59(7)	0.30(3)	0.46(5)	1.35(9)
c) Ernst(70)	5	LST VdG	9.9	Yes	1.40(20)	0.55(7)	0.30(4)	0.34(5)	1.19(10)
Fröhner(79)	16				1.25(20)				
d) Allen(76,79)	7,17	C_6F_6 Linac	8.2	Yes	1.60(30)	0.66(7)	0.28(3)	0.38(4)	1.32(9)
e) Gayther(79)	6	LST Linac	51.0 17.0 4.1	Yes	0.89(13)	0.52(8)	0.24(4)	0.33(5)	1.09(10)
final					0.85(13)				
f) Moxon(65)	10	MR Linac	16.9 3.6 1.3	Yes	<1.3 0.75(23)				
m					0.80(25)				
g) Allen (80)	11	MR VdG	18.5	No	0.82(11)				1.19(15)
m					0.78(11)				
h) Wisshak(81)	12	MR VdG	5.3 2.6 1.4	No	1.01(5)	0.52(5)	0.32(5)	0.31(5)	1.15(5)*
m					1.07(6)				
i) Brusegan(80)	8	C_6D_6 Linac	15.0	Yes	0.80(20)	0.54(8)	0.23(3)	0.34(5)	1.11(10)
final	18				1.04(6)				

m - Values modified in this paper.
PBG - Prompt background; VdG - Van de Graaff accelerator.
Linac - Linear accelerator; MR - Moxon-Rae; LST - Liquid scintillator tank.
C_6F_6, C_6D_6 - Liquid scintillators with pulse height weighting.
* - Systematic error.

DIFFERENTIAL FISSION PRODUCT CAPTURE CROSS SECTION MEASUREMENTS SINCE BOLOGNA

by

Robert C. Block
Gaerttner Linac Laboratory
Nuclear Engineering Department
Rensselaer Polytechnic Institute
Troy, New York

Abstract

Differential capture cross section measurements of fission products are reviewed for the time period since the 1979 Bologna Specialist's Meeting on Neutron Cross Sections of Fission Products. Fission product capture data from nine laboratories in seven countries have been reported, and these results are discussed in regard to fast reactor applications.

I. Introduction

I have been given the task of reviewing the progress of fission product capture measurements since the 1979 Bologna Specialist's Meeting on Neutron Cross Sections of Fission Product.(1) However, before I plunge into the details of this progress, it is perhaps better to review first the situation at the conclusion of the Bologna meeting. In Table 1 I have summarized the request, status and action for fast differential fission product capture data which was made by the working group at the 1979 meeting.(2) Thirty four entries are listed in this table, referring to the 34 separate categories of fission product data which were summarized as the most important for fast reactor applications. Of these 34 requests, approximately 11 were considered completed and 23 still required additional measurements. Of those requiring additional measurements, 9 were requests for radioactive nuclei and 14 for stable isotopes.

Thus, one measure of the progress since Bologna is to review what new measurements have been reported in the remaining 23 requests that were not met. I have written friends and colleagues requesting information on their recent fission product capture measurements and I have spent some time in the library searching for recent publications. Although I do not claim I have found all of the recent experimental results, I do feel that I have found a significant fraction of them and that I can draw some conclusions from my

survey. Nine laboratories from 7 countries have reported recent measurements on 38 fission products. Of these, 10 measurements were made upon a total of 8 nuclei which are listed in Table 1. These nuclei are indicated by the asterisk (*) in the first column of the table. All but one of these 'important' measurements were for stable nuclei. The experimental techniques were very similar, if not identical, to the techniques used in the pre-Bologna days. In addition, several laboratories who have been active in fission product measurement, such as Rensselaer Polytechnic Institute, are no longer making these measurements, probably as the result of funding restrictions and programatic changes.

I therefore conclude that the emphasis on fission product capture differential measurements is diminishing. Of a total of 38 reported new measurements, only 10 or the order of 20% addressed the important needs of the fast reactor program, and only one of these measurements was for a radioactive nucleus. Many of these measurements were for only a few energies and did not address the energy ranges required. Perhaps there are as yet unreported activities which could change these conclusions, but as of the writing of this paper I see a diminishing emphasis in this area of research.

II. Recent Capture Measurements

The fission product capture measurements reported from the nine laboratories are summarized in Table 2 according to the laboratory, or country, in which the measurement was carried out (column 1), the experimental method used (column 2), the isotope of naturally abundant element that was measured (column 3) and the neutron energy range, or discrete neutron energies, reported (column 4).

The results of these measurements are as follows:

(1) Oak Ridge National Laboratory (ORNL) -- Neutron capture cross section measurements have been reported for ^{86}Kr up to 90 keV; ^{99}Tc, ^{107}Ag and ^{109}Ag from 2.6 keV to 2 MeV, and ^{133}Cs from 2.6 keV to 600 keV. These measurements were carried out by time-of-flight (TOF) at the ORELA linear accelerator with two C_6F_6 weighted-spectrum scintillator detectors located about the samples at a flight path of 40.12 meters. The neutron flux was measured with a ^{6}Li glass scintillator and capture normalization (i.e. product of neutron-flux-times-capture-efficiency)was made with saturated capture in the 4.9 eV Au resonance. An overall uncertainty of the order of 3 to 5% (1σ) is quoted for the errors based on relative capture efficiency, relative neutron flux, and normalization. In the higher energies counting statistical errors become important.

For ^{86}Kr the capture data were analyzed up to 90 keV, whereas the transmission data indicated 41 resonances up to 400 keV.(3) Thus, only a limited number of resonances were observed in capture, and the authors estimate that the effective capture cross section calculated over a Maxwellian energy distribution and from the resonance data resulted in an estimated uncertainty of less than 30%. A total of 183 resonances were resolved in the capture measurements upon ^{99}Tc between 2.6 and 5.1 keV, and capture areas under these resonances were determined.(4) The capture data were averaged over 21 energy

groups between 3 keV and 2 MeV, and these data are plotted in Fig. 1 along with the evaluated JENDL-1 and ENDF/B-V (mod 1) data. As can be seen in Fig. 1, the new experimental data fall between the two evaluations below 40 keV, but agree better with JENDL-1 evaluation between 40 keV and 700 keV and with the ENDF/B-V (mod 1) evaluation above 900 keV. It would appear, based on these measurements, that the ^{99}Tc capture cross section evaluation should be reviewed.

Preliminary measurements have been reported[5] for ^{107}Ag and ^{109}Ag, and the group-averaged cross section for ^{109}Ag is shown in Fig. 2 along with the ENDF/B-V and JENDL-1 evaluations. Here the recent experimental results fall below both evaluations below 300 keV, although the data lie closer to the ENDF/B-V evaluation. Although the experimental data agree with ENDF/B-V in the limited energy range from about 300 to 800 keV, the experimental data decrease monotonically above this energy while both evaluations develop a shoulder near 2MeV. This lack of a high-energy shoulder in the experimental data suggest that the evaluation be reviewed.

In the measurements of ^{133}Cs a total of 167 resonances were resolved up to 6 keV, and the average cross section was determined for 17 energy groups between 3 and 600 keV.[6] The group averaged data are plotted in Fig. 3. As can be seen in Fig. 3, the recent data are in good agreement with the JENDL-1 evaluation and slightly poorer agreement with ENDF/B-V. Although Macklin's recent results are in good agreement with the JENDL-1 data, which was strongly influenced by the measurements reported at Bologna by Asami and Yamamuro,[7] the expected strong onset of inelastic scattering above 600 keV would make an extension of these measurements to higher energies desirable to provide a guide to the higher energy evaluation.

(2) Kernforschungszentrum Karlsruhe (KFK) -- Capture cross section measurements were carried out with the Karlsruhe 3 MV pulsed Van de Graaff accelerator using the ^{7}Li(p,n) reaction, the TOF method and a Moxon-Rae detector with a graphite converter.[8] Measurements were reported[9] from 10 to 70 keV for fission product nuclei ^{93}Np and ^{103}Rh. These measurements were normalized to capture in Au, and the total uncertainty is estimated at ~4% for most of the data. The results are plotted in Figures 4 and 5, respectively, for ^{93}Nb and ^{103}Rh, along with other recent measured data,[10,11,13-15] the ENDF/B-V and RCN[12] evaluations, and a theoretical fit based on Hauser-Feshbach and optical models. The experimental error bars indicate only the uncertainty in the ratio of capture to that of Au.

The results for ^{93}Nb in Fig. 4 show that all the experimental results are very close to each other, and since these results were obtained at different laboratories and with different detectors and standards, one may conclude that the capture in ^{93}Np appears known to the order 5 to 10%. The RCN evaluation lies only slightly above the experimental data below 20 keV, but the ENDF/B-V evaluation falls well below the measured data and consideration should be given for a reevaluation. In Fig. 5 where the ^{103}Rh results are displayed, the new experimental data fall slightly below the bulk of the other experimental data, but still the agreement is within the 10% range. Below 20 keV the RCN evaluation appears to pass through the center of all of the experimental data while the ENDF/B-V evaluation favors the Hockenbury et al.[13] and Macklin and Halperin[15] data more.

The calculated cross sections, shown as the solid curves in Figures 4 and 5, were determined by a consistent set of parameters which fit a large amount of data in this mass range. Although the calculated curves do not pass through the center of the experimental data, they certainly fall within the error bands that are suggested by the clustering of the different sets of measurements, and this approach then provides a consistent data base for reliable model calculations.

Activation measurements using the ^{7}Li(p,n) reaction and the Van der Graaff accelerator were reported at 25 keV.[16] The capture cross sections of the fission products, ^{132}Xe, ^{134}Xe, ^{152}Sm, ^{151}Eu, ^{158}Gd and ^{160}Gd were determined relative to capture in Au; the quoted uncertainties ranged from 6 to 9%.

(3) Central Bureau for Nuclear Measurements, Geel (CBNM) -- Average capture cross section measurements have been carried out on isotopically enriched samples of ^{105}Pd and ^{108}Pd at the Gelina facility at Geel.[17] The measurements spanned the energy range from 10 eV to 600 keV and both ^{6}Li and ^{10}B were used to determine the neutron flux. Normalization was made to low-energy resonances in ^{105}Pd where the resonance parameters are well known. These results will be presented at this meeting.

(4) Bruyères-le-Châtel (BRC) -- Neutron capture cross sections have been reported at selected energies between 0.5 and 3 MeV for zirconium, lanthanum and terbium.[18,19] The measurements were carried out with the pulsed 4 MV Van de Graaff accelerator, a ^{7}Li(p,n) or T(p,n) target to produce pulses of monoenergetic neutrons, the TOF method to suppress gamma-ray background, and a NaI detector surrounded by annular NaI to detect capture gamma rays.[20,21] Both anti-compton and first-escape pulse-height data are recorded, and the data were unfolded to produce both the capture spectrum and the capture cross section. Uncertainties of the order of 10% have been reported for these measurements.

The capture cross section for the fission products Zr and Tb are shown in Fig. 6 (along with data for Sc and Re). The Zr experimental data appear discrepant by 30 to 50% in the overlap region of the BRC data from 0.5 to 1 MeV, and it is difficult to evaluate the impact of the BRC data here. However, the BRC datum at 2.5 MeV does serve to guide the evaluation in the high energy region. Indeed, the evaluation of Benzi et al.[22] passes very close to the 2.5 MeV point. The Tb (or ^{159}Tb, since this element is monoisotopic) data appear to follow the low-energy trend of the experimental data from other laboratories. The solid curve is an eyeball fit to the BRC data, and this is compared with the Benzi et al. and ENDF/B-IV evaluations. Below 1 MeV the experimental data fall between the two evaluations, while near 3 MeV the Benzi et al. evaluation comes closer to the BRC results.

In addition to determining the capture cross section, the BRC measurements also provide information on the capture gamma ray spectrum. From these data the gamma-ray strength functions of ^{94}Nb and ^{160}Tb have been deduced.[23] This information adds to the consistent set of data from which the model calculations, such as used at Karlsruhe[9] and Argonne,[24] can be used to provide a better overall evaluation of the experimental data (where such data exist) and in the region where no experimental data exist.

(5) Institute for Nuclear Research, Warsaw -- Neutron activation measurements were made with neutrons from the T(p,n) reaction using a 3 MV Van der Graaff accelerator.[25] Data are reported at neutron energies of 0.53 ± 0.14, 0.86 ± 0.21, 1.20 ± 0.15 and 1.31 ± 0.07 MeV for the fission product (target) nuclei ^{78}Se, ^{80}Se, ^{82}Se, ^{108}Pd, ^{110}Pd, ^{114}Cd and ^{116}Cd. Uncertainties of ≥10% are indicated for these results.

The authors did not compare their results with evaluated data, although they did note that their ^{80}Se cross section is about half of that reported by Tolstikov et al.[26,27] but that they are in agreement with the results of Lindner et al.[28] for ^{114}Cd and with the results of Weston et al.[29] for ^{108}Pd. The main thrust of this research was to compare their measured capture cross sections with calculations based on the statistical model according to the approach of Tepel et al.[30] Although the authors did get reasonable fits to their data, it would be interesting to see how their data compare to the bulk of the measured, evaluated and calculated data in the mass range of their data.

(6) Japan Atomic Energy Research Institute, Tokai (JAERI) -- Capture cross section measurements were carried out by the TOF method at the JAERI linac with a 3500 liter liquid scintillator detector located at their 52 meter flight path.[7,31] Both ^{6}Li and ^{10}B was used to determine the relative neutron flux, and normalization was by the saturated capture method. Recent measurements have been reported for enriched isotopes of ^{107}Ag and ^{108}Ag over the energy range 3.2 to 700 eV.[32] The average capture cross sections of ^{107}Ag, ^{109}Ag and ^{nat}Ag are listed in Table 3 for 36 energy groups. In Table 4 are listed the uncertainties, and in Table 5 are listed the covariance matrix for these data.

The JAERI results for natural Ag and ^{107}Ag are in good agreement with earlier data. However, their ^{109}Ag results lie between two previous discrepant measurements, 30% higher than those of Weston et al.[29] and 35% lower than those of Kononov et al.[33] However, these new results are in fairly good agreement with the recent ORNL results.[5]

(7) Kyoto University Research Reactor Institute (KURRI) -- Capture cross sections were made by the TOF technique using the 46-MeV linac and a pair of pulse-weighting C_6D_6 detectors at an 11.7 meter flight path. The neutron flux was determined relative to ^{10}B(n,αγ).[7,11] Measurements were also made near 24 keV with an Fe-filtered TOF beam, and the continuous TOF data were normalized to the 24 keV data.[34] A measurement has been reported for ^{165}Ho over the energy range from 3.2 to 80 keV.[11] The capture cross section results are shown in Fig. 7 along with the experimental data of Konks and Fenin,[35] Asghar et al.,[36] Czirr and Stelts[37] and Macklin[38] and the ENDF/B-IV evaluation. The agreement between these sets of experimental results is within the order of 10%.

Additional measurements using 24 keV Fe-filtered and 55 and 146 keV Si-filtered beams are also being used for capture measurements.[39] Measurements of the relative capture cross section at these three energies have been reported for ^{93}Nb, ^{127}I, ^{133}Cs and ^{165}Ho.

Gamma ray spectra have been determined by unfolding the C_6D_6 pulse-height data, and this again provides useful information on the capture mechanism for these fission product nuclei.[40] The spectrum obtained for neutron capture between 1.5 and 75 keV are shown in Fig. 8. The solid curve is calculated assuming pure electric dipole transitions and using the giant resonance parameters from Berman,[41] the level density formulation of Gilbert and Cameron[42] and one pigmy resonance. The measured spectrum exhibits the same bump near 5 MeV that has been observed by Bergqvist et al.[43] and Brzosko et al.[44]

(8) Tokyo Institute of Technology -- This group has recently installed a 3MV Pelletron accelerator. Neutron capture measurements were reported for ^{165}Ho at 200, 300, 460 and 610 keV using a novel pulse-height weighting detector and normalizing relative to capture in Au.[45] The detector consists of an annulus of NE-213 which has an inner diameter of 17 cm, an outer diameter of 37 cm and is 13 cm long. An annular graphite sleeve of 7 cm inner diameter and 19.5 cm long is located inside the NE213 annulus. The graphite liner serves as a gamma ray absorber much in the same sense as the graphite liner in a Moxon-Rae detector, and like the Moxon-Rae detector this detector has an almost linear weighting function. The experimental results are shown in Fig. 9, along with the data of Johnsrud et al.,[46] Brzosko et al.,[44] Czirr et al.[37] and Macklin and Winters.[47] An overall uncertainty of ∿5% is estimated for the annular detector data, and the agreement is quite good with the Johnsrud and Macklin data.

(9) India Institute of Technology (IIT) -- Activation measurements have been reported for ^{69}Ga, ^{80}Se, ^{107}Ag, ^{110}Pd and ^{154}Sm at 388, 415, 460 and 650 keV using the T(p,n) reaction and the IIT Van der Graaff accelerator.[48] An overall uncertainty between 6 and 20% is quoted for these results.

III. Status of Fast Capture Requests

The eight nuclei measured which were on the Bologna workshop list[2] are ^{99}Tc, ^{105}Pd, ^{109}Ag, ^{127}I, ^{133}Cs, ^{132}Xe, ^{152}Sm and ^{151}Eu. Although it will require a thorough evaluation of all of the data to see if these recent measurements satisfy the requests, it is still worthwhile to speculate on their impact. The ^{99}Tc data from ORNL[4] will have to be compared with the measurements of Little and Block[49] and Chou and Werle[50] to see if the present discrepancy can be resolved to the requested 10% requirement. The higher energy range of the ORNL data should provide a good benchmark for the evaluation. The ^{105}Pd data from CBNM[17] will be presented at this meeting, and it remains to be seen if the requested 10% requirement will now be met.

The ^{109}Ag results from ORNL[5] and JAERI[32] appear to be in good agreement, and together with earlier measurements may be able to resolve the existing discrepancies and satisfy the 10 to 20% request. For ^{127}I only the ratio of capture cross sections was provided,[39] but the quoted errors are ∿5% and may provide enough information to satisfy the 10% request. However, it is very doubtful that these data can satisfy the 5% request. The capture cross section of ^{133}Cs has been measured by TOF at ORNL[6] and ratios at three energies at KURRI,[39] and it is possible that the 10% request may now be satisfied. The ^{132}Xe (request: 30%), ^{152}Sm (request: 20%) and ^{151}Eu

(request: 5%) were addressed by KFK measurements at 25 keV only.[16] These measurements may help satisfy the ^{132}Xe and ^{152}Sm requests, but it appears doubtful that the ^{151}Eu request is now met.

IV. Conclusions

I have reviewed post-Bologna measurements of 38 fission products from 9 laboratories, and only the order of 20% of these measurements were concerned with the high priority requests for fast reactor applications.[2] Only one radioactive nucleus was measured, ^{99}Tc, and this nucleus presents few problems to most capture detectors. No effort seems to have been made to do the more difficult capture measurements, both from the standpoint of getting an adequate sample or by designing a detector to handle the activity. For example, a gamma-multiplicity detector, such as the Romashka detector developed at the Kurchatov Institute[51] or the Crystal Ball detector developed at SLAC,[52] might be useful to select high-multiplicity capture events from low-multiciplicity gamma rays from a radioactive sample. However, it is the opinion of this author that it is quite likely that there may not be sufficient funding to carry out some of these more difficult measurements in the near future.

In conclusion, I want to thank the organizers of this meeting for the opportunity to present this paper and my special point of view.

References

1. NEANDC Specialist's Meeting on Neutron Cross Sections of Fission Product Nuclei, Dec. 12-14, 1979, Bologna, Italy, Report NEANDC(E)-209.

2. "Status of the Capture Cross Section for the Most Important FP Nuclei," ibid., Report of Working Group 1, pg. 403.

3. B. Fogelbert, J.A. Harvey, R.L. Macklin, S. Raman and P.H. Stelson, "Neutron Resonance Study of ^{86}Kr," Proc. of 4th Int'l. Symposium on Neutron-Capture Gamma Ray Spectroscopy and Related Topics, Sept. 7-11, 1981, Grenoble.

4. R.L. Macklin, "^{99}Techniciun Neutron Capture Cross Section" (to be published).

5. R.L. Macklin (private communication).

6. R.L. Macklin, "^{133}Cesium Neutron Capture Cross Section" (to be published).

7. N. Yamamuro and A. Asami, "Measurements of Capture Cross Sections in the FP Mass Range," ref. 1, page 19.

8. K. Wisshak and F. Käppeler, Nucl. Sci. & Eng. 77, 58 (1981) and Nucl. Sci. & Eng. 76, 148 (1980).

9. G. Reffo, F. Fabbri, K. Wisshak and F. Käppeler," Fast Neutron Capture Cross Sections and Related Gamma Ray Spectra of ^{93}Nb, ^{103}Rh, and ^{181}Ta," (to be published).

10. R.L. Macklin, Nucl. Sci. & Eng. 59, 12 (1976).

11. N. Yamamuro, K. Saito, T. Emoto, T. Wada, Y. Fujita and K. Kobayashi, "Neutron Capture Cross Section Measurements of Nb-93, I-127, Ho-165, Ta-181 and U-238," J. Nucl. Sci. & Technol. 17, 582 (1980).

12. H. Gruppelaar, "Tables of RCN-2 Fission Product Cross Section Evaluation, Vol. 1," ECN-13 Netherlands Energy Research Foundation (1977).

13. R.W. Hockenbury, H.R. Knox and N.N. Kaushal, Proc. Conf. Nucl. Cross Sections & Technol., Wash. D.C., March 3-7, 1975, NBS Spec. Publ. 425 (1975).

14. C. LeRigoleur, A. Arnaud and J. Taste, "Absolute Capture Cross Section Measurements for ^{23}Na, Cr, ^{55}Mn, Fe, Ni, ^{103}Rh, Ta, ^{197}Au, ^{238}U from 10 to 600 keV," Report CEA-R-4788, Centre d'Etudes Nucleaires de Cadarache, France (1976).

15. R.L. Macklin and J. Halperin, Nucl. Sci. & Eng. 73, 174 (1980).

16. H. Beer, F. Käppeler and G. Reffo, "Capture Cross Section Measurements on Xe, Sm, Eu and Gd-Isotopes with the Activation Method", Prog. Rep't. on Nucl. Res. in the Federal Republic of Germany, April 1, 1980 to March 31, 1981, NEANDC(E)-222U Vol, V (1981).

17. G. Rohr, C. Bastian, E. Cornelius, R. Shelley, F. van der Veen and G. Vanpraet, "Average Capture Cross Section of the Fission Product Nuclei ^{105}Pd and ^{108}Pd," (to be presented at this meeting).

18. J. Voignier, S. Joly and G. Grenier, "Neutron Capture Cross Sections for Scandium, Zirconium, Terbium and Rhenium Between 0.5 and 2.5 MeV," Proc. of 4th Int'l. Symposium on Neutron-Capture Gamma Ray Spectroscopy and Related Topics, Sept. 7-11, 1981, Grenoble.

19. G. Grenier (private communication).

20. S. Joly, J. Voignier, G. Grenier, D. Drake and L. Nilsson, Nucl. Instr. & Methods 153, 493 (1978).

21. S. Joly, J. Voignier, G. Grenier, D. Drake and L. Nilsson, Nucl. Sci. & Eng. 70, 53 (1979).

22. Benzi et al., Report DOC-CEC(71)9.

23. S. Joly, "Photon Strength Functions for ^{90}Y, ^{94}Nb, ^{160}Tb and ^{182}Ta," Proc. of 4th Int'l. Symposium on Neutron-Capture Gamma Ray Sepctroscopy and Related Topics," Sept. 7-11, 1981, Grenoble.

24. W.P. Poenitz, "Fast Neutron Capture Cross Section Measurements, Evaluation and Model Calculation of Fission Product Nuclei," ref. 1, page 85.

25. M. Herman and A. Marcinkowski, "Cross Sections for Fast Neutron Capture on the Se, Pd, Cd, Os and Pt Isotopes," Nucl. Phys. A357, 1 (1981).

26. W.A. Tolstikov, W.P. Koroleva, W.E. Kolesov and A.G. Dovbienko, Atomnaya Energia 23, 576 (1967).

27. W.A. Tolstikov, W.P. Koroleva and W.E. Kolesov, Atomnaya Energia 24, 187 (1968).

28. M. Lindner, R.J. Nagle and J.H. Landrum, Nucl. Sci. & Eng. 59, 381 (1976).

29. L.W. Weston, K.K. Seth, E.G. Bilpuch and H.W. Newson, Ann. of Phys. 10, 477 (1960).

30. J.W. Tepel, H.M. Hofmann and H.A. Weidenmuller, Phys. Lett. 49B, 1 (1974).

31. M. Mizumoto, "Neutron Resonance Parameters and Radiative Capture Cross Sections of ^{147}Sm and ^{149}Sm," Nucl. Phys. A357, 90 (1981).

32. M. Mizumoto (private communication).

33. V.N. Kononov et al., Proc. of Conf. on Nuclear Data for Reactors, Paris (1966).

34. N. Yamamuro, T. Doi, T. Miyagawa, Y. Fujita, K. Kobayashi and R.C. Block, J. Nucl. Sci. Technol. 15, 637 (1978).

35. V.A. Konks and Yu. I. Fenin, Proc. Int'l. Conf. Nucl. Struc. Study Neutrons, pg. 576 (1965).

36. M. Asghar, C.M. Chaffey and M.C. Moxon, Nucl. Phys. A108, 535 (1968).

37. J.B. Czirr and M.L. Stelts, Nucl. Sci. & Eng. 52, 299 (1973).

38. R.L. Macklin, ibid. 59, 231 (1976).

39. Y. Fujita (private communication).

40. N. Yamamuro, M. Igashira, H. Shirayanagi, Y. Fujita and K. Kobayashi, "Gamma-Rays from Radiative Capture Reactions in ^{133}Cs, ^{181}Ta and ^{197}Au," (to be published).

41. B.L. Berman, "Atlas of Photoneutron Cross Sections Obtained with Monoenergetic Photons," UCRL-78482 (1976).

42. A. Gilbert and A.G. W. Cameron, Can. J. Phys. 43, 1446 (1965).

43. I. Bergqvist and N. Starfelt, Nucl. Phys. 39, 529 (1962).

44. J.S. Brzosko, E. Gierlik, A. Soltan, Jr., Z. Szeflinski and Z. Wilhelmi, Acta. Phys. Polonica B2, 489 (1971).

45. N. Yamamuro, M. Igashira and M. Shimizu, "Fast Neutron Capture Cross Section Measurement with Pulse-Height Weighting Technique," (to be published).

46. A.E. Johnsrud, M.G. Silbert and H.H. Barschall, Phys. Rev. 116, 927 (1959).

47. R.L. Macklin and R.R. Winters, Nucl. Sci. & Eng. 78, 110 (1981).

48. H.M. Agrawal, M. Afzal Ansari, M. Wasim and M.L. Sehgal, "Neutron Capture Cross-Sections in the KeV Energy Region," Nuovo Cimento 61A, 142 (1981).

49. R.C. Little and R.C. Block, "Neutron Capture Cross-Section Measurements of ^{99}Tc up to 80 keV," Trans. Am. Nucl. Soc. 26, 574 (1974).

50. J. Chou and H. Werle, "(n,γ) Cross Section Measurements of ^{99}Tc, Eu, Sm and Fe in the Energy Range 1 eV to 50 keV with a Slowing-Down Time Spectrometer," J. Nucl. Energy 27, 811 (1973).

51. G.V. Muradyan, "The Spectrometry of Multiplicity of Secondary Radiation as a Method of Measurement of Neutron Cross-Section and Investigation of Nuclei," Proc. of Nucl. Cross Sections for Technol., October 22-26,1979, Knoxville, Tenn., pg. 521, NBS Spec. Publ. 594 (1980).

52. M.J. Oreglia, "A Study of the Reactions $\psi' \to \gamma\gamma\psi$," SLAC-236 (1980).

Table 1. Request, Status and Action for Fast Differential Capture Data
(As summarized at 1979 Specialist's Mtg. on Fission Product Nuclei)

	Nuclide	Request	Status	Action
1.	^{93}Zr	20%	Not met	
2.	^{95}Mo	10%	New data, but not met	Measure above 100keV
3.	^{97}Mo	10%	New data	Measure above 100keV
4.	^{98}Mo	20%	New data	
5.	^{99}Mo	[ρ(t)]		Reevaluate
6.	^{100}Mo	20%		Resolve discrepancies
7.*	^{99}Tc	10%	Not met	Measure from 1 to 500keV
8.	^{101}Ru	10%	New data	
9.	^{102}Ru	20%	New data	
10.	^{103}Ru	20%	Not met	
11.	^{104}Ru	20%	New data	
12.	^{103}Rh	10%	New data	
13.	^{105}Rh			Reevaluate
14.*	^{105}Pd	10%	New data	Measure from 100eV to 10eV
15.	^{107}Pd	10%	Not met	
16.*	^{109}Ag	10%-20%	Many discrepancies in keV region; not met	
17.*	^{127}I	10% 5%	Status 20% New data	Need more keV data for secondary standard
18.	^{129}I	20%	Not met	
19.	^{131}Xe	20%	Not met	
20.*	^{132}Xe	30%	Not met	
21.*	^{133}Cs	10%	Not met	
22.	^{135}Cs	10%	Not met	
23.	^{139}La	20%	Met	

	Nuclide	Request	Status	Action
24.	^{141}Pr	20%	Probably met	
25.	$^{143-150}Nd$	10%(BU)	Status 15%	
26.	^{147}Pm	10%	Not met	keV data required
27.	^{148m}Pm		Probably met	
28.	^{14a}Pm	[ρ(t)]	No data	Reevaluate
29.	^{149}Sm	10%	New data, but discrepant	Resolve discrepancy; one measurement at ∿100 keV
30.	^{151}Sm	10%	No keV data	PHENIX data made available
31.*	^{152}Sm	20%	New data (not met)	
32.	^{153}Eu	20%	New data, but discrepant: not met	
33.*	^{151}Eu	5%	New data, not met	
	^{152}Eu	20%		
	^{153}Eu	5%	New data	
	^{154}Eu	20%		
	Eu(nat)	?	New data	
34.	^{155}Eu	20%	Not met	

*New measurements reported since Bologna

Table 2. FP Capture Measurements (Reported After the 1979 Bologna Meeting).

Laboratory	Method	Nuclei	Neutron Energy
ORNL	Linac,TOF,C_6F_6 det.	^{86}Kr, ^{99}Tc, ^{107}Ag, ^{109}Ag, ^{133}Cs	2.6keV-2000keV
KFK	VdG,TOF,Moxon-Rae det.	^{93}Nb, ^{103}Rh	10keV-70keV
	VdG, Activation	$^{132,134}Xe$, ^{152}Sm, ^{151}Eu, $^{158,160}Gd$	25keV
CBNM	Linac,TOF,C_6D_6 det.	^{105}Pd, ^{108}Pd	.01keV-600keV
Bruyères-le-Châtel	VdG,TOF,NaI det.	Zr, ^{139}La, ^{159}Tb	0.5,0.7,1,2,2.5,3MeV
Inst. Nuclear Res., Warsaw	VdG, Activation	$^{78,80,82}Se$, $^{108,110}Pd$, $^{114,116}Cd$	0.5,0.9,1.2,1.3MEV
JAERI	Linac,TOF,Large scint. det.	^{107}Ag, ^{109}Ag	3.2keV-700keV
KURRI	Linac,TOF,C_6D_6 det.	^{165}Ho	3.2keV-80keV
		^{93}Nb, ^{127}I, ^{133}Cs, ^{165}Ho	24,55,146keV
Tokyo Inst.Tech.	VdG,TOF, C + scint. det.	^{165}Ho	200,300,460,610keV
India Inst.Tech.	VdG, Activation	^{69}Ga, ^{80}Se, ^{107}Ag, ^{110}Pd, ^{154}Sm	388,415,460,650keV

Table 3. Average Capture Cross Sections of ^{107}Ag, ^{109}Ag and ^{nat}Ag (32)

E_n (keV)	^{107}Ag (barn)	^{109}Ag (barn)	^{nat}Ag a) (barn)
3.2 - 4	1.810 (0.9) b)	1.851 (1.0) b)	2.221 (1.1) b)
4 - 5	1.765 (0.5)	1.713 (0.5)	1.973 (0.6)
5 - 6	1.568 (0.5)	1.629 (0.5)	1.778 (0.6)
6 - 7	1.490 (0.5)	1.671 (0.6)	1.737 (0.6)
7 - 8	1.246 (0.6)	1.391 (0.6)	1.455 (0.7)
8 - 9	1.407 (0.5)	1.637 (0.5)	1.620 (0.6)
9 - 10	1.352 (0.6)	1.320 (0.6)	1.445 (0.7)
10 - 12	1.186 (0.4)	1.349 (0.4)	1.345 (0.5)
12 - 14	1.138 (0.5)	1.171 (0.5)	1.207 (0.6)
14 - 16	1.068 (0.5)	1.309 (0.6)	1.101 (0.6)
16 - 18	1.062 (0.5)	1.075 (0.6)	1.112 (0.7)
18 - 20	1.037 (0.5)	1.061 (0.6)	1.068 (0.7)
20 - 25	0.963 (2.6)	1.010 (2.7)	0.988 (3.1)
25 - 30	0.911 (2.8)	0.855 (3.2)	0.888 (3.4)
30 - 35	0.825 (3.5)	0.816 (3.8)	0.814 (4.3)
35 - 40	0.762 (3.9)	0.748 (4.3)	0.732 (4.9)
40 - 45	0.683 (4.1)	0.681 (4.4)	0.696 (5.0)
45 - 50	0.679 (3.8)	0.623 (4.4)	0.667 (4.7)
50 - 60	0.593 (3.9)	0.575 (3.3)	0.586 (3.7)
60 - 70	0.554 (3.0)	0.518 (3.3)	0.536 (3.7)
70 - 80	0.525 (3.8)	0.477 (4.3)	0.502 (4.8)
80 - 90	0.484 (4.0)	0.438 (4.5)	0.441 (5.1)
90 - 100	0.451 (3.9)	0.419 (4.4)	0.439 (5.1)
100 - 120	0.403 (2.8)	0.375 (3.2)	0.382 (5.2)
120 - 140	0.366 (3.0)	0.337 (3.4)	0.344 (5.5)
140 - 160	0.347 (3.5)	0.316 (4.0)	0.309 (6.7)
160 - 180	0.314 (3.6)	0.291 (4.0)	0.293 (6.6)
180 - 200	0.292 (3.7)	0.285 (4.1)	0.268 (6.6)
200 - 250	0.271 (2.6)	0.257 (2.9)	0.249 (4.6)
250 - 300	0.246 (2.8)	0.232 (3.1)	0.233 (4.4)
300 - 350	0.230 (3.0)	0.213 (3.3)	0.213 (4.6)
350 - 400	0.193 (3.5)	0.179 (4.0)	0.171 (5.6)
400 - 450	0.177 (4.0)	0.157 (4.5)	0.153 (6.2)
450 - 500	0.142 (4.0)	0.133 (4.5)	0.135 (5.0)
500 - 600	0.113 (3.3)	0.109 (3.6)	0.110 (6.1)
600 - 700	0.094 (3.9)	0.091 (4.3)	0.101 (6.1)

a) The systematic uncertainty for the capture cross sections of natural isotope is large compared with the values for separated isotope, mainly due to the difficulty of calculations of self-shielding and multiple scattering correction.

b) Statistical standard deviations given in percentage. Systematic uncertainties are discussed separately.

Table 4. Uncertainties of measured capture cross sections of silver isotopes for each group[32]

Group number	Energy (keV)	^{107}Ag (%)	^{109}Ag (%)	^{nat}Ag (%)
1	1100 - 800	7.41	7.61	8.53
2	800 - 630	7.14	7.19	8.29
3	630 - 500	6.89	6.93	8.08
4	500 - 400	6.63	6.69	7.86
5	400 - 310	6.51	6.57	7.79
6	310 - 250	6.40	6.48	7.73
7	250 - 200	6.32	6.44	7.71
8	200 - 150	6.23	6.42	7.71
9	150 - 120	6.12	6.41	7.60
10	120 - 100	6.08	6.46	7.57
11	100 - 77.3	6.14	6.81	7.08
12	77.3 - 59.8	6.06	6.53	6.97
13	59.8 - 46.5	6.11	6.69	7.25
14	46.5 - 36.0	6.19	6.84	7.48
15	36.0 - 21.5	6.18	6.89	7.84
16	21.5 - 16.6	6.15	6.50	7.96
17	16.6 - 12.9	6.33	7.12	8.78
18	12.9 - 10.0	4.71	4.83	4.24
19	10.0 - 7.73	4.77	4.87	4.83
20	7.73 - 5.98	4.83	4.97	4.96
21	5.98 - 4.65	4.97	5.13	5.13
22	4.65 - 3.60	4.96	5.33	5.00

Table 5. Covariance matrix (x100) for capture cross sections of Ag isotopes.[32]

Group	1	2	3	4	5	6	7	8	9	10	11	12	13	14	15	16	17	18	19	20	21	22
1	100																					
2	68	100																				
3	62	67	100																			
4	56	62	66	100																		
5	58	64	65	68	100																	
6	58	60	64	64	66	100																
7	60	60	63	65	66	66	100															
8	57	60	62	64	65	65	66	100														
9	58	60	61	62	63	64	65	66	100													
10	57	57	59	61	62	63	64	66	66	100												
11	52	57	57	59	60	61	63	66	64	68	100											
12	52	55	56	59	60	61	63	65	66	67	69	100										
13	50	52	54	56	58	59	62	64	66	67	69	68	100									
14	51	53	55	58	60	61	64	67	69	72	75	73	77	100								
15	44	47	49	52	54	55	58	61	64	65	69	62	69	71	100							
16	44	46	49	51	53	58	57	62	62	64	67	66	67	68	68	100						
17	38	40	43	45	47	49	53	54	57	58	61	60	59	68	64	63	100					
18	49	51	53	55	56	57	58	58	58	58	55	58	56	60	55	59	53	100				
19	48	51	53	55	56	57	57	57	57	57	54	57	56	59	54	58	52	100	100			
20	47	50	53	54	55	56	56	55	56	56	54	56	55	58	54	57	51	99	99	100		
21	44	49	51	53	54	54	55	55	55	55	52	55	54	57	50	56	50	98	98	99	100	
22	46	49	51	53	54	54	55	51	55	55	52	55	54	57	50	56	48	98	98	99	99	100

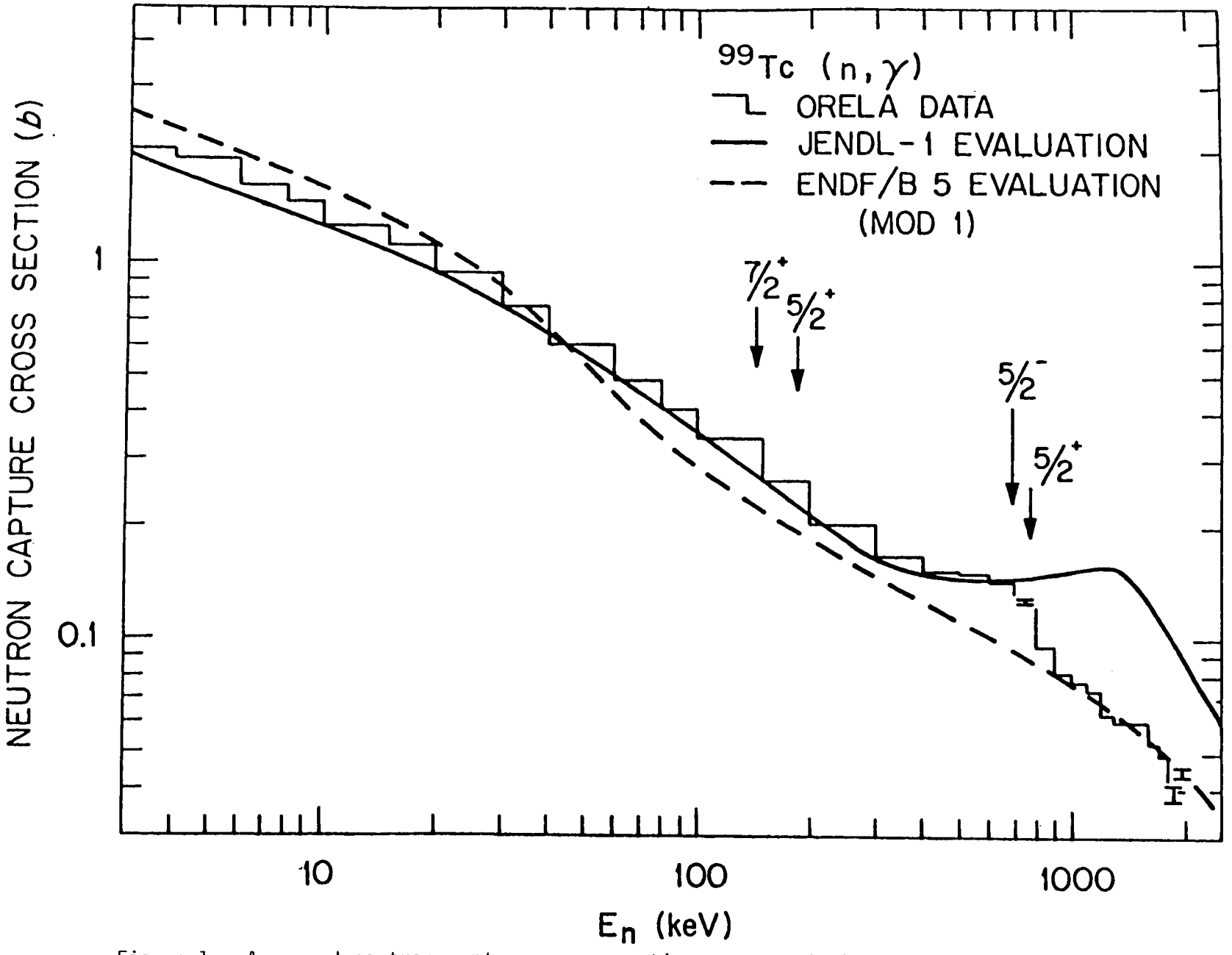

Figure 1. Averaged neutron capture cross sections compared with two recent evaluations. Arrows indicate thresholds for inelastic scattering.

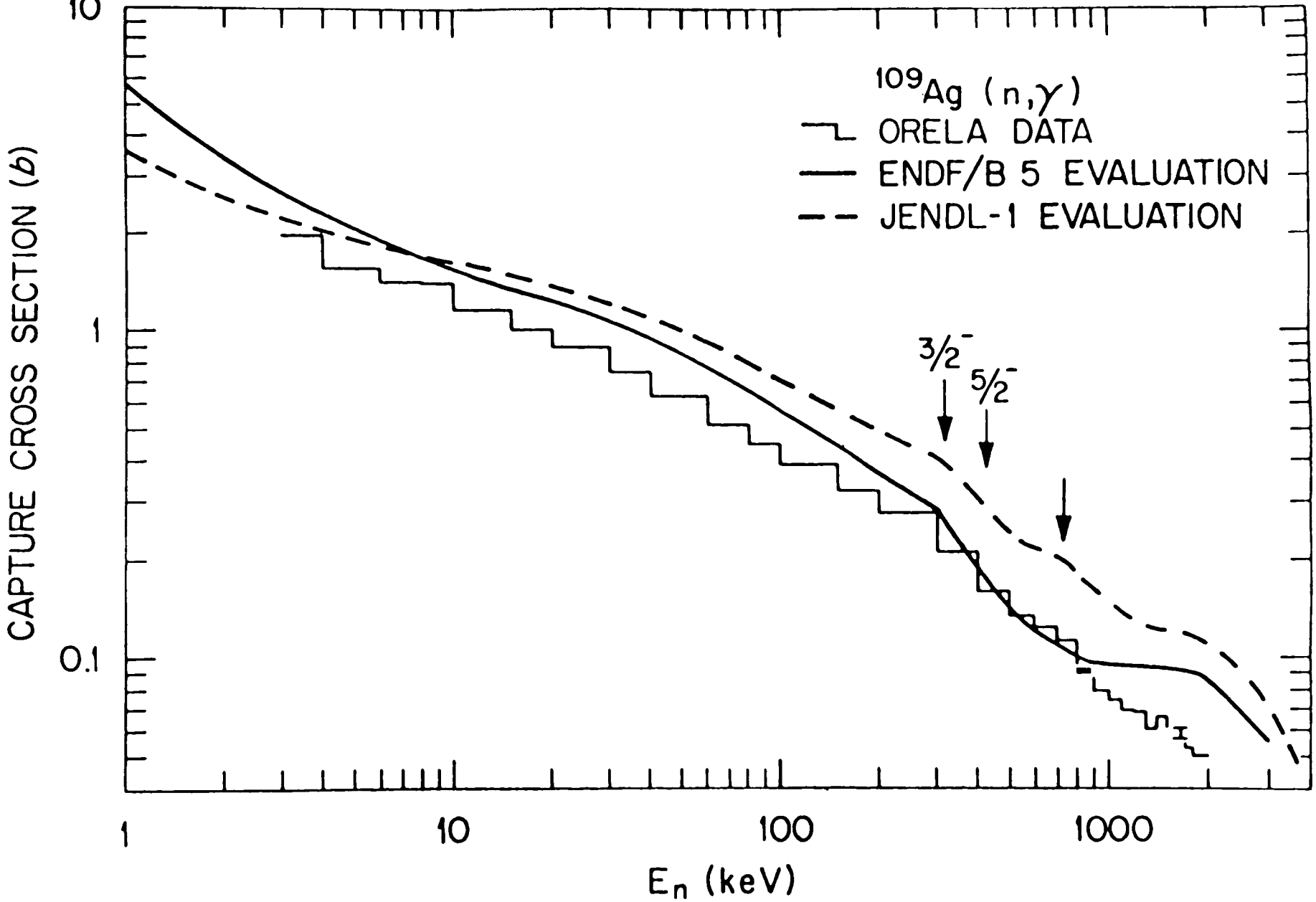

Figure 2. Averaged neutron capture cross sections compared with two recent evaluations. Arrows indicate thresholds for inelastic scattering.

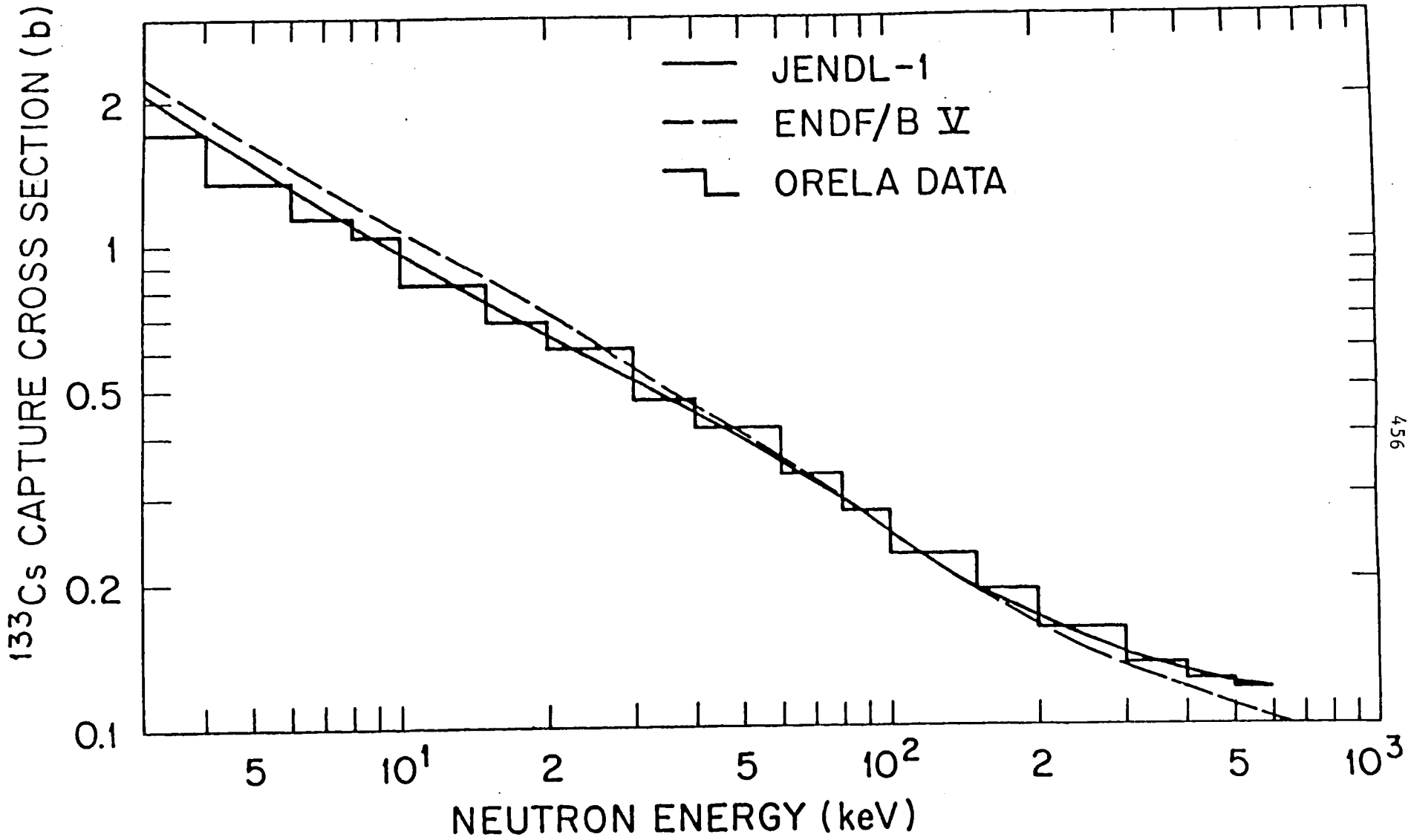

Figure 3. Averaged neutron capture cross sections compared with two recent evaluations. The solid curve is based on average parameters Γ_γ = 118 meV, $D_{\ell=0}$ = 23.2 eV, $10^4 S_0$ = 1.42, $10^4 S_1$ = 1.39 and fits the present data fairly well, though a small increase in S_1($\sim$10%) appears likely to improve the fit.

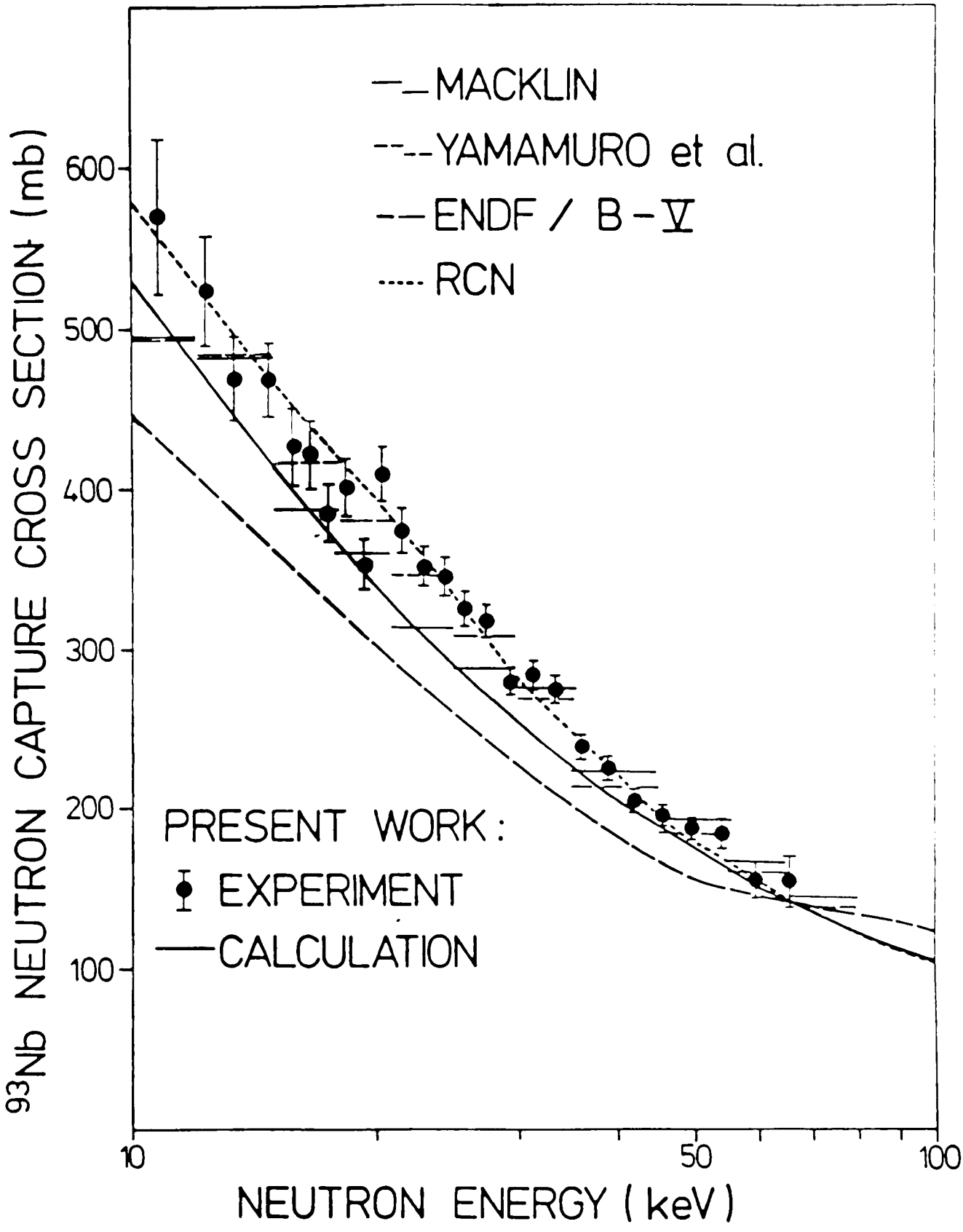

Figure 4. The measured neutron capture cross section of ^{93}Nb compared to the data of Macklin[10] and Yamamuro et al.,[11] the ENDF/B-V and RCN[12] evaluations, and a calculation based on Hauser-Feshbach and optical models.

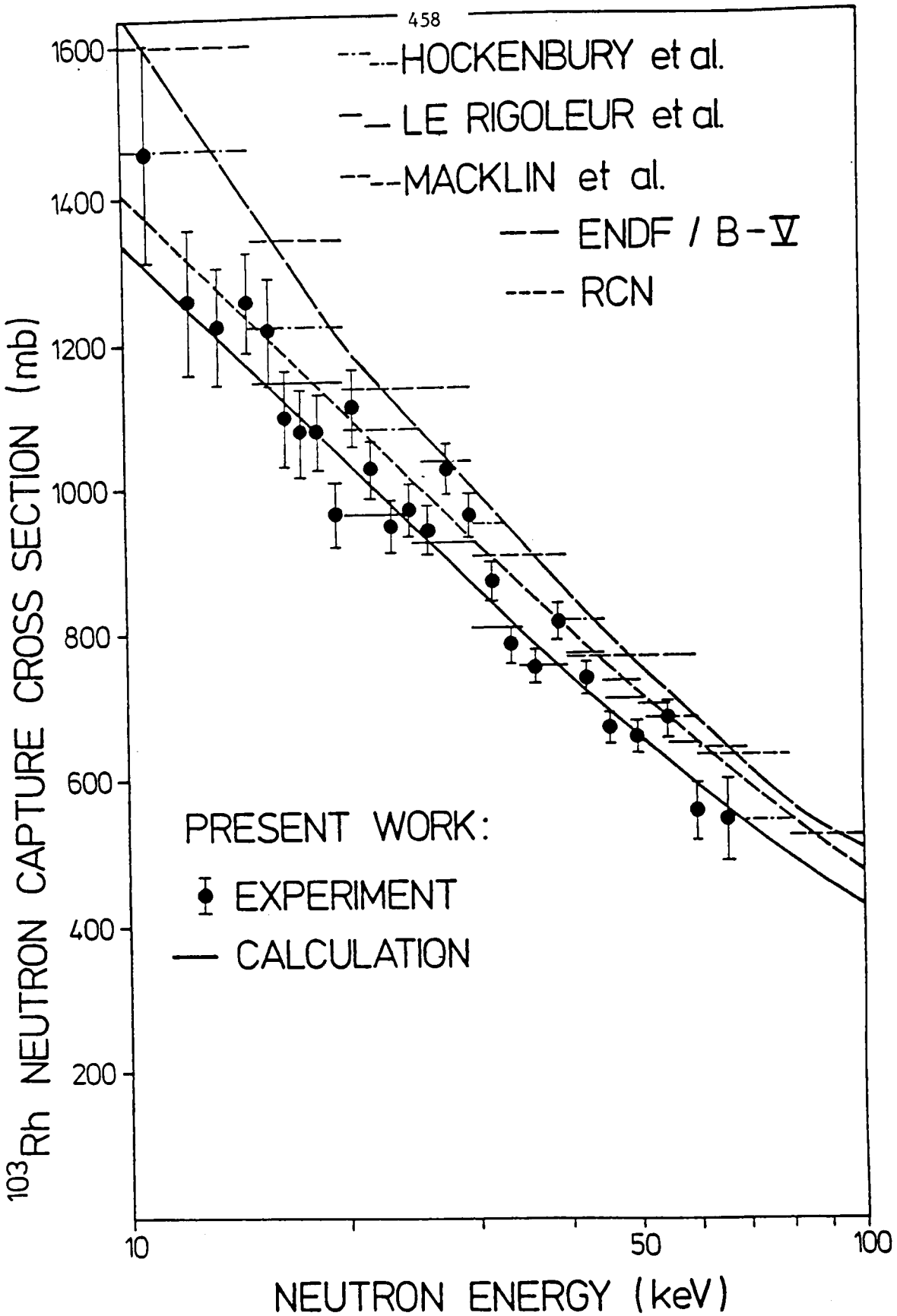

Figure 5. The measured neutron capture cross section of ^{103}Rh compared with the data of Hockenbury et al.,[13] LeRigoleur et al.,[14] Macklin and Halperin,[15] the ENDF/B-V and RCN[12] evaluations, and a calculation based on Hauser-Feshbach and optical models.

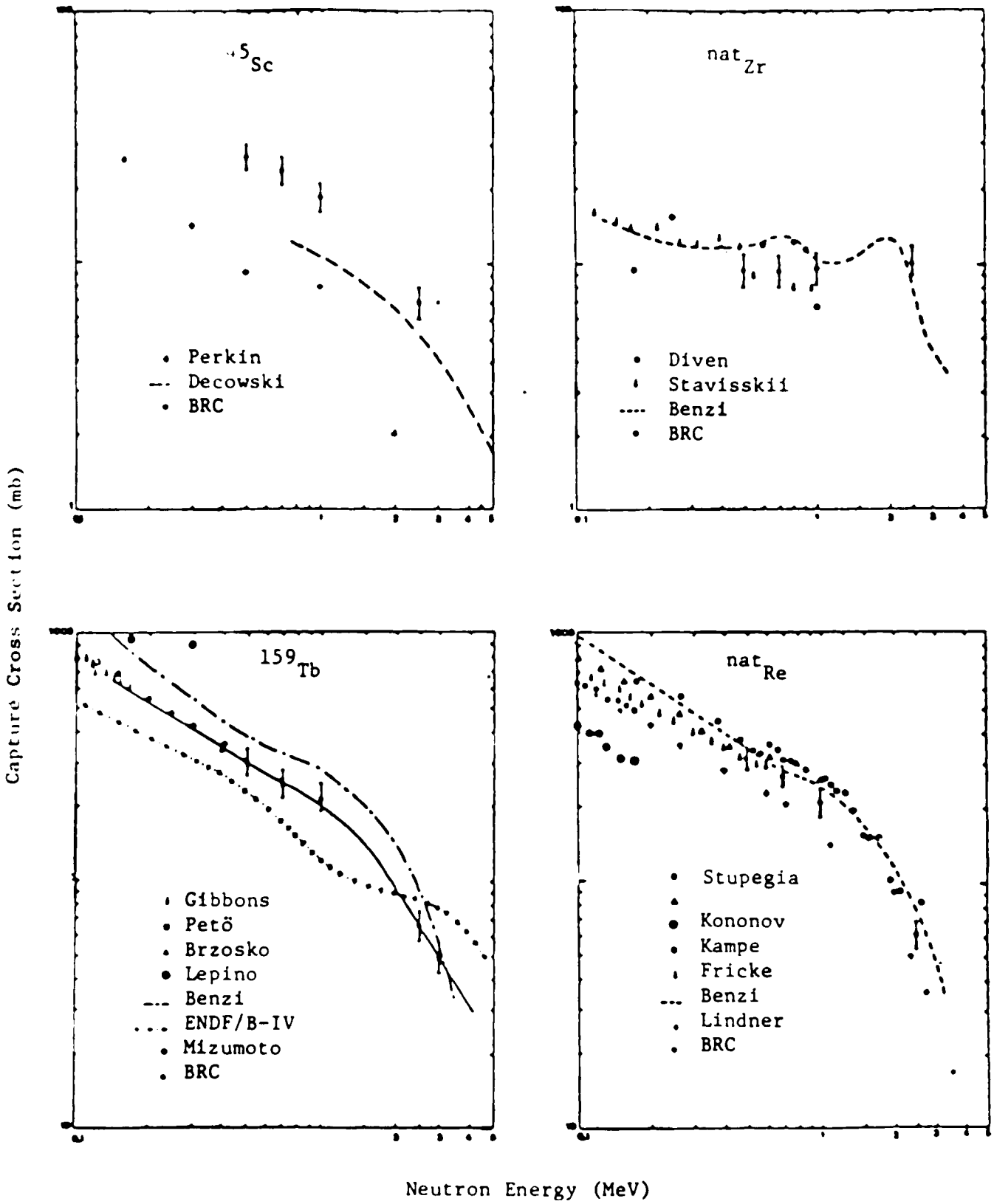

Figure 6. Neutron capture cross sections of Sc, Zr, Tb and Re.

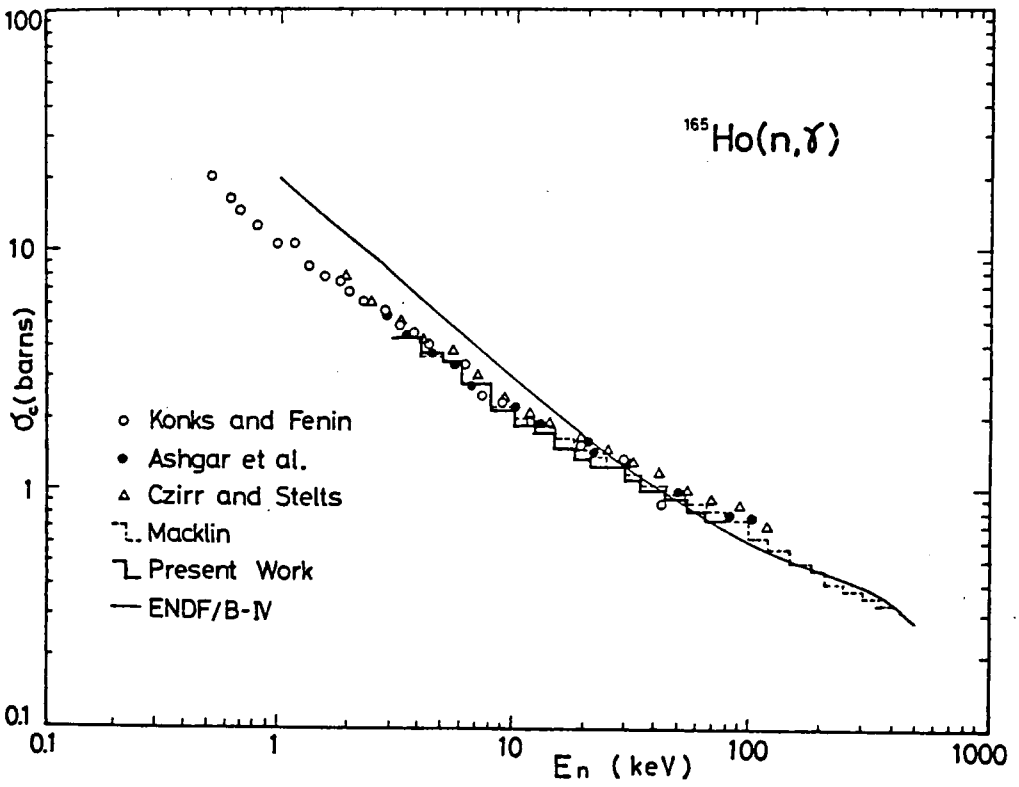

Figure 7. Average capture cross sections of ^{165}Ho as a function of neutron energy.

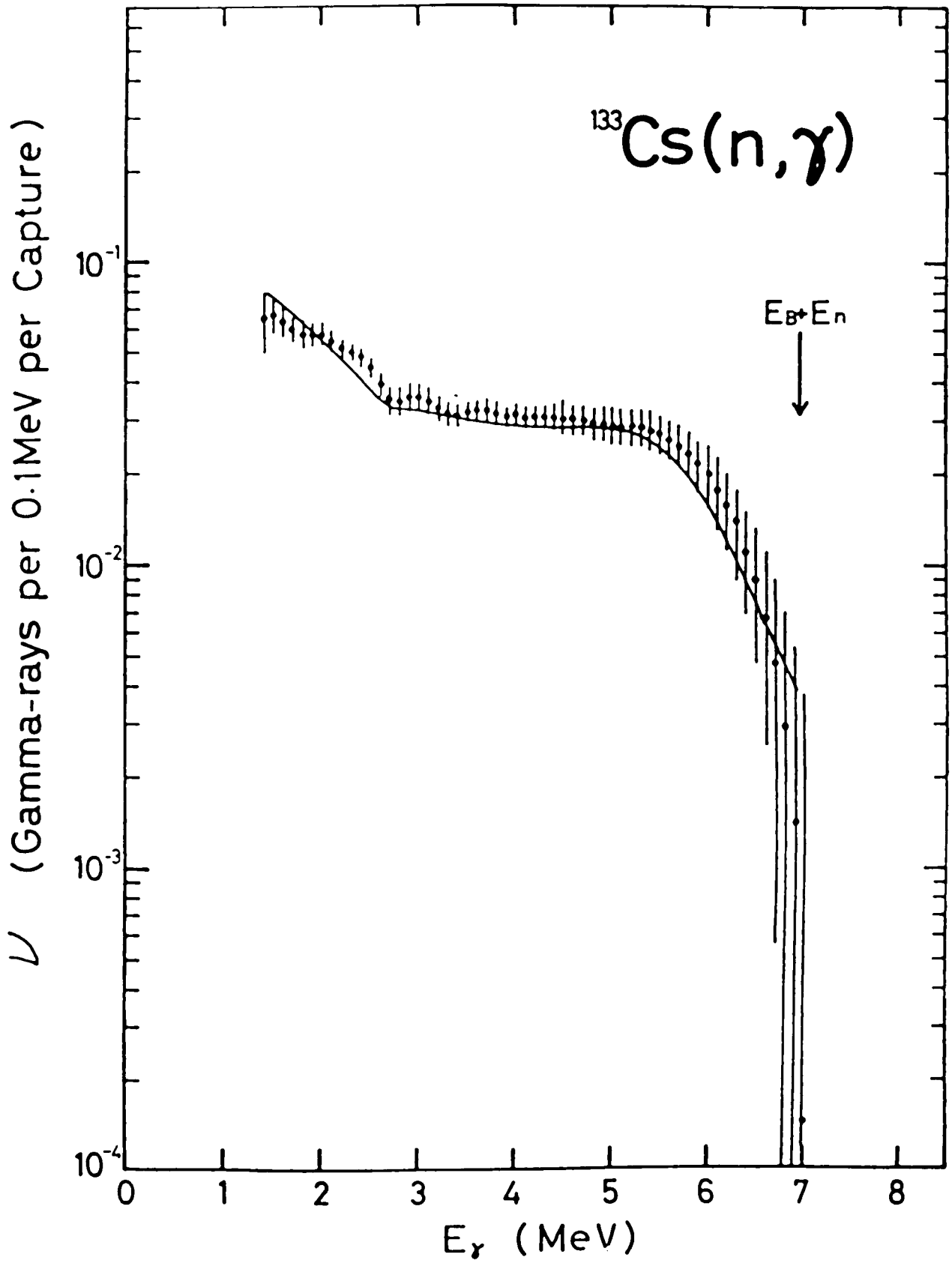

Figure 8. Gamma ray spectrum from neutron capture by ^{133}Cs. The solid line is calculated from the giant dipole resonance data,[41] level density[42] and one pigmy resonance.

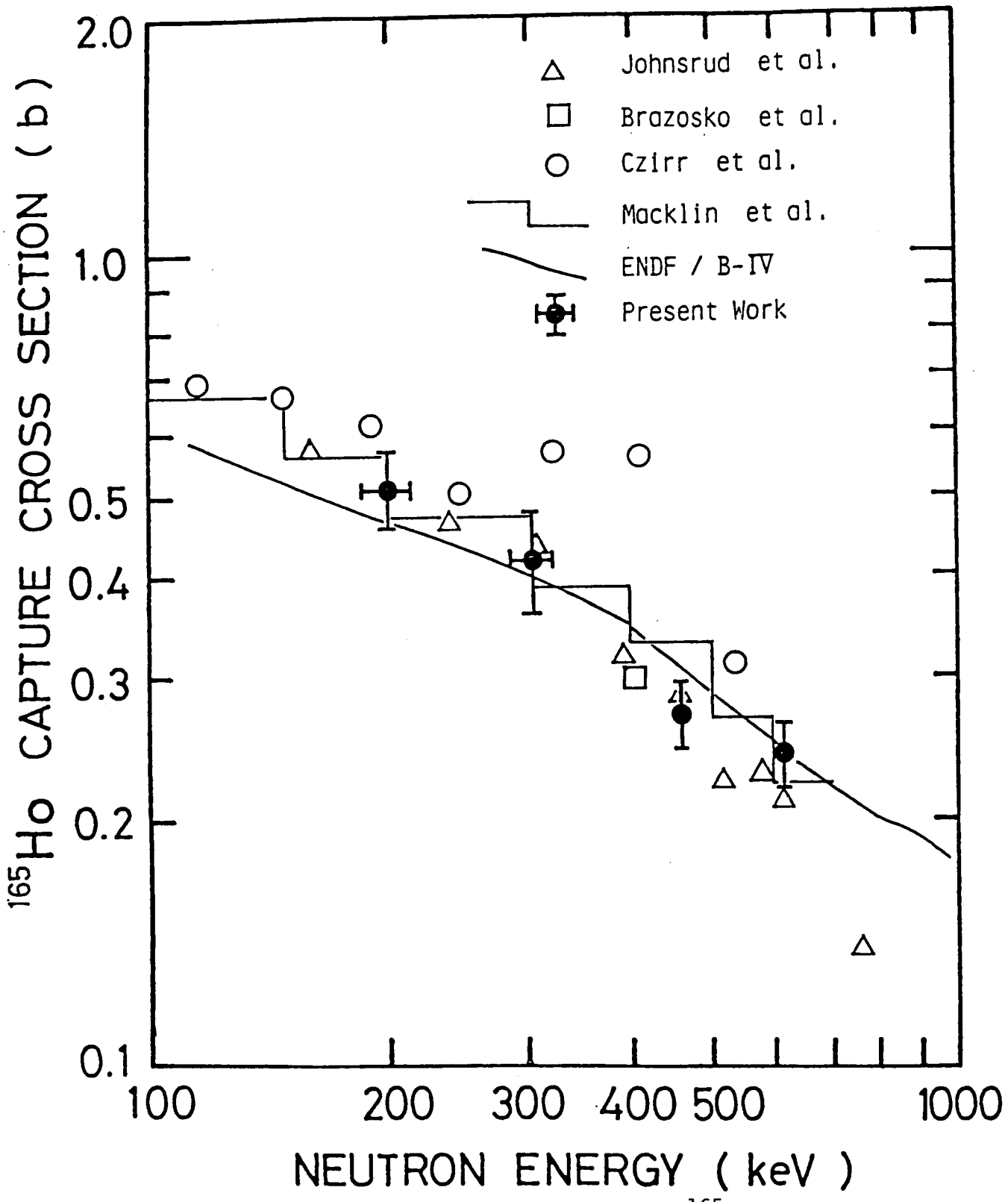

Figure 9. Neutron capture cross sections of ^{165}Ho.

Discussion

QUESTION: R. Schenter
Do you have the cross section values for the recent experiments quoted in your table?

ANSWER: R. Block
Yes.

AVERAGE CAPTURE CROSS SECTION OF THE FISSION PRODUCT NUCLEI ^{105}Pd AND ^{108}Pd

by

G. Rohr, C. Bastian, E. Cornelis*, R. Shelley*
T. van der Veen and G. Vanpraet
CEC - JRC, Geel Establishment
Central Bureau for Nuclear Measurements, B-2440, Geel, Belgium

Abstract

Neutron capture cross section measurements on enriched stable isotopes have been performed at the 30 m station of Gelina in the energy range of 10 eV up to 600 keV. The neutron flux shape was determined with a 0.5 mm ^{6}Li-glass scintillator and a 0.6 mm thick $^{10}B_4C$-slab. The time dependent background was evaluated by using the yields from a 0.5 mm ^{208}Pb capture sample. The present data analysis covers the energy range between 10 keV and 300 keV.

I. Introduction

Neutron cross sections of fission products are of great importance for predicting long term characteristics of fast reactors. Among these nuclei, seven palladium isotopes are listed on the ENDF/B-V data files for fission product nuclides as important absorbers for fast and thermal reactors (1). Of these isotopes, ^{105}Pd ranks first on the list of the 25 most important fission product absorbers in a fast breeder reactor core. On the other hand, ^{108}Pd is listed among important nuclide absorbers in LWR's because it contributes more than 0.1 % to the thermal, epithermal or total absorption at some deflection time. In this paper we present capture cross sections for ^{105}Pd and ^{108}Pd in regard to this poisoning effect. As in a large fast reactor, the energy range below several keV is important and should not be neglected, these measurements have been performed in the energy range of 4 eV up to 600 keV. The present data analysis however covers the energy range between 3 keV and 300 keV.

---

* R.U.C.A. University of Antwerp, Belgium

II. Experimental Technique

The C.B.N.M. 150 MeV electron linear accelerator at Geel, GELINA (2), has been used with the characteristics listed in Table I for this experiment.

Intense neutron bursts are produced in a mercury cooled natural U-target through a photonuclear reaction, and moderated by two halfmoon shaped polyethyleen discs, placed one on top and one below the target. To suppress the detector paralyzing γ-flash effect of the bremsstrahlung, blocks of copper and lead are shielding the U-target in its horizontal plane through the beam line.

Enriched samples of ^{105}Pd and ^{108}Pd were investigated at the 30 m time-of-flight station linked to the target bunker by an evacuated flight path tube, equipped with neutron beam collimators. The beam line was perpendicular to the target moderator that is entirely viewed by the capture sample. The detection of prompt γ-rays following neutron capture is carried out by two cylindrical C_6D_6 liquid scintillators, of 10.2 cm diameter and 7.5 cm thickness each, coupled to an EMI photomultiplier. This capture detector is characterized by a low prompt sensitivity to sample scattered neutrons. This has been achieved by reducing the amount of materials around the capture detector to a minimum. The distance from the neutron source moderator assembly was determined to be 28.398 m. The electronic signals, carrying time and amplitude information are registered with the time-of-flight start signals derived from the electron bursts and sorted electronically in a Nuclear Data ND 6600 acquisition system linked to a C.B.N.M. built 2ns digital time coder (3). This two-parameter experiment is required by the Mayer-Leibnitz weighting technique (4). In this method, the detector events are assigned an importance proportional to the energy of detected photons and is independent of the gamma decay mode. This results in a detector response proportional to the total energy research in the capture process.

Amplitude calibration and amplifiers gain have been controlled regularly with the Compton edge from the (Pu,Be)$^{13}C^*$ 6.8 MeV gamma rays. A 200 keV bias was set for the pulse height amplitude by suppressing the first 4 channels. For the weighting, the events are sorted in 16 PH-groups of 8K TOF each.

Monitoring the shape of the neutron flux was done by putting permanently in the neutron beam, 75.0 cm in front of the capture sample, a ^{6}Li-loaded glass scintillator of 0.05 cm thickness and 10 cm diameter. It was contained in a thin Al-foil cylinder acting as a reflector and viewed by 2 EMI photomultipliers. The relative neutron flux measured with a $^{10}B_4C$ slab, 0.06 cm thick and of 8 cm diameter, used as a capture sample by measuring the 478 keV photons associated with the neutron absorption $^{10}B(n,\alpha\gamma)^7Li$ reaction.

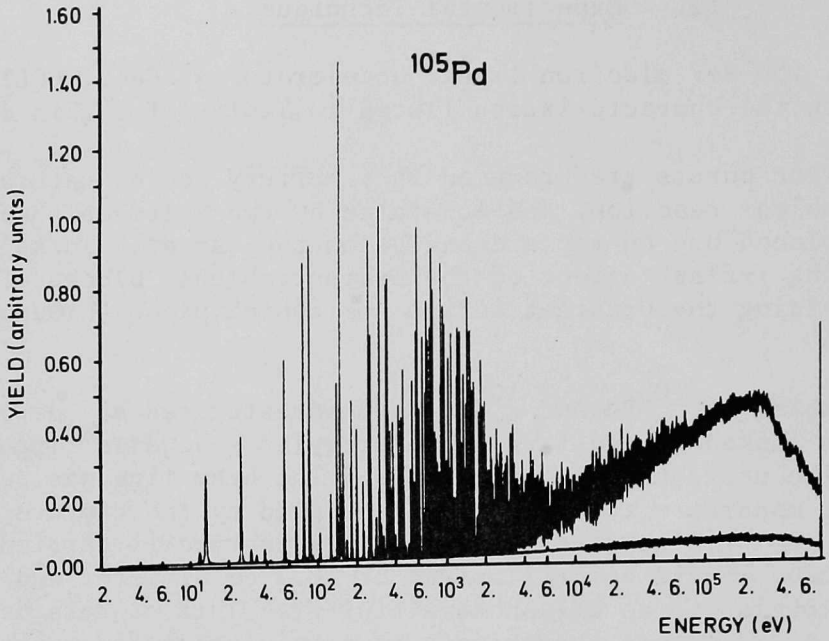

Fig. 1 Capture yield and background obtained for ^{105}Pd as a function of energy.

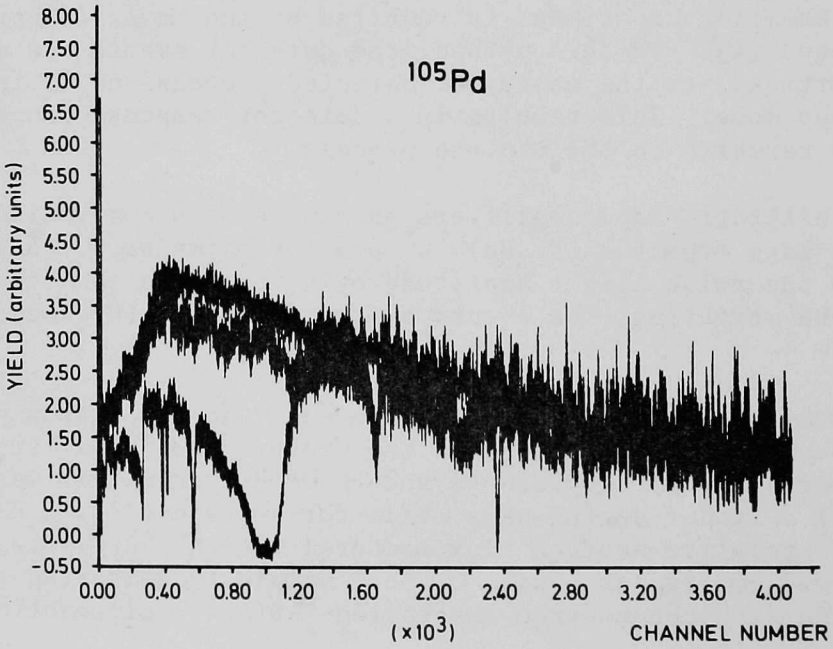

Fig. 2 Capture yield in ^{105}Pd obtained without filter, with Na filter and with all black resonance filters respectively top, middle and bottom curve after being corrected for ^{208}Pb background.

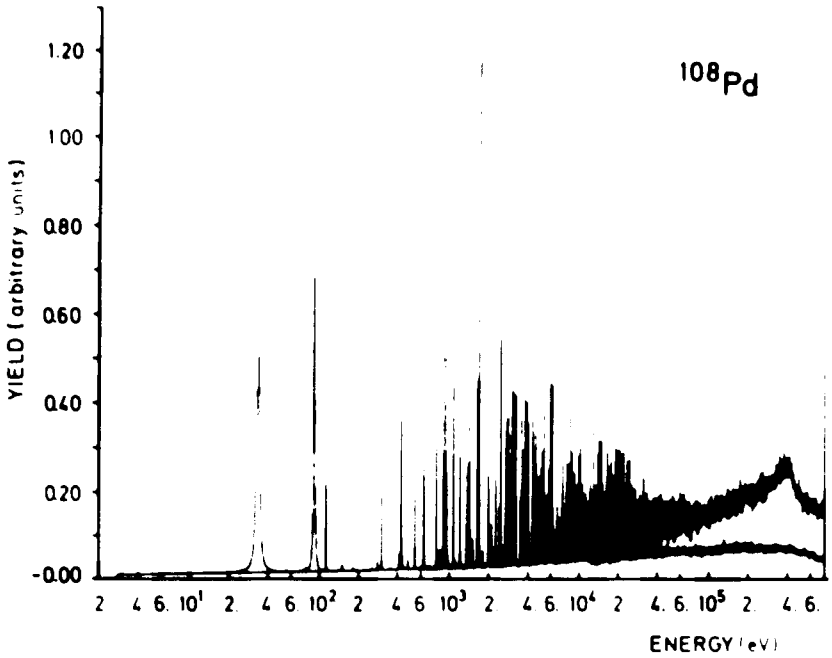

Fig. 3 idem as for fig. 1, but now for ^{108}Pd.

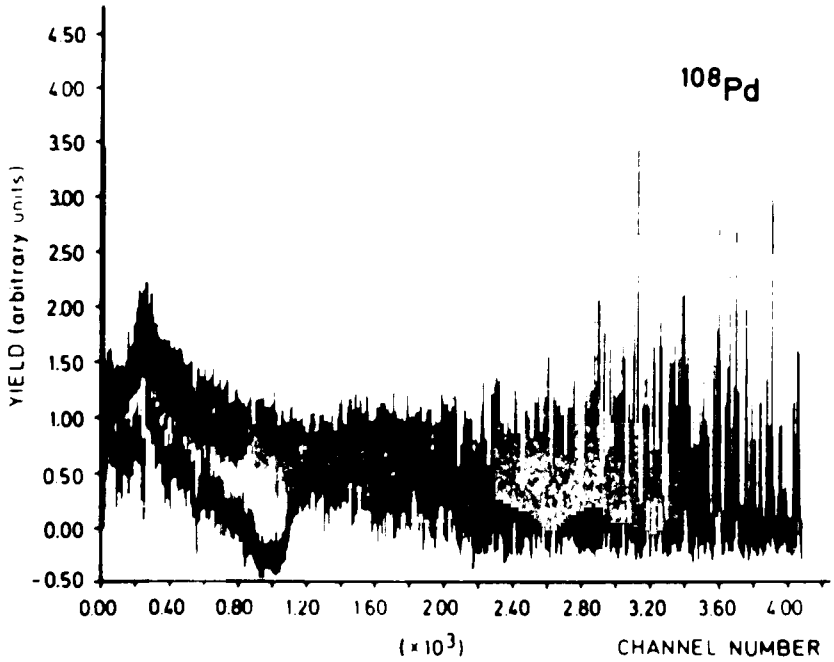

Fig. 4 idem as for fig. 2, but now for ^{108}Pd.

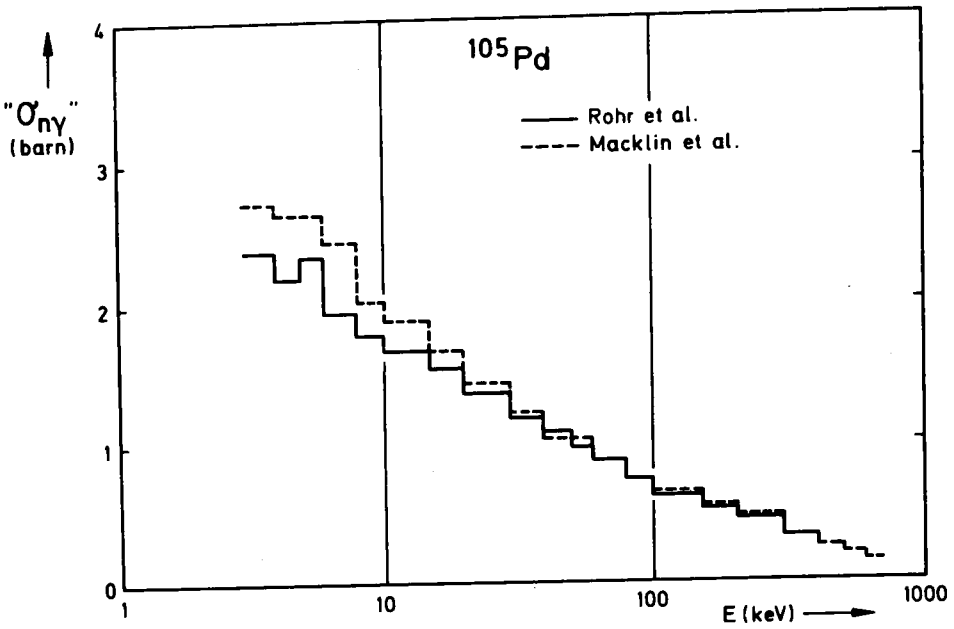

Fig. 5 Average Capture Cross Section as histogram for ^{105}Pd.

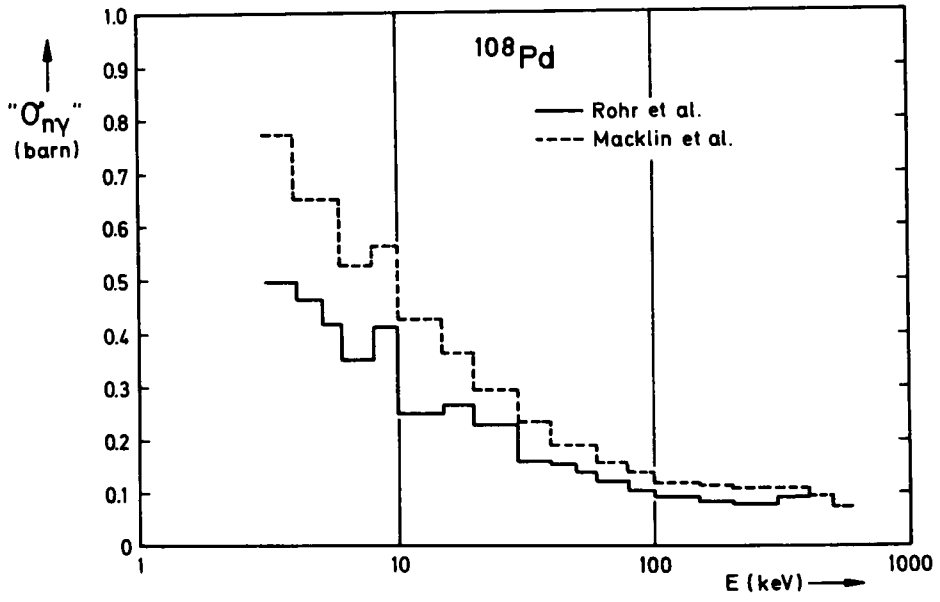

Fig. 6 Average Capture Cross Section as histogram for ^{108}Pd.

III. Analysis

Some effort has been devoted in obtaining a critical evaluation of the time dependent background with black resonance filters S, Na, Co, W and Ag and the yield obtained with a 0.05 cm thick ^{208}Pb sample of 8 cm diameter. For the latter case it was found that the actual background was higher when compared to the results obtained with the thick sulphur filter. This filter depleted the incident neutron flux by an average of about 30 % outside the 102 keV resonance. Fig. 1 shows typical results obtained for ^{105}Pd in the upper curve and for ^{208}Pb on the lower curve both normalized per monitor count. In Fig. 2, three different spectra are shown after subtracting the yield per monitor count obtained with ^{208}Pb; the upper curve is the ^{105}Pd capture yield without black resonance filters; the middle one with the Na filter and the bottom one was obtained with all filters. For this case the background evaluation by using the black resonance technique is off by 7 % compared to that obtained with the lead sample at the sulphur resonance. The channel numbers cover the energy range from 600 keV down to 10 keV. Similar figures for ^{108}Pd are shown in Figs. 3 and 4. For this case a discrepancy of about 35 % for this energy region was found.

IV. Normalization

To normalize the capture data, the value of $2g\Gamma_n$ = (6.70 ± 0.04) meV for the resonance at 55.2 eV in ^{105}Pd was taken from recent C.B.N.M. transmission data (5). Hence, corrections for γ absorption of photons in the capture sample can be disregarded. Further confidence in the normalization procedure was obtained by cross calibration to the results obtained with a 0.05 cm thick Au sample, using the ENDF/B-V file at 200 keV. Palladium sample characteristics are as follows: ^{105}Pd (97.38 %, 2.440 x 10^{-3} at/barn) and ^{108}Pd (98.88 %, 0.899 x 10^{-3} at/barn). The agreement of both calibration procedures was found to be within 1 %. For ^{108}Pd the normalization was only carried out relative to the standard cross section of Au. No corrections for self-protection and multiple scattering effects have been applied. Since our samples are at least three times thinner than those used at O.R.N.L., these effects can only contribute for a small possible systematic error. Statistically good data have been obtained with these relative thin Pd-samples, especially for ^{105}Pd. Average capture cross sections are shown in the histograms of Fig. 5 and Fig. 6. The numerical results for which statistical and systematic errors are estimated to be smaller than 5 % are given in Table 2.

V. Conclusions

For ^{105}Pd, the O.R.N.L. results (6) show a systematic deviation relative to the C.B.N.M. data of approximately + 8.5 % below 15 keV neutron energy whereas at higher energies the data are in agreement within ± 5 %. For ^{108}Pd however, below 15 keV a systematic deviation of about + 40 % is found for the O.R.N.L. results. This deviation reduces to 20 % in the higher energies region. No explainable evidence for the observed discrepancy could be found on the base of our experimental investigations.

References

(1) R.E. Schenter et al. Proc. Specialists' Meeting on Neutron Cross Sections of Fission Product Nuclei, Bologna 1979, p. 253.

(2) J. Salomé and K. Böckhoff, Proc. Knoxville Conf. on Nuclear Cross Sections for Technology, 1979, p. 534.

(3) S. de Jonge, Fast Time Coder Type 7602D, Internal Report GE/IN/DE/72/81, C.B.N.M. Geel

(4) R.L. Macklin and J.H. Gibbons, Phys. Rev. 159 (1967) 1009.

(5) P. Staveloz et al., Proc. Specialists' Meeting on Neutron Cross Sections of Fission Product Nuclei, Bologna 1979, p. 53.

(6) R.L. Macklin, Private Communication Nov. 7, 1980 concerning corrections to publication N.S.E. 71, (1979) 205.

Table 1. Experimental Parameters

burst width	4 ns	Moderator thickness		4 cm
repetition rate	800 Hz	Gamma flash filter	lead	30 cm
electron energy	100 MeV		copper	20 cm
beam power	5 kW	Time overlap filter	5.68×10^{-3}	^{10}B at/b

Table 2. Average cross sections

Energy Range (eV)		Aver. Cross-Section (barn)	
		^{105}Pd	^{108}Pd
3000.	4000.	2.38	.493
4000.	5000.	2.19	.459
5000.	6000.	2.36	.413
6000.	8000.	1.93	.348
8000.	10000.	1.78	.407
10000.	15000.	1.66	.244
15000.	20000.	1.54	.268
20000.	30000.	1.35	.227
30000.	40000.	1.17	.157
40000.	50000.	1.06	.147
50000.	60000.	.968	.132
60000.	80000.	.852	.117
80000.	100000.	.713	.098
100000.	150000.	.611	.089
150000.	200000.	.501	.082
200000.	300000.	.427	.079
300000.	400000.	.331	.089

Discussion

QUESTION: S. Mughabghab
I have two questions. First, in your comparison with the ORNL data, is this the renormalized ORNL data? Second, have you least-square fitted the capture data to obtain average resonance parameters? If so, what are the values of these parameters.

ANSWER: G. Rohr
1. Yes, these are the renormalized ORNL data.
2. Up to now no least-square fits have been performed for the Pd isotopes.

QUESTION: R. Block
I note that for ^{105}Pd you normalized to a low energy resonance. In our recently published 23 eV self-indication-capture measurements we noted (and measured) a several per cent difference in the capture-detection efficiency when the capture changed from surface capture at resonance to volume capture off resonance. Is this a problem for your measurements?

ANSWER: G. Rohr
The capture in the 55 eV resonance of ^{105}Pd with a sample thickness of $n = 2.44 \times 10^{-3}$ at/b cannot be considered as surface capture.

QUESTION: T. Ryves
Can you comment on the ± 5% uncertainty on your measurements, which presumably include the error in the Au standard?

ANSWER: G. Rohr
The ± 5% uncertainty on the numerical results (Table 2) includes the error of the Au standard. A description of the systematic error can only be given, when the corrections for self-protection and multiple-scattering effects have been applied.

STATUS OF RECENT FAST CAPTURE CROSS SECTION EVALUATIONS FOR IMPORTANT FISSION PRODUCT NUCLIDES

by

Harm Gruppelaar
Netherlands Energy Research Foundation ECN
P.O. Box 1, 1755 ZG Petten, The Netherlands

Abstract

A comparison is made between recent evaluations of fission-product cross sections as given in the CNEN/CEA, ENDF/B-IV, ENDF/B-V, JENDL-1, RCN-2 and RCN-3 data libraries. The intercomparison is restricted to 24 important fission products in a fast power reactor. The evaluation methods used to obtain the various data files are reviewed and possible shortcomings are indicated. A survey is given of the experimental data base used in the various evaluations. Some graphs are included showing the new ENDF/B-V and RCN-3 fast capture cross-section evaluations. Further intercomparisons are made by means of multi-group and one-group cross sections. It is shown that lumped fission-product cross sections calculated from the most recent versions of the data files are in quite good agreement with each other. This review concludes with a discussion on oberved discrepancies and requests for new measurements.

I. INTRODUCTION

In this report a comparison is made between evaluations of fission-product cross sections recently made in Italy (cooperation with France) [1-3], Japan [4-6], the Netherlands [7,8] and the U.S.A. [9-12] for 24 of the most important fission products with respect to their reactivity contribution in a fast power reactor.

Some *characteristics of these evaluations* are given in Table 1. The most extensive data libraries are ENDF/B-IV and -V, which include cross section data for about 190 fission products and decay data and fission yields for more than 800 nuclides. Most libraries have the ENDF/B format, except the RCN-2,3 evaluations which are given in KEDAK format. The dates of the evaluations vary from nuclide to nuclide; the "date of release" in Table 1 refers to availability from the NEA Data Bank at Saclay.

For a number of nuclides revisions [3] have been applied to the CNEN/CEA set. An extensive re-evaluation programme is underway in Japan (JENDL-2 [6]). In these revised evaluations results from comparisons between evaluated data and *integral* experiments have been introduced. The RCN-3 and ENDF/B-V versions have been obtained by *adjusting* the previous versions to fit integral data. In addition, some other revisions have been applied to account for results of a vast amount of recent differential data. In the case of ENDF/B-V the adjustments were applied simultaneously to fit integral and differential data. A recent review of these and other adjustment methods has been presented in Ref. [13].

The CNEN/CEA and RCN-2 evaluations have been used to calculate *group constants* [14,16], which were adjusted to fit integral data. The adjusted group constant libraries, CARNAVAL-IV [15] and RCN-2A [16,17] have recently been intercompared [18]. The capture cross sections calculated from the RCN-3 evaluation are very close to those from RCN-2A.

Various *intercomparisons* between the evaluations of CNEN/CEA, JENDL-1, RCN-2, RCN-2A and ENDF/B-IV have been made: The most recent intercomparison is given in the report of Kikuchi et al. [5]. In Ref. [14] a graphical and numerical intercomparison between 25-group constants is given. Other intercomparisons can be found e.g. in the proceedings of the Petten-1977 conference [19-22]. A somewhat older intercomparison was given in Ref. [23]. This paper supplements these references mainly with comments on the newest versions of these evaluations.

The *evaluation methods* used to obtain the various data files are only slightly different; they are reviewed in Sect. II, together with suggestions for possible improvements. In Sects.III and IV some *global comparisons* based upon the experimental data base and energy-group averaged cross sections are presented. An overall intercomparison between the above-mentioned evaluations is obtained by calculating *pseudo fission-product* group cross sections (Sect. IV C). The latest report of this type is Ref. [24]. Some comments which apply to *individual nuclides* are given in Sect. V. In a number of cases large discrepancies are found. These are summarized in Table 6. Some requests for new measurements have been listed in Table 7. The most important conclusions of this report are summarized in Sect. VI.

II. EVALUATION METHODS

The existing evaluations of fast capture cross sections for fission products are all based upon statistical-model calculations [7,25-28] of which the parameters are obtained from experimental data, systematics [29] or theory. Whenever possible, the parameters are adjusted to fit available experimental point cross sections (and/or integral data). In the following we discuss the various aspects of the evaluation procedure. For a review on adjustment methods we refer to Ref. [13].

A. Average parameters from resolved resonance parameters

In the fission-product mass range resolved resonance parameters are used to represent the capture cross sections upto a few keV. This region is also of great importance to the calculation of *fast* capture cross sections. Prior to the cross section calculation the average parameters $\langle\Gamma_{\gamma\ell}\rangle$ (average total capture width for ℓ-wave resonances), D_{obs} (observed s-wave level

spacing) and S_ℓ (ℓ-wave neutron strength function) are extracted from the resonance parameters ($\ell = 0$ or 1).

Due to the sharp distribution of total capture widths of resonances the determination of $\langle\Gamma_{\gamma\ell}\rangle$ is quite simple. However, at the time most evaluations were performed, the number of nuclides with a large fraction of measured s- and p-wave capture widths was quite small. This applies in particular to p-wave capture. At present the situation is much better in this respect (see 4th edition of BNL-325 [30]). The average p-wave capture widths are still quite uncertain for even-mass isotopes with $A \approx 90$, due to the enhanced possibility of "non-statistical" effects [31].

The evaluation of D_{obs}, S_0 and S_1 is usually based upon the statistics of neutron widths and level energies. This process can be quite complicated due to missed resonances, strong mixture of s- and p-wave resonances, unresolved doublets and "non-statistical" effects. At present sophisticated methods exist to estimate these average parameters, see review of Fort et al. at the Bologna meeting [32] and the more recent review of Liou [33]. Last year, an international "benchmark" study was performed to check the various codes used for this purpose [34]. This study was based upon carefully prepared sets of statistically generated resonance parameters. The initial results showed quite large disagreements for cases which are typical for nuclides with $A \simeq 100$, where there is a strong mixture of s- and p-wave resonances (with unassigned ℓ-values). After applying some modifications to the code (and with the knowledge of the "true" values!) more satisfactory agreement was obtained by some authors.

As an example we show some results obtained at our laboratory before and after this exercise. We have used the code CAVECN [35] which is a slightly modified version of the original CAVE code by Stefanon [36,37]. In this code all resonances having reduced neutron widths above a threshold $t\,\eta(E)$ are analysed, where initially t is taken as unity. In Fig. 1 the values of D_{obs}, S_0 and S_1 have been plotted for values of t from 1 to 150 (open symbols). These values should be independent of t. This is not so, as a result of statistical fluctuations. Utilization of additional information from the ℓ-assignments of strong resonances ($t > 20$) improves this behaviour, see black symbols in Fig. 1 [38]. Still, a departure from the "true" values (horizontal lines in Fig. 1) is observed when the set of analysed data is reduced to the strongest resonances ($t > 50$).

An extensive report of the results of this international exercise will be published this year [39]. It is expected that the new methods - together with the increased amount of experimental information [30] - will improve the results of capture cross section evaluations in the near future. At our laboratory we have made an attempt in this direction by reanalysing (old) resonance parameters for 18 fission-product nuclei [35]. Recently, we have also analysed [8] the new CBNM data for the Pd isotopes [40].

B. Systematics of average resonance parameters

The existing evaluations of fission-product capture cross sections are partly based upon systematics of average resonance parameters, e.g. for the calculation of cross sections of unstable nuclides and for the calculation of inelastic scattering competition in the continuum (level density of target). This systematics has been obtained from "eye-guided" curves through experimental data points in a limited mass range ("local" syste-

matics). Commonly, new (reduced) parameters were defined using theoretical dependences of energy and nuclear mass.

1. R', S_0 and S_1

With regard to the potential scattering radius R' and the neutron strength functions S_0 and S_1 one could say that, although standard optical-model calculations may give the global trend [30], local variations with mass are much more difficult to predict. In practice simple eye-guided curves have been used to obtain the local systematics of neutron strength functions from experimental values of neighbouring isotopes or nuclides. It is expected that more refined optical-model calculations, e.g. with deformed potentials could improve this situation [30].

2. Level-density parameters

All authors use the composite level-density formula of Gilbert and Cameron [41], though in slightly different forms (Sect. II D). At high excitation energies (Fermi-gas formula) its important parameters are a and the pairing energy shift P. The parameter a is derived from the level spacing D_{obs} assuming a value of P from Ref. [41]. Global systematics is obtained by plotting a as a function of the neutron number N [29]. Such a plot clearly reflects the shell effects near the magic number N = 50 and N = 82. Closer inspection reveals a significant Z-dependence, in particular for N just above 50 and 82. In these cases local systematics as given in Fig. 2 has been used in the evaluations. It was also found that there exist odd-even effects in a for the Nd and Sm isotopes (vol. 3 of [7]), indicating that the reported values of the energy shifts [41] between odd- and even-mass nuclides are inadequate. Similar effects were recently found for the Pd isotopes (bottom part of Fig. 4). These problems indicate that the Gilbert-Cameron formula with the original table of pairing energies is not a very good basis for a reliable systematics of the level density.

A survey of possible improvements in the description of level-density parameters and their systematics is beyond the scope of this paper. We refer here to a forthcoming IAEA meeting on this issue, provisionally planned in 1983 at Brookhaven.

3. Radiative capture widths and γ-ray strength functions

In the statistical-model codes used for the various evaluations the total radiative capture widths are calculated according to slightly different versions of Brink-Axel formula (Sect. IID). The results were normally renormalized to fit the experimental value of the total radiative capture widths at the neutron separation energy. If experimental data were lacking this value was obtained from simple local systematics of $\langle\Gamma_{\gamma\ell}\rangle$. At CNEN the Brink-Axel formula was used to predict unknown radiative capture widths [42, 43], assuming experimental values or systematics of electric-dipole giant resonance parameters (neglecting M1 and E2 transitions). In a more recent report Reffo [29] has provided quite useful systematics of giant resonance parameters as a function of A and the nuclear deformation parameter β (two Lorentzian peaks for deformed nuclei).

The results of these calculations reflect the uncertainties of the input parameters, i.e. level scheme data, level-density parameters and giant resonance parameters. Moreover, the validity of the Brink-Axel estimate is

not very well-established and non-statistical effects [31] are not accounted for. The model used at CNEN [43] gives $\langle\Gamma_\gamma^{J\Pi}\rangle$ as a function of spin and parity. For even-even compound nuclei there may be quite a strong parity dependence, due to a possible predominance of one parity at low-lying states, which therefore are mainly populated from the opposite-parity compound state. Consequently, different renormalizations for s- and p-wave capture widths may be required. This was for instance performed in the RCN-2,3 evaluations. Moreover, if necessary, a p-wave valency component was added, according to the systematics of Allen and Musgrove [31] or older systematics of Weigmann [44].

The above-mentioned approach is not always satisfactory. As an example we show in the upper part of Fig. 4 some results of calculations of $\langle\Gamma_{\gamma 0}\rangle$ for the Pd isotopes [8], using the Brink-Axel model [43], adopting simple systematics for the single-peak giant-dipole resonance parameters [43]: $\Gamma_r = 5$ MeV, $E_r = 163\sqrt{NZ}\,A^{4/3}$ MeV, $\sigma_r = 0.0535\,(NZ/A\Gamma_r)$b. The experimental data shown in Fig. 4 have been adopted from recent measurements at RPI [45] and CBNM [40]. They show a significant odd-even effect. The calculated curves fail to reproduce it (small effect in opposite direction) and the mass-dependence is also completely wrong. Very large and unrealistic adjustments of the model parameters would be needed to force consistency between calculations and measurements. Probably nuclear structure effects play an important role.

Possible improvements could be obtained by adopting a modified shape of the E1-strength function f_{E1} as proposed by Gardner and Dietrich [45]. It was also stressed [46] that since the γ-ray strength function is the most important parameter to calculate the radiative capture cross section, it might be better to concentrate on the systematics of f_{E1}, rather than to evaluate $\langle\Gamma_\gamma\rangle$ and D_{obs} separately. The systematics of Gardner and Dietrich for f_{E1} was used to calculate capture cross sections of various medium-mass nuclei [46,47]. In this respect we also mention some recent work performed at our laboratory by Kopecky on the systematics of E1, M1 and E2 strength functions [48,49]. Further developments on the systematics of radiative widths have recently been reviewed by Moore [50].

C. Optical-model parameters

For the bulk of the fission products a spherical optical model with a global set of parameters was used. The parameters of Igarasi et al.[51] have been used throughout the JENDL-1 evaluation and for many nuclides also in the CNEN/CEA and RCN-2,3 evaluations. In ENDF/B-IV,V the potential of Moldauer [52] was adopted for most evaluations performed at HEDL. For some important nuclides other global potentials have been selected in the CNEN/CEA, RCN-2,3 and ENDF/B-IV,V evaluations. In recent Japanese work [6] the potentials of individual nuclides were fitted to experimental data by means of the "SPRT method". For a review on possible improvements using the SPRT method in the fission-product mass range we refer to Lagrange [53].

We note that the use of a "strength function model" (Sect. 2.4.2) at low neutron energies, adopting experimental values for R', S_0 and S_1, partly compensates for the deficiencies of global optical models at low neutron energies (upto 50 to 100 keV). Such models have been applied throughout the CNEN/CEA and RCN-2,3 evaluations and for important nuclides in the ENDF/B-IV,V evaluations. At higher energies discrepancies in σ_c due to the use of different global optical-model parameters are usually within 10% [6].

D. Statistical-model calculations

1. Width fluctuation effects

In all evaluations the Hauser-Feshbach formula has been used with width-fluctuation correction. In most evaluations the "classical" integration method was used with one degree of freedom ν for each outgoing particle channel T, assuming the γ-ray transmission coefficient as a non-fluctuating quantity, see review article [54]. Moldauer [55] has shown that the number of degrees of freedom should be increased up to 2 when the absorption increases. This means that for a large number of channels (> 20) the enhancement factor of the compound elastic scattering $w = 1 + 2/\nu$ approaches 2 rather than 3. In the alternative statistical-model description of Tepel et al. [56] which is valid for medium and strong absorption, the elastic enhancement factor has been parametrized [57]. On the basis of some calculations with these new theories [55-57] it was concluded in 1977 that for the computation of neutron radiative capture cross sections the use of the "classical" integration method with $\nu = 1$ is still a good approximation [54].

Meanwhile, Moldauer [58] has given a useful parametrization of the number of degrees of freedom:

$$\nu = 1.78 + (T^{1.212} - 0.78)\ \exp[-0.228\Sigma T'],$$

where $\Sigma T'$ is the total transmission coefficient of all competing channels. This equation clearly shows that only for weakly absorbing channels ($T \ll 1$) and few competing channels ($\Sigma T' < 1$) the approximation $\nu = 1$ is valid (elastic scattering at low energies). Therefore, it seems better to use the above-mentioned parametrization of ν, which is valid for weak, medium and strong absorption. At higher energies also the updated expressions of Tepel et al. [59] could be adopted. A formalism to include width fluctuation corrections in the continuum has been discussed in Ref. [54].

2. Strength function models

Differences between the various statistical models used for fission-product cross section evaluations at low neutron energies are mainly due to the calculation of neutron transmission coefficients either from the optical model or from a "strength function model". In the RCN-2,3 evaluations this model simply implies that the s- and p-wave neutron transmission coefficients are overwritten by values calculated from

$$T_\ell^n = \frac{2\pi\, S_\ell \sqrt{E}\, \nu_\ell}{(1 + \frac{\pi}{2} S_\ell \sqrt{E}\, \nu_\ell)^2 + (R_\ell^\infty \rho\, \nu_\ell)^2},$$

where ν_ℓ is the penetration factor and R^∞ describes the effect of distant resonances ($R' = R[1 - R^\infty]$). At low neutron energies this relation leads to the usual expression $T_\ell^n = 2\pi\, S_\ell \sqrt{E}\, \nu_\ell$; at higher energies T_ℓ^n remains less than unity. In this context we mention that S_1 strongly depends upon the selected value of the channel radius a. A more appropriate definition of S_1, recently suggested by Moldauer [60], is obtained by reducing the p-wave neutron widths with $E^{-3/2}$ or $E^{-3/2}[1+(ka)^2]$ instead of with $E^{-\frac{1}{2}}/\nu_\ell = E^{-\frac{1}{2}}[1+(ka)^2]/(ka)^2$.

In the CNEN/CEA and ENDF/B-IV,V evaluations the prescribed ENDF/B unresolved resonance description has been adopted, at least for the important nuclides. We note that this description has recently been revised [61]. In JENDL-1 no strength function model has been used.

3. Different forms of level-density formulas

The differences in the adopted composite level-density formulas [41] are discussed in this section. As has been noted previously [6,21,23] the adopted expressions for the spin cut-off parameter σ^2 differ in the various evaluations:

ENDF/B, JENDL-1 : $\sigma^2(E) = 0.0888\sqrt{a(E-P)}\ (E \geq E_x)$,

$\sigma^2(E) = \sigma^2(E_x) \qquad (E < E_x)$.

CNEN/CEA, RCN, JENDL-2: $\sigma^2(E) = 0.146\sqrt{a(E-P)}\ (E \geq E_x)$,

$\sigma^2(E) = \sigma^2_{exp} + (\sigma^2(E_x) - \sigma^2_{exp})E/E_x \quad (E < E_x)$,

where E_x is the dividing energy of the composite Gilbert and Cameron formula [41] and σ^2_{exp} follows from the spin distribution of low-lying levels [26]. The use of σ^2_{exp} leads to quite large differences in the capture cross section above an energy E_c, where inelastic scattering competition to the continuum commences.

The continuum parity distribution p_π is usually assumed to be 1/2. This distribution is quite important to calculate the ℓ-dependence of $\langle\Gamma_{\gamma\ell}\rangle$. In the JENDL evaluation the expression of Igarasi [25] has been adopted:

$$p_\pi(E) = \frac{f_\pi + 0.5\exp[(E-E_o)/\delta]}{1+\exp[(E-E_o)/\delta]},$$

where f_π is the fraction of discrete levels with parity π, $E_o = (E_x + E_c)/2$ and $\delta = |E_x - E_c|/8$.
Reffo [29] has proposed

$$p_\pi(E) = \exp\{a_\pi E + b_\pi\} \quad \text{at } E < E_{\frac{1}{2}},$$

where a_π and b_π are fitted to obtain agreement at low-energy discrete levels and $E_{\frac{1}{2}}$ is the energy above which $p_\pi = \frac{1}{2}$ is assumed.

We note that the Japanese evaluators [6] have adopted a significantly different formulation of the low-energy part of the Gilbert and Cameron formula: $\rho(E) = C\exp[(E-E_o)/T]$, where C and T are fitted to the staircase plot of low-lying levels and the dividing energy E_x is obtained by adjustment of these parameters"to obtain a smooth continuation with the Fermi-gas level density". In the original prescription of Gilbert and Cameron the value $C = 1/T$ is adopted and E_x is obtained from the requirement of continuity of ρ and ρ' at E_x. The Japanese method could give a better description at the lowest energies, but problems may occur to define the value of E_x. In some cases no smooth connection between the constant-temperature formula and the Fermi-gas formula could be found [6].

Other problems with the Gilbert-Cameron formula may occur when E_x exceeds the neutron separation energy. In that case the calculated value of D_{obs} (from the constant-temperature formula) may become different from

the originally introduced experimental value, used to fit a, applying the Fermi-gas formula. In the RCN-2,3 evaluations we still have adopted this value of a for the renormalization of the capture γ-ray transmission coefficient.

4. Gamma-ray transmission coefficient

In all evaluations the γ-ray transmission coefficient is obtained from the Brink-Axel formula. A rather complete representation is used in the CNEN codes [27,28,43]:

$$T_\gamma^{J\Pi} = \frac{2\pi}{3(\pi\hbar c)^2} \left[\sum_n \sum_{j_n} \delta_{\pi_n,-\Pi} (B - E_n)^2 \sigma_L (B - E_n) + \right.$$

$$\left. + \int_0^{B-E_c} \varepsilon_\gamma^2 \sigma_L(\varepsilon_\gamma) \sum_j \rho(B - \varepsilon_\gamma, j, -\Pi) d\varepsilon_\gamma \right] .$$

In this equation the spin and parity of the compound state at energy B (binding energy) are denoted by capital J and Π. The primary γ-ray emission to states with excitation energy less than E_c (discrete level excitation) is calculated in the first term, assuming that only E1-transitions are possible. The spin and parity of the discrete states are denoted by j_n and π_n. The second term gives the contribution of E1-transitions from the compound state to levels with excitation energy above E_c. The γ-ray energy is denoted by ε_γ. The Lorentzian function $\sigma_L(\varepsilon_\gamma)$ is given by

$$\sigma_L(\varepsilon_\gamma) = \sum_{i=1}^{2} \frac{\varepsilon_\gamma^2 \sigma_i \Gamma_i}{(\varepsilon_\gamma^2 - E_i^2)^2 + \varepsilon_\gamma^2 \Gamma_i^2} ,$$

where the giant resonance parameters σ_i, E_i and Γ_i refer to the peak cross section, peak energy and half-maximum width, respectively.

In the ENDF/B, JENDL and RCN evaluations the following approximations were made: only the continuum part is calculated ($E_c = 0$); only one Lorentzian peak is adopted; equal parity distribution of ρ is assumed; the summation over j is performed in an approximate way. As a result the radiation width (*not* $T_\gamma^{J\Pi}$) is independent of spin and parity. This could partly be compensated by the introduction of different normalization factors for each spin and parity. In the RCN-2,3 evaluations a parity dependence is introduced in this way. We note that a renormalization to experimental data is performed in *all* evaluations (Sect. II B).

Possible non-statistical effects could also be incorporated in parity-dependent renormalization factors. In the RCN-2,3 evaluations a valency component was introduced (Sect. II B). The statistical-model expression was modified by taking into account the correlation between the neutron and capture widths, leading to a different value of the width fluctuation factor [23].

5. High-energy region

Above a few MeV, where the competition of inelastic scattering is described by a continuum model ($E > E_c$), the adopted models may deviate for a variety of reasons. The most important one seems to be the effect of the

spin distribution of the level density (Sect. II D.3). Other effects which should not be neglected are the (n,2γ) contribution, the direct and collective contribution and the competition of charged-particle emission cross sections. The last-mentioned effects are important only above about 5 MeV. The status with regard to charged-particle emission cross sections has already been reviewed at Bologna [62]. We feel that more attention should be paid to evaluation methods and codes at energies above E_c.

6. Uncertainties

The subject of uncertainty evaluations is closely connected to adjustment procedures. We therefore refer to the recent review [13] and references therein. The uncertainties of adjusted RCN-2A capture group constants are given in Refs. [16,17]. The adjusted ENDF/B-V capture cross sections have also been supplied with error estimates [10,11].

III. COMPARISON BASED UPON EXPERIMENTAL DATA BASE

A. Resolved resonance parameters

Since 1973, the date of publication of version 3 of the BNL-compilation, many resolved resonances have been remeasured, see version 4 [30] and Table 2, column 2 (CINDA notation). However, most of these data have not yet been used in the evaluations. This also holds for ENDF/B-V. Exceptions are indicated in Table 2. It has to be noted that the new resolved resonance parameters may lead to important improvements for ^{99}Tc, ^{101,102,104}Ru, ^{105,107}Pd and ^{151}Sm. Moreover, the average resonance parameters deduced from these data could have important implications in the statistical-model calculations (particularly for ^{107}Pd, ^{151}Sm). For many other nuclides, given in Table 2, the new resonance parameters refer to the higher energies, where at present the evaluations are based upon statistical-model calculations. Application of this new information is not so straightforward, because of the large possibility of missed resonances. The average capture data may be more useful in this respect.
See Sect. V for a detailed discussion on each nuclide.

B. Differential capture measurements

Recently, a large number of differential measurements has been performed in the energy range from 1 keV to about 500 keV. These measurements are summarized in column 2 of Table 3 (data released after publication of BNL-compilation, 1976). As can be seen from Table 2 a large fraction of these data have been measured at ORELA, and have been analysed at Oak Ridge (ORL) or Lucas Heights (AUA). These data might need a correction [63]. Part of the data have been plotted in Figs. 5b-16b. Most of the new measurements have been included in ENDF/B-V by means of an adjustment of the ENDF/B-IV capture cross section, taking into account recent differential data and integral data [10,11]. They have also been considered in the most recent other evaluations (i.e. in part of RCN-2, RCN-3, 1979-revisions of CNEN/CEA, preliminary JENDL-2). The recent differential data have important implications for ^{98,100}Mo, ^{99}Tc, ^{101,102,104}Ru, ^{133}Cs, ^{143}Nd, ^{148}Nd and ^{149}Sm; see corresponding figures. No data at all exist for ^{93}Zr, ^{103}Ru and ^{135}Cs. Note that there are large discrepancies between differential data, even when

only recent measurements are considered.

C. Integral measurements

A recent review of the integral data base is given by Anderl at this meeting [63]. Older reviews are given in Refs. [22,65-67]. The integral STEK and CFRMF data have been used in the ENDF/B-V and RCN-3 evaluations. In addition, EBR-2 integral data were used to adjust the ^{143}Nd, ^{145}Nd and ^{149}Sm cross sections [66,67]. The revisions of CNEN/CEA are based upon an analysis of STEK, CFRMF and French integral data [3]. Revisions for JENDL-2 [6] are partly also based upon integral data (STEK†, CFRMF). Integral data can be used for adjustments; they are also extremely useful as a selection criterion between the various differential data set.

Some clear examples showing that integral data may help to select between different data sets (CINDA notation) are given in Figs. 5b, 6b, 11b and 12b for ^{99}Tc (RPI-77 rather than KfK-73), ^{101}Ru (ORL-80 rather than RPI-75), ^{109}Ag (DKE-60 rather than FEI-65) and ^{133}Cs (LEB-62 and KTO-69 rather than KfK-69, respectively.

IV. INTERCOMPARISON OF GROUP CONSTANTS

A. Multi-group cross sections

A graphical intercomparison was made between 26-group cross sections with a micro-flux weighting spectrum as used for calculations of the DeBeNe SNR-300 fast power reactor, which is under construction at Kalkar, FRG. Some examples of this intercomparison for ENDF/B-IV, ENDF/B-V and RCN-2A* are given in Figs. 5a to 16a. The results generally show rather good agreement between the adjusted data files ENDF/B-V and RCN-2A in the important energy range from 500 eV to 500 keV; exceptions are ^{98}Mo and ^{151}Sm (Sect. V). However, there are large differences in the resolved resonance range (^{97}Mo, ^{99}Tc, ^{101}Ru, ^{105,107}Pd, ^{149,151}Sm) and in the high-energy range (^{102}Ru, ^{109}Ag, ^{147}Pm, ^{148}Nd, ^{149,151}Sm). Therefore it is concluded that more effort is needed to evaluate the recent experimental resonance parameters and the capture cross sections at high energies [71].

B. One-group cross sections

In Table 4 average capture cross sections have been listed for the 24 most important fission product nuclides. These data represent average cross sections in the fast reactor spectrum of SNR-300. The most interesting observation from Table 4 is that for many nuclides the ENDF/B-V cross sections

---

† Note: The problems of calculating self-shielding of STEK samples mentioned in Ref. [6] are due to the circumstance that no perturbed spectra $\underline{\psi}^*$ have been used to calculate integral data, i.e. $\underline{\Sigma}.\underline{\psi}$ instead of $\underline{\Sigma}.\underline{\psi}^*$. In Refs. [16,17] the elements of $\underline{\Sigma}$ were multiplied by the ratio ψ_i^*/ψ_i.

* Adjusted *group* constant set. Capture group cross sections obtained from RCN-3 are almost identical to those from RCN-2A for most nuclides.

have been increased (compared to ENDF/B-IV) with quite large amounts, to become much closer to the results from the other data libraries. This has important consequences for lumped fission-product cross sections calculated from ENDF/B-V, see Sect. IV C.

The average cross sections calculated from ENDF/B-V, RCN-2, RCN-2A, JENDL-1 and CNEN/CEA are in quite good agreement, i.e. almost always within the standard deviations of the RCN-2 data set and often within the standard deviations of the adjusted RCN-2A data set (exceptions are indicated by underlined numbers in Table 4).

The agreement between ENDF/B-V and RCN-2A is very good; this is mainly due to the fact that these data are partly based upon the same integral data (i.e. STEK and CFRMF).

The revised 1979 evaluations of CNEN/CEA, in which Dutch and French integral data were considered, improve the agreement between the average capture cross section of CNEN/CEA and RCN-2A for ^{105}Pd, ^{143}Nd and ^{149}Sm. For ^{151}Sm the situation is worse, since no satisfactory integral data measurements are available (sample problems).

Preliminary revisions for the JENDL-2 library indicate higher cross sections for ^{143}Nd, ^{149}Sm and ^{151}Sm [6], yielding better agreement with RCN-2A for ^{143}Nd and ^{151}Sm. The one-group value for ^{149}Sm calculated from the revised JENDL-2 library is probably higher than that of RCN-2 (indications from a graph in Ref. [6]).

C. Lumped fission-product cross sections

Pseudo fission-product cross sections have been calculated to simulate the effect of fission-products from ^{239}Pu in a fast power reactor. The concentrations of 169 fission-product nuclides in a large power reactor at a burn-up of 41 MWd/kg (460 days irradiation time) were taken from Ref. [68]. The calculated capture cross sections for the lumped fission-product mixture based upon ENDF/B-V are given in the second column of Table 5. In the first column the previous results [68,62], based upon the adjusted RCN-2A cross sections (supplemented mainly with ENDF/B-IV data) are listed. The differences are quite small. This could partly be ascribed to the fact that both ENDF/B-V and RCN-2A were obtained by adjustment to the same set of integral data (STEK and CFRMF).

The last line of Table 5 gives the predicted average capture cross sections in the core of SNR-300. The difference is only 0.24%. It has to be noted that the ENDF/B-IV library gave 10% lower average cross sections [24]. The CNEN/CEA and JENDL-1 libraries yield values which differ less than 1% from the RCN-2A and ENDF/B-V results [24]. This excellent agreement between results of recent data files is quite satisfactory. The CARNAVAL-IV results are about 5% higer [18] which is still within the expected uncertainty limits.

The increase of the ENDF/B lumped fission-product cross sections is mainly caused by increased cross sections for ^{99}Tc, ^{101}Ru, ^{107}Pd, ^{109}Ag, ^{145}Nd and ^{149}Sm. This, in turn, is to a large extend due to the use of integral data in the evaluation.

V. DISCUSSION †

A. Most important fission products

In this section the most recent ENDF/B and RCN evaluations are discussed. A summary of observed discrepancies between the various experimental data is given in Table 7a. In Table 8a some requests for new measurements are formulated. For each nuclide two figures are given, one with group cross sections (26-group ABBN scheme, SNR-300 flux weighting) and one with point-wise given data and experimental data. The solid, dotted and dashed curves correspond to ENDF/B-V, ENDF/B-IV and RCN-2A or -3, respectively. The RCN-2A group cross sections have been obtained from a direct adjustment of RCN-2 cross sections to fit integral STEK and CFRMF data. The RCN-3 data file is a point-wise given file, always quite close to RCN-2A in the smooth energy range. Significant differences between RCN-2A and RCN-3 are indicated in the text. When experimental data have been averaged the symbol "A" is given in the legend box.

1. ^{99}Tc (Fig. 5)

In the resolved resonance range there is a large discrepancy between the evaluations in the range from 20 eV to 0.5 keV (Fig. 5a). In ENDF/B-V the new RPI resonance parameters have been adopted upto 791 eV. However, it seems that the adopted Γ_n values in ENDF/B-V are a factor of 2 too small at $E > 25$ eV (at least compared to the new BNL-compilation [30]). In the RCN-2A,-3 evaluations the Russian (KUR-73) resolved resonance parameters have been adopted upto 1.1 keV. These data are in good agreement with the RPI-77 data [69]. There is also good agreement with the low-energy data ($E < 25$eV) obtained at Kiel (KIL-78, KIG-81). The data given in the third edition of BNL-325 should not be used (too high values of Γ_γ [70]). More values of Γ_γ are needed for resolved resonances at $E > 300$ eV.

From Fig. 5b it follows that the ENDF/B-V and RCN-3 evaluations are in favour of the RPI-77 data. They are higher than the KFK-73 data (discrepancy RPI-77 > KFK-73). Fischer et al. [70] have mentioned problems with the ^{99}Tc sample used to obtain the KFK data. The ENDF/B-V and RCN-3 evaluations are partly based upon integral STEK data; the CFRMF data indicate lower fast capture cross sections. There seems to be a discrepancy between STEK and CFRMF data [6]. More experimental data are needed at 1 to 500 keV. *This request has been satisfied with ORL-82 data reported at this meeting.*

2. ^{101}Ru (Fig. 6)

For this nuclide the RCN-3 evaluation has not yet been completed. From Fig. 6a it follows that RCN-2A is much larger than ENDF/B-IV and -V in the range from 100 to 600 eV. This arises from the fact that the resolved resonance range in RCN-2A extends upto 666 eV, whereas in ENDF/B-IV,V the high-energy limit of the resonance range is at 113 eV. Meanwhile, new resonance parameters have been published, with neutron widths upto about 1 keV (DUB-80). These data should be included in future evaluations. At higher energies only values of $g\Gamma_n\Gamma_\gamma/\Gamma$ are known. There might be a need for new transmission measurements at energies above about 1 keV to determine the neutron widths of resolved resonances.

The RCN-2A and ENDF/B-V curves in Fig. 6b are close to the ORL-80 data, that are significantly lower than the RPI-75 data (discrepancy ORL-80 and RPI-75). The normalization of the RCN-2A curve is mainly based upon the STEK

†Comments in recent data presented at this meeting have been added in *italics*.

integral data, which seem to be in agreement with the ORL-80 differential measurements.

3. ^{102}Ru (Fig. 7)

For this nuclide the RCN-3 evaluation has not yet been completed. In the existing evaluations only three resonances (up to 1.3 keV) have been included. The discrepancy at 0.5 to 1.0 keV (Fig. 7a) is due to the use of different background functions. In future updatings the resolved resonance range should be extended up to at least 10 keV, using the new data (DUB-80, ORL-80), accounting for missed resonances. However, neutron widths are lacking for many resonances at $E > 0.5$ keV.

The ENDF/B-V evaluation is in agreement with the ORL-80 data (Fig. 7b). The RPI-75 data are significantly higher at 15 to 30 keV (discrepancy ORL-80 and RPI-75). The normalization of the RCN-2A curve is mainly based upon the STEK integral data (agreement with ORL-80 data at 10 to 100 keV). The adjustment from RCN-2 to RCN-2A was quite large and the shape has been deformed; therefore a re-evaluation is needed (RCN-3, in progress). Fig. 7a shows the large discrepancy between ENDF/B and RCN-2A in the MeV range.

4. ^{103}Rh (Fig. 8)

In the RCN-2A,-3 evaluations the resolved resonance range has been terminated at about 1 keV; in ENDF/B-V this limit is at about 1.5 keV. The differences between the evaluations are small up to 1.5 keV (Fig. 8a). Meanwhile, new resolved resonances have become available [30] at 2.6 to 4.2 keV (ORL-79). However, this range is probably better described by a smooth curve.

In Fig. 8b the experimental data published after 1970 have been plotted. The ORL data have been corrected [63]. The mutual agreement between the plotted data is reasonably good. The ENDF/B-V and RCN-3 evaluations are within the spread of the experimental data. In the important range from 2 to 20 keV the RCN-3 evaluation is somewhat lower than ENDF/B-V (Fig. 8a). There is, however, quite good agreement between RCN-3 and the measured points (GA-71). We also note that the RCN-3 evaluation is in excellent agreement with STEK and CFRMF integral measurements. Very recently, measurements have been obtained at KfK in the range 10 to 70 keV [74]. These measurements are in excellent agreement with the RCN-3 evaluation.

5. ^{105}Pd (Fig. 9)

A serious discrepancy between the evaluations is observed in the range from 0.1 to 1 keV (Fig. 9a). The upper limit of the resonance range is 92 eV in ENDF/B-IV,-V and 155 eV in RCN-2A. This range has been extended up to 2 keV in RCN-3 using the recent resonance parameters measured at Geel (GEL-79). Still, there are only minor differences between RCN-2A and RCN-3 in this range [8]. We conclude that the ENDF/B-IV,-V values need to be increased at 100 eV to 1 keV. We also note that recently the thermal capture cross section at 0.0253 eV has been measured. The new value, $\sigma_\gamma = 22.0 \pm 1.1$ b [72] has been used to fit the RCN-3 cross sections. This value is appreciably higher than the previously recommended value of 14 b. Other new data: DUB-78, ORL-79.

After the recent correction of the ORL-data [63] good overall agreement is obtained between the various experimental data (Fig. 9b). Possibly the Australian data need also corrections. The ENDF/B-V and RCN-3 [8] evaluations agree with most data within their errors at energies from 3 to 500 keV. In the MeV range the RCN-2A curve is below that of ENDF/B-V (Fig. 9a). We note

that French integral data indicate higher average capture cross sections in a fast reactor spectrum (discrepancy STEK-French data) [18]. *New data: GEL-82.*

6. ^{107}Pd (Fig. 10)

The new resolved resonance parameters measured at RPI [73] up to 655 eV have been included in the RCN-3 evaluation [8], see Fig. 10b. These data have been measured with the STEK fission-product sample, containing only 15.7 % of ^{107}Pd. They are the main source of differential data available. From an analysis of these data [73] it follows that $D_{obs} \approx 10.7$ eV, $\langle\Gamma_\gamma\rangle$ = 125 meV. However, the fraction of missed s-wave levels is probably quite high [18]. Therefore, more measurements have to be recommended. This requires a better sample with a higher enrichment of ^{107}Pd. Recently, new data (NIR-80) have been reported up to 45 eV. The RCN-2A and ENDF/B-V evaluations are still based upon theoretical models in the entire energy range (Fig. 10a).

The calculated fast cross-sections of RCN-2A and RCN-3 (Fig. 10b) have been adjusted to fit the integral STEK data. In the case of RCN-3 the value of D_{obs} has been decreased to 6.1 eV [8]; the adopted value of $\langle\Gamma_\gamma\rangle$ was 125 meV. The RCN-3 values have been increased compared to RCN-2A in the range from 0.6 to 10 keV by adopting $S_o = (0.69 \pm 0.30) \times 10^{-4} eV^{-\frac{1}{2}}$, obtained from an analysis of the new RPI data. The previous value of S_o was 0.45×10^{-4}. More experimental data are required. We recommend integral transmutation measurements with highly-enriched samples in well-defined intense neutron fields [18].

7. ^{109}Ag (Fig. 11)

There is a good agreement in the resolved resonance range up to about 0.5 keV (Fig. 11a). At 0.5 to 1.0 keV there is a discrepancy (ENDF/B-IV,V lower than RCN-2A,3). *New data reported at this meeting: ORL-82, JAE-82.*

In the smooth energy range (Fig. 11b) there is a significant discrepancy between experimental data (DKE-60 > FEI-65). The RCN-3 and ENDF/B-V evaluations are in agreement with STEK and CFRMF integral data. We recommend new measurements from 1 to 500 keV. *This request has been satisfied with ORL-82, JAE-82 data reported at this meeting.* Integral data with high accuracy would also be helpful [18].

8. ^{133}Cs (Fig. 12)

The resolved resonance range of ^{133}Cs extends up to about 2.5 keV in ENDF/B-IV,-V and 3.5 keV in RCN-2A,-3. The RCN-2A cross section has been adjusted to STEK (and CFRMF) integral data, resulting in a positive adjustment in the resolved resonance range, particularly at 1 eV to 3.5 keV. A similar adjustment has been applied to the RCN-3 point-wise given cross sections leading to increased cross sections in this range (see Fig. 12a). By this adjustment the resonance integral has been increased from 376 to 406 b, i.e. closer to the experimental value of 437 ± 26 b [30]. We note that recently [30] the low-energy part of the resonance range has been revised (RPI-77, NIR-77, KIG-81). There still is a lack of capture data in the resolved resonance range above 40 eV.

In the smooth energy range the effect of adjustment to integral STEK and CFRMF data is a decrease in cross section. The RCN-2 and ENDF/B-IV evaluations were based upon the KFK-69 data, which are much higher than the old Russian data (LEB-62). The recent Japanese data (KTO-79) confirm the relatively low values adopted in RCN-3 and ENDF/B-V. *Note: The ORL-82 data reported at this meeting are also in agreement with KTO-79.*

9. ^{143}Nd (Fig. 13)

There are no important differences between the evaluations shown in Fig. 13a up to 500 keV. In the RCN-3 evaluation the resolved range extends up to 4 keV, using the AUA-78 parameters at 2.5 to 4 keV. The ENDF/B-V resolved resonance range is limited to 0.6 keV (BNL-325, third ed.). The newest BNL-compilation [30] includes the recent data (GEL-75, AUA-78, RPI-79).

In the smooth energy range (Fig. 13b) there is a good agreement between the various experimental data and evaluations up to about 70 keV. At higher energies the experimental data (AUA-77, JAE-79) indicate quite low cross sections, in disagreement with the model calculations. There are also discrepancies between RCN-3 and ENDF/B-IV,V evaluations, probably due to the uncertainties in the level scheme of ^{143}Nd [5]. Besides a re-evaluation of this level scheme, accounting for possible missed levels, there is a need for additional experimental data at 0.1 to 3 MeV. There is good agreement with the existing STEK data.

10. ^{147}Pm (Fig. 14)

The resolved resonance parameters (up to 316 eV) adopted in the available evaluations are based upon the work of Kirouac et al. [75]. The more recent Russian data (NIR-78) need to be combined in future evaluations.

The smooth range (Fig. 14b) is obtained from model calculations. Adjustments have been applied to fit integral STEK and CFRMF data. The shape of the ENDF/B-IV,-V curves from 0.1 to 0.7 MeV is quite different from that of RCN-3. The reason is not very clear, since the adopted level schemes are the same up to 400 keV [5]. This discrepancy should be investigated by means of model calculations. Some experimental data in the range 1 to 500 keV would be helpful. Integral data performed at STEK were obtained with a sample containing 30% to 40% ^{147}Sm. This adds some uncertainty to the results. New integral data with a fresh ^{147}Pm sample are recommended [18].

11. ^{149}Sm (Fig. 15)

Resolved resonances have been adopted in RCN-3 and ENDF/B up to 150 eV and 100 eV, respectively. Their main source is BNL-325 (third edition), with some updatings, e.g. in the thermal range up to 12 eV (BNL-74). There is a discrepancy with ENDF/B-IV,-V at 20 to 100 eV (Fig. 15a) probably due to the use of different values of Γ_γ (62 meV in RCN-3; 49 meV in ENDF/B-V). In future updatings the resolved resonance range should be re-evaluated using recent information (JAE-81). Radiation widths are known only up to 31 eV ($\langle\Gamma_\gamma\rangle = 62$ meV).

In the smooth energy range (Fig. 15b) there exists a discrepancy between the Russian data (FEI-75) and other recent experimental data (RPI-75, JAE-79) at energies up to 30 keV. All evaluated curves are still lower than these experimental points. The RCN-3 curve has been adjusted to fit the integral STEK measurements. ENDF/B-V is based upon a combined adjustment to differential data (RPI-75) and integral data (STEK). French integral data lead to an adjusted average cross section quite close to the RCN-2A (and ENDF/B-V) value [18]. Since the adjusted curves are below the recent experimental data there could be a discrepancy between differential and STEK data. We suggest new average capture measurements in the range 0.5 to 30 keV. In the high-energy range different level schemes have been used in the evaluations [5]. A critical quantity in the spin of the second excited state at 277 keV, which is probably 5/2 (RCN-3) rather than 3/2 (ENDF/B-IV,V) [5].

12. ^{151}Sm (Fig. 16)

The resolved resonance parameters in ENDF/B-V are still based upon BNL-325 (third edition) with a maximum energy of only 6.5 eV. In RCN-3 this range has been extended up to 105 eV with new data (KAP-75). Recently, it was pointed out [32] that the number of missed resonances is quite high in these data. Therefore, a correction for missed resonances might be needed in future updatings. More recent data have been obtained at Dimitrovgrad (NIR-77) up to 18 eV.

The value of D_{obs} adopted in most evaluations also needs a significant correction [32], leading to quite high capture cross sections in the smooth energy range. These corrections need to be applied in new evaluations. There are no differential data available. The situation with respect to integral data is unsatisfactory [18]: the STEK sample contains only 6.13 % ^{151}Sm and the PHENIX sample consisted mainly of ^{149}Sm (multiple capture in intense neutron flux). A large discrepancy was reported between RCN-2A and CARNAVAL-IV [18], indicating that the RCN-3 cross section should be higher. The ENDF/B-V value is appreciably higher than RCN-3. Evidently, more (integral) measurements with enriched ^{151}Sm samples are needed. There are large discrepancies between ENDF/B-IV, V and RCN-3 above 100 keV due to the use of different level schemes for ^{151}Sm (missed levels in ENDF/B-V) [5]. We also mention that the ground-state spin of ^{151}Sm should be 5/2 rather than 7/2 as adopted in BNL-325 and ENDF/B-V.

B. Less important fission products

Some observed discrepancies between recent experimental data have been listed in Table 6b. They have been obtained from unpublished intercomparisons [78] and from inspection of graphs given in Refs. [5,6,8,76]. A general observation from Table 6 is that the FEI-75 data are usually higher than the other data, particularly at the lower neutron energies.

A few requests for new data have been listed in Table 7b. Many of these requests refer to unstable nuclides, for which samples are difficult to obtain. For the even-mass Pd isotopes average capture measurements are underway at Geel. These measurements have been requested by the author, in order to solve the systematic discrepancies [8] between the average cross section data obtained by Macklin et al. [63] and results from model calculations [8] based upon resonance parameters measured by Staveloz et al. [77]. *From results presented at this meeting by Rohr for ^{108}Pd it seems that most of these discrepancies have been resolved.*

VI. CONCLUSIONS

(1) Theoretical models and methods used to predict capture cross sections of fission-product nuclei in the MeV range need to be re-evaluated. Particular attention is needed for the description of spin- and parity distributions of target levels in the continuum. There are significant differences between various evaluations in the MeV range.

(2) Serious discrepancies between the recent capture cross section evaluations occur in the resolved resonance range. Many new data (Table 2) should be inserted in these evaluations. This applies in particular to ENDF/B-V.

(3) Recent differential capture cross sections in the smooth energy range

(Table 3) have been considered only in the newest versions of the nuclear data files (e.g. ENDF/B-V).

(4) Integral data have successfully been used to adjust the ENDF/B-V and RCN-2A, -3 data libraries. Other recent evaluations have been revised as a result of integral data tests (CNEN and JENDL updates). One-group cross sections of ENDF/B-V and RCN-2A are in quite good agreement (Table 4).

(5) Lumped fission-product capture cross sections calculated from CNEN/CEA, ENDF/B-V, JENDL-1 and RCN-2A, -3 are in very good agreement. The one-group cross sections agree within about 1%.

(6) Discrepancies between experimental data (Table 6) indicate problems for a large number of cases. Only a combination of model calculations, differential data and integral data leads to acceptable results.

(7) Some requests for new measurements (Table 7) refer to gaps in the nuclear data for stable nuclei. For long-lived unstable nuclei only very few data are available. Sample problems could prevent differential measurements; integral (irradiation) measurements in intense neutron fluxes are recommended in these cases.

VII. ACKNOWLEDGEMENTS

The author would like to thank Mr. H.A.J. van der Kamp and Mr. H.Ch. Rieffe for important contributions to this review.

The author is grateful to the members of the Scientific Coordination group of the European-Japanese Joint Evaluated File (JEF) for valuable discussions.

This work has been performed in the framework of DeBeNe-cooperation on fast power reactors.

VIII. REFERENCES

[1] M. Darrouzet et al., An evaluated fission product library for Super-Phenix project, Proc. Int. Conf. on Neutron Physics and Nuclear Data for Reactors and Other Applied Purposes, Harwell, Sept. 1978, p. 1146, OECD 1978.

[2] A. Montaguti and M. Vaccari, Tables of neutron resonance data and parameters for 63 fission products evaluated and compiled at the Bologna Centre (1977), RT/FI(78)23.

[3] M. Vaccari, Tables of neutron resonance parameters and multigroup cross sections for PD-105, Nd-143, Sm-149, Sm-151 (1979 evaluation), CNEN-RT/FI(80)1 and private communication (E. Menapace, 1981).

[4] S. Iijima et al., Evaluation of neutron cross sections of 27 fission product nuclides important for fast reactor, J.Nucl.Sci.Techn. 14 (1977) 161.

[5] Y. Kikuchi et al., Neutron cross sections of 28 fission product nuclides adopted in JENDL-1, JAERI-1268 (1981).

[6] S. Iijima et al., Fission product neutron cross section evaluations for JENDL and the integral tests, Proc. Specialists'Meeting on Neutron cross sections of fission product nuclei, Bologna 1979, NEANDC(E)209"L"., p. 317.

[7] H. Gruppelaar, Tables of RCN-2 fission product cross section evaluations, vol. 1: ECN-13 (1977), vol. 2: ECN-33 (1977) and vol. 3: ECN-65 (1979).

[8] H.A.J. van der Kamp and H. Gruppelaar, Evaluation of neutron cross sections for the Pd isotopes (RCN-3 data library), ECN-108 (1981); other reports to be published.

[9] National Neutron Cross Section Center (Brookhaven), Evaluated Nuclear Data File B, version IV (1975).

[10] R.E. Schenter and T.R. England, ENDF/B-5 fission product cross section evaluations, Proc. Specialists' Meeting on Neutron cross sections of fission-product nuclei, Bologna, Dec. 1979, NEANDC(E)209"L", 1980, p. 253.

[11] R.E. Schenter et al., Evaluations of fission product capture cross sections for ENDF/B-V, Proc. of the Int. Conf. on Nuclear Cross Sections and Technology, Knoxville, 1979, NBS-SP594(1980), p. 662.

[12] R. Kinsey (comp.), ENDF/B summary documentation, ENDF-201 (1979).

[13] H. Gruppelaar and J.B. Dragt, Cross section adjustments using integral data, Workshop on Evaluation Methods and Procedures, Brookhaven, September 1980; BNL-NCS-51363, vol.1(1981), p. 133.

[14] A. Montaguti et al., Multigroup cross-sections of 63 fission product nuclei from different nuclear data files, RT/FI(78)16.

[15] J.P. Chaudat et al., Data adjustments for fast reactor design, Trans. Am. Nucl. Soc. 27 (1977) 877.

[16] J.W.M. Dekker, Tables and figures of adjusted and unadjusted capture group cross sections based on the RCN-2 evaluation and integral measurements in STEK, vol. 1: ECN-14 (1977), vol. 2: ECN-30 (1977) and vol. 3: ECN-54 (1979).

[17] J.W.M. Dekker and H.Ch. Rieffe, Adjusted cross sections of fission product nuclides from STEK reactivity worths and CFRMF activation data, vol. 1: ECN-28 (1977) and vol. 2: ECN-55 (1979).

[18] H. Gruppelaar et al., Intercomparison of adjusted data sets for capture cross sections of fission products, Proc. Specialists' Meeting on Neutron cross sections of fission product nuclei, Bologna 1979, NEANDC(E)209"L", p. 299.

[19] E. Fort, Status of neutron reaction cross sections of fission products in the energy range of resolved and unresolved resonances, Proc. of the second advisory group meeting on Fission Product Nuclear Data (FPND) - 1977, Petten, IAEA-213 (1978), vol. 1, p. 139.

[20] H. Gruppelaar, Impact of integral measurements on the capture cross section evaluations of individual fission product isotopes, ibid, vol. 1, p. 219 and ECN-24.

[21] S. Iijima, Status of neutron reaction cross sections of fission products, ibid., vol. 1, p. 279.

[22] M. Bustraan et al., Integral determination of fission product neutron capture cross sections, ibid., vol. 2, p. 627.

[23] H. Gruppelaar et al., Intercomparison of recent evaluations for the capture cross sections of some fission-product nuclides, ECN-12 (1976),

[24] R.J. Heijboer and A.J. Janssen, Status of fission-product cross sections for fast reactors; sensitivity study for sodium void effect, Proc. Specialists' Mtg. on Neutron Cross Sections of Fission Product Nuclei, Bologna 1979, NEANDC(E)209"L" (1980), p. 375.

[25] S. Igarasi, On the modified methods of the neutron cross-section calculations. J. Nucl. Sci. Techn . 12 (1975) p. 67.

[26] F.A. Schmittroth, Theoretical calculations of fast neutron capture cross sections, HEDL-TME-71-016 (1971).

[27] F. Fabbri and G. Reffo. CERBERO - A Fortran programme for the calculation of nuclear reaction cross sections, CNEN-report RT/FI(74)36 and supplement RT/FI(77)6.

[28] F. Fabbri and G. Reffo, ERINNI: An optical model FORTRAN-IV code for the calculation of multiple cascading particle emission, CNEN-report RT/FI/77) 4.

[29] G. Reffo, Parameter systematics for statistical theory calculations, Proc. of the course on Nuclear Theory for Applications, Trieste, 1978, IAEA-SMR-43 (1980).

[30] S.F. Mughabghab, M. Divadeenam and N.E. Holden, Neutron cross sections, vol. 1. Neutron resonance parameters and thermal cross sections, part A: Z = 1-60, Academic Press (1981).

[31] B.J. Allen and A.R. de L. Musgrove, Valence and doorway mechanisms in resonance neutron capture, Advances in Nuclear Physics, Plenum Press N.Y., vol. 10 (1978), p. 129.

[32] E. Fort, H. Derrien and D. Lafond, Review of the different methods to derive average spacing from resolved resonance parameter sets, Proc. of the Specialists' Meeting on Neutron cross sections of fission product nuclei, Bologna, Dec. 1979, NEANDC(E)209"L".

[33] H.I. Liou, Evaluations of average level spacings, Proc. of the Conf. on Nuclear data evaluation methods and procedures, Brookhaven, Sept. 1980, BNL-NCS-51363, vol. 1 (1981) p. 463.

[34] P. Ribon, Set of statistically generated resonance parameters, available from NEA Data Bank, 1981.

[35] G. Delfini and H. Gruppelaar, Maximum likelihood analysis of resolved resonance parameters for 18 fission product nuclides, ECN-82 (1980) and Proc. of the Specialists' Meeting on Neutron cross sections of fission product nuclei, Bologna, 1979, NEANDC(E)209"L" (1980) p. 169.

[36] M. Stefanon, Statistical analysis of neutron resonance parameters, Proc. of the Specialists' Meeting on Neutron cross sections of fission product nuclei, Bologna, 1979, NEANDC(E)209"L" (1980), p. 161 and private communication (1980-191).

[37] M. Stefanon, Description of a statistical method of analysis of neutron resonance data, Nucl. Inst. and Meth. 174 (1980) p. 243.

[38] Gruppelaar, H., Note on the results of the benchmark test of code CAVECN, Contr. to the Proc. of the Workshop on Intercomparison of methods to determine average parameters from resolved resonance parameters, NEA Data Bank, Saclay, October 15-16, 1981.

[39] NEA Data Bank, to be published.

[40] P. Staveloz et al., Neutron resonances for Palladium isotopes, Proc. of the Specialists' Meeting on Neutron Cross Sections of Fission Product Nuclei, Bologna, Dec. 1979, NEANDC(E) 209"L", 1980, p. 53 and private communication (1981).

[41] A. Gilbert and A.G.W. Cameron, A composite nuclear level-density formula with shell corrections, Can. J. of Phys. 43 (1965) p. 1446.

[42] V. Benzi, G. Reffo and M. Vaccari, On the calculation of total radiative widths of neutron resonances, Proc. of a panel on Fission Product Nuclear Data (FPND), Bologna 1973, vol. 3, IAEA-169 (1974) p. 123.

[43] G. Reffo and M. Vaccari, LARA: A Fortran-IV code for the calculation of the compound nucleus contribution to the total radiative width in medium and heavy nuclei based on the Brink-Axel model, CNEN-report RT/FI/74/17 (1974).

[44] H. Weigmann and G. Rohr, Systematics of total radiative widths of neutron resonances, Proc. Symp. on Nuclear Physics with Thermal and Resonance Neutrons, Petten, 1973, RCN-203 (1973) p. 194.

[45] D.G. Gardner and F.S. Dietrich, A new parameterization of the E1 gamma-ray strength function, Proc. of the Int. Conf. on Nuclear cross sections for technology, Knoxville, Oct. 1979, p. 770 and D.G. Gardner et al., Lawrence Livermore Laboratory report UCID-18759, 1980 (unpublished).

[46] M.A. Gardner and D.G. Gardner, Calculated neutron capture cross sections for the ground state and isomers of ^{93,94}Nb, Proc. of the Int. Conf. on Neutron physics and nuclear data, Harwell (1978) p. 1121.

[47] M.A. Gardner and D.G. Gardner, Capture cross section and gamma-ray spectrum calculations for medium-weight nuclei, Proc. of the Int. Conf. on Nuclear cross sections for technology, Knoxville, Oct. 1979, p. 752.

[48] J. Kopecky, Mass dependence of the giant resonance model, Contr. to the 4th Int. Symp. on Neutron capture gamma-ray spectroscopy and related topics, Sept. 1981, Grenoble.

[49] J. Kopecky, Quadrupole radiation strength in neutron capture, ECN-88 (1981) and Contr. to the 4th Int. Symp. on Neutron capture gamma-ray spectroscopy and related topics, Sept. 1981, Grenoble.

[50] M. Moore, Systematics of s- and p-wave radiative widths, Proc. of the Conf. on Nuclear data evaluation methods and procedures, Brookhaven, Sept. 1980, BNL-NCS-S1363, vol. 1 (1981) p. 449.

[51] Japanese Nuclear Data Committee, Evaluation of fission product nuclear data for fast reactor, JAERI-M5752 (1974).

[52] P.A. Moldauer, Optical model of low energy neutron interactions with spherical nuclei, Nucl. Phys. 47 (1963) p. 65.

[53] Ch. Lagrange, On optical model calculations in the mass region A = 80 to A = 170, Proc. of the Specialists' Meeting on Neutron Cross Sections of fission product nuclei, Bologna 1979, NEANDC(E)209"L", p. 233.

[54] H. Gruppelaar and G. Reffo, Some properties of the width fluctuation factor, Nucl. Sc. and Eng. 62 (1977) 756.

[55] P.A. Moldauer, Why the Hauser-Feshbach formula works, Phys. Rev. C11 (1975) 426.

[56] J.W. Tepel, H.M. Hofmann and H.A. Weidenmüller, Hauser-Feshbach formulas for medium and strong absorption, Phys. Lett. 49B (1974) p. 1.

[57] H.M. Hofmann et al., Direct reactions and Hauser-Feshbach theory, Annals of Physics 90 (1975) p. 403.

[58] P.A. Moldauer, Statistics and the average cross section, Nucl. Phys. A344 (1980) p. 185.

[59] J.W. Tepel, H.M. Hofmann and M. Herman, Improved formulas for compound nucleus cross sections, Proc. of the Int. Conf. on Nuclear cross sections for technology, Knoxville, 1979, NBS-SP594 (1980) p. 762.

[60] P. Moldauer, Neutron strength functions: The link between resolved resonances and the optical model, Proc. of the Conf. on Nuclear data evaluation methods and procedures, Brookhaven, Sept. 1980, BNL-NCS-51363, vol. 1 (1981) p. 433.

[61] R. Kinsey (rev.), Data formats and procedures for the evaluated nuclear data file, ENDF, ENDF-102 (1979).

[62] H. Gruppelaar and B.P.J. van den Bos, The contribution of (n,p) and (n,α) cross sections to fission-product capture cross sections, Proc. of the Specialists' Mtg. on Neutron cross sections of fission product nuclei, Bologna, Dec. 1979, NEANDC(E) 209"L", p. 5 and ECN-78 (1979).

[63] R.L. Macklin and R.R. Winters, Stable isotope capture cross sections from the Oak Ridge electron linear accelerator (corrigendum), Nucl. Sc. and Eng. 78 (1981) p. 110.

[64] R.A. Anderl, Review paper on Integral measurements and tests of fission-product neutron capture cross sections, this meeting.

[65] G. Langlet and L. Martin-Deidier, The French programme on the determination of the effect of fission products in fast reactors, Second advisory group meeting on Fission Product Nuclear Data (FPND) - 1977, INDC(NDS)-87/GO+Sp (1978), p. 293.

[66] Y.D. Harker and R.A. Anderl, Integral cross-section measurements on fission-products in fast neutron fields, Proc. Specialists' Meeting on Neutron cross sections of fission product nuclei, Bologna, Dec. 1979, NEANDC(E)209"L", 1980, p. 5.

[67] R.A. Anderl and Y.D. Harker, Neodymium, Samarium and Europium capture cross section adjustments based on EBR-II measurements, ibid., p. 363.

[68] R.J. Heijboer, Pseudo fission-product cross sections for a 1300 MWe fast breeder reactor (status July 1978), ECN-52 (1978).

[69] R.C. Little and R.C. Block, Neutron capture cross-section measurements of ^{99}Tc upto 80 keV, Trans. Am. Nucl. Soc. 26 (1977) p. 574.

[70] P. Fischer et al., Neutron resonance parameters of ^{99}Tc in the energy range between 4.5 and 25 eV, Atomkernenergie-Kerntechnik 38 (1981) p. 63.

[71] W.P. Poenitz, Fast neutron cross section measurements, evaluations and model calculations of fission product nuclei, Proc. of the Specialists' Mtg. on Neutron cross sections of fission product nuclei, Bologna, Dec. 1979, NEANDC(E), p. 85 (1980).

[72] F. Corvi, CBNM, Geel, private communication (1981).

[73] U.N. Singh, R.C. Block and Y. Nakagome, Neutron capture and transmission measurements on fission product Palladium-107, Nucl. Sci. Eng. 67 (1978) p. 54.

[74] G. Reffo et al., Fast neutron cross sections and related gamma ray spectra of ^{93}Nb, ^{103}Rh and ^{181}Ta, to be publ. (1981).

[75] G.J. Kirouac et al., Resonance and thermal-neutron total cross sections for Promethium-147 and Promethium-148m, Nucl. Sci. Eng. 52 (1973) p. 310.

[76] N. Yamamuro and A. Asami, Measurments of capture cross sections in the FP mass region, Proc. of the Specialists' Mtg. on Neutron cross sections of fission product nuclei, Bologna, Dec. 1979, NEANDC(E), p. 19 (1980).

[77] P. Staveloz et al., Neutron resonance parameters for Palladium isotopes, Proc. of the Specialists' Mtg. on Neutron cross sections of fission product nuclei, Bolgona, Dec. 1979, NEANDC(E), p. 53 (1980) and private communication CBNM, 1981.

[78] H. Gruppelaar and H.A.J. van der Kamp, ECN-report, to be published.

Table 1. Characteristics of recent fission-product nuclear data evaluations.

Item	CNEN/CEA	JENDL-1	RCN-2 (KEDAK-3)	RCN-3	ENDF/B-IV	ENDF/B-V
References	[1-3]	[4-6]	[7]	[8]	[9]	[10-12]
Number of materials	63	63	44	37	825 a)	834 a)
Format	ENDF/B	ENDF/B	KEDAK	KEDAK	ENDF/B	ENDF/B
Date of release	1978	1975-1977	1977-1979	1981	1975	1979-1980
Availability	NEA-Data Bank, except for recent updatings [3]	NEA-Data Bank, except for recent updatings to 80 f.p. (JENDL-2 [6])	NEA-Data Bank	NEA-Data Bank	NEA-Data Bank	NEA-Data Bank
Use of integral data	only for recent updatings Nd-143, Sm-149, Sm-151, Pd-105, Pd-107	only in JENDL-2	unadjusted	adjusted to STEK and CFRMF data	unadjusted	adjusted to STEK, CFRMF
Group constants	25 groups [14] adj. version CARNAVAL-IV [15]		26 groups [16] with adjusted version RCN-2A [16,17]			
Decay data, yields	no	no	no	no	yes	yes

a) Cross sections for 196 nuclides.

Table 2a. Adopted sources of low-energy resolved resonance parameters in various evaluations for the most important fission products.

Nuclide	Most recent data[a)]	ENDF/B-V	RCN-2	RCN-3	CNEN/CEA	1979-1982 versions	JENDL-1
^{99}Tc	KUR-73,RPI-77,KIL-78, KIG-81,*ORL-82*	RPI-77	KUR-73	KUR-73	KUR-73	-	
^{101}Ru	(RPI-75),DUB-80, ORL-80			in progress		-	
^{102}Ru	(RPI-75),DUB-80, ORL-80			in progress		-	
^{103}Rh	(ORL-79)					-	
^{105}Pd	DUB-78,GEL-79,ORL-79			GEL-79		GEL-79	
^{107}Pd	RPI-78, NIR-80	(no res.par.)	(no res.par.)	RPI-78	(no res.par.)	RPI-78	(no res.par.)
^{109}Ag	*ORL-82,JAE-82*					-	
^{133}Cs	(RPI-77),NIR-77,KIG-81					-	
^{143}Nd	GEL-75,(RPI-79),AUA-78		GEL-75,AUA-78	GEL-75,AUA-78	GEL-75	AUA-78	
^{147}Pm	NIR-78					-	
^{149}Sm	BNL-74,JAE-81		BNL74	BNL-74			
^{151}Sm	KAP-75,NIR-77		KAP-75	KAP-75		KAP-75	

Table 2b. Adopted sources of low-energy resolved resonance parameters in various evaluations for less important fission products.

Nuclide	Most recent data[a)]	ENDF/B-V	RCN-2	RCN-3	CNEN/CEA	JENDL-1
^{93}Zr	(only one resonance known)	(no res.)	-	-	(1 res.)	(1 res.)
^{95}Mo	AUA-76,(RPI-77)			-		
^{97}Mo	AUA-76,(RPI-77)			-		
^{98}Mo	AUA-76, ORL-76		ORL-76	-		-
^{100}Mo	AUA-76, ORL-77,79			-		-
^{103}Ru	(no resonances known)	(no res.)	-	-	(random)	-
^{104}Ru	(RPI-75), (DUB-79), ORL-80			-		
^{135}Cs	KIL-79 (1 res.)	(no res.)	-	-	(random)	
^{141}Pr	(RPI-79),(AUA-79)					
^{145}Nd	(RPI-75), (AUA-77), (NIR-79)					b)
^{148}Nd	AUA-77		AUA-77	AUA-77	(+random)	b)
^{153}Eu	NIR-79		-	-		

a) Data not given in BNL-325, vol. 1, third ed., 1973. Note that the Oak Ridge data have recently been revised [63]. These corrections are important for ^{103}Rh (-5%) and ^{105}Pd (+11%). Corrections may also be needed in the ORELA data analysed in Australia. Most of the unpublished data (indicated in parenthesis) are given in Ref. [30].

Table 3a. Adopted sources of differential capture data (E>1 keV) in various evaluations for the most important fission products.

Nuclide	Most recent data[a)]	ENDF/B-V	RCN-2	RCN-3	CNEN/CEA	1979-1982 versions	JENDL-1	1979 version
^{99}Tc	RPI-77, *ORL-82*	RPI-77				-		-
^{101}Ru	RPI-75, ORL-80	RPI-77, ORL-80		in progr.		-		-
^{102}Ru	RPI-75, ORL-80	RPI-77, ORL-80		in progr.		-		-
^{103}Rh	RPI-75, CAD-76, BRC-79 ANL-79, ORL-80, (KFK-81)	RPI-75, ORL-80	RPI-75, CAD-75	RPI-75, ORL-80	CAD-75	RPI-75, AUA-78		-
^{105}Pd	RPI-75, AUA-78, ORL-81, *GEL-82*	RPI-75, ORL-79		RPI-75, AUA-78, ORL-81 [c)]		RPI-75, AUA-78		-
^{107}Pd	(no data)	(no data)	(no data)	(no data)	(no data)	(no data)	(no data)	-
^{109}Ag	*ORL-82, JAE-82*					-		-
^{133}Cs	KTO-79, (BRC-80), *ORL-82, KURRI-82*			KTO-79		-		-
^{143}Nd	(RPI-77), AUA-78, JAE-78	AUA-77	AUA-78, JAE-78	AUA-78, JAE-78		AUA-78, JAE-78		AUA-78, JAE-79
^{147}Pm	(no data)	(no data)	(no data)	(no data)	(no data)	-	(no data)	-
^{149}Sm	RPI-75, FEI-77, JAE-79	RPI-75	RPI-75, FEI-76	RPI-75, FEI-76		RPI-75, FEI-76		RPI-75, JAE-79
^{151}Sm	(no data)	(no data)	(no data)	(no data)	(no data)	(no data)	(no data)	(no data)

Table 3b. Adopted sources of differential capture data (E>1 keV) in various evaluations for less important fission products.

Nuclide	Most recent data[a)]	ENDF/B-V	RCN-2	RCN-3	CNEN/CEA	JENDL-1
^{93}Zr	(no data)	(no data)	-	-	(no data)	(no data)
^{95}Mo	(RPI-77), AUA-78	AUA-78		-		
^{97}Mo	(RPI-77), AUA-78	AUA-78		-		
^{98}Mo	AUA-78	AUA-78		-		
^{100}Mo	AUA-78	AUA-78		-		
^{103}Ru	(no data)	(no data)	-	-	(no data)	-
^{104}Ru	(RPI-75), ORL-80	(RPI-75), ORL-80		-		
^{135}Cs	(no data)	(no data)	-	-	(no data)	(no data)
^{141}Pr	(RPI-78), AUA-79			AUA-79		
^{145}Nd	(RPI-75), AUA-78, JAE-78-80	(RPI-75)	(RPI-75)	(RPI-75), AUA-78, JAE-78-80		b)
^{148}Nd	FEI-78, AUA-78, JAE-78-80	AUA-78		FEI-78, AUA-78, JAE-78-80		b)
^{153}Eu	(RPI-75), HAR-76, FEI-77, JAE-79	(RPI-75), HAR-76, FEI-77	-	-		

a) Data not given in BNL-325, vol. 2, third ed., 1976. Note that the Oak Ridge data have recently been revised [63]. These corrections are important for ^{103}Rh (-5%) and ^{105}Pd (+11%). Corrections may also be needed in the ORELA data analysed in Australia. Some of the unpublished data (indicated in parentesis) are available from the NEA Data Bank.

b) New evaluation in progress [6].

c) Corrected data used [63].

Table 4a. Average capture cross sections in a fast power reactor (SNR-300) from various nuclear data libraries for the most important fission products.

Nuclide	Order of importance[a]	$\bar{\sigma}_c$ [b] (b)					
		ENDF/B-IV	ENDF/B-V	RCN-2	RCN-2A	CNEN/CEA	JENDL-1
^{99}Tc	4	0.49	0.61	0.54(18%)	0.59(9%)	0.54	0.54
^{101}Ru	2	0.53	0.71	0.69(21%)	0.67(10%)	0.75	0.71
^{102}Ru	13	0.19	0.16	0.20(39%)	0.16(15%)	0.22	0.22
^{103}Rh	3	0.70	0.68	0.64(8%)	0.64(6%)	0.63	0.65
^{105}Pd	1	0.83	0.85	0.81(15%)	0.88(7%)	0.84 [c]	0.76
^{107}Pd	6	0.57	0.81	0.96(92%)	0.94(17%)	0.79 [c]	0.75
^{109}Ag	14	0.48	0.74	0.68(17%)	0.73(10%)	0.65	0.81
^{133}Cs	5	0.48	0.46	0.50(12%)	0.49(8%)	0.49	0.45
^{143}Nd	12	0.30	0.31	0.32(8%)	0.30(7%)	0.34 [c]	0.29 [d]
^{147}Pm	8	1.25	1.21	1.04(24%)	1.29(7%)	1.07	1.08
^{149}Sm	7	1.41	2.27	2.24(23%)	2.21(13%)	1.76 [c]	1.99 [d]
^{151}Sm	9	2.21	2.54	2.13(8%)	1.80(11%)	2.11 [c]	2.07 [d]

Table 4b. Average capture cross sections in a fast power reactor (SNR-300) from various nuclear data libraries for less important fission products.

Nuclide	Order of importance[a]	$\bar{\sigma}_c$ (b) [b]					
		ENDF/B-IV	ENDF/B-V	RCN-2	RCN-2A[c]	CNEN/CEA	JENDL
^{93}Zr	32	0.087	0.087	-	-	0.11	0.16
^{95}Mo	16	0.29	0.30	0.30(17%)	0.28 (8%)	0.27	0.30
^{97}Mo	10	0.28	0.29	0.30(17%)	0.30 (9%)	0.28	0.31
^{98}Mo	19	0.10	0.11	0.086(9%)	0.087(6%)	0.10	-
^{100}Mo	22	0.078	0.085	0.10(26%)	0.074(8%)	0.082	-
^{103}Ru	27	0.43	0.43	-	-	1.10	-
^{104}Ru	17	0.14	0.14	0.17(29%)	0.14 (7%)	0.18	0.16
^{135}Cs	24	0.067	0.067	-	-	0.21	0.27
^{141}Pr	21	0.15	0.13	0.13(12%)	0.12 (7%)	0.13	0.12
^{145}Nd	11	0.33	0.43	0.46(8%)	0.48 (7%)	0.36	0.34[d]
^{148}Nd	36	0.18	0.14	0.14(11%)	0.14 (7%)	0.16	0.18[d]
^{153}Eu	15	2.29	2.46	-	-	2.47	2.43

a) According to ENDF/B-V. Total contribution in fast reactor (conc. * $\bar{\sigma}_c$) is 81.1%.

b) For the RCN-2 and RCN-2A values the relative uncertainties are indicated in parenthesis; underlined values differ more than one standard deviation from the RCN-2A values.

c) The revised evaluations (1979) yield enhanced values for ^{105}Pd, ^{107}Pd, ^{149}Sm and ^{151}Sm and a reduced value for ^{143}Nd [3]. These modifications are partly based upon integral data analysed by the French group at Cadarache.

d) The preliminary JENDL-2 evaluations [6] yield enhanced values for ^{143}Nd, ^{145}Nd, ^{149}Sm and ^{151}Sm and a reduced value for ^{148}Nd.

Table 5. Capture cross sections[a)] of the pseudo fission product for ^{239}Pu at 41 MWd/kg (irradiation time 460 days).

group number	RCN-2A, supplemented with ENDF/B-IV [b)]	ENDF/B-V
1	0.003 (0.0063) [c)]	0.006 (0.0092) [c)]
2	0.014 (0.015) [c)]	0.015 (0.016) [c)]
3	0.033	0.039
4	0.058	0.067
5	0.084	0.090
6	0.120	0.118
7	0.182	0.174
8	0.256	0.248
9	0.383	0.378
10	0.588	0.601
11	0.875	0.916
12	1.308	1.365
13	1.931	1.993
14	3.054	3.009
15	4.637	4.419
16	9.68	8.25
17	12.58	10.93
18	20.75	17.72
19	27.68	28.23
20	57.32	64.96
21	145.21	146.89
22	21.54	19.58
23	105.09	93.43
24	63.97	58.34
25	64.78	61.12
26	1066	1040
$\bar{\sigma}_c$ [d)]	0.4995	0.4983

a) In barn/fission, 26-group ABBN scheme.

b) See ref. [68].

c) Data corrected for σ_{np} and $\sigma_{n\alpha}$ contributions [62].

d) This is the one-group cross section averaged over the SNR-300 neutron spectrum (table 3.1. of [68]).

Table 6a. Observed discrepancies between recent experimental data sets for the most important fission-product nuclides.

Nuclide	Energy range	Discrepancies
^{99}Tc	resonance range	Use BNL-325, fourth edition; Γ_n in ENDF/B-V too small (E>25 eV)
	4 - 50 keV	RPI-77 > KFK-73 (KFK-73 data may need corrections for composition of capsule [70]. *New ORL-82 data in between.*
	fast	STEK > CFRMF (integral data) [6]
^{101}Ru	5 - 100 keV	RPI-75 > ORL-80 (ORL-80 in agreement with STEK)
^{102}Ru	15 - 30 keV	RPI-75 > ORL-80 ?
^{105}Pd	fast	PHENIX > STEK (integral data) [18]
^{109}Ag	30 - 150 keV	DKE-60 >> FEI-65. *New ORL-82, JAE-82 data in between.*
^{133}Cs	10 - 200 keV	KFK-69 > other data.
^{143}Nd	70 - 200 keV	AUA-77, JAE-79 too low?
^{149}Sm	7 - 30 keV	FEI-75 > RPI-75, JAE-79
	fast	STEK data predict lower average cross-sections
^{151}Sm	fast	PHENIX > STEK (integral data) [18]

Table 6b. Observed discrepancies between recent experimental data for the less-important fission-product nuclides.

Nuclide	Energy range	Discrepancies
^{98}Mo	5-200 keV	ANL-68 > AUA-76[a)]
$^{104,106}Pd$ $^{108,110}Pd$	5-10 keV	ORL-81 > GEL-80 (resonance parameters) [8]
^{141}Pr	100-400 keV	ANL-68 > IJI-71
^{145}Nd	50-100 keV	AUA-77[a)] < RPI-75, JAE-79 [76]
^{148}Nd	8-20 keV	FEI-75 > JAE-78, AUA-77[a)] [76]
^{147}Sm	4-200 keV	FEI-75 >> JAE-79 [76]
^{153}Eu	7-150 keV	FEI-75 > RPI-75 [76]
	40-100 keV	JAE-79 > RPI-75 [76]
	≈ 100 keV	HAR-74 > RPI-75

a) Corrections might be needed [33].

Table 7a. Suggested requests for capture cross section measurements for the most important fission-product nuclides[a].

Nuclide	Energy range	Accuracy[b]	Request
^{99}Tc	0.3-1.5 keV	±10%	Γ_γ of resolved resonances
	1 - 500 keV	±10%	average cross sections *(request satisfied: ORL-82)*
	fast	± 5%	integral data
^{101}Ru	1 - 5 keV	±10%	$2g\Gamma_n$ of resolved resonances
^{102}Ru	0.5-10 keV	±10%	$g\Gamma_n$ of resolved resonances
^{105}Pd	fast	± 5%	integral data, see [18]
^{107}Pd	thermal-500 keV	±10%	thermal cross section, resonance integral resonance parameters, average cross sections (sample problems)
	fast	± 5%	integral data (transmutation measurements)
^{109}Ag	1-500 keV	±10%	average cross sections *(request satisfied: ORL-82)*
	fast	± 5%	integral data, see [18]
^{133}Cs	40 eV-4 keV	±10%	Γ_γ of resolved resonances
^{143}Nd	0.1 - 3 MeV	±10%	average cross sections
	fast	± 5%	integral data [18]
^{147}Pm	1 - 500 keV	±10%	average cross sections (sample problems)
	fast	± 5%	integral data, see [18]
^{149}Sm	0.5-30 keV	±10%	average cross sections
^{151}Sm	0.1-100 keV	±10%	average cross sections (sample problems)
	fast	± 5%	integral data (transmutation measurements, see [18])

Table 7b. Suggested requests for capture cross section measurements for the less-important fission-product nuclides[a]

Nuclide	Energy range	Accuracy[b]	Requests
^{93}Zr	1 eV - 200 keV	±15%	resolved resonances, average cross sections (sample problems
	fast	±10%	integral data
$^{108,110}Pd$	1 - 100 keV	±15%	average capture cross sections (underway at CBNM, Geel; *see data for ^{108}Pd at this meeting)*
^{129}I	0.1 - 100 keV	±15%	average capture cross sections *(planned ORL-KFK)*
	fast	±10%	integral data
^{131}Xe	4 - 200 keV	±15%	average capture cross sections (sample problems)
	fast	±10%	integral data
^{135}Cs	50 eV - 200 keV	±15%	resolved resonances, average cross sections (sample problems)
	fast	±10%	integral data

a) For many fission products the most urgent needs with regard to reactivity calculations for fast reactors have already been fulfilled by means of results from various integral measurements. The requested data are needed: (1) to meet additional requirements for future fast power reactors; (2) to improve or to check the present evaluations and (3) to solve some discrepancies between experimental data (see Table 6).

b) Accuracy requirements refer to the average cross section in a typical fast power-reactor-flux spectrum. For integral data a higher accuracy is required, due to uncertainties in the shape of response functions.

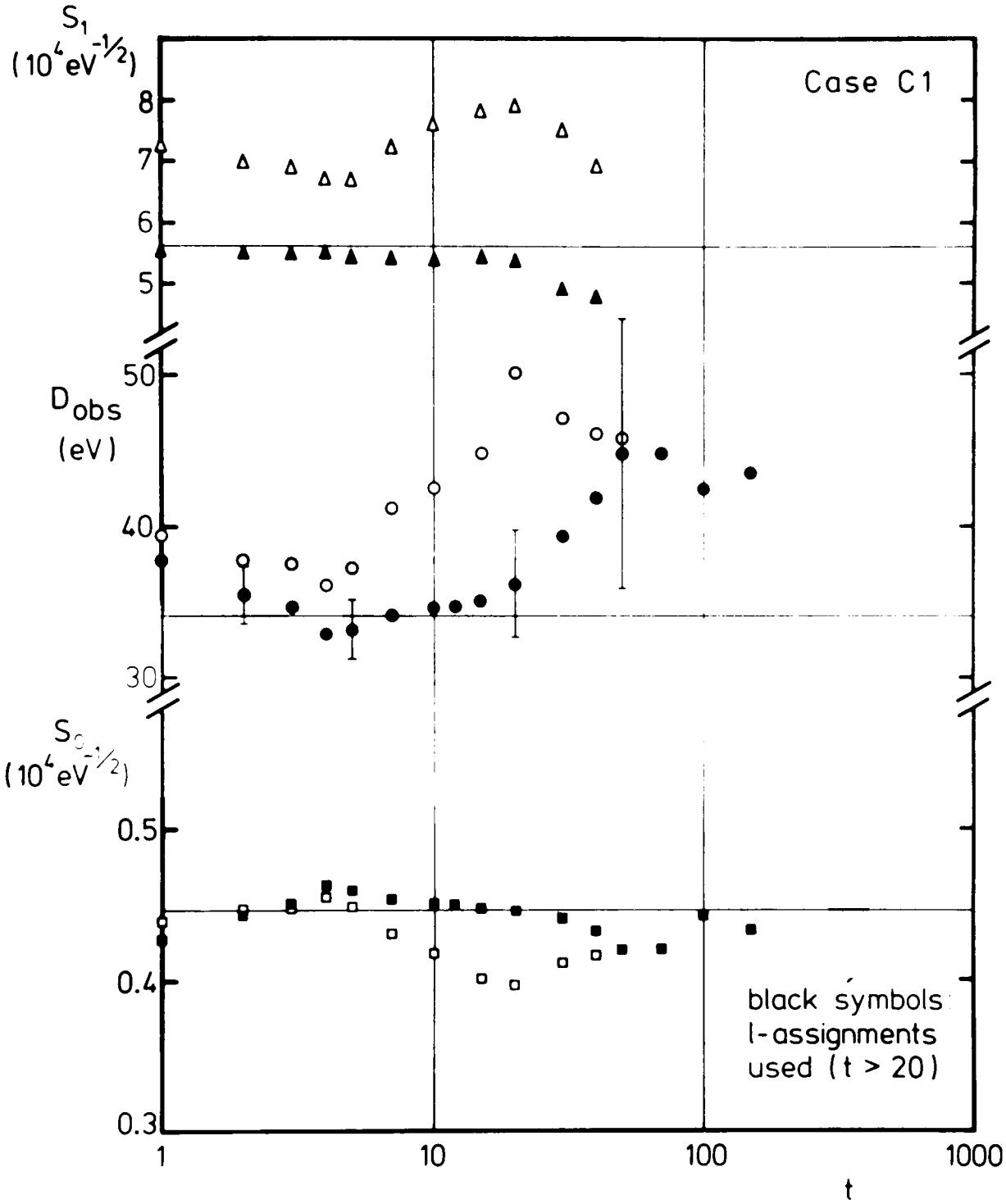

Fig. 1. Benchmark test of code CAVECN [38] for case C1.
Determination of D_{obs}, S_0 and S_1 for values of threshold multiplication factors t = 1 to 150 (Case C1). The open data points were obtained without knowledge of the "true" average values, indicated by solid lines. At $t \geq 70$ the value of $\langle g\Gamma_n^1 \rangle$ was fixed in the analysis. Black points refer to an analysis using ℓ-assignments for strong resonances (i.e. those with $g\Gamma_n/\sqrt{E} > 20\eta(E)$).
Note: Recently a revision has been applied to the code, leading to slightly different results when using ℓ-assignments.

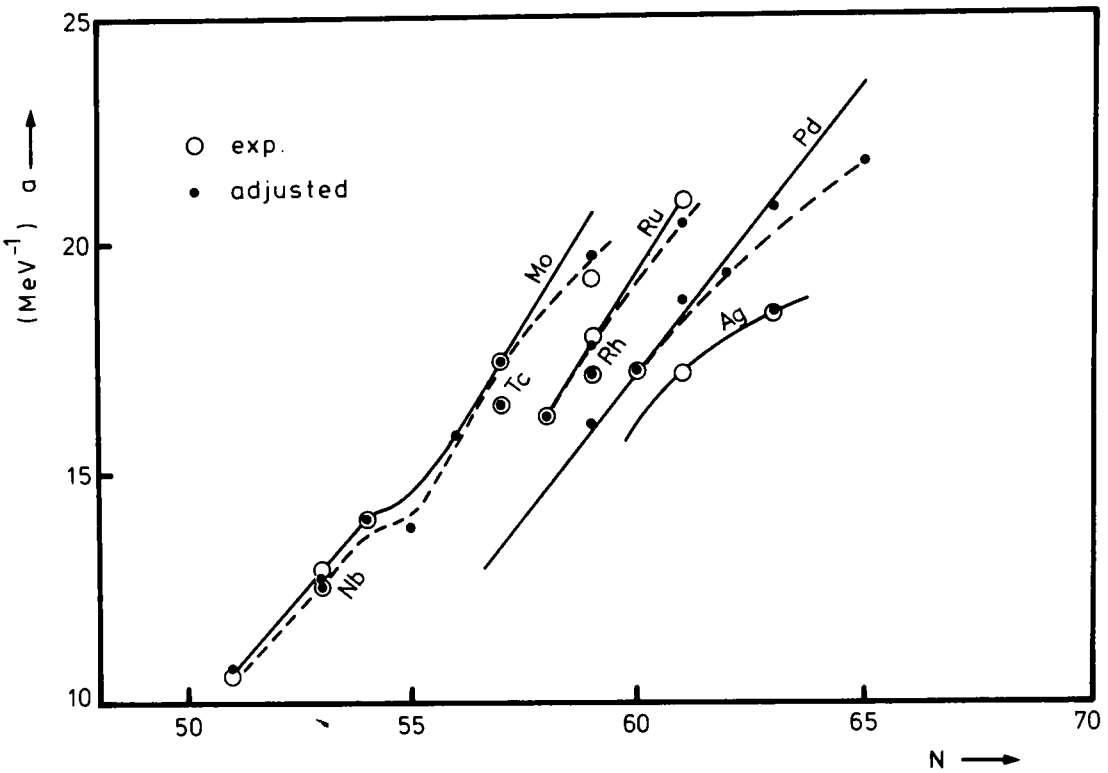

Fig. 2. Local systematics of the level-density parameter a for nuclides with neutron number N above the magic number 50. Solid and dashed curves correspond to adopted systematics in the RCN-2 and adjusted RCN-2A data files, respectively. See Fig. 4 for more recent systematics of a of the Pd-isotopes (RCN-3 evaluation).

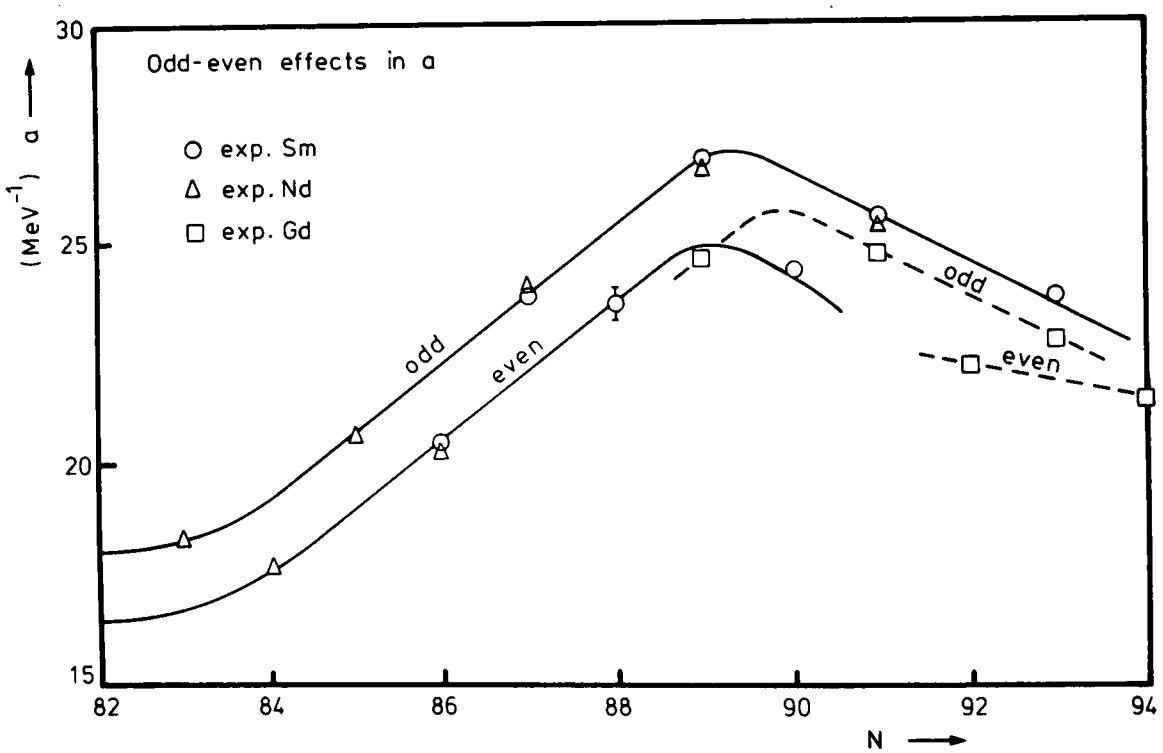

Fig. 3. Odd-even effects in the level-density parameter a for nuclides with neutron number N above the magic number 82. Solid and dashed curves correspond to adopted systematics in the RCN-2 data file for odd-mass and even-mass compound nuclei, respectively.

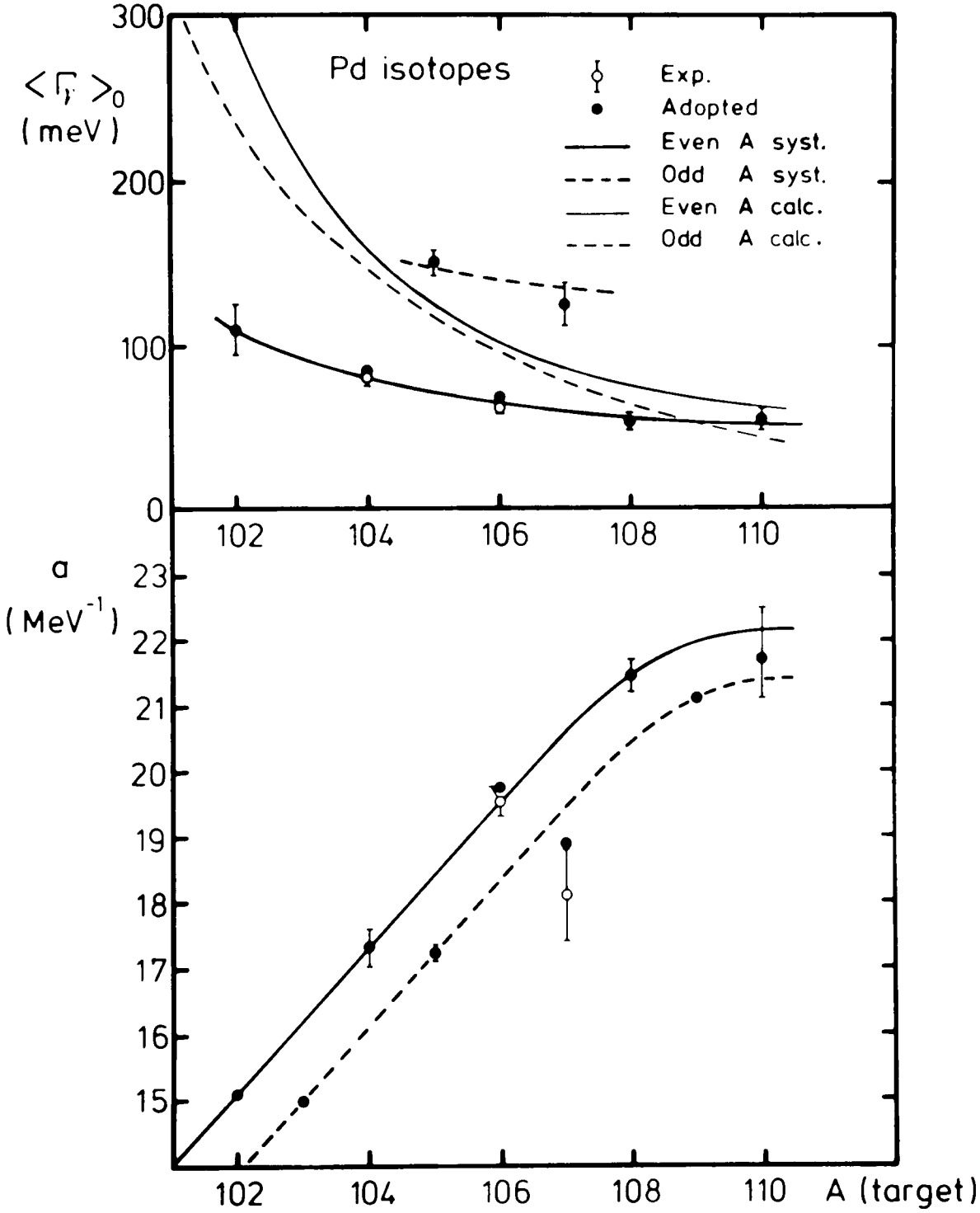

Fig. 4. Suggested systematics of radiation width ($\ell = 0$) and level-density parameter for even and odd target isotopes of Pd. Experimental data are indicated by points with error bars. The solid dots refer to data adopted in statistical-model calculations [8]. In the calculation of $\langle\Gamma_\gamma\rangle_0$ the systematics of a was used rather than the experimental data points.
Note: The experimental data of $\langle\Gamma_\gamma\rangle_0$ for the even-mass isotopes need to be increased (normalization problems).

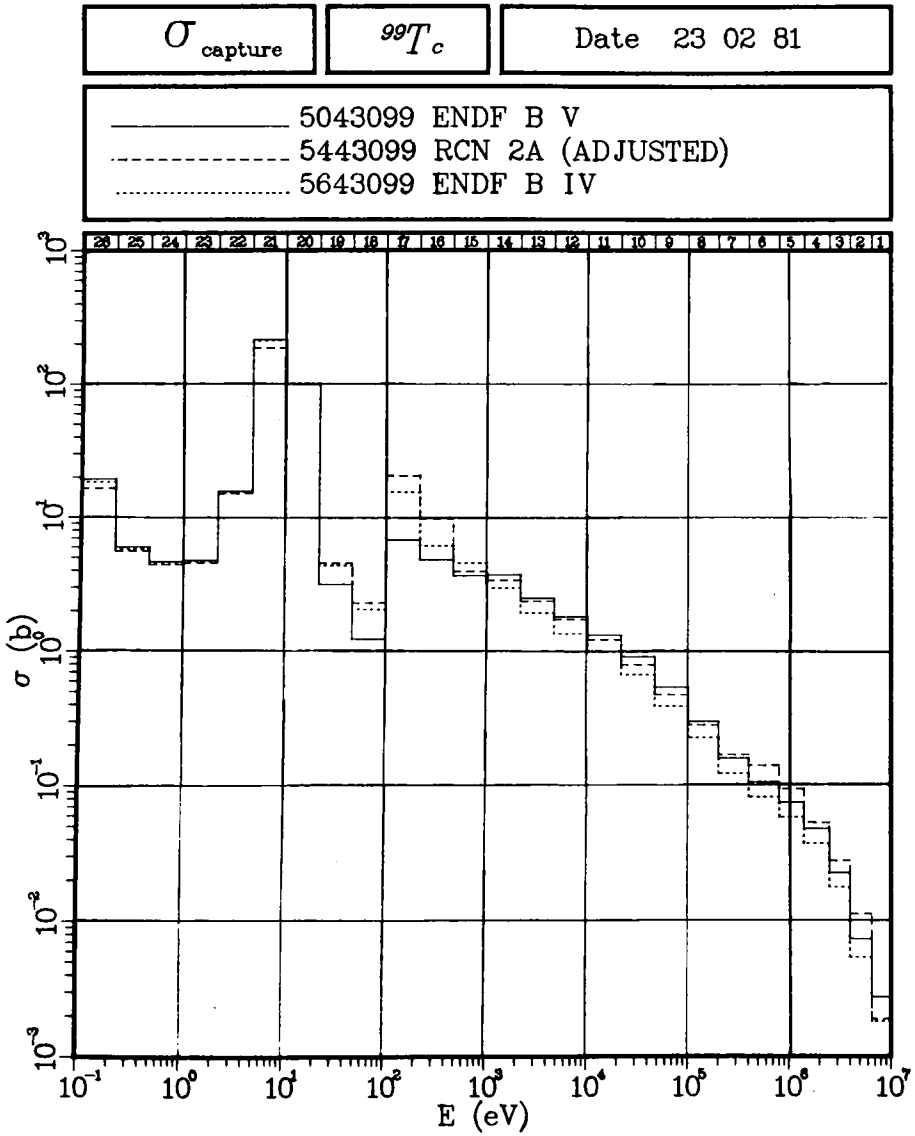

Fig. 5a. Discrepancy 20-400 keV: see text.

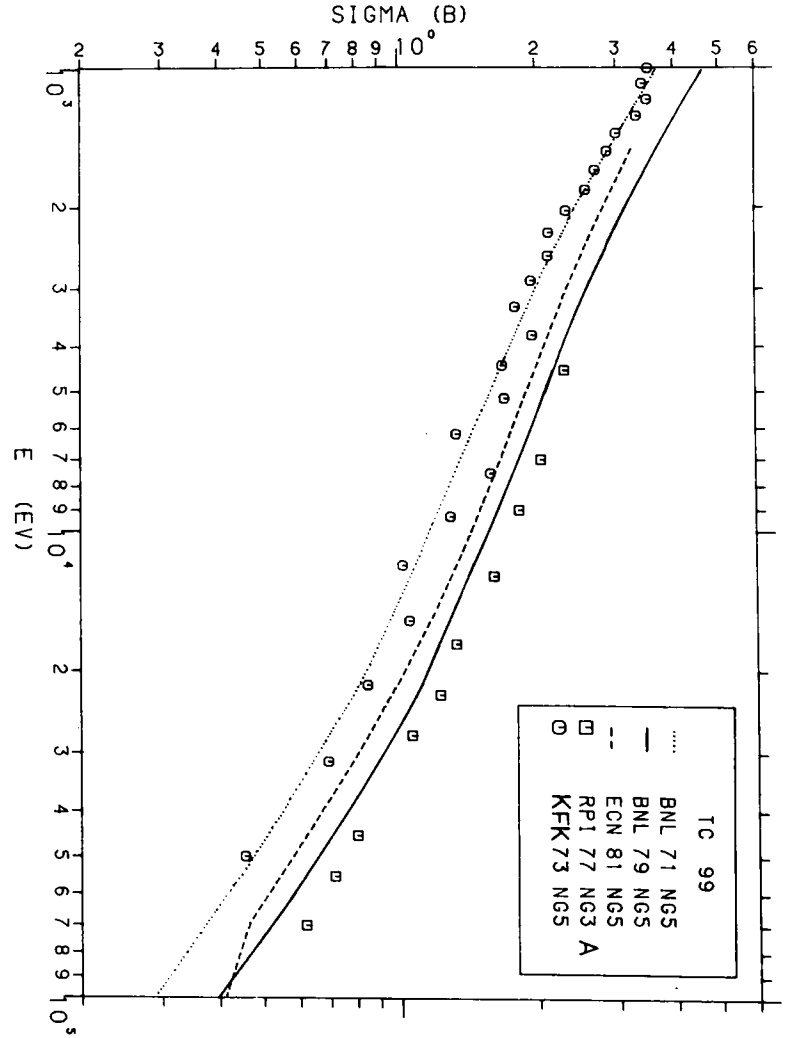

Fig. 5b. *Not plotted: ORL-82 (this meeting).*

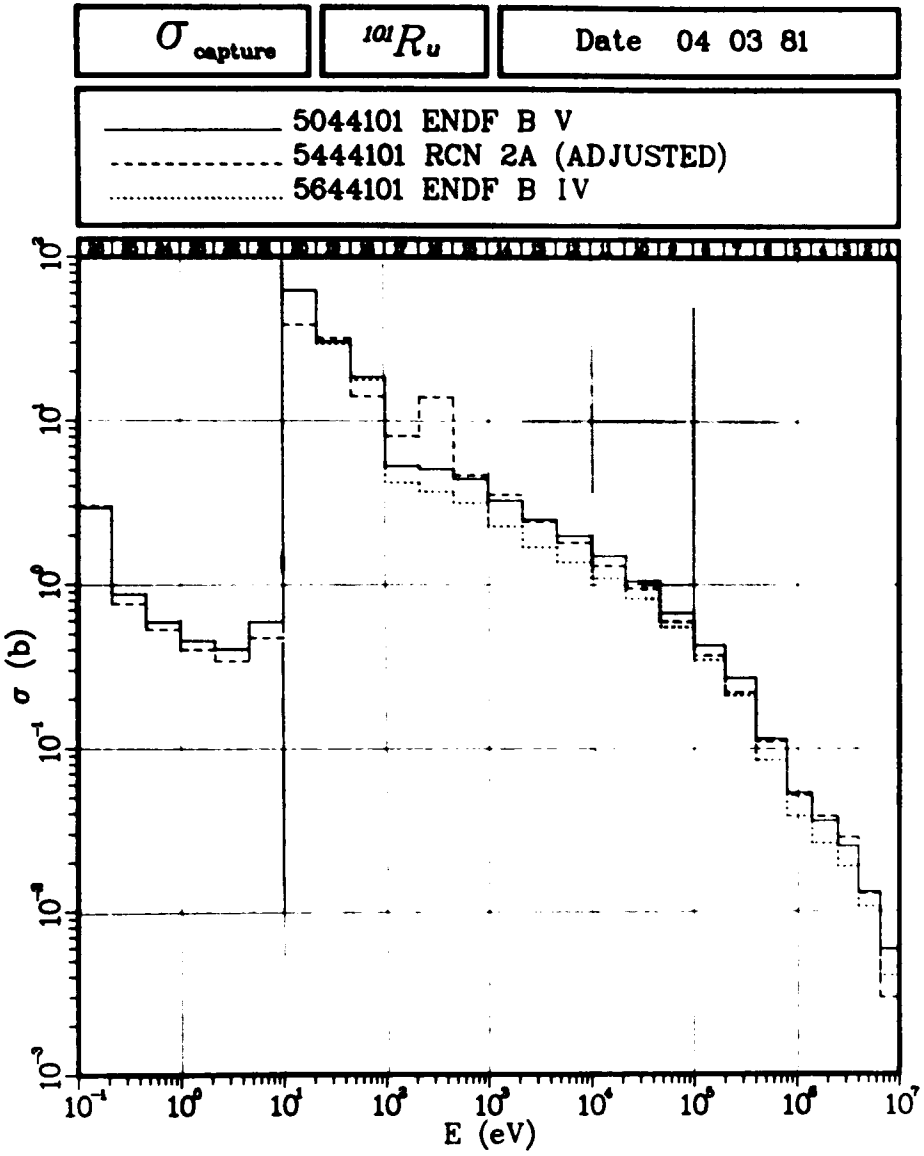

Fig. 6a. Discrepancy 100-200 keV: see text.

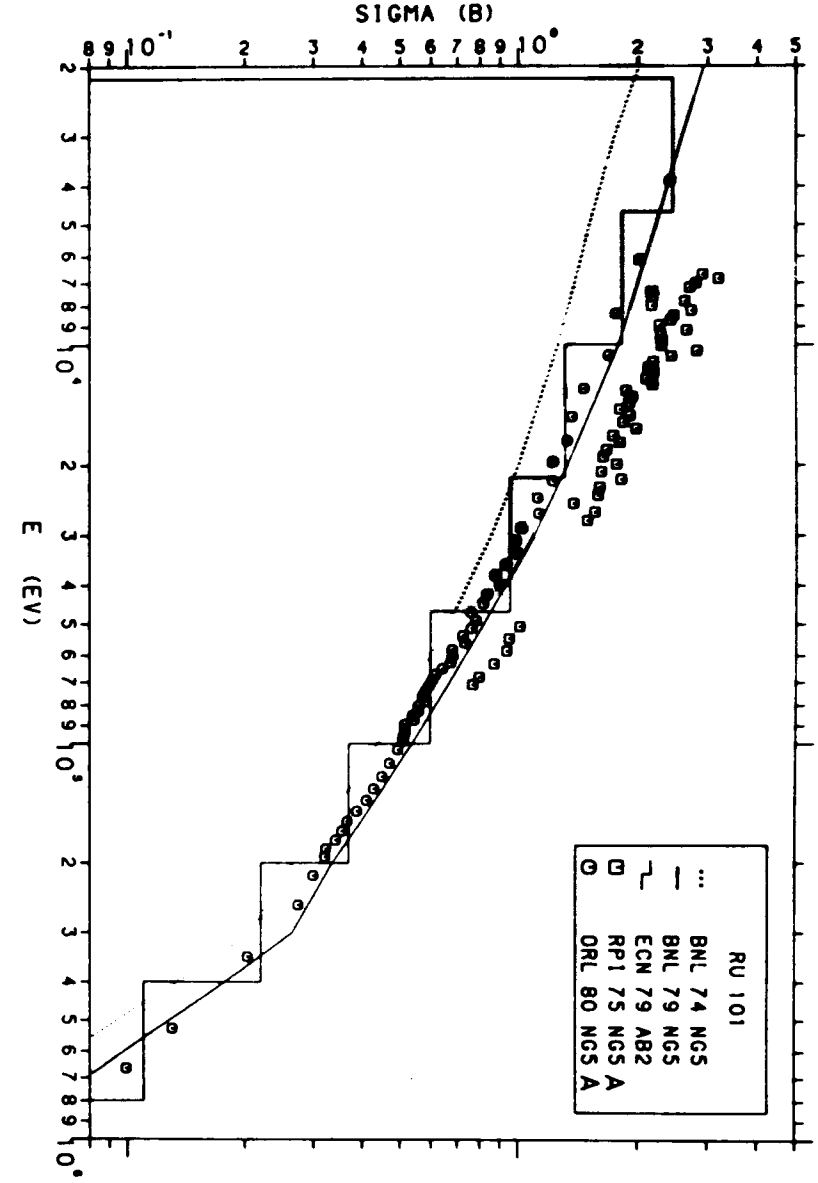

Fig. 6b. Histogram represents RCN-2A.

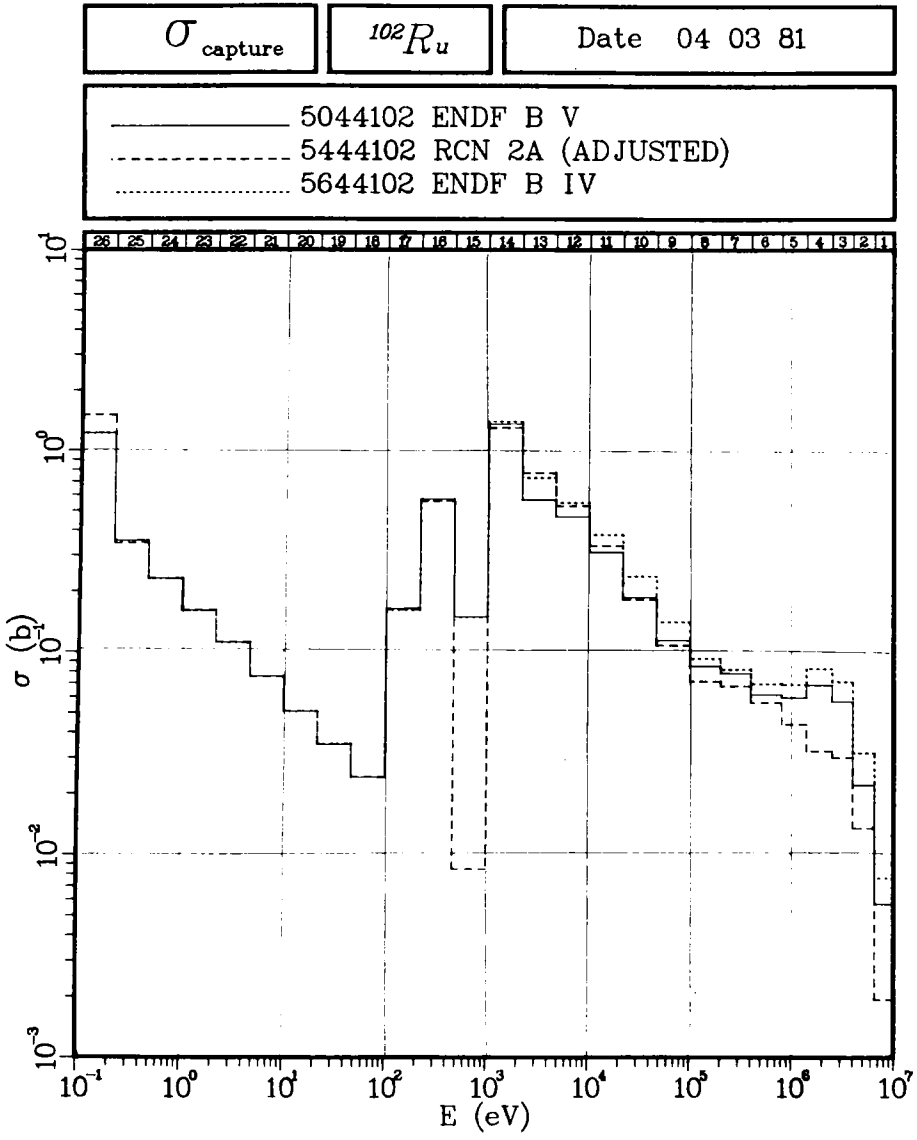

Fig. 7a. Discrepancy 0.5-1.0 keV: RCN-2A too low.

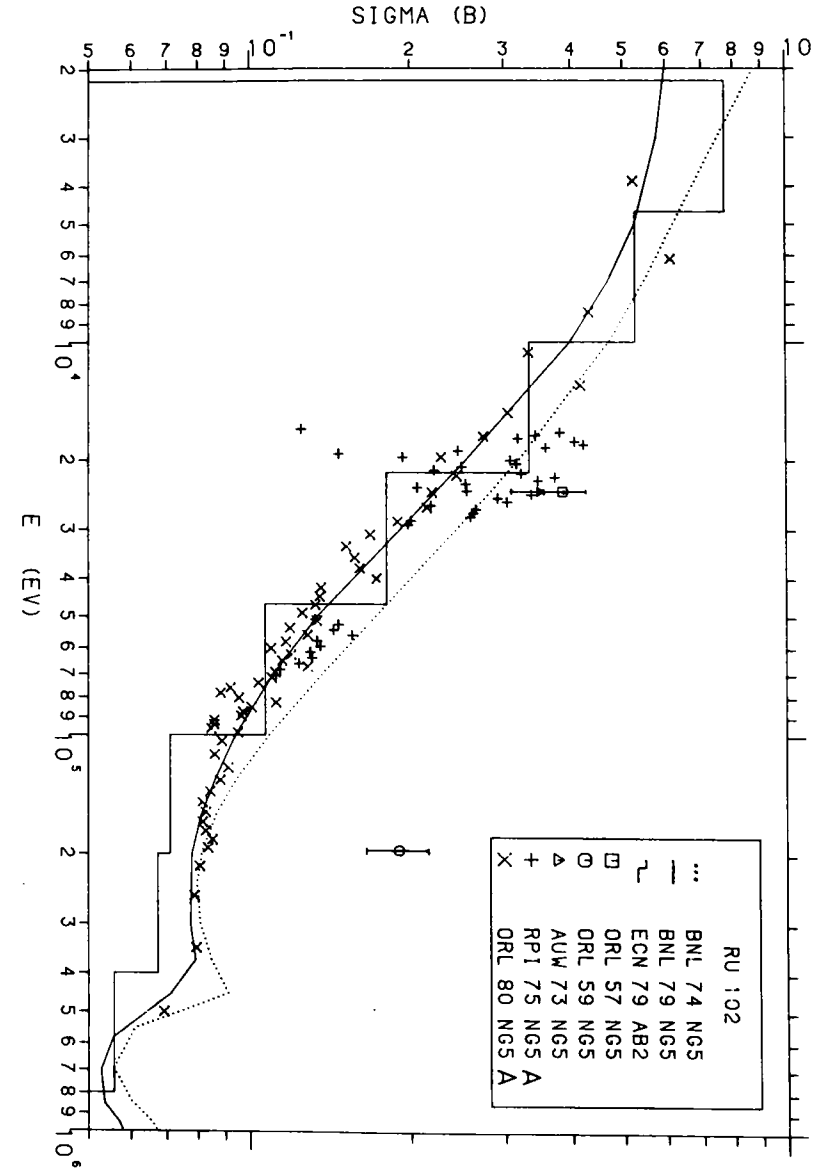

Fig. 7b. Histogram represents RCN-2A.

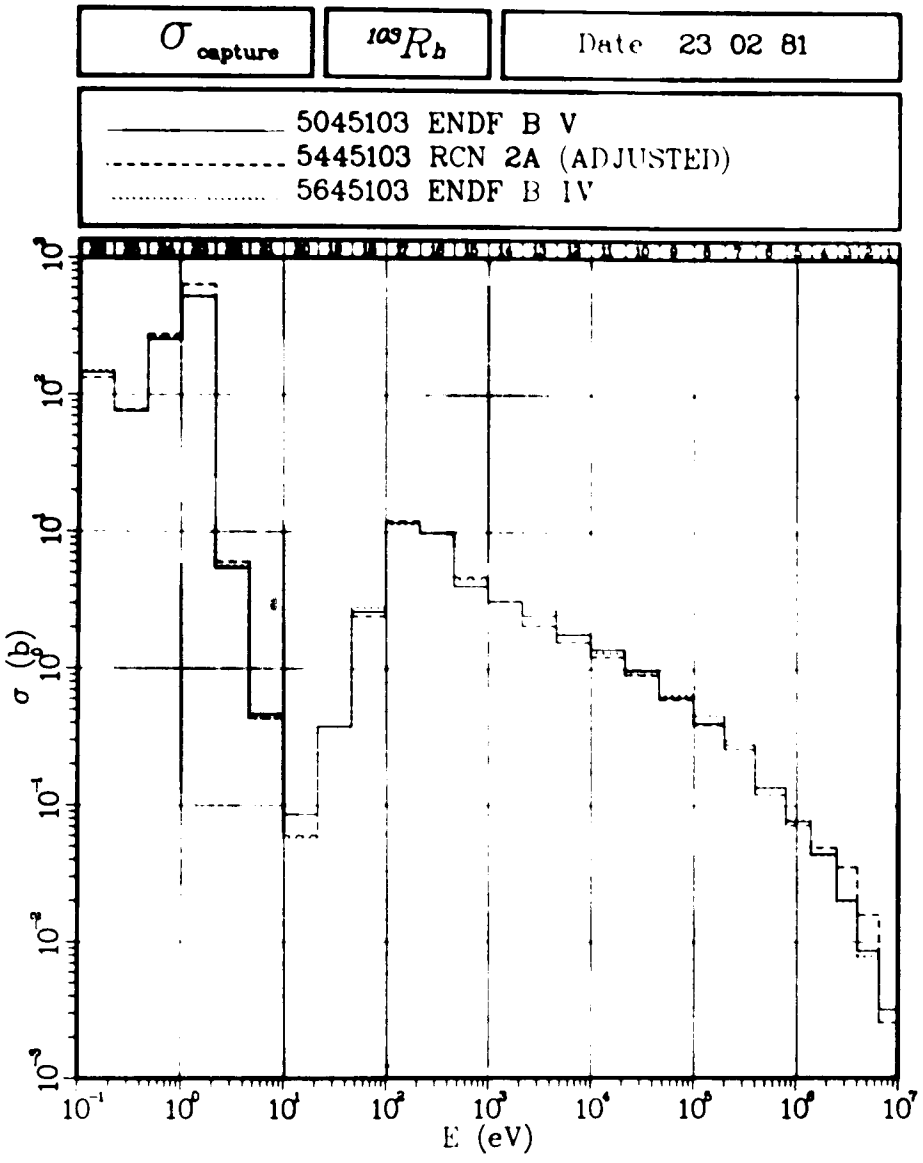

Fig. 8a. Satisfactory agreement.

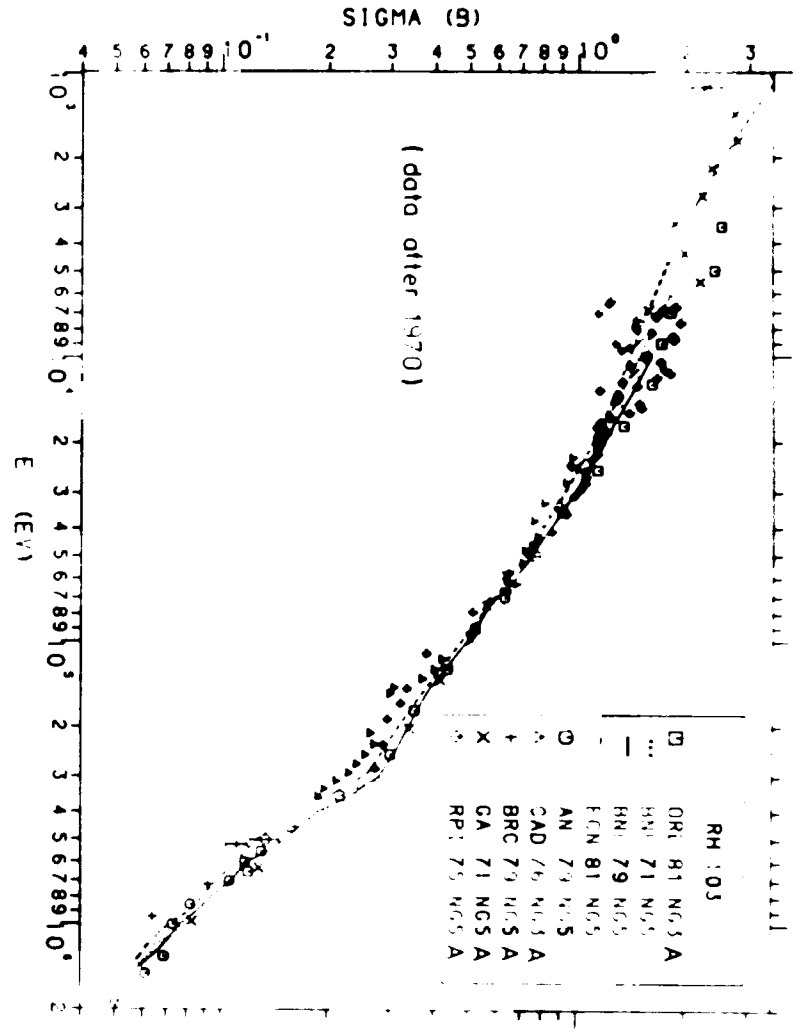

Fig. 8b. Not plotted: KFK-82 [74].

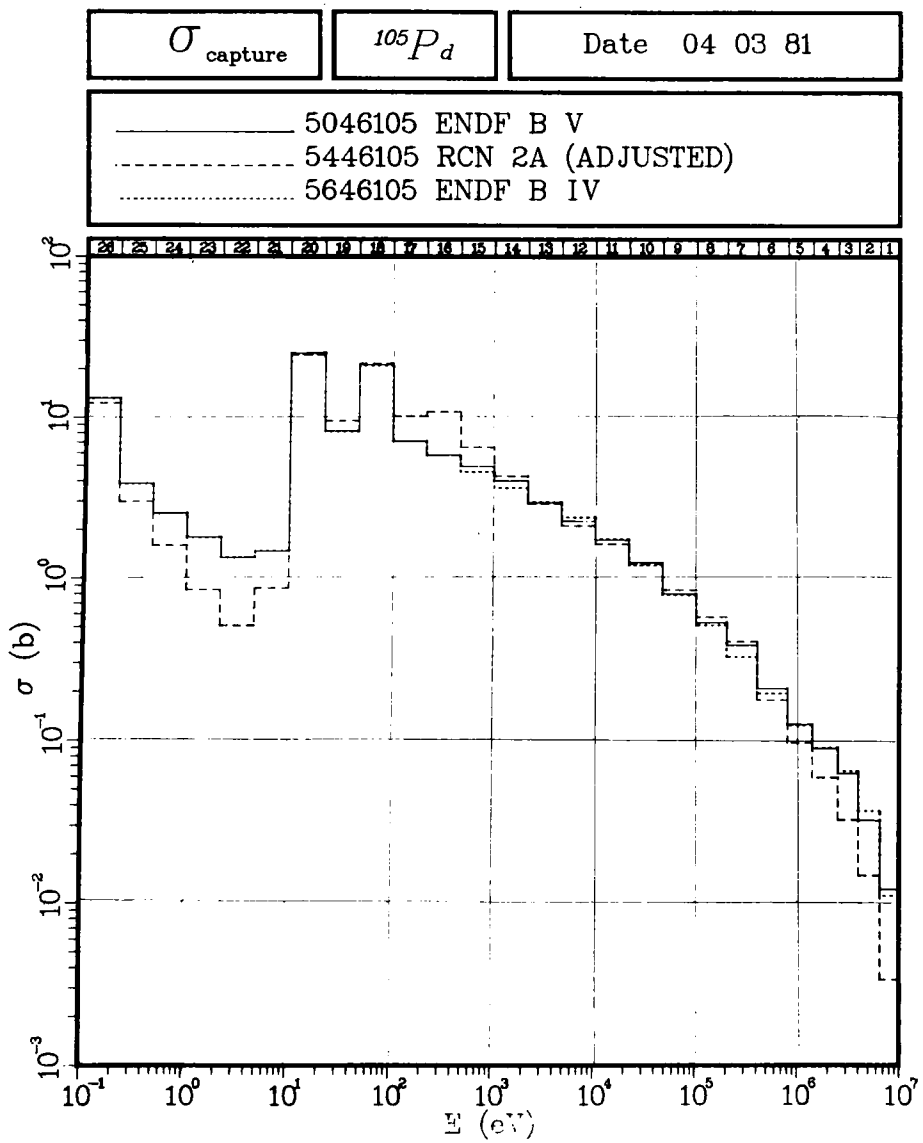

Fig. 9a. Note: RCN-3 contains recent res. pars. (GEL-79).

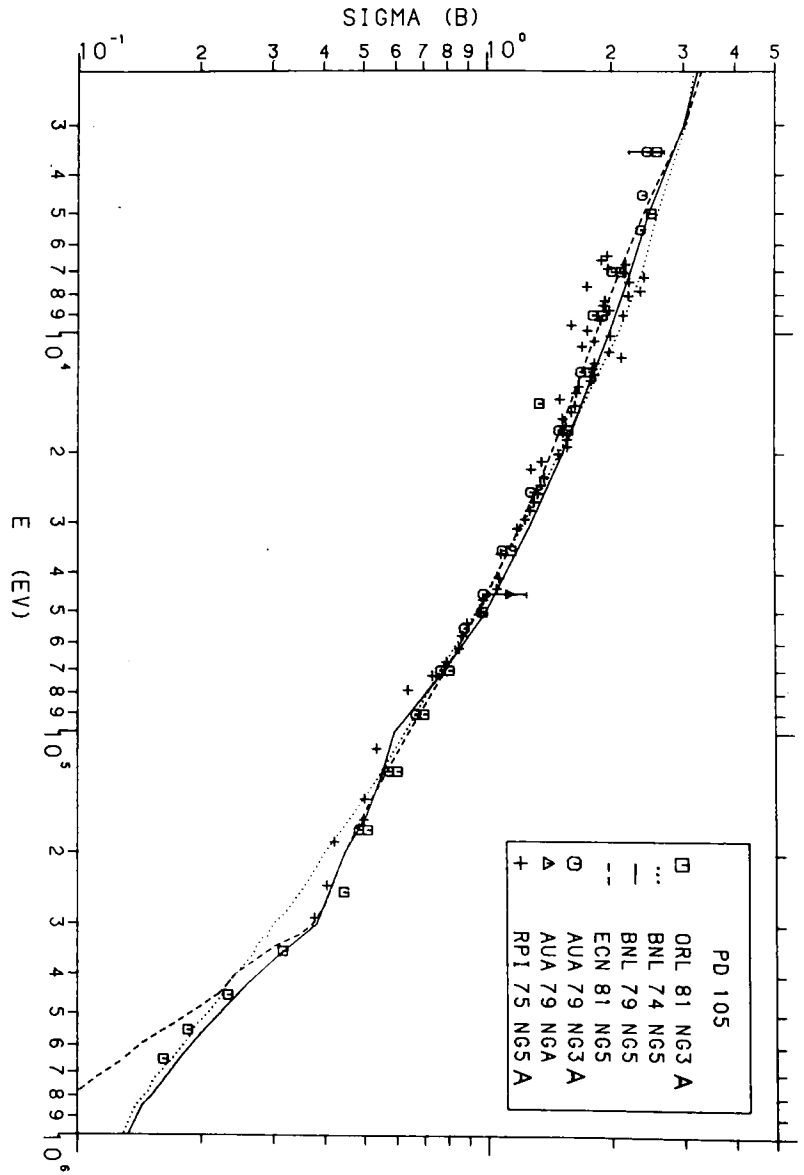

Fig. 9b. *Not plotted: GEL-82 (this meeting).*

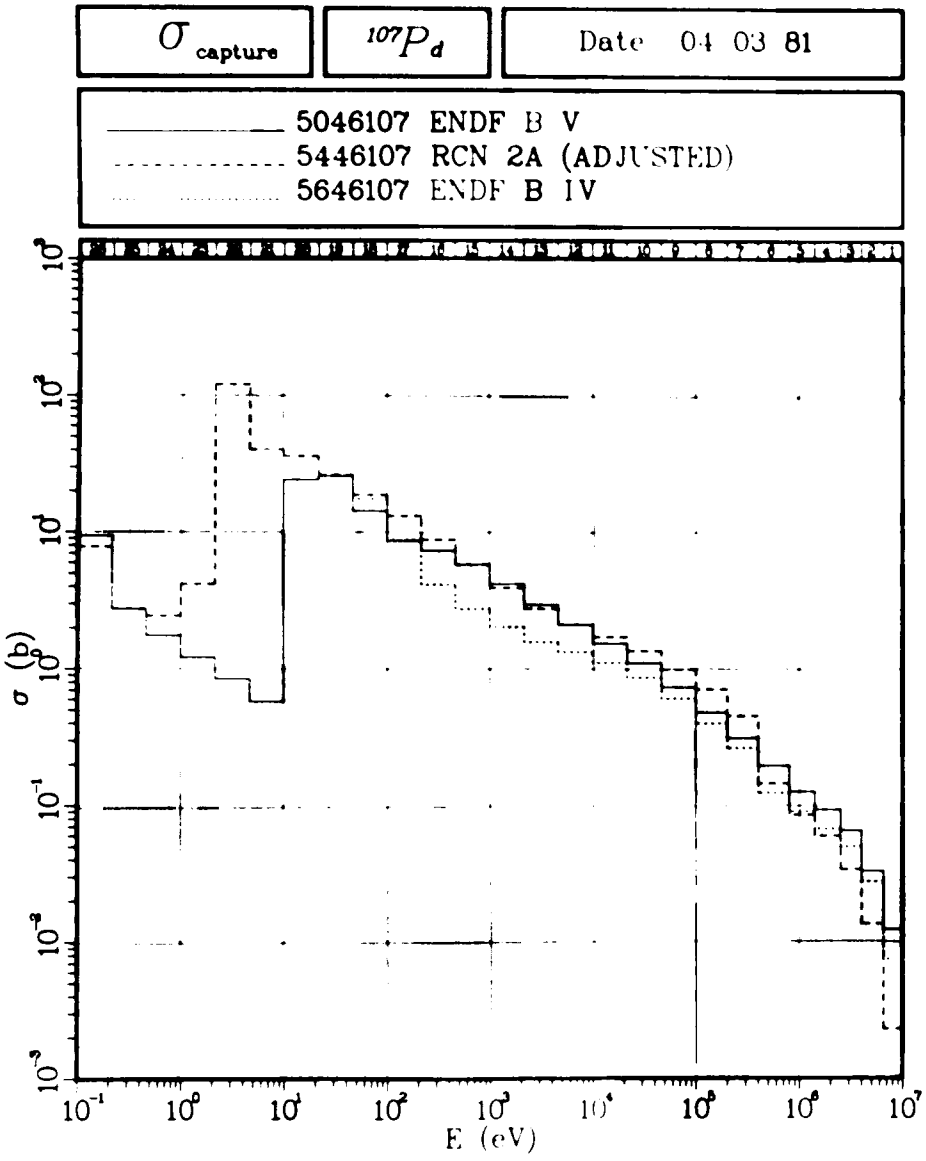

Fig. 10a. Note: RCN-3 contains recent res. pars. (RPI-78).

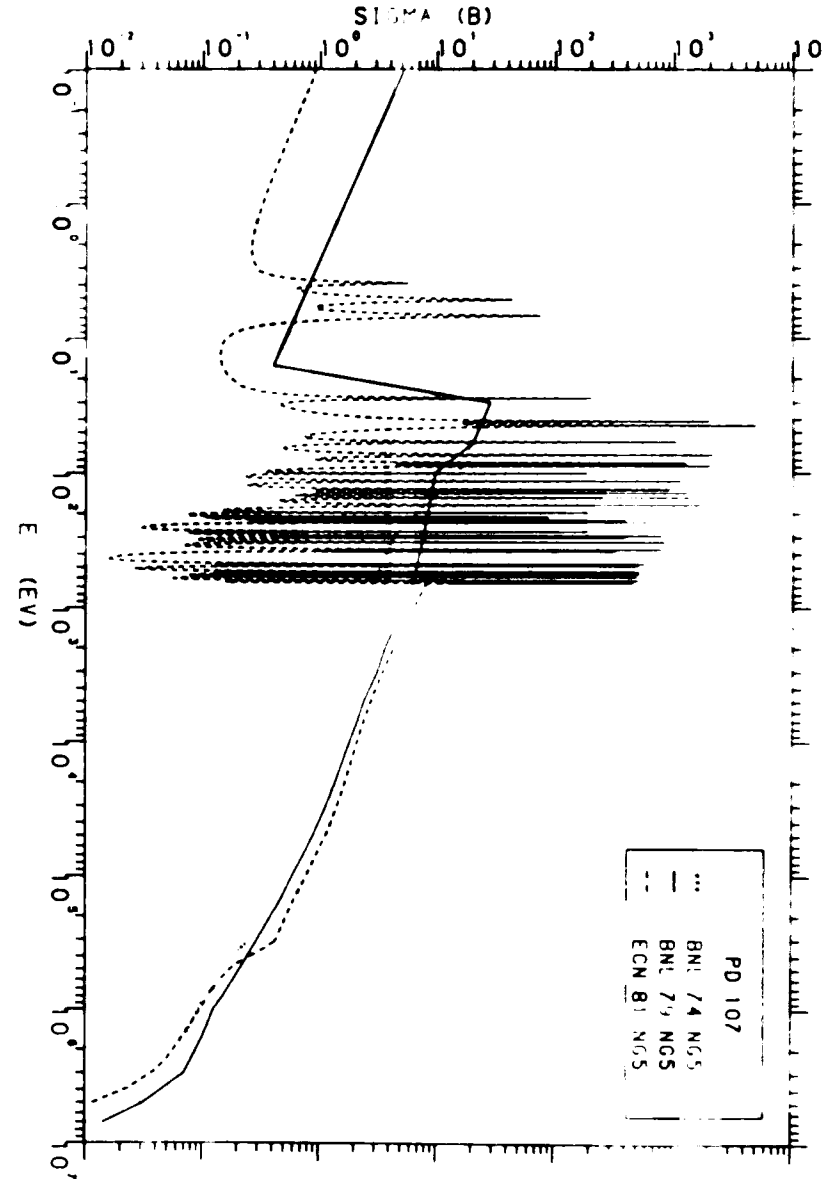

Fig. 10b. Resonance parameters: RPI-78.

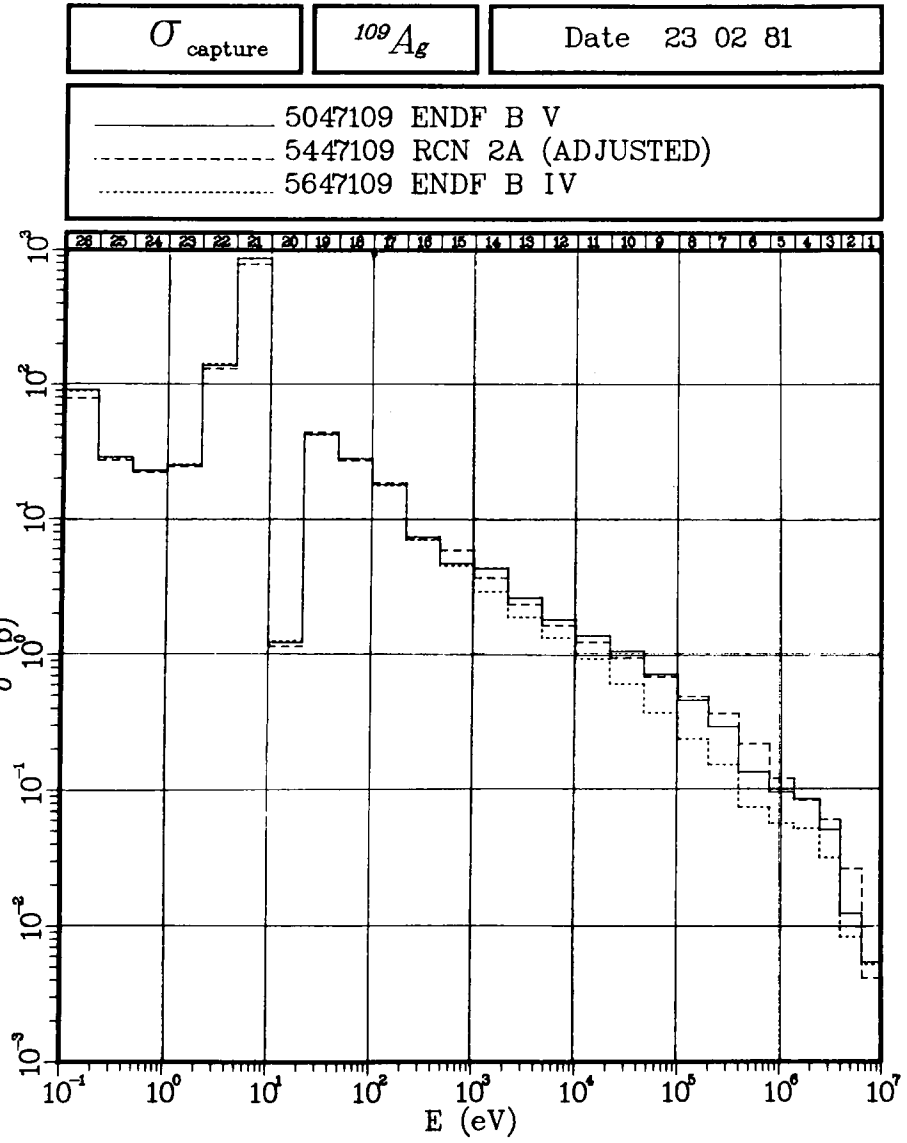

Fig. 11a. Satisfactory agreement in resonance range.

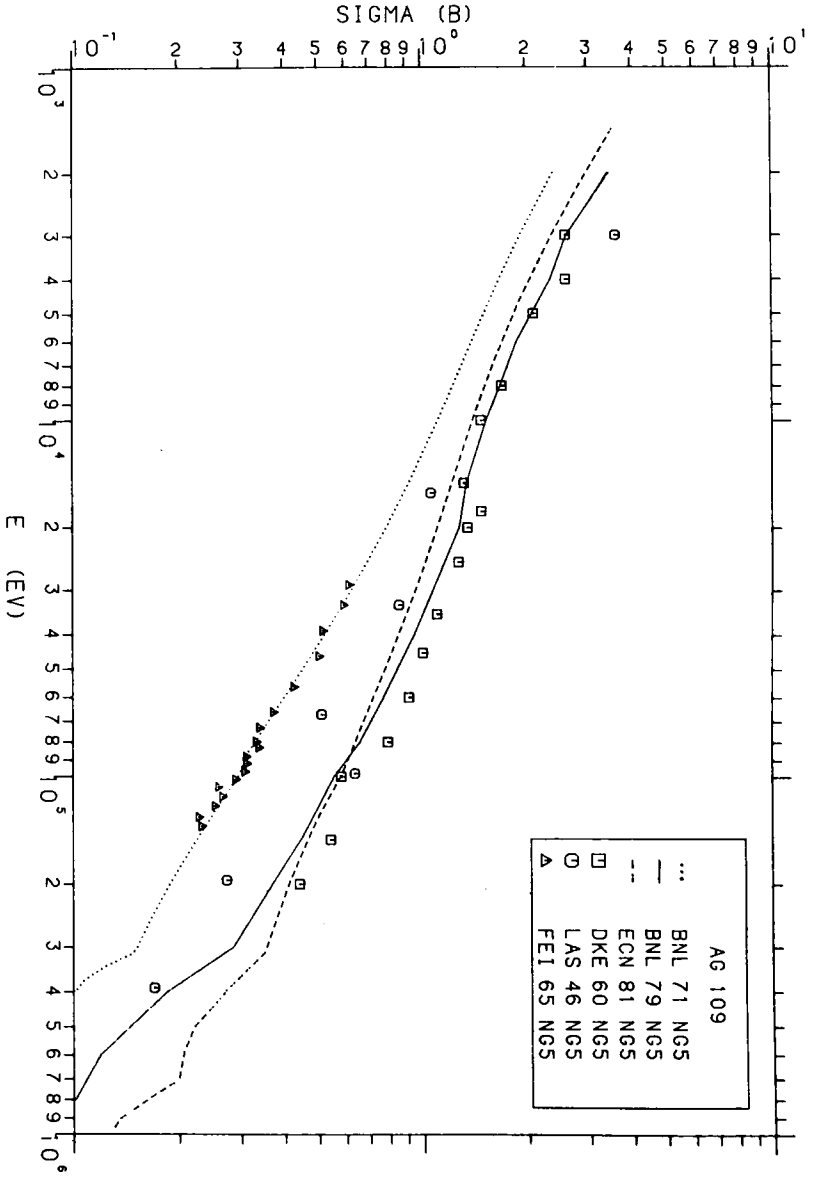

Fig. 11b. *Not plotted: ORL-82, JAE-82 (this meeting).*

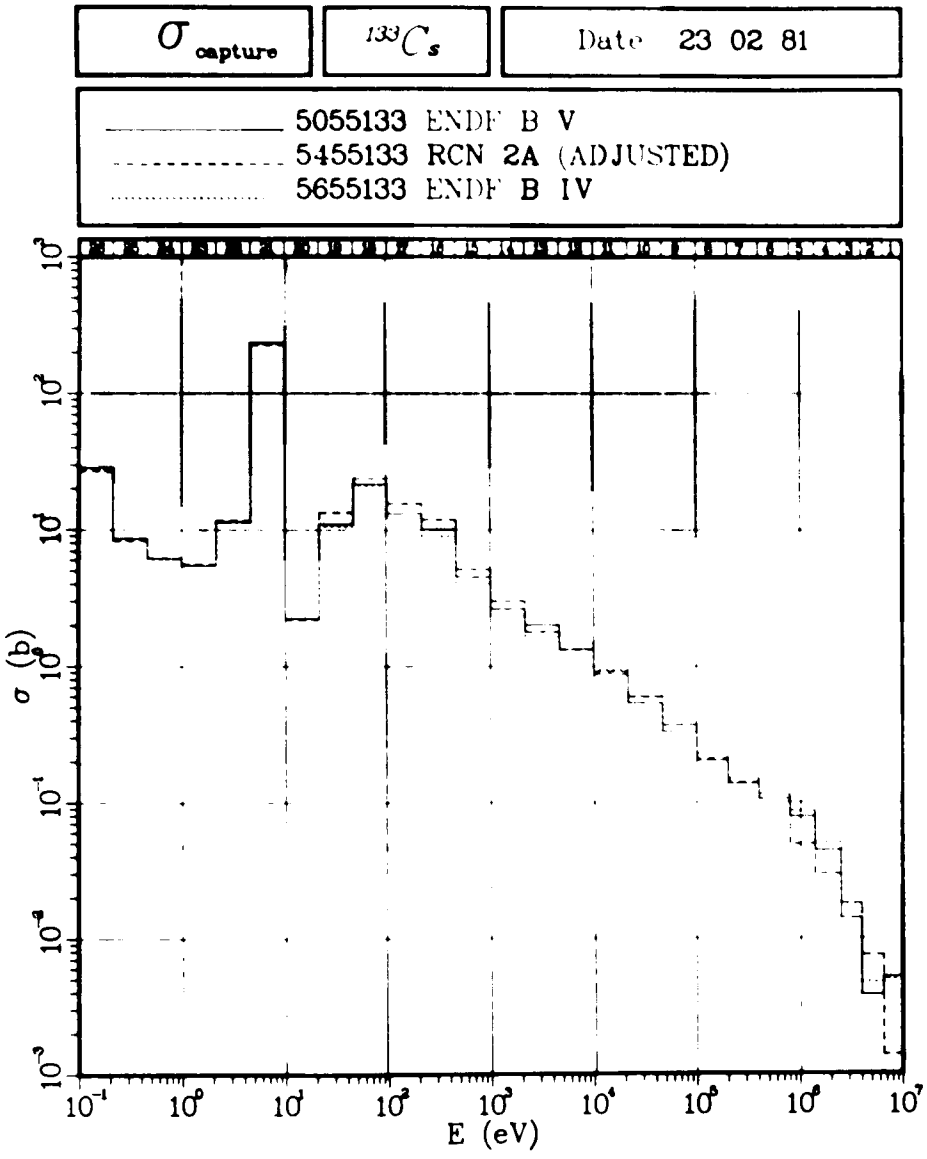

Fig. 12a. RCN-2A adjustments in resonance range.

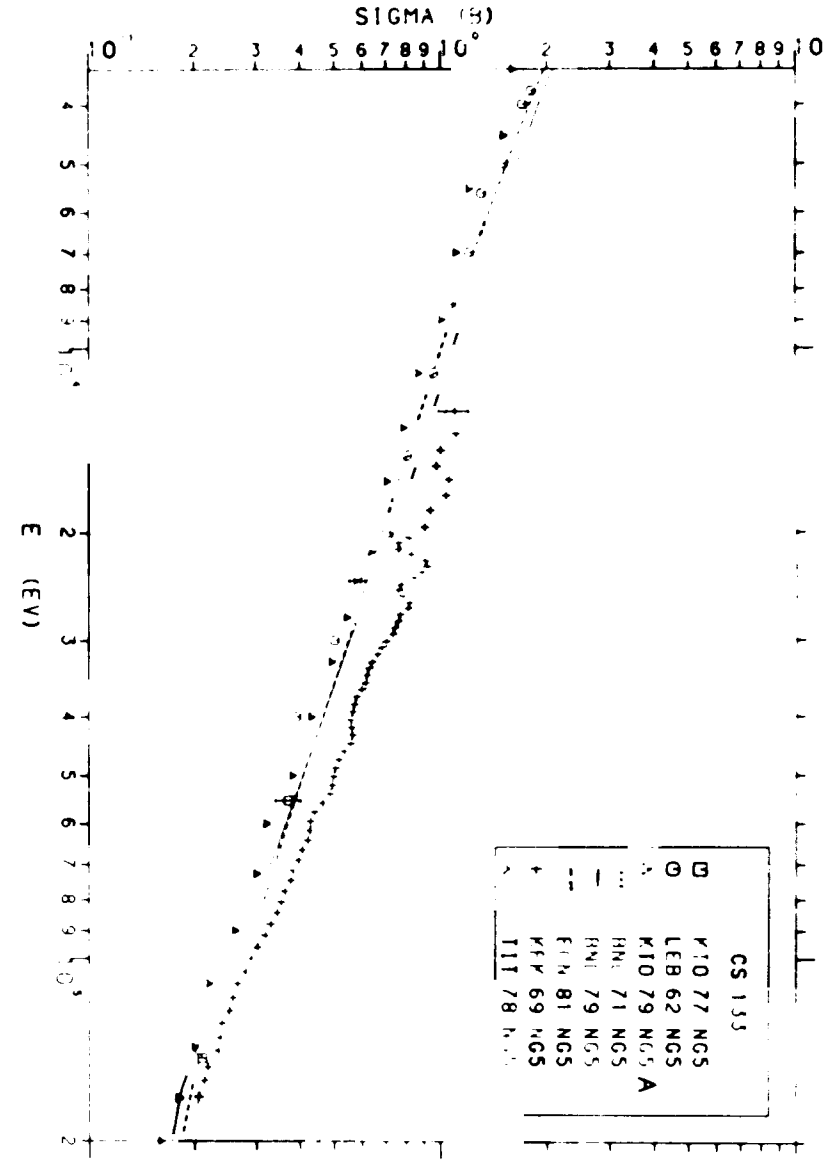

Fig. 12b. *Not plotted: ORL-82, KURRI-82 (this meeting).*

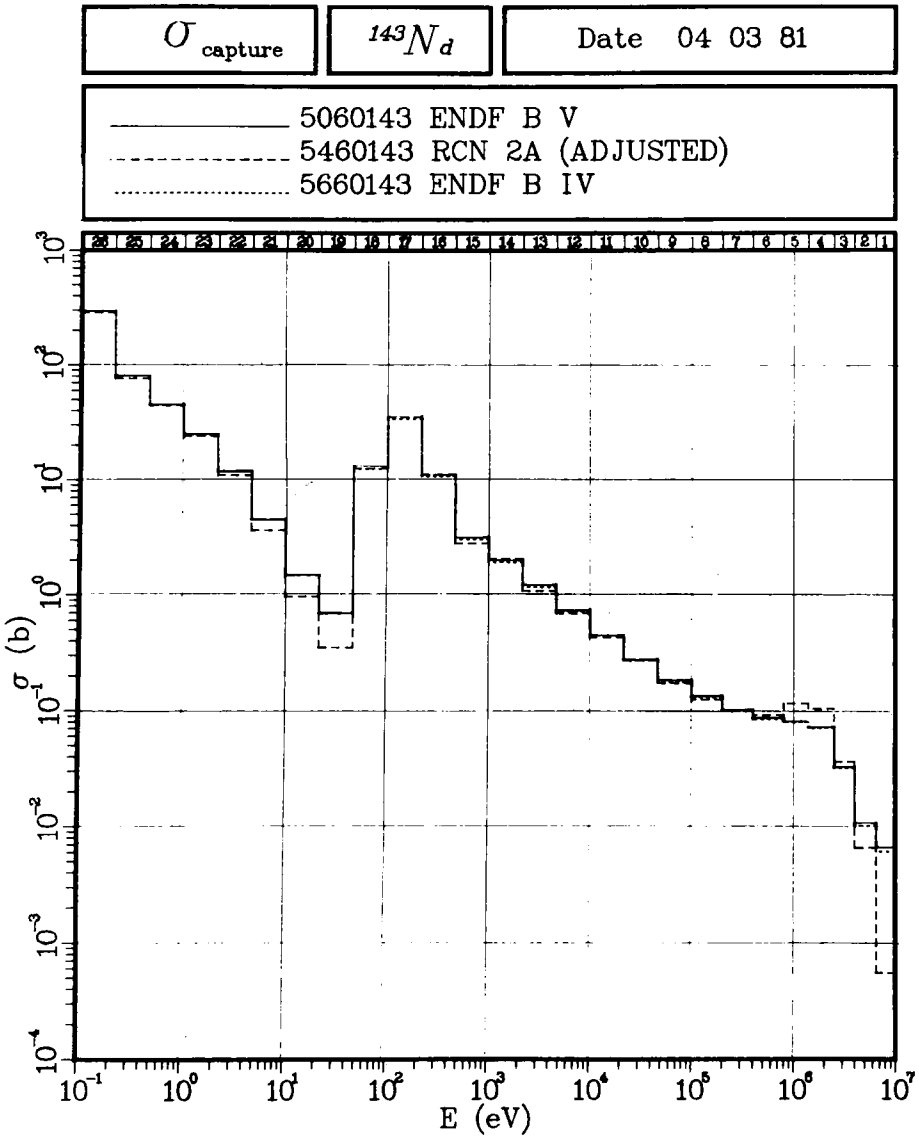

Fig. 13a. Satisfactory agreement < 0.8 MeV.

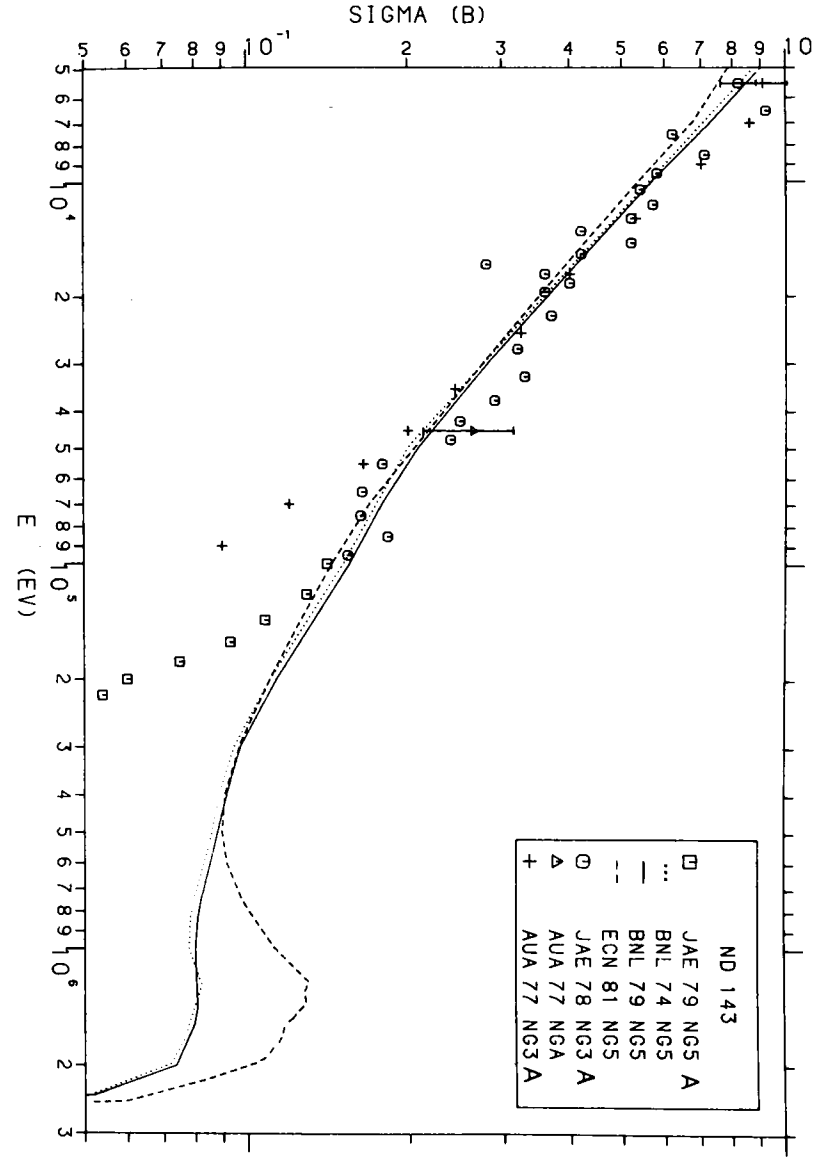

Fig. 13b. Discrepancy in level scheme data.

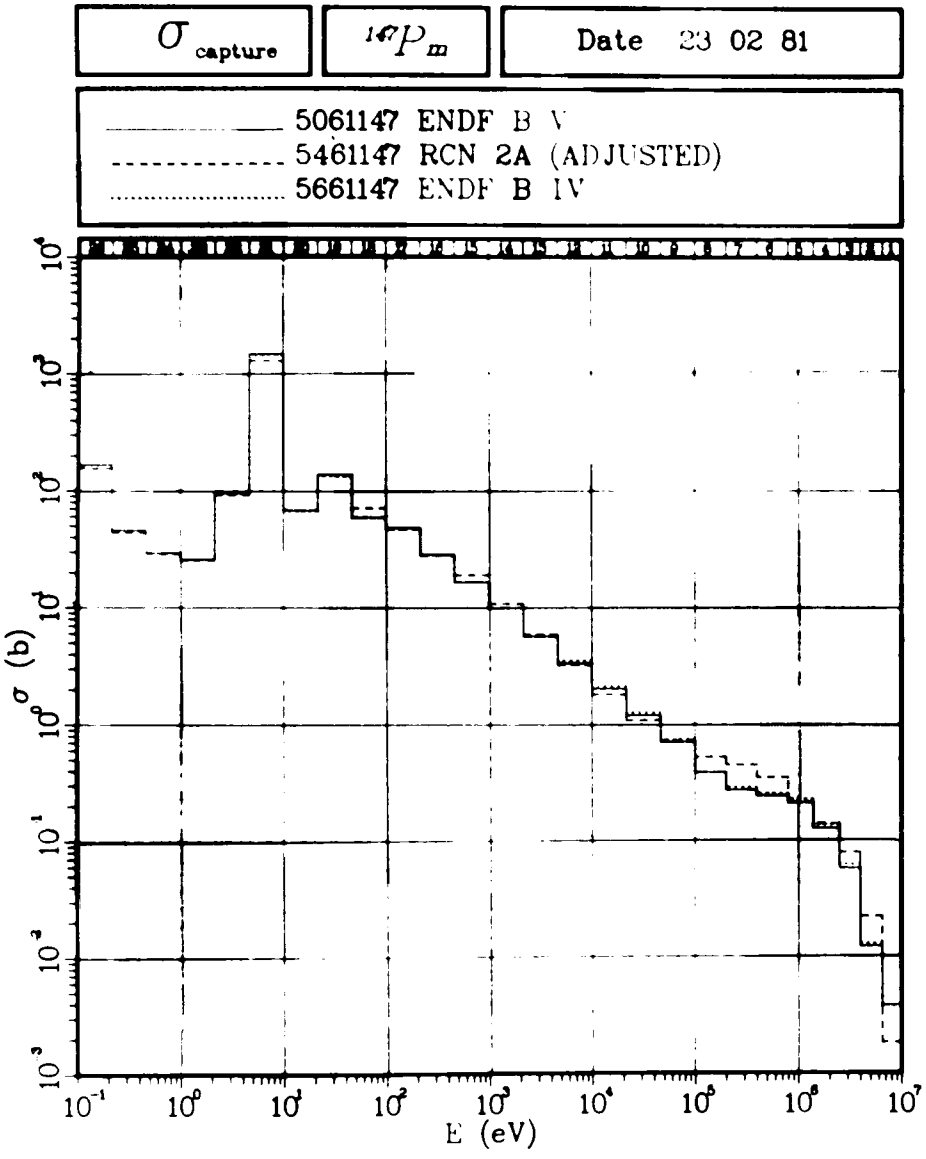

Fig. 14a. Satisfactory agreement up to 100 eV.

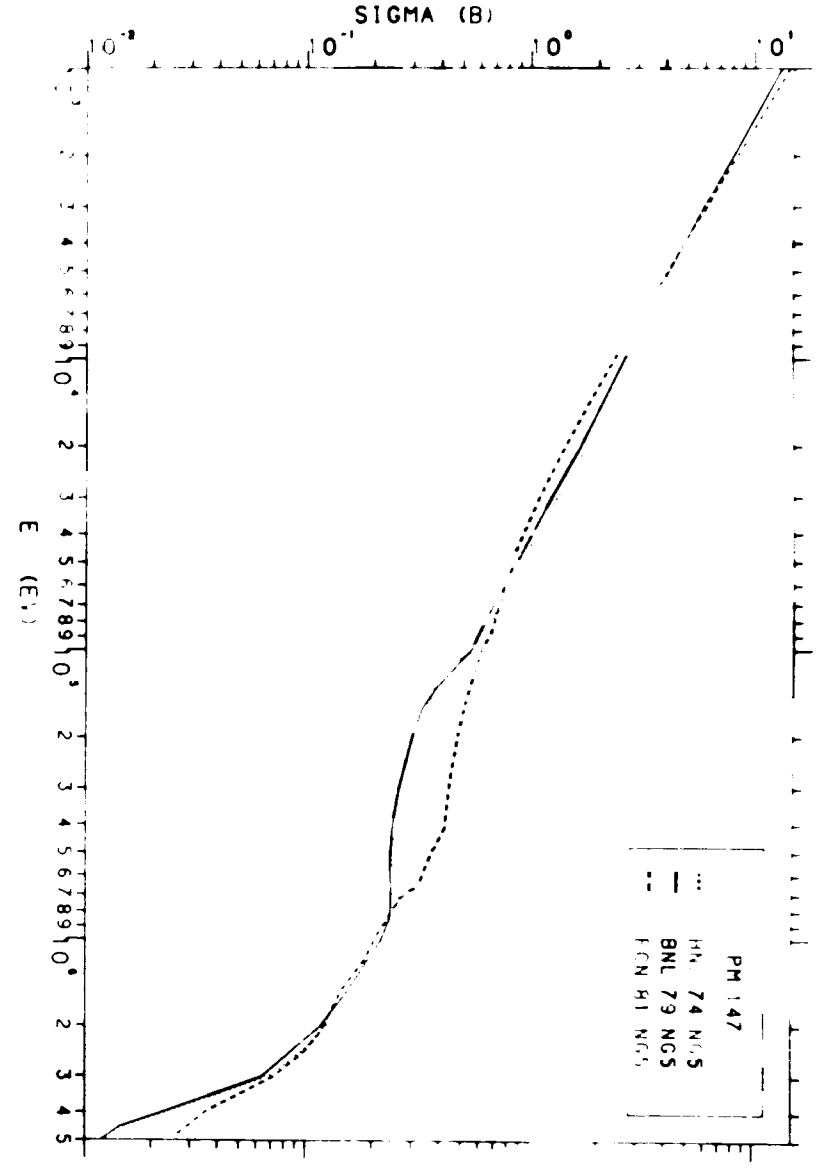

Fig. 14b. Discrepancy 100-700 keV.

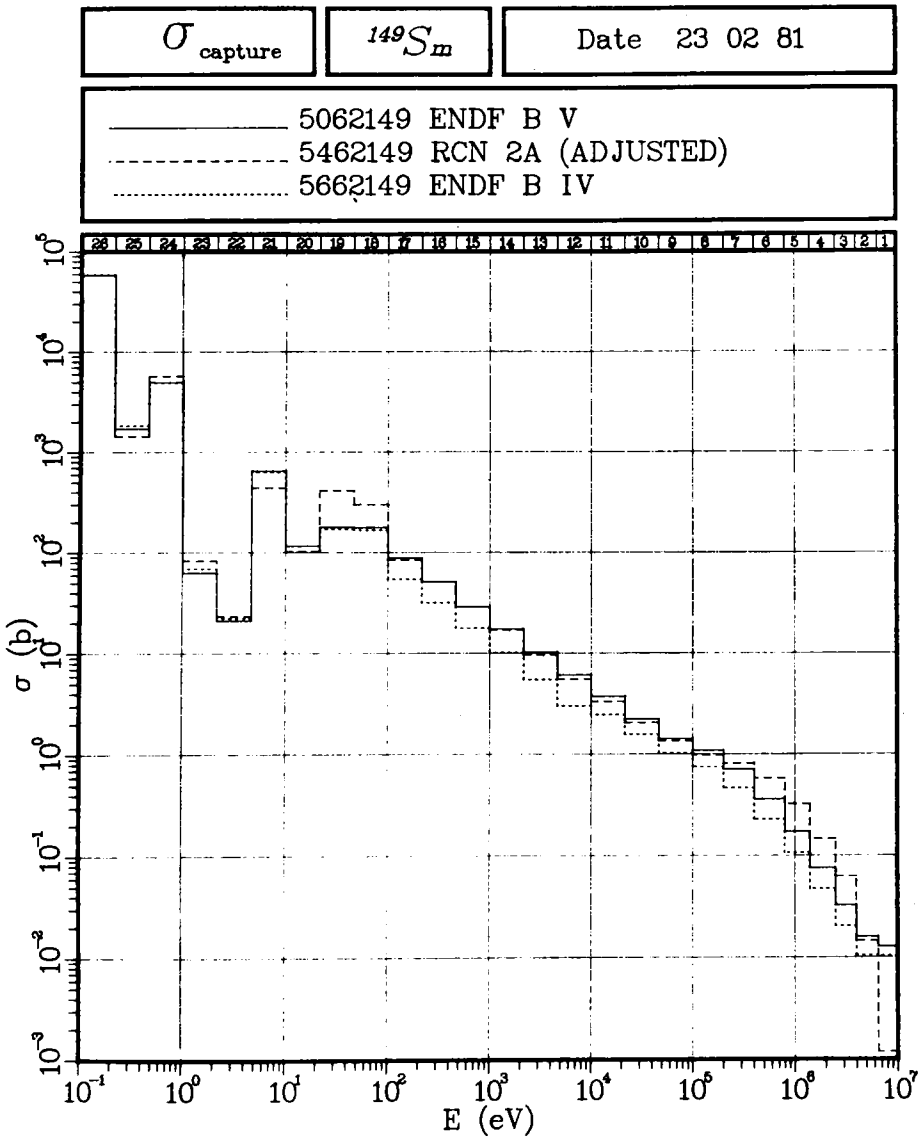

Fig. 15a. Discrepancy 20-100 eV: see text.

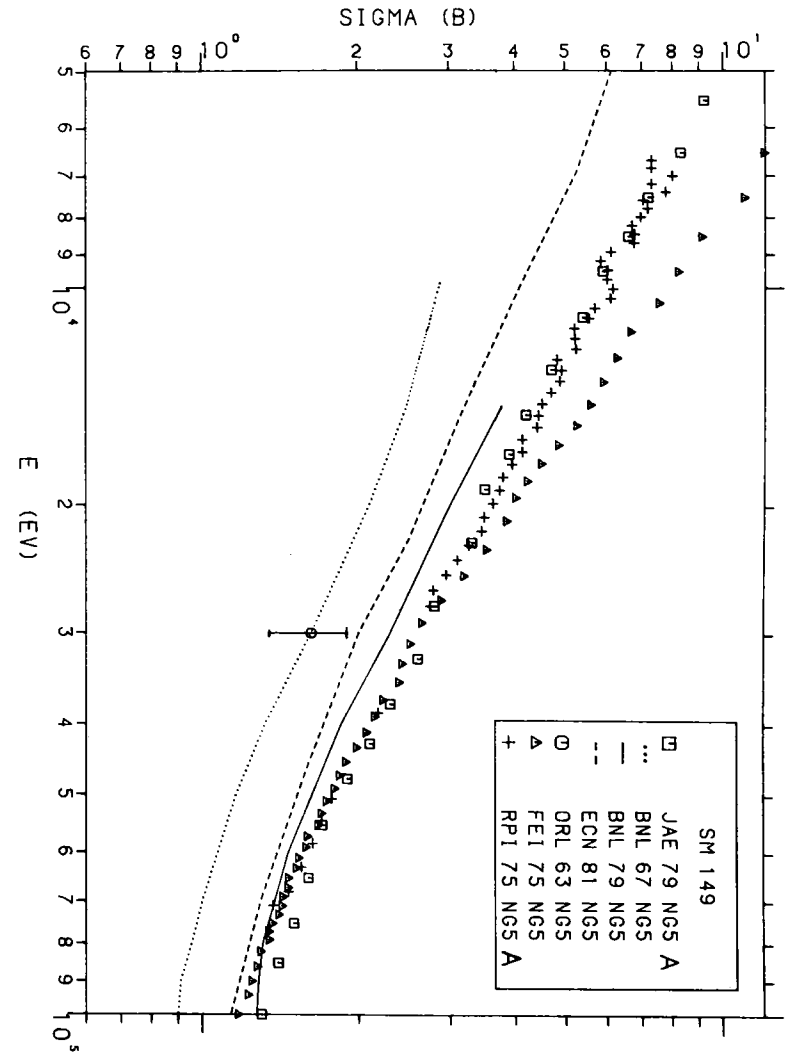

Fig. 15b. Problems at low energies.

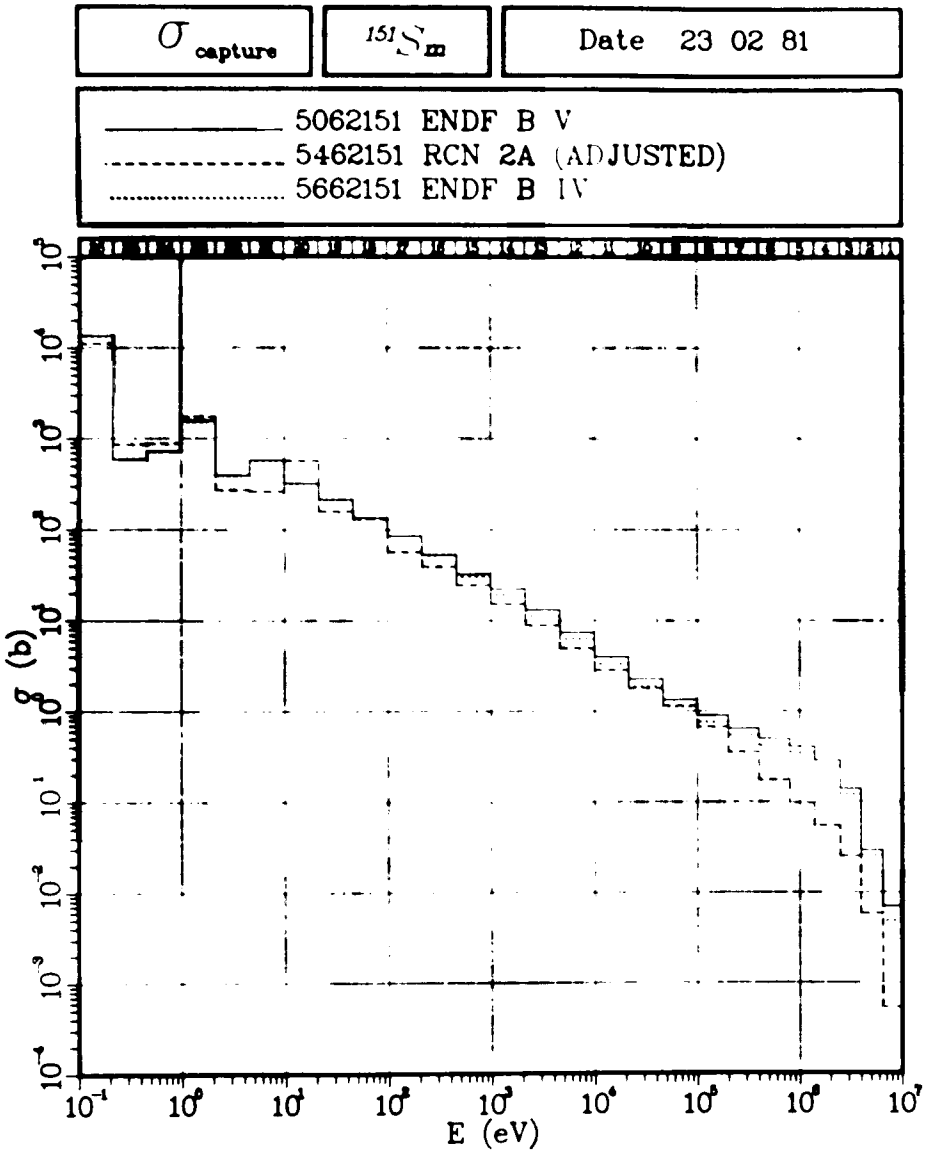

Fig. 16a. Discrepancies < 105 eV: see text.

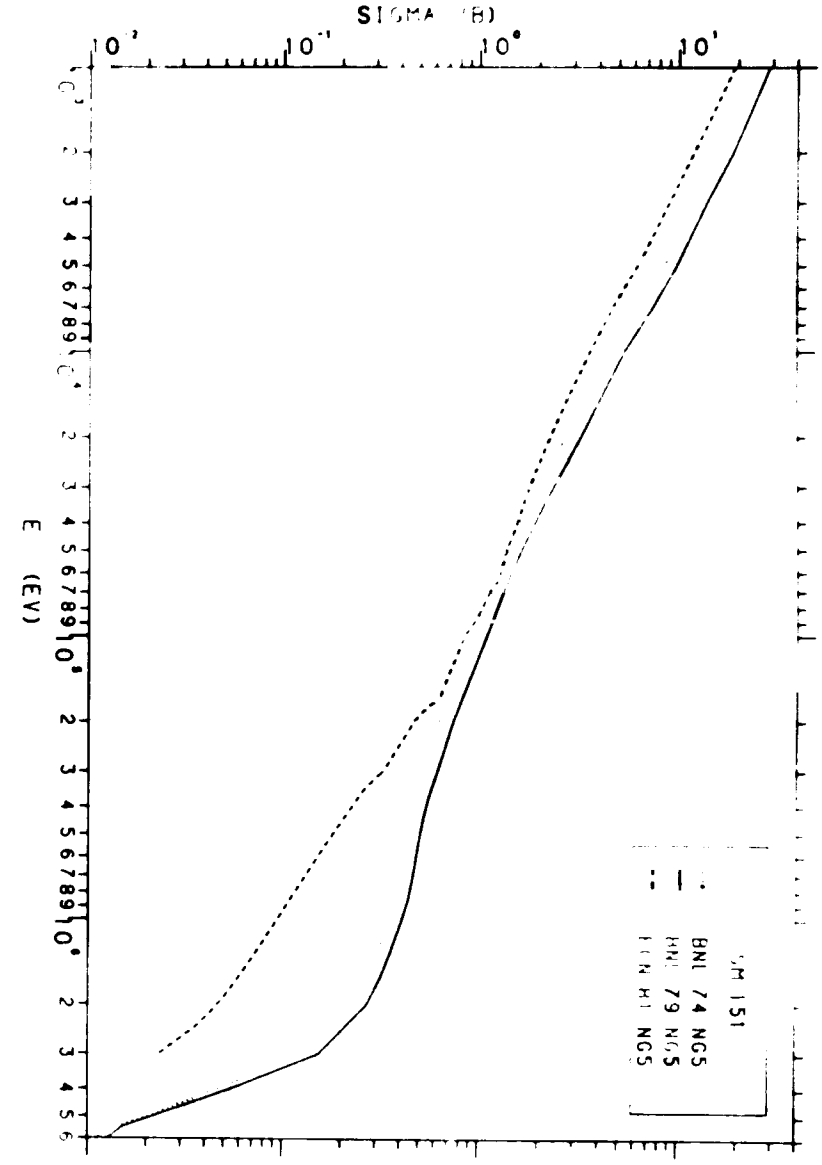

Fig. 16b. Discrepancy in level scheme data.

Discussion

QUESTION: E. Menapace
Indications from integral measurements were taken into account in FP evaluations by CNEN/CEA with reference to 21 most important nuclides for capture estimates in fast breeders. According to these indications the evaluations of 5 nuclides (the only ones in disagreement) were revised with a proper consideration of basic parameters. Do you adopt a similar approach with respect to integral data or do you adopt a fitting procedure to both differential and integral data (as made for ENDF/B-V evaluations through the FERRET code)?

ANSWER: H. Gruppelaar
We have adopted a generalized least-squares adjustment method to obtain adjusted model parameters. These parameters have been used to recalculate the fast capture cross sections (adjusted RCN-3 data library). In a few cases we have further modified the model parameters to account for results from recent differential measurements.

QUESTION: S. Mughabghab
I am pleased to find out that a measurement of the thermal capture cross section of ^{105}Pd was finally carried out. Who carried out the measurement, what is the value and its uncertainty, and, (finally) the technique? I may point out that the recommended value of "BNL-325" 4th edition is σ_γ = 20.0 ± 3.0 b which is derived from consistency considerations. In addition, I would like to make the comment that you would expect to find differences between in the s-wave radiative widths of odd and even target Pd isotopes because of differences in the neutron separation energies. The T_γ's of ^{105}Pd and ^{107}Pd are expected to be larger than those of ^{106,108,110,}Pd.

ANSWER: Dr. Corvi
The measurement of ^{105}Pd thermal capture cross section was carried out in Geel using Au(n,γ) as a standard. At the same occasion we measured σ_γ of ^{108}Pd. The data measured are in agreement with the thermal capture cross section of the natural element. The data are to be found in the 1981 Geel Progress Report.

QUESTION: G. Reffo
Did you check whether the wrong A-dependence of $\langle\Gamma_\gamma\rangle$ you mentioned in Pd could not in part be due to wrong deformation parameters on which giant resonance parameters depend and which might bring in a wrong mass dependence.

ANSWER: H. Gruppelaar
In our calculations only a single giant-dipole resonance peak has been assumed. I don't think that the use of your recent systematics (using two giant dipole peaks, depending upon the deformation) will explain the observed odd-even effect in $\langle\Gamma_\gamma\rangle$.

COMMENT: S. Mughabghab
You would expect that the Γ_γ of the odd isotopes to be higher than for the even isotopes because you have a higher excitation energy.

COMMENT: H. Gruppelaar
That is an important effect. The binding energy is different.

COMMENT: S. Mughabghab
For ^{105}Pd it is 7-8 MeV, for the even isotopes it is ~ 5.8 MeV.

INTEGRAL MEASUREMENTS AND TESTS OF FISSION-PRODUCT NEUTRON CAPTURE CROSS SECTIONS*

by

R. A. Anderl

EG&G Idaho, Inc.
Idaho National Engineering Laboratory
Idaho Falls, Idaho 83415

Abstract

This paper reviews the current status of measured integral data for fission-product fast-neutron capture and the application of those integral measurements for cross-section testing. The various types of integral experiments are described and an assessment is made of the utility of the measured data for testing cross sections. Although the integral data base is surveyed as completely as possible, specific emphasis is given to those integral data which have been published since the 1979 Bologna specialist's meeting on fission-product nuclei. As a second thrust of this paper, the utilization of measured integral data for cross-section adjustment and for conventional C/E testing is discussed. Specifically, the role of measured integral data for the ENDF/B-V evaluation of fission-product capture cross sections is addressed. A detailed discussion is presented of a study made to assess the consistency of the ENDF/B-V cross sections and the measured integral data from experiments in the Coupled Fast Reactivity Measurements Facility (CFRMF) and in the Experimental Breeder Reactor-II (EBR-II). We conclude the paper with a summary of the outstanding integral test discrepancies and point out the areas for improving consistency between integral data and evaluated cross sections.

I. INTRODUCTION

Over the past 12 years a significant effort has been made to improve the accuracy of fast-neutron capture cross sections for fission-product nuclides. The primary motivation for this effort was to improve the

* Work performed under the auspices of the USDOE under DOE Contract No. DE-AC07-76ID01570.

accuracy for prediction of fission-product absorption effects in fast reactor systems. Fission-product absorption affects both burnup and reactivity for fast reactors and, as such, impacts the economics considerations for reactor and fuel cycle design. For this reason, a design target accuracy of ± 10% has been suggested for prediction of global fission-product absorption[1,2,3]. This requirement translates into a ± 10% accuracy on bulk fission-product spectrum-averaged cross sections and, because of possible systematic effects, places a requirement of ± 10% accuracy on spectrum-averaged cross sections for important individual fission products[3]. More recently, design target accuracy requirements of ± 7%[4] and ± 5%[5] have been recommended for global fission-product absorption.

Integral measurements for individual fission-product samples in fast neutron fields have provided an important data base for use in the evaluation of the fission-product capture cross sections with the expressed purpose of meeting the above design target accuracy requirement. Key integral measurement programs are identified in Table 1. Comprehensive reviews of these measurements have been made by Bustraan[6,7], Langlet and Martin-Deidier[8], and Harker and Anderl[9]. The impact of integral measurements on cross-section evaluations has been reviewed by Gruppelaar and Dekker[10]. A comparison of fission-product capture cross-section evaluations that have incorporated integral data has been made by Gruppelaar et. al[11]. This latter work demonstrated the importance of including the integral measurements in the preparation of fast-reactor-design cross-section libraries if the design target accuracy for global fission-product absorption is to be met.

The present paper is an extension of the above review papers concerning integral measurements and their application to cross-section evaluation. The purpose of this paper is two fold: (1) to review the current status of the integral data base, with an emphasis on highlighting the integral data reported since the Bologna fission-product meeting in 1979, (2) to discuss the role of integral data in the cross-section evaluation process, with an emphasis on integral testing for ENDF/B-V fission-product capture cross sections. In Section II of this paper, a general review of integral measurements is given. This includes a discussion of various measurement techniques, a description of the measurement programs which have generated the integral data base and an identification of the measured integral data for the 50 most important fission-product nuclides in a fast reactor. The applications of integral data to cross-section evaluation are reviewed in Section III. The discussion treats integral tests and cross-section adjustment applications. Principal results of an integral testing study for ENDF/B-V fission-product capture cross sections are presented in Section IV. Finally, in Section V we conclude with a summary of the status of integral capture measurements for fission-products and an identification of integral test discrepancies which point out areas for future work.

II. REVIEW OF INTEGRAL MEASUREMENTS

A. Measurement Techniques

In general, the integral data used for fast capture cross-section evaluation purposes are capture reactivity worths derived from reactivity worth

measurements and integral capture cross sections derived from measurements of the integral capture rates using activation or transmutation techniques. Each of these techniques will be discussed in the following paragraphs with an emphasis on those unique features which differentiate the three approaches and which impact their utilization for improving the capture cross-section data base.

1. Reactivity Worth Measurements

In measurements utilizing reactivity techniques, the sample is placed in a critical assembly and the reactivity effect due to introduction of the sample is measured. The reactivity effect is typically deduced in one of two ways: (1) from the time behavior of the neutron flux (inverse kinetic method) as the sample is oscillated through the core, (2) by balancing the reactivity effect of the sample by a small control member (auto-rod technique) which is calibrated by a kinetic measurement[6]. According to first order perturbation theory, the reactivity effect of a nonfissionable sample is composed of absorption and scattering contributions and is represented by

$$\rho = \int_{V_s} (ABS + SCAT)\, d\vec{r} \,/NI \tag{1}$$

where

$$ABS = -\int_E \Sigma_a(E)\, \phi\, (E,\vec{r})\, \phi^+\, (E,\vec{r})\, dE \tag{2}$$

$$SCAT = \int_E \int_{E'} \Sigma_{sc}\, (E \rightarrow E')\, \phi\, (E,\vec{r}) \left\{ \phi^+\, (E',\vec{r}) - \phi^+\, (E,\vec{r}) \right\} dE dE' \tag{3}$$

$$NI = \int_{V_r} \int_E \int_{E'} \nu\, \Sigma_f(E)\, \phi\, (E,\vec{r})\, \chi_f(E')\, \phi^+\, (E',\vec{r})\, dE dE' d\vec{r} \tag{4}$$

In these expressions V_s and V_r represent volumes of the sample and reactor, respectively; $\Sigma_a(E)$ and $\Sigma_{sc}(E)$ represent macroscopic absorption and scattering cross sections for the sample; $\phi(E,\vec{r})$ and $\phi^+(E,\vec{r})$ represent the real and adjoint fluxes; and NI, the normalization integral for the reactor, includes the macroscopic fission cross section, Σ_f, the prompt fission neutron spectrum, χ_f, and the average number of neutrons per fission, ν, for the fuel in the assembly. Typically, the normalization integral is determined by calculation or it is eliminated from the analysis by making the reactivity measurements relative to reactivity measurements for suitable standards[6]. Some of the unique features of this measurement approach are outlined in Table 2. Uncertainties in the measured quantities range from 3-10% or larger depending on the magnitude of the measured reactivity effect for the sample.

As discussed in some detail by Bustraan[6,7], the interpretation of reactivity worth measurements is difficult. Consequently, their application to the improvement of capture cross sections is somewhat complex[10]. One observes from a glance at equations 1-3 that the following items are particularly important to a successful application of the reactivity data

to capture cross-section improvement: (1) an accurate determination of the spatial and energy dependence of both the real and adjoint fluxes, $\phi(E,r)$, and $\phi^{+}(E,r)$, (2) the determination of a correction to account for elastic and inelastic scattering in the sample and (3) an estimation of flux depression and resonance self-shielding corrections for each sample. In general the specification of the real and adjoint spectra is based principally on neutronics calculations for the assemblies in which the measurements were made. These spectra have inherent uncertainties because of modelling errors and uncertainties in the nuclear data used for the calculations. As pointed out by Gruppelaar et. al.[11], these uncertainties are not always included in subsequent analyses which utilize reactivity integral data. Scattering effects can result in large corrections, as much or greater than the capture effects, especially for weak to moderate absorbers (for example, Zr, Mo and Pd) in the harder neutron spectra. If the adjoint flux increases significantly with energy, the scattering reactivity associated with the sample and with trace quantities of moisture in the sample can dominate the total worth of a sample and render the reactivity data nearly unusuable for testing capture cross sections[7]. Finally, for the fast thermal coupled facilities like ERMINE, STEK and CFRMF, large samples are required to get a measurable reactivity effect. Consequently, the reactivity worth measurements include the effects of flux depression and significant resonance self-shielding (especially in the softer STEK cores). These effects have been estimated to range from 10% to 40% for the STEK data[11]. In spite of the complexity in the interpretation and application of reactivity integral data, Gruppelaar et. al[10,11] and Schenter et. al[12] have demonstrated the importance of including these integral data in schemes to improve fast capture cross sections for fission-product nuclides.

2. Activation Measurements

According to this approach, the capture effect for a sample is based on the measurement of the specific activity of a radioactive capture product produced from an irradiation of the sample in a well characterized neutron field. Gamma-ray spectrometry using Na(I) or Ge(Li) detectors is used to determine the specific activity of the irradiated samples[13]. For the case of a stable sample and a single radioactive capture product (no isomers), the analysis of the activation measurement is based on equation 5,

$$\bar{\phi}\cdot\bar{\sigma}_c = \frac{A}{b.\varepsilon}\cdot\frac{1}{N}\cdot\left\{\frac{T'}{T}\cdot\frac{\lambda}{1-e^{-\lambda T'}}\cdot\frac{e^{\lambda\tau}}{1-e^{-\lambda\tau}}\right\}\cdot\frac{1}{\pi_i\ \delta_i} \qquad (5)$$

where the neutron flux, $\bar{\phi}$, and the spectrum-averaged or integral cross section, $\bar{\sigma}_c$, are given by equations 6 and 7, respectively.

$$\bar{\phi} = \int_E \phi(E)\ dE \qquad (6)$$

$$\bar{\sigma}_c = \left\{\int_E \phi\ (e)\ \sigma_c\ (E)\ dE\right\}\Big/\bar{\phi} \qquad (7)$$

The parameters in equation 5 are defined as follows: A is the peak area of a characteristic gamma ray with branching ratio b for the radioactive capture product; ε is the detector efficiency, N is the number of target atoms in the sample; the term in brackets accounts for the irradiation, decay and count time history for the measurement; and the δ_i correspond to corrections to account for effects like gamma-ray self absorption and attenuation, random summing and live timer losses, neutron resonance self-shielding in the sample and interfering gamma rays. Generally, sample sizes are kept small to minimize self-shielding effects. Activation integral data are typically reported as integral reaction rates $\bar{\phi}\cdot\bar{\sigma}_c$ which are measured relative to the integral reaction rates for standards or they are reported as integral cross sections derived from measured integral rates by equation 7. In the latter case, an independent determination of the flux ϕ is made for some power level and this flux value is related to the specific integral experiment by means of power level monitors, for example the relative activation of ^{197}Au. Some features of this measurement approach are outlined in Table 2. Representative uncertainties in the measured reaction rates range from 3-10% with the largest uncertainty contributions generally due to uncertainties in the nuclear data required for the analysis.

It is clear from equations 5-7 that the application of activation measurements to the improvement of capture cross sections depends in a direct way on: (1) an accurate determination of the energy dependence of the neutron flux spectrum in the sample and (2) accurate neutron flux determination or accurate integral reaction rate measurements for applicable standard materials. Integral measurements by the activation method have been made generally in fast neutron fields for which a substantial experimental and calculational effort was made to accurately characterize the neutron environment both in terms of spectral shape and flux level. For example, errors in the spectrum shape characterization for the Coupled Fast Reactivity Measurements Facility (CFRMF)[14,15] have been estimated to contribute ~ 2% to the uncertainty in a calculated spectrum-averaged cross section for fission-product capture[16]. From a flux transfer type experiment based on the ^{239}Pu fission cross section and fission chamber measurements in the CFRMF and NBS ^{252}Cf standard neutron field, the integrated neutron flux level in CFRMF has been determined to an accuracy of $\pm$ 2.7%[17].

3. Transmutation Measurements

Transmutation experiments are very similar to activation experiments except that the capture product need not be radioactive. This method hinges on using mass-spectrometric techniques to measure the isotopic atom ratios of the capture products with respect to the target nuclide concentration. For the case of a stable, isotopically enriched sample whose capture product is stable, the integral reaction rate $\bar{\phi}\cdot\bar{\sigma}_c$ is related to the post irradiation isotope ratio of the capture product to target nuclide, namely N_2/N_1, by the following expression,

$$\bar{\phi}\cdot\bar{\sigma}_c = \left\{\ln\left(1 + N_2/N_1\right)\right\}\Big/ t \qquad (8)$$

where t is the irradiation time. Equation 8 assumes that multiple capture effects are negligible and that the neutron flux is constant over the irradiation time. Similar, but considerably more complex, expressions can be derived which take into consideration features like the use of samples which are not isotopically enriched and depletion of the primary capture product either by radioactive decay or neutron capture. The sensitivity of the current state-of-the-art mass spectrometry dictates that high power irradiation facilities and samples with reasonably high isotopic enrichment are used for transmutation experiments. Some features of this measurement approach are presented in Table 2. In principle, this approach is capable of producing very accurate measured integral data with uncertainties between 1% and 2% in the simplest cases represented by equation 8 [18,19]. Transmutation experiments in which the analysis is complicated by neutron capture to isomeric and ground states, or by depletion of the capture product by decay or burnup, uncertainties in the measured integral data can range from 5% to 10% [20].

The application of transmutation data to cross-section evaluation requires: (1) an accurate determination of the neutron flux spectrum in the sample and (2) an accurate determination of the neutron flux level or of integral reaction rates for standard materials irradiated simultaneously with the sample. This does present some difficulty for experiments in high flux test reactors in which the neutron environment is not as well characterized as it is in a fast neutron "benchmark type" field. In general, neutron spectrum shape characterization for high power reactor experiments relies heavily on neutronics calculations. Modelling simplifications which are often required to make the calculations can give rise to significant uncertainty in the computed neutron spectra. It is possible however to refine the calculated spectrum shape by utilizing passive neutron dosimetry [19,21]. In this way, uncertainties in the neutron fluxes can be determined to $\pm$ 3% to $\pm$ 5%. In addition, contribution of the spectrum shape uncertainty to calculated spectrum-averaged cross sections for irradiated specimens can be determined to $\pm$ 5%. So, derived integral cross sections from transmutation experiments that have been made to date are known to $\pm$ 6% to $\pm$ 7%.

B. Measurement Programs

Programs for measuring integral capture data for individual fission products in fast neutron fields have been carried out in Sweden, the Netherlands, the USA and in France. A breakdown of these programs in terms of facilities used and the types of measurements made is given in Table 1. Table 3 provides a semi-quantitative characterization of some of the central fast neutron fields used in these programs as compared to core and blanket spectra for a typical 1000 MW LMFBR [22]. A graphical illustration of representative fast neutron spectra is given in Figure 1. In the following paragraphs, the facilities used in each measurement program will be briefly described and the corresponding integral measurements documentation will be cited.

1. Swedish Program

Reactivity measurements for 10 fission-product isotopes were made by the oscillation technique in FRO [23]. These measurements were completed prior

to the 1973 Bologna meeting on fission products and no further measurements have been carried out. FRO was a fast critical reactor which used 20% enriched ^{235}U as fuel and graphite, stainless steel, aluminum and polyethylene as moderator materials. Reactivity measurements were made in three different cores with different neutron spectra. The fission-product worth measurements were normalized to reactivity worth of a sample of ^{235}U enriched to 93%. The central neutron spectra were derived from neutronics calculations. Documentation for this work is found in Reference 23.

2. Netherlands Program

The largest body of integral capture data for fission-product isotopes was measured in the STEK facility[24] located at Petten, The Netherlands. The measurement phase of this program was completed prior to 1974 and a report[25] was issued in 1976 documenting the measured worths for all samples. Since this early measurement period, there has been an on-going effort at Petten related to capture cross-section evaluation and the utilization of the STEK integral data for generating adjusted cross-section libraries[26].

STEK was a fast-thermal-coupled critical facility built specifically for the integral determination of fission-product capture cross sections in fast reactor spectra. Central reactivity worths measurements were made by the oscillation technique for 57 fission-product isotopes in five different STEK cores. The cores were built up from highly enriched uranium fuel and graphite moderator material. Five different atom ratios of carbon to ^{235}U were used to establish central fast zone spectra with varying degrees of hardness, STEK-4000, -3000, -2000, -1000, -500. An extensive program of spectrum measurements and neutronics calculations was carried out. The spectra recommended for use with the measured integral data are those resulting from neutronics calculations with slight adjustments to fit a selected set of reaction-rate and reactivity measurements[27]. Covariance matrices based upon uncertainties in the nuclear data used for the neutronics calculations were evaluated for the spectra.

The measured integral data correspond to reactivity worths in the five cores for samples of various sizes and compositions. Scattering contributions were calculated for all measurements and they were subtracted from the measured total reactivity effect to yield "measured" absorption reactivity worths. For weak-to-moderate absorbers (for example, Zr, Mo and Pd), scattering effects resulted in corrections which were as much or greater than the capture effects. For strong absorbers, the scattering corrections were considerably less than this. No self-shielding corrections were applied to reduce the "measured" absorption reactivity worths to worths at infinite dilution. In view of this point, it should be noted that for both integral test and cross-section adjustment applications which utilize the STEK integral data, self-shielded capture cross sections associated with each nuclide in a sample with a unique size are required in the computation of calculated worths. The reader is referred to References 24, 25 and 27 for a more complete description of the facility, the measuring techniques, and the detailed integral results.

3. US Program

Integral capture measurements for fission-product nuclides have been made using the fast neutron fields of the CFRMF[14] and the Experimental

Breeder Reactor-II, EBR-II[28], located at the Idaho National Engineering Laboratory, INEL. Both activation and reactivity measurements were made in the CFRMF in the mid-seventies[29]. The integral data obtained from the EBR-II experiment were measured by the transmutation approach[19].

The CFRMF is a zoned-core critical assembly with a fast-neutron spectrum zone in the center of an enriched ^{235}U, water-moderated, thermal "driver". The thermal driver zone fuel elements are conventional plate elements of aluminum clad 93% enriched ^{235}U. The central fast zone is produced by a water-free filter assembly which tailors the neutron energy spectrum incident on it from the thermal driver. The filter consists primarily of a large depleted uranium block clad externally with stainless steel and boral. Access to the center of the filter assembly is provided by an axial experiment hole through the block. The experiment hole is lined with stainless-steel clad concentric cylinders of ^{10}B and ^{235}U. This facility is a Cross Section Evaluation Working Group (CSEWG) benchmark field for data testing dosimeter, fission-product and actinide cross sections for the US Evaluated Nuclear Data File (ENDF/B). Specification of the central neutron spectrum has been established by means of a comprehensive program involving neutronics calculations, active neutron spectrometry and passive neutron spectrometry[14,30]. Figure 2 illustrates a comparison of a broad group CFRMF spectrum obtained from a transport calculation to a fine group representation that includes fine structure due to resonances in the cross sections for the materials which comprise the facility. A sensitivity and uncertainty analysis has been made to determine a central neutron spectrum flux covariance matrix related to the uncertainties and correlations in the nuclear data for the materials which comprise the facility[15]. For more complete details describing the facility and the central spectrum recommended for data testing, the reader is referred to References 14, 15, 29, 30 and 31.

Integral capture data based on the activation method were reported originally[29] for 38 fission-product nuclides. These integral data were reported as ratios of the capture rates with respect to the measured fission rate for ^{235}U. Subsequently, these data were updated for the 1979 Bologna meeting on fission-products with an emphasis given to using current decay data and a flux normalization scheme which was consistent with that for the dosimeter integral data base for CFRMF. In the reanalysis effort, some of the earlier measurements were judged suspect and were eliminated from the CFRMF data base used for cross-section testing. Integral cross sections reported in Reference 9 were derived by dividing the measured integral reaction rates by a neutron flux value established by means of a power level monitor based on measured ^{197}Au activation and a flux transfer using the $^{239}Pu(n,f)$ reaction and the NBS ^{252}Cf standard source[17]. The integral cross sections reported in Reference 9 have uncertainties ranging from $\pm$ 5% to $\pm$ 7%, whereas the overall uncertainties for the original integral data[29] were ~ $\pm$ 10%.

Reactivity measurements have also been made with the CFRMF for several fission-product nuclides. The data exist only as an internal company document. The reactivity effects were measured by a control rod calibrated against periods. These measurements are probably not suitable for evaluating capture cross sections because of the difficulty in reducing the measured total worth to an accurate capture worth. The reasons for this are as follows: (1) the CFRMF has a low reactivity sensitivity to absorption effects for

samples placed in the fast filter assembly, consequently large samples are required to get a measurable effect and the result is significant flux perturbation in the sample; and (2) the CFRMF has a high reactivity sensitivity to scattering because the adjoint spectrum increases significantly with increasing neutron energy, consequently scattering effects often dominant absorption effects. It has been suggested that these reactivity measurements could be useful for testing the scattering cross sections for important fission product nuclides[9].

Integral capture measurements for selected isotopes of Nd, Sm and Eu have been reported for an irradiation experiment in the EBR-II[18,19]. EBR-II is a liquid metal cooled high power fast test reactor that has been a cornerstone for fuels and materials testing important to the US fast reactor program[28]. In this experiment isotopically enriched samples were located both at midplane and in the reflector. Integral capture reaction rates were obtained by the transmutation method using post-irradiation mass-spectrometric analyses. The neutron spectra and fluxes for the samples were characterized using passive neutron dosimetry and spectrum-unfolding with the FERRET least-squares data analysis code[32,33]. Preliminary results of the work are found in Reference 18 and the comprehensive final report[19] has recently been published.

4. French Program

An extensive series of integral measurements for individual fission-product nuclides is being carried out by the French using the fast-thermal-coupled reactor ERMINE, the fast critical reactor MASURCA, and the high power LMFBR PHENIX. An overview of this program is found in Reference 8. Both reactivity measurements by the oscillation technique and activation measurements have been made with the ERMINE facility. Only reactivity measurements have been made in MASURCA. Integral data obtained from the irradiation experiment in PHENIX were measured by the transmutation method. Some phases of this work have been reported[20,34]. However, in general, integral results from the French program are not available in sufficient detail to the international fast reactor community for use in their own laboratories.

C. Integral Data Base

An identification summary of the integral capture data base for 50 fission-product nuclides of most importance to fast reactor systems is given in Table 4. This summary provides an indication of the coverage of integral measurements generated by the programs described in the last subsection. The reader is referred to the references cited in that subsection for specific details concerning the measured integral data. The ordering of the nuclides in Table 4 is according to estimated percent contribution to total fission-product absorption in a large fast reactor after 300 days of operation[22]. In the table, A, R and T stand for the type of integral measurement made, namely, activation, reactivity and transmutation, respectively. It should be noted that of all the measurements indicated in Table 4, final results for the transmutation experiments in EBR-II were the only "new" data reported since the 1979 Bologna meeting on fission

products. Additional experiments are underway at PHENIX but the results are not available. The emphasis since 1979 has been more on the application of integral data than on the measurements of new data.

III. APPLICATIONS OF INTEGRAL DATA

Integral data have been used in a variety of ways for the improvement of fission-product capture cross sections. These include: (1) cross-section normalization, (2) integral testing and (3) adjustment schemes. Integral cross sections were used in the preparation of ENDF/B-IV to normalize differential curves based on model calculations for several fission product class nuclides[35]. This approach was taken because the measured differential data base was sparce or non-existent for many nuclides and the model calculations had significant normalization uncertainties. Integral testing in which measured integral data are compared with integral data computed using differential cross sections and spectrum representations is the traditional approach used for ENDF/B and JENDL to assess the consistency between evaluated cross sections and the measured integral data. Adjustment procedures have been developed and applied in which the integral data are directly incorporated in the improvement of capture cross sections by means of model parameter adjustment, pointwise cross-section adjustment and multigroup cross-section adjustment. Integral testing and adjustment schemes are discussed in more detail in the following two subsections.

A. Integral Tests

The primary objective of an integral test is to make a "consistency check" of an evaluated differential cross section by comparing the measured integral datum to that computed using the differential cross section for the reaction in question and the neutron spectrum of the field in which the measurement was made. Although the following development emphasizes the use of integral cross sections derived from activation or transmutation experiments, most of the discussion applies also to the use of reactivity data for integral test applications. Typically, multigroup representations of the cross section and spectrum are used in the computation of the calculated integral datum. For example, this computation takes the form of equation 9 for an integral cross section $\bar{\sigma}_c$ where ϕ_i and σ_i are group-average quantities for the fluxes and cross sections, respectively, and the group index i is summed over all groups.

$$\bar{\sigma}_c = \Sigma_i \sigma_i \phi_i \Big/ \Sigma_i \phi_i \qquad (9)$$

The "consistency test" then entails computing the ratio of the calculated-to-the-measured quantity, C/M, and assessing whether the ratio indicates a discrepancy outside the error determined for the C/M ratio. Typically in the past for fission-product capture cross sections, only the error on the measured quantity was quoted[29]. A discrepancy outside this error was then used as a guide to point to an inadequacy in the differential data base originating from either the cross section or the neutron spectrum. As a first approximation this discrepancy was assumed to be primarily due to normalization problems in the model calculations or in the measured differential data. Bearing in

mind that the integral test, as such, provides no information about detailed shapes of cross sections, this assessment of an integral test discrepancy assumes that the shapes of the tested cross section and the spectrum are known very accurately. This may not always hold true. Caution is then demanded concerning the interpretation of the integral test because apparent consistency or unconsistency between differential data and integral data can result if either the cross-section or spectrum shapes are significantly incorrect.

A more rigorous assessment of integral tests requires a comprehensive treatment of all the major sources of error which contribute to the uncertainties in the C/M ratios. This treatment should include an evaluation of the measured integral data base, a determination of uncertainties and correlations for the spectrum shape, estimates of the uncertainties and correlations for the evaluated cross sections, and an assessment of computational errors. Standard error propagation rules can then be used to estimate the various uncertainty contributions for the computed integral datum, for example, an integral cross section based on equation 9. The uncertainty in the C/M ratio can then be viewed as the quadrature sum of the error in the measured quantity and the error in the computed quantity. An example of this approach to integral testing for fission-product capture cross sections on ENDF/B-V is found in Reference 16. The principal results of that study are included in this paper in Section IV.

Computational errors related to the use of processed multigroup cross sections can, in some cases, provide a significant bias to the C/M ratio. A minimization of this source of error demands that when collapsing cross-section data into multigroup format that a weighting function be used which is representative of the actual spectrum in which the measurements were made. This requirement is particularly crucial for cases in which there is significant overlap between the spectrum structure and the cross-section resonances. Such errors, as large as seven percent, were noted in the integral testing study[16] for fission products when a comparison was made of integral cross sections computed using cross sections processed with a 1/E + fission spectrum type weighting and cross sections processed using actual CFRMF spectrum weighting.

In recent ENDF/B-V evaluations[12] for fission products, integral data have had a direct influence on the generation of evaluated capture cross sections. Under these circumstances one may question the interpretation or validity of an integral test analysis. This question is examined in Section IV.

Finally, the interpretation of an integral test analysis and its application to evaluating a cross section should be made with some knowledge of the reaction energy response in the neutron spectrum. This serves to point out those neutron energy ranges over which the integral assessment applies. Examples of reaction energy responses in the CFRMF spectrum for some fission-product reactions are given in Figures 3, 4 and 5. The top half of each figure shows a 72-group representation of a specific cross section and the bottom half shows the relative energy response of that reaction in the CFRMF central spectrum. The area under each response histogram is normalized to 1.0. Hence one can readily note the fractional response from each group.

The primary purpose of showing the cross-section response plots is to illustrate the variability and complexity of the reaction response, especially when resolved resonances contribute substantially to the total response. As illustrated in Figure 3, the response for ^{99}Tc in CFRMF is relatively broad with minor structure due principally to structure in the CFRMF spectrum. The case for ^{102}Ru, Figure 4, shows the onset of resolved resonance response contributing approximately six percent to the total response. A more dramatic case of significant resolved resonance response is that for ^{108}Pd, Figure 5, in which the two resonances at .03 keV and .09 keV contribute approximately 11% and 15% respectively to the total reaction response. This resonance response is in an energy range of the neutron spectrum where the flux is falling off rapidly and where significant structure is present in the flux spectrum (see Figure 2). The example of ^{108}Pd points to the need for accurate treatment of cross-section processing in terms of spectrum weighting and accurate resonance self-shielding.

Integral test analyses have played an important role in the generation of evaluated fission-product capture cross sections in the USA and in Japan. Reference 29 includes the results of data testing for ENDF/B-IV fission product cross sections. As stated earlier, an integral testing study[16] based on CFRMF and EBR-II integral data, was made for ENDF/B-V cross sections. Some of the results of that work are included here in Section IV. At the Bologna meeting in 1979, Iijima reported[36] on a comprehensive data testing study of the JENDL-1 library based on CFRMF and STEK integral data. Data testing for JENDL-2 against this same integral data base was not completed for use at this fission-product specialist meeting[37].

B. Adjustment Applications

There are two distinct viewpoints of cross-section adjustment as related to data evaluation. One generally accepted viewpoint is that integral measurements are useful to adjust multigroup cross sections and that these adjusted cross sections are then valid in limited applications that are very similar to the integral experiments. Because the adjustments may reflect modelling errors or other undetected problems, the adjustments are not viewed as improvements of the basic cross section itself[38]. Another viewpoint is that if all significant sources of error are identified and estimated, one is justified in applying integral measurements to improve the microscopic cross sections[10,12]. Typically integral data have been used in three ways: (1) to adjust multigroup representations of the cross sections, (2) to adjust nuclear model parameters and (3) for adjustment of pointwise cross sections. The methodology associated with each of these three approaches has been reviewed in detail by Gruppelaar[39]. A common denominator in each approach is the utilization of a least-squares adjustment formalism and a treatment of uncertainties and correlations for the measured data, the differential cross sections and the neutron spectra.

Integral data have been used by the French and the Dutch in the applications-oriented approach in the generation of the CARNAVAL-IV and RCN-2A adjusted multigroup cross-section libraries, respectively, for design of fast reactors[11]. According to this approach, evaluated pointwise cross sections are based on differential measurements and nuclear model calculations. The pointwise cross sections are expressed in a multigroup

representation and group constants adjustments are made based on integral data measured in "benchmark" fast neutron facilities whose neutron spectra are similar to those in a typical fast power reactor. Integral data from MASURCA, ERMINE, PHENIX, STEK, CFRMF and FRO were used to obtain adjusted group constants for CARNAVAL-IV. The RCN-2A adjusted library is based on integral data from STEK and CFRMF. Gruppelaar et. al.[11] have demonstrated the importance of this approach for achieving the target design accuracy for prediction of global fission-product absorption in a fast power reactor.

Capture cross sections for fission products in the forthcoming Dutch RCN-3 evaluation[40] are based on a procedure which utilizes integral data in a least-squares-adjustment of important statistical model parameters (radiation widths, level spacings, strength functions). According to this approach, differential data and nuclear systematics are used to establish the a priori model parameters, namely those for RCN-2. Model parameter adjustments are then made based on STEK and CFRMF integral data. The adjusted model parameters are then used in a statistical model prescription to generate an evaluated pointwise curve above the resolved resonance region[10].

Integral data have also been used simultaneously with differential data in a least-squares-adjustment analysis of microscopic differential cross sections derived from earlier evaluations or from nuclear model calculations. Several of the fission-product capture evaluations for ENDF/B-V were made in this way using the STEK and CFRMF integral data base[12].

The least-squares-adjustment methodology developed for cross-section adjustments applications referred to above provides an important tool for analysis of integral experiments in high power test reactors in which the usual spectrum characterization is not detailed to the specific neutron environment of each experiment. A direct benefit of this approach is the generation of integral data and spectra with complete covariances for use in integral test analysis or for the generation of adjusted multigroup cross sections with associated covariances which can be used directly in cross-section adjustment evaluation applications. An example of this approach is given in the following paragraphs for an integral experiment in EBR-II which has been recently documented[19].

The experiment consisted of the following: (1) row 8 irradiation of isotopically-enriched samples of Nd, Sm and Eu and passive dosimetry sets in different neutron spectra (midplane, reflector), (2) mass-spectrometric determination of the integral capture reaction rates for the rare-earth samples, (3) and radiometric determination of the integral reaction rates for the dosimeters. Flux/cross-section adjustment analyses were made with the FERRET code[32] utilizing the measured integral data for the dosimeter and rare-earth samples. A priori data input to those analyses included multigroup cross sections for the dosimeters and fission products based on ENDF/B-IV, multigroup neutron spectra derived from neutronics calculations for EBR-II, and flux and cross-section covariance matrices based on a parametric representation for the correlations between groupwise uncertainties[32].

Basically two types of analyses were made: (1) neutron spectra characterization - neutron spectra in the experiment capsules were obtained by a simultaneous adjustment of the input spectra and the dosimeter cross

sections within the constraints specified by the measured integral data for the dosimeters and the a priori uncertainty and correlation specification for the input data, (2) simultaneous adjustment of all cross sections and spectra - data input were the same as for type 1 but expanded to include appropriate fission product cross sections, covariances and integral data.

The principal results of the first analysis namely adjusted spectra and associated covariances, are a much improved characterization of the neutron spectra for the fission-product integral data. As such, they can be used by the evaluator, along with the measured fission-product integral data to integrally test microscopic cross sections. The principal results of the second analysis, namely adjusted fission-product cross sections and associated covariances, can be utilized directly in a microscopic cross-section evaluation. The latter application provides a direct comparison of the information contained in the integral experiment to the body of measured differential data or model calculations. Results from both types of applications are given here. The utilization of the EBR-II integral data for integral test analyses is included in Section IV. A comparison of the adjusted multigroup cross sections to recent differential data for the most important fission-product cross sections in the experiment is given in Figures 6-10.

Shown in Figures 6 and 7 are plots comparing the EBR-II adjusted capture cross sections for ^{143}Nd and ^{145}Nd to other data spanning the energy range from 1 keV to 10 MeV. The STEK adjusted cross sections in both figures were taken from Reference 26. The differential data included: for ^{143}Nd, measurements by Nakijima et. al.[41] and Musgrove et. al.[42]; for ^{145}Nd measurements by Nakijima et. al.[41] and by Shaw and collaborators[43,44]. In general for ^{143}Nd and ^{145}Nd, there is good agreement between the EBR-II adjusted cross sections, the STEK adjusted cross sections and the differential data. Differences between the STEK and EBR-II adjusted cross sections above ~800 keV, especially for ^{143}Nd, are most likely related to the significant shape differences in this energy range between RCN-2 and ENDF/B-IV cross sections used as a priori data in respective analyses[40]. The shape differences are traceable to nuclear model calculation differences. The need for upward adjustment of the ENDF/B-IV fast capture cross section for ^{145}Nd is demonstrated.

Figures 8 and 9 illustrate the data comparison for ^{147}Sm and ^{149}Sm, respectively, over the energy range from 1 keV to 10 MeV. The STEK adjusted cross sections are from Reference 26. The differential data included: for ^{147}Sm, measurements by Mizumoto[45]; and for ^{149}Sm, measurements by Mizumoto[45] and by Shaw et. al.[43,44]. Figure 8 indicates good agreement between both adjusted multigroup cross sections and the differential data and points to the need for a re-evaluation of the ENDF/B-IV ^{147}Sm fast capture cross section. As illustrated in Figure 9, the recent differential data and the adjusted multigroup cross sections indicate the need for re-evaluating the fast cross section for ^{149}Sm. However, the EBR-II adjusted cross section appears to be discrepant with the other data, especially below 10 keV. The source of this inconsistency is traceable to the choice of a priori correlations used to describe the unresolved and smooth energy regions which join at 10 keV[19]. A chi-square test which utilizes the full covariance matrix for the EBR-II adjusted cross section demonstrated its consistency with respect to the other data[19]. This example points out that the interpretation and application of adjusted cross sections can be misleading

if one ignores the underlying correlations imposed by the integral data.

Finally, in Figure 10 we illustrate a comparison of the EBR-II adjusted curve for ^{153}Eu to the most recent differential data, that of Mizumoto et. al.[46]. Both the EBR-II adjusted curve and the measured differential data indicate the need for some upward adjustment of the ENDF/B-IV fast capture cross section for ^{153}Eu.

IV. INTEGRAL TESTS FOR ENDF/B-V FISSION PRODUCTS

An integral-testing study[16] has been done for fission-product capture cross sections in ENDF/B-V. This study is an integral part of the forthcoming formal ENDF/B-V Data Testing Report. A summary of the work follows.

The analysis used integral cross-section data derived from measurements in CFRMF and EBR-II. The STEK results were not used because the reactivity worth data, as reported[25], have not been corrected for resonance self-shielding effects and do not correspond to capture worths at infinite dilution. For the CFRMF related data testing, multigroup spectrum representations based on transport calculations with both ENDF/B-IV and ENDF/B-V nuclear data for the materials which comprise the facility were used in the calculation of spectrum-averaged cross sections. Fine structure effects were included in the spectrum representations. Neutron spectra used for the EBR-II related data-testing were based on multigroup spectrum representations obtained from spectrum unfolding analyses as described in Section III. Calculated spectrum-averaged cross sections were obtained using both ENDF/B-IV and ENDF/B-V capture data. Where possible, calculations were made to estimate the uncertainty in the calculated integral cross sections because of uncertainties and correlations in the input fluxes. No attempt was made to include estimates of the uncertainties for the evaluated differential cross sections because that information was not available. Sources of error related to spectrum shape changes and weighting function effects were evaluated and quantified. Ratios of calculated-to-measured integral cross sections were computed and an uncertainty for each C/M ratio was determined. Response plots as a function of energy were generated for all capture reactions to provide the cross-section evaluator with a guide for applying the integral test results to applicable evaluation problems.

A summary of some of the integral test results from the above study are given here in Table 5. The results are arranged in order of increasing atomic number for the nuclides. An importance ranking based on the Table 4 listing of percent contribution to total fission-product absorption in a fast reactor is given in column 2. For example, ^{98}Mo is the twenty-first nuclide in the list of Table 4. Under column 3 EBR-II-M and EBR-II-R stand for integral data corresponding to midplane and reflector positions, respectively, in EBR-II. Ratios of calculated-to-measured integral cross sections are tabulated in column 4 along with estimates of the percent error in each quantity given in parenthesis. Each error value represents the quadrature sum of the error in the measured integral datum and the spectrum uncertainty contribution to the calculated integral cross section. The column labelled "discrepancy range" indicates whether an integral test discrepancy is < 1, 1-2, 2-3, 3-4 or > 4 times the uncertainty in the integral test C/M ratio. Discrepancy range values > 1 indicate an inconsistency between the measured integral

data and the evaluated cross sections. The numbers tabulated in column 6 are ratios of integral cross sections calculated with ENDF/B-V fission-product capture cross section data relative to ENDF/B-IV capture data. These values provide an indication of the changes made in the fast capture cross sections for the fission product nuclides in going from the ENDF/B-IV evaluation to the ENDF/B-V evaluation. An assessment of the change in consistency between the measured integral data and the evaluated cross sections in going from ENDF/B-IV to ENDF/B-V is given by the three columns under the heading "Consistency IV-V". This means for example that the significant changes in the capture cross section for ^{99}Tc, (V/IV ratio = 1.21), resulted in less consistency between the measured integral data and the ENDF/B-V evaluation than between the measured integral data and the ENDF/B-IV evaluation. In fact, for ^{99}Tc, the measured integral data and the ENDF/B-IV evaluation are consistent.

From a global sense the results in Table 5 indicate that the changes in the fast capture cross sections for the selected fission products in going from ENDF/B-IV to ENDF/B-V resulted in more consistency for twenty-one of the integral data, less consistency for seven of the integral data and no change for four of the integral data. This point is not too surprising because integral data from STEK and CFRMF were used directly in the FERRET least-squares-adjustment analyses made as part of the evaluation of fission-product capture cross sections for ENDF/B-V[12].

The impact of CFRMF integral data on the ENDF/B-V evaluations relative to the influence of other input data (differential measurements and STEK integral measurements) was investigated by comparing the results of least-squares analyses which included CFRMF integral data to analyses which did not include CFRMF integral data. The comparison was not made in a differential sense, that is, adjusted cross sections from the two types of analyses were not directly compared. Rather, the comparison was made in an integral sense, that is, spectrum-averaged cross sections, computed with the two types of adjusted differential curves, were compared. A summary of the results of this comparison for nine important fission-product nuclides is shown in Table 6. Columns 2, 3 and 4 tabulate ratios of calculated-to-measured CFRMF integral cross sections. The results are presented this way because they indicate not only the influence of the CFRMF integral data on the evaluated cross section (comparison of columns 3 and 4), but they demonstrate the magnitude of the impact relative to the influence of the other measured data used in the least-squares-adjustment analyses (comparison of columns 3 and 2). This comparison is more transparent in the information presented in columns 5 and 6. Column 5 provides an indication of the influence of all of the measured data (differential and integral, including CFRMF) in the adjustment of the <u>a priori</u> ENDF/B-IV cross section. Adjustments in the capture cross sections were made which resulted in changes in computed spectrum-averaged cross sections ranging from 0% for ^{104}Ru to 43% for ^{109}Ag. The values in column 5 indicate that the exclusion (or inclusion) of CFRMF integral data resulted in changes in computed spectrum-averaged cross sections ranging from 0% for ^{98}Mo to 6% for ^{146}Nd. Clearly, the measured differential data and the STEK integral data have dominated the least-squares-adjustment analyses for these fission-product capture cross sections. This is probably due to the use of relatively large uncertainties for the measured CFRMF integral data (quoted uncertainty +5%) in the least-squares analyses[22].

V. SUMMARY AND CONCLUDING REMARKS

In this paper, the current status of the measured integral data base for fission-product fast-neutron capture was reviewed. Integral capture data have been reported for 40 of the 50 most important fission-product nuclides. The data were obtained from activation, reactivity worth or transmutation measurements in the fast neutron fields of STEK, FRO, MASURCA, ERMINE, CFRMF, PHENIX and EBR-II. Most of the integral data were available at the 1979 Bologna meeting on fission products. The only "new" integral data that have been reported since 1979 are integral measurements for isotopes of Nd, Sm and Eu which were irradiated in EBR-II. Preliminary results of this work had been reported in 1979[18] and a final report has been published recently[19]. It has been reported that new experiments in PHENIX were underway at the time of the 1979 Bologna fission-product meeting, but the results of that work were not available at the time of this meeting[11].

As a second thrust to this paper, the role of integral data in the cross-section evaluation process was discussed with an emphasis on integral data testing and cross-section adjustment applications. Criteria for carrying out and interpreting an integral testing analysis were identified and discussed. In this framework a summary of an integral testing study for ENDF/B-V fission-product capture cross sections using CFRMF and EBR-II integral data was presented here. The study, which included analyses for 26 important fission-product nuclides and 32 applicable integral data, revealed that the changes in the fast capture cross sections in going from ENDF/B-IV to ENDF/B-V resulted in more consistency between measured and calculated integral cross sections for twenty-one, less consistency for seven and no change for four of the fission-product integral tests. Outstanding discrepancies (discrepancy greater than twice the uncertainty in C/M ratio) between the measured integral data and the ENDF/B-V cross sections were noted for ^{108}Pd, ^{109}Ag, ^{134}Xe, ^{137}Cs, ^{142}Ce, ^{145}Nd, ^{146}Nd, ^{148}Nd, ^{150}Nd, ^{149}Sm and ^{153}Eu.

As an alternate approach to conventional C/M integral testing, the use of adjusted cross sections in the cross-section evaluation process was presented. The example presented utilized adjusted multigroup cross sections based on integral measurements in EBR-II for isotopes of Nd, Sm and Eu. A comparison of the adjusted cross sections to recent differential capture measurements and to the RCN-2A adjusted library indicated good agreement between all of the compared information for ^{143}Nd, ^{145}Nd, ^{147}Sm, ^{149}Sm, and ^{153}Eu. The implication is that when the more recent differential data are incorporated into re-evaluation of the ENDF/B-V capture cross sections, some of the outstanding discrepancies identified in the above paragraph will be resolved.

At the 1979 Bologna meeting for fission products, discrepancies between different integral measurements were noted for the following nuclides: ^{99}Tc, ^{105}Pd, ^{108}Pd, ^{127}I, ^{151}Sm, ^{147}Pm, ^{109}Ag and ^{104}Ru. New measurements were not made to resolve these discrepancies prior to the present meeting. It should be noted that an attempt will be made to do so in the near future for applicable CFRMF integral data. New measurements with the CFRMF, with an emphasis in accuracy and precision, are underway for ^{99}Tc, ^{127}I, ^{147}Pm, ^{109}Ag and ^{104}Ru.

New integral experiments would be helpful to improve the capture cross sections for important radioactive fission-product cross sections. These include ^{107}Pd, ^{135}Cs, ^{106}Ru, ^{151}Sm, ^{144}Ce, ^{103}Ru, ^{154}Eu and ^{95}Zr.

With the availability of new and more complete resonance information[47] for important fission product nuclides, it would be useful to compute resonance self-shielding correction factors for the STEK integral data to obtain capture reactivity worths at infinite dilution. Such integral data would be helpful for future integral testing applications.

Finally, it should be noted that although there were few new integral measurements made since the 1979 Bologna meeting, there was considerable activity in the application of the existing integral data base to cross-section evaluations. Gruppelaar[1] reported on a comparison of several of the evaluated files at this meeting. One outstanding conclusion of that work is that to achieve a design target accuracy of ± 10% for the prediction of global fission-product absorption in a fast reactor, one must utilize cross-section libraries that have been adjusted with integral data. In addition, it has been shown that measured integral data are very useful to resolve discrepancies between measured differential data[1,4]. The primary motivation to improve and utilize integral measurements lies with both of these points.

Acknowledgements

The author would like to acknowledge Bob Schenter of HEDL for many conversations about the substance of this paper and for making the FERRET runs related to investigating the impact of CFRMF integral data on some fission-product capture cross section evaluations for ENDF/B-V. Y. D. Harker provided assistance and support in interpreting the measured integral data.

REFERENCES

1. P. Greebler, B. A. Hutchins, C. L. Cowan, "Implications of Nuclear Data Uncertainties to Reactor Design," Second International Conference on Nuclear Data For Reactors, Helsinki, June, 1970, IAEA-CN-26/102,17 (1970).

2. J. L. Rowlands, "Nuclear Data for Reactor Design, Operation and Safety," Proc. Int. Conf. on Neutron Physics and Nuclear Data for Reactors, Harwell, United Kingdom, September, 1978, OECD, p.7, (1978).

3. J. L. Rowlands, "Needs and Accuracy Requirements for Fission-Product Nuclear Data in the Physics Design of Power Reactor Cores," RP3 in Proc. of Second Advisory Group Meeting on Fission Product Nuclear Data, Petten, The Netherlands, September 5-9, 1977, IAEA-213, Vol. I, 41 (1977).

4. R. J. Heijboer and A. J. Janssen, "Status of Pseudo Fission-Product Cross Sections for Fast Reactors; Sensitivity Study for Sodium Void Effect," Proc. Specialists' Meeting on Neutron Cross Sections of Fission-Product Nuclei, Bologna, Italy, December 12-14, 1979, NEANDC(E)-209"L",375 (1980).

5. Ph. Hammer, "Besoins en Donnies Nucleair des Products de Fission et Actinides pour les Calculs de Reacteurs de Puissance a Neutrons Rapides," Proc. Int. Conf. on Neutron Physics and Nuclear Data for Reactors, Harwell, United Kingdom, September, 1978, OECD, p. 551, (1978).

6. M. Bustraan, "Integral Determination of Neutron Absorption by Fission Products," RP14 in Proc. of a Panel on Fission-Product Nuclear Data, Bologna, Italy, November 26-30, 1973, IAEA-169, Vol. II, p. 53 (1974).

7. M. Bustraan, J. W. M. Dekker, R. J. Heijboer and A. J. Janssen, "Integral Determination of Fission-Product Neutron Capture Cross Sections for Application in Fast Reactors," RP14 in Proc. of Second Advisory Group Meeting on Fission-Product Nuclear Data, Petten, The Netherlands, September 5-9, 1977, IAEA-213, Vol. II, p. 677 (1978).

8. G. Langlet and L. Martin-Deidier, "The French Program on the Determination of the Effect of Fission Products in Fast Reactors," Contribution to Second Advisory Group Meeting on Fission-Product Nuclear Data - 1977, IAEA, INDC(NDS)-87/GO+Sp, p. 293 (1978).

9. Y. D. Harker and R. A. Anderl, "Integral Cross-Section Measurements on Fission Products in Fast Neutron Fields," in Proc. Specialists' Meeting on Neutron Cross Sections of Fission-Product Nuclei, Bologna, Italy, December 12-14, 1979, NEANDC(E)-209"L",5 (1980).

10. H. Gruppelaar and J.W.M. Dekker, "Impact of Integral Measurements on the Capture Cross-Section Evaluations of Individual Fission-Product Isotopes," RP8 in Proc. of Second Advisory Group Meeting on Fission-Product Nuclear Data, Petten, The Netherlands, September 5-9, 1977, IAEA-213, Vol. I, p. 219 (1978).

11. H. Gruppelaar, P. Hammer and L. Martin-Deidier, "Intercomparison of Adjusted Data Sets for Capture Cross Sections of Fission Products," in Proc. Specialists' Meeting on Neutron Cross Sections of Fission-Product Nuclei, Bologna, Italy, December 12-14, 1979, NEANDC(E)-209"L", 299 (1980).

12. R. E. Schenter and T. R. England, "ENDF/B-5 Fission-Product Cross-Section Evaluations," in Proc. Specialists' Meeting on Neutron Cross Sections of Fission-Product Nucli, Bologna, Italy, December 12-14, 1979, NEANDC(E)-209"L",253 (1980). R. E. Schenter, D. L. Johnson, F. M. Mann, F. Schmittroth, and H. Gruppelaar, "Evaluations of Fission-Product Capture Cross Sections for ENDF/B-V" in Proc. Int. Conf. on Nuclear Cross Sections for Technology, Knoxville, Tennessee, October 22-26, 1979, NBS Special Publication 594, NBS, 662 (1980).

13. R. C. Greenwood, R. G. Helmer, J W Rogers, N. D. Dudy, R. J. Popek, L. S. Kellogg and W. H. Zimmer, Nucl. Tech. 25, 275 (1975).

14. J W Rogers, D. A. Millsap and Y. D. Harker, Nucl. Tech. 25, 330 (1975).

15. J. M. Ryskamp, R. A. Anderl, B. L. Broadhead, W. E. Ford III, J. L. Lucius, J. H. Marable and J. J. Wagschal, Nucl. Tech. 57, 20 (1982).

16. R. A. Anderl, "INEL Integral Data-Testing Report for ENDF/B-V Fission-Product and Actinide Cross Sections," US DOE Report EGG-PHYS-5406, INEL (April, 1981).

17. R. A. Anderl, D. A. Millsap, J W Rogers, and Y. D. Harker, "INEL Integral Data-Testing Report for ENDF/B-V Dosimeter Cross Sections," US DOE Report EGG-PHYS-5608, INEL (October, 1981).

18. R. A. Anderl, Y. D. Harker, and F. Schmittroth, "Neodymium, Samarium and Europium Capture Cross-Section Adjustements Based on EBR-II Integral Measurements," in Proc. Int. Conf. on Nuclear Cross Sections for Technology, Knoxville, Tennessee, October 22-26, 1979, NBS Special Publication 594, NBS, 557 (1980).

19. R. A. Anderl, F. Schmittroth and Y. D. Harker, "Integral Capture Measurements and Cross-Section Adjustments for Nd, Sm and Eu," US DOE Report EGG-PHYS-5182, INEL (1981).

20. A. Giacometti, M. Darrouzet, P. Hammer, M. Lucas, F. Prost-Marechal, M. Robin, "Measure de Sections Integrales de Capture par L'Irradiation PROFIL dans PHENIX," in Proc. of an Intl. Symposium on Fast Reactor Physics 1979, Aix-en-Province, September 24-28, 1979, IAEA-SM-244/22,521 (1980).

21. W. N. McElroy and L. S. Kellogg, Nucl. Tech. 25, 180 (1975).

22. R. E. Schenter, Hanford Engineering Development Laboratory (HEDL), Private communication (1971, 1981).

23. T. L. Anderson, "Integral Measurement of Fission-Product Reactivity Worths in Some Fast Reactor Spectra," Aktiebolaget Atomenergi, AE-428 (1971).

24. H. Th. Klippel and J. Smit, "The Coupled Fast-Thermal Critical Facility STEK," RCN-209 (1974).

25. J. J. Veenama and A. J. Janssen, "Small Sample Reactivity Worths of Fission-Product Isotopes and Some Other Materials Irradiated in STEK," ECN-10 (1976).

26. J.W.M. Dekker, "Tables and Figures of Adjusted and Unadjusted Capture Group Cross Sections Based on the RCN-2 Evaluation and Integral Measurements in STEK," Vol. 1: ECN-14(1977), Vol. 2: ECN-30(1977) and Vol. 3: ECN-54(1970).

27. J.W.M. Dekker, J. B. Dragt, A. J. Janssen, R. J. Heijboer, and H. Th. Klippel, "Adjusted Neutron Spectra of STEK Cores for Reactivity Calculations," ECN-35(1978).

28. L. J. Koch, W. B. Loewenstein, and H. O. Monson, "Addendum to Hazard Summary Report, Experimental Breeder Reactor-II (EBR-II)," US AEC Report ANL-5719 (Addendum), Argonne National Laboratory (1964).

29. Y. D. Harker, J W Rogers, and D. A. Millsap, "Fission-Product and Reactor Dosimetry Studies at Coupled Fast Reactivity Measurements Facility," US DOE Report TREE-1259, INEL (1978).

30. J W Rogers, D. A. Millsap and Y. D. Harker, "The Coupled Fast Reactivity Measurements Facility (CFRMF)," in Proc. of IAEA Consultants Meeting on Integral Cross-Section Measurements for Reactor Dosimetry, IAEA, Vienna, Austria, November 15-19, 1976, IAEA-208, Vol. II, 117 (1976).

31. R. A. Anderl, D. A. Millsap, J W Rogers, Y. D. Harker, "Addendum to Integral Data Testing Report for ENDF/B-V Dosimeter Cross Sections," US DOE Report EGG-PHYS-5668, INEL (1981).

32. F. Schmittroth, "FERRET Data Analysis Code," HEDL-TME-79-40, Hanford Engineering Development Laboratory (1979).

33. F. Schmittroth, Nucl. Sci. Eng. 72, 19 (1979).

34. L. Martin-Deidier, M. Darrouzet, P. Hammer, and E. Fort, "Measures Integrales de La Capture des Produits de Fission dans les Spectres de Reacteurs Eau et de Reacteurs a Neutrons Rapides," Proc. Intl. Conf. on Neutron Physics and Nuclear Data for Reactors, Harwell, United Kingdom, September 1978, OECD, 1016 (1978).

35. R. E. Schenter, HEDL, Private communication (1975).

36. S. Iijima, T. Watanabe, T. Yoshida, Y. Kikuchi and H. Nishimura, "Fission-Product Neutron Cross-Section Evaluations for JENDL and the Integral Tests," in Proc. Specialists" Meeting on Neutron Cross Sections of Fission-Product Nuclei, Bologna, Italy, December 12-14, 1979, NEANDC(E)209"L",317 (1980).

37. S. Iijima, NAIG Nuclear Research Laboratory, Japan, Private Communication (1982).

38. S. Pearlstein, Nucl. Sci. Eng. 74, 215 (1980).

39. H. Gruppelaar and J. B. Dregt, "Cross-Section Adjustments Using Integral Data," in Proc. Workshop on Evaluation Methods and Procedures, Brookhaven National Laboratory, September 22-25, 1980, BNL-NCS-51363, Vol. 1, p. 133 (1981).

40. H. Grupppelaar, "Status of Recent Fast Capture Cross-Section Evaluations for Important Fission-Product Nuclides," contribution to this meeting.

41. Y. Nakajima, A. Asami, Y. Kawarasaki, Y. Furuta, T. Yamamoto and Y. Kanda, "Neutron Capture Cross-Section Measurements for ^{143}Nd, ^{145}Nd, ^{146}Nd and ^{148}Nd," in Proc. Intl. Conf. Neutron Physics and Nuclear Data for Reactors, Harwell, United Kingdom, September 1978, OECD, 438 (1980).

42. A. R. de L. Musgrove, B. J. Allen, J. W. Boldeman and R. L. Macklin, "Recent Measurements of Neutron Capture Cross Sections in the Fission-Product Mass Region," Proc. Intl. Conf. Neutron Physics and Nuclear Data for Reactors, Harwell, United Kingdom, OECD, 449 (1978).

43. Shaw, et. al., Data in NEUDADA, NEA Data Bank.

44. R. W. Hockenberry, et. al., Bull. Am. Phys. Soc. 20, 560 (1975).

45. M. Mizumoto, Nucl. Phys. A357, 90 (1981).

46. M. Mizumoto, et. al., J. Nucl. Sci. Tech., 16, 711 (1979).

47. F. F. Mughabghab, M. Divadeevam, and N. E. Holden, Neutron Cross Sections, Vol. I, Neutron Resonance Parameters and Thermal Cross Sections, Part A:Z=1-60, Academic Press (1981).

Table 1. Summary of Integral Measurement Programs

Country	Facilities	Measurement Types	Status
USA	CFRMF[a]	Activation, Reactivity	Ongoing
	EBR-II[b]	Transmutation	
The Netherlands	STEK: 5 Cores	Reactivity	Ended
Sweden	FRO: 3 Cores	Reactivity	Ended
France	ERMINE/MINERVE	Activation, Reactivity	Ongoing
	MASURCA	Reactivity	
	PHENIX	Transmutation	

a. CFRMF: Coupled Fast Reactivity Measurements Facility

b. EBR-II: Experimental Breeder Reactor-II

Table 2. Comparison of Measurement Techniques

Feature	Reactivity	Activation	Transmutation
Applicability	General	Limited (Radioactive)	Limited
Sample Req.			
Size	g (1-100)	mg	ug-mg
Enrichment	High	Natural	High
Reactor Facility			
Power	Critical	Low (10^9-10^{11} n/cm^2-S)	High (10^{14} n/cm^2-S)
Spectrum	ϕ, ϕ^+ - Required	ϕ - Required	ϕ - Required
	Neutronics Calculation	Neutronics Calculation	Neutronics Calculation
	Active and Passive Dosimetry	Active and Passive Dosimetry	Passive Dosimetry
Analysis Limitations	Scattering Effects	Decay Data	Production/Depletion
	Flux Perturbations		Corrections
	Self-Shielding	Self-Shielding	
Normalization	^{252}Cf or ^{235}U Fission Rates	^{235}U(n,f), ^{239}Pu(n,f)	^{238}U(n,γ) Reaction
	^{235}U Worth	^{238}U(n,γ) Reactions	Passive Dosimetry
Measurement Uncertainty	3-10%	3-10%	2-10%

Table 3. Characterization of Fast Neutron Fields

Neutron Field	Mean Neutron Energy (keV)	Median Neutron Energy (keV)	95% Range		$\frac{^{235}U(n,f)}{^{238}U(n,f)}$
			E_L (keV)	E_H (keV)	
CFRMF	760	375	4.6	4000	20
STEK					
- 500	808	272	2.4	5210	17
- 4000	537	74	0.06	4230	63
EBR-II					
- Midplane	555	172	3.5	3710	34
- Reflector	233	60	0.05	1670	345
1000 MW LMFBR					
- P1	427	75	0.9	2760	50
- P25	216	27	0.2	2230	190

Table 4. Integral Data Base For Important Fission-Product Nuclides

Nuclide	% Contribution[a]	Integral Measurements					
		FRO	CFRMF	STEK	EBR-II	ERMINE	PHENIX
^{105}Pd	9.9	-	-	R	-	R	T
^{99}Tc	8.6	R	A	R	-	R	-
^{101}Ru	7.7	R	-	R	-	-	T
^{107}Pd	6.2	-	-	R	-	-	-
^{103}Rh	5.5	R	A	R	-	R	-
^{133}Cs	4.9	R	A	R	-	R	T
^{147}Pm	3.5	R	A	R	-	R	-
^{149}Sm	3.4	R	R	R	T	-	T
^{145}Nd	3.4	-	R	R	T	-	T
^{102}Ru	3.3	R	A	R	-	R,A	-
^{135}Cs	3.0	-	-	-	-	-	-
^{97}Mo	2.9	R	R	R	-	-	T
^{109}Ag	2.7	-	A,R	R	-	R	-
^{106}Ru	2.3	-	-	-	-	-	-
^{143}Nd	2.3	-	R	R	T	-	-
^{131}Xe	1.9	-	-	R	-	-	-

a. Estimated percent contribution to total fission-product absorption in a fast reactor.

Table 4. Integral Data Base For Important Fission-Product Nuclides (Cont'd)

Nuclide	% Contribution	Integral Measurements					
		FRO	CFRMF	STEK	EBR-II	ERMINE	PHENIX
^{151}Sm	1.9	-	-	R	-	-	T
^{95}Mo	1.5	R	R	R	-	-	T
^{104}Ru	1.3	R	A	R	-	A	-
^{153}Eu	1.3	-	A	-	T	-	-
^{98}Mo	1.2	-	A,R	R	-	A	-
^{144}Ce	1.1	-	-	-	-	-	-
^{129}I	1.0	-	A	R	-	-	-
^{100}Mo	0.9	-	A,R	R	-	A	-
^{141}Pr	0.9	-	A	R	-	A,R	-
^{93}Zr	0.8	-	-	R	-	-	-
^{108}Pd	0.8	-	A	R	-	A	-
^{103}Ru	0.8	-	-	-	-	-	-
^{155}Eu	0.7	-	-	-	-	-	-
^{95}Zr	0.7	-	-	-	-	-	-
^{148}Nd	0.7	-	A,R	R	T	A	-
^{150}Nd	0.7	-	A,R	R	-	A	-

Table 4. Integral Data Base For Important Fission-Product Nuclides (Cont'd)

Nuclide	% Contribution	Integral Measurements					
		FRO	CFRMF	STEK	EBR-II	ERMINE	PHENIX
^{132}Xe	0.6	-	A	-	-	-	-
^{134}Xe	0.6	-	A	-	-	-	-
^{146}Nd	0.6	-	A	R	T	A	-
^{111}Cd	0.6	-	-	-	-	-	-
^{152}Sm	0.6	-	A,R	R	-	A	-
^{137}Cs	0.5	-	A	R	-	-	-
^{106}Pd	0.5	-	-	R	-	-	T
^{83}Kr	0.4	-	-	-	-	-	-
^{96}Zr	0.4	-	-	R	-	-	-
^{127}I	0.4	-	A,R	R	-	-	-
^{142}Ce	0.4	-	A	R	-	A	-
^{95}Nb	0.4	-	-	-	-	-	-
^{139}La	0.4	-	A	R	-	A	-
^{147}Sm	0.4	-	R	R	T	R	-
^{85}Rb	0.3	-	-	-	-	-	-
^{140}Ce	0.3	-	A	R	-	-	-
^{157}Gd	0.3	-	-	R	-	-	-
^{156}Gd	0.3	-	-	R	-	-	-

Table 5. Integral Tests for ENDF/B-V Fission-Product Capture Cross Sections

Nuclide	Importance	Neutron Field	C/M	Discrepancy Range	V/IV	Consistency IV-V More	Consistency IV-V Less	Consistency IV-V No Change
^{98}Mo	21	CFRMF	1.09(7)	1-2	0.97	-	X	-
^{100}Mo	24	CFRMF	0.86(17)	< 1	1.03	X	-	-
^{99}Tc	2	CFRMF	1.15(15)	1-2	1.21	-	X	-
^{102}Ru	10	CFRMF	1.12(7)	1-2	0.87	X	-	-
^{104}Ru	19	CFRMF	1.04(7)	< 1	1.02	-	X	-
^{108}Pd	27	CFRMF	1.20(7)	2-3	1.37	-	X	-
^{109}Ag	13	CFRMF	0.86(10)	2-3	1.53	X	-	-
^{127}I	42	CFRMF	1.16(10)	1-2	1.02	X	-	-
^{129}I	23	CFRMF	1.07(7)	1-2	0.87	X	-	-
^{132}Xe	33	CFRMF	1.10(8)	1-2	1.00	-	-	X
^{134}Xe	34	CFRMF	1.70(7)	> 4	1.04	-	X	-
^{133}Cs	6	CFRMF	1.02(7)	< 1	0.97	X	-	-
^{137}Cs	38	CFRMF	0.08(25)	> 4	1.00	-	-	X
^{139}La	45	CFRMF	1.10(6)	1-2	0.90	X	-	-
^{142}Ce	43	CFRMF	1.34(8)	> 4	1.00	-	-	X
^{141}Pr	25	CFRMF	1.01(15)	< 1	0.82	X	-	-

Table 5. Integral Tests for ENDF/B-V Fission-Product Capture Cross Sections (Cont'd)

Nuclide	Importance	Neutron Field	C/M	Discrepancy Range	V/IV	Consistency IV-V More	Consistency IV-V Less	Consistency IV-V No Change
^{143}Nd	15	EBR-II-M	0.85(8)	1-2	0.99	-	-	X
		EBR-II-R	0.86(15)	< 1	0.96	-	X	-
^{145}Nd	9	EBR-II-M	0.77(8)	2-3	1.20	X	-	-
		EBR-II-R	0.80(17)	1-2	1.12	X	-	-
^{146}Nd	35	CFRMF	1.24(7)	3-4	0.81	X	-	-
^{148}Nd	31	CFRMF	1.30(14)	2-3	0.75	X	-	-
^{150}Nd	32	CFRMF	1.45(12)	3-4	0.70	X	-	-
^{147}Pm	7	CFRMF	1.12(13)	< 1	0.97	X	-	-
^{147}Sm	46	EBR-II-M	0.87(9)	1-2	1.31	X	-	-
		EBR-II-R	1.06(20)	< 1	1.20	X	-	-
^{149}Sm	8	EBR-II-M	0.77(9)	2-3	1.31	X	-	-
		EBR-II-R	0.84(19)	< 1	1.12	X	-	-
^{152}Sm	37	CFRMF	1.18(7)	2-3	1.17	-	X	-
^{153}Eu	20	CFRMF	1.00(7)	< 1	1.06	X	-	-
		EBR-II-M	0.89(9)	1-2	1.08	X	-	-
		EBR-II-R	0.90(17)	< 1	1.02	X	-	-

Table 6. Ratios of Calculated-to-Measured CFRMF Integral Cross Sections For Various Evaluated Differential Data

Nuclide	Unadjusted[a]	Adjusted[b] W/O-CFRMF	Adjusted[b] W-CFRMF	W/UN[c]	W/(W/O)[d]
^{98}Mo	1.061	1.005	1.005	0.95	1.00
^{99}Tc	0.993	1.187	1.170	1.18	0.99
^{102}Ru	1.359	1.224	1.168	0.86	0.95
^{104}Ru	1.090	1.119	1.091	1.00	0.97
^{108}Pd	1.059	1.374	1.363	1.29	0.99
^{109}Ag	0.572	0.784	0.822	1.43	1.05
^{129}I	1.298	1.088	1.061	0.82	0.98
^{146}Nd	1.393	1.188	1.115	0.80	0.94

a. Unadjusted: Ratio of calculated-to-measured integral cross sections, calculated cross section computed with ENDF/B-IV fission-product capture cross section.

b. Adjusted: Ratio of calculated-to-measured integral cross sections, W/O-CFRMF implies calculated cross section was computed with differential data which did not include CFRMF measured integral data for adjustment analysis, W-CFRMF implies that calculated cross section was computed with differential data which did include CFRMF measured integral data in adjustment analysis.

c. W/UN: Ratio of column 3 to 2.

d. W/(W/O): Ratio of column 4 to 3.

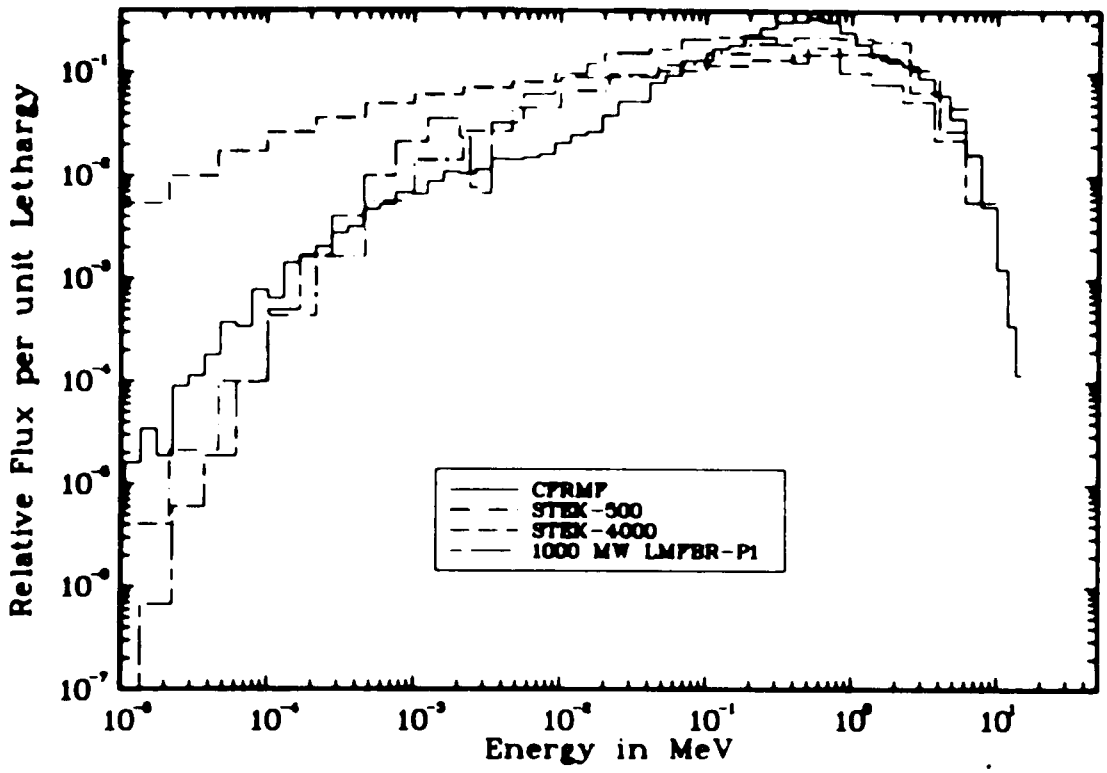

Figure 1. Comparison of Reactor Fast Neutron Fields.

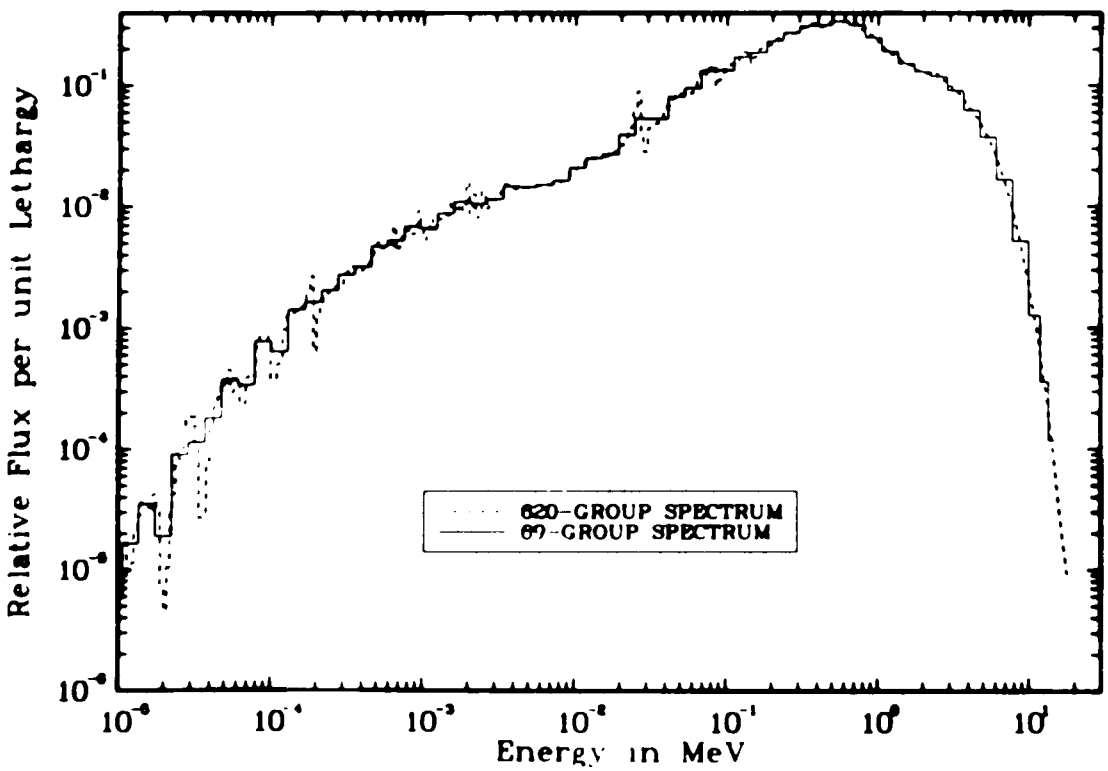

Figure 2. Comparison of Broad-Group and Fine-Group Representations for CFRMF Central Neutron Spectrum.

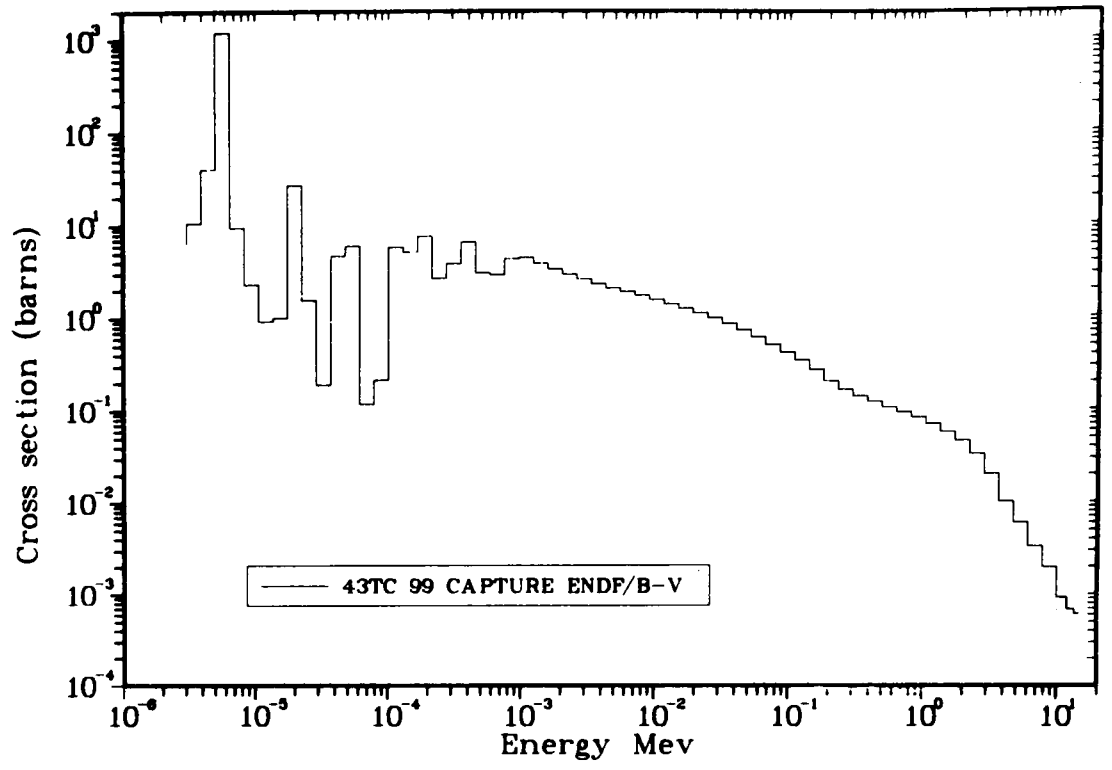

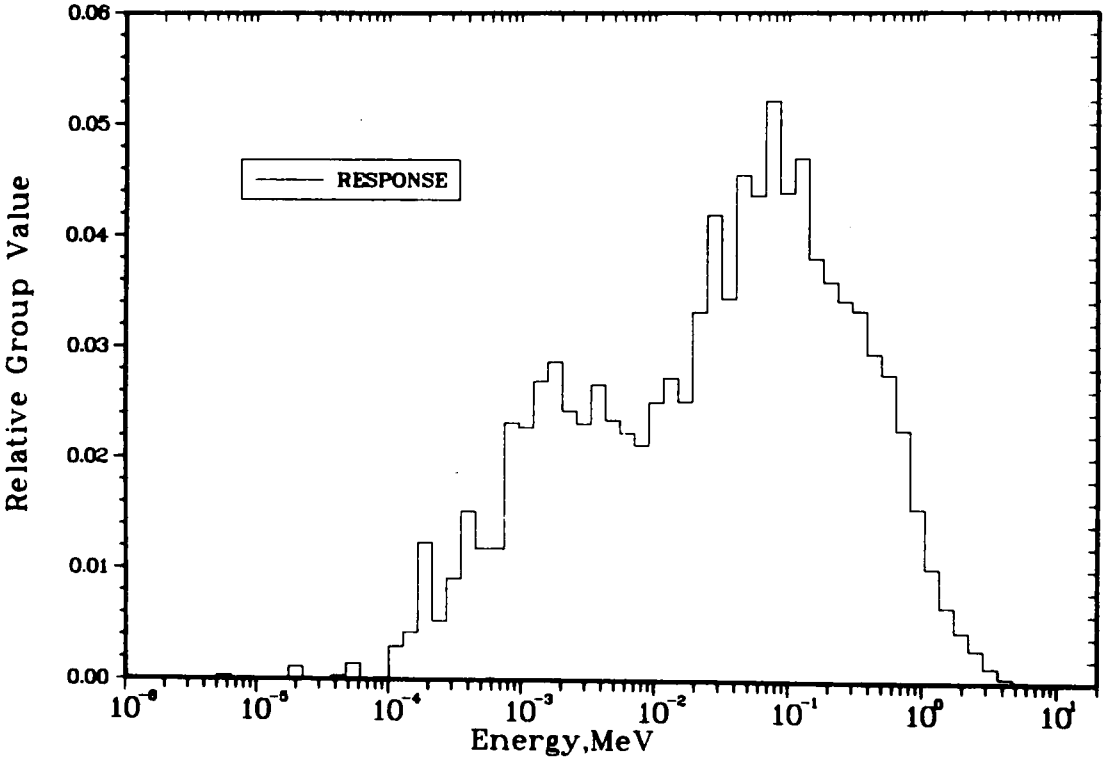

Figure 3. ENDF/B-V Cross Section for $^{99}Tc(n,\gamma)$ and Response in CFRMF.

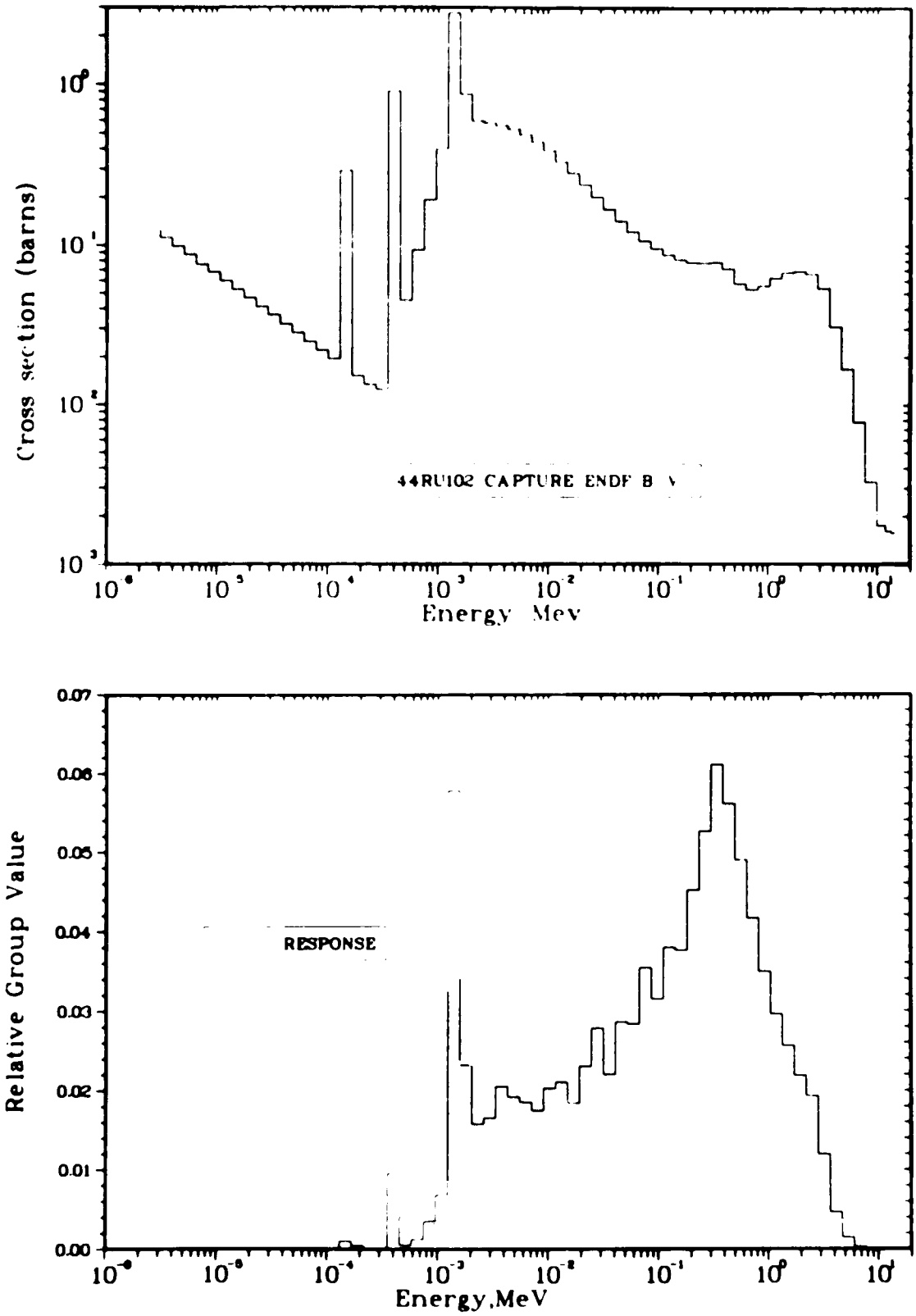

Figure 4. ENDF/B-V Cross Section for $^{102}Ru(n,\gamma)$ and Response in CFRMF.

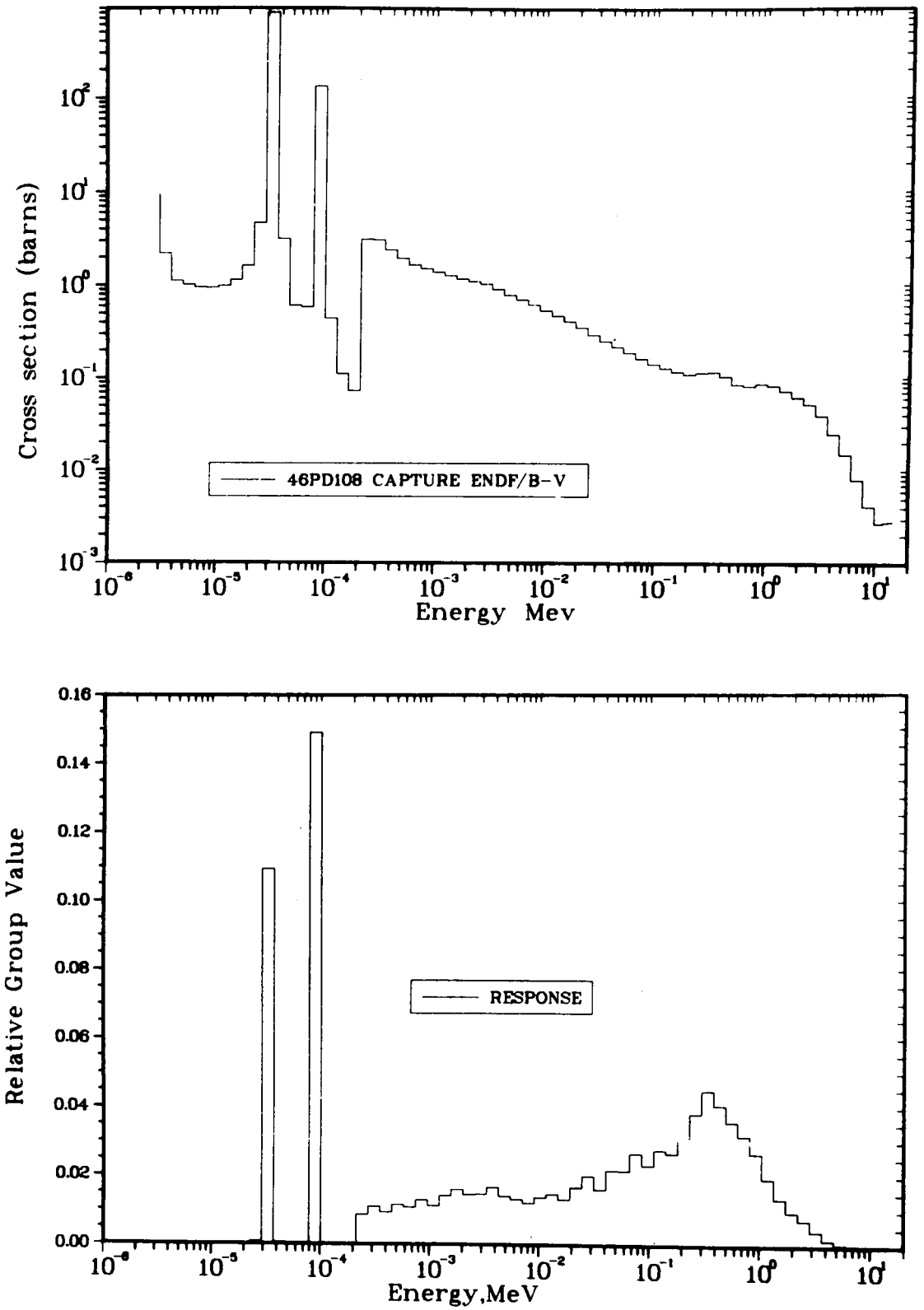

Figure 5. ENDF/B-V Cross Section for $^{108}Pd(n,\gamma)$ and Response in CFRMF.

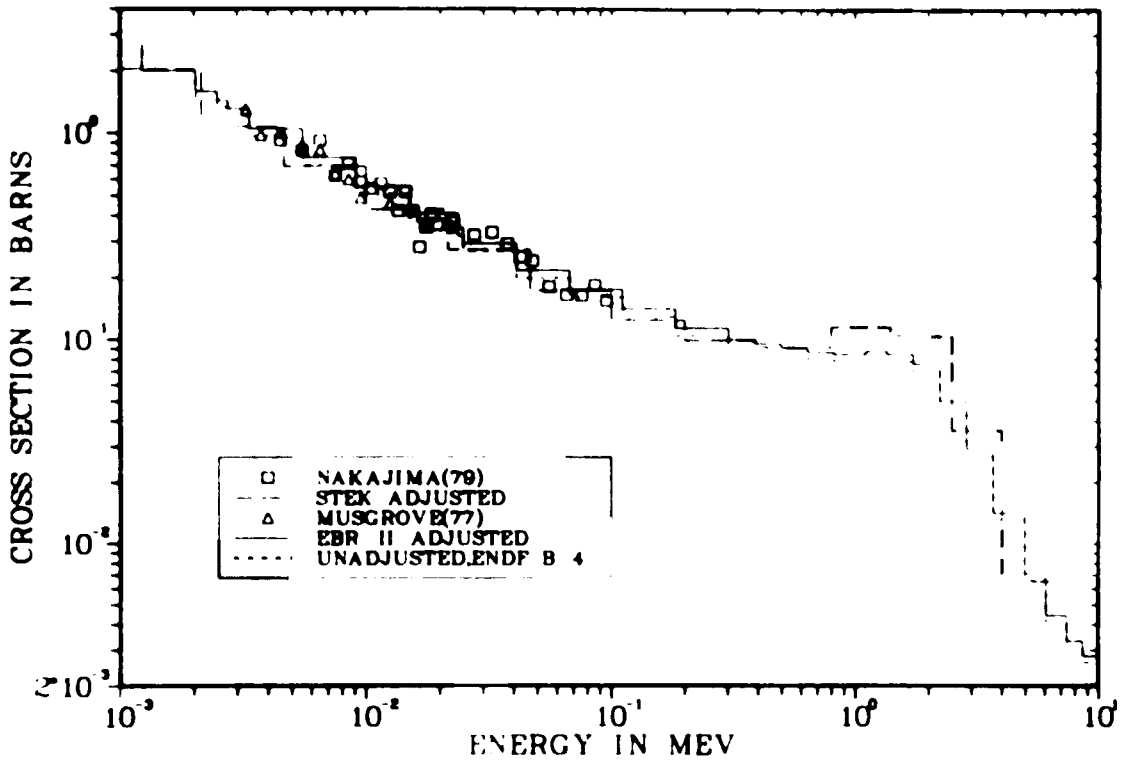

Figure 6. Comparison of EBR-II Adjusted Cross Section for ^{143}Nd to Other Data.

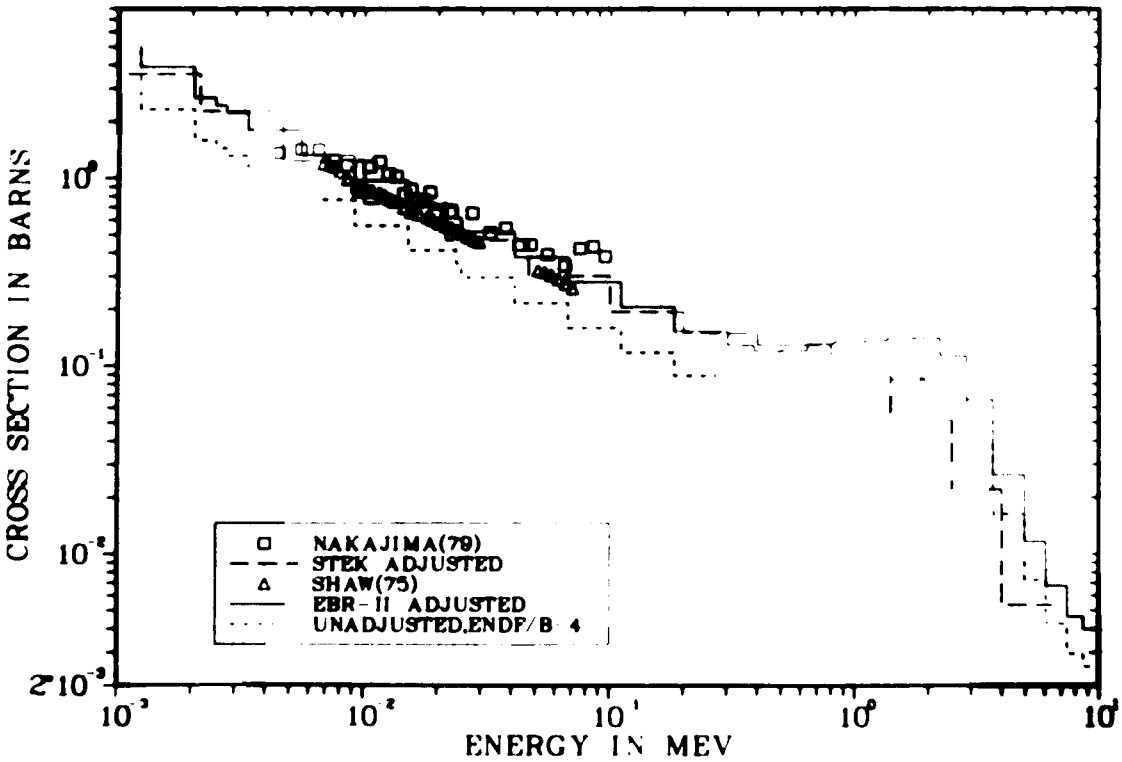

Figure 7. Comparison of EBR-II Adjusted Cross Section for ^{145}Nd to Other Data.

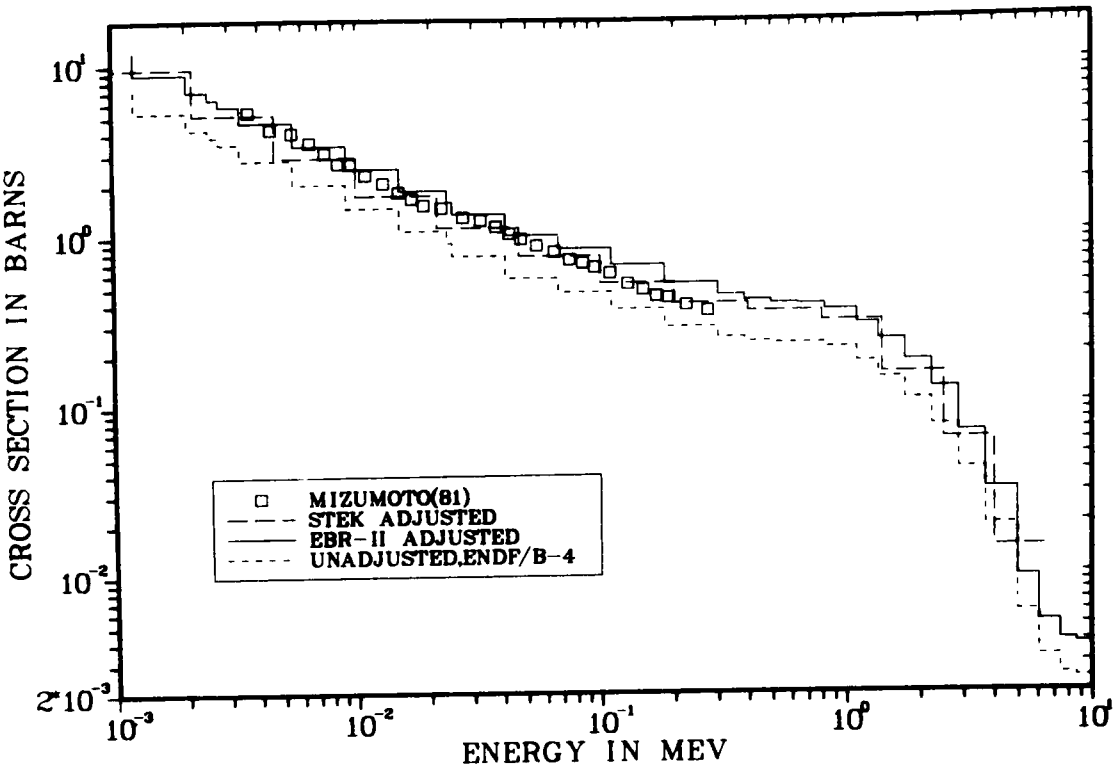

Figure 8. Comparison of EBR-II Adjusted Cross Section for ^{147}Sm to Other Data.

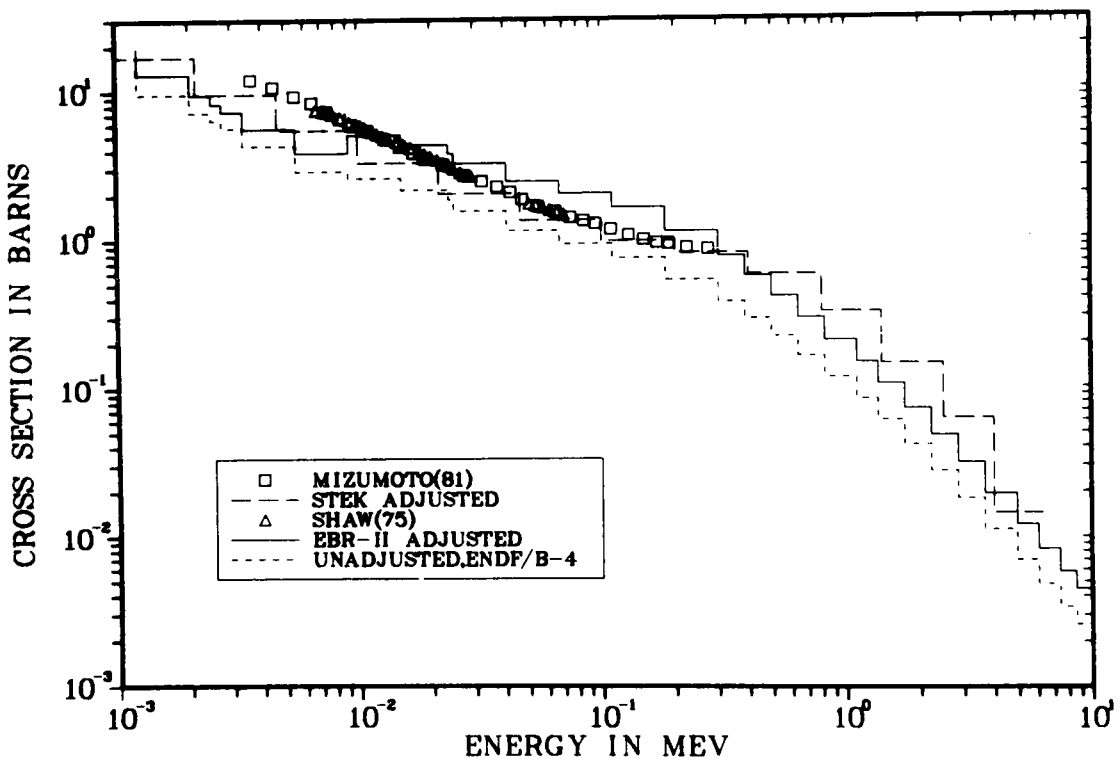

Figure 9. Comparison of EBR-II Adjusted Cross Section for ^{149}Sm to Other Data.

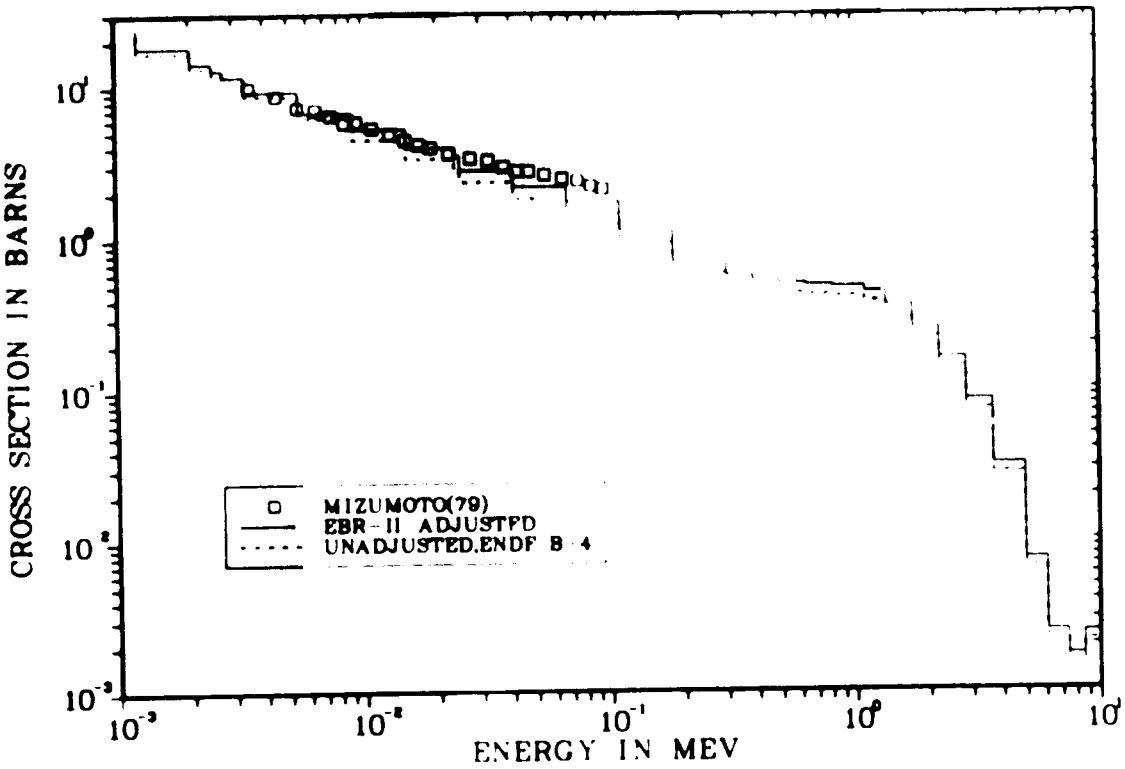

Figure 10. Comparison of EBR-II Adjusted Cross Section for ^{153}Eu to Other Data.

Discussion

COMMENT: A. Smith
I recall that somebody at this laboratory a while back made a study of fuel cycle economics using a lumped fission product data set based on an ancient Babcock-Wilcox set and than used ENDF/B-V and the result, I guess, was a big yawn. It did not have much punch to it. So are the problems discussed here, concerning small differences, really important. Do we take the requests for 5 or 10% accuracies seriously?

COMMENT: R. Schenter
I think it was just a coincidence that the Babcock-Wilcox lumped fission product value agreed with ENDF/B-V. Between Babcock-Wilcox and ENDF/B-V was version IV and there was about a 10% difference there. The ENDF/B-IV data represented a large number of differential data and nuclear model calculations. Then the version V included differential and integral values and there was a change. I think it is just a coincidence that Babcock-Wilcox agreed with V. There is a lot of concern about the FP absorption. Collins showed that they have an important impact on things like breeding ratio etc. The uncertainties of the FP absorption is important for the enrichment specifications, with large economic consequences in the order of millions of dollars. These people didn't yawn.

COMMENT: H. Gruppelaar
The uncertainty in the lumped fission-product cross section is difficult to estimate. Due to the large number of isotopes the statistical uncertainty in the fast capture cross section is probably small. The remaining error is of a systematical nature. In the case of adjusted data sets, this systematical error might be close to the systematical error in the integral data, i.e. the uncertainty in the normalization and that in the shape of the flux spectrum of the reactor core. This error is estimated to be about 5%. We have assumed a total uncertainty of 6 to 9% in the lumped fission-product average cross section in a fast power-reactor spectrum (see Bologna-1979).

Report of the Working Group on

FAST-NEUTRON CAPTURE IN FISSILE AND FERTILE NUCLIDES

Chairman: R. W. Peelle
Participants: F. Corvi, H. Derrien, G. Grenier, E. Menapace, W. Poenitz, L. Weston, S. Whetstone and R. Peelle.
Also in attendance for portions of the discussions; P. Collins, R. Howerton, P. Moldauer, P. Persiani and A. Smith

INTRODUCTION

Extensive graphical and numerical presentations, available to the working group, assisted us in exploring the rich data base established through the labors of many skilled persons. Consistent with the meeting setting, the working group discussion concentrated on data for fast-breeder reactor (FBR) applications. All but 1-3% of the magnitude of cross section sensitivities of FBR parameters come from the energy region below ≈ 1.5 MeV, so the statistical model is the relevant theoretical concept. The Meeting emphasizes energies above ≈ 10 keV where resonance fluctuations are not a dominant factor. However, we should remember that approximately half the FBR sensitivity to ^{238}U capture data, as reflected in integral parameters, lies below 25 keV where resonance fluctuations are strong and resonance self-protection is a most important consideration in reactor physics. There are similar low-energy aspects to ^{239}Pu capture in that ≈ 30% of the FBR-parameter data sensitivity lies below ≈ 4 keV. Even with the discussion largely confined to the ≈ 10-1500 keV region, the working group could only scratch the surface of the available body of information. The reader is referred to the papers presented at the Meeting and to the references contained therein in order to obtain a more detailed understanding of current issues related to fissile and fertile fast-neutron capture.

ACCURACY GOALS

Enunciation of appropriate accuracy goals is very difficult, so they probably never will be stated in a fully satisfactory manner. The working group primarily relied upon an interpretation of the goals set forth by P. Collins at the Meeting. It seemed to be the consensus of the experimentalists present that achieving the most stringent basic-data accuracy goals so far set forth will be trying but not impossible using differential data alone. Critical-integral experiments will continue to serve as "quality assurance" checks of the differential data.

Accuracy goals can be briefly summarized for one-group FBR cross sections. Such a simple formulation, taken from Rowlands (Conf. on Neut. Phys. and Nucl. Data, Harwell, 1978), is given in Table 1. Here and elsewhere it is unclear what goal should apply for neutron capture in ^{240}Pu.

Table 1. One-group FBR Fissile-Fertile Capture Goals*

Fertile (n,γ) cross sections	± 3%
Fertile (n,γ)/Fissile (n,f) ratio	± 1.5%
Fissile (n,γ) cross sections	± 4%
Other (n,γ) cross sections	± 10%

*In a conventional U-Pu FBR system, fertile = ^{238}U and fissile = ^{239}Pu. Rowlands' table leaves ambiguous the required accuracy for the capture cross section of ^{240}Pu. It is helpful to put accuracy requirements in terms of one-group cross sections so that the reader will notice that there is no need to meet the tolerance at each energy of interest.

The primary FBR capture sensitivity lies below 500 keV, so the above goals can be relaxed at higher energies. The estimates are explicitly relevant to the U-Pu FBR systems. However, if the Th-U FBR cycle again becomes of interest, similar statements are applicable to ^{232}Th (fertile) and ^{233}U (fissile) data. Rowlands notes that the energy dependences are a concern in the case of some integral parameters.

More detailed lists of accuracy goals are to be found in the literature. The present speaker believes that k_{eff}-reset sensitivities can be used in assessing some of the ultimate data needs and such considerations may result in some relaxation of basic-data accuracy goals. On the other hand, most of the present goals are based on needs for founding rather than optimizing a fast reactor industry.

The above guidelines are inclusive of fuel-cycle and safeguards interests. The latter need for cross sections to permit correct calculation of the isotopic content of spent fuel was outlined for the working group by P. Persiani.

Finally, the sometimes quoted 10% accuracy goals for ^{233,235}U alpha (ratio capture/fission) above 1 MeV (see recent draft NEANDC/NEACRP priority request list) are difficult to understand. It is suggested that these fissile-U requirements be re-examined. They will be very difficult to meet.

USE OF NUCLEAR THEORY

The modes of use of nuclear theory in cross section evaluation are; i) to provide information where experimental data do not exist, ii) to check the

reasonableness of incomplete data sets, iii) to assist in achieving consistency among partial cross sections, and at the minimum iv) to indicate a physically plausible energy-averaged cross-section behavior to guide evaluations. Below 1 MeV, the region of most concern here, the statistical processes predominate although direct reaction mechanisms are of importance for inelastic scattering. Apparently the primary theoretical problems are associated with fission, resulting in difficulty in accurately calculating the fission competition with other compound-nucleus channels. There is a similar, though less serious problem associated with inelastic-channel competition with the capture process as there remain uncertainties in the calculation of inelastic scattering itself.

In summary, in this mass-energy region the theoretical framework for calculating energy-averaged cross sections is sound in the absence of fission; however, results are sensitive to the choice of model-parameter values that are not well known. In the presence of fission the situation is far more complex and uncertain. Therefore, calculations alone cannot provide the highly quantitative capture data required for the isotopes of major interest.

EXPERIMENT

Well developed experimental techniques can probably meet the capture-data needs of the lesser isotopes as those needs are presently formulated. For the major isotopes the contemporary goals are challenging indeed and will be achieved only through the most arduous application of a combination of the finest techniques available. For measurements of alpha in fissile nuclides, emphasis should be given to measurements using techniques capable of differentiating between fission and capture (e.g. use of multiplicity detectors or high-efficiency fission chambers). Especially for ^{238}U capture, we must try hard for a replication of experiments that take advantage of favorable experimental opportunities where nature provides us with a potential for the highest precision (e.g. $\approx$ 30 keV measurements using the $^{7}Li(p,n)$ associated-activity method, coupled with activation detector calibration based on the α-activity of a sample of the natural parent). We must also keep in mind the special importance of the ratio of cross sections for ^{238}U capture and ^{239}Pu fission.

Since the most important goals will be achieved with difficulty, we must stress careful reporting of results, for example by including sensitivities of results to input parameters used in the analysis. Uncertainty and covariance information should be explicitly stated. Particularly for ^{238}U capture, more attention should be given to assure that self-shielded as well as infinite dilution cross sections can be obtained from the reported results.

EVALUATION TECHNIQUES

The workshop participants were encouraged to note the increased use of theory in the evaluation process as well as the wider application of relatively rigorous numerical methods in the combination of experimental data. It seems essential to continue and expand these trends if evaluated cross sections are to represent our global knowledge.

STATUS OF THE DATA

The working group reviewed the status of fissile and fertile capture data. This review was in summary and support of the papers presented at the Meeting. The situation is briefly summarized as follows:-

^{233}U

The existing data below 2 keV and above 30 keV seem reasonable. The gap without direct experimental data between these two energies should not be allowed to remain indefinitely. Even data of relatively low accuracy would be helpful to limit the magnitude of possible future surprises.

^{235}U

Corvi showed, at this Meeting, that selected data sets obtained using contemporary state-of-the-art techniques display a wide spread in alpha. Corvi's recent data and the data of Muradyan (1979 Knoxville Conference) fall well below the Gwin data that have guided many evaluations (Corvi more than 10% lower over the 5-50 keV region and Muradyan up to 20% lower at all energies). The normalization problem for ^{235}U alpha is relatively severe compared to that of ^{239}Pu measurements. Indeed, the best normalization technique is a matter of some controversy among the experts. It appears that the requested one-group accuracy of ± 4% has not been met unless it is appropriate to renormalize some of the data sets. The ± 4% tolerance is assumed to apply because of the extensive past use of ^{235}U in fast reactor test assemblies.

^{239}Pu

Agreement among the results of measurements selected for the review of Corvi is better than for the above ^{235}U case, perhaps because the normalizations are easier and the alpha values larger at low energies. The evaluations now appear to be converging. However, the inherent difficulty of these measurements, the problems seen in the results from similar but easier experimental work for ^{235}U, the quoted uncertainties, and the importance of accurate results all suggest that new ^{239}Pu alpha measurements be undertaken using refined techniques.

^{238}U

The long standing shape and magnitude differences among the various data sets have not been resolved. However, Poenitz, in his paper at this meeting, estimates a contemporary ± 5% uncertainty in the 10-500 keV energy range, increasing to ± 10% at 1 MeV. At the higher energies the data needs are met, but in the central and lower-energy regions that is not so. One should also recall that self-shielding is important, even for the gross reaction rate, and

that ≈ 30% of the typical FBR sensitivity to ^{238}U capture lies below ≈ 10 keV where uncertainties are larger. Vigorous experimental efforts using improved techniques are required for reaching ^{238}U capture accuracy goals, as indicated above.

^{232}Th

The data situation appears to be similar to that of ^{238}U, though the measured results reported at this meeting appear to be just significantly larger than the consensus of previously reported values. Since Th-cycle fast reactors are not presently proposed, the urgency for Th-data improvement is not as strong as that for ^{238}U.

^{240}Pu

The present situation is questionable if high-^{240}Pu-content fuels are to be used in FBR systems. A one-group accuracy requirement of ± 10% may be met, but not the 3% requirement suggested by Hammer (1979 Knoxville).

^{241}Pu

There is only one direct measurement and its results seem reasonable. Confirmation would be appropriate if superior techniques, proven in ^{239}Pu measurements where the requirements are more stringent, can be employed. Note that Hammer suggests a one-group uncertainty tolerance of ± 5% that is not likely met at present.

^{242}Pu

The measured data seem in sufficient agreement to meet the one-group accuracy requirement of ±10%.

^{241}Am

The data of Wisshak, of Gayther, and of Weston provide a satisfactory basis for meeting the usually stated needs, though the Weston data are lower by up to 20% in the 10-100 keV region. The Weston data are the easiest to fit with theory, but Derrien stated that integral results obtained at Cadarache support the higher values which were used in their (French) evaluation. The above situation may soon improve since new microscopic data are expected from CBNM.

^{237}Np

Derrien reported that the data of Weston and of Lindner support an evaluation at Cadarache that is theoretically reasonable and believed valid to about 5% at low energies and to perhaps 10% at 1 MeV. Consideration should be given to a revision of the ENDF/B-V ^{237}Np evaluation. Generally, known experimental data needs appear to be met in this case.

^{238}Pu

There appear to be no reliable microscopic data. It was noted that the explosive-source results of Silbert et al. seem to have been subject to large background effects, at least in the resonance region. Derrien reported a new capture evaluation which goes more than 25% below ENDF/B-V but which is in agreement with Masurca and Phenix integral results.

^{243}Am

At present there appears to be available only one data set and that is preliminary in nature. This is not a satisfactory situation.

The above status is summarized in the following table:-

Table 2. DATA-STATUS SUMMARY
Are FBR Neutron-Capture Needs Met?

Nuclide	Probably-YES	MAYBE+	Probably-NO
^{232}Th			X*
^{233}U			X*
^{235}U			X
^{238}U			X
^{237}Np	X		
^{239}Pu			X
^{240}Pu		X	
^{241}Pu		X	
^{242}Pu	X		
^{241}Am	X		
^{243}Am			X

+Following re-evaluation.

*If Th-cycle systems are a consideration.

RECOMMENDATIONS

1. New ^{238}U capture measurements, made with advanced techniques, are needed below approximately 100 keV. Some of these measurements should concentrate on obtaining 2% uncertainties, exploiting favorable experimental opportunities. One of the latter may be the $^{7}Li(p,n)$ source reaction near threshold (i.e. $\approx$ 30 keV neutron energy). It must be assured through other efforts that self-shielding effects and the methods for their interpretation are adequately treated.

2. ^{239}Pu capture (or alpha) data are probably in deceptive agreement. Therefore, measurements with improved techniques should be undertaken (for "tuneup", or if equivalent need for ^{235}U capture data exists, similar efforts should be applied to ^{235}U).

3. For the most important nuclides that correspond to demanding accuracy goals, routine repetition of measurements using old techniques will not be worthwhile.

4. There is only a single data set available for ^{241}Pu capture and only a preliminary set for ^{243}Am. This is an unsatisfactory situation and experimental confirmation is desirable.

5. Consideration should be given to revising the evaluations (including neutron capture) for at least ^{232}Th, ^{235}U, ^{239}Pu and ^{240}Pu.

6. Nuclear-model codes should be applied to a greater extent in the evaluation process in order to assist in determining physical shapes and the consistency among partial cross sections. Model codes are not now, and will not soon be, sufficiently accurate to provide the accurate absolute values sought for the more important nuclides.

7. The validity of seemingly unreal requests for alpha data for fissile nuclides at high energies is questioned and the need should be further justified.

Report of the Working Group on

FAST-NEUTRON CAPTURE IN STRUCTURAL MATERIALS

Chairman: F.H. Fröhner
Participants: D. Gayther, G. Nordborg, R. Macklin, G. Rohr, K. Wisshak and (part time) F. Corvi

1. Scope of Discussions

The discussions of developments in the field of capture data of structural materials since the 1977 Geel meeting were mainly based on the invited paper presented by G. Rohr and on information from the other participants about their own activities. There was not much input about recent work in Japan, where the new version JENDL-2 of the Japanese Evaluated Nuclear Data Library has been issued, or on the resonance analysis work on iron and nickel isotopes going on at ORNL. Moreover, the discussion was restricted to the three principal structural material elements Cr, Fe and Ni. Some of the remaining structural materials such as Zr and Mo were covered by the Working Group on Fission Product Nuclides.

2. Long-term goals

The review of accuracy requirements for LMFBR and similar applications presented by P. Collins in essence confirmed the picture drawn by Hammer et al. at Geel in 1977. This means that fast-neutron capture cross sections are needed with about 5% accuracy for Fe, 8% for Ni and 10-12% for Cr. Although considerable progress has been made since, these target accuracies have not been reached by experimenters except perhaps in limited energy ranges. Many of the persisting problems are related to the pronounced resonance structure and the extremely high scattering-to-capture ratios across s-wave resonances of the main structural materials (Fe, Ni, Cr) in the technologically most important energy range from 0 up to about 300 keV. Another source of difficulties are the γ-spectrum fluctuations from resonance to resonance exhibited by by the structural-material nuclides. One conclusion from the subsequent discussions was that

- the target goals for reactor applications cannot be reached without further substantial experimental effort especially in the resonance region.

With the new techniques refered to below a reduction of present errors to a level satisfying most user requests seems to be achievable during the coming years at least for Cr and Ni. To reach 5% uncertainty for Fe certainly requires a special effort, but in view of new results for the 27.7 keV resonance of ^{56}Fe this goal appears not completely unrealistic.

3. Recent Measurements

Following recommendations of the 1977 Geel meeting the prompt neutron background due to very severe scattering across broad s-wave resonances has been studied experimentally at several laboratories. A technique originally proposed by Macklin was used at the Van de Graaff accelerators at Lucas Heights and especially at Karlsruhe, namely time-of-flight discrimination between capture events in the sample and counts caused by capture of resonance-scattered neutrons in and near the detectors. This discrimination is achieved with very short primary flight paths (few cm) and similar secondary flight paths between sample and detectors, in conjunction with tailored quasi-monoenergetic neutron spectra, as explained in K. Wisshak's contribution. At Karlsruhe several metallic, isotopically pure samples with different thicknesses were used in measurements on ^{56}Fe, ^{58}Ni and ^{60}Ni. The spectra were tailored so as to cover just one of the strong s-wave resonances in each case, and Moxon-Rae detectors with three different converters were employed. Deviations of the detector efficiency at small γ-ray energies from the ideal energy-independence were corrected for with the help of theoretical capture γ-ray spectra specially calculated by the Bologna group. The resonance shapes including multiple-collision and resolution effects were fitted with the FANAC code. The reported (still preliminary) results show excellent consistency: the radiation widths obtained with different sample thicknesses or neutron spectra or converters agree within few percent. They agree also quite well with the older KfK scintillator tank results of Ernst, Fröhner et al. showing that in spite of the substantial corrections for multiple collisions and prompt neutron background the older results do not appear to contain any serious errors . Finally, for the strong 27.7 keV resonance of ^{56}Fe they are consistent with the evaluation of all previous measurements which B. Allen sent to the present meeting:

Target Nucleus	Resonance Energy (keV)	Radiation Width (eV)	Detector, Method	Authors	Year
^{58}Ni	15.4	1.46 ± .22	Tank	Fröhner/Ernst	1975
		1.55 ± .04	Moxon-Rae	Wisshak et al.	1982
^{60}Ni	12.5	2.73 ± .50	Tank	Fröhner/Ernst	1975
		2.89 ± .05	Moxon-Rae	Wisshak et al.	1982
^{56}Fe	27.7	1.25 ± .20	Tank	Fröhner/Ernst	1975
		1.08 ± .02	Moxon-Rae	Wisshak et al.	1982
		1.00 ± .04	Evaluation	Allen	1982

Note: - Errors given by Wisshak et al. are statistical only. Their preliminary rough estimate of systematic errors is 5% .

The radiation widths for the 27.7 keV resonance of ^{56}Fe listed here have to be compared with values reported until 1977 ranging from 0.6 to 1.6 eV. The demonstrated progress is due mainly to recognition of prompt neutron background as a main source of errors. It was realised that in measurements of the structural-material capture cross sections it is essential to determine the sensitivity of the detector to prompt scattered neutrons.

- It is recommended that this be done experimentally, if necessary with the aid of detailed analytical or Monte Carlo calculations for interpolation between experimental points. At Van de Graaff accelerators one should use time-of-flight discrimination between capture γ-rays and scattered neutrons together with tailored neutron spectra whenever possible.

The latter technique permits practically complete elimination of prompt neutron background. Its usefulness is, however, restricted to a limited number of strong s-wave resonances in the lower keV region due to the modest energy resolution achievable. In any case the recommendation of the 1977 Geel meeting still remains valid:

- Experimenters should check their ability to account for sensitivity of their detectors to prompt scattered neutrons and for multiple-collision effects by determining radiation widths for a list of resonances for which $\Gamma_n \gg \Gamma_\gamma$.

The difficulties caused by fluctuations of the γ-ray spectra from resonance to resonance and by the need to determine the neutron flux accurately were put in evidence by G. Rohr. He compared capture areas for p- and d-wave resonances of ^{54}Fe, ^{56}Fe and ^{57}Fe obtained at ORNL, RPI, Harwell, KfK and Geel. He found that the ^{56}Fe capture areas from ORNL are systematically higher by about 17% than those from Geel. They agree, however, with the KfK values for levels with a soft capture γ-ray spectrum, whereas the Geel values agree with the KfK results if the capture γ-ray spectrum is hard. A comparison with results from Harwell indicates inconsistencies in flux shape between Oak Ridge on one side and Geel/Harwell on the other at energies below 30 keV. It appears that the discrepancies can not be blamed on inadequate weighting functions used for the total-energy detectors at Geel and ORNL. On the other hand, black-resonance normalisation at Geel based on the first resonances of Au and Ag gave flux calibrations that differed from those based on the measured transmission dip area of the 1.15 keV resonance of ^{56}Fe. In order to locate the source of the trouble it is recommended to

- check the flux shape determination at ORNL (perhaps in the same manner as at Harwell and Geel),

- check the KfK corrections for the influence of harder or softer γ-ray spectra on the intrinsic tank efficiency (these were based on observed γ-ray spectra for individual resonances and on tank

escape calculations performed for different γ-cascades by Kompe),

- check the transmission dip area of the 1.15 keV resonance of ^{56}Fe. (Two determinations at Geel agreed but had limited statistical accuracy and differed from results obtained elsewhere.) This check should be performed at laboratories other than Geel, e. g. at ORNL,

- check whether the black-sample normalisation based on Au and Ag resonances reproduces the correct thermal cross section of ^{56}Fe (in progress at Geel),

- check geometry effects for Moxon-Rae and total-energy detectors which could result from the expected differences in multiplicity and anisotropy between γ-ray spectra differing in hardness.

Many of the problems encountered in measurements of structural-material capture cross sections are caused by limited neutron source strength, necessitating for instance fairly thick samples for which multiple-scattering and γ-ray self-absorption corrections are substantial. K. Wisshak mentioned a study made at KfK which indicates that the new techniques applied to discriminate against prompt neutron background at Van de Graaff accelerators could also be used with modern high-current ion accelerators that are being sold commercially off the shelf. He suggested that possibilities be explored to replace weaker electrostatic accelerators by such modern and relatively inexpensive machines.

4. Theory

The question was discussed whether simple resonance theory, without explicit account of valence nucleon effects and direct capture, is adequate to deal with structural materials such as Cr, Fe and Ni. Thanks to the progress achieved with respect to prompt neutron background it has become clear that many of the Γ_n-Γ_γ correlations thought to be due to valence nucleon transitions are in fact spurious, caused by inadequate account for, or complete neglect of, prompt detection of resonance-scattered neutrons. This is even true for some of the nuclei with high p-wave and low s-wave strength functions such as Zr which are often cited as providing typical examples for valence capture.

- The conclusion, therefore, was that the simple resonance theory, without valence or direct capture, appears to be quite adequate for a quantitative description of neutron capture by structural-material nuclei.

Following a recommendation of the 1977 Geel meeting three main codes employed for resonance analysis of structural-material capture data, viz. REFIT, FANAC and the ORNL/RPI code, were compared at Harwell. In a very severe test with several hundred percent multiple-collision correction the calculated first-collision yields agreed perfectly while

the total capture areas agreed to better than 4% . In more typical cases agreement was said to be of the order of 1% or better, indicating a comparable accuracy of the multiple-collision treatment. In order to improve portability of the codes it is recommended to

- create clear-cut interfaces to plotting and other subroutines that may be available only at the originating laboratory,
- provide adequate documentation (user manuals, documented test cases etc.)

where these are not already available.

The use of γ-ray spectra calculated from nuclear models where no other spectral data exist to correct for nonlinearities in Moxon-Rae detector response or to construct weighting functions for total-energy detectors has led to encouraging improvements. In this context

- it is recommended to explore the possibility of operating Moxon-Rae detectors as total-energy detectors, i. e. of straightening out their non-constant efficiency at low γ-ray energies by means of pulse-height weighting.

Among the problems recognised at the 1977 Geel meeting but not tackled yet is the influence on resonance analysis of anisotropic emission of capture γ-rays.

- It is again recommended that this problem be studied. It exists for p- and d-wave levels in general and for s-wave levels at higher energies where potential scattering amplitudes for p- and d-waves are high enough to interfere appreciably with s-wave amplitudes.

5. Evaluations and Compilations

It was noted that in contrast to the 1977 KEDAK evaluation and the new JENDL-2 evaluation for Fe inelastic scattering by ^{57}Fe is disregarded in ENDF/B-V, although its threshold is as low as 14 keV. This leads to wrong transfer matrices and difficulties in the interpretation of integral measurements at facilities containing large amounts of Fe and should be remedied.

It was further noted that the new Barn Book (4th edition of BNL 325) is affected by the same deficiency. Inelastic scattering widths for ^{57}Fe, still given in the 3rd edition, have now vanished. In general it appears that the new edition is already outdated with respect to structural materials because results available since the 1975 Washington conference and the 1977 Geel meeting are not included. Examples are radiation widths and capture areas for Fe and Ni. The radiation width listed for the 27.7 keV resonance of ^{56}Fe is more than twelve years old. Nevertheless the new compilation is clearly quite important.

- It is recommended to distribute the computer file associated with the new edition of the Barn Book to the data centres.

It was realised that there may be problems since unmeasured quantities (spins, partial widths etc.) have been generated for the computer file by Monte Carlo sampling and similar methods to furnish complete tables for computer calculations. But this should not impede dissemination as the book can be used to identify such artificial data.

Measurements relative to gold require careful account of the structure in the Au capture cross section. The known structure at keV energies, e.g. the steplike feature at 279 keV discussed by T. Ryves, should be included in the evaluated files.

The last problem addressed was the unsatisfactory situation in the field of nuclear data evaluation. The US embargo on much of ENDF/B-V caused an alternative file to be assembled which includes European and Japanese evaluations. Inevitably this creates a great deal of rather unnecessary duplication of effort. The unanimous opinion was that

- ways should be explored to restore the former free exchange of evaluated data information as soon as possible.

Report of Working Group on

FAST-NEUTRON CAPTURE CROSS SECTIONS FOR THE MOST IMPORTANT FISSION-PRODUCT NUCLEI

Chairman: H. Gruppelaar
Secretary: R. Schenter
Participants: R. Anderl, I. Bergqvist, R. Block, P. Collins, Y. Fujita, D. Gardner, R. Joly, R. Macklin, E. Menapace, S. Mughabghab and R. Reffo

I. INTRODUCTION

The main activity of the fission-product (FP) Working Group was the discussion of the current status of neutron capture knowledge of the most important FP nuclides, including the formulation of recommendations toward improved understanding. The results of the discussion are summarized in Table 1. General conclusions and recommendations are given in the following sections. The status of integral data was summarized by R. Anderl (see Sec. V). Nuclear models and calculations were reviewed by D. Gardner and G. Reffo (see Sec. VIII) and some of their conclusions are relevant to the areas of the other Working Groups.

II. GENERAL REQUIREMENTS

Collins, at this Meeting, reviewed the accuracy requirements for FP cross sections. These are essentially the same as expressed at the Bologna Meeting (1979); i.e. 5-10% in the lumped FP capture cross sections averaged over a typical fast-power-reactor (FBR) spectrum. More specific requirements are given in Collins' paper. The following comments are relevant to the above need.

For the calculation of the Na-void effect, FP capture in the range 100 eV to 10 keV (i.e. near the 2.8 keV Na resonance) is of importance. Strong FP resonances, those contributing a distinct peak to the lumped FP cross section near the 2.8 keV Na resonance, should be resolved. The importance of such resonances was demonstrated by Koyama et al. (IAEA-SM-249/24, Vol. 1, 1979), who used a mockup FP sample consisting of natural elements in the FP mass region. The very prominent ^{142}Nd resonance at 2.5 keV strongly influenced Na voiding. From these considerations, the Working Group recommends that FP capture be described as resolved resonances up to $\approx$ 10 keV in those cases where there are strong resonances near 2.8 keV (i.e.

near the Na resonance).

Most of the above cited requirements are relevant to Na-cooled FBR systems. For the development of advanced water-cooled reactors (APWR) the requirements may be different due to the different core spectra. The resolved resonance region is probably much more important for such reactors but the detailed requirements have not been assessed. The need for capture-branching calculations (and information) should also be assessed. Such data could have an impact on radioactive-inventory calculations.

III. RESOLVED RESONANCE PARAMETERS

There has been a large improvement with respect to FP resolved resonance parameters since the Bologna Meeting ('79). Most of the new data are given in the 4th Edition of BNL-325. Additional data have very recently become available, as indicated by the review of Gruppelaar at this Meeting. Since most of these new data have not been used in FP evaluations, it is recommended that evaluated FP files be updated using recent resonance-parameter information, taking into account the possibility of missed resonances. Specific instances relative to particular nuclides are cited in Table 1.

IV. ENERGY-AVERAGE CAPTURE-CROSS-SECTION DATA

The results of post-Bologna measurements were reviewed by Block at this Meeting. Measurements for 38 FP from 9 laboratories were considered in that review. About 20% of these experimental results dealt with high-priority FP data requests. Only one radioactive nuclide (^{99}Tc) was included. Block concluded that "no effort seems to have been made to do the more difficult capture measurements."

Gruppelaar (at this Meeting) compared evaluated and recent experimental data for the most important FP nuclides. Some discrepancies were noted, discussed in detail by the Working Group and defined in Table 1. It may well be possible that an evaluation of new data (including resonance and integral data) using nuclear models with updated parameters will show that requests for the most important stable FP data have been met. Many new data are relevant to natural elements and such information is useful in the isotopic evaluation process.

It was recommended that an attempt be made to measure energy-average capture cross sections of some unstable nuclides. For example, useful results could perhaps be obtained with an available ^{107}Pd sample. This sample contains only $\approx$ 16% ^{107}Pd, a large proportion of ^{105}Pd and

some other Pd isotopes. Gruppelaar suggests a mockup of the stable FPs with the same abundance as the active ^{107}Pd sample. A difference measurement between the mockup and ^{107}Pd-containing samples could give useful results. Generally, the feasibility of making measurements with enriched radioactive samples should be investigated. Measurements with ^{129}I and ^{151}Sm are being planned at ORNL and KFK, respectively.

Bergqvist reported on capture measurements in the MeV range. The systematics of the capture process near 14 MeV seem well established ($\sigma \approx 1$ mb). However, this high-energy region is of little FBR interest.

Experimentalists are strongly urged to provide uncertainty and covariance information relevant to their data. A full covariance matrix is not required. What is needed are the basic elements requisite to the calculation of covariances. In the simplest cases these are represented by statistical and systematic uncertainties (e.g. uncertainties associated with the reference standard). It is recommended that any corrections or normalizations applied to data be communicated to the regional data centers. Superseded or suspect data sets should be "flagged" in center files.

V. INTEGRAL DATA

Fast-neutron integral data for individual FP nuclides have been measured in STEK, FRO, MASURCA, ERMINE, CFRMF, PHENIX and EBR-II. Most of the integral data were available at the Bologna Meeting ('79). However, since that time the final results of the integral measurements of the isotopes of Nd, Sm, and Eu in EBR-II have been reported (R. Anderl et al., EGG-PHYS-5182 (1981)). In addition, new experiments with important FPs have been carried out in PHENIX (M. Darrouget and M. Martin Deider, INDC(NDS)-116/G+P(1981)), but the results are not easily available.

The integral-experimental data have been used in the preparation of the evaluated FP files; RCN-2A, RCN-3, ENDF/B-V, CNEN/CEA-80, CARNAVAL-IV and JENDL-2. Gruppelaar, at this Meeting, compared several of these evaluated files. It was pointed out that the use of multi-group cross sections, adjusted with integral data, makes an important contribution to the reduction of uncertainties in the "global" FP absorption in FBR systems.

A summary of integral testing of ENDF/B-V FP cross sections using CFRMF and EBR-II integral data was given by Anderl at this Meeting (see also EGG-PHYS-5406 (1981)). It appears that many of the discrepancies between integral data and ENDF/B-V cross sections will vanish with evaluations based upon differential data reported since 1979. Adjusted multi-group cross sections, based upon EBR-II integral data, appear in good agreement with recent differential data for ^{143}Nd, ^{145}Nd, ^{147}Sm, ^{149}Sm, ^{151}Eu and ^{153}Eu. Integral tests for these nuclides indicate discrepancies with ENDF/B-V

beyond the integral-test uncertainties. There does not appear to be sufficient differential data to resolve ENDF/B-V integral-test discrepancies for: ^{137}Cs, ^{142}Ce, ^{134}Xe, ^{146}Nd, ^{148}Nd, ^{150}Nd and ^{154}Eu. At the Bologna Meeting discrepancies were noted between different integral measurements for the nuclides: ^{99}Tc, ^{105}Pd, ^{108}Pd, ^{127}I, ^{151}Sm, ^{147}Pm, ^{109}Ag and ^{104}Ru. These discrepancies had not been resolved prior to the present Meeting. It should be noted that measurements, emphasizing accuracies, are planned at CFRMF for '82, including ^{99}Tc, ^{127}I, ^{147}Pm, ^{109}Ag and ^{104}Ru.

With the availability of new and more complete resonance information for important FP nuclides, it would be useful to report resonance self-shielding correction factors of group cross sections used to analyse the STEK integral data. The results would be helpful in future integral testing. New integral experiments (transmutation measurements) would be helpful in improving capture cross sections of important radioactive FPs, including ^{107}Pd, ^{135}Cs, ^{106}Ru, ^{151}Sm, ^{144}Ce, ^{103}Ru, ^{155}Eu, ^{93}Zr and ^{95}Zr.

VI. EVALUATIONS

The status of FP fast-capture evaluations was reviewed by Gruppelaar. He concluded that there are serious discrepancies between recent evaluations in both the resolved-resonance and MeV regions. New data should be considered in re-evaluations. At high energies there are also large differences due to the use of different level schemes (for example, many ENDF/B-V calculations were made about ten years ago with older level information). From Table 1 it follows that some re-evaluation effort is needed including new experimental information. A covariance analysis is needed to assess the accuracies. It is possible that many requirements will be met when all the available information is combined. Data for the natural elements should be used to obtain consistent evaluations for both isotopes and elements. Cases where the element consists of many isotopes must be treated with care.

The evaluator should give average resonance parameters suitable for self-shielding calculations as such corrections are important in the analysis of integral data involving thick samples.

VII. LUMPED FP CROSS SECTIONS

The average capture cross sections in a FBR spectrum due to lumped FPs, as calculated from CNEN/CEA, ENDF/B-V, JENDL-1, REN-2A and RCN-3, differ by less than 1%. The estimated uncertainty is 6-9%. This agreement is very satisfactory. It should be noted that the previous ENDF/B-IV results tended to be about 9% low.

For calculations of the Na-void effect, it may be necessary to represent the lumped FP cross sections in five groups near the Na resonance.

Because FP nuclides migrate within a fuel pin after they are produced, consideration should be given to generating multi-lumped FP sets (gaseous, semi-volitile, non-volitile, etc.). These data sets could be used to interpret the results of FBR integral measurements.

Recently, interest has been shown in the use of multi-group lumped FP cross sections and their associated covariance matrixes. For example, they were used to determine the enrichment of the Clinch River Breeder Reactor (see Collins' paper at this Meeting.)

VIII. NUCLEAR MODEL CODES

There now exist a number of nuclear-model computer codes with which both statistical and non-statistical neutron capture mechanisms may be treated in varying degrees of detail. Since the Bologna Meeting ('79), the major areas of progress seem to be; i) the testing of codes, ii) the development of dependable methods for obtaining the radiation width (or average strength functions), and iii) the application of the codes to calculations involving isomeric states (not only to the calculations of isomeric populations in the daughter nucleus but also to the calculations involving isomers as the target states.)

In discussing capture calculations, it is convenient to divide the incident-neutron energy into three regions, i) the resonance region, ii) the range from overlapping resonances to perhaps 5 MeV, and iii) the region above 5 MeV. For the purpose of calculating capture cross sections for fission-reactor applications; it appears that, in addition to a vanishing Hauser-Fesbach component, relatively simple models of the direct-semidirect capture processes above $\approx$ 5 MeV will be adequate, unless detailed information about the capture-gamma-ray spectrum is required. In the low-energy region it is difficult to make theoretical cross-section estimates that are reliable to within an order of magnitude unless some experimental resonance information is available. It is the intermediate energy region, where statistical-model calculations of the Hauser-Feshbach type apply, that benefits most from careful theoretical calculation. In this region it is fair to say that the accuracies of the calculated capture cross sections are not limited by currently available computer codes but rather by the need for accurate and complete input data. Under favorable conditions, it is possible to achieve results for FP targets that are accurate to perhaps 25%.* In particular, models provide us with the correct shape of the capture cross section when the discrete level scheme of the target nucleus is available.

With regard to statistical-model calculations, there are a number of comments that can be made with some confidence. In the region of over-

* Not for fissile targets, for which it is usually necessary to have some experimental information on the competing fission channels in order to achieve similar uncertainties in the capture cross section.

lapping resonances we feel that the valence-capture mechanism may safely be ignored (although it is certainly useful for obtaining a better understanding of resonance parameters). The most important parameter in capture calculations is Γ_γ/D. This may best be obtained from calculations involving absolute gamma-ray strength functions rather than from separate calculations or systematics of Γ_γ and D. The experimental parity dependence of the observed radiation width should be correctly accounted for by the calculations. In general, only dipole transitions are important in the continuum, although higher multipoles may be required when treating transitions between the continuum and discrete low-lying levels. For transitions between discrete levels it is usually necessary to invoke experimental measurements or detailed model calculations (e.g. shell model or interacting-boson model).

Another important quantity for statistical-model calculations is the neutron optical-model potential. It appears that a spherical global potential may be adequate, even for moderately deformed nuclei, if only the capture cross section is required. We favor the SPRT approach, developed by Brúyeres-le-Châtel, and note that transmission coefficients should be obtained using a potential with a spin-orbit term. Often it is not adequate to average transmission coefficients over channel spin to obtain values that are only functions of orbital angular momentum. This is particularly true if isomer populations are to be calculated.

With regards to the width-fluctuation correction, it is the opinion of the Working Group that the method of Moldauer is best. Lumping of channels should be considered in order to save computing time.

The remaining requirements involve discrete level information for each nucleus and level-density formulation for the excitation-energy region above the discrete levels. There is no adequate way in which a level-density experession can reproduce the first 20 or so levels in a nucleus, particularly in the deformed-mass region. Not only are the discrete levels required for proper calculation of the competition from inelastic-scattering, but they may also be important in determining the magnitude of the radiation width for each incident-neutron partial wave. In the continuum region we tend to favor the Gilbert and Cameron level-density formulation, in which a constant-temperature model at low energies is smoothly joined to a Fermi-gas model at an excitation energy somewhat below the neutron-binding energy. All parameters in the Gilbert and Cameron formulation follow well-defined systematics which allow calculation and uncertainty estimates when no level and/or resonance schemes are available. The parameters of this model should well represent discrete-level information, not only with regard to the number of levels but also with respect to their spin and parity distributions. In particular, the energy dependence of the spin-cut-off factor should be carefully accounted for over the entire energy range. An adequate Yrast treatment is also important in a number of situations.

Perhaps the strongest recommendation from the point of view of calculation is the requirement for the complete definition of the first 20 or so levels. Often this implies supplementing experimental information with theoretically calculated levels. The above is a minimum requirement. For deformed nuclei it may be necessary that the collective levels (such as the

rotational band) be extended to rather high spins if isomer populations are required. In addition, there are circumstances where gamma-branching information is required. It may be necessary to create a request list of nuclear-structure information for the most important FP nuclei if complete calculations are to be made.

IX. SUMMARY OF RECOMMENDATIONS

The following items summarize the recommendations cited throughout the above text. Appropriate action is encouraged.

1. Recent differential and integral results should be incorporated in new evaluations as indicated in Table 1 and Sections IV and VI (above).

2. Recent resonance-parameter data should be incorporated in new evaluations (see Section III).

3. Nuclear-model calculations for the higher-energy region should be updated to reflect improved input data and models (see Section VIII).

4. New differential measurements of fast capture (mainly radioactive nuclei) should be undertaken as indicated in Table 1 and Section IV.

5. New integral measurements of fast capture should be performed as indicated in Table 1 and Section V.

6. Attention should be given to resolved-resonance descriptions in the region of the Na resonance for selected nuclei (see Section III).

7. Use of enriched radioactive samples should be investigated (see Section IV).

8. Experimentalists should provide uncertainty and covariance information (see Section IV.)

9. Data corrections and renormalizations should be communicated. to the regional centers (see Section IV).

10. Selfshielding correction factors should be reported to facilitate the integral-data analysis (see Section V).

11. Covariance analysis should be used to assess the accuracy of evaluations (see Section VI).

12. Elemental data should be used in obtaining consistent evaluations for individual isotopes (see Section VI).

13. Lumped FP cross sections should be represented with a fine mesh in the region of the Na resonance (see Section VII).

14. Multiple lumped FP data sets should be generated to account for FP migration (Section VII).

15. Extend low-energy level schemes, supplementing with theoretical information as necessary (see Section VIII).

16. Create a request list for nuclear-structure information for the most important FP nuclides (see Section VIII).

Table 1: Summary Status, FP-Capture Data[a]

Nuclide, ^{93}Zr

Accuracy, ± 15%
Status,
a) Resolved resonances; one resonance known.
b) Average cross section; no data.
c) Integral data; STEK results (not yet analyzed).
d) Evaluation (ENDF/B-V); based upon model calculations (JENDL-1 is much larger).

Actions,
1) Analyze STEK data.
2) Attempt differential measurements.
3) Use systematics of neighboring isotopes in evaluation.
4) Integral data required (transmutation).

Conclusion,
Needs not met.

Nuclide, ^{95}Mo (similiar remarks apply to ^{97}Mo)

Accuracy, ± 10 to ± 15%
Status,
a) Resolved resonances; new data from AUA-76 and RPI-77. There is a gap in the data from 1.9 - 3.06 keV.
b) Average cross sections; new data from RPI-77 and AUA-78. Fairly good agreement.
c) Integral data; STEK results in agreement with new differential information.
d) Evaluation (ENDF/B-V); in agreement with experimental information.

Action,
None required.

Conclusion,
Accuracies of better than ± 15% have been achieved.

---

a. This table reflects the results of discussions in the Working Group. The choice of nuclides is somewhat arbitrary although the ten most important FP are discussed. See the Bologna Meeting and the FP papers presented at this Meeting for information on other nuclides.

Remarks as to evaluated data files usually refer to ENDF/B-V. See, for comparisons with other evaluations, Gruppelaar's paper and references quoted therein.

The references to experimental data are easily found in the CINDA-82 data index by inspecting the quantities "Reson Params" and "(n,γ)" for the given nuclides, using the laboratory and year keys.

Nuclide, ^{98}Mo

Accuracy, ± 20%
Status,
a) Resolved resonances; recent data AUA-76 and ORL-76. Resonances known up to 52 keV.
b) Average cross sections; recent data, AUA-78 and BNL-76 (at 24 keV). There is agreement between cross sections calculated from resolved resonances and AUA-78 average cross sections up to 10 keV; at higher energies missed resonances occur. The older ANL-68 data appears systematically too high. A. B. Smith suggests that this older information should be used with caution, possibly excepting the relative shape.
c) Integral data; STEK data, large corrections due to scattering.
d) Evaluation (ENDF/B-V); Agreement with AUA-78 results, level scheme should be checked.

Actions,
1) Re-evaluate in the resolved resonance region.
2) Check level scheme used in the evaluation.

Conclusions,
Needs probably met after re-evaluation.

Nuclide, ^{99}Tc

Accuracy, ± 10%
Status,
a) Resolved resonances; recent data from; KUR-73, RPI-77, KIL-78, KIG-81 and ORL-82 (to be published in NS&E).
b) Average cross sections; recent data from RPI-77 and ORL-82. There is a discrepancy with RPI-77 being larger than ORL-82 which is larger than KFK-73. KFK-73 data may need corrections for sample composition (Priesmeyer, Bologna 1979). Original RPI-77 values are 15% lower (improved background correction in 1978 by R. C. Little) and in agreement with ORL-82 results.
c) Integral data; discrepancy between STEK and CFRMF results. High uncertainty in CFRMF results (± 15%) and new measurements are planned.
d) Evaluation (ENDF/B-V); updating needed in the resolved range, good agreement with RPI-77 and STEK results in the keV range, updating needed in the MeV range using improved level schemes.

Actions,
1) Correction to the KFK data, inspection of RPI correction.
2) Re-evaluate.
3) New CFRMF measurements (planned).

Conclusion,
Needs probably met after action 1 and new evaluation.

Nuclide, ^{101}Ru

Accuracy, ± 10%
Status,
a) Resolved resonances; recent data from RPI-75, DUB-80, and ORL-80. Useful up to 1 keV.
b) Average cross sections; recent data from RPI-75 and ORL-80. Discrepant, with RPI results larger than ORL values. This discrepancy does not exist (or is smaller) for ^{102}Ru and ^{104}Ru.
c) Integral data; STEK results agree with ORL-80 differential values.
d) Evaluation (ENDF/B-V); updating needed in the resolved resonance range.

Action,
Re-evaluation the resolved-resonance range.

Conclusion,
Needs probably met with new resonance information, ORL and STEK results.

Nuclide, ^{102}Ru (similar remarks for ^{104}Ru)

Accuracy, ± 10% (^{102}Ru) and ± 20% (^{104}Ru)
Status,
a) Resolved resonances; recent data from RPI-75, DUB-80, and ORL-80. Not enough Γ_n values above 0.5 keV.
b) Average cross sections; recent data from RPI-75 and ORL-80. Satisfactory agreement (small discrepancy at 15-30 keV?).
c) Integral data; STEK and CFRMF results agree with differential data.
d) Evaluation (ENDF/B-V); updating needed in the resolved range.

Actions,
1) Measure Γ_n values in the 0.5 - 5.0 keV range.
2) Re-evaluate resolved resonance region.

Conclusion,
Needs nearly met.

Nuclides, ^{103}Rh

Accuracy, ± 10%
Status,
a) Resolved resonances; recent data from ORL-79 (2.6 - 4.2 keV). No discrepancies.
b) Averaged cross sections; many new data. Recent KFK-81 and CAD-76 data lower than ENDF/B-V.
c) Integral data; STEK and CFRMF results in agreement with ENDF/B-V (a somewhat lower evaluated cross section would be an improvement).
d) Evaluation (ENDF/B-V); ENDF/B-V could be lowered by a few %.

Action,
Check evaluation with newest data.

Conclusion,
Accuracy requirements met.

Nuclide, ^{105}Pd

Accuracy, ± 10%
Status,
a) Resolved resonances; recent data from DUB-78, GEL-79 and ORL-79. New thermal cross section (GEL-81). Resolved range satisfactory to 2 keV.
b) Average cross sections; recent data from RPI-75, AUA-78, ORL-81 and GEL-82 (this Meeting); quite good agreement.
c) Integral data; STEK results are in agreement with differential data. There is a discrepancy with French integral data.
d) Evaluation (ENDF/B-V); ENDF/B-V too low in the resolved range (0.1 - 1.0 keV), slightly too high above 1 keV. Improvements may be possible above 0.5 MeV.

Actions,
1) Re-evaluate the resolved range.
2) Re-evaluated the energy-average range.
3) Update level schemes.

Conclusion,
Needs probably met after re-evaluation.

Nuclide, ^{107}Pd

Accuracy, ± 10%
Status,
a) Resolved resonances; recent data from RPI-78 (up to 655 eV); and NIR-80 (up to 45 eV); comparison needed. Thermal cross section and resonance integral unknown.
b) Average cross sections; no data available.
c) Integral data; STEK results, sample only 15.7% ^{107}Pd.
d) Evaluation (ENDF/B-V); based upon model calculations using parameters from systematics. RCN-3 is partly based upon model and parameters from the RPI data, particularly S_0.

Actions,
1) Compare RPI-78 and NIR-80 data.
2) Update level scheme.
3) Use model parameters from RPI-78 data.
4) Attempt an average cross section measurement with isotopic and mockup samples (see Section IV).
5) Attempt an integral transmission measurement with a small highly-enriched sample in a fast-power reactor spectrum.

Conclusions,
Needs not met, more data needed.

Nuclide, ^{109}Ag

Accuracy, ± 15%
Status,
a) Resolved resonances; recent data from ORL-82 (in press NS+E) and JAE-82, to be combined with previous data.
b) Average cross sections; recent ORL-82 and JAE-82 results are in very good agreement. Older DKE-60 data much higher and FEI-65 data much lower.
c) Integral data; STEK and CFRMF results indicate relatively high cross sections.
d) Evaluation (ENDF/B-V); shape of cross section not in agreement with some recent data.

Actions,
1) Combine new resonance parameter information with previous data and use in re-evaluation.
2) Re-evaluate smooth energy range.
3) Attempt to obtain agreement with elemental Ag data (ANL-82, this Meeting) using new ^{107}Ag data (ORL-82, in press NS+E).

Conclusion,
Re-evaluation needed, needs then probably met.

Nuclide, ^{129}I

Accuracy, ± 20%
Status,
a) Resolved resonances; few parameters known.
b) Average cross sections; no data.
c) Integral data; STEK and CFRMF results in good agreement.
d) Evaluation (ENDF/B-V); adjusted to integral results.

Action,
New measurements planned ORNL.

Conclusion,
Wait for new differential data.

Nuclide, ^{133}Cs

Accuracy, ± 10%
Status,
a) Resolved resonances; recent data from RPI-77, NIR-77, KIG-81 and ORNL-82 (in press, NS+E). The problem is that the capture widths are not well-known. STEK results indicate missed strength.

b) Average cross sections; recent results from KTO-79, BRC-80 ORL-82 (in press, NS+E), and filtered-beam results from KTO-82 (see review of Block at this Meeting). New results are in good agreement and also with the older LEB-62 data. There is a discrepancy with the KFK-69 data (too high).
c) Integral data; STEK and CFRMF results agree with the newest differential data.
d) Evaluation (ENDF/B-V); satisfactory in the smooth range up to 200 eV.

Actions,
1) New resolved resonace data should be used in re-evaluation, possibly capture widths should be increased.
2) Check level scheme data used in evaluation.
3) Capture widths for isolated resonances required from 40 eV to 4 keV.

Conclusions,
Needs almost met.

Nuclide, ^{135}Cs

Accuracy, ± 20%
Status,
a) Resolved resonances; one resonance known with value of capture width.
b) Averaged cross sections; no data known.
c) Integral data; STEK results (to be analyzed, sample composition needs to be re-determined).
d) Evaluation(ENDF/B-V); based upon old systematics, probably capture cross section is much too low.

Actions,
1) Differential and integral measurements recommended.
2) Should be re-evaluated with new systematics.
3) Analyze STEK data.

Conclusion,
Needs not met.

Nuclide, ^{137}Cs

Accuracy, ± 20%
Status,
a) Resolved resonances; no known data.
b) Average cross sections; no known data.
c) Integral data; CFRMF data available, STEK data needs analysis.
d) Evaluation (ENDF/B-V); based upon old systematics, capture cross section probably too low.

Actions,
1) Analyze STEK and CFRMF integral data.
2) Re-evaluate with new systematics.

Conclusion,
Needs not met.

Nuclide, ^{143}Nd

Accuracy, ± 10%
Status,
a) Resolved resonances; recent data from RPI-79 and AUA-78. Useful up to 4 keV.
b) Average cross sections; recent data from AUA-77 and JAE-79 agree up to 100 keV. (There are problems with the data in the range 100-200 keV.)
c) Integral data; STEK and EBR-II results are consistent with recent differential data.
d) Evaluation (ENDF/B-V); evaluation is satisfactory except near 1 MeV where RCN-3 gives a bump; level scheme needs to be checked.

Actions,
1) Re-evaluate MeV region, check level scheme.
2) Check data above 100 keV with the authors, (see b).
3) Inelastic-scattering data at low energies could be useful for checking level scheme.

Conclusion,
Needs not met.

Nuclide, ^{147}Pm

Accuracy, ± 10%
Status,
a) Resolved resonances; parameters available up to 316 eV, recent NIR-78 results need to be included.
b) Average cross sections; no known data.
c) Integral data; STEK sample contained 30-40% ^{147}Sm. CFRMF uncertainties are 13%. STEK and CFRMF results are in reasonable agreement.
d) Evaluation (ENDF/B-V); based upon STEK and CFRMF results, level scheme uncertain above 100 keV.

Actions,
1) Use NIR-78 resonance data in re-evaluation.
2) Re-evaluated average capture cross section using updated level scheme.
3) Consider possible average capture-cross section measurements.
4) New CFRMF measurements (planned).

Conclusion,
Needs not met.

Nuclide, ^{149}Sm

Accuracy, ± 10%
Status,
a) Resolved resonances; recent data from JAE-81. Average capture width = 62 meV.
b) Average cross sections; recent data from RPI-75, FEI-77 and JAE-80. RPI and JAE results are in good agreement, FEI values are high up to 25 keV.
c) Integral data; EBR-II data in good agreement with RPI and JAE differential results. STEK data may indicate lower cross sections. Analysis is difficult due to high response in the low-energy range, updated resonance information could improve the results.
d) Evaluation (ENDF/B-V); Complete re-evaluation needed.

Action,
Re-evaluation of entire energy range recommended.

Conclusion,
Needs not met.

Nuclide, ^{151}Sm

Accuracy, ± 10%
Status,
a) Resolved resonances; recent data from KAP-75 and NIR-77, up to 105 and 18 eV, respectively.
b) Average cross sections; no known data.
c) Integral data; STEK data, sample contained only 6.13% ^{151}Sm. Large discrepancy with PHENIX results (^{149}Sm sample with multiple capture.)
d) Evaluation (ENDF/B-V); based upon model calculations. D_{obs} needs correction for missed resonances and the consequence will be an increased cross section. Very large discrepancies in the MeV range (check level scheme and ground-state spin of ^{151}Sm).

Actions,
1) Re-evaluate over entire energy range using improved model parameters and systematics.
2) New differential measurements needed (planned ORL-KFK cooperative effort in '82).
3) Recommend integral transmutation measurement with enriched sample in fast power-reactor spectrum.

Conclusion,
Needs not met.

SOME SUMMARY REFLECTIONS

A. B. Smith
Argonne National Laboratory

I come to this podium as a modest substitute for a distinguished scientist, Dr. André Michaudon. A few days ago he had to cancel his attendance here but he extends his best wishes for a successful Meeting. My reflections are, in a sense, of virgin purity as I cannot recall ever having made a capture-cross-section measurement and my theoretical endeavors are certainly elementary. It is from this "unbiased" viewpoint that I consider the proceedings of the past few days.

Thermal reactors are mature and proprietary animals. Fusion systems lie over the distant horizon and their neutronic characteristics are, in many ways, similar to those of the fast-breeder reactor(FBR). Thus, the major applied data need remains the FBR system. Looking back over more than a decade, one is impressed by how little the FBR capture-data needs have changed and how variable the progress toward the most important data goals has been. For example, consider---

FBR Data Uncertainties (%); Status and Goals

Type	Status		Goal	
	1970[a]	Present[b]	1970[a]	Present[b]
$^{238}U(n,\gamma)$	10	5-8	2	3
$^{239}Pu(n,\gamma)$	20	10+	3	4
$^{240}Pu(n,\gamma)$	30	15+	10	3
(n,γ) Fission-Products	40	10+	10	5-10
(n,γ) Struct.-Materials	30	15+	10	5-10

a. Greebler et al., Proc. Inter. Conf. on Nucl. Data for Reactors, Helsinki (1970), IAEA Press, Vienna.

b. From this meeting, particularly the paper by Collins.

Knowledge of the very important $^{238}U(n,\gamma)$ data has improved by several percentage points but falls far short of the accuracy goal. Uncertainties in ^{239}Pu alpha have been reduced by a factor of perhaps two but remain 3-4 times larger than the desired objective. The accuracy goal for ^{240}Pu capture is now much more stringent due to the consideration of realistic

fuel cycles, and we are far from achieving it. Fission-product (FP) and structural-material capture objectives have been only partially achieved. There remain particularly disturbing discrepancies between differential and integral data; for example $^{238}U(n,\gamma)$ or the ratio $^{238}U(n,\gamma)/^{239}Pu(n,f)$. The progress to this point suggests a need for a increased emphasis on the precise determination of a relatively few key FBR capture quantities.

This is the golden anniversary of the discovery of the neutron. The physical understanding of neutron capture is at least half that old. There are essentially no new concepts, only experimental verification of old ideas. There has been impressive improvement in our ability to model and calculate with a good degree of consistency. However, the models are parameter sensitive and, as more accuracy is sought, the acceptable parameter sets depart from "global" toward "regional" representations and finally to explicit experimental parameterizations absolutely dependent upon underlying observations. Physical uncertainties remain troubling (for example, the value of $\langle\Gamma_\gamma/D\rangle$, statistical level properties and discrete-level-structure specification) and there is very little basic-research interest in resolving these issues. It is disturbing to note that calculations which describe capture well can be very deficient in representing other aspects of the neutron-nucleus interaction (e.g. large discrepancies in FP inelastic scattering). Theoretical calculations provide for excellent physical interpolation between measured values but are far less reliable for extrapolation. Typically, there are uncertainties of 20% or more which are too large to meet the more important FBR capture needs. It is well to remember that physics is an observational science, and that is especially true in the context of the precise applied capture-data needs.

There are two measurement regimes: i) specific high-accuracy, high-importance values (e.g. $^{238}U(n,\gamma)$), and ii) broad-scope results to modest accuracies (e.g. $FP(n,\gamma)$). Where nature is kind, it seems clear that the activation method offers the most promise for achieving the high-accuracy goals. With contemporary technologies flux and activity determinations can be made to $\approx$ 1% accuracies, and this should provide capture cross sections accurate to the 2-3% level. Such accuracies have been achieved in dealing with the somewhat anologous $^{235}U(n,f)$ process. Where nature is not so kind (or where lesser accuracies will suffice) recourse is made to prompt-detection techniques. Their potential seems to have reached a plateau at the 5-8% accuracy level with little, if any, promise that 2-3% accuracies can soon be achieved.

Given the above measurement potential, the gold-capture standard situation is disturbing. This is an ideal case for activation measurements, and it is a reference standard for work reported at this Meeting. Yet, the gold situation seems to have deteriorated since the 1970 Standards Symposium and certainly the potential for (and desired) accuracies of several percent has not been realized. The situation is similar for the key $^{238}U(n,\gamma)$ cross section; the FBR goal is achievable, yet nothing seems to have been done for more than three years, with the result that the contemporary knowledge is probably no better than a

decade ago. These two examples (and there are others) are very disturbing. Diligent engineering application of established techniques should have produced far better results. It is clear that only measurements capable of achieving few-percent accuracies will have a substantive effect on the contemporary understanding in these precise cases (e.g. $^{238}U(n,\gamma)$).

Equal concern can be expressed for the status of fissile-alpha values, but the experimental course is not nearly as clear. The 10-20% discrepancies between recent ^{235}U alpha results is startling. It is disturbing to note that the same general techniques, and even personnel, have been involved in the important ^{239}Pu alpha measurements, where the FBR accuracy goals are precise. Not only have the latter not been achieved, but it seems very likely that the present understanding is far more uncertain than previously estimated. Yet, there has been no work on ^{239}Pu alpha for five years or more. The ^{233}U alpha status is at least as unsatisfactory, with no experimental effort for approximately a decade. ^{240}Pu capture is important in realistic FBR fuel cycles, yet the capture cross section remains essentially unknown above several hundred keV. Concern for alpha is endemic thoughout the fissile nuclei. The accuracy goals for the most important cases clearly exceed theoretical capabilities. No experimental method has the proven potential for achieving the desired 2-3% accuracies, nor does an experimental breakthrough appear imminent. The outlook for precise fissile-alpha values is not optimistic.

Following the 1977 Specialists Meeting at CBNM, knowledge of structural-material capture has shown much progress. Experimental perturbations due to scattering are now largely understood. Spectral sensitivities of a variety of detector systems are better delineated, in part by careful coordination of measurements and calculations. Glaring discrepancies in the radiation widths of "classic" resonances are being removed, with results converging to common values. Unfortunately, the new results have not yet been assimilated by most of the users (e.g. 27 keV resonance in ^{56}Fe). There remain some experimental background and flux issues, but the goal of determining structural-material-capture to 5-10% accuracy appears consistent with contemporary capability, and will be reasonably-well achieved. With this relatively good situation, it is difficult to understand some of the integral discrepancies. It was pointed out that stainless-steel capture, as given in various multigroup libraries, can differ by as much as 60% (Collins' paper). Recent NEACRP intercomparisons showed large differences between iron transport cross sections generated at various laboratories (up to 25% at even the one-group level). Then, there is the problem of self-shielding in the unresolved resonance region, with peculiar conclusions frequently drawn from studies of neutron transmission through thick media. These and similar problems do not seem consistent with the relatively goo

uncertainties may tend to compensate in the average. FP capture data has improved considerably over a decade, with a very modest impact on calculated FBR performance. However, the improved data sharply reduce uncertainties in performance predictions, with potentially large fiscal benefits. Despite some large discrepancies, the continuing need for stable-FP capture data appears relatively small. A number of governing stable-FP data uncertainties are now often associated with processes other than capture: e.g., with inelastic scattering. Active-FP capture is another matter, and the primary source of differential data will doubtlessly remain microscopic calculations since the prospects for active-FP capture measurements with any degree of accuracy and scope are not promising. Integral studies of active-FP capture are more attractive and, generally, integral measurements provide useful tests of differential FP results. However, one should bear in mind that fission yields vary with energy and can be significantly dependent on the particular integral spectrum involved.

Evaluation plays a key interface role between producer and user. It should be approached in a wholistic, physical manner which precludes confinement to any particular provincial area (e.g. capture). Glaring physical shortcomings in the evaluation process are all too frequent: e.g., omission of significant isotopes (e.g. ^{57}Fe), actinide inelastic-scattering errors of 30-50% with a sharp impact on integral predictions, and "background" resonances in the structural materials that approach or exceed those of the "foreground", etc. We should give more attention to the physical content of the evaluations to assure that our results are being properly communicated to the user. Some consideration of integral calculations themselves also seems to be in order. Cooperation in and comparison of evaluations is wise, but with independent thought. Some the the evaluation comparisons made over the past few days appear to be somewhat incestuous.

I am indebted to all of you participants who so liberally gave of your time and talent, to the working group chairmen who led the fruitful discussions that have just been summarized, and, particularly, to Dr. Wolfgang Poenitz whose skill and energy were a prominent contribution to this Meeting. It has been very much our pleasure to be your host. I hope you have found the Meeting of value and leave now with new knowledge and renewed enthusiasm. To each of you go my very best wishes.

CAPTURE MEETING PARTICIPANTS

R. ANDERL, Idaho Natl. Eng. Lab., E.G.&G. Idaho, Inc., Idaho Falls, Idaho USA.

I. BERGQVIST, University of Lund, Sweden.

R. BLOCK, Rensselaer Polytechnic Institute, Troy, New York USA.

R. CHRIEN, Brookhaven National Laboratory, Upton Long Island, New York USA.

P. COLLINS, Argonne National Laborabory - West, Idaho Falls, Idaho USA.

F. CORVI, Bureau Central de Measures Nucleaires, Geel, Belgium.

H. DERRIEN, Centre d'Etudes Nucleaires de Cadarache, France.

F. FROEHNER, Kernforschungszentrum Karlsruhe, Germany.

Y. FUJITA, Tokyo Institute of Technology and Kyoto University, Japan.

D. GARDNER, Lawrence Livermore National Laboratory, Livermore, California USA.

D. GAYTHER, Nuclear Physics Division, A.E.R.E., Harwell, United Kingdom.

D. GRADY, Systems Group of TRW, Redondo Beach, California USA.

G. GRENIER, Centre d'Etudes de Nucleaires, Bruyères-le-Châtel, France.

H. GRUPPELAAR, Netherlands Energy Research Foundation, Netherlands.

R. HOWERTON, Lawrence Livermore National Lab., Livermore, California USA.

S. JOLY, Centre d'Etudes Nucleaires, Bruyères-le-Châtel, France.

L. LESAGE, Argonne National Laboratory, Argonne, Illinois USA.

G. KNOLL, The University of Michigan, Ann Arbor, Michigan USA.

R. MACKLIN, Oak Ridge National Labortory, Oak Ridge, Tennessee USA.

J. MEADOWS, Argonne National Laboratory, Argonne, Illinois USA.

E. MENAPACE, Centro di Calcolo del C.N.E.N., Bologna, Italy.

P. MOLDAUER, Argonne National Laboratory, Argonne, Illinois USA.

S. MUGHABGHAB, Brookhaven National Lab., Upton, Long Island, New York USA.

C. NORDBORG, NEA Data Bank, Saclay, France.

R. PEELLE, Oak Ridge National Laboratory, Oak Ridge, Tennessee USA.

P. PERSIANI, Argonne National Laboratory, Argonne, Illinois USA.

W. POENITZ, Argonne National Laboratory, Argonne, Illinois USA.

G. REFFO, ENEA, Bologna, Italy.

G. ROHR, Central Bureau de Measures Nucleaires, Geel, Belgium.

T. RYVES, National Physical Laboratory, United Kingdom.

R. SCHENTER, Westinghouse Hanford Company, Richmond, Washington USA.

A. B. SMITH, Argonne National Laboratory, Argonne, Illinois USA.

D. L. SMITH, Argonne National Laboratory, Argonne, Illinois USA.

L. WESTON, Oak Ridge National Laboratory, Oak Ridge, Tennessee USA.

S. WHETSTONE, U. S. Dept. of Energy, Washington, D.C. USA.

K. WISSHAK, Kernforschungszentrum, Karlsruhe, Germany.

Distribution for ANL-83-4 (NEANDC(US)-214L)

Internal:

W. E. Massey
C. E. Till
L. G. LeSage
H. Henryson
M. J. Lineberry
D. S. Gemmell
P. J. Collins
J. W. Meadows
P. A. Moldauer
P. J. Persiani
W. P. Poenitz
A. B. Smith (12)
D. L. Smith
ANL Contract File
ANL Patent Dept.
ANL Libraries (2)
TIS Files (2)

External:

DOE-TIC (27)
Manager, Chicago Operations Office, DOE
R. Anderl, EG&G Idaho, Inc.
I. Bergqvist, U. Lund, Sweden
R. Block, Rensselaer Polytechnic Inst.
F. Corvi, Bu. Central de Measures Nucleaires, Geel, Belgium
H. Derrien, Centre d'Etudes Nucleaires, Cadarache, France
F. Froehner, Kernforschungszentrum, Karlsruhe, Germany
Y. Fujita, Research Reactor Inst., Kyoto U., Japan
D. Gardner, Lawrence Livermore National Lab.
D. Gayther, AERE Harwell, United Kingdom
D. Grady, TRW Systems Group, Redondo Beach
G. Grenier, Centre d'Etudes de Nucleaires, Bruyéres-le-Châtel, France
H. Gruppelaar, Netherlands Energy Research Foundation, The Netherlands
R. Howerton, Lawrence Livermore National Lab.
S. Joly, Centre d'Etudes Nucleaires, Bruyéres-le-Châtel, France
G. Knoll, U. Michigan
R. Macklin, Oak Ridge National Lab.
E. Menapace, Centro di Calcolo del C.N.E.N., Bologna, Italy
S. Mughabghab, Brookhaven National Lab.
C. Nordborg, NEA Data Bank, Saclay, France
R. Peelle, Oak Ridge National Lab.
G. Reffo, ENEA, Bologna, Italy
G. Rohr, Bu. Central de Measures Nucleaires, Geel, Belgium
T. Ryves, National Physical Lab., United Kingdom
R. Schenter, Westinghouse Hanford Co.
L. Weston, Oak Ridge National Lab.
K. Wisshak, Kernforschungszentrum, Karlsruhe, Germany
T. Thom, AERE Harwell, United Kingdom
N. Yamamuro, Tokyo Inst. of Technology, Japan
M. Igashira, Tokyo Inst. of Technology, Japan
M. Shimizu, Tokyo Inst. of Technology, Japan
H. Shirayanagi, Tokyo Inst. of Technology, Japan
G. Baldwin, U. Michigan
F. Fabbri, Kernforschungszentrum, Karlsruhe, Germany
L. Calabretta, Bu. Central de Measures Nucleaires, Geel, Belgium
M. Merla, Bu. Central de Measures Nucleaires, Geel, Belgium
T. van der Veen, Bu. Central de Measures Nucleaires, Geel, Belgium
Y. Harker, EG&G Idaho, Inc.
J. Rodgers, EG&G Idaho, Inc.
C. Bastian, Bu. Central de Measures Nucleaires, Geel, Belgium
G. Cornelis, Bu. Central de Measures Nucleaires, Geel, Belgium

R. Shelley, Bu. Central de Measures Nucleaires, Geel, Belgium
G. Vanpraet, Bu. Central de Measures Nucleaires, Geel, Belgium
J. Schmidt, International Atomic Energy Agency, Vienna
W. G. Cross, Atomic Energy of Canada Ltd., Chalk River
S. Igarasi, Japan Atomic Energy Research Inst., Tokai-Mura
R. E. Chrien, Brookhaven National Lab.
S. L. Whetstone, U. S. Department of Energy, Washington
H. T. Motz, Los Alamos National Lab.
F. G. Perey, Oak Ridge National Lab.
K. H. Böckhoff, Bu. Central de Measures Nucleaires, Geel, Belgium
C. Conceva, Comitato Nazionale per l'Energia Nucleare, Bologna, Italy
S. Cierjacks, Kernforschungszentrum, Karlsruhe, Germany
E. Fort, Commissariat a l'Energie Atomique, Cadarache, France
A. Michaudon, Commissariat a l'Energie Atomique, Centre d'Etudes de Limeil, France
S. M. Qaim, Kernforschungsanlage Jülich GmbH, Germany
M. G. Sowerby, AERE Harwell, United Kingdom
J. Rowlands, AEE Winfrith, United Kingdom
H. Condé, National Defense Research Inst., Stockholm, Sweden
H. Vonach, Institut für Radiumforschung und Kernphysik, Vienna
S. Pearlstein, National Nuclear Data Center, Brookhaven National Lab.
P. B. Hemmig, U. S. Department of Energy, Washington
J. Rosen, OECD Nuclear Energy Agency, Paris
N. Tubbs, OECD Nuclear Energy Agency, Paris
R. Haight, Lawrence Livermore National Lab.
O. Ozer, Electric Power Research Inst., Palo Alto
R. Heath, EG&G Idaho, Inc.
J. Anderson, Lawrence Livermore National Lab.
P. Young, Los Alamos National Lab.
A. Carlson, National Bu. of Standards, Washington
S. Berk, U. S. Department of Energy, Washington
D. Auton, Defense Nuclear Agency, Washington
J. Voignier, Centre d'Etudes de Nucleaires, Bruyéres-le-Châtel, France
B. Goel, Kernforschungszentrum, Karlsruhe, Germany
U. Fischer, Kernforschungszentrum, Karlsruhe, Germany
P. W. Dickson, Jr., Clinch River Breeder Reactor Project, Oak Ridge
K. D. Lathrop, Los Alamos National Lab.
D. A. Meneley, Ontario Hydro, Toronto, Canada
J. E. Meyer, Massachusetts Inst. Technology
R. Sher, Stanford U.
D. B. Wehmeyer, Detroit Edison Co.
M. Salvatores, Centre d'Etudes Nucleaires, Cadarache, France
J. Debrue, C.E.N./S.C.K., Mol, Belgium
P. Garvey, Atomic Energy of Canada Ltd., Chalk River
H. Rief, Centre Commun. de Recherche, C.C.E., Ispra, Italy
J. Bouchard, Centre d'Etudes Nucleaires, Cadarache, France
H. Küsters, Kernforschungszentrum, Karlsruhe, Germany
T. Asaoka, Japan Atomic Energy Research Inst., Tokai-Mura
K. Shirakata, PNC, Tokyo, Japan
J. Askew, AEE Winfrith, United Kingdom
F. Maienschein, Oak Ridge National Lab.
R. Martinelli, ENEA, Italy
M. Bustraan, Energy Research Foundation, Petten, The Netherlands
K. Jirlow, ABA Studsvik, Sweden

P. Wydler, EIR Wuerenlingen, Switzerland
B. Allen, A.A.E.C. Research Establishment, Sutherland, Australia
M. S. Moore, Los Alamos National Lab.
K. Kobayashi, Research Reactor Institute, Kyoto U., Japan
H. H. Neltrup, Risø National Lab., Roskilde, Denmark

ARGONNE NATIONAL LAB WEST
3 4444 00023007 8